

(NASA-CR-134207) STUDY TO DEFINE LOGIC
ASSOCIATED WITH CMGS TO MANEUVER AND
STABILIZE AN ORBITING SPACECRAFT Final
Report (Bendix Corp.) 528 p HC \$29.50

N74-19515

Unclas

CSCI 22B G3/3. 32549

The
Bendix
Corporation


Navigation and
Control Division
Denver Operations

Study to Define Logic
Associated With CMGs
to Maneuver and
Stabilize an Orbiting
Spacecraft

Approved by:


S. Calvin Rybak
Program Manager


O. Taylor
Technical Manager


M. Brown
Manager
Denver Operations

Final Report

September 4, 1973

Prepared For:

Johnson Space Center
Houston, Texas

NASA Contract No.
NAS9-13085

FOREWORD

This Final Report is submitted in accordance with requirements of NASA-JSC, Contract No. NAS9-13085.

CONTENTS

	<u>Page</u>
Foreword.	ii
Contents.	iii
 1. INTRODUCTION.	 1-1
1.1 General	1-1
1.2 Study Objectives.	1-1
1.3 Relationship to Other Efforts	1-2
1.4 Method of Approach and Principal Assumptions.	1-3
1.5 Basic Study Output and Significant Results.	1-4
1.6 Study Limitations	1-5
1.7 Suggested Additional Effort	1-5
 2. STUDY PLAN.	 2-1
 3. VEHICLE AND BASELINE RCS.	 3-1
3.1 Vehicle Dynamics.	3-1
3.2 Baseline Reaction Control Subsystem (RCS)	3-2
3.3 Baseline Vehicle Orbit.	3-2
 4. MISSION REQUIREMENTS.	 4-1
4.1 Vehicle Pointing and Stabilization.	4-1
4.2 Vehicle Attitudes	4-8
4.3 CMG Momentum Desaturation	4-10
4.4 Vehicle Maneuver Capability	4-10
4.5 Baseline Reaction Control Subsystem (RCS) for On-Orbit Vehicle Stabilization.	4-10
4.6 Mission Requirements Summary.	4-19
4.7 Notes	4-19
4.7.1 Symbols and Abbreviations	4-19
4.7.2 References.	4-20
 5. CMG SYSTEM REQUIREMENTS	 5-1
5.1 Impact of Mission Requirements on CMG Attitude Control System.	5-1
5.2 CMG Torque and Momentum Requirements.	5-2
5.2.1 Vehicle Torque Environment.	5-2
5.2.2 X Axis Perpendicular to the Orbital Plane (X-POP)	5-3
5.2.3 X Axis in the Orbital Plane (X-IOP)	5-8
5.2.4 Acquiring and Maintaining Local Vertical.	5-14
5.2.5 Tracking An Earth Target.	5-19
5.2.6 Maneuvering	5-25
5.2.7 Aerodynamic Torques	5-29
5.2.8 Summary of CMG Torque and Momentum Requirements.	5-29

CONTENTS (Continued)

	<u>Page</u>
5.3	CMG Redundancy. 5-32
5.4	Notes 5-32
5.4.1	Symbols and Abbreviations 5-32
5.4.2	References. 5-33
6.	CMG CONFIGURATION STUDY 6-1
6.1	CMG Types 6-1
6.2	CMG Output Torque 6-1
6.3	CMG Survey. 6-4
6.3.1	Double Gimbal CMGs. 6-4
6.3.2	Single Gimbal CMGs. 6-10
6.4	CMG Configuration Selection 6-16
6.5	Symbols and Abbreviations 6-19
7.	CMG SYSTEM STABILITY. 7-1
7.1	Vehicle Control Law 7-1
7.2	Vehicle Control Loop. 7-2
7.3	Notes 7-18
7.3.1	Symbols 7-18
7.3.2	Reference 7-19
8.	CMG MANEUVER CONTROL LAWS 8-1
8.1	Vehicle Control Law 8-1
8.2	Quaternion Maneuver Control Law 8-1
8.2.1	Quaternion Definition 8-2
8.2.2	Quaternion Strapdown Equations. 8-9
8.2.3	Quaternion Maneuver 8-15
8.2.4	Quaternion Vehicle Attitude Error 8-18
8.3	Direction Cosine Maneuver Control Law 8-19
8.3.1	Direction Cosine Definition 8-19
8.3.2	Direction Cosine Strapdown Equations. 8-19
8.3.3	Direction Cosine Vehicle Attitude Error 8-22
8.3.4	Direction Cosine Maneuver 8-23
8.4	Euler Angle Maneuver Control Law. 8-27
8.4.1	Euler Angle Definition. 8-27
8.4.2	Euler Angle Strapdown Equations 8-29
8.4.3	Euler Angle Vehicle Attitude Error. 8-31
8.4.4	Euler Angle Maneuver. 8-39
8.5	Strapdown Equation Initialization and Update. 8-42
8.6	Comparison of Candidate Maneuver Control Laws 8-50
8.7	Selected CMG Maneuver Control Law Signal Flow Diagram 8-53
8.8	Notes 8-57
8.8.1	Symbols and Abbreviations 8-57
8.8.2	References. 8-58

CONTENTS (Continued)

		<u>Page</u>
9.	CMG CONTROL LAWS AND SINGULARITY AVOIDANCE	
	TECHNIQUES.	9-1
9.1	CMG Configurations.	9-1
9.2	CMG Torque Equations.	9-3
9.3	CMG Control Laws and Singularity Avoidance.	9-14
9.4	CMG Control Laws.	9-17
9.4.1	Cross Product CMG Control Law	9-17
9.4.2	H-Vector CMG Control Law.	9-28
9.4.3	Decoupled Scissored Pair CMG Control Law.	9-35
9.4.4	Decoupled Pseudo-Inverse CMG Control Law.	9-52
9.5	CMG Singularity Avoidance Laws.	9-61
9.5.1	Arbitrary Torquing of CMGs Away From Singularity	9-62
9.5.2	Isogonal CMG Distribution Law	9-73
9.5.3	Optimal CMG Distribution Law.	9-85
9.6	Combined CMG Gimbal Rate Command Law.	9-101
9.7	Selection of CMG Control Law and Singularity Avoidance Scheme.	9-110
9.8	Logic Flow Diagram for Recommended CMG Control Law and Singularity Avoidance System.	9-113
9.9	Notes	9-120
9.9.1	Abbreviations and Symbols	9-120
9.9.2	References.	9-121
10.	CMG SYSTEM MOMENTUM MANAGEMENT.	10-1
10.1	Shuttle and Baseline RCS Models	10-1
10.2	Prediction of CMG Momentum Profile.	10-1
10.3	Reaction Control System (RCS) CMG Desaturation Systems	10-14
10.3.1	System 1: CMG Attitude Control	10-14
10.3.2	System 2: RCS Attitude Control	10-24
10.3.3	Comparison of RCS CMG Desaturation Systems	10-34
10.3.4	Recommended RCS CMG Desaturation Signal Flow Diagram.	10-37
10.4	Gravity Gradient CMG Desaturation Systems	10-40
10.4.1	Orbit, Coordinate Frames, and Coordinate Transformations	10-40
10.4.2	Small Angle CMG Desaturation Law.	10-45
10.4.3	A Single Axis Large Angle Desaturation Control Law	10-54
10.4.4	A Reflexive Control Law for Desaturation From An Arbitrary Attitude.	10-69

CONTENTS (Continued)

	<u>Page</u>
10.4.5 A Gravity Tracking Control Law for Desatura- tion From An Arbitrary Attitude	10-85
10.4.6 Gravity Gradient CMG Desaturation Law Comparison.	10-98
10.4.7 Small Angle Gravity Gradient Z-LV Desatura- tion Law.	10-98
10.4.8 Gravity Gradient CMG Desaturation Law Signal Flow Diagrams.	10-110
10.5 Selection of Baseline CMG Desaturation System . . .	10-113
10.6 Pseudo-Axis Alignment Scheme.	10-114
10.6.1 Derivation of Inertial X-POP Pseudo-Axis Alignment Control Law	10-115
10.6.2 Derivation of Inertial X-IOP Pseudo-Axis Alignment Control Law	10-118
10.7 Notes	10-122
10.7.1 Symbols and Abbreviations	10-122
10.7.2 References.	10-124
11. REVIEW OF SELECTED CMG CONTROL LOGIC.	11-1
12. COMPUTER VERIFICATION	12-1
12.1 Simulated CMG Control System.	12-1
12.2 Computer Study Results.	12-3
12.2.1 System Response Runs.	12-6
12.2.2 Singularity Avoidance Runs.	12-6
12.2.3 Orbital Runs.	12-7
13. CONCLUSIONS	13-1
 <u>Figure</u>	
2.1 Study Plan Logic Flow Diagram	2-2
2.2 CMG Control Logic Block Diagram	2-4
3.1 Sketch of Shuttle RCS Thruster Locations.	3-3
4.1 Shuttle Astronomy Sortie Missions Experiment Mounts.	4-7
4.2 Sketch of RCS Attitude Deadband	4-13
5.1 Sketch of Shuttle X-POP Attitudes	5-4
5.2 Angular Momentum Vs Time (X-POP Attitude)	5-7
5.3 Sketch of X-IOP Shuttle Attitude.	5-9
5.4 Elliptical Orbit Geometry	5-16
5.5 Tracking Earth Target	5-22
5.6 Example Vehicle Maneuver.	5-27
6.1 Sketches of a Single and a Double Gimbal CMG.	6-2
6.2 Sketch of SG and DG CMG Torque Loci	6-3

CONTENTS (Continued)

	<u>Page</u>
6.3 Candidate MA-6000D DGCMG Mounting Configuration . . .	6-8
6.4 Candidate MA-2300 DGCMG Mounting Configuration. . . .	6-9
6.5 Typical SGCMG Pyramid Mounting Configuration.	6-11
6.6 Sketch of Potential SGCMG Desaturation Problem Associated With Nonspherical Momentum Envelope.	6-13
6.7 Three-Scissored Pair SGCMC Mounting Configuration	6-17
7.1 Vehicle Control Loop.	7-3
7.2 Disturbance Due to Crew Motion.	7-4
7.3 Simplified Vehicle Control Loop Signal Flow Diagram	7-6
7.4 Magnitude Vs Frequency (Bode) Plot of Simplified Open Vehicle Control Loop	7-7
7.5 Magnitude Vs Frequency Plot of Simplified Vehicle Control Loop Using Typical SGCMG's ($\tau=0.002$ sec)	7-10
7.6 Signal-Flow Graph of Rigid DGCMG.	7-11
7.7 Simplified Vehicle Control Loop (Using Quadratic Approximation to DGCMG)	7-12
7.8 Magnitude Vs Frequency Plot of Simplified Vehicle Control Loop Using Typical DGCMG's.	7-13
7.9 Typical Attitude Errors	7-17
8.1 Rigid Body Coordinate Systems	8-3
8.2 Rotational Displacement θ of $X_v Y_v Z_v$ From $x'y'z'$	8-5
8.3 Euler Rotations ψ, η, ϕ	8-10
8.4 Direction Cosines Associated With Vehicle Frame $X_v Y_v Z_v$ and Reference Frame XYZ.	8-20
8.5 Sketch of Direction Cosine Maneuvers.	8-24
8.6 Euler Angles.	8-28
8.7 CMG Quaternion Maneuver Control Logic Flow Diagram (3 sheets).	8-54
9.1 Proposed CMG Mounting Configuration	9-2
9.2 CMG Assembly.	9-4
9.3 Singularity Conditions for a Double Gimbal CMG System.	9-16
9.4 Relationship Between Cross Product CMG Control Torque \vec{T}_{CMG} and \vec{T}_{COM}	9-18
9.5 Cross Product CMG Control Law Vehicle Control Loops	9-19
9.6 Relative Orientations of $\vec{\omega}_{Ii}$, \vec{H}_{Ii} , and \vec{H}	9-21

CONTENTS (Continued)

	<u>Page</u>
9.7 H-Vector CMG Control Law Vehicle Control Loop	9-29
9.8 Cross Product and H-Vector CMG Control Law Block Diagrams.	9-32
9.9 Decoupled Scissored Pair CMG Control Law Vehicle Control Loop.	9-36
9.10 CMG Scissored Pair 1, 2	9-37
9.11 Sketch of \vec{H}_x , \vec{H}_y , and \vec{H}_{xy}	9-45
9.12 Decoupled Pseudo-Inverse CMG Control Law Control Loop.	9-53
9.13 Detection of \vec{H}_1 and \vec{H}_2 Approaching Anti-Parallel Condition	9-63
9.14 Block Diagram of Arbitrary Torquing CMGs Away From Singularity Scheme	9-66
9.15 Signal Flow Logic Diagram for Arbitrary Torquing of CMGs Away From Singularity (Slaved CMG Mode of Operation) (2 sheets).	9-67
9.16 Signal Flow Logic Diagram for Arbitrary Torquing of CMGs Away From Singularity (Six Individual CMG Mode) (2 sheets).	9-71
9.17 Sketch of an Isogonal CMG Distribution.	9-74
9.18 CMG Pair 1, 2	9-75
9.19 Functional Block Diagram of Isogonal CMG Distribu- tion Law.	9-78
9.20 Block Diagram of Optimal CMG Distribution Law	9-86
9.21 Pseudo-Inverse CMG Control Law and Optimal CMG Distribution Law Logic Flow Diagram (5 sheets). . . .	9-114
10.1 Recommended CMG Mounting Configuration.	10-4
10.2 Sketch of Inertial X-IOP Attitude	10-7
10.3 Logic Flow Diagram For Predicting Future CMG Momentum Profiles	10-12
10.4 Potential Implementations of RCS Desaturation System, System 1.	10-15
10.5 Sketches of CMG Isogonal Distribution and RCS Desaturation Torque \vec{T}_{RCS} and Resultant CMG Torque \vec{T}_{CMG}	10-19
10.6 Sketches of \vec{T}_{RCS} , \vec{T}_{CMG} , $\vec{\alpha}$, $\vec{\omega}$, and $\vec{\theta}$	10-21
10. Alternative Implementation RCS Desaturation System, System 1.	10-25
10.8 Sketch of RCS Desaturation System, System 2 Modulated Pulse	10-33

CONTENTS (Continued)

	<u>Page</u>
10.9 System 2: Phase Plane $\omega_y(t)$ Versus $\theta_y(t)$	10-35
10.10 Logic Signal Flow Diagram for Recommended RCS CMG Desaturation System	10-38
10.11 Vehicle Reference Frame $X_R Y_R Z_R$	10-41
10.12 Orbital Reference Frame $X_O Y_O Z_O$	10-43
10.13 Relation of a Vector (Axis) Directed Toward a Celestial Target with Respect to the $X_R Y_R Z_R$ Frame	10-44
10.14 Vehicle Desaturation Maneuvers for the Single Axis Large Angle Law.	10-55
10.15 Orientation of the Intermediate Coordinates	10-58
10.16 The Gravity Torque Plane.	10-87
10.17 Torque Vector Orientation	10-88
10.18 Control Switching for the Gravity Tracking Method	10-94
10.19 Z-LV Inertial Orbital Reference Frames.	10-104
10.20 Internal Small Angle Gravity Gradient Desatura- tion Law Logic Flow Diagram	10-111
10.21 Z-LV Small Angle Gravity Gradient CMG Desatura- tion Law Logic Flow Diagram	10-112
12.1 Selected CMG Mounting Configuration	12-2
12.2 CMG Attitude Control System Block Diagram	12-4
12.3 Impulse and Step Response Runs With X-POP, Z-TT (3 sheets)	12-12
12.4 Singularity Avoidance Runs With X-POP, Z-TT (3 sheets).	12-15
12.5 Inertial Orbital Run With X-IOP and Z-TT. No CMG Desaturation (3 sheets)	12-18
12.6 Inertial Orbital Run With X-IOP and Z-TT (3 sheets).	12-21
12.7 Inertial Orbital Run With X-IOP and Z-TT (Nominally) and 1/2 Degree Vehicle Offset on Each Axis (3 sheets)	12-24
12.8 Inertial Orbital Run With X-POP and Z-TT. No CMG Desaturation (3 sheets)	12-27
12.9 Inertial Orbital Run With X-POP and Z-TT (3 sheets).	12-30
12.10 Inertial Orbital Run With X-POP and Z-TT (Nominally) and 1/2 Degree Vehicle Offset on Each Axis (3 sheets)	12-33
12.11 Z-LV Orbital Run With X-IOP. No CMG Desatura- tion (3 sheets)	12-36

CONTENTS (Concluded)

	<u>Page</u>
12.12 Z-LV Orbital Run With X-IOP (3 sheets)	12-39
12.13 Z-LV Orbital Run With X-IOP (Nominally) and 1/2 Degree Vehicle Offset on Each Axis (3 sheets)	12-42
12.14 Z-LV Orbital Run With X-POP (3 sheets)	12-45
12.15 Z-LV Orbital Run With X-POP (Nominally) and 1/2 Degree Vehicle Offset on Each Axis (3 sheets)	12-48
 <u>Table</u>	
3.1 Baseline RCS Characteristics	3-4
4.1 RAM Sortie Payloads and Requirements (4 sheets) . . .	4-2
4.2 Shuttle Mission Requirements	4-18
5.1 Torque and Momentum Requirements for Z-LV ($h_a = 100$ n.m.; $h_p = 100 - 1,000$ n.m.)	5-20
5.2 CMG Torque and Momentum Requirements for Tracking an Earth Target	5-24
5.3 CMG Torque and Momentum Maneuver Requirements	5-26
5.4 Summary of Worst Case Torque and Momentum Requirements	5-30
6.1 Bendix Double-Gimbal Control Moment Gyros	6-6
6.2 Total Candidate DGCMG System Characteristics	6-6
6.3 Bendix Single-Gimbal Control Moment Gyros	6-15
6.4 Candidate Shuttle CMG Configuration and Requirements	6-18
8.1 CMG Maneuver Control Laws	8-51
10.1 Assumed Shuttle RCS and Vehicle Characteristics . . .	10-2
10.2 Advantages and Disadvantages of RCS Desaturation Systems System 1 and 2	10-36
13.1 Mission Requirements	13-2

1. INTRODUCTION

1.1 General - The orbiting of Skylab has marked the beginning in a series of large manned orbiting spacecraft that will be used as bases from which a variety of experiments will be performed. These experiments include astronomy, Earth resources, biomed, space physics, and various other technology areas. The orbital environment will enable measurements and observations to be made over extended periods of time that were not possible from the Earth or high flying aircraft due to atmospheric obscuration, the gravity environment, and limited observation times. These observations, measurements, and experiments conducted in space will contribute significantly to the understanding of the universe, its origin and dynamic behavior, as well as the Earth, its resources, weather, and its complex dynamic life cycles.

The Space Shuttle presently being planned by NASA will not only be a logistics vehicle, but will also serve a crucial role as a manned experiment base. In this role the Shuttle will orbit the Earth from 7 to 30 days performing various experiments with equipment mounted in the cargo bay and/or deployed on various types of booms and isolation mechanisms. Examination of the experiments proposed for performance in low Earth orbit attached to a manned orbiting spacecraft such as Shuttle indicates that attitude stabilization of one degree or better is required by approximately 65 percent of the payloads with many of them primarily in the astronomy area requiring pointing stabilities of an sec or better. In addition, all of the astronomy and plasma physics experiments proposed are extremely sensitive to contamination. A CMG system that will stabilize large orbiting spacecraft such as the Shuttle is very attractive since it would provide a contamination free environment and simplify the experiment integration equipment needed to meet the stringent pointing stability requirements of the astronomy and some of the physics experiments.

This study titled "Study to Define Logic Associated With CMGs to Maneuver and Stabilize an Orbiting Spacecraft" will define a CMG system capable of controlling a large orbiting spacecraft such as a Shuttle and develop all of the software required to satisfactorily manage and control such a system.

1.2 Study Objectives - The objectives of this study were the following:

- a. Define mission requirements and feasible attitudes for a Shuttle-like vehicle that will meet mission objectives.

- b. Determine the CMG actuator type (i.e., Single Gimbal CMGs or Double Gimbal CMGs) and system configuration that will best meet overall mission requirements.
- c. Define all of the software required to manage and control the selected CMG system.
- d. Verify by computer simulation the adequacy of the selected CMG system and specified software package in meeting the overall mission requirements.

All of the above objectives were met during the course of the study.

1.3 Relationship to Other Efforts - The Bendix Corporation has been critically involved with the Skylab program since its inception, performing studies in the areas of communications, mission operations, experiment integration, stabilization and control, human factors, and test and reliability. Bendix has also furnished the double gimbal CMGs, double gimballed star tracker and the experiment pointing electronics assembly (EPEA) which form a critical part of the total Skylab attitude and pointing control system (APCS) in addition to the C&D console used to operate and command virtually all systems aboard Skylab. During the course of the Skylab program detailed studies have been made into the behavior of CMG systems and the software required to satisfactorily control and manage such a system. Valuable experience and insight into the behavior and idiosyncracies of CMG systems has been gained over the seven years that these studies were performed, and was directly applicable to the performance of the present study.

Data generated during the course of the Research and Applications Module (RAM) study (May 1971 - June 1972) in which Bendix was a prime participant, provided valuable input to the present study in the area of proposed experiment payloads for the Shuttle vehicle and the requirements placed upon that vehicle due to those payloads. In addition the experience gained in the analysis and design of candidate CMG control systems for RAM applications is directly applicable to the present study.

The Astronomy Sortie Mission (ASM) Definition Study (December 1971 - March 1973) in which Bendix was a prime participant, also provided valuable inputs to the present study in the area of Shuttle vehicle requirements due to proposed astronomy experimentation and in the design of possible attitude control systems which included reaction control, CMG, and experiment isolation systems that could be used to meet these requirements.

The experience and technical expertise gained during the performance of Skylab, RAM, and ASM formed the technological base which the present study was able to draw upon to further advance CMG technology for Shuttle-like vehicle applications thus yielding the basis for the design of a realistic hardware and software package that could be used for this purpose.

1.4 Method of Approach and Principal Assumptions - The approach taken in the performance of the present study was to make maximum use of the results obtained in the RAM and ASM programs. These outputs still assumed applicable were used to specify the requirements placed upon a Shuttle type vehicle by the experimentation programs defined in these studies. In addition whatever developed hardware (i.e., CMGs) available from Skylab and other programs would be given maximum consideration for use in the present application in order to obtain an optimum and cost effective system. The software packages designed for Skylab, RAM, and ASM were used as a starting point for the present study which helped to optimize both system performance and computational requirements for the software package specified to meet the present overall mission specifications.

Verification of the specified CMG control system and associated software package was accomplished on a hybrid computer. The reason for choosing a hybrid machine to perform system verification was to enable the faithful simulation of the A/D and D/A interfaces that would be encountered in an actual flight control system. Effects of quantization and sampling time were taken into account in the specification of overall system performance.

The Shuttle as defined in the July 1972 time frame was the vehicle for which the CMG control system design was defined. The Shuttle was modeled as a rigid body which was another assumption of the present study. Modeling the vehicle in this manner obviated the need for bending mode filters that might be required to yield satisfactory vehicle stability when flexibility is taken into account. These bending mode filters would probably be implemented in the digital computer aboard the vehicle and therefore represent an added software load. In addition the vehicle pointing stability would be somewhat degraded when vehicle flexibilities are taken into account. However, all of the software developed for managing and controlling the CMG system specified would still apply when vehicle flexibility is considered.

1.5 Basic Study Output and Significant Results - The study results and significant conclusions are listed below:

- a. The Shuttle attitudes that will meet mission requirements can be divided into two classes, pseudo-inertial and local vertical. The pseudo-inertial orientations are longitudinal vehicle axis perpendicular to the orbital plane (X-POP), and the longitudinal axis of the vehicle in the orbital plane (X-IOP). In the local vertical orientation, the vehicle Z axis is local vertical with the vehicle X axis in the orbital plane (X-IOP, ZLV) or perpendicular to the orbital plane (X-POP, ZLV).
- b. CMG system is sized to allow attitude hold for one orbit under the worst case gravity gradient momentum accumulation.
- c. The CMG system chosen for Shuttle attitude control consists of six Skylab double gimbal CMGs modified with slip rings to enable unlimited gimbal freedom. Each of these CMGs have a momentum capability of 2,300 ft-lb-sec and provides fail operational, fail safe capability.
- d. A rate plus position control law is recommended for vehicle stabilization with a closed loop bandwidth of 0.127 rad/sec and a damping ratio of 0.7.
- e. The Pseudo-Inverse CMG Control Law is recommended for commanding appropriate CMG gimbal rates. This gimbal rate steering law will give decoupled vehicle control while minimizing the energy expended.
- f. The Optimal CMG Distribution Singularity Avoidance Control Law is defined in order to avoid CMG singularity conditions. This type of control will maximize the distance from a singularity condition for a particular CMG system momentum state and is compatible with the Pseudo-Inverse CMG Control Law.
- g. Gravity gradient desaturation is the recommended means of CMG momentum unloading. This will yield a contamination free environment required by a number of the proposed experiment payloads. The gravity gradient desaturation control law selected maneuvers the vehicle through small angles (i.e., <15 deg) in order to achieve momentum dump. This type of control law minimizes computational requirements and the momentum required to affect the gravity gradient maneuvers.

- h. A hybrid computer simulation verified the adequacy of the chosen CMG system configuration and associated software package in meeting overall mission requirements.

1.6 Study Limitations - The present study was primarily geared to define the software package required to manage and control a representative CMG system that could be used to control the attitude of a Shuttle type vehicle. Although trade studies were performed to select a candidate CMG system configuration from several alternatives, they did not constitute a major portion of the study and hence were top level in nature. When the design of an actual CMG system for Shuttle is contemplated, considerably more effort would be required in trading various candidate CMG system configurations in order to determine the optimum configuration that would meet overall Shuttle requirements in a cost effective manner. Shuttle mass characteristics should be updated to reflect the present Shuttle configuration. Additionally the latest experiment payloads slated to fly in a sortie mode should be examined in order to better ascertain and update the requirements placed upon the Shuttle by these experiments. However it should be noted that all of the techniques and some of the control laws (i.e., gravity gradient desaturation) developed in this study will be directly applicable to any CMG configuration that may finally result for Shuttle attitude control.

Although the pointing stability achievable by the CMG system selected has been estimated, the pointing performance that could ultimately be obtained would require a more comprehensive simulation for its determination. This simulation would include vehicle flexibility, CMG dynamics including all nonlinearities, and adequate representation of man motion disturbances. A more accurate determination of the pointing stability achievable by the CMG system is desirable since it would have a very strong effect on the type and complexity of the required experiment integration equipment. This in turn can appreciably effect the overall cost of the Shuttle experiment program.

1.7 Suggested Additional Effort - The following additional effort is suggested:

- a. Review the experiments that are presently candidates for the Shuttle sortie mode and revise/update Shuttle mission requirements.
- b. Define candidate CMG control system configurations that could meet Shuttle mission requirements. Perform indepth trade studies between the various CMG control system configurations in order to determine the optimum CMG configuration that will meet overall mission requirements in a cost effective manner. These studies should include detailed hardware trade offs with respect to size,

weight, power consumption, reliability and cost as well as the impact various CMG configurations have on software complexity and overall software cost. In addition candidate types of control logic (e.g., CMG gimbal rate control laws, singularity avoidance laws, etc.) required to satisfactorily manage the CMG control system should be evaluated from the standpoint of software complexity, and required computer capacity for implementation as well as overall performance. These software trades will be of key significance in determining whether a dedicated or the central Shuttle computer be used to drive the chosen CMG system configuration.

c. Define the software package required to satisfactorily manage and control the resulting CMG system configuration. The amount of revision to the candidate CMG control logic described in this study will depend on the final configuration of the Shuttle CMG control system. If the configuration consists of a cluster of double gimbal CMGs, the modifications required to the defined control laws would be minimal. If the chosen CMG system consists of a cluster of single gimbal CMGs or a mixture of single and double gimbal CMGs the required software modification would be more extensive. However, regardless of the CMG configuration chosen, all of the techniques used to derive the various control laws required to manage a CMG system detailed in this report still applies.

d. Determine the accuracy that can be achieved by the CMG system and the impact this accuracy has on the type and complexity of required experiment integration equipment.

2. STUDY PLAN

Figure 2.1 is the study flow diagram describing the logic flow used to perform this study. The study was initiated as shown in block 1 by first selecting an appropriate vehicle that would benefit from a control moment gyro (CMG) attitude control system. The vehicle selected was the Space Shuttle. The assumed Shuttle vehicle dynamics and baseline reaction control subsystem (RCS) characteristics used in this study are contained in section 3. Proceeding onto block 2, the next objective is to determine the vehicle mission requirements and how they impact the proposed CMG control system. For this analysis, the Shuttle sortie missions defined in the General Dynamics/Convair Phase B Research and Application Module (RAM) program were used. The results of this analysis are contained in section 4. In block 3 of the study flow, the mission requirements defined in the previous task are translated into appropriate CMG system requirements, such as output torque, momentum storage, and system redundancy requirements. The analysis and the resultant CMG system requirements are documented in section 5. After the CMG system requirements have been defined, the next step in the logic flow is to perform a survey of available CMG actuators. In this study a survey of both double gimbal and single gimbal CMGs was performed. From this survey, a number of candidate CMG systems were configured to meet the CMG system requirements defined in section 5. A recommended CMG configuration was selected based on system weight, power, volume, availability, and software complexity. This task is documented in section 6. In block 5, a CMG system stability analysis is performed. In this task, a vehicle control law is defined along with a set of appropriate control law gains that insure CMG control system stability. The resultant vehicle control law analysis is documented in section 7.

In block 6 of this study flow diagram, a trade study is performed to select the CMG control logic needed to implement the CMG control system configured and designed in blocks 4 and 5. The required CMG control logic consists of three components; they are: (1) a CMG maneuver control law, (2) a CMG gimbal rate command law, and (3) a CMG system momentum management scheme. The general relationships of these three CMG control logic functions are illustrated in the block diagram shown in figure 2.2. In sections 8 thru 10 of this report, various candidates for the above CMG control logic functions are derived. From each set of candidates, a law is selected based primary on computational complexity and performance.

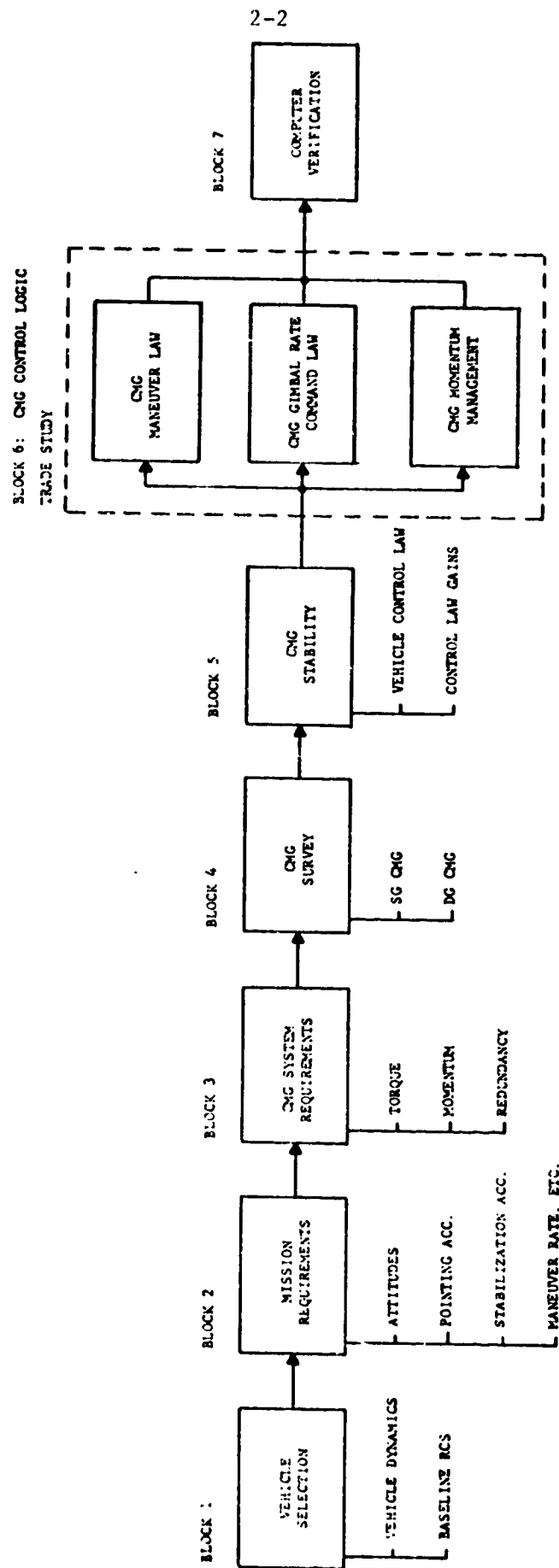


Figure 2.1. Study Plan Logic Flow Diagram

In section 8, three candidate CMG maneuver control laws are derived; these three laws are based on (1) quaternion, (2) direction cosine, and (3) Euler angle strapdown implementations for describing the attitude of a spacecraft. The function of these three methods for computing the strapdown equations of motion is to generate the appropriate error signals that will enable the vehicle to maintain or track specific attitudes and to perform particular maneuvers from one attitude to another. The resultant attitude error $\Delta \vec{\theta}$ and/or rate maneuver command $\vec{\omega}_D$ are implemented by inputting these signals into the vehicle control law as shown in figure 2.2.

The CMG gimbal rate command law shown in figure 2.2 consists of two components; they are: (1) a CMG control law and (2) a CMG singularity avoidance scheme. The CMG control law generates a set of CMG gimbal rate commands as a function of the CMG gimbal state that will produce the desired CMG torque \vec{T}_{COM} as computed by the vehicle control law. The purpose of the CMG singularity avoidance scheme is to drive the CMG system away from singularity points in its CMG gimbal space where the CMG system is physically unable to generate a three axis control torque. In other words, the function of the CMG singularity avoidance scheme is to insure that the CMG system is always capable of generating the desired CMG torque \vec{T}_{COM} whenever the system is not in saturation. The singularity avoidance scheme generates an additional set of CMG gimbal rate commands that drive the CMG system away from singularity without applying a net CMG torque to the vehicle. The sum of the CMG control law and singularity avoidance scheme gimbal rate commands $\vec{\omega}_c$ are routed to the appropriate CMG actuators as shown in figure 2.2. In section 9 of this report, various candidate CMG control laws and CMG singularity avoidance schemes are derived and from these candidates a CMG control law and a singularity avoidance scheme is selected.

The function of the CMG momentum management scheme depicted in figure 2.2 is to insure that the CMG momentum exchange system does not saturate. Two types of laws are described in section 10, accomplishing the above objective in different ways. The first law described is a CMG desaturation law which desaturates the CMG system by applying a torque to the vehicle which reduces the magnitude of the momentum stored in the CMG system. In section 10, two general types of CMG desaturation systems are described; they are (1) a reaction jet desaturation system utilizing the baseline Shuttle

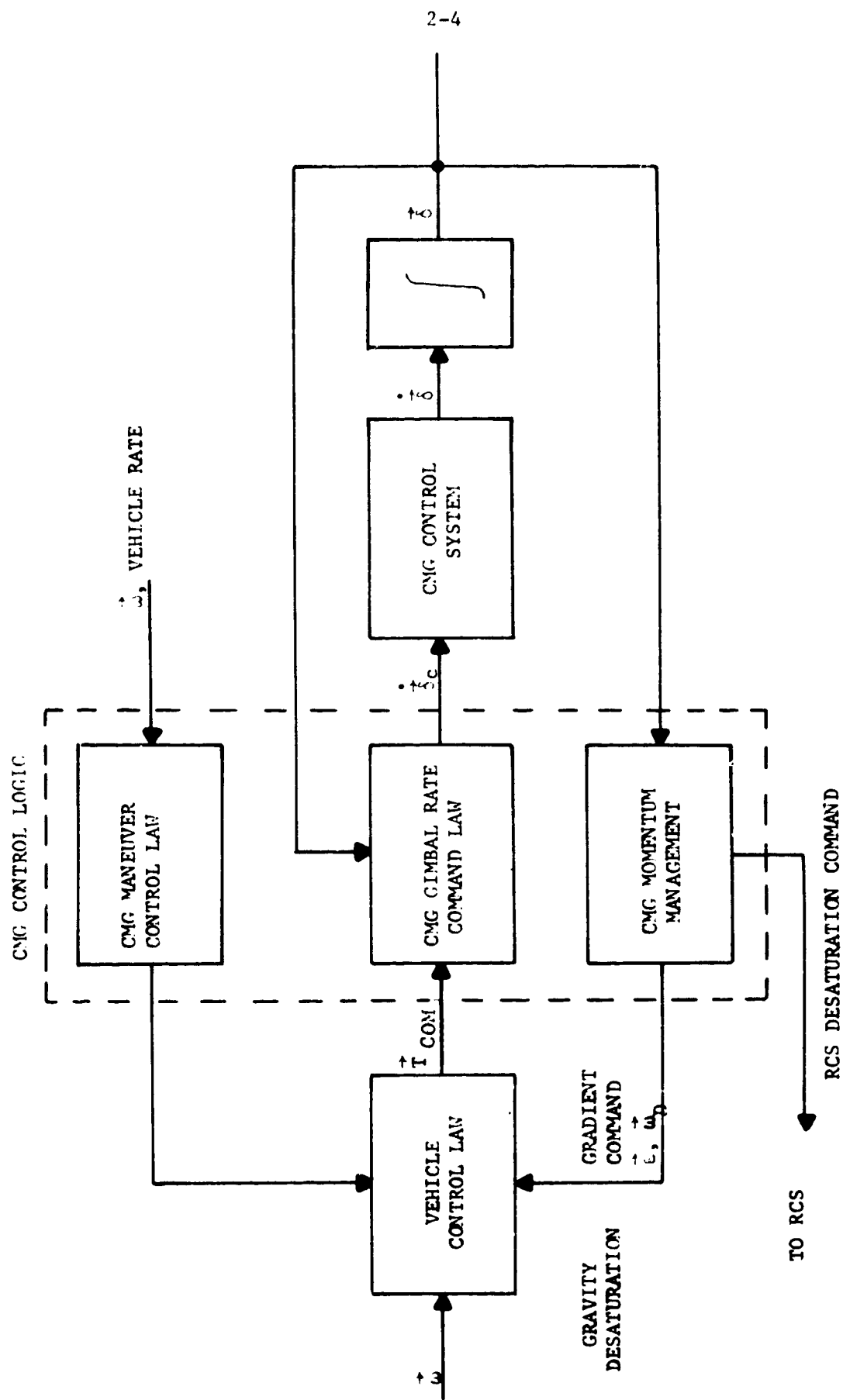


Figure 2.2 CMG Control Logic Block Diagram

RCS and (2) a gravity gradient desaturation system which uses the gravity gradient torques acting on the vehicle. As illustrated in figure 2.2, a RCS desaturation system desaturates the CMG system by sending appropriate jet firing commands to the baseline RCS. For a gravity gradient desaturation system, CMG desaturation is accomplished by sending the appropriate vehicle maneuver command \vec{c} and rate command $\vec{\omega}_D$ to the vehicle control law where these commands are implemented. In section 10, from among the various RCS and gravity gradient desaturation systems, a preferred desaturation law is selected. The second law described in section 10 is a pseudo-axis alignment scheme which attempts to compensate for the momentum build-up in the CMG system resulting from vehicle principal and control axis misalignments. In this way, the pseudo-axis alignment scheme minimizes the momentum that the CMG desaturation law must "dump" for any particular attitude.

In block 7 of the study flow, all of the selected components of the CMG control system are brought together into a hybrid computer simulation. This hybrid computer simulation is used to verify the effectiveness of the selected CMG control logic and to demonstrate the overall operations of the selected CMG attitude control system. The results of this computer simulation are documented in section 12.

3. VEHICLE AND BASELINE RCS

The vehicle used in this study is assumed to be the Space Shuttle. Using the Shuttle as the baseline vehicle, the mission requirements and the sizing of the CMG attitude control system are determined in the following sections. Since at the beginning of this study no final Shuttle design existed, the vehicle dynamics and baseline reaction control subsystem (RCS) listed in this section are assumed to be representative of a final design.

3.1 Vehicle Dynamics - The Shuttle is assumed to be a rigid body with the following moments of inertia:

$$I_{xx} = 1.04 \times 10^6 \text{ slug ft}^2$$

$$I_{yy} = 8.21 \times 10^6 \text{ slug ft}^2$$

$$I_{zz} = 8.55 \times 10^6 \text{ slug ft}^2$$

The vehicle cross products of inertia I_{xy} , I_{xz} , and I_{yz} are assumed to be negligible.

The vehicle dynamics are governed by the following Euler equation of motion:

$$\vec{T}_v = [I]\dot{\vec{\omega}} + \vec{\omega} \times [I]\vec{\omega} \quad (1)$$

\vec{T}_v is the total resultant torque acting on the vehicle; \vec{T}_v consists of all disturbance torques \vec{T}_D , torques \vec{T}_{RCS} exerted on the vehicle by the baseline RCS, and the CMG control torques \vec{T}_{CMG} ($\vec{T}_v = \vec{T}_D + \vec{T}_{RCS} + \vec{T}_{CMG}$). $[I]$ is the vehicle inertia tensor; $[I]$ equals

$$[I] = \begin{bmatrix} I_{xx} & 0 & 0 \\ 0 & I_{yy} & 0 \\ 0 & 0 & I_{zz} \end{bmatrix} \quad (2)$$

Note that because the cross products of inertia are zero, the X, Y, and Z vehicle geometric control axes are also the vehicle principal axes. $\vec{\omega}$ and $\dot{\vec{\omega}}$ are the vehicle angular rate and acceleration, respectively.

$$\dot{\omega} = \begin{bmatrix} \dot{\omega}_x \\ \dot{\omega}_y \\ \dot{\omega}_z \end{bmatrix} \quad (3)$$

3.2 Baseline Reaction Control Subsystem (RCS) - Figure 3.1 is a sketch of the Space Shuttle showing the locations of the baseline on-orbit reaction control subsystem. This system is assumed to consist of three pods, a single forward pod containing 16 thrusters and two aft pods containing 12 thrusters each. The forward pod thrusters in conjunction with the aft pod thrusters control both pitch and yaw while the two aft pod thrusters control roll. The normal control torque operating mode for this RCS system is to fire thruster pairs. A thruster pair firing consists of two thrusters fired simultaneously in opposite directions so that no net translational force is produced; the resulting pure control torque equals the engine thrust level times the corresponding moment arm between the two thrusters. The baseline RCS operating characteristics such as thrust level, attitude deadband, etc..., are listed in table 3.1.

3.3 Baseline Vehicle Orbit - The vehicle is assumed to be stabilized in a 270 nautical mile circular orbit.

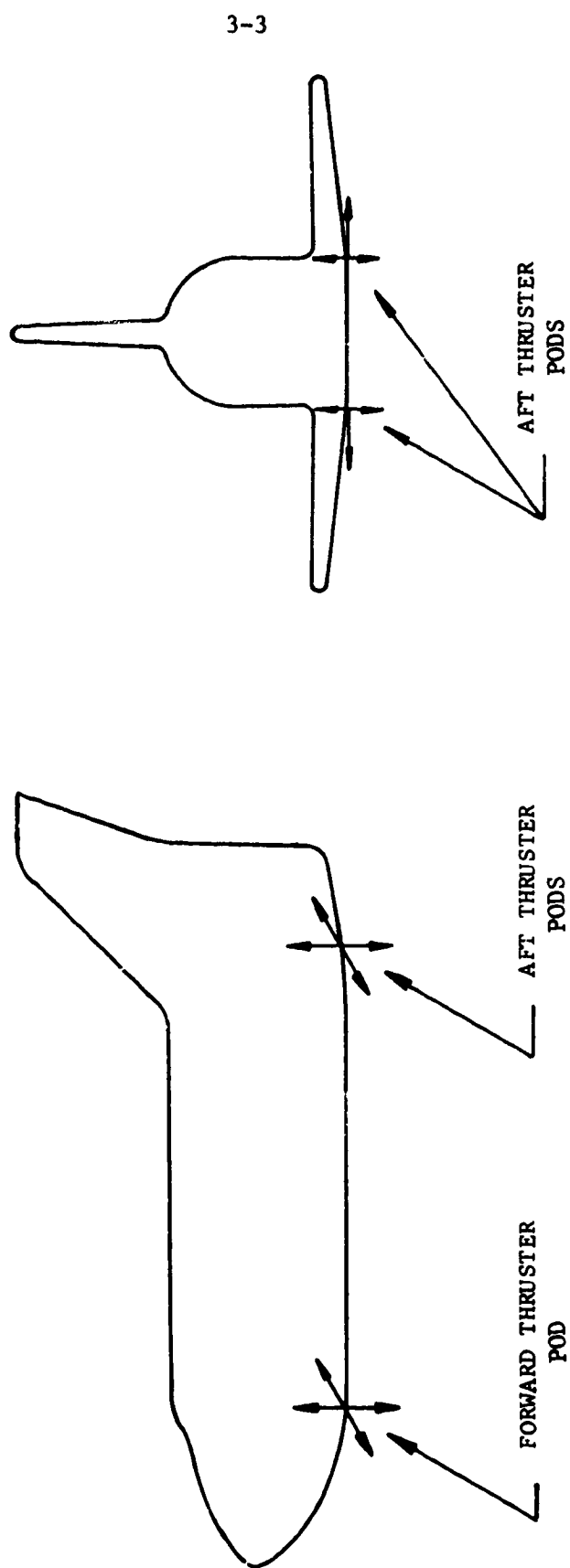


Figure 3.1 Sketch of Shuttle RCS Thruster Locations

Table 3.1. Baseline RCS Characteristics

Thrust level, F : 400 lbf.

Minimum pulse duration, t_f : 0.1 sec

Minimum attitude deadband, θ_o : ± 0.5 deg

Fuel: Monopropellant hydrazine with a specific
impulse I_{sp} of 200 seconds

Roll moment arm, l_x : 20.7 ft

Pitch moment arm, l_y : 100 ft

Yaw moment arm, l_z : 100 ft

4. MISSION REQUIREMENTS

In this section, typical Shuttle mission requirements are defined that impact and influence the design of a CMG attitude control system. These mission requirements are used in sections 5.0, 6.0, and 7.0 to size, configure, and design a Shuttle CMG control system.

4.1 Vehicle Pointing and Stabilization - The vehicle pointing and stabilization capabilities of a CMG control system are in general much superior to those of a reaction jet attitude control system. The addition of a CMG attitude control system to a vehicle like the Shuttle can drastically improve its pointing and stabilization capabilities and convert the vehicle into an accurately stabilized on-orbit experimental base. For this study, a CMG attitude controlled Shuttle base stabilization capability of three arc minutes is assumed. This projected stabilization capability is a conservative value because other studies for similar vehicles, reference 1, indicate that a stabilization capability of less than one arc minute is feasible. The accuracy with which this vehicle can be pointed using a CMG control system is assumed to be approximately equal to its stabilization capability of three arc minutes. In general, the accuracy with which a vehicle can be pointed is limited by the accuracy of its attitude determination sensors; these sensors therefore will need to have accuracies of three arc minutes or less.

Listed in table 4.1 are thirty-seven Shuttle sortie payloads defined in the General Dynamics/Convair Phase B Research and Application Modules (RAM) Study, reference 2. These payloads are listed in table 4.1 by disciplines: astronomy, physics, Earth observations, communications and navigation, materials science, technology, and life sciences. Also listed are the payload's pointing accuracy, stabilization, maximum observation, orientation, and contamination control requirements. It should be noted that the stabilization requirements listed in table 4.1 are specified either in terms of maximum allowable angular velocity (e.g., 0.5 $\hat{\text{sec}}/\text{second}$) or angular displacement (e.g., 1 $\hat{\text{sec}}/\text{observation}$). This latter method of specifying a stability criteria is preferred because angular displacement usually determines the success or failure of an observation. Stability requirements are specified in terms of angular velocity only in cases of very short observation intervals where an angular rate limit is essential. In the following paragraphs, the impact of this proposed Shuttle CMG attitude control system on the payloads listed in table 4.1 are investigated by scientific disciplines.

Table 4.1. RAM Sortie Payloads and Requirements

Discipline	Payload No.	Payload Title	Pointing		Maximum Observation Time (hr.)	Orientation	Contamination	
			Accuracy	Stability			Particles (Class)	Gas (toirs)
Astronomy	A3S1B	Austere Solar Astronomy (Photoheliograph)	10 sec	1 sec/obs	0.8	Solar	10,000	10^{-6}
	A6S1B	Austere IR Astronomy (ARC Telescope)	1 sec	0.5 sec/obs	5	Stellar	10,000	10^{-7}
	A8S1V	Combined Austere Astronomy Photoheliograph	10 sec	1 sec/obs	0.8	Solar	10,000	10^{-6}
		High Energy Array	1 min	30 sec/obs	3	Stellar	10,000	10^{-6}
	A8S1X	Combined Austere Astronomy Narrow-Field UV Telescope	1 sec	1 sec/obs	0.8	Stellar	10,000	10^{-6}
		High Energy Array	1 min	30 sec/obs	3	Stellar	10,000	10^{-6}
	A9S1J	Combined Austere Astronomy Solar Telescope	10 sec	2.5 sec/obs	0.75	Solar	10,000	10^{-7}
		High Energy Array	6 min	1 min/obs	0.75	Stellar	10,000	10^{-7}
	A8S1W	Combined Austere Astronomy Wide-Field UV Telescope	5 sec	1 sec/obs	1	Stellar	10,000	10^{-6}
		High Energy Array	6 min	6 min/obs	10	Stellar	10,000	10^{-6}
	A8S1Z	Combined Austere Astronomy IR Telescope	1 sec	1 sec/obs	0.75	Stellar	10,000	10^{-7}
		High Energy Array	5 min	1 min/obs	0.75	Stellar	10,000	10^{-7}

Table 4.1. RAM Sortie Payloads and Requirements (Continued)

Discipline	Payload No.	Payload Title	Pointing		Maximum Observation Time (hr.)	Orientation	Contamination	
			Accuracy	Stability			Particles (Class)	Gas (torrs)
Astronomy	A8S1U	Combined Austere Astronomy ARC Telescope	1 sec	0.5 sec/ obs	5	Stellar	10,000	10^{-7}
		High Energy Array	15 min	1.5 min/ obs	5	Stellar	10,000	10^{-7}
Physics	P5S1B	Combined Austere Space/Plasma Physics	2 min	12 sec/ sec	1.6	Earth		
	P5S2A	Combined Median Space/Plasma Physics	1.6 sec	0.5 sec/ sec	1	Stellar		
	P7S1A	Combined Austere Cosmic Ray/Physics & Chemistry	1 deg	0.1 deg/ sec	10	Away From Earth		
	P7S3A	Combined (Advanced) Cosmic Ray/Physics & Chemistry	1 deg	0.1 deg/ sec	10	Away From Earth		
Earth Observation	P8S2B	Combined (Median) Space/Plasma/Cosmic Ray Physics	1 deg	15 sec/ sec	0.3	Inertial	NS	
	E1S1N	Earth Observation (Weather)-Austere	0.5 deg	0.01 deg/ sec	0.25	Earth		
	E1S1O	Earth Observation (World Land Use Mapping) - Austere	0.5 deg	0.05 deg/ sec	0.45	Earth		
	E1S1P	Earth Observation (Air and Water Pollution) - Austere	0.5 deg	0.05 deg/ sec	0.2	Earth		
	E1S1Q	Earth Observations (Resource Location) - Austere	0.5 deg	0.05 deg/ sec	0.05	Earth		

Table 4.1. RAM Sortie Payloads and Requirements (Continued)

Discipline	Payload No.	Payload Title	Pointing		Maximum Observation Time (hr.)	Orientation	Contamination	
			Accuracy	Stability			Particles (Class)	Gas (torrs)
Earth Observation	ELS1R	Earth Observations (Disaster Assessment) - Austere	0.5 deg	0.05 deg/sec	0.25	Earth		
	ELS1S	Earth Observation (Ocean Resources) - Austere	0.5 deg	0.05 deg/sec	0.25	Earth		
Communications/Navigation	CLS1F	Communication/Navigation (Lab I) - Austere	0.5 deg	0.1 deg/sec	0.25	Earth		
	CLS1E	Communication/Navigation (Lab I) - Austere	0.5 deg	1 deg/sec	0.25	Earth	NS	
	CLS2C	Communication/Navigation (Lab II) - Median	0.5 deg	0.1 deg/sec	1	Earth/Stellar	NS	
Material Science	MLS1E	Material Science Configuration 1 - Operations Level 1	N/A	N/A	N/A	N/A		
	MLS1F	Material Science Configuration 1 - Operations Level 2	N/A	N/A	N/A	N/A		
	MLS1G	Material Science Configuration 1 - Operations Level 3	N/A	N/A	N/A	N/A		
	MLS2B	Material Science Configuration 2 - Operations Level 3	N/A	N/A	N/A	N/A		
Technology	TLS3A*	Complete Contamination Measurements	0.5 deg	0.05 deg/sec	14	Solar		
	T2S1A	Propellant Transfer Experiment	N/A	N/A	N/A	N/A		
	T2S2E	Combined Cryogenic Storage and Fluid Systems Experiment	N/A	N/A	N/A	N/A		

Table 4.1. RAM Sortie Payloads and Requirements (Concluded)

Discipline	Payload No.	Payload Title	Pointing		Maximum Observation Time (hr.)	Orientation	Contamination	
			Accuracy	Stability			Particles (Class)	Gas (torrs)
Technology	T3S1A*	Astronaut Maneuvering Unit Experiment	N/A	N/A	N/A	N/A		
	T3S2B	Maneuverable Work Platform Experiment	N/A	N/A	N/A	N/A		
	T4S1A*	Advanced Spacecraft Systems Test-Short Duration	NS	NS		NS		
	T5S2B	Teleoperator Shuttle Sortie	N/A	N/A	N/A	N/A		
	T2(D)2B	Detached Long-Term Cryogenic Storage Experiment	N/A	N/A	N/A	Inertial/Earth		
	L8S1B	Life Sciences Lab	N/A	N/A	N/A	N/A		
Life Sciences	L8S2B	Life Sciences Lab (MINI-30)	N/A	N/A	N/A	N/A		

* This payload is a "suitcase" type payload and flies piggy back with other experimental payloads.

sec - arc second sec/obs - arc seconds per observation IR - infrared N/A - not applicable

min - arc minute min/obs - arc minutes per observation UV - ultraviolet NS - not specified

deg - degree deg/sec - degrees per second ARC - Ames Research Center

Eight astronomy sortie payloads are defined in table 4.1. Six of these payloads consist of a telescope and a separate high energy array; the two remaining payloads, A3S1B and A6S1B, consist of a single telescope. The pointing accuracy and stabilization requirements associated with each telescope and high energy array are listed separately in table 4.1. In general, these pointing accuracies and stability requirements are more stringent than the corresponding projected vehicle capabilities thus, an additional fine pointing and stabilization system is required to meet these requirements. Another problem associated with the combined telescope and high energy array payloads is that some of the telescopes and high energy arrays need to be pointed at separate targets. For example, payload A8S1V consists of a telescope, a photoheliograph, that must be pointed at the sun and a high energy array that must be pointed at various stellar energy sources. This latter problem implies that the telescope and the arrays must have the capability of being pointed independently. These pointing and stabilization problems were solved in the RAM and the subsequent NASA Astronomy Sortie Missions (ASM) programs by mounting the telescope and the high energy arrays on separate experiment mounts located in the Shuttle bay as illustrated in figure 4.1. Built into each mount are: (1) a wide angle gimbaling system so that each telescope and array can be accurately and independently pointed and (2) a fine stabilization system to provide the additional stabilization required. From table 4.1, note that the high energy array stability requirements range from 0.5 to 6 arc minutes. If the eventual Shuttle base stabilization can be improved to within 0.5 arc minute using a CMG control system, the high energy array mount can be simplified by removing its fine stabilization system; the array and vehicle stabilization requirements and capabilities will then be compatible. In any case, stabilizing the Shuttle to three arc minutes simplifies the design problems associated with these mounts and therefore from the standpoint of the astronomy payloads pointing and stabilization requirements, the addition of a CMG control system to the Shuttle is desirable.

Five physics payloads are defined in table 4.1. Three of these payloads' pointing and stabilization requirements can be met by a CMG stabilized Shuttle. The two remaining physics payloads have pointing and stability requirements that exceed the projected Shuttle capabilities. To these two payloads, additional fine pointing and stabilization systems will have to be added to their affected scientific instruments in order to achieve these instruments' pointing and stabilization requirements.

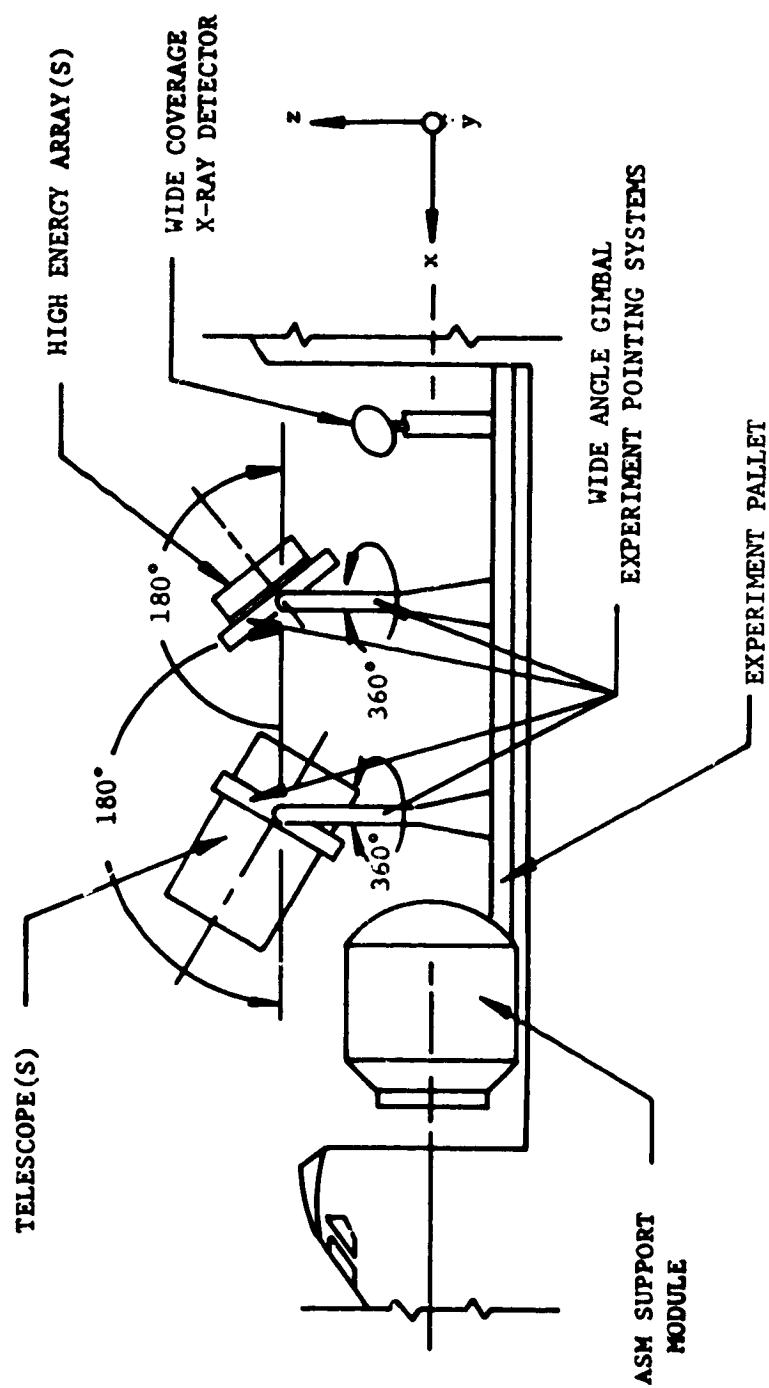


Figure 4.1. Shuttle Astronomy Sortie Missions Experiment Mounts

Six Earth observation and three communications and navigation payloads are listed in table 4.1. All of these payloads have pointing and stabilization requirements that are compatible with the projected CMG stabilized Shuttle capabilities. Only one other payload contained in table 4.1 has definite pointing and stabilization requirements; this payload is the technology payload T1S3A. Its pointing and stability requirements are also compatible with the projected CMG Shuttle capabilities.

Of the thirty-seven sortie payloads defined in the RAM program, twenty-three have definite pointing and stabilization requirements. Ten of these payloads' pointing and stability requirements can be directly met by the projected pointing and stabilization capabilities of a CMG stabilized Shuttle. These payload pointing and stability requirements cannot be realistically met by the baseline RCS system defined in section 3.0. The remaining thirteen payloads will require additional fine pointing and stabilization systems. The complexity of these additional systems can be simplified due to the improved Shuttle base pointing and stabilization capabilities afforded by a CMG control system. In total, the pointing and stabilization requirements of twenty-three of the thirty-seven sortie payloads listed in table 4.1 can be met or partially met by the projected Shuttle CMG control system.

4.2 Vehicle Attitudes - The Shuttle payloads listed in table 4.1 requires two types of attitudes; they are: (1) an inertial attitude which allows the experimental payloads to be pointed towards the sun or a distant celestial target and (2) a local vertical attitude with one of the Shuttle axes normally the Z axis pointed towards or away from the Earth. Three Shuttle attitudes were selected, two inertial and one local vertical, for meeting the above payload pointing requirements. The three selected attitudes are:

- a. An inertial attitude with the X axis perpendicular to the orbital plane (X-POP).
- b. An inertial attitude with the X axis in the orbital plane (X-IOP).
- c. A local vertical attitude with the Z axis aligned along the local vertical (Z-LV).

The stellar and solar payloads can be pointed and stabilized using either inertial attitudes a or b. These two inertial attitudes impact with the designs of the CMG attitude control and experiment pointing systems in different ways. For an inertial X-POP attitude, attitude a, the vehicle's Y and Z axes are constrained to the orbital plane thus reducing the spacecraft's rotational degrees-of-freedom from three to one. The vehicle can be rotated about only the X axis. In order to permit a hemispherical experiment coverage capability to within an accuracy of three arc minutes, at least one wide angle gimbal (range: ≈ 180 degrees) must be added to the experimental instrument to provide the second degree-of-freedom required. For an inertial X-IOP attitude, attitude b, the vehicle's X axis is constrained to the orbital plane thus reducing the vehicle's rotational degrees-of-freedom from three to two. The vehicle can be rotated about the X axis and an axis normal to the orbital plane. Because the vehicle still has two rotational degrees-of-freedom, the experiment package can be pointed anywhere in the celestial sphere hardmounted to the spacecraft; no wide angle gimbal is required. The cost of this additional rotational degree-of-freedom for an X-IOP attitude is a large increase in the CMG momentum storage requirement per orbit over that required by an X-POP attitude. This increase momentum storage requirement significantly impacts the size of the CMG control system; it can be directly related to additional CMGs required and more frequent CMG momentum desaturation "dumps". Depending on the experiment payload and its pointing and stabilization requirements, one of these two inertial attitudes may be required or exhibit certain characteristics that are particularly attractive for this specific mission or class of missions. For example, if on-orbit access to the payload's sensors or other components by the experimenter is required it may be impossible to add the wide angle gimbal to the experiment required by the X-POP attitude therefore, a X-IOP Shuttle attitude would have to be utilized in order to provide a hemispherical pointing capability.

The Z local vertical attitude, attitude c, is required by certain experiments such as Shuttle payloads C1S1F and P7S3A that must either remain pointed towards or away from the Earth. Payload C1S1F is a Communication and Navigation payload that must remain oriented towards the Earth while payload P7S3A, the Combined Cosmic Ray Physics and Chemistry Laboratory, must be kept pointed away from the Earth. By mounting these payloads along the Shuttle Z axis, the experiments can be either pointed towards or away from the Earth using this Z local vertical attitude.

4.3 CMG Momentum Desaturation - CMG momentum desaturation will be performed by either firing the vehicle's baseline reaction jets or by performing gravity gradient desaturation maneuvers. The select CMG desaturation system is assumed to have the capability of desaturating the CMG system once an orbit. Therefore, the maximum momentum that the CMG system must be sized to absorb corresponds to the maximum momentum that the CMG system must store during one orbit for the worst possible vehicle orientation. The possible vehicle orientations are limited to those contained in the classes of vehicle attitudes listed in section 4.2.

4.4 Vehicle Maneuver Capability - The Shuttle is assumed to have a maximum maneuver rate capability of a 0.1 degree per second about each vehicle control axis. It is further assumed that this maneuver rate can be achieved in 15 seconds.

4.5 Baseline Reaction Control Subsystem (RCS) for On-Orbit Vehicle Stabilization - In this section, the on-orbit fuel requirements for stabilizing the Shuttle with the baseline reaction control subsystem described in section 3.0 are computed. Using the baseline RCS for stabilizing the vehicle while on-orbit is a viable alternative to adding a CMG control system to a vehicle like Shuttle.

To compute the fuel consumed by the baseline RCS during one orbit, the number of reaction jet actuations per orbit must be determined. The vehicle's on-orbit torque environment is assumed to be comprised of only gravity gradient torques. The resultant counteracting RCS control torques are generated by expelling mass. The minimum rate at which this mass is expelled corresponds to the case where the resultant RCS control torques just counteract the effects of the gravity gradient torques. For this case, the amount of fuel consumed is directly proportional to the rectified gravity gradient momentum acting on the vehicle. If on the other hand the RCS system is continuously limit cycling back and forth through the RCS deadbands, the resultant fuel consumption can be excessive.

The maximum average rectified gravity gradient torques that can exist along the Shuttle X, Y, and Z axis are:

$$T_{gx}|_{ra} = \frac{3}{\pi} \omega_o^2 (I_{zz} - I_{yy}) \quad (1)$$

$$T_{gy}|_{ra} = \frac{3}{\pi} \omega_o^2 (I_{zz} - I_{xx}) \quad (2)$$

$$T_{gz}|_{ra} = \frac{3}{\pi} \omega_o^2 (I_{yy} - I_{xx}) \quad (3)$$

where

$$\omega_o^2 = \frac{gR}{r^3} \quad (4)$$

ω_o is the vehicle orbital rate, g is the gravitational acceleration of the Earth, R is the mean radius of the Earth ($R = 3.48$ nautical miles), and r is the distance between the center of the Earth and the vehicle center of mass.

For a 270 nautical mile circular orbit,

$$\omega_o^2 = 1.23 \times 10^{-6} \frac{1}{\text{sec}^2}$$

$$\omega_o = 1.11 \times 10^{-3} \frac{1}{\text{sec}} \quad (5)$$

$T_{gx}|_{ra}$, $T_{gy}|_{ra}$, and $T_{gz}|_{ra}$ equal

$$T_{gx}|_{ra} = 0.396 \text{ ft-lb} \quad (6)$$

$$T_{gy}|_{ra} = 8.75 \text{ ft-lb} \quad (7)$$

$$T_{gz}|_{ra} = 8.36 \text{ ft-lb} \quad (8)$$

The minimum angular momentum impulse bit $(MIB)_i$, $i = x, y, z$, that can be imparted along the vehicle X, Y, and Z control axes due to firing the appropriate RCS pairs equal

$$(MIB)_i = F l_i t_f \quad i = x, y, z \quad (9)$$

Using the RCS parameters defined in section 3.0, the minimum impulse bits $(MIB)_i$ equal

$$(MIB)_x = 828 \text{ ft-lb-sec} \quad (10)$$

$$(MIB)_y = 4000 \text{ ft-lb-sec} \quad (11)$$

$$(MIB)_z = 4000 \text{ ft-lb-sec} \quad (12)$$

The vehicle body rates ω_i along the X, Y, and Z vehicle axes due to firing the appropriate momentum impulse bits $(MIB)_i$ equal

$$\omega_i = \frac{(MIB)_i}{I_{ii}} \quad (i = x, y, z) \quad (13)$$

where

ω_i is the angular rate along the i^{th} vehicle axis,
radians per second

I_{ii} is the vehicle moment of inertia about the i^{th} axis,
slug-ft²

Using the vehicle inertias given in section 3.0, ω_x , ω_y , and ω_z equal

$$\omega_x = 0.796 \text{ m rad/second} \quad (14)$$

$$\omega_y = 0.487 \text{ m rad/second} \quad (15)$$

$$\omega_z = 0.468 \text{ m rad/second} \quad (16)$$

Assume that the Shuttle is in a torque-free environment. In this environment, the vehicle will limit cycle between the limits of the baseline RCS attitude deadband $\pm\theta_o$. Figure 4.2 is a sketch of one of the RCS deadbands. The lower limit, $-\theta_o$, is designated state a, and the upper limit, $+\theta_o$, is designated state b. Assume the i^{th} vehicle axis is at state a. At this point, the appropriate RCS thrusters will fire one $(MIB)_i$ sending the i^{th} axis towards state b. As the i^{th} axis traverses the deadband from a to b, the i^{th} axis angular velocity ω_{ab} equals

$$\omega_{ab} = \omega_i + \omega_{ab}(0) \quad (17)$$

where $\omega_{ab}(0)$ is the i^{th} axis velocity just before the appropriate i^{th} axis RCS reaction jets are fired. The resultant angular displacement of the i^{th} axis within this attitude deadband equals

$$\theta_{ab} = [\omega_i + \omega_{ab}(0)]t - \theta_o \quad (18)$$

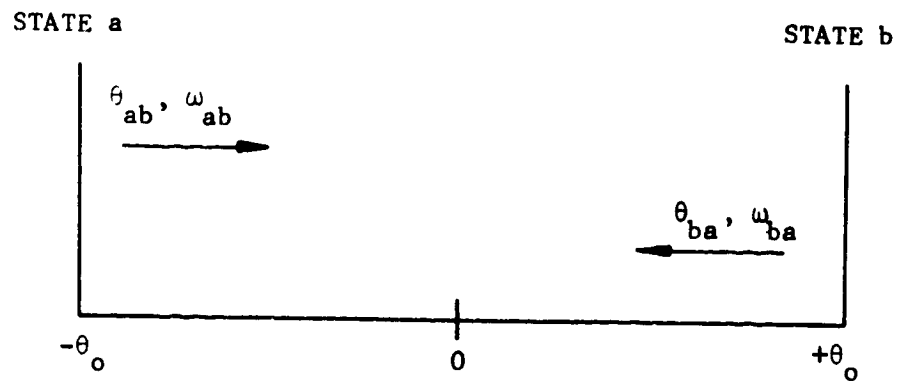


Figure 4.2. Sketch of RCS Attitude Deadband

When the i^{th} axis reaches state b, another set of RCS thrusters will fire sending the i^{th} axis back towards state a. The corresponding angular velocity ω_{ba} and displacement θ_{ba} as the i^{th} axis travels back towards state a equal

$$\omega_{ba} = -\omega_i + \omega_{ba}(0) \quad (19)$$

$$\theta_{ba} = [-\omega_i + \omega_{ba}(0)]t + \theta_o \quad (20)$$

$\omega_{ba}(0)$ is the angular velocity of the i^{th} axis just prior to the reaction jet firings sending this vehicle axis back towards state a. From equation 18, the time t_{ab} for the i^{th} axis to traverse the deadband from state a to state b equals

$$\theta_{ab} = \theta_o = [\omega_i + \omega_{ab}(0)]t_{ab} - \theta_o$$

$$t_{ab} = \frac{2\theta_o}{\omega_i + \omega_{ab}(0)} \quad (21)$$

From equation 20, the time t_{ba} to return to state a equals

$$\theta_{ba} = -\theta_o = [-\omega_i + \omega_{ba}(0)]t_{ba} + \theta_o$$

$$t_{ba} = \frac{2\theta_o}{\omega_i - \omega_{ba}(0)} \quad (22)$$

Under steady state conditions

$$t_{ab} = t_{ba} \quad (23)$$

Therefore, from equations 21, 22, and 23,

$$\omega_{ab}(0) = -\omega_{ba}(0) \quad (24)$$

Because the angular velocity of the i^{th} axis cannot change instantaneously at either boundary of the deadband, the following expressions can be written using equations 17 and 19,

$$\omega_{ba}(0) = \omega_i + \omega_{ab}(0) \quad (25)$$

$$\omega_{ab}(0) = -\omega_i + \omega_{ba}(0) \quad (26)$$

Solving equations 24, 25, and 26 for $\omega_{ab}(0)$ and $\omega_{ba}(0)$ in terms of ω_i , $\omega_{ab}(0)$ and $\omega_{ba}(0)$ equal

$$\omega_{ab}(0) = -\frac{\omega_i}{2} \quad (27)$$

$$\omega_{ba}(0) = \frac{\omega_i}{2} \quad (28)$$

Substituting the above expressions into either equation 21 or 22 yields the time t_{Ti} required to transverse the i^{th} axis attitude deadband, $2\theta_o$.

$$t_{Ti} = t_{ab} = t_{ba} = \frac{4\theta_o}{\omega_i} \quad (i = x, y, z) \quad (29)$$

For the baseline RCS described in section 3.0, θ_o equals 8.75 m rad (0.5 degrees). Substituting the values of ω_i given in equations 14 thru 16 into equation 29 yields the transit times to traverse the X, Y, and Z axis RCS attitude deadbands, respectively.

$$t_{Tx} = 39 \text{ seconds} \quad (30)$$

$$t_{Ty} = 63.6 \text{ seconds} \quad (31)$$

$$t_{Tz} = 66.2 \text{ seconds} \quad (32)$$

The assumption that the vehicle is in a torque-free environment is valid if the actual gravity gradient torques acting on the vehicle are unable to prevent the baseline RCS from limit cycling with every RCS actuation. The gravity gradient decelerating angular momentum impulse, H_{gi} , for the above deadband transit times, t_{Ti} , equal

$$H_{gi} = (T_{gi}|_{ra}) t_{Ti} \quad (i = x, y, z) \quad (33)$$

Substituting the appropriate values of $T_{gi}|_{ra}$ and t_{Ti} into equation 33, H_{gi} corresponding to the three vehicle axes equal

$$H_{gx} = 15.4 \text{ ft-lb-sec} \quad (34)$$

$$H_{gy} = 556 \text{ ft-lb-sec} \quad (35)$$

$$H_{gz} = 554 \text{ ft-lb-sec} \quad (36)$$

Note that the above values of H_{gi} are less than one-seventh of the corresponding RCS minimum momentum impulse bit $(MIB)_i$ indicating that the gravity gradient torque environment cannot prevent the baseline RCS from limit cycling. The assumption that the vehicle is in a torque free environment is therefore valid. Because the vehicle can be considered to be in a torque-free environment, the rate of fuel consumption is independent of the vehicle attitude and only depends on the average time t_{Ti} it takes to traverse the RCS deadband.

The number of engine firings per orbit equals

$$NEF/\text{orbit} = 2T_o \sum_i \frac{1}{t_{Ti}} = \frac{T_o}{2\theta_o} \sum_i \frac{(MIB)_i}{I_{ii}} \quad (i = x, y, z) \quad (37)$$

where T_o is the period in seconds of one complete orbit.

$$T_o = \frac{2\pi}{\omega_o} \quad (38)$$

For a 270 nautical mile circular orbit, T_o equals

$$T_o = 5 \text{ 700 seconds} \quad (39)$$

The weight of fuel per orbit equals

$$\begin{aligned} \text{WOF/orbit} &= (\text{NEF/orbit}) \frac{F_{t_f}}{I_{sp}} \\ &= \frac{T_o F_{t_f}}{2\theta_o I_{sp}} \sum_i \frac{(\text{MIB})_i}{I_{ii}} \quad (i = x, y, z) \end{aligned} \quad (40)$$

For the baseline RCS described in section 3.0, the weight of fuel per orbit required to stabilize the vehicle within a ± 0.5 degree attitude deadband equals

$$\text{WOF/orbit} = 114 \text{ lb/orbit} \quad (41)$$

The amount of fuel consumed per day equals

$$\text{WOF/day} = 1,730 \text{ lb/day} \quad (42)$$

The conclusions from the above analysis are: (1) the baseline RCS fuel consumption rate necessary to hold the Shuttle attitude within a ± 0.5 degree deadband is too large and (2) the resultant RCS contaminants produced are excessive. Increasing the baseline RCS deadband can drastically reduce the fuel consumption and therefore the RCS contaminants produced but, at the expense of vehicle pointing and stabilization. Contamination is an important consideration because the astronomy payloads listed in table 4.1 require a clean vehicle environment. Three possible alternative exist to this contamination problem; they are: (1) eliminate the astronomy payloads, (2) add a low thrust RCS system, or (3) add a CMG attitude control system to the Shuttle. The first alternative is unacceptable because the astronomy payloads are one of the principal reasons for having a Shuttle sortie program. The second alternative, adding a low thrust RCS, can improve the vehicle pointing and stabilization capabilities and reduce RCS contaminants. This potential answer is not a "sure proof" solution because although RCS contaminants are reduced, they are not eliminated. Even with a low thrust RCS, the astronomy payloads might still have to be eliminated from the list of potential Shuttle sortie missions due to RCS contaminants. The third alternative, the addition of a CMG attitude control system, can drastically improve the vehicle's long term pointing and stabilization capabilities without contributing to the experiment contamination problem because CMGs are contamination "free" devices. From a total program standpoint, the costs of a CMG control system versus a low thrust RCS are very competitive.

Table 4.2. Shuttle Mission Requirements

Absolute Shuttle Pointing Requirement: 3 min
Shuttle Stabilization Requirement: $3 \text{ min/observation}$

Potential Shuttle Attitudes:

X-POP Inertial

X-IOP Inertial

Z-LV

CMG System Momentum Desaturation: Once an orbit capability

Vehicle Maneuver Rate Capability: $0.1 \text{ degree/second}$

about each vehicle control axis (rate must be attainable
in 15 seconds)

Contamination Control:

Particles: 10,000 class

Gas: 10^{-6} to 10^{-7} torrs.

From a preliminary examination, the total costs including operational and refurbishment costs appear to favor a CMG system over an add-on low thrust RCS. This third alternative, the addition of a CMG attitude control system, is the preferred solution.

4.6 Mission Requirements Summary - The mission requirements defined in this section are summarized in table 4.2. These mission requirements are used in subsequent sections as guidelines to size, configure, and design an appropriate CMG attitude control system.

4.7 Notes

4.7.1 Symbols and Abbreviations

ARC	Ames Research Center
ASM	Astronomy Sortie Missions
CMG	Control Moment Gyro
deg	Degree
F	RCS thrust level
g	Gravitational acceleration of the Earth (32.2 ft/sec)
H_{gi}	i^{th} axis rectified average gravity gradient momentum ($i = x, y, z$)
I_{ii}	vehicle moments of inertia ($i = x, y, z$)
IR	Infrared
I_{sp}	RCS fuel specific impulse
l_i	RCS vehicle moment arms ($i = x, y, z$)
$(MIB)_i$	i^{th} axis minimum RCS angular momentum impulse ($i = x, y, z$)
\overline{min}	Arc minute
\overline{min}/obs	Arc minute per observation
N/A	Not applicable
NEF/orbit	Number of RCS engine firings per orbit
NS	Not specified
R	Mean radius of the Earth
RAM	Research Application Modules
RCS	Reaction Control Subsystem
r	Distance between the center of the Earth and the vehicle center of mass
\overline{sec}	Arc second
\overline{sec}/obs	Arc second per observation
$T_{gi ra}$	i^{th} axis rectified average gravity gradient torque ($i = x, y, z$)

T_o	Orbital period in seconds
t	Time in seconds
t_{ab}	Time for vehicle axis to traverse RCS attitude deadband from "a" to "b"
t_{ba}	Time for vehicle axis to traverse RCS attitude deadband from "b" to "a"
t_f	Minimum RCS pulse duration
t_{Ti}	Time to traverse i^{th} axis RCS deadband ($i = x, y, z$)
UV	Ultra-violet
WOF/day	Weight of fuel per day
WOF/orbit	Weight of fuel per orbit
X-IOP	X axis in the orbital plane
X-POP	X axis perpendicular to the orbital plane
Z-LV	Z axis aligned along the local vertical
θ_{ab}	Angular displacement as vehicle axis traverses RCS attitude deadband from "a" to "b"
$\theta_{ab}(0)$	Initial value of θ_{ab} at "a"
θ_{ba}	Angular displacement as vehicle axis traverses RCS attitude deadband from "b" to "a"
$\theta_{ba}(0)$	Initial value of θ_{ba} at "b"
θ_o	RCS attitude deadband limit ($\pm\theta_o$)
π	Physical constant, 3.141593
ω_{ab}	Angular velocity as vehicle axis traverses RCS attitude deadband from "a" to "b"
$\omega_{ab}(0)$	Initial value of ω_{ab} at "a"
ω_{ba}	Angular velocity as vehicle axis traverses RCS attitude deadband from "b" to "a"
$\omega_{ba}(0)$	Initial value of ω_{ba} at "b"
ω_i	i^{th} axis angular velocity due to a single (MIB) $_i$ ($i = x, y, z$)
ω_o	Orbital rate

4.7.2 References

1. High-Accuracy Stabilization and Control, MT-2383, Bendix Corporation, Navigation & Control Division, Denver Facility, December 14, 1971.

2. Research and Applications Module (RAM) Phase B
B Study, GDCA-DDA71-003, General Dynamics/
Convair Aerospace Division, San Diego, California,
August 28, 1971.
3. Astronomy Sortie Missions Definition Study, Final
Report, Volume III, Book 1, Martin Marietta
Aerospace/Denver Division, September 1972.

5. CMG SYSTEM REQUIREMENTS

Using the mission requirements defined in section 4.0, the size of the proposed CMG attitude control system and the role that it is to play in meeting these requirements are determined. The CMG control system torque and momentum storage requirements are computed so that a CMG system can be selected and configured in section 6.0.

5.1 Impact of Mission Requirements on CMG Attitude Control System - For convenience, the mission requirements specified in section 4.0 are listed below:

- a. Pointing: 3 arc-minutes
- b. Stabilization: 3 arc-minutes/observation
- c. Contamination
 - Particles: 10,000 class
 - Gas: 10^{-7} to 10^{-6} torrs
- d. Attitudes:
 - Inertial X-POP
 - Inertial X-IOP
 - Z local vertical
- e. CMG Desaturation Capability: once an orbit
- f. Vehicle Maneuvering: 0.1 degree/second maneuver rate capability about each vehicle axis; this rate should be attainable in 15 seconds.

From a potential experiment payload standpoint, adding a CMG attitude control system converts a vehicle like Shuttle from a poorly stabilized experimental base to a rather good one. The resultant CMG vehicle pointing and stabilization capabilities should exceed the mission requirements a and b listed above. Unlike the baseline RCS or a small reaction jet system, CMGs are contamination free devices and therefore will not add contaminants to the vehicle environment. This means that adding a CMG control system will reduce contamination and thus make the problem of meeting the mission contamination requirement, requirement c, more easily attainable. The remaining mission requirements d thru f directly impacts the size of the CMG control system. The following sub-sections deal with the sizing of this CMG attitude control system.

5.2 CMG Torque and Momentum Requirements

5.2.1 Vehicle Torque Environment - The CMG system momentum storage requirements are sized based on the gravity gradient momentum that must be stored per orbit. Because the vehicle cross products of inertia are assumed to be negligible, the gravity gradient torque equation \vec{T}_{gg} reduces to

$$\vec{T}_{gg} = \begin{bmatrix} T_{gx} \\ T_{gy} \\ T_{gz} \end{bmatrix} = 3\omega_o^2 \begin{bmatrix} a_y a_z (I_{zz} - I_{yy}) \\ a_x a_z (I_{xx} - I_{zz}) \\ a_x a_y (I_{yy} - I_{xx}) \end{bmatrix} \quad (1)$$

T_{gx} , T_{gy} , and T_{gz} are the components of \vec{T}_{gg} along the vehicle X, Y, and Z axes, respectively. ω_o is the vehicle orbital rate, the rate at which the vehicle orbits the Earth. For a 270 n.m. circular orbit, ω_o equals 1.11×10^{-3} radians per second. a_x , a_y , and a_z are the components of the local vertical vector \hat{a} in vehicle coordinates. \hat{a} is a unit vector directed from the center of the Earth towards the vehicle center of mass. I_{xx} , I_{yy} , and I_{zz} are the vehicle moments of inertia. The resulting gravity gradient momentum \vec{H}_{gg} that must be stored in the CMG system equals

$$\vec{H}_{gg} = \int \vec{T}_{gg} dt \quad (2)$$

The CMG control system needs only be sized to store the maximum momentum \vec{H}_{gg} that can occur during a single orbit because the CMG system can be desaturated every orbit (mission requirement e).

It should be evident from the definition of \hat{a} , the local vertical vector, that if the vehicle is stabilized in a Z-LV attitude, a_x and a_y are both zero. The resultant components of \vec{T}_{gg} are zero and therefore, no gravity gradient momentum \vec{H}_{gg} storage requirement exists. The same result occurs if either of the two other vehicle axes X or Y are aligned along \hat{a} . For the

other candidate vehicle attitudes X-POP and X-IOP, the components of \vec{T}_{gg} are not zero and therefore, the CMG control system must be sized in order to accommodate the resultant angular momentum \vec{H}_{gg} .

5.2.2 X Axis Perpendicular to the Orbital Plane (X-POP) -
An inertial X-POP attitude where the X roll axis remains perpendicular to the orbital plane is desirable from a momentum storage standpoint because the resultant gravity gradient torque \vec{T}_{gg} remains low. Assume that the Shuttle is stabilized in the X-POP attitude depicted in figure 5.1. The components of the local vertical vector \hat{a} equals

$$a_x = 0 \quad (3)$$

$$a_y = \cos \omega_o t \quad (4)$$

$$a_z = \sin \omega_o t \quad (5)$$

where t is the elapsed time in seconds (see figure 5.1).

Substituting the above components of \hat{a} into the gravity gradient torque equation, equation 1, T_{gx} , T_{gy} , and T_{gz} equal

$$\begin{aligned} T_{gx} &= 3\omega_o^2 (I_{zz} - I_{yy}) \sin \omega_o t \cos \omega_o t \\ &= 0.626 \sin 2\omega_o t \text{ ft-lb} \end{aligned} \quad (6)$$

$$T_{gy} = 0 \quad (7)$$

$$T_{gz} = 0 \quad (8)$$

The resultant gravity gradient momentum \vec{H}_{gg} that must be stored in the CMG system equals the time integral of the above torque components. Because the Y and Z components of \vec{T}_{gg} are zero, the change in \vec{H}_{gg} occurs only along the X axis. H_{gx} equals

$$\begin{aligned} H_{gx} &= \int_0^t T_{gx} dt = \frac{0.626}{2\omega_o} (\cos 2\omega_o t - 1) \\ &= 282 (\cos 2\omega_o t - 1) \text{ ft-lb-sec} \end{aligned} \quad (9)$$

For this ideal X-POP attitude, the momentum H_{gx} is purely cyclic and therefore bounded. Ideally, given a CMG system large enough to store H_{gx} , no CMG desaturation system would be required since no accumulative momentum build-ups exist.

Given an ideal X-POP attitude, the maximum values of torque, 0.626 ft-lb, and momentum, 564 ft-lb-sec, that the CMG system would have to absorb are small. A reasonable question is does small angular departures from an ideal X-POP attitude lead to excessive CMG torque and/or momentum storage requirements. To answer this question, assume that the vehicle is rotated through a small angle ϵ about the Z axis. The local vertical vector \hat{a} equals

$$\hat{a} = \begin{bmatrix} 1 & \epsilon & 0 \\ -\epsilon & 1 & 0 \\ 0 & 0 & 1 \end{bmatrix} \begin{bmatrix} 0 \\ \cos\omega_o t \\ \sin\omega_o t \end{bmatrix} = \begin{bmatrix} \epsilon \cos\omega_o t \\ \cos\omega_o t \\ \sin\omega_o t \end{bmatrix} \quad (10)$$

The resultant components of the gravity gradient torque are:

$$\begin{aligned} T_{gx} &= 3\omega_o^2 (I_{zz} - I_{yy}) \sin\omega_o t \cos\omega_o t \\ &= 0.626 \sin 2\omega_o t \text{ ft-lb} \end{aligned} \quad (11)$$

$$\begin{aligned} T_{gy} &= 3\omega_o^2 \epsilon (I_{xx} - I_{zz}) \sin\omega_o t \cos\omega_o t \\ &= -13.9 \epsilon \sin 2\omega_o t \text{ ft-lb} \end{aligned} \quad (12)$$

$$\begin{aligned} T_{gz} &= 3\omega_o^2 \epsilon (I_{yy} - I_{xx}) \cos^2\omega_o t \\ &= 13.2 \epsilon (1 + \cos 2\omega_o t) \text{ ft-lb} \end{aligned} \quad (13)$$

Assume ϵ corresponds to a one degree offset ($\epsilon = 1.745 \times 10^{-2}$ radian).
 T_{gy} and T_{gz} equal

$$T_{gy} = -0.242 \sin 2\omega_0 t \text{ ft-lb} \quad (14)$$

$$T_{gz} = 0.230 (1 + \cos 2\omega_0 t) \text{ ft-lb} \quad (15)$$

The magnitude of \vec{T}_{gg} ($|\vec{T}_{gg}| = \sqrt{(T_{gx})^2 + (T_{gy})^2 + (T_{gz})^2}$) is a maximum when $\omega_0 t$ equals 0.458π ; the peak magnitude of \vec{T}_{gg} equals 0.715 ft-lb. This magnitude of \vec{T}_{gg} is small and therefore does not pose a sizing problem for the CMG system.

The resultant components of the angular momentum \vec{H}_{gg} are:

$$H_{gx} = \int_0^t T_{gx} dt = 282 (\cos 2\omega_0 t - 1) \text{ ft-lb-sec} \quad (16)$$

$$H_{gy} = \int_0^t T_{gy} dt = 109 (\cos 2\omega_0 t - 1) \text{ ft-lb-sec} \quad (17)$$

$$H_{gz} = \int_0^t T_{gz} dt = 207 (\omega_0 t + 0.5 \sin 2\omega_0 t) \text{ ft-lb-sec} \quad (18)$$

Note that a non-cyclic momentum build-up occurs along the Z axis; the components of momentum along the X and Y axes are cyclic. After one complete orbit, $\omega_0 t = 2\pi$, the momentum build-up along the Z axis equals

$$H_{gz}|_a = 0.230t = 1300 \text{ ft-lb-sec} \quad (19)$$

It is this accumulated momentum build-up $H_{gz}|_a$ that a CMG desaturation system would have to "dump" per orbit. The time histories of the components of \vec{H}_{gg} , H_{gx} , H_{gy} , and H_{gz} , are illustrated in figure 5.2. From this figure, it is estimated that the magnitude of the gravity gradient momentum \vec{H}_{gg} is a maximum after 7/8 of

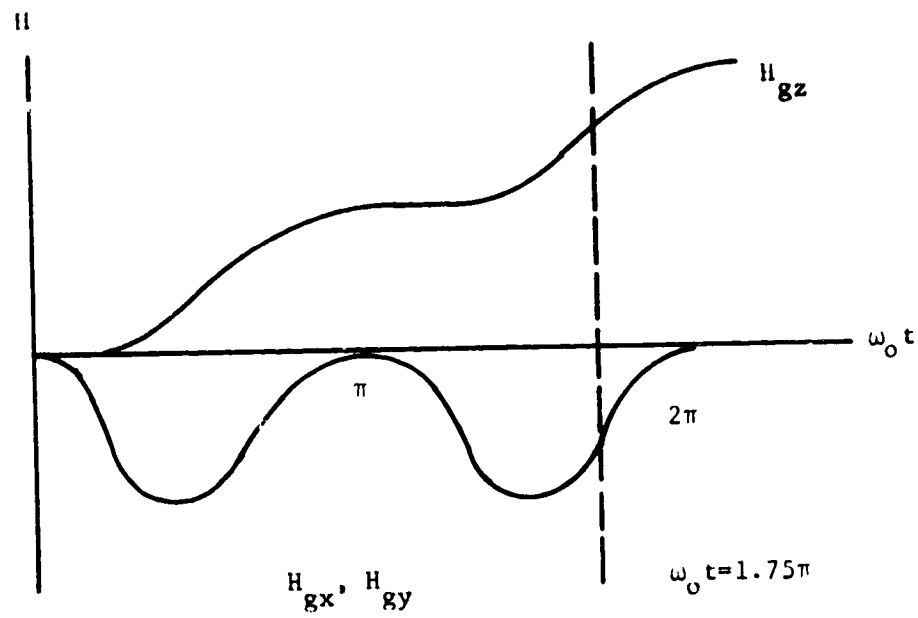


Figure 5.2. Angular Momentum vs.
Time (X-POP Attitude)

an orbit has been traversed; H_{gz} is near its peak and H_{gx} and H_{gy} are at half their peak values. The magnitude of the peak gravity momentum stored in the CMG system during a single orbit equals

$$H_{MAX} = [(282)^2 + (109)^2 + (1,300)^2]^{1/2} \\ = 1,330 \text{ ft-lb-sec} \quad (20)$$

This value of H_{MAX} will be greater in successive orbits because of the momentum build-up along the Z axis unless means are provided for desaturating the CMG control system. Continuous operation in this X-POP attitude for several orbits without desaturating the CMG system is plausible and is a reasonable mission requirement.

5.2.3 X Axis in the Orbital Plane (X-IOP) - Maintaining the vehicle inertially fixed with its long axis, the X axis, in the orbital plane significantly increases the CMG torque requirements over those required to stabilize the same vehicle in a X-POP attitude. The gravity gradient momentum build-up accumulated during an orbit is small as long as the moments of inertia of the vehicle transverse axes are approximately equal which is the case for the vehicle used in this study.

Assume the Shuttle is stabilized in the X-IOP attitude depicted in figure 5.3. The minimum angle between the vehicle Z axis and the orbital plane is denoted by the parameter λ . The corresponding local vertical vector \hat{a} equals

$$\hat{a} = \begin{bmatrix} \cos \omega_o t \\ -\sin \lambda \sin \omega_o t \\ -\cos \lambda \sin \omega_o t \end{bmatrix} \quad (21)$$

Substituting the components of \hat{a} into equation 1, the gravity gradient torque components T_{gx} , T_{gy} , and T_{gz} are:

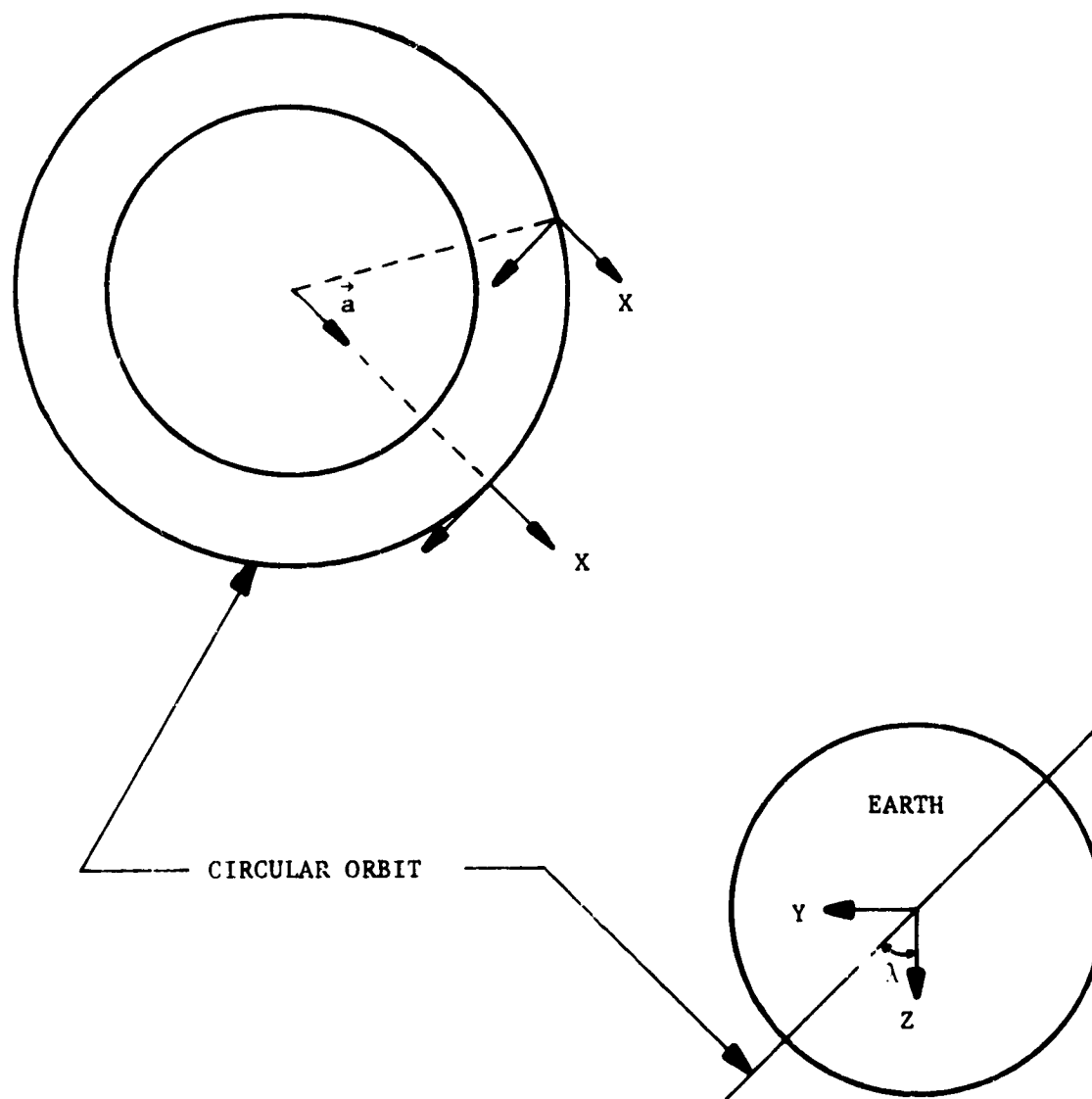


Figure 5.3 Sketch of X-IOP Shuttle Attitude

$$T_{gx} = 3\omega_o^2 (I_{zz} - I_{yy}) \sin\lambda \cos\lambda \sin^2 \omega_o t \quad (22)$$

$$T_{gy} = -3\omega_o^2 (I_{xx} - I_{zz}) \cos\lambda \sin\omega_o t \cos\omega_o t \quad (23)$$

$$T_{gz} = -3\omega_o^2 (I_{yy} - I_{xx}) \sin\lambda \sin\omega_o t \cos\omega_o t \quad (24)$$

Substituting the appropriate vehicle inertia's and orbital rate ω_o corresponding to a 270 n.m. circular orbit into equations

22 thru 24, T_{gx} , T_{gy} , and T_{gz} equal

$$T_{gx} = 0.313 \sin 2\lambda (1 - \cos 2\omega_o t) \text{ ft-lb} \quad (25)$$

$$T_{gy} = 13.9 \cos\lambda \sin 2\omega_o t \text{ ft-lb} \quad (26)$$

$$T_{gz} = -13.2 \sin\lambda \sin 2\omega_o t \text{ ft-lb} \quad (27)$$

Because the magnitude of T_{gx} is much smaller than those of T_{gy} and T_{gz} , assume that the gravity gradient torque \vec{T}_{gg} consists of only two components T_{gy} and T_{gz} . The peak magnitude of \vec{T}_{gg} , T_{max} , occurs when $\omega_o t$ equals 0.25π and λ equals zero; T_{max} equals

$$T_{max} = 13.9 \text{ ft-lb} \quad (28)$$

This minimum CMG system torque requirement T_{max} is over twenty-two times larger than its corresponding value for the X-POP attitude (0.626 ft-lb) described in section 5.2.2.

The corresponding components of the gravity gradient angular momentum \vec{H}_{gg} are:

$$H_{gx} = \int_0^t T_{gx} dt = 282 \sin 2\lambda (\omega_o t - 0.5 \sin 2\omega_o t) \text{ ft-lb-sec} \quad (29)$$

$$H_{gy} = \int_0^t T_{gy} dt = -6,260 \cos\lambda (\cos 2\omega_o t - 1) \text{ ft-lb-sec} \quad (30)$$

$$H_{gz} = \int_0^t T_{gz} dt = 5,950 \sin\lambda (\cos 2\omega_o t - 1) \text{ ft-lb-sec} \quad (31)$$

Note that an accumulative momentum build-up occurs along only the X axis, $H_{gx}|_a$ equals

$$H_{gx}|_a = 282 \omega_o t \sin 2\lambda \text{ ft-lb-sec} \quad (32)$$

This accumulated momentum build-up increases at its maximum rate when λ equals 45 degrees. After a complete orbit, $\omega_o t$ equals 2π , and for a λ of 45 degrees, $H_{gx}|_a$ equals

$$H_{gx}|_a = 1,770 \text{ ft-lb-sec for } \omega_o t = 2\pi, \lambda = 45^\circ \quad (33)$$

$H_{gx}|_a$ is the maximum momentum for an ideal X-IOP attitude that would have to be "dumped" on a per orbit basis by the CMG desaturation system.

The maximum gravity gradient momentum that is stored in the CMG system on a per orbit basis H_{MAX} corresponds to an orbital elapsed time t approximately equal to $\frac{1.5\pi}{\omega_o}$. Because H_{gx} is much smaller than either H_{gy} or H_{gz} , H_{MAX} can be approximated by

$$\begin{aligned} H_{MAX} &= (H_{gy}^2 + H_{gz}^2)^{1/2} \\ &= [(12,520)^2 \cos^2 \lambda + (11,900)^2 \sin^2 \lambda]^{1/2} \\ &\text{for } \omega_o t = 1.5\pi \end{aligned} \quad (34)$$

For λ equal to 45 degrees which corresponds to the maximum rate of momentum accumulation along the X axis, H_{MAX} equals

$$H_{MAX} = 12,210 \text{ ft-lb-sec} \quad (35)$$

The effects of a small angular departure from a ideal X-IOP attitude must also be considered. Assume that the X axis is rotated out of the orbital plane through a small angle ϵ about the Z axis, the corresponding local vertical vector \hat{a}' equals

$$\begin{aligned}
 \hat{a}' &= \begin{bmatrix} 1 & \epsilon & 0 \\ -\epsilon & 1 & 0 \\ 0 & 0 & 1 \end{bmatrix} \begin{bmatrix} \cos \omega_o t \\ -\sin \lambda \sin \omega_o t \\ -\cos \lambda \sin \omega_o t \end{bmatrix} \\
 &= \begin{bmatrix} \cos \omega_o t - \epsilon \sin \lambda \sin \omega_o t \\ -\epsilon \cos \omega_o t - \sin \lambda \sin \omega_o t \\ -\cos \lambda \sin \omega_o t \end{bmatrix} \quad (36)
 \end{aligned}$$

The prime (') superscript is used to denote the offset X-IOP attitude from the ideal X-IOP attitude; all unprimed functions in this section 5.2.3 correspond to the ideal X-IOP attitude.

Substituting the above components of \hat{a}' , into equation 1 and neglecting all terms that are multiplied by ϵ^2 ($\epsilon^2 \sim 0$), the resultant gravity gradient torque components T_{gx}' , T_{gy}' , and T_{gz}' equal

$$\begin{aligned}
 T_{gx}' &= 1.5 \omega_o^2 (I_{zz} - I_{yy}) [\epsilon \cos \lambda \sin 2\omega_o t \\
 &\quad + 0.5 \sin 2\lambda (1 - \cos 2\omega_o t)] \\
 &= T_{gx} + 1.5 \omega_o^2 \epsilon (I_{zz} - I_{yy}) \cos \lambda \sin 2\omega_o t \quad (37)
 \end{aligned}$$

$$\begin{aligned}
 T_{gy}' &= 1.5 \omega_o^2 (I_{xx} - I_{zz}) [0.5 \epsilon \sin 2\lambda (1 - \cos 2\omega_o t) \\
 &\quad - \cos \lambda \sin 2\omega_o t] \\
 &= T_{gy} + 0.75 \omega_o^2 \epsilon (I_{xx} - I_{zz}) \sin 2\lambda (1 - \cos 2\omega_o t) \quad (38)
 \end{aligned}$$

$$\begin{aligned}
 T_{gz}' &= -1.5 \omega_o^2 (I_{yy} - I_{xx}) [0.5 \epsilon (1 + \cos 2\lambda) (1 - \cos 2\omega_o t) \\
 &\quad + \sin \lambda \sin 2\omega_o t] \\
 &= T_{gz} - 0.75 \omega_o^2 \epsilon (I_{yy} - I_{xx}) (1 + \cos 2\lambda) (1 - \cos 2\omega_o t) \quad (39)
 \end{aligned}$$

T_{gx} , T_{gy} , and T_{gz} are the gravity gradient torque components corresponding to the ideal X-IOP attitude illustrated in figure 5.3. The components of the gravity gradient momentum \vec{H}_{gg} are:

$$\begin{aligned} H_{gx}' &= \int_0^t T_{gx}' dt \\ &= 0.75 \omega_o (I_{zz} - I_{yy}) [\sin 2\lambda (\omega_o t - 0.5 \sin 2\omega_o t) \\ &\quad - \epsilon \cos \lambda (\cos 2\omega_o t - 1)] \\ &= H_{gx} - 0.75 \omega_o \epsilon (I_{zz} - I_{yy}) \cos \lambda (\cos 2\omega_o t - 1) \quad (40) \end{aligned}$$

$$\begin{aligned} H_{gy}' &= \int_0^t T_{gy}' dt \\ &= 0.75 \omega_o (I_{xx} - I_{zz}) [\epsilon \sin 2\lambda (\omega_o t - 0.5 \sin 2\omega_o t) \\ &\quad + \cos \lambda (\cos 2\omega_o t - 1)] \\ &= H_{gy} + 0.75 \omega_o \epsilon (I_{xx} - I_{zz}) \sin 2\lambda (\omega_o t - 0.5 \sin 2\omega_o t) \quad (41) \end{aligned}$$

$$\begin{aligned} H_{gz}' &= \int_0^t T_{gz}' dt \\ &= 0.75 \omega_o (I_{yy} - I_{xx}) [\sin \lambda (\cos 2\omega_o t - 1) \\ &\quad - \epsilon (1 + \cos \lambda) (\omega_o t - 0.5 \sin 2\omega_o t)] \\ &= H_{gz} - 0.75 \omega_o \epsilon (I_{yy} - I_{xx}) (1 + \cos \lambda) (\omega_o t - 0.5 \sin 2\omega_o t) \quad (42) \end{aligned}$$

Assume that ϵ corresponds to a one degree offset ($\epsilon = +1.745 \times 10^{-2}$ radian). Substituting ϵ , the vehicle moments of inertia, and the orbital rate ω_o corresponding to a 270 n.m. circular orbit into equations 37 thru 42, the components of \vec{T}_{gg}' and \vec{H}_{gg}' are:

$$T_{gx}' = T_{gx} \pm (1.1 \times 10^{-2}) \cos \lambda \sin 2\omega_o t \quad (43)$$

$$T_{gy}' = T_{gy} \mp 0.121 \sin 2\lambda (1 - \cos 2\omega_o t) \quad (44)$$

$$T_{gz}' = T_{gz} \mp 0.155 (1 + \cos 2\lambda)(1 - \cos 2\omega_o t) \quad (45)$$

$$H_{gx}' = H_{gx} \mp 4.93 \cos \lambda (\cos 2\omega_o t - 1) \quad (46)$$

$$H_{gy}' = H_{gy} \mp 109 \sin 2\lambda (\omega_o t - 0.5 \sin 2\omega_o t) \quad (47)$$

$$H_{gz}' = H_{gz} \mp 140 (1 + \cos \lambda) (\omega_o t - 0.5 \sin 2\omega_o t) \quad (48)$$

Comparing the above components of \vec{T}_{gg}' and \vec{H}_{gg}' with those for \vec{T}_{gg} and \vec{H}_{gg} given in equation 25 thru 27 and 29 thru 31, respectively, no significant change in the magnitude of the resultant gravity gradient torque or momentum is produced due to this one degree ϵ offset.

5.2.4 Acquiring and Maintaining Local Vertical - It was pointed out in section 5.2.1 that the magnitude of the gravity gradient torque acting on the vehicle is zero when one of its principal axes is aligned with the local vertical. To keep this principal axis aligned with the local vertical, the spacecraft must rotate at the orbital rate ω_o about an axis perpendicular to the orbital plane. If this axis perpendicular to the orbital plane is also a principal axis, no dynamic torque due to spinning the vehicle is produced, but if the vehicle is spun around a non-principal axis a constant dynamic torque is generated that must be absorbed by the CMG system. This statement can be verified by the following Euler equation of vehicle motion contained in section 3.1.

$$\vec{T}_v = [I]\dot{\vec{\omega}} + \vec{\omega} \times [I]\vec{\omega} \quad (49)$$

\vec{T}_v is the total resultant torque acting on the vehicle due to all disturbance and control torques, $[I]$ is the vehicle inertia tensor, and $\vec{\omega}$ and $\dot{\vec{\omega}}$ are the vehicle angular velocity and acceleration, respectively. The terms $[I]\dot{\vec{\omega}}$ and $\vec{\omega} \times [I]\vec{\omega}$ in equation 49 are

the two dynamic torque terms due to the angular motion of the vehicle. Because for a local vertical attitude the vehicle is spinning at a constant velocity $\vec{\omega}$, $\dot{\vec{\omega}}$ is zero and the first term $[I]\dot{\vec{\omega}}$ is zero. If the vehicle is rotating about a principal axis, the vehicle angular momentum $[I]\vec{\omega}$ is a vector quantity along the angular velocity vector $\vec{\omega}$ therefore, the second term, the cross product of $\vec{\omega}$ into $[I]\vec{\omega}$, is also zero. If on the other hand the vehicle is not rotating about a principal axis, the dynamic torque $\vec{\omega} \times [I]\vec{\omega}$ is a constant because $\vec{\omega}$ and $[I]\vec{\omega}$ are not aligned. This constant torque $\vec{\omega} \times [I]\vec{\omega}$ in vehicle coordinates must be absorbed by the CMG system. The above discussion emphasizes the need for spinning the vehicle about either the X or Y principal axis when the spacecraft is in a Z local vertical attitude (Z-LV).

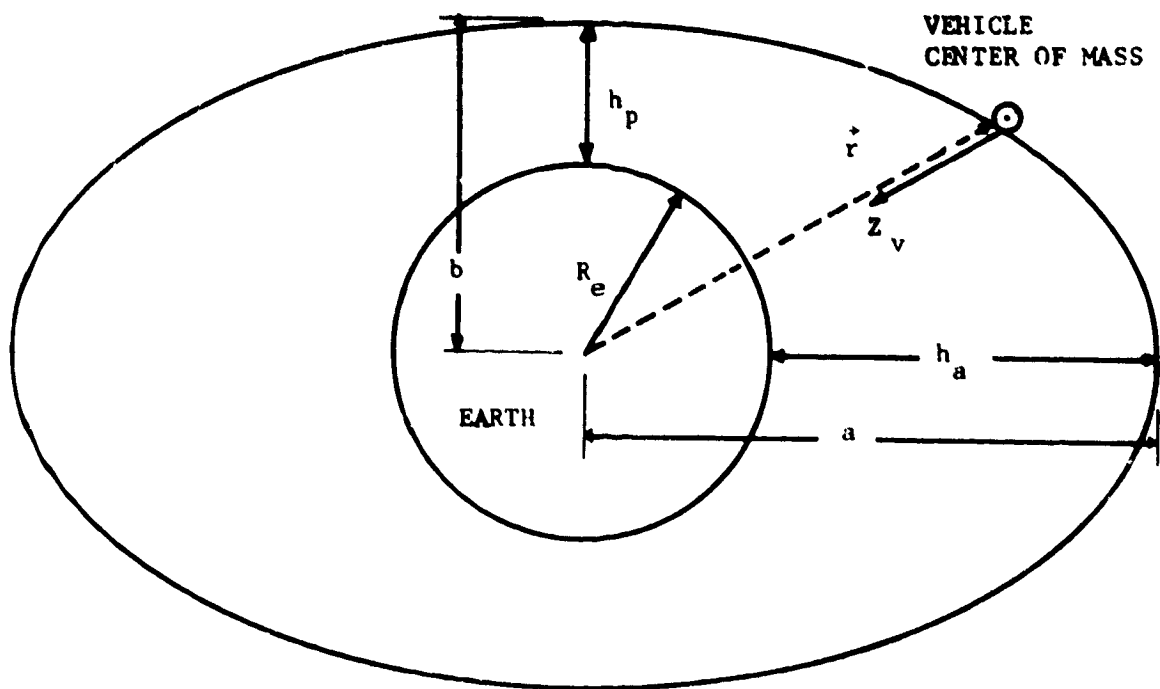
For a 270 n.m. circular orbit, the vehicle angular momentum that the CMG system would have to impart to the vehicle in order to acquire a Z-LV attitude is a function of whether the vehicle is spun around the X or Y principal axis. The corresponding momentum requirements needed to acquire these two Z-LV attitudes, X-POP Z-LV and X-IOP Z-LV, are:

$$\text{X-POP Z-LV: } H_x = I_{xx} \omega_o = 1,154 \text{ ft-lb-sec} \quad (50)$$

$$\text{X-IOP Z-LV: } H_y = I_{yy} \omega_o = 9,111 \text{ ft-lb-sec} \quad (51)$$

From strictly a momentum standpoint, a X-POP Z-LV attitude is preferred because it requires the smallest expenditure of momentum to acquire.

Assume that the vehicle is stabilized in a Z-LV attitude and that its orbit is elliptical rather than circular. As the vehicle travels along this elliptical path, the angular velocity $\dot{\theta}$ and acceleration $\ddot{\theta}$ of its spin axis perpendicular to the orbital plane varies as a function of its orbital position. Because the vehicle is in a Z-LV attitude, the Z vehicle axis remains pointed towards the center of Earth along the vector \vec{r} shown in figure 5.4.



$$\text{ECCENTRICITY, } e = \frac{\sqrt{a^2 - b^2}}{a}$$

Figure 5.4. Elliptical Orbit Geometry

In other words, the vehicle is stationary with respect to \vec{r} and therefore, the rotational velocity and acceleration of \vec{r} equals those of the vehicle's spin axis. The rotational motion $\dot{\theta}$ of this spin axis can be described by the following four equations contained in reference 2.

$$r^2 \dot{\theta} = h = \text{constant} \quad (52)$$

$$r = \frac{a(1-e^2)}{1+e\cos\theta} \quad (53)$$

$$h = na^2 \sqrt{1-e^2} \quad (54)$$

$$n = \sqrt{\frac{gR_e^2}{a^3}} \quad (55)$$

where

r is the magnitude of \vec{r}

h is the angular momentum of the vehicle about the center of the Earth

θ is the angle from perigee describing the location of \vec{r}

a is the semimajor axis of the orbit

e is the eccentricity of the orbit

n is the mean motion, i.e., a constant angular velocity having the same period as the orbit

R_e is the mean radius of the Earth

g is the gravitational acceleration of the Earth (32.2 ft/sec)

Combining equations 52 and 53,

$$\dot{\theta} = \frac{h(1+e\cos\theta)^2}{a^2(1-e^2)^2} \quad (56)$$

Substituting equation 54 into 56,

$$\dot{\theta} = \frac{n(1+e\cos\theta)^2}{(1-e^2)^{3/2}} \quad (57)$$

If e is small, the above expression can be simplified,

$$\dot{\theta} = \frac{n(1+2e\cos\theta)}{1-3/2e^2} \quad (58)$$

The extreme values of $\dot{\theta}$ occur when $\theta=0$ and $\theta=\pi$. Consequently, the total change in $\dot{\theta}$ equals

$$\begin{aligned} \Delta\dot{\theta} &= \frac{n(1+2e\cos 0 - 1 - 2e\cos\pi)}{1-3/2e^2} \\ &= \frac{4ne}{1-3/2e^2} \end{aligned} \quad (59)$$

Differentiating equation 57 results in the angular acceleration $\ddot{\theta}$

$$\ddot{\theta} = \frac{-2n^2e(1+e\cos\theta)^3\sin\theta}{(1-e^2)^3} \quad (60)$$

which for small values of e can be simplified to

$$\ddot{\theta} = \frac{-2n^2e(1+3e\cos\theta)\sin\theta}{1-3e^2} \quad (61)$$

The magnitude of $\ddot{\theta}$ is a maximum when θ equals $\frac{\pi}{2}$ or $-\frac{\pi}{2}$; the maximum value of $\ddot{\theta}$, $\ddot{\theta}_{\max}$, equals

$$\ddot{\theta}_{\max} = \frac{2n^2e}{1-3e^2} \quad (62)$$

The orbit of an artificial satellite is often described in terms of its altitude at apogee h_a and perigee h_p . From the geometry of an ellipse, the orbit's semimajor axis a and eccentricity e can be written in terms of h_a and h_p .

$$a = R_e + \frac{1}{2}(h_a + h_p) \quad (63)$$

$$e = (a - R_e - h_p) / a \quad (64)$$

Using the above expressions for a and e , the maximum torque, $T_{\max} = I_{ii} \ddot{\theta}_{\max}$, and the maximum change in vehicle momentum, $\Delta H_{\max} = I_{ii} \Delta \dot{\theta}$ ($i = x, y$), were computed for a class of elliptical orbits where the orbit's perigee h_p equals 100 n.m. and its apogee h_a ranges from 100 to 1,000 n.m. The corresponding values of T_{\max} and ΔH_{\max} for these orbits are tabulated in table 5.1. These values of T_{\max} and ΔH_{\max} appear to be well within the capabilities of a CMG control system. For apogee altitudes h_a greater than 1,000 n.m., the assumption that the orbital eccentricity e is small is no longer valid and the approximations made in this section are not appropriate.

5.2.5 Tracking An Earth Target - Tracking a point on the surface of the Earth is an experimental requirement for a number of potential experimental payloads. One possible method of tracking such a target is to maneuver the vehicle from a Z-LV attitude so that the experiment's line of sight is always pointed at the target. The vehicle angular velocity, acceleration, and the corresponding CMG system torque and momentum requirements are computed below.

Assume that the vehicle is in a 100 n.m. circular orbit. The orbital angular velocity ω_o equals

$$\omega_o = \sqrt{\frac{g R_e^2}{r^3}} \quad (65)$$

The magnitude of the vehicle's linear velocity v_o equals

$$v_o = r \omega_o = R_e \sqrt{\frac{g}{r}} \quad (66)$$

Table 5.1. Torque and Momentum Requirements for Z-LV
 ($h_a = 100$ n.m.; $h_p = 100 - 1,000$ n.m.)

APOGEE	X-IOP ($i = y$)		X-POP ($i = x$)	
ALTITUDE n.m.	MOMENTUM CHANGE, ΔH FT.LB.SEC. ^{max}	MAX. TORQUE, T_{max} FT.LB.	MOMENTUM CHANGE, ΔH FT.LB.SEC. ^{max}	MAX. TORQUE, T_{max} FT.LB.
100	0	0	0	0
200	533	0.3	67	0.04
300	1023	0.57	130	0.07
400	1615	0.80	205	0.10
500	1950	1.08	247	0.14
600	2340	1.25	296	0.16
800	3090	1.57	391	0.20
1000	3740	1.89	474	0.24

and neglecting the Earth's rotational rate, the maximum vehicle tracking rate $\dot{\alpha}_{\max}$ is the ratio of its linear velocity v_o to its altitude.

$$\dot{\alpha}_{\max} = \frac{R_e}{r-R_e} \sqrt{\frac{g}{r}} \quad (67)$$

$$= 0.0419 \text{ rad/sec (2.40 deg/sec)}$$

This maximum vehicle angular tracking rate $\dot{\alpha}_{\max}$ can be translated into the following CMG momentum storage requirements ΔH_{\max} . For a X-POP Z-LV attitude,

$$\Delta H_{\max} = I_{xx} \dot{\alpha}_{\max} = 4.35 \times 10^4 \text{ ft-lb-sec} \quad (68)$$

and for a X-IOP Z-LV attitude,

$$\Delta H_{\max} = I_{yy} \dot{\alpha}_{\max} = 3.44 \times 10^5 \text{ ft-lb-sec} \quad (69)$$

The vehicle's maximum angular acceleration $\ddot{\alpha}_{\max}$ can be estimated by assuming the spacecraft is moving in a straight horizontal line over the target as shown in figure 5.5. Using this figure, the tracking angle α equals

$$\alpha = \arctan (v_o t / a_E) \quad (70)$$

where a_E is the altitude of the orbit above the Earth and the time t is measured in seconds from the point directly above the target. Differentiating equation 70 twice, the angular acceleration $\ddot{\alpha}$ equals

$$\ddot{\alpha} = \frac{-2a_E v_o^3 t}{a_E^4 + 2a_E^2 v_o^2 t^2 + v_o^4 t^4} \quad (71)$$

Substituting the appropriate values of a_E and v_o into equation 71, $\ddot{\alpha}$ equals

$$\ddot{\alpha} = \frac{-47.3t}{3.14 \times 10^5 + 1.122 \times 10^3 t^2 + t^4} \quad (72)$$

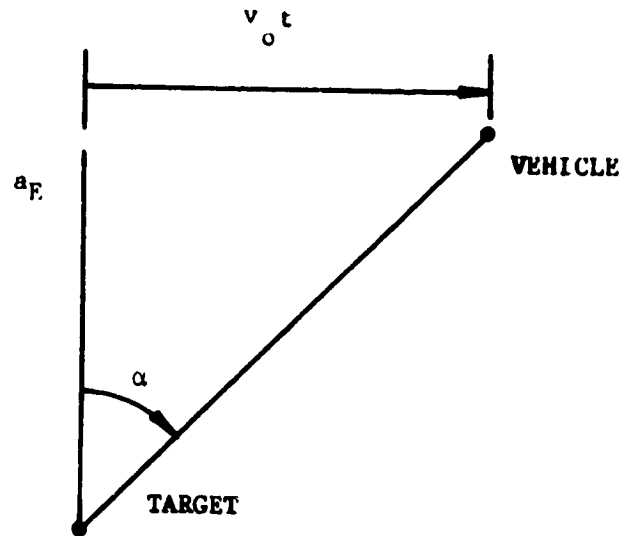


Figure 5.5. Tracking Earth Target

To determine the time t when $\ddot{\alpha}$ is a maximum, $\ddot{\alpha}$ is differentiated once more and then set equal to zero.

$$\ddot{\alpha} = \frac{47.3(-3.14 \times 10^5 + 1.122 \times 10^3 t^2 + 3t^4)}{\text{denominator}} = 0 \quad (73)$$

The denominator of $\ddot{\alpha}$ need not be evaluated in order to determine that $\ddot{\alpha}$ equals zero when t equals 13.7 seconds. Substituting this value of t into equation 72, the maximum magnitude of the vehicle angular acceleration $\ddot{\alpha}_{\max}$ equals

$$\ddot{\alpha}_{\max} = 1.07 \times 10^{-3} \text{ rad/sec}^2 (6.12 \times 10^{-2} \text{ deg/sec}^2) \quad (74)$$

This maximum vehicle angular acceleration $\ddot{\alpha}_{\max}$ can be converted into the following CMG torque requirements T_{\max} . For a X-POP Z-LV attitude,

$$T_{\max} = I_{xx} \ddot{\alpha}_{\max} = 1.11 \times 10^3 \text{ ft-lb} \quad (75)$$

and for a X-IOP Z-LV attitude,

$$T_{\max} = I_{yy} \ddot{\alpha}_{\max} = 8.79 \times 10^3 \text{ ft-lb} \quad (76)$$

Summarized in table 5.2 are the CMG torque and momentum requirements associated with tracking a target fixed to the surface of the Earth. These CMG torque and momentum requirements are excessive indicating that a reasonably sized CMG control system would be incapable of tracking such a target by maneuvering the Shuttle. All of these experimental payloads would have to provide a separate tracking system for tracking an Earth target while the vehicle is held in a Z-LV attitude. This separate tracking system could be either internal or external to the experimental instrument. An internal tracking system would correspond to an image motion compensation system within the instrument while an external system would correspond to a mechanical gimbaling system that would physically rotate the instrument with respect to the vehicle base.

Table 5.2. CMG Torque and Momentum Requirements
for Tracking an Earth Target

ATTITUDE	
X-POP Z-LV	$T_{\max} = 1.11 \times 10^3 \text{ ft-lb}$ $\Delta H_{\max} = 4.35 \times 10^4 \text{ ft-lb-sec}$
X-IOP Z-LV	$T_{\max} = 8.79 \times 10^3 \text{ ft-lb}$ $\Delta H_{\max} = 3.44 \times 10^5 \text{ ft-lb-sec}$

5.2.6 Maneuvering - The maximum maneuver rate defined for the Shuttle in section 4.0 is 0.1 degree per second (1.745×10^{-3} rad/sec) about each vehicle control axis; this rate should be attainable in 15 seconds (mission requirement f). The CMG torque $T_i^{(m)}$ and momentum $H_i^{(m)}$ requirements necessary to meet this above maneuver requirement along each axis can be readily computed using the following expressions

$$T_i^{(m)} = 1.162 \times 10^{-4} I_{ii} \quad (i = x, y, z) \quad (77)$$

$$H_i^{(m)} = 1.745 \times 10^{-3} I_{ii} \quad (i = x, y, z) \quad (78)$$

Using these equations, the CMG torque and momentum requirements necessary to attain a maneuver rate of 0.1 degree per second about each axis in 15 seconds were computed and tabulated in table 5.3.

A 0.1 degree per second maneuver rate corresponds to a very slow maneuver. Because of this slow maneuver rate capability, the gravity gradient torque acting on the vehicle during the maneuver interval can result in an appreciable momentum accumulation in the CMG system. As an illustration, assume the vehicle is maneuvered between the two attitudes shown in figure 5.6. Initially, the vehicle is oriented so that its positive Z axis is pointed away from the Earth and its Y axis is perpendicular to the orbital plane directed out of the page. The vehicle is maneuvered to its desired attitude by rotating the vehicle in a clockwise direction about its Y axis until the Z axis is aligned along the local vertical as shown in figure 5.6. This particular maneuver can be associated with a transition from an inertial X-IOP attitude to an Earth observation X-IOP Z-LV attitude.

Assume that during this maneuver the position of the vehicle in the orbit does not significantly change. The local vertical vector \hat{a} during the maneuver therefore can be approximated by

$$\hat{a} = \begin{bmatrix} \cos \omega_m t \\ 0 \\ -\sin \omega_m t \end{bmatrix} \quad (79)$$

Table 5.3. CMG Torque and Momentum Maneuver Requirements

CONTROL AXIS i	T_i (m) FT-LB	H_i (m) FT-LB-SEC
x	121	1,815
y	955	14,350
z	995	14,920

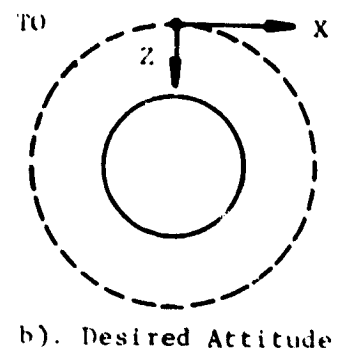
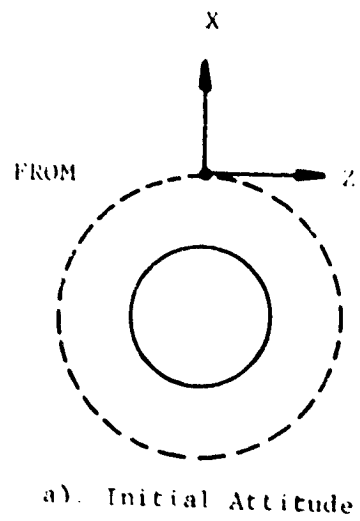


Figure 5.6. Example Vehicle Maneuver

where ω_m is the maneuver rate in radians per second ($\omega_m = 1.745 \times 10^{-3}$ radian/second). Substituting the above components of \hat{a} into the gravity gradient torque equation, equation 1, the components of \vec{T}_{gg} are

$$T_{gx} = 0 \quad (80)$$

$$T_{gy} = \frac{3\omega_o^2}{2} (I_{zz} - I_{xx}) \sin 2\omega_m t \quad (81)$$

$$T_{gz} = 0 \quad (82)$$

The gravity gradient momentum accumulated during this 90 degree maneuver occurs only along the Y axis; this accumulated momentum $H_{gy}^{(m)}$ equals

$$H_{gy}^{(m)} = \int_0^{\frac{\pi}{2\omega_m}} T_{gy} dt = \frac{3\omega_o^2}{2\omega_m} (I_{zz} - I_{xx}) \quad (83)$$

Substituting the appropriate Shuttle moments of inertia, maneuver rate ω_m , and orbital rate ω_o corresponding to a 270 n.m. circular orbit into equation 83, $H_{gy}^{(m)}$ equals

$$H_{gy}^{(m)} = 7,930 \text{ ft-lb-sec} \quad (84)$$

Adding this accumulated gravity gradient momentum $H_{gy}^{(m)}$ to the 14,350 ft-lb-sec (table 5.3) needed to accelerate the Shuttle's Y axis to a maneuver rate of 0.1 degree per second increases the total CMG momentum requirement needed to perform the maneuver shown in figure 5.6 to 22,280 ft-lb-sec. A CMG system with this large momentum capability is feasible although it would be very expensive from a cost, weight, and power standpoint. As an alternative, the baseline RCS because of its large torque and momentum capabilities should be used to maneuver the vehicle. In this mode, the CMG system would be used to provide fine maneuver control by reducing system overshoots and settling times.

5.2.7 Aerodynamic Torques - At the present time, information concerning the aerodynamic coefficients of the Shuttle is not available. Nevertheless, on the basis of previous experience with vehicles of similar size like Skylab, the aerodynamic torques acting on the Shuttle can be estimated to be an order of magnitude smaller than their corresponding gravity gradient torques. A rough estimate of the CMG aerodynamic torque and momentum requirements is 1.0 ft-lb and 1,200 ft-lb-sec for a X-POP attitude and 0.7 ft-lb and 800 ft-lb-sec for a X-IOP attitude. The differences in these CMG torque and momentum requirements between a X-POP and a X-IOP attitude can be explained by noting that the projected vehicle area perpendicular to the vehicle's translational velocity vector \vec{v}_0 is larger for a X-POP attitude than for a X-IOP attitude.

5.2.8 Summary of CMG Torque and Momentum Requirements - Summarized in table 5.4 are the CMG system torque and momentum requirements derived in this section. Tabulated in column 2 as a function of Shuttle attitude is the accumulative gravity gradient momentum that is stored in the CMG system on a per orbit basis. It is this accumulative momentum that a CMG desaturation system must be able to "dump" per orbit.

The CMG system torque and momentum requirements listed in table 5.4 for tracking stationary targets on the surface of the Earth and for maneuvering the vehicle at a rate of 0.1 degree per second are excessive and beyond the reasonable capabilities of a Shuttle designed CMG system. Therefore, these two functions will not be charged against the CMG control system. It is recommended that payloads that must track objects on the surface of the Earth provide their own tracking mechanisms. This tracking mechanism can be an internal system such as an image motion compensation system or an external gimbaling system that tracks the target line-of-sight by rotating the affected scientific instrument with respect to the Shuttle base. To provide the 0.1 degree per second maneuver rate requirement needed to maneuver the vehicle between its various attitudes, the baseline RCS should be used because of its high torque and momentum capabilities.

The CMG system momentum storage requirement should be based on the peak gravity gradient momentum that the CMG system must store. From table 5.4, the peak gravity gradient momentum occurs for the worst case X-IOP attitude and equals 12,210 ft-lb-sec. For the X-IOP attitude illustrated in figure 5.3, the expressions for the components of the gravity gradient momentum \vec{H}_{GG} are given in equation 29 thru 31. As a review, these expressions are reproduced below.

Table 5.4. Summary of Worst Case Torque and Momentum Requirements

OPERATION	PEAK OR TRANSIENT MOMENTUM FT.LB.SEC.	ACCUMULATED MOMENTUM PER ORBIT FT.LB.SEC.	PEAK TORQUE FT.LB.
Maintain X-POP	564	0	0.6
Maintain X-POP (1° Misalignment)	1330	1300	0.7
Maintain X-IOP Z 45° from OP	12210	1770	13.9
Maintain X-IOP Z 45° from OP (1° Misalignment)	12210	2400	14.1
Acquire Z-LV from Inertial Hold X-POP	1154		
Acquire Z-LV from Inertial Hold X-IOP	9111		
Maintain Z-LV in Elliptic Orbit X-IOP 100 to 1000 n.m. Altitude	3740		1.9
Track Earth Target X-POP Z-LV	4.35×10^4		1110
Track Earth Target X-IOP Z-LV	3.44×10^5		8790
Slew At 0.1 deg/sec (Z-axis)	14920		
Accelerate at 0.1 deg/sec in 15 sec (Z-axis)			995
Gravity-Gradient Effect During Maneuver	7930		13.9
Aerodynamic Torque X-POP	1200		1
Aerodynamic Torque X-IOP	800		0.7
OP - Orbital Plane			

$$H_{gx} = 282 \sin 2\lambda (\omega_o t - 0.5 \sin 2\omega_o t) \text{ ft-lb-sec} \quad (29)$$

$$H_{gy} = -6,260 \cos \lambda (\cos 2\omega_o t - 1) \text{ ft-lb-sec} \quad (30)$$

$$H_{gz} = 5,950 \sin \lambda (\cos 2\omega_o t - 1) \text{ ft-lb-sec} \quad (31)$$

Note that on a single orbit basis, the momentum that the CMG system must store occurs principally along the Y and Z axes. Also note that these components are cyclic and that their algebraic signs do not change but, vary between zero and their peak magnitudes. Because the gravity gradient momentum \vec{H}_{gg} acting on the vehicle is predictable and basically cyclic and because the algebraic signs of the principal components of \vec{H}_{gg} , H_{gy} and H_{gz} , do not change, the CMG system momentum storage capability can effectively be doubled by properly initializing the CMG system so that the stored momentum along each axis is periodic about zero. The CMG system can also be initialized so that the momentum stored along the X axis varies over a range centered around zero.

Based on the aerodynamic and gravity gradient momentum that the CMG system must be capable of storing, a CMG system spherical momentum requirement of 13,000 ft-lb-sec was selected. Assuming proper CMG initialization, this momentum capability can provide: (1) a sufficient momentum storage capability to enable the vehicle to remain in a X-POP, a X-IOP, or a Z-LV attitude for several orbits without desaturating the CMG system, (2) an adequate safety margin, and (3) sufficient momentum to permit small angle CMG gravity gradient desaturation maneuvers. From a CMG torque standpoint, a double gimbal CMG can be expected to develop a torque of 60 ft-lb per 1,000 ft-lb-sec of wheel momentum. In general, a single gimbal CMG can generate a larger torque per 1,000 ft-lb-sec of wheel momentum than a double gimbal CMG. Based on the torque requirements listed in table 5.3 and on the specified 13,000 ft-lb-sec CMG system momentum storage requirement, a CMG system torque requirement of 200 ft-lb along each axis is more than adequate and can be reasonably produced by any CMG configuration with a 13,000 ft-lb-sec spherical momentum storage capability. In summary, the CMG system momentum and torque requirements determined in this section are:

Momentum: 13,000 ft-lb-sec (spherical)

Torque: 200 ft-lb about each axis

5.3 CMG Redundancy - The CMG system redundancy criteria selected is a "fail operational, fail safe" philosophy. If a single CMG should fail, the remaining CMG system must be capable of successfully completing the mission. If a second failure should occur, this failure must not endanger the crew or vehicle. This "fail safe" condition is inherent because the baseline RCS is always available to return the crew and Shuttle to Earth.

5.4 Notes

5.4.1 Symbols and Abbreviations

a	Elliptical orbit semimajor axis
\hat{a}	Local vertical vector in vehicle space
a_x, a_y, a_z	Components of \hat{a}
\hat{a}'	Local vertical vector \hat{a} after small angle rotation
CMG	Control momentum gyro
e	Orbital eccentricity
ft-lb	Foot pound(s)
ft-lb-sec	Foot pound second(s)
g	Gravitational acceleration of the Earth
\vec{H}_{gg}	Gravity gradient angular momentum
H_{gx}, H_{gy}, H_{gz}	Components of \vec{H}_{gg}
\vec{H}'_{gg}	\vec{H}_{gg} after a small angle vehicle rotation
$H'_{gx}, H'_{gy}, H'_{gz}$	Components of \vec{H}'_{gg}
H_{max}	Maximum angular momentum
ΔH_{max}	Maximum change in momentum
h	Vehicle angular momentum about center of Earth
h_a	Altitude at apogee
h_p	Altitude at perigee
\bar{I}_{ii}	Vehicle moments of inertia ($i=x,y,z$)
$[I]$	Vehicle inertia tensor
n	Mean motion of vehicle in orbit
n.m.	Nautical mile(s)
RCS	Reaction control (sub) system
R_e	Mean radius of the Earth

\vec{r}	Vector from the center of the Earth to vehicle center of mass
\vec{T}_{gg}	Gravity gradient torque
T_{gx}, T_{gy}, T_{gz}	Components of T_{gg}
\vec{T}'_{gg}	T_{gg} after a small angle vehicle rotation
$T'_{gx}, T'_{gy}, T'_{gz}$	Components of \vec{T}'_{gg}
T_{max}	Maximum torque
t	Time (seconds)
v_o	Linear velocity of vehicle in orbit
X-POP	X axis perpendicular to the orbital plane
X-IOP	X axis in the orbital plane
Z-LV	Z axis along the local vertical
α	Angle between line of sight and vertical
$\dot{\alpha}_{max}$	Maximum vehicle tracking rate
ϵ	Small angle vehicle rotation
θ	Rotational displacement about spin axis
$\dot{\theta}$	Rotational velocity about spin axis
$\Delta\dot{\theta}$	Incremental change in $\dot{\theta}$
$\ddot{\theta}$	Rotational acceleration about spin axis
θ_{max}	Maximum θ
λ	Angle Z axis is rotated out of the orbital plane for X-IOP
$\vec{\omega}$	Vehicle angular rate
$\dot{\omega}$	Vehicle angular acceleration
ω_m	Vehicle maneuver angular rate
ω_o	Orbital rate

5.4.2 References

1. Routh, E. J., Advanced Dynamics of a System of Rigid Bodies, Dover, 1905.
2. Battin, R. H., Astronautical Guidance, McGraw-Hill, 1964.

6. CMG CONFIGURATION STUDY

The purpose of this section is to survey the types and sizes of control moment gyros (CMGs) that are available and to configure an appropriate CMG control system that can meet the momentum, torque, and CMG redundancy requirements defined in section 5. These CMG system requirements are:

Momentum: 13,000 ft-lb-sec (spherical)

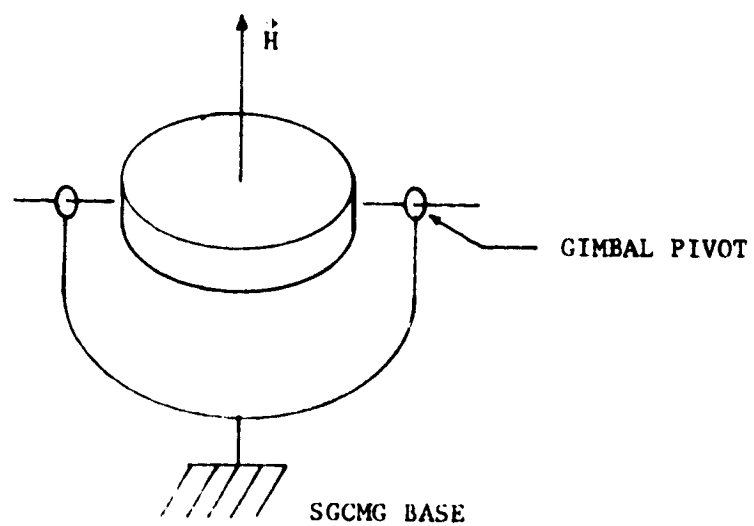
Torque: 200 ft-lb about each control axis

Redundancy: fail operational, fail safe

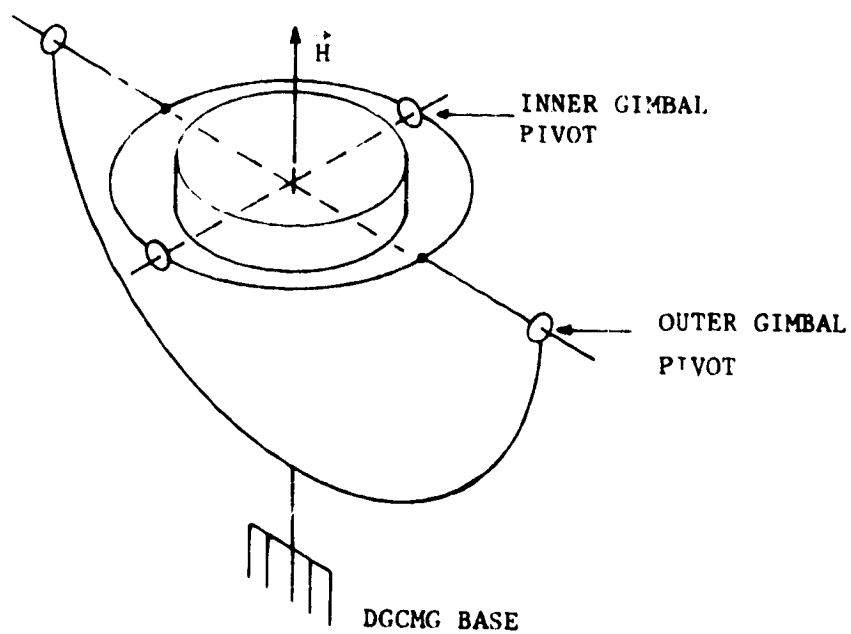
6.1 CMG Types - There are two principal types of CMGs: (1) a single gimbal CMG (SGCMG) and a double gimbal CMG (DGCMG). Sketches of these two types of CMGs are shown in figure 6.1. A SGCMG has a single gimbal between its wheel and its base, its gimbal axis is perpendicular to its wheel momentum vector \vec{H} . A DGCMG has two gimbals between its wheel and base and is essentially a SGCMG with an additional outer gimbal as illustrated in figure 6.1(b). A SGCMG has a single degree-of-freedom while a DGCMG due to its additional gimbal has two degrees-of-freedom.

6.2 CMG Output Torque - Because a SGCMG has only one rotational degree-of-freedom, its output torque \vec{T}_{CMG} ($\vec{T}_{CMG} = \vec{\omega}_g \times \vec{H}$) is constrained to lie along the straight line that is orthogonal to both its gimbal axis and wheel momentum \vec{H} . This straight line shown in figure 6.2(a) is referred to as the SGCMG output torque axis. Adding a second gimbal as shown in figure 6.1(b), a DGCMG can generate an effective gimbal rate $\vec{\omega}_g$ anywhere in the plane perpendicular to \vec{H} and therefore, an output torque \vec{T}_{CMG} anywhere in this plane as illustrated in figure 6.2(b).

The gyroscopic torques in a SGCMG are perpendicular to the gimbal axis and therefore there is no torque component along the gimbal axis. Thus, the loading capacity of the gimbal bearing is the factor that limits CMG output torque. The gimbal actuators must only accelerate the gimbal and overcome the small gyroscopic torques due to vehicle rotation. Because there are no large gyroscopic torques acting along the gimbal axis, relatively large gimbal rates can be obtained and therefore, large output torques. Using present technology, gimbal rates as large as 1.7 radians per second can be generated which means that the magnitude of the maximum CMG output torque $|\vec{T}_{CMG}|_{max}$ can equal 1.7 times the magnitude of the wheel momentum \vec{H} ($|\vec{T}_{CMG}|_{max} = 1.7|\vec{H}|$).

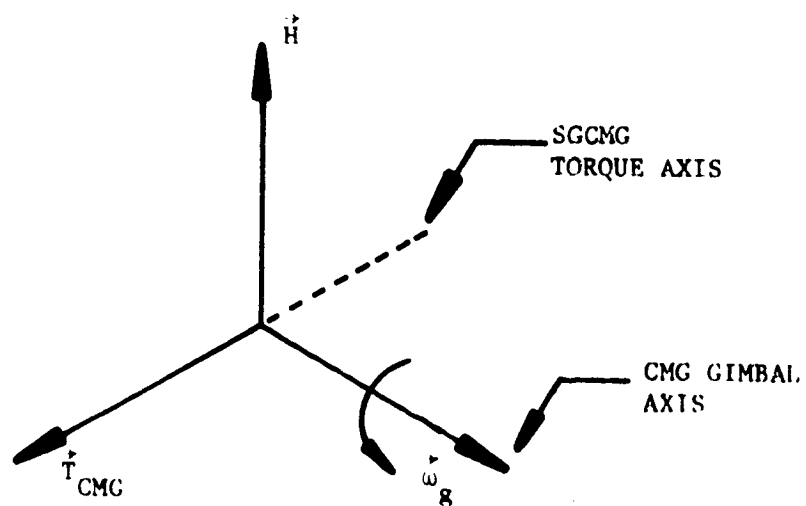


(a) SINGLE GIMBAL CMG

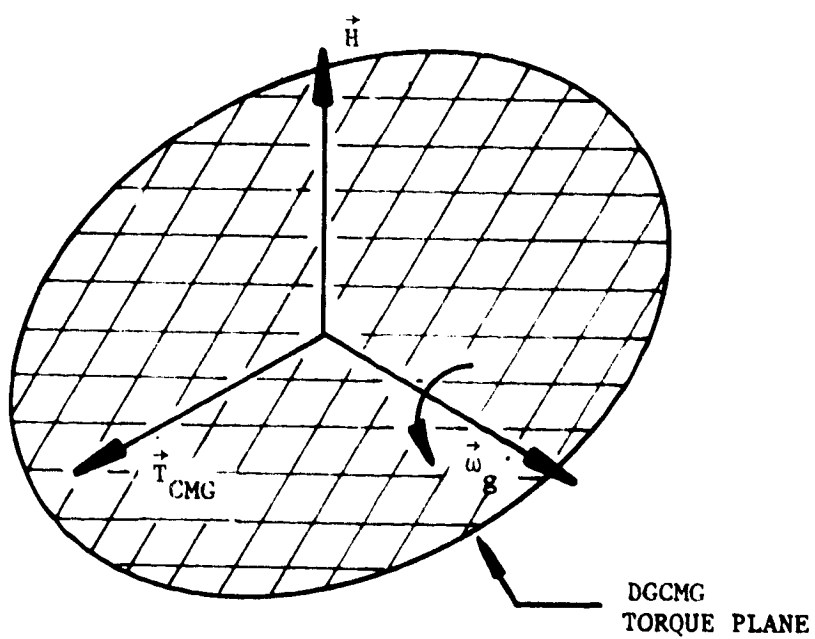


(b) DOUBLE GIMBAL CMG

Figure 6.1 Sketches of a Single and a Double Gimbal CMG



(a) SGCMG TORQUE AXIS



(b) DGCMG TORQUE PLANE

Figure 6.2 Sketch of SG and DG CMG Torque Loci

For a DGCMG, the CMG gyroscopic torques acting on the gimbals always have a component along one of these two gimbal axes. The CMG output torque \vec{T}_{CMG} transmitted to the base is therefore limited due to the possible saturation of one of the gimbal actuators. The maximum CMG output torque $|\vec{T}_{CMG}|_{max}$ is therefore much smaller than for a corresponding SGCMG with the same CMG wheel momentum. For example, the DGCMG developed for Skylab has a wheel momentum of 2,300 ft-lb-sec and a maximum output torque $|\vec{T}_{CMG}|_{max}$ of only 122 ft-lb. This value of $|\vec{T}_{CMG}|_{max}$ corresponds to a maximum gimbal rate of approximately 0.05 radian per second which is much smaller than the 1.7 radians per second capability of a SGCMG. A SGCMG with the same wheel momentum and a maximum gimbal rate of 1.7 radians per second has a maximum torque capability of 3,910 ft-lb. Another significant difference between a SG and a DGCMG are their structural integrity. Because of the additional outer gimbal, a DGCMG is structurally less rigid, more flexible than a corresponding SGCMG. The resultant DGCMG bending modes and mechanical cross coupling tend to limit the servo bandwidth to a value lower than that of a SGCMG with the same momentum rating.

In general, SGCMGs are used where high output torques are of prime consideration and DGCMGs where large momentum storage capabilities are required and low CMG output torques are acceptable. This latter case is the present situation. Any reasonable CMG system, SG or DG, that is sized to meet the CMG momentum storage requirement of 13,000 ft-lb-sec can also easily meet the 200 ft-lb torque requirement. Therefore, the final selection of CMG type and configuration is made on the basis of CMG system momentum and redundancy requirements.

6.3 CMG Survey

6.3.1 Double Gimbal CMGs - DGCMGs are presently available without gimbal stops. The elimination of gimbal stops simplifies the CMG system software requirements because additional control logic is not needed to avoid gimbal stops. As a result of the unlimited gimbal rotation, the available momentum in any direction is the algebraic sum of the individual CMG wheel momentum. The resultant CMG system momentum envelope is spherical. Therefore, the number of DGCMGs required are determined primarily on the basis of available DGCMG sizes, CMG redundancy, and singularity avoidance.

For a DGCMG system, singularity occurs when all of the CMG wheel spin axes are parallel. In this condition, it is impossible for the CMG system to develop a control torque directed parallel to the spin axes. If the spin axes are all pointed in the same direction, the system is saturated and the CMG system must be desaturated. If the spin axes are parallel but, with some axes pointed in opposite directions, the resultant singularity condition is referred to as an "anti-parallel" condition. This "anti-parallel" singularity can in general be avoided by redistributing the CMG gimbal angles without generating a net CMG torque.

If the system is comprised of only two DGCMG, the "anti-parallel" condition occurs when the total CMG system momentum is zero. Redistribution of the gimbal angles is impossible because any gimbal motion away from this singularity condition results in a net CMG torque. However, because the torques acting on the vehicle are to a large extent predictable, the CMG gimbal angles can be initialized so as to prevent all three components of the total CMG momentum from simultaneously passing through zero. In this way, the "anti-parallel" condition can be avoided. With three or more DGCMGs, the "anti-parallel" singularity conditions occur at an infinite number of points in the CMG momentum space. But, because a sufficient number of CMG rotational degrees-of-freedom are available, singularity can be avoided without generating a net CMG torque by redistributing the CMG gimbal angles. For a DGCMG system, singularity avoidance is not a critical problem.

The "fail operational, fail safe" CMG redundancy criteria can be satisfied with a minimum of three DGCMGs. After a single CMG failure, the total CMG system momentum capability is reduced and proper CMG gimbal initialization will be necessary to avoid singularity but, the system is still operational. After a second failure, CMG attitude control is lost, but because the baseline RCS is available to return the crew and Shuttle to Earth, the "fail safe" criteria is satisfied.

Listed in table 6.1 are the momentum, torque, weight, volume, and power characteristics of the four Bendix DGCMGs that are either presently available or will be in the near future. For each DGCMG model listed in table 6.1, the number of CMGs required to meet the system requirement of 13,000 ft-lb-sec plus, the resultant CMG system momentum capability, weight, volume, and power characteristics associated with each system are tabulated in table 6.2.

The MA-1000 DGCMG system listed in table 6.2 requires thirteen CMGs. The software computational requirements associated with this system are excessive because of the large number of CMGs required

Table 6.1. Bendix Double-Gimbal Control Moment Gyros

MODEL	MOMENTUM FT LB SEC	PEAK TORQUE FT LB	WEIGHT** LB	VOLUME CU FT	POWER WATTS		
					SPIN-UP	NOMINAL OPERATING	PEAK TORQUE
MA-1000	1,000	175	230		400	54	275
MA-2000	1,000 to 3,000	175	558	18.0			
MA-2300	2,300	122	418	18.0	240	65	280
MA-6000D	3,000 to 9,000	500*	900*	28*	625	70*	750*

* Estimated value

** Weight does not include CMG inverter assemblies

Table 6.2. Total Candidate DDCMG System Characteristics

MODEL	NUMBER OF UNITS	SYSTEM MOMENTUM FT LB SEC	SYSTEM** WEIGHT LB	SYSTEM VOLUME CU FT	POWER, WATTS	
					SPIN-UP	NOMINAL OPERATING
MA-1000	13	13,000	2,990			
MA-2000	5	5,000 - 15,000	2,790	90	2,000	270
MA-2300	6	13,800	2,508	108	1,440	390
MA-6000D	3	9,000 - 27,000	2,700*	84*	1,875	210*

* Estimated value

** Weight does not include CMG inverter assemblies

and therefore, this system is eliminated from further consideration. The DGCMG system utilizing CMG model MA-2000 is also eliminated because of its high spin-up power requirement and also because its remaining system characteristics are very similar to those exhibited by the DGCMG system using CMG model MA-2300. The two remaining DGCMG systems are discussed in detail in the following paragraphs.

The MA-6000D DGCMG system can be mounted as illustrated in figure 6.3 and because there are only three CMGs, the minimum allowable by the CMG redundancy requirement, the software computational requirements can be kept to a minimum. Note that the MA-6000D CMG has a variable CMG wheel speed and therefore, a variable CMG wheel momentum. If this DGCMG system is operating with a CMG momentum capability of 13,000 ft-lb-sec and a CMG should fail, the remaining CMG wheel speeds can be increased so that the total system momentum capability is returned to 13,000 ft-lb-sec. For this two CMG operational mode, the CMG gimbal angles must also be initialized to avoid the "anti-parallel" zero momentum singularity condition. The MA-6000D DGCMG is being developed and at present, only the CMG wheel and gimbal assemblies have been built and tested. Therefore, the CMG wheel spin-up power is the only measured quantity contained in tables 6.1 and 6.2; the remaining parameters are estimated. The chief drawbacks of this system are: (1) the MA-6000D DGCMG has not been fully developed and may not be and (2) the system's wheel spin-up power requirement is high as compared to the MA-2300 DGCMG system. The principal advantage of the MA-6000D CMG system over the MA-2300 one is that it has an estimated lower operating power requirement. The MA-6000D system has an operating power requirement of 210 watts as compared to a 390 watts for the MA-2300 system. This advantage is not very significant because both operating power requirements are reasonable requirements that a Shuttle power system might be expected to set aside for a CMG control system.

The MA-2300 DGCMG system listed in table 6.2 consists of six CMGs or twice as many as needed using the MA-6000D DGCMGs. If these six CMGs are operated as six individual CMGs, the logic associated with the CMG control law and singularity avoidance scheme would approximately double over that required by three DGCMGs, e.g., the MA-6000D system. The logic associated with the vehicle, maneuver, and CMG desaturation control laws would essentially remain unchanged. A possible CMG mounting configuration for the six MA-2300 CMGs is illustrated in figure 6.4. Two CMGs are identically mounted along each of the three vehicle control axes. The advantage of this configuration is that each axial CMG pair can be slaved together so that they act as a single CMG with a wheel momentum of $2H$ ($H=2,300$ ft-lb-sec). This effective reduction in the number of CMGs from six

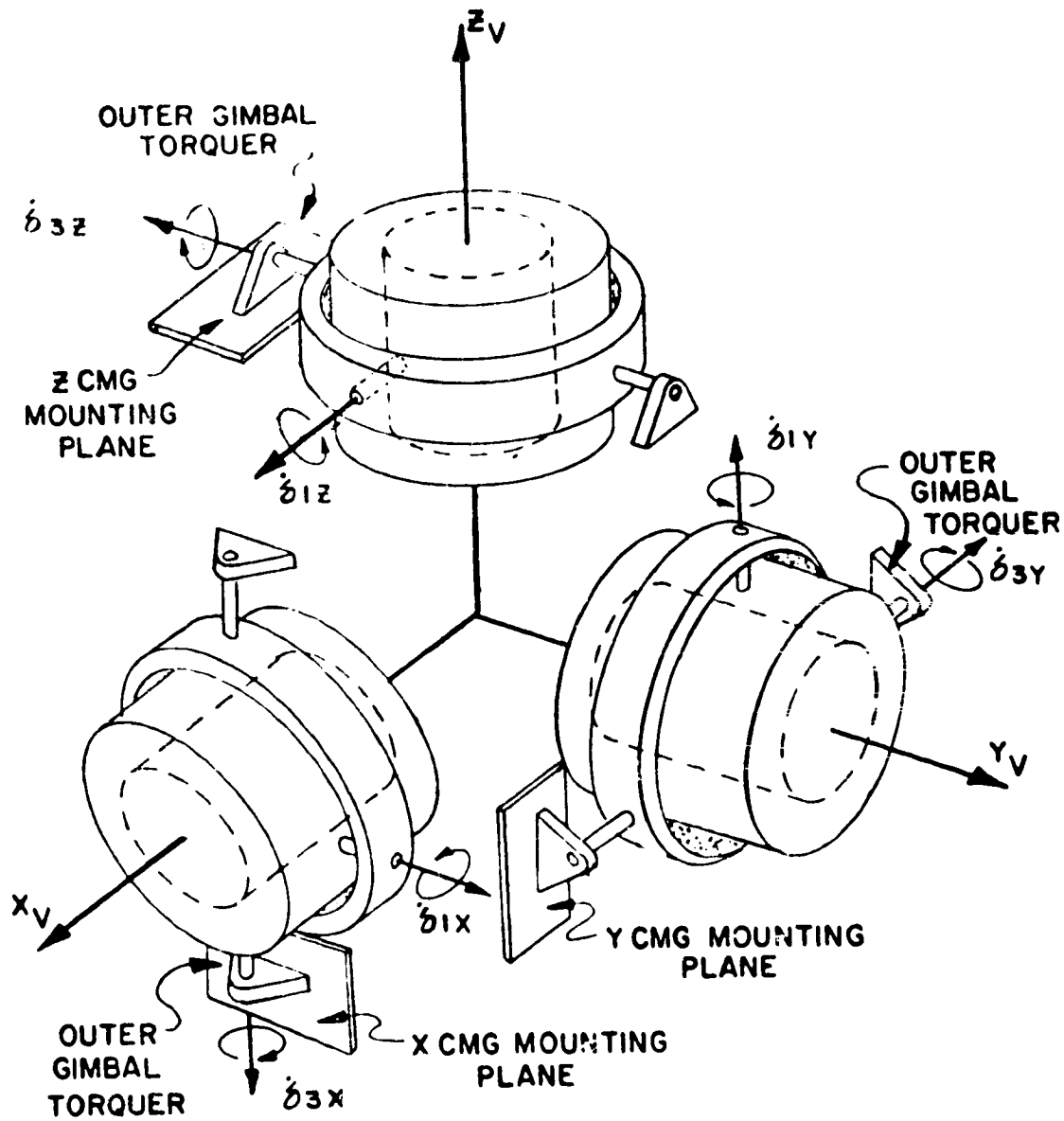


Figure 6.3 Candidate MA-6000D DGCMS Mounting Configuration

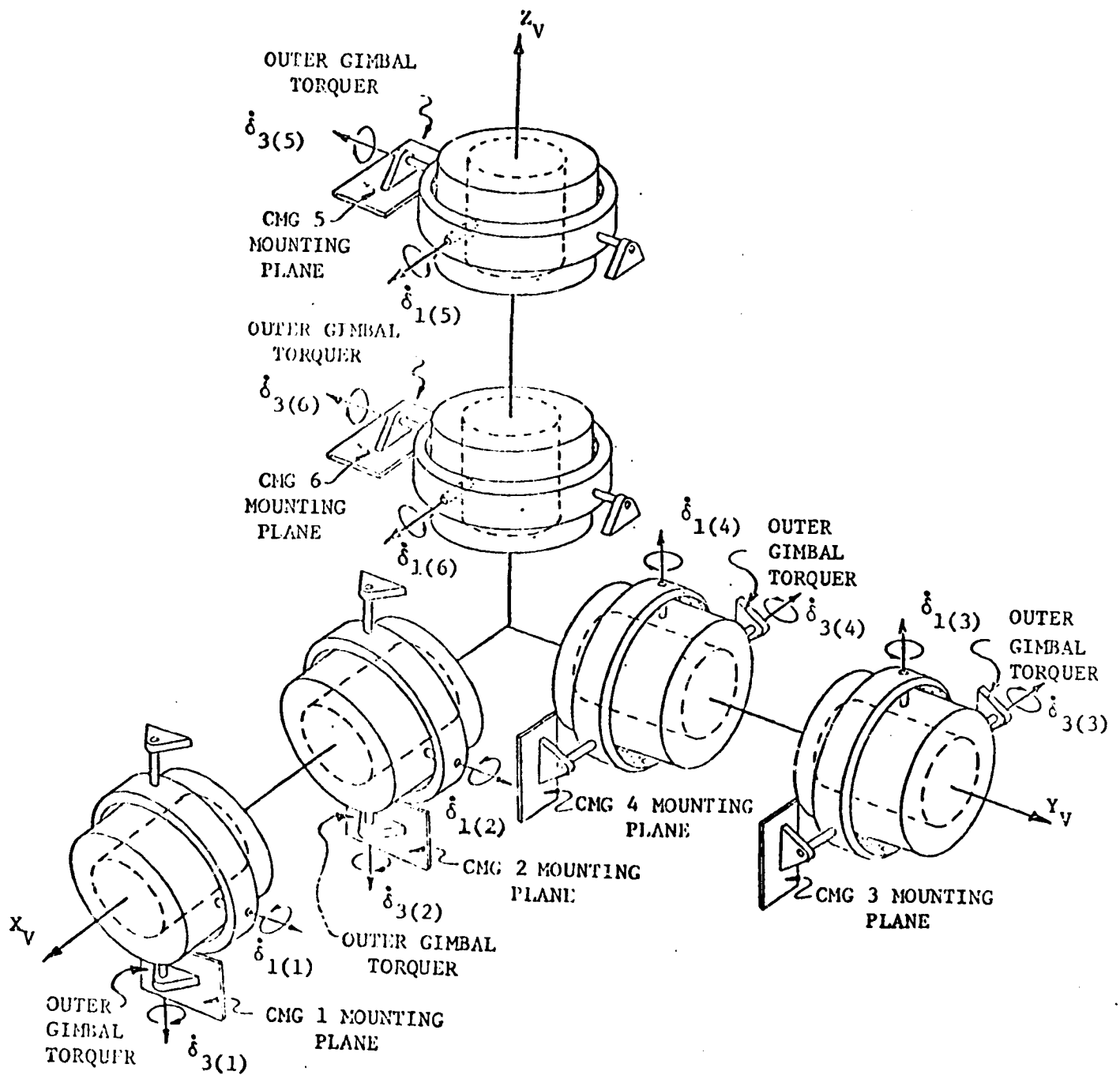


Figure 6.4. Candidate MA-2300 DGCMS Mounting Configuration

to three reduces the computational complexity of the CMG control law and singularity avoidance scheme to essentially that required for three DGCMGs or the MA-6000D CMG system. This slaved CMG operational mode is neither recommended or disapproved of; it is just a method of reducing the computational complexity of the CMG control logic.

With the six MA-2300 CMG system, if a single CMG fails, the CMG system momentum capability is reduced from 13,800 to 11,500 ft-lb-sec which should still be adequate to successfully complete the mission. No special gimbal angle initialization procedure is needed to avoid the "anti-parallel" singularity condition because five DGCMGs are still operational.

One of the principal advantages of configuring a CMG control system using the MA-2300 DGCMG is that this CMG has been developed and built. The MA-2300 DGCMG is primarily the same CMG that is used to control the attitude of NASA's first manned orbiting space station Skylab. The only significant difference between the proposed MA-2300 CMG and the Skylab ATM CMG is that it has no gimbal stops.

6.3.2 Single Gimbal CMGs - Because a SGCMG has only one gimbal, its wheel momentum vector \vec{H} is constrained to lie in the plane perpendicular to its gimbal axis. Therefore, the momentum envelope for a SGCMG system is not spherical with a radius equal to the sum of the individual CMG wheel momentums as in the case of a DGCMG system. A SGCMG system momentum envelope is a function of the number of CMGs, their orientations, and their wheel momentums. Figure 6.5 is a typical SGCMG mounting configuration; the SGCMGs are mounted on the faces of an imaginary pyramid. The SGCMG configuration illustrated in figure 6.5 consists of a six-sided pyramid; each CMG gimbal axis is perpendicular to its corresponding pyramid face as shown. The X, Y, and Z axes shown in this figure are assumed to be the vehicle control axes. The vehicle's roll axis, its X axis, is perpendicular to the base of the pyramid. The shape of the momentum envelope is a function of the angle β , the angle formed by the sides of the pyramid with the base. As β decreases, the envelope becomes flatter with its momentum capability along the X axis decreasing. For a β of 53 degrees, the momentum envelope is approximately spherical.

The 13,000 ft-lb-sec momentum requirement computed in section 5 is primarily based on the momentum storage capability needed in the Y-Z plane. The actual momentum requirements along the X axis is considerably less than 13,000 ft-lb-sec because the vehicle moments of inertia about the Y and Z axes, I_{yy} and I_{zz} , are

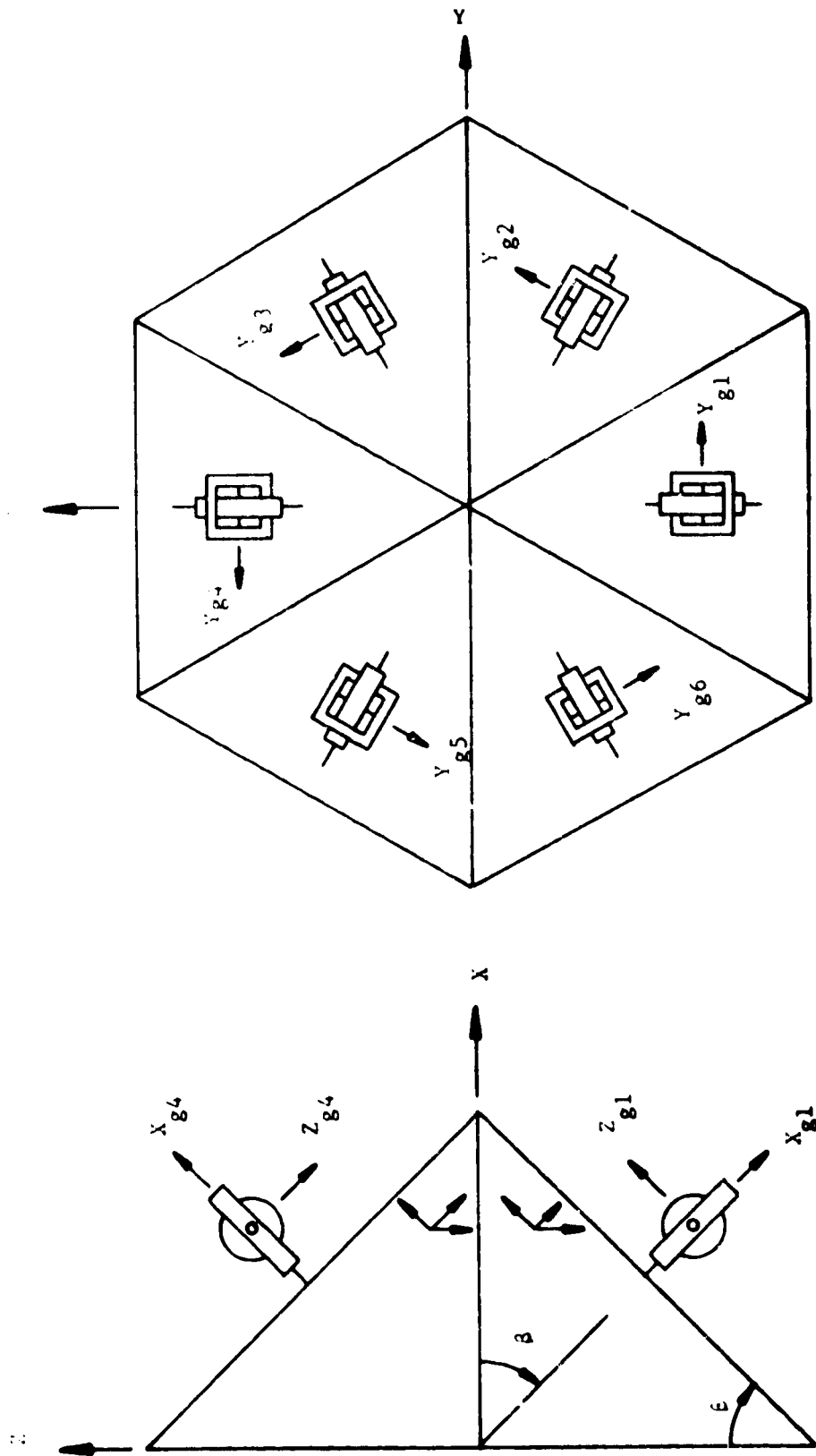


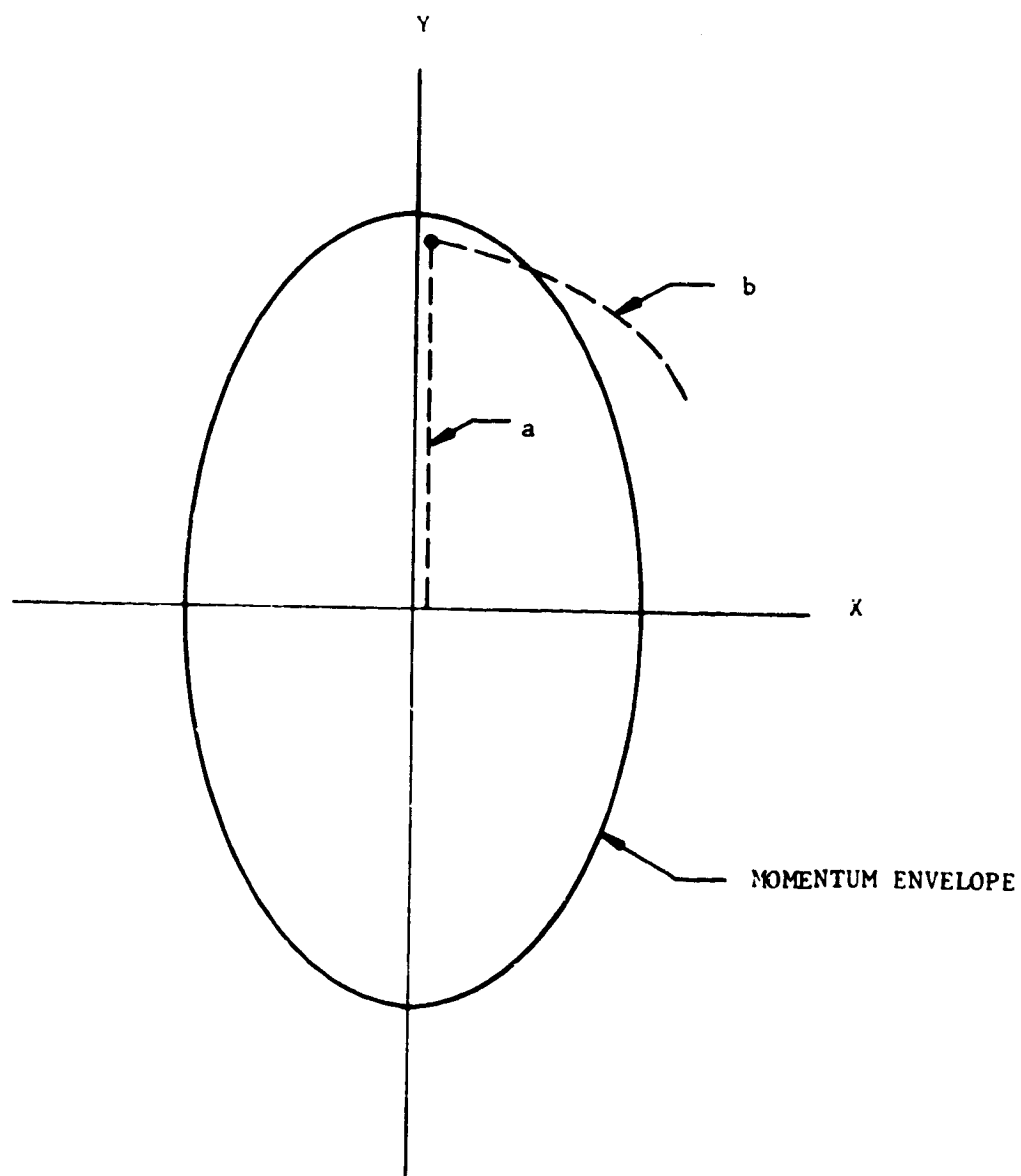
Figure 6.5 Typical SCQM Pyramid Mounting Configuration

approximately equal and much larger than I_{xx} , the X axis moment of inertia. A spherical momentum envelope is therefore not really necessary. For instance, if each SGCMG shown in figure 6.5 had a wheel momentum of 2,300 ft-lb-sec and β equals 25 degrees, the momentum capabilities along the Y and Z axes would be 13,100 ft-lb-sec and 5,800 ft-lb-sec along the X axis. This momentum envelope would be adequate, but its nonspherical shape introduces a new problem. Assume that this SGCMG system is approaching saturation along the Y axis as illustrated in figure 6.6. If a reaction jet system is used to desaturate the CMG system, a torque can readily be applied directly to the Y axis thus, reducing the momentum along this axis without difficulty. On the other hand, if CMG desaturation is accomplished using either a magnetic or a gravity gradient system, the only torque that may be available with a component along the Y axis may also have an unavoidable component along the X axis. Although the magnitude of the momentum stored in the CMG system may be decreasing, its direction may also be moving towards rather than away from saturation as shown in figure 6.6 due to the nonspherical shape of the momentum envelope. For this reason, the SGCMG systems configured in this section will have momentum envelopes that are approximately spherical.

A SGCMG configuration similar to the pyramid array shown in figure 6.5 can include as many SGCMGs and pyramid faces as needed to meet the CMG system momentum requirements. The minimum number of SGCMGs required is determined on the basis of CMG singularity avoidance and the "fail operational, fail safe" CMG redundancy requirements. Singularity for a SGCMG system occurs when all of the CMG output torque axes are coplanar. In this condition, it is impossible for the CMG system to generate a torque perpendicular to this plane and therefore, three axis control is lost.

Singularity for a SGCMG system can be avoided by over sizing the CMG system and then limiting its operating range to a small region of the potentially large momentum envelope where no singularity conditions exist. This procedure can be performed when the momentum that must be stored in the CMG system is predictable by properly initializing the CMG gimbal angles to insure that the system will operate in the desired momentum region. The main problem with this singularity avoidance scheme is that it is very wasteful of the potential CMG momentum capability because the CMG system is constrained to operate in only a small portion of the total CMG momentum space. For the above reason, this method of providing singularity avoidance is not desirable.

Another method of avoiding singularity is to develop a scalar function that is a measure of the "distance" from singularity. A CMG gimbal rate control law is then developed that attempts to



- a PATH OF DESATURATION BY REACTION JETS
- b POSSIBLE PATH OF DESATURATION BY MAGNETIC TORQUE

Figure 6.6 Sketch of Potential SGCMG Desaturation
Problem Associated With Nonspherical Momentum Envelope

maximize this function without generating a net torque. In this way, singularity is avoided. In order to keep the computational requirements within reason, the scalar function is driven to a local rather than a global maximum which unfortunately may not be very far from a potential singularity condition. At least four SGCMGs are required to avoid singularity. With three SGCMGs, all three gimbal rotational degrees-of-freedom are needed to generate the desired CMG torque command \vec{T}_{COM} ; no additional degree-of-freedom is available to provide for singularity avoidance. To provide a singularity avoidance capability, at least one additional SGCMG or a total of four SGCMGs is needed so that a single degree-of-freedom is available for singularity avoidance. To meet the "fail operational, fail safe" CMG redundancy criteria, a minimum of five SGCMGs are needed in order to provide for a single CMG failure.

If a SGCMG fails, the shape of the momentum envelope is altered which in turn creates a nonspherical momentum envelope. The resultant shape of the momentum envelope is a function of which SGCMG fails. This nonspherical momentum envelope results in the same CMG desaturation problem previously discussed.

Listed in table 6.3 are the SGCMGs that have been built or are presently being developed by Bendix along with their corresponding wheel momentum, peak torque capability, weight, volume, and power requirements. To meet the 13,000 ft-lb-sec system momentum requirement, these SGCMGs can be arranged into pyramid array configurations similar to the one shown in figure 6.5.

One possible configuration is to mount five MA-6000D SGCMGs to the faces of a five-sided pyramid. Note that five is the minimum number of SGCMGs that can be used and still meet the "fail operational, fail safe" CMG redundancy requirement. If the angle β , the angle between the pyramid base and sides, equals 45 degrees, the maximum available CMG momentum capability along the three vehicle axes are:

$$H_x = 21,200 \text{ ft-lb-sec}$$

$$H_y = 25,800 \text{ ft-lb-sec}$$

$$H_z = 25,600 \text{ ft-lb-sec}$$

The momentum capability of this array far exceeds the CMG system momentum requirement of 13,000 ft-lb-sec.

Table 6.3. Bendix Single-Gimbal Control Moment Gyros

MODEL	MOMENTUM FT LB SEC	PEAK TORQUE FT LB	WEIGHT** lb	VOLUME CU FT	POWER WATTS		
					SPIN-UP	NOMINAL OPERATING	PEAK TORQUE
MA-450	450	80	179	4.6	128	34	48
MA-500	500	500	145	2.5	170	22	132
MA-1300	1,300	2,000	261		224	36	810
MA-6000D	3,000 to 9,000		800*		625	70*	

* Estimated value

** Weight does not include CMG inverter assemblies

Twelve MA-1300 SGCMGs can also be used to meet the CMG system momentum requirement. These SGCMGs can either be uniformly distributed on the sides of a twelve-sided pyramid or arranged in parallel pairs on the faces of a six-sided pyramid. The former arrangement provides a much smoother momentum envelope while the latter configuration can result in a reduction in the CMG control law computational requirements associated with these configurations if the SGCMGs comprising a CMG pair are slaved together. For a β of 45 degrees, the maximum available CMG momentum capability along the vehicle axes for both potential configurations equals:

$$H_x = 11,050 \text{ ft-lb-sec}$$

$$H_y = 14,200 \text{ ft-lb-sec}$$

$$H_z = 14,200 \text{ ft-lb-sec}$$

Thirty MA-450 or MA-500 SGCMGs could also be used to provide the required CMG system momentum capability. But because of the large number of units needed and the resultant system complexity associated with this many SGCMGs, these two SGCMGs are eliminated as potential candidates for a Shuttle CMG control system.

Another alternative SGCMG configuration is the scissored pair configuration illustrated in figure 6.7. A scissored pair consists of two SGCMGs either geared or servoed together to rotate in opposite directions at the same rate. The resultant momentum vector associated with a SGCMG pair can vary in magnitude but not in direction. Three orthogonally mounted scissored pairs as shown in figure 6.7 can generate a control torque in any direction and requires only a simple control law because each CMG pair generates a torque along only one of the vehicle control axes. Another advantage of this configuration is that no singularity condition exists because the torque axes associated with the CMG pairs are always orthogonal. This configuration's momentum envelope is a cube with a momentum capability of $2H$ along each orthogonal axis. The problem with this configuration is that if a SGCMG should fail, the system as it is presently being operated is inoperative and three axis control is lost. The CMG "fail operational" redundancy requirement cannot therefore be met with this type of a system.

6.4 CMG Configuration Selection - Tabulated in table 6.4 are the four remaining candidate CMG configurations, two DG and two SG systems, along with the number of CMGs needed, system weight, volume, and power requirements. Note that the SGCMG system weights and spin-up power requirements greatly exceed those associated with the candidate DG systems.

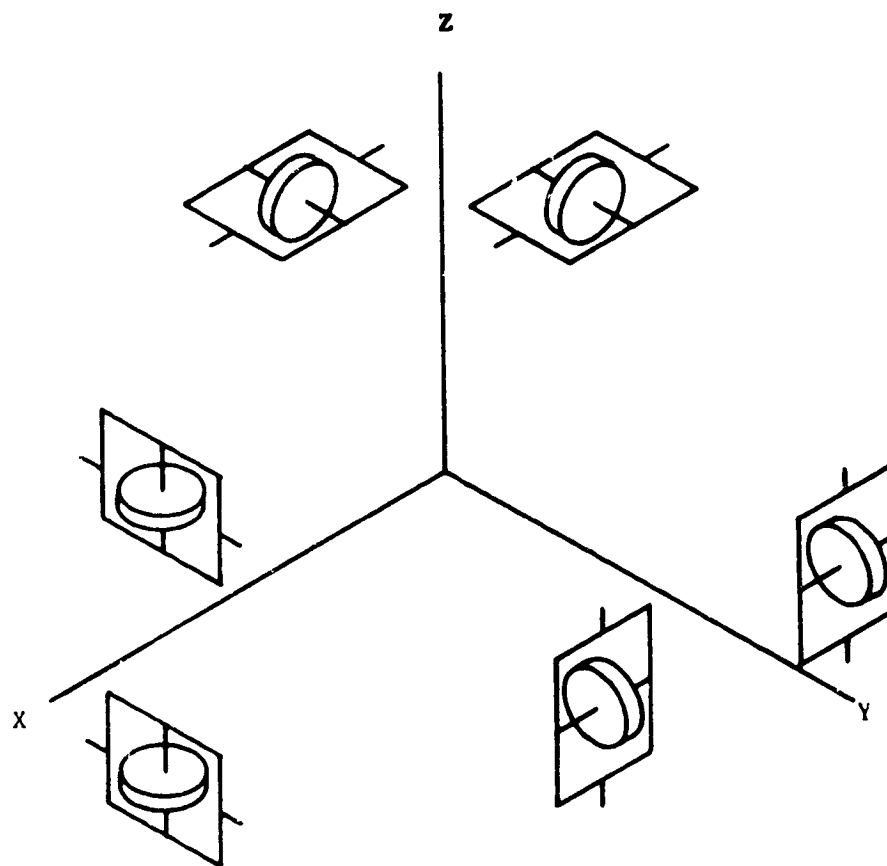


Figure 6.7 Three-Scissored-Pair SGCMG Mounting Configuration

Table 6.4. Candidate Shuttle CMG Configuration and Requirements

TYPE	MODEL	NUMBER OF UNITS	WEIGHT** lb	VOLUME CU FT	POWER WATTS	
					SPIN-UP	NOMINAL OPERATING
DG	MA-2300	6	2,508	108	1,440	390
DG	MA-6000D	3	2,700*	84*	1,875	210*
SG	MA-1300	12	3,132		2,688	432
SG	MA-6000D	5	4,000*		3,125	350*
* Estimated value						
** Does not include weight of CMG inverter assemblies						

The chief advantage of a SGCMG system is its high system torque capability. Its principal disadvantages besides its system weight and spin-up power requirements are: (1) a single CMG failure will result in a nonspherical momentum envelope which may either prevent or make CMG desaturation with either a magnetic or gravity gradient system very difficult, and (2) singularity avoidance is a complex problem and can therefore result in excessive computational requirements. Although compared to a SGCMG system, the torque capabilities of a DGCMG system are much smaller, it does not exhibit the above problems associated with a SGCMG system. If a DGCMG should fail, the system momentum envelope is reduced but, its shape remains spherical and therefore, CMG desaturation can still be performed with no increase in complexity by either a magnetic or gravity gradient desaturation system. Singularity avoidance for a DGCMG system is not a major problem and therefore can easily be accomplished unlike a SGCMG system. Because of the above problems associated with a SGCMG system and because the CMG system torque requirements are not large and can be met by either a SG or DGCMG system, the two SGCMG candidate systems listed in table 6.4 are eliminated as potential candidates.

Of the two remaining CMG systems, the system weight and spin-up power requirements favor the MA-2300 DGCMG system but, on the other hand, the system volume and nominal operating power requirements favor the MA-6000D DGCMG system. The system comparisons between these two systems are very similar and do not favor one system over the other. The final CMG system selection is therefore made on availability. The MA-2300 DGCMG system is selected over the MA-6000D system because the MA-2300 DGCMG is a unit that has been built whereas the MA-6000D DGCMG has not yet been fully developed. The recommended CMG mounting configuration is the CMG pair mounting configuration shown in figure 6.4.

6.5 Symbols and Abbreviations

ATM	Apollo Telescope Mount
CMG	Control Moment Gyro
CU FT	Cubic Feet
DGCMG	Double Gimbal CMG
ft-lb	foot pound(s)
ft-lb-sec	foot pound second(s)
H	CMG wheel momentum
H _x , H _y , H _z	CMG system momentum storage capabilities along X, Y, and Z vehicle axes
I _{ii}	Vehicle moments of inertia (i = x, y, z)

lb	pounds
RCS	Reaction Control (sub) System
SGCMG	Single gimbal CMG
\vec{T}_{CMG}	CMG output torque
$ \vec{T}_{CMG} _{max}$	maximum CMG output torque
β	Angle between the base and sides of a SGCMG pyramid mounting configuration (see figure 6.5)
$\vec{\omega}_g$	CMG gimbal rate in inner gimbal space

7. CMG SYSTEM STABILITY

The objective of this section is to specify a vehicle control law along with an appropriate set of control law gains. The control law gains are selected so as to keep the vehicle stable as opposed to unstable and to meet the three arc-minute vehicle stabilization goal specified in section 4.1. The control law gains are computed so that the vehicle can meet this three arc-minute stabilization goal under the influence of both gravity gradient and worst case man disturbance torques.

7.1 Vehicle Control Law - The main function of the vehicle control law is to compute a CMG torque command \vec{T}_{COM} from sensed body motion that will compensate for the disturbance torques acting on the vehicle resulting in unwanted vehicle motion. The vehicle control law is also used to implement any CMG maneuver command generated by the CMG maneuver control law. The selected vehicle control law is a standard rate plus position control law. This vehicle control law is given in equation 1.

$$\vec{T}_{COM} = [K_r](\vec{\omega}_D - \vec{\omega}) + [K_p](\Delta\vec{\theta} + \vec{\epsilon}) \quad (1)$$

$\vec{\omega}$ is the sensed vehicle angular velocity. $\vec{\omega}_D$ and $\Delta\vec{\theta}$ are the desired vehicle rotational rate and attitude error, respectively; both $\vec{\omega}_D$ and $\Delta\vec{\theta}$ are computed by the CMG maneuver control law. $\vec{\epsilon}$ is a vehicle attitude offset command; $\vec{\epsilon}$ can be a gravity gradient CMG desaturation maneuver command. $[K_r]$ and $[K_p]$ are the vehicle control law rate and position gain matrices, respectively.

$$[K_r] = \begin{bmatrix} K_{rx} & 0 & 0 \\ 0 & K_{ry} & 0 \\ 0 & 0 & K_{rz} \end{bmatrix} \quad (2)$$

$$[K_p] = \begin{bmatrix} K_{px} & 0 & 0 \\ 0 & K_{py} & 0 \\ 0 & 0 & K_{pz} \end{bmatrix} \quad (3)$$

K_{rx} , K_{ry} , and K_{rz} and K_{px} , K_{py} , and K_{pz} are the rate and position gains associated with the three vehicle control axes. These gains are determined in the following section.

7.2 Vehicle Control Loop - Figure 7.1 shows the general arrangement of the vehicle control loop. To compute the gain matrices $[K_r]$ and $[K_p]$, the following assumptions are made: (1) all control sensors are perfect, (2) the vehicle is rigid, (3) interaxis vehicle dynamic coupling does not exist, and (4) the CMG dynamics can be represented by a first-order lag. After a preliminary set of values for K_{rx} , K_{ry} , K_{rz} , K_{px} , K_{py} , and K_{pz} have been computed, the above assumptions will be reexamined.

The largest projected disturbance torque acting on the Shuttle is assumed to be due to a wall pushoff by a crewman moving from one side of the crew quarters to the other. The projected disturbance force profile F_w is shown in figure 7.2. Assume that this force acts along the Z axis causing a disturbance torque about the Y axis. Assume an effective moment arm L of 50 feet, the distance along the X axis from the vehicle center of mass to the line of action of the force F_w . The change in the angular rate about the Y axis due to a single wall pushoff equals

$$\Delta\omega_y = \frac{L}{I_{yy}} \cdot \int F_w dt = 1.096 \times 10^{-4} \text{ rad/sec} \quad (4)$$

If the pushoffs occur periodically with a crewman pushing off one wall and then off the opposite wall, the incremental change in the velocity $\Delta\omega_y$ varies in a steady state condition between plus and minus 5.48×10^{-5} radians per second. The angular displacement during a half cycle, $P/2$, approximately equals

$$\Delta\theta_y = 5.48 \times 10^{-5} (P/2) = 2.74 \times 10^{-5} P \text{ radians} \quad (5)$$

One of the mission requirements described in section 4.0 is that the vehicle attitude must be stabilized to three arc-minutes during each observation. Because wall pushoffs are by far the largest disturbances expected, an error of two arc-minutes from this source is tolerable. Substituting the appropriate value for $\Delta\theta_y$, 5.82×10^{-4} radian, corresponding to two arc-minutes into

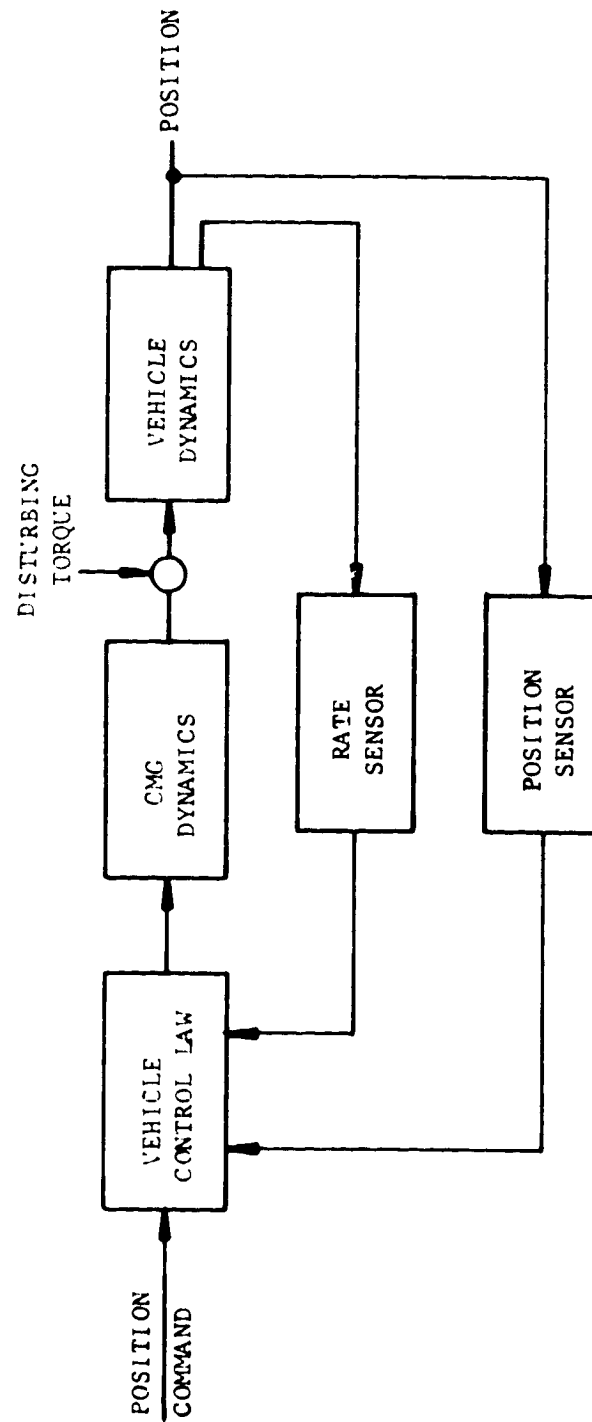


Figure 7.1. Vehicle Control Loop

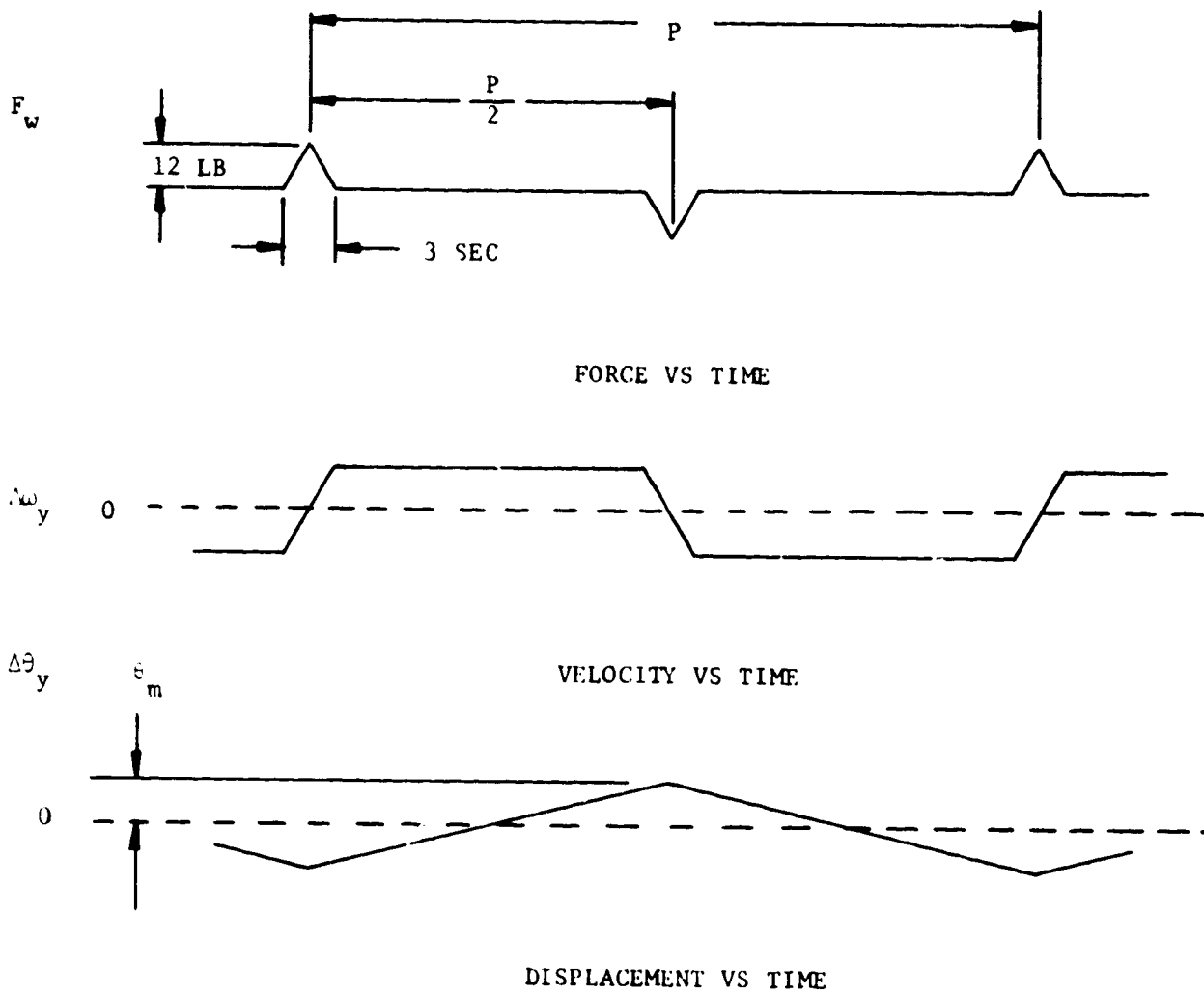


Figure 7.2. Disturbance Due to Crew Motion

equation 5, the period P equals 21.3 seconds. This period P corresponds to a principal frequency of 0.295 radian per second. If the period P is made shorter than 21.3 seconds, the corresponding principal frequency would increase but, because the angular displacement $\Delta\theta_y$ decreases as the frequency increases, the resulting $\Delta\theta_y$ will not exceed the two arc-minute limitation. Therefore, the vehicle control loop must only be effective for frequencies less than 0.3 radian per second.

Consider the signal flow diagram of the simplified control system shown in figure 7.3. Applying Mason's method to this signal flow diagram, the transfer function with the outer loop open is

$$\begin{aligned}\frac{\theta_o}{\epsilon} &= \frac{K_p}{s(\tau_g s^2 + Is + K_r)} \\ &= \frac{K_p/K_r}{s(s^2/\omega_r^2 + 2\zeta_r s/\omega_r + 1)}\end{aligned}\quad (6)$$

where ω_r and ζ_r are the natural frequency and damping ratio of the rate loop, respectively. A Bode diagram of this transfer function is shown in figure 7.4. A rule of thumb is that the closed loop will be stable if the open-loop transfer function crosses the zero-db axis at a point where (1) its slope is 20 db per decade and (2) there are no breakpoints within an octave. The crossover will be set at 0.3 radian per second to provide the bandwidth specified in the previous paragraph. If ω_r is set at 1.0, it will be more than an octave from the crossover, and setting ζ_r equal to 0.707 will prevent the occurrence of resonant peaks. For rotational motion about the pitch axis, Y axis, the vehicle moment of inertia I , I_{yy} , equals 8.21×10^6 slug feet². Substituting these values of ω_r , ζ_r , and I into equation 6, τ_g and K_r equal

$$\tau_g = 1/(2\zeta_r\omega_r) = 0.707 \text{ sec} \quad (7)$$

$$K_r = \omega_r^2 \tau_g I = 5.82 \times 10^6 \text{ ft-lb/(rad/sec)} \quad (8)$$

The asymptote of figure 7.4 has a magnitude of -9.5 db, or 0.30, at ω equal to one. At ω equal to one, the magnitude of the denominator of equation 6 equals one and therefore its numerator K_p/K_r equals the above value, 0.3. Using the value of K_r given in equation 8, K_p equals 1.745×10^6 ft-lb/radian.

Figure 7.3. Simplified Vehicle Control Loop Signal Flow Diagram

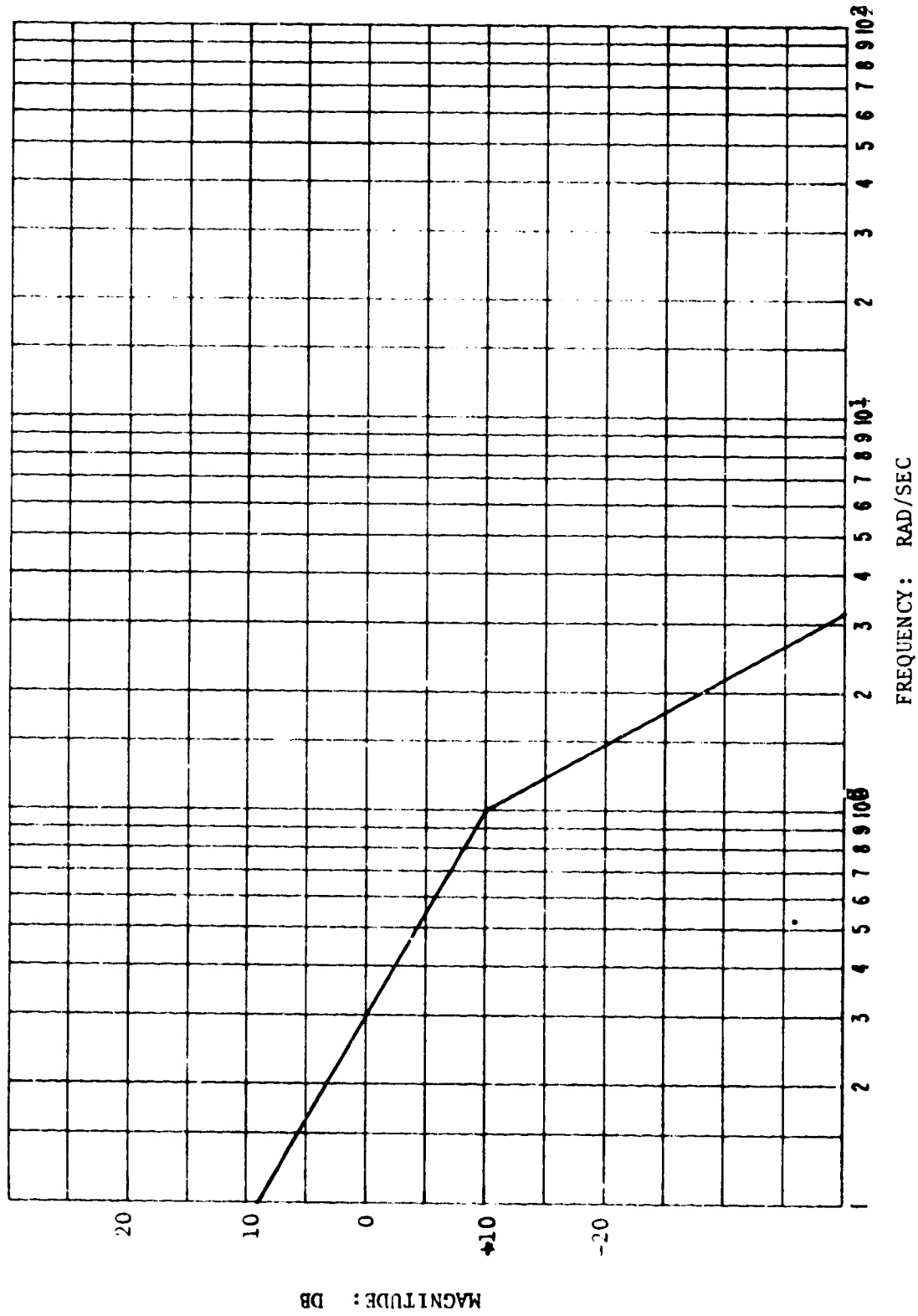


Figure 7.4. Magnitude Vs Frequency (Bode) Plot of Simplified Open Vehicle Control Loop

This preliminary analysis has specified approximate gains K_r and K_p that satisfy stabilization requirements in the presence of assumed crew motion. Other disturbances, particularly gravity gradient torques must be considered. The gravity gradient torque acting on the vehicle has a maximum component of 13.9 ft-lb about the Y axis (X-IOP attitude) and varies so slowly that it may be considered constant. The steady state displacement $\Delta\theta_y^{(gg)}$ due to this torque equals

$$\begin{aligned}\Delta\theta_y^{(gg)} &= T_{gy}/K_p = 13.9/1.745 \times 10^6 \\ &= 7.95 \times 10^{-6} \text{ rad} = 0.00273 \text{ arc minute}\end{aligned}\quad (9)$$

which is negligible. Angular displacement due to aerodynamic torques are even smaller than $\Delta\theta_y^{(gg)}$. The assumed rate and position control law gains are therefore adequate, and error integration is not required.

Another source of error is the dead zones inherent in each CMG due to Coulomb friction and various electronic dead zones. In the case of a 2,300 ft-lb-sec DGCMG, the minimum output torque is 0.25 ft lb. A pessimistic assumption is that six of these gyros break away simultaneously, providing a total dead zone of 1.5 ft lb. A position error of 0.003 arc minute or a rate error of 0.009 arc minute per second will generate enough signal to drive the CMG out of the dead zone. The error is so small that further consideration of the limit cycle caused by CMG dead zones is unnecessary.

The first-order lag is a reasonable approximation to the transfer function of a SGCMG at low frequencies. However, a typical time constant is 0.02 second. It could be increased to 0.7 second, as required by the foregoing analysis, by reducing the gain of the gimbal servo; but an undesirable result would be an increase in the dead zone due to Coulomb friction. A CMG time constant of 0.02 second and the previously computed rate-loop gain (5.82×10^6) give the following transfer function.

$$\begin{aligned}\frac{\theta}{\epsilon} &= \frac{1.745 \times 10^6}{s(0.02 \times 8.21 \times 10^6 s^2 + 8.21 \times 10^6 s + 5.82 \times 10^6)} \\ &= \frac{0.3}{s(s/0.72 + 1)(s/49.3 + 1)}\end{aligned}\quad (10)$$

The Bode diagram of this function shown in figure 7.5 is still satisfactory.

In the case of a DGCMG, the preliminary estimates may be improved by use of a more exact gyro model. Figure 7.6 is a signal flow diagram of a DGCMG in which all mechanical parts are rigid. The corresponding transfer function derived from this diagram is

$$\frac{\dot{\delta}_1}{\dot{\delta}_{lc}} = \frac{NK_v G_1 (J_{e3}s + G_3 NK_v)}{J_{e1} J_{e3} s^2 + NK_v (G_1 J_{e3} + G_3 J_{e1}) s + H^2 \cos^2 \delta_1 + G_1 G_3 N^2 K_v^2} \quad (11)$$

If the compensation functions G_1 and G_3 are unity, $\frac{\dot{\delta}_1}{\dot{\delta}_{lc}}$ becomes

$$\frac{\dot{\delta}_1}{\dot{\delta}_{lc}} = \frac{\tau_n s + 1}{s^2/\omega_g^2 + 2\zeta_g s/\omega_g + 1} \quad (12)$$

The vehicle control loop including the transfer function $\frac{\dot{\delta}_1}{\dot{\delta}_{lc}}$ is shown in figure 7.7. One more application of Mason's method gives the open loop transfer function $\frac{\theta_o}{\epsilon}$.

$$\frac{\theta_o}{\epsilon} = \frac{K_p (\tau_n s + 1)}{s [I s^3/\omega_g^2 + 2I\zeta_g s^2/\omega_g + (I + K_r \tau_n) s + K_r]} \quad (13)$$

In a typical CMG, τ_n is about 1 millisecond. $K_r \tau_n$ is, consequently, negligible by comparison to I . Using the values of K_r and K_p estimated by the first-order approximation and setting ω_g equal to $1/\tau_g$, 1.414 rad/sec, the transfer function $\frac{\theta_o}{\epsilon}$ equals

$$\frac{\theta_o}{\epsilon} = \frac{0.3(s/1000+1)}{s(s/1.30+1)(s^2/1.045^2 + 2 \times 0.335s/1.045+1)} \quad (14)$$

The Bode diagram of this transfer function shown in figure 7.8, indicates a stable system but, the damping ratio 0.335 is inadequate.

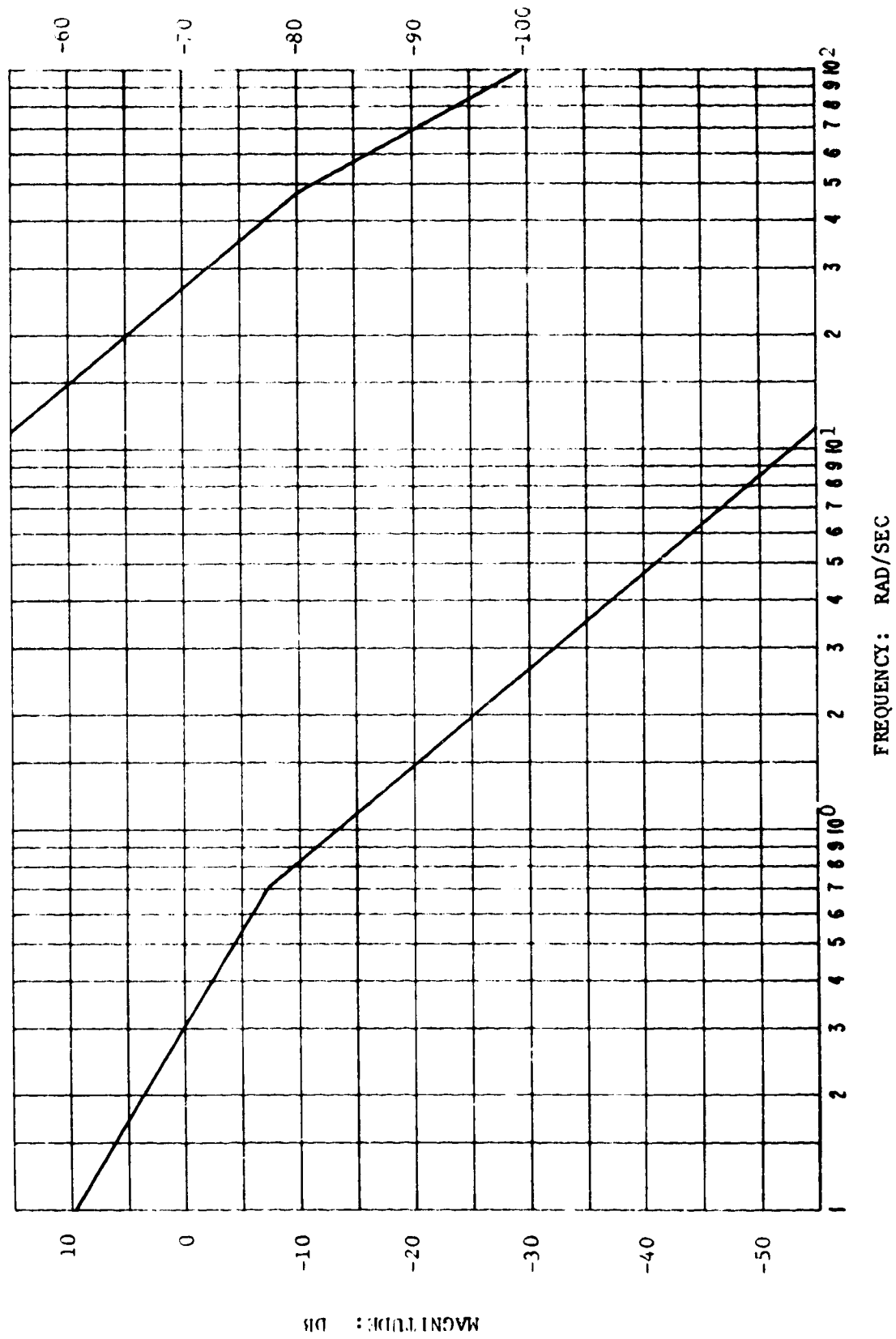
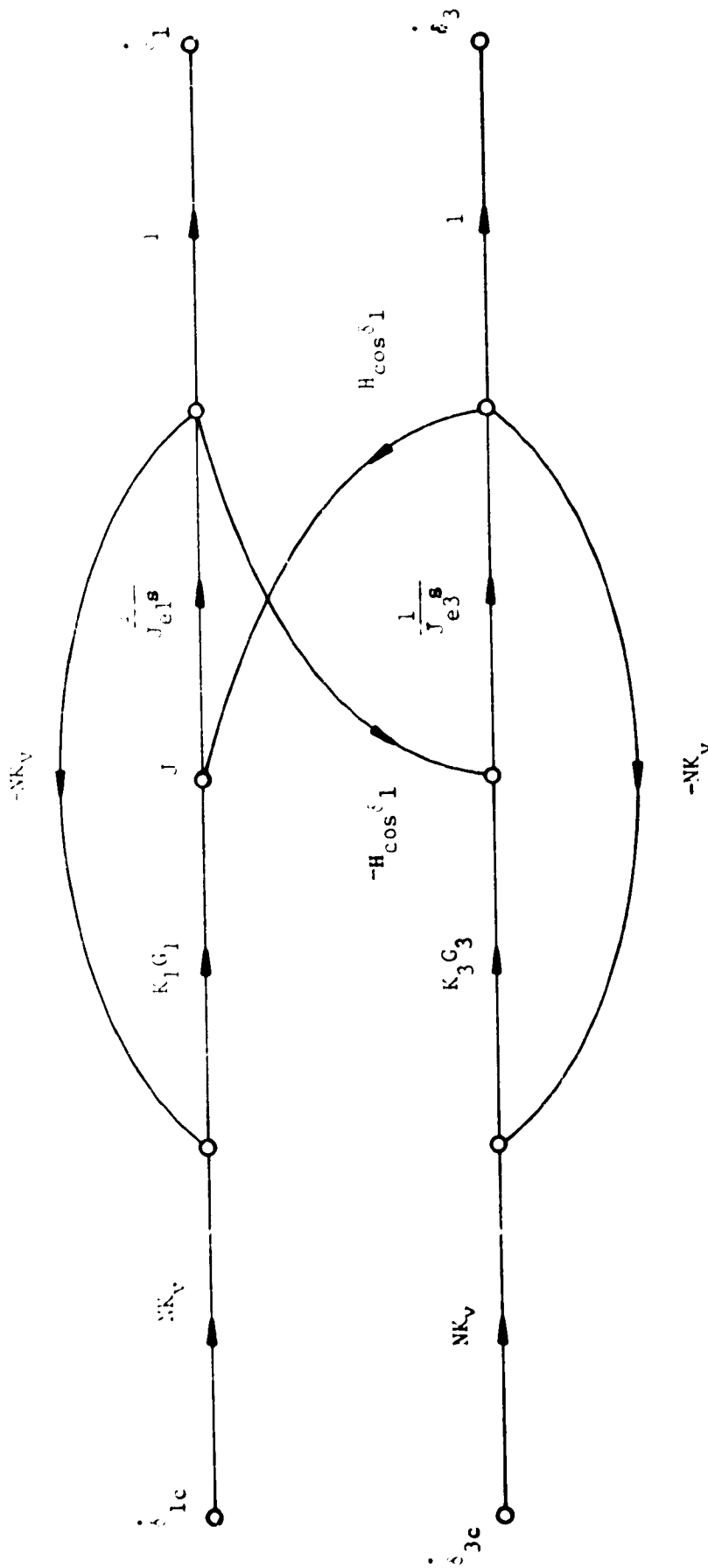


Figure 7.5. Magnitude Vs Frequency Plot of Simplified Vehicle Control Loop Using Typical SGCMG's ($\tau = 0.002$ sec)



SUBSCRIPTS 1 AND 3 REFER TO INNER AND OUTER GIMBALS, RESPECTIVELY.

- s LAPLACE VARIABLE
 G COMPENSATION FUNCTION
 H SPIN MOMENTUM
 J_e EQUIVALENT MOMENT OF INERTIA OF WHEEL AND GIMBAL
 K AMPLIFIER AND MOTOR GAIN
 K_v TACHOMETER GAIN
 N GEAR RATIO
 δ GIMBAL ANGLE
 δ_c GIMBAL-ANGLE COMMAND

Figure 7.6. Signal-Flow Graph of Rigid DGCMG

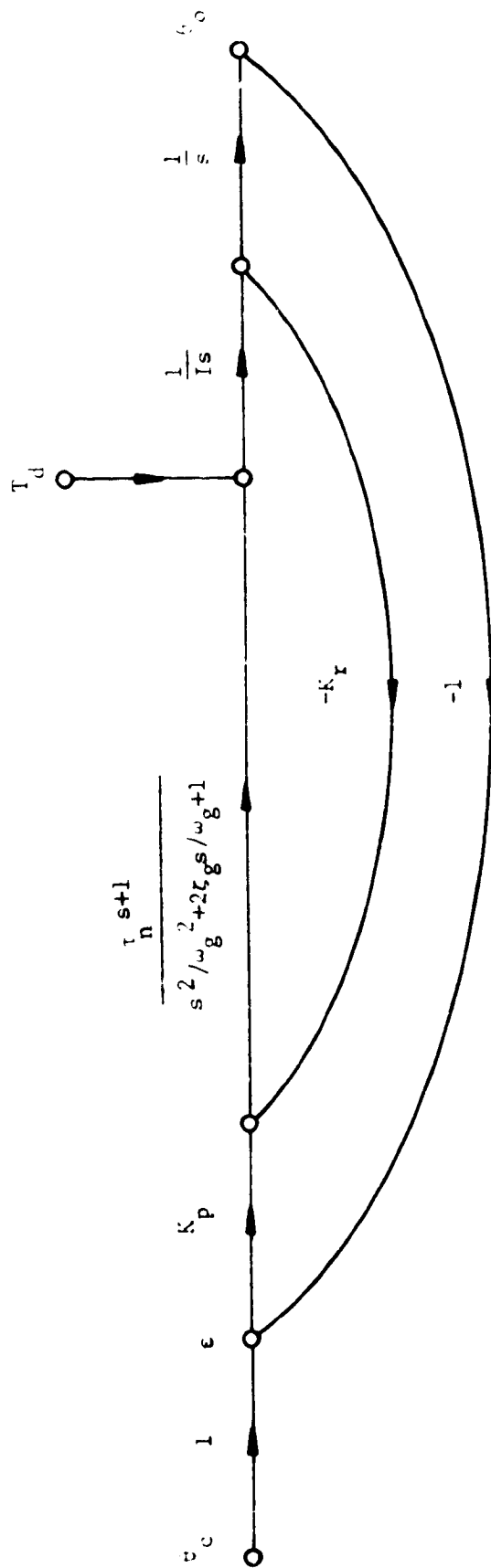


Figure 7.7. Simplified Vehicle Control Loop (Using Quadratic Approximation to DGCMG)

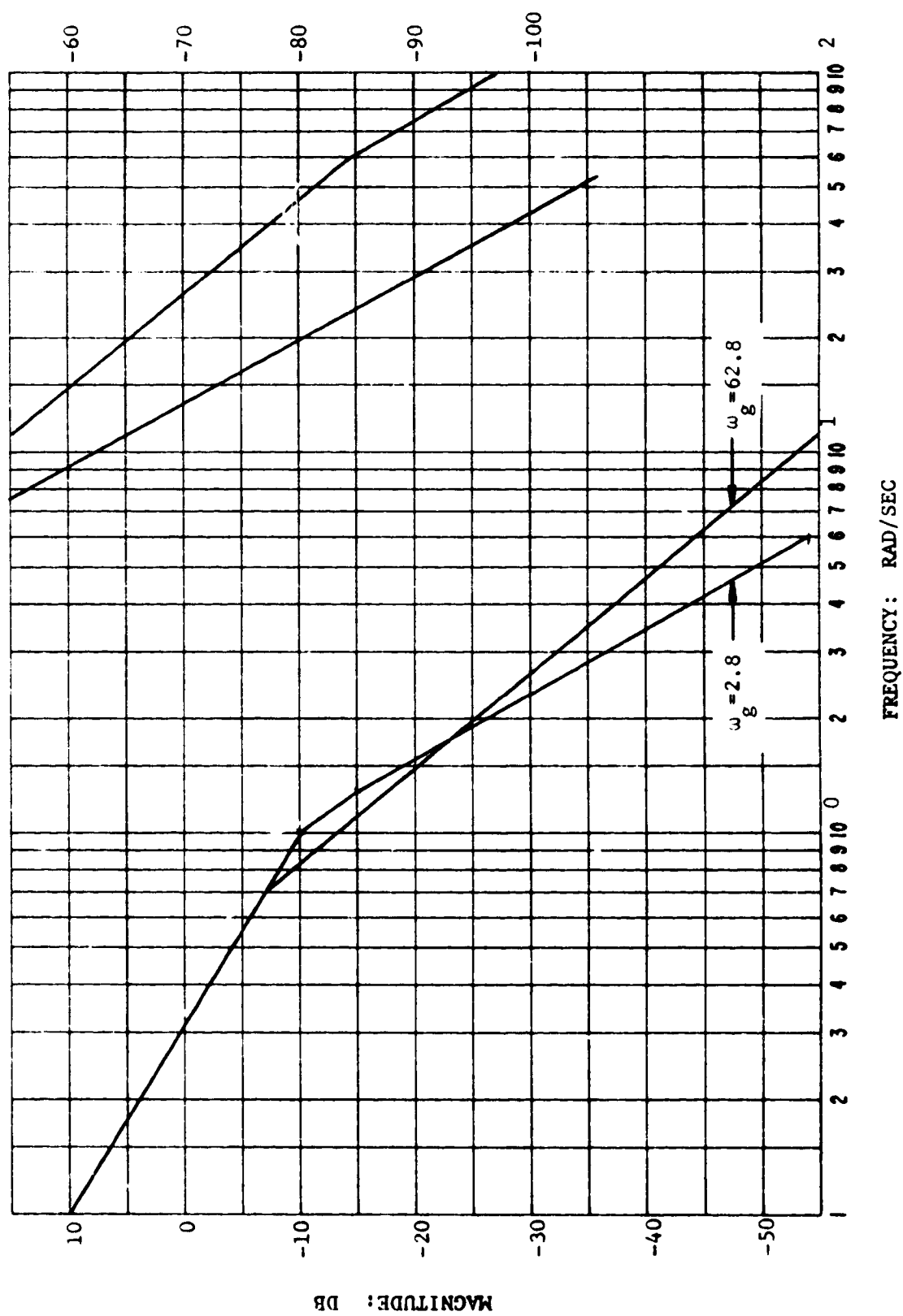


Figure 7.8. Magnitude Vs Frequency Plot of Simplified Vehicle Control Loop Using Typical DCCMG's

CMGs are usually designed to have a natural frequency much greater than 1.414 radians per second. Ten Hz, or 62.8 radians per second, is a typical value of ω_g . If this is used, the vehicle transfer function $\frac{\theta_o}{\epsilon}$ equals

$$\frac{\theta_o}{\epsilon} = \frac{0.3(s/1000+1)}{s(s/0.72+1)(s^2/62.3^2+2 \times 0.705s/62.3+1)} \quad (15)$$

The corresponding Bode diagram also shown in figure 7.8 indicates a more satisfactory system.

Another matter of interest is the effect of crew motion disturbances on the model shown in figure 7.7. The transfer function relating vehicle displacement θ_o to disturbance torque equals

$$\frac{\theta_o}{T_d} = \frac{(s^2 + 2\zeta_g \omega_g s + \omega_g^2)/I}{s^4 + 2\zeta_g \omega_g s^3 + \omega_g^2 (1 + \tau_n K_r/I) s^2 + \omega_g^2 (K_r + \tau_n K_p) s + \omega_g^2 K_p/I} \quad (16)$$

The previously established values for the parameters contained in equation 16 are:

$$I = 8.21 \times 10^6 \text{ slug ft}^2$$

$$K_p = 1.745 \times 10^6 \text{ ft lb/rad}$$

$$K_r = 5.82 \times 10^6 \text{ ft lb/(rad/sec)}$$

$$\zeta_g = 0.707$$

$$\tau_n = 0.001 \text{ sec}$$

$$\omega_g = 62.4 \text{ rad/sec}$$

Substituting these values into the transfer function $\frac{\theta_o}{T_d}$,

$$\frac{\theta_o}{T_d} = \frac{(s^2 + 88.8s + 3940)/8.21 \times 10^6}{(s^2 + 0.707s + 0.213)(s^2 + 88.1s + 3880)} \quad (17)$$

The quadratic factor in the numerator is essentially identical to one in the denominator therefore they can be assumed to cancel.

The resulting transfer function $\frac{\theta_o}{T_d}$ equals

$$\frac{\theta_o}{T_d} \approx \frac{1.22 \times 10^{-7}}{s^2 + 0.707s + 0.213} \quad (18)$$

The time response to a unit impulse of torque can be readily computed; $\theta_o(t)$ equals

$$\theta_o(t) = 4.12 \times 10^{-7} e^{-0.354t} \sin 0.295t \quad (19)$$

The crew motion disturbance mentioned previously generates alternating impulses of 900 ft lb sec each. The resulting displacement, in arc minutes, is therefore

$$\begin{aligned} \theta_o(t) &= 4.12 \times 10^{-7} \times 900 \times 57.3 \times 60 e^{-0.354t} \sin 0.295t \quad (20) \\ &= 1.275 e^{-0.354t} \sin 0.295t \end{aligned}$$

which has a maximum value of 0.36 arc minute when $t=2.5$ seconds.

Although this is the largest disturbance that has been considered, it is much smaller than the allowable disturbance. A reduction of vehicle loop gains might therefore be considered. By neglecting CMG dynamics, it is estimated that values of 2.43×10^5

and 2.08×10^6 for K_p and K_r , respectively, will allow the disturbance

to increase to 1.0 arc minute while maintaining a damping ratio of 0.7. Substitution of these values into equation 16 leads to

$$\begin{aligned} \frac{\theta_o}{T_d} &= \frac{(s^2 + 88.8s + 3940) / 8.21 \times 10^6}{(s^2 + 0.253s + 0.0296)(s^2 + 88.8s + 3940)} \\ &= \frac{1.22 \times 10^{-7}}{s^2 + 0.253s + 0.0296} \quad (21) \end{aligned}$$

The time response $\theta_o(t)$ corresponding to a 900 ft lb sec. impulse in arc minutes equals

$$\theta_o(t) = 3.11 e^{-0.217t} \sin 0.172t \quad (22)$$

$\theta_o(t)$ has a maximum value of 1.0 arc minute at t equal to 4.56 seconds.

The cancellation of the quadratic terms in equation 21 indicates that the affects of CMG dynamics on the vehicle attitude control loop is negligible. The revised value of K_p for the Y axis changes the angular displacement due to gravity gradient disturbance torques as computed in equation 9 to 0.197 arc minute; this angular displacement is still negligible. The attitude error attributed to CMG dead zones is increased to 0.02 arc minutes which is also insignificant. These attitude errors along with those due to crew motion are illustrated in figure 7.9. Note that the total attitude error depicted in this figure is well within the desired three arc minute stablization goal.

The revised rate and position gains K_{ri} and K_{pi} , $i=x,y,z$, are:

$$\begin{aligned} K_{ri} &= 0.243 I_{ii} \\ K_{pi} &= 0.0295 I_{ii} \end{aligned} \quad (23)$$

Substituting the appropriate vehicle moments of inertia I_{ii} into the above expressions K_{ri} and K_{pi} equal

$$\begin{aligned} K_{rx} &= 2.52 \times 10^5 \text{ ft-lb/(rad/sec)} \\ K_{ry} &= 1.995 \times 10^6 \text{ ft-lb/(rad/sec)} \\ K_{rz} &= 2.078 \times 10^6 \text{ ft-lb/(rad/sec)} \\ K_{px} &= 3.068 \times 10^4 \text{ ft-lb/rad} \\ K_{py} &= 2.422 \times 10^5 \text{ ft-lb/rad} \\ K_{pz} &= 2.522 \times 10^5 \text{ ft-lb/rad} \end{aligned} \quad (24)$$

The above control law gains result in a closed loop control system with a natural frequency of 0.127 radian per second (0.027 Hz) and a damping ratio of 0.7. These CMG vehicle control law gains are used in the computer verification task documented in section 12.0. The purpose of the computer verification task is to demonstrate the feasibility using a hybrid computer simulation of the selected control logic associated with this CMG control system.

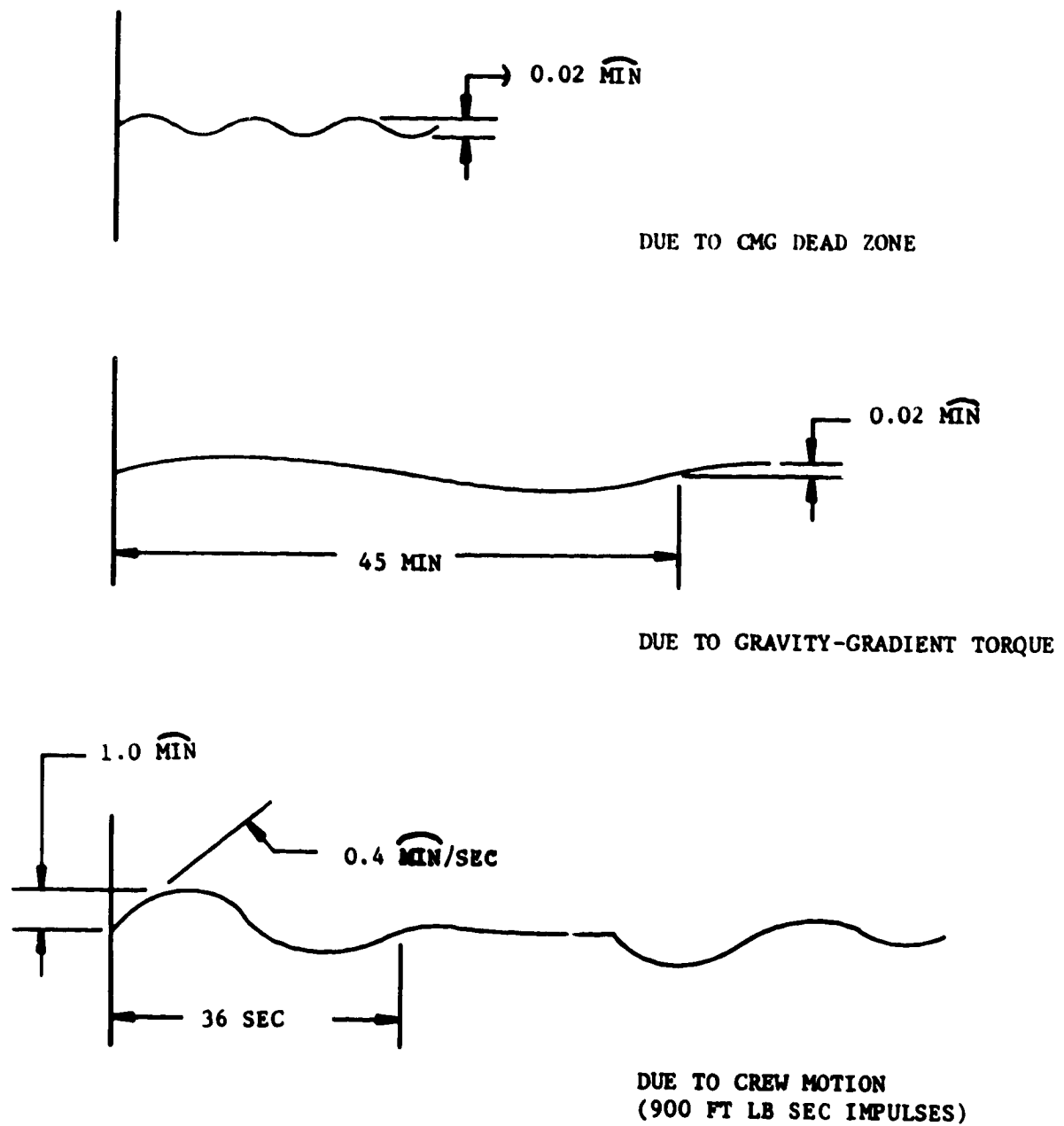


Figure 7.9. Typical Attitude Errors

7.3 Notes

7.3.1 Symbols

CMG	Control moment gyro
db	Decibel(s)
DGCMG	Double gimbal CMG
ft-lb	Foot pound(s)
Γ_w	Crew wall pushoff disturbance force
G	CMG servo compensation function
H	Wheel spin momentum
Hz	Hertz
I	Vehicle moment of inertia
[I]	Vehicle inertia tensor
I_{ii}	Vehicle moment of inertia ($i=x,y,z$)
J_e	Equivalent moment of inertia of CMG wheel and gimbal
K	CMG amplifier and motor gain
$[K_p]$	Vehicle control law position gain matrix
K_{px}, K_{py}, K_{pz}	Components of $[K_p]$
$[K_r]$	Vehicle control law rate gain matrix
K_{rx}, K_{ry}, K_{rz}	Components of $[K_r]$
K_v	CMG tachometer gain
L	Effective moment arm corresponding to crew wall pushoff disturbance
$\overset{\text{min}}{\curvearrowright}$	Arc minute(s)
$\frac{\text{min}}{\text{sec}}$	Arc minute(s) per second
N	CMG gear train ratio
P	Period between crew pushoffs
s	Laplace transform operator
sec	Second(s)
SGCMG	Single gimbal CMG
t	Time (seconds)
\vec{T}_{COM}	CMG torque command
T_d	Disturbance torque
δ	Gimbal angle
δ_i	Gimbal angle ($i=1$, inner; $i=3$, outer)
$\dot{\delta}_i$	Gimbal rate ($i=1$, inner; $i=3$, outer)
$\dot{\delta}_{ic}$	Gimbal rate command ($i=1$, inner; $i=3$, outer)
$\vec{\epsilon}$	Vehicle attitude error or offset command
ζ_r	CMG servo damping ratio
θ_c	Vehicle angular displacement command
θ_o	Vehicle angular displacement

$\Delta \delta$	vehicle attitude error
$\Delta \theta_y$	incremental change in vehicle angular displacement due to crew wall pushoffs
τ_g	CMG time constant (seconds)
$\vec{\omega}$	vehicle angular velocity
$\vec{\omega}_D$	desired vehicle angular velocity
ω_r	CMG servo natural frequency
$\Delta \omega_y$	incremental change in vehicle angular velocity due to crew wall pushoffs

7.3.2 Reference

1. Mathematical Models for Orbiting Space Station Control System Analysis, Report No. 70-4, Bendix Corp., Research Laboratories, Southfield, Michigan, January 1971

8. CMG MANEUVER CONTROL LAWS

Three methods of implementing the attitude strapdown equations of motion for a large Earth orbiting spacecraft are described in this section; they are based on (1) quaternion, (2) direct cosines, and (3) Euler angle implementations for describing the attitude of a spacecraft. The function of the strapdown equations is to generate sufficient vehicle attitude information that will enable the vehicle to maintain or track specific attitudes and to perform vehicle maneuvers. The output of this section is to select one of these CMG maneuver control laws on the basis of software complexity, computational case, and system performance.

8.1 Vehicle Control Law - The vehicle control law utilizes the attitude information computed by the CMG maneuver control law to generate the appropriate CMG torque commands \vec{T}_{COM} . The CMG torque command \vec{T}_{COM} that is sent to the CMG control system is governed by the following rate plus position vehicle control law described in section 7.1.

$$\vec{T}_{COM} = [K_r](\vec{\omega}_D - \vec{\omega}) + [K_p](\Delta\vec{\theta} + \vec{\epsilon}) \quad (1)$$

$\vec{\omega}$ is the vehicle angular rate as measured by the rate gyros mounted to the vehicle, $\vec{\omega}_D$ and $\Delta\vec{\theta}$ are the desired vehicle rate and vehicle attitude error as determined by the CMG maneuver control law. The gains matrices $[K_r]$ and $[K_p]$ are the corresponding vehicle rate and position vehicle control law gains defined in section 7.0 and $\vec{\epsilon}$ is a vehicle attitude offset command.

8.2 Quaternion Maneuver Control Law - The attitude of a spacecraft with respect to some reference frame can be described by a set of four parameters called quaternions. These four parameters are based on Euler's theorem that states that the rotational displacement of a rigid body from some initial orientation can be described by a single rotation about a fixed axis. This axis is referred to as an eigenaxis because it is common to both the reference and vehicle coordinate frames. The quaternions describe the attitude of a spacecraft by defining the eigenaxis and the appropriate angular displacement about this axis necessary to transfer from the reference frame to vehicle space.

8.2.1 Quaternion Definition - Assume that the rigid body shown in figure 8.1 is rotated with respect to some reference frame XYZ about an eigenaxis \vec{E} defined by the three directional angles α , β , and γ through an angular displacement θ . Assume that \vec{E} is a unit vector.

$$\vec{E} = \cos\alpha \hat{i} + \cos\beta \hat{j} + \cos\gamma \hat{k} \quad (2)$$

where \hat{i} , \hat{j} , and \hat{k} are unit vectors along the X, Y, and Z axes, respectively. Let the reference coordinates x, y, z define the location of a point P in the body prior to the rotation θ about \vec{E} .

Define a second coordinate system $x'y'z'$ such that x' lies along the eigenaxis \vec{E} , y' lies in the YZ plane, and z' forms the remaining axis of the orthogonal coordinate triad $x'y'z'$. Let \hat{i}' , \hat{j}' , and \hat{k}' be unit vectors along x' , y' , and z' , respectively. \hat{i}' , \hat{j}' , and \hat{k}' in terms of \hat{i} , \hat{j} , and \hat{k} equal

$$\hat{i}' = \vec{E} = \cos\alpha \hat{i} + \cos\beta \hat{j} + \cos\gamma \hat{k} \quad (3)$$

$$\hat{j}' = \frac{\hat{i} \times \hat{i}'}{\sin\alpha} = -\frac{\cos\gamma}{\sin\alpha} \hat{j} + \frac{\cos\beta}{\sin\alpha} \hat{k} \quad (4)$$

$$\begin{aligned} \hat{k}' = \hat{i}' \times \hat{j}' = \frac{1}{\sin\alpha} [(\cos^2\beta + \cos^2\gamma)\hat{i} \\ - \cos\alpha \cos\beta \hat{j} - \cos\alpha \cos\gamma \hat{k}] \end{aligned} \quad (5)$$

The transformation from $x'y'z'$ to XYZ space can be defined by the following transformation:

$$\begin{bmatrix} X \\ Y \\ Z \end{bmatrix} = [\phi_{R \rightarrow R'}] \begin{bmatrix} x' \\ y' \\ z' \end{bmatrix} \quad (6)$$

where

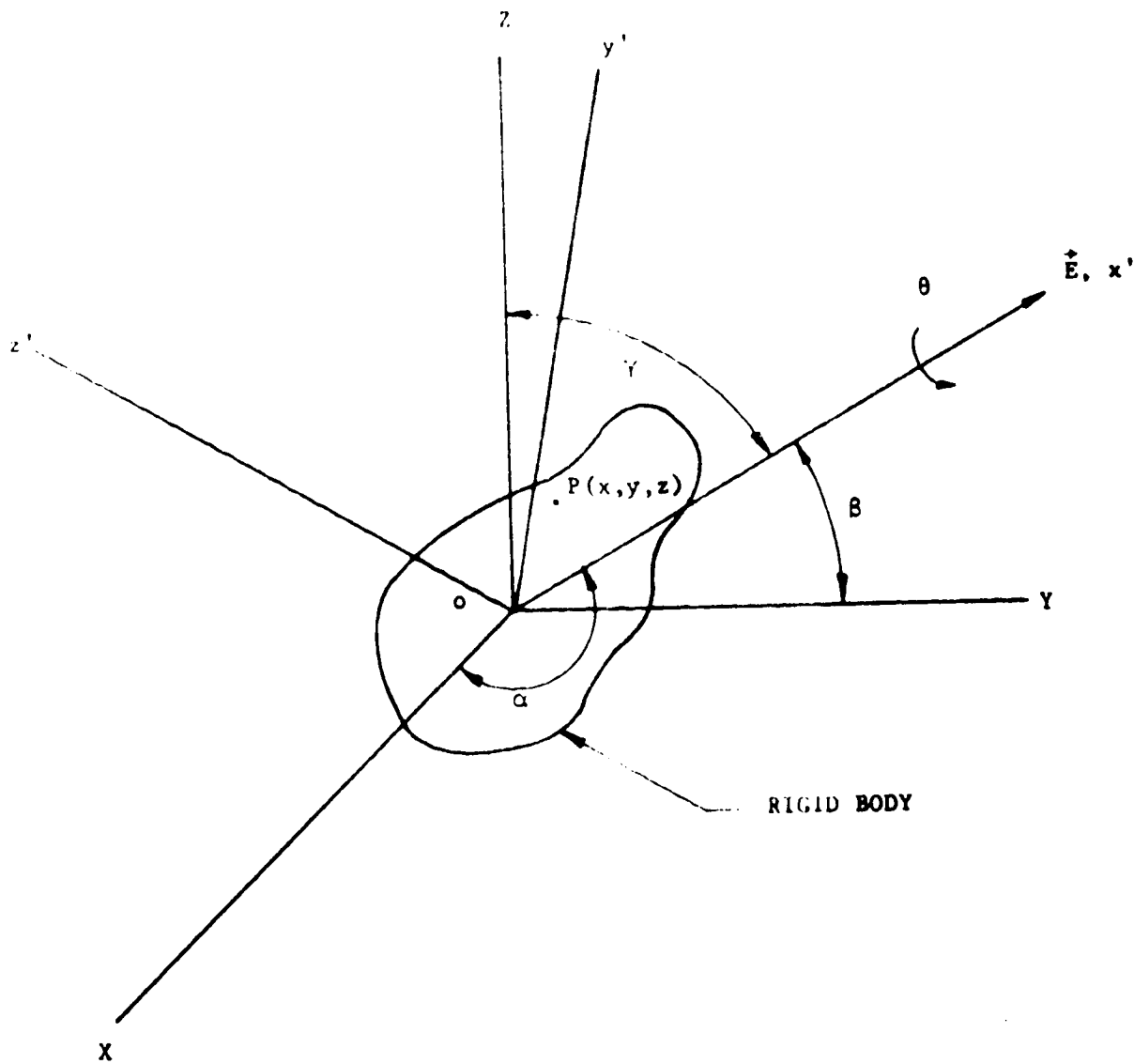


Figure 8.1 Rigid Body Coordinate Systems

$$[\phi_{R \leftarrow R'}] = \begin{bmatrix} \cos \alpha & 0 & \frac{\cos^2 \beta + \cos^2 \gamma}{\sin \alpha} \\ \cos \beta & -\frac{\cos \gamma}{\sin \alpha} & -\frac{\cos \alpha \cos \beta}{\sin \alpha} \\ \cos \gamma & \frac{\cos \beta}{\sin \alpha} & -\frac{\cos \alpha \cos \gamma}{\sin \alpha} \end{bmatrix}$$

Define a third coordinate system $X_v Y_v Z_v$ that is fixed to the rigid body. Assume that prior to the rotation θ about \vec{E} , that the two coordinate systems $x'y'z'$ and $X_v Y_v Z_v$ are aligned. The coordinates of point P in body space $X_v Y_v Z_v$ are

$$\begin{bmatrix} X_v \\ Y_v \\ Z_v \end{bmatrix} = [\phi_{R \leftarrow R'}] \begin{bmatrix} x \\ y \\ z \end{bmatrix} \quad (7)$$

where

$$[\phi_{R' \leftarrow R}] = \begin{bmatrix} \cos \alpha & \cos \beta & \cos \gamma \\ 0 & -\frac{\cos \gamma}{\sin \alpha} & \frac{\cos \beta}{\sin \alpha} \\ \frac{\cos^2 \beta + \cos^2 \gamma}{\sin \alpha} & -\frac{\cos \alpha \cos \beta}{\sin \alpha} & -\frac{\cos \alpha \cos \gamma}{\sin \alpha} \end{bmatrix}$$

Now assume the rigid body is rotated about the eigenaxis \vec{E} (X_v axis) through the angle θ . This rotation can be thought of as a transformation from the $x'y'z'$ coordinate frame to the new location of the $X_v Y_v Z_v$ coordinate system as shown in figure 8.2.

The resulting transformation from $X_v Y_v Z_v$ to $x'y'z'$ is

$$\begin{bmatrix} x' \\ y' \\ z' \end{bmatrix} = [\phi_{R' \leftarrow v}] \begin{bmatrix} X_v \\ Y_v \\ Z_v \end{bmatrix} \quad (8)$$

where

$$[\phi_{R' \leftarrow v}] = \begin{bmatrix} 1 & 0 & 0 \\ 0 & \cos \theta & -\sin \theta \\ 0 & \sin \theta & \cos \theta \end{bmatrix}$$

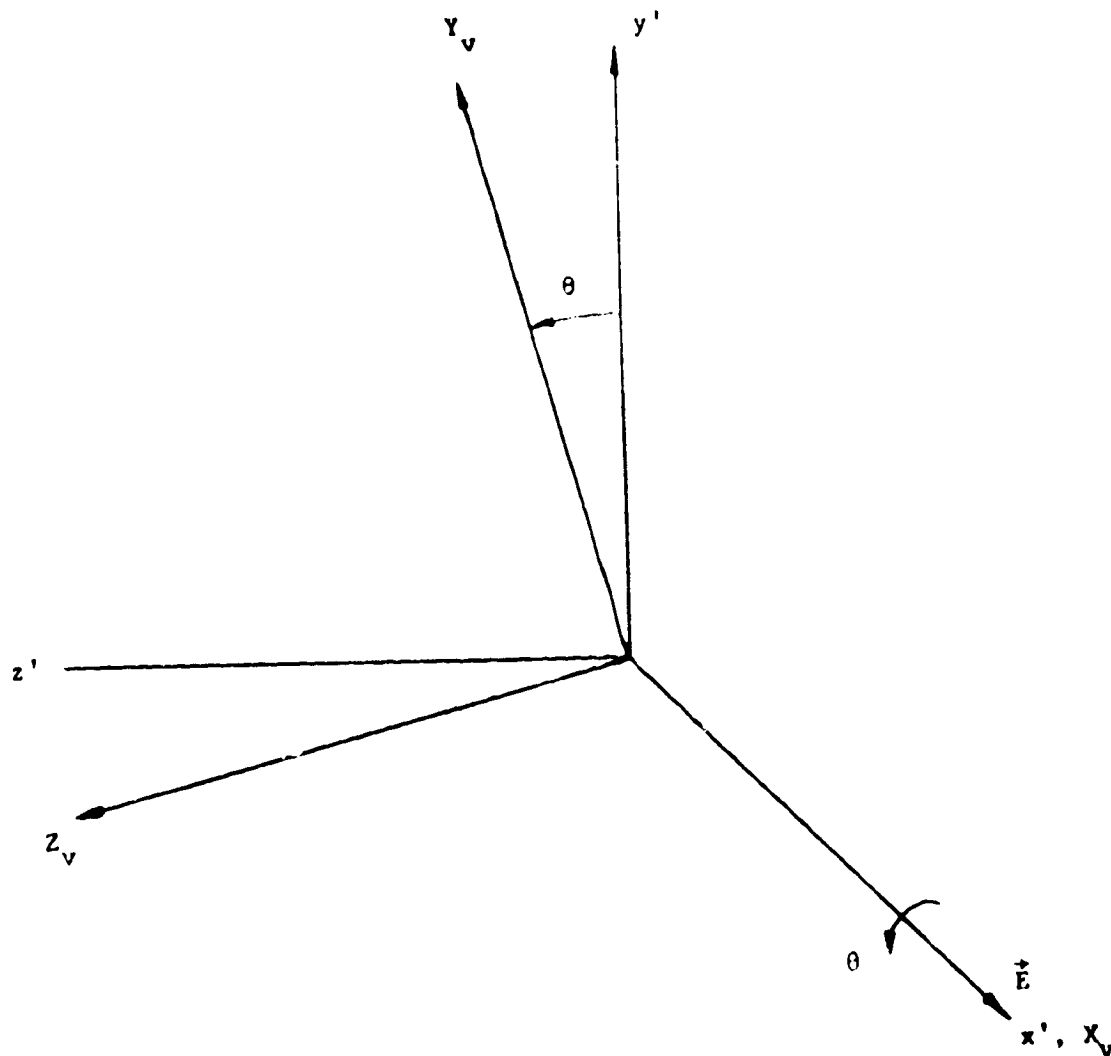


Figure 8.2 Rotational Displacement θ of $x_v y_v z_v$
From $x'y'z'$

The new location of point P in the XYZ reference frame due to the rotational displacement θ about \vec{E} is given by the following transformation.

$$\begin{bmatrix} X \\ Y \\ Z \end{bmatrix} = [\phi_{R+R'}][\phi_{R'+V}][\phi_{R'+R}] \begin{bmatrix} x \\ y \\ z \end{bmatrix} \quad (9)$$

Let

$$[\phi] = [\phi_{R+R'}][\phi_{R'+V}][\phi_{R'+R}] \quad (10)$$

such that

$$\begin{bmatrix} X \\ Y \\ Z \end{bmatrix} = [\phi] \begin{bmatrix} x \\ y \\ z \end{bmatrix} \quad (11)$$

The transformation $[\phi]$ describes the new location of the rigid body with respect to the XYZ reference frame. $[\phi]$ equals

$$[\phi] = \begin{bmatrix} a_{11} & a_{12} & a_{13} \\ a_{21} & a_{22} & a_{23} \\ a_{31} & a_{32} & a_{33} \end{bmatrix} \quad (12)$$

where

$$\begin{aligned} a_{11} &= 1 - 2\sin^2\left(\frac{\theta}{2}\right)\sin^2\alpha \\ a_{12} &= 2\left[\sin^2\left(\frac{\theta}{2}\right)\cos\alpha\cos\beta - \sin\left(\frac{\theta}{2}\right)\cos\left(\frac{\theta}{2}\right)\cos\gamma\right] \\ a_{13} &= 2\left[\sin^2\left(\frac{\theta}{2}\right)\cos\alpha\cos\gamma + \sin\left(\frac{\theta}{2}\right)\cos\left(\frac{\theta}{2}\right)\cos\beta\right] \\ a_{21} &= 2\left[\sin^2\left(\frac{\theta}{2}\right)\cos\beta\cos\alpha + \sin\left(\frac{\theta}{2}\right)\cos\left(\frac{\theta}{2}\right)\cos\gamma\right] \\ a_{22} &= 1 - 2\sin^2\left(\frac{\theta}{2}\right)\sin^2\beta \\ a_{23} &= 2\left[\sin^2\left(\frac{\theta}{2}\right)\cos\beta\cos\gamma - \sin\left(\frac{\theta}{2}\right)\cos\left(\frac{\theta}{2}\right)\cos\alpha\right] \end{aligned}$$

$$a_{31} = 2[\sin^2(\frac{\theta}{2})\cos\gamma\cos\alpha - \sin(\frac{\theta}{2})\cos(\frac{\theta}{2})\cos\beta]$$

$$a_{32} = 2[\sin^2(\frac{\theta}{2})\cos\gamma\cos\beta + \sin(\frac{\theta}{2})\cos(\frac{\theta}{2})\cos\alpha]$$

$$a_{33} = 1 - 2\sin^2(\frac{\theta}{2})\sin^2\gamma$$

The relative orientation of the two coordinate systems, $X_v Y_v Z_v$ with respect to XYZ, can be specified by either the transformation $[\phi]$ or by the single axis rotation defined by \vec{E} and θ that would align both coordinate frames. The following four parameters q_1 , q_2 , q_3 , and q_4 can be used to specify \vec{E} and θ .

$$q_1 = \cos(\frac{\theta}{2}) \quad (13)$$

$$q_2 = E_x \sin(\frac{\theta}{2}) \quad (14)$$

$$q_3 = E_y \sin(\frac{\theta}{2}) \quad (15)$$

$$q_4 = E_z \sin(\frac{\theta}{2}) \quad (16)$$

These four parameters are referred to as the four Euler rotational quaternions. E_x , E_y , and E_z are the directional cosines that define \vec{E} ($E_x = \cos\alpha$, $E_y = \cos\beta$, $E_z = \cos\gamma$). The four quaternions q_1 , q_2 , q_3 , and q_4 are often written in the form of a complex number \vec{q} .

$$\vec{q} = q_1 + q_2 \hat{i} + q_3 \hat{j} + q_4 \hat{k} \quad (17)$$

where \hat{i} , \hat{j} , and \hat{k} are the unit vectors along the X, Y, and Z reference axes, respectively.

These four quaternions q_1 , q_2 , q_3 , and q_4 are sufficient to determine completely the transformation $[\phi]$. It can be shown that the nine elements of $[\phi]$ a_{11} , a_{12} , ..., a_{33} can be written in terms of these four quaternions.

$$a_{11} = q_1^2 + q_2^2 - q_3^2 - q_4^2 \quad (18)$$

$$a_{12} = 2(q_2 q_3 - q_1 q_4) \quad (19)$$

$$a_{13} = 2(q_2 q_4 + q_1 q_3) \quad (20)$$

$$a_{21} = 2(q_2q_3 + q_1q_4) \quad (21)$$

$$a_{22} = q_1^2 - q_2^2 + q_3^2 - q_4^2 \quad (22)$$

$$a_{23} = 2(q_3q_4 - q_1q_2) \quad (23)$$

$$a_{31} = 2(q_2q_4 - q_1q_3) \quad (24)$$

$$a_{32} = 2(q_1q_2 + q_3q_4) \quad (25)$$

$$a_{33} = q_1^2 - q_2^2 - q_3^2 + q_4^2 \quad (26)$$

Since the transformation $[\Phi]$ describes the attitude of the rigid body shown in figure 8.1 with respect to the XYZ reference frame and since $[\Phi]$ can also be written in terms of q_1 , q_2 , q_3 , and q_4 , these four quaternions also completely specify the orientation of the $X_v Y_v Z_v$ coordinate frame.

Given $[\Phi]$, the quaternions q_1 , q_2 , q_3 , and q_4 can be computed from its elements a_{11} , a_{12} , ..., a_{33} . To compute q_1 , q_2 , q_3 , and q_4 , one needs only to determine the eigenaxis \vec{E} and the rotational displacement θ about the axis as specified by $[\Phi]$. θ can be computed using the unique property that the trace of $[\Phi]$ equals $1 + 2\cos\theta$.

$$\text{trace of } [\Phi] = \sum_{i=1}^3 a_{ii} = 1 + 2\cos\theta \quad (27)$$

θ equals

$$\theta = \cos^{-1}[0.5(a_{11} + a_{22} + a_{33} - 1)] \quad (28)$$

The eigenaxis \vec{E} is defined by the three direction cosines, $\cos\alpha$, $\cos\beta$, and $\cos\gamma$ designated E_x , E_y , and E_z , respectively. Using equations 18 thru 26, it can be shown that E_x , E_y , and E_z equal

$$E_x = \cos\alpha = \frac{a_{32} - a_{23}}{4\cos(\frac{\theta}{2})\sin(\frac{\theta}{2})} \quad (29)$$

$$E_y = \cos\beta = \frac{a_{13} - a_{31}}{4\cos(\frac{\theta}{2})\sin(\frac{\theta}{2})} \quad (30)$$

$$E_z = \cos \gamma = \frac{a_{21} - a_{12}}{4 \cos(\frac{\theta}{2}) \sin(\frac{\theta}{2})} \quad (31)$$

Using the results of equations 28 thru 31, the quaternions q_1 , q_2 , q_3 , and q_4 as a function of the elements of $[\Phi]$ equal

$$q_1 = \cos(\frac{\theta}{2}) \text{ where } \theta = \cos^{-1} [0.5(a_{11} + a_{22} + a_{33} - 1)] \quad (32)$$

$$q_2 = E_x \sin(\frac{\theta}{2}) = \frac{a_{32} - a_{23}}{4q_1} \quad (33)$$

$$q_3 = E_y \sin(\frac{\theta}{2}) = \frac{a_{13} - a_{31}}{4q_1} \quad (34)$$

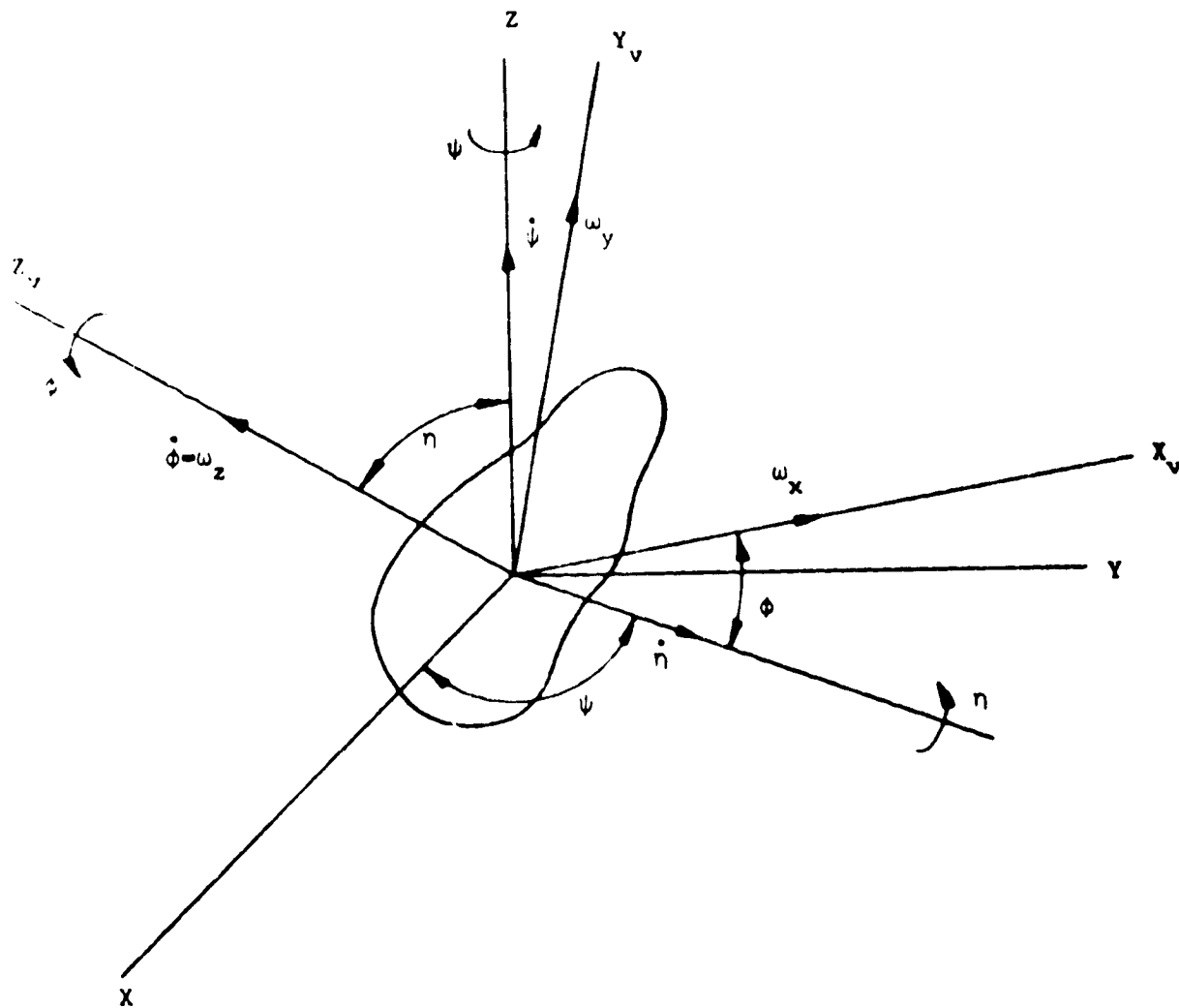
$$q_4 = E_z \sin(\frac{\theta}{2}) = \frac{a_{21} - a_{12}}{4q_1} \quad (35)$$

8.2.2 Quaternion Strapdown Equations - The strapdown equations are a set of equations that are used to digitally compute the four quaternions by using sensed body rates. In the case of a spacecraft, these body rates ω_x , ω_y , and ω_z are normally sensed and measured by at least three rate gyros rigidly mounted to the vehicle.

Assume that the orientation of the rigid body shown in figure 8.3 is due to the Euler rotations ψ , η , and ϕ . The order of these rotations is (1) an angular rotation ψ about the Z axis, (2) a η rotation about the displaced X axis, and (3) a ϕ rotation about the displaced Z axis. The three Euler rotations ψ , η , and ϕ correspond to the following transformations $[\Phi]_\psi$, $[\Phi]_\eta$, and $[\Phi]_\phi$, respectively.

$$[\Phi]_\psi = \begin{bmatrix} \cos \psi & \sin \psi & 0 \\ -\sin \psi & \cos \psi & 0 \\ 0 & 0 & 1 \end{bmatrix} \quad (36)$$

$$[\Phi]_\eta = \begin{bmatrix} 1 & 0 & 0 \\ 0 & \cos \eta & \sin \eta \\ 0 & -\sin \eta & \cos \eta \end{bmatrix} \quad (37)$$

Figure 8.3 Euler Rotations ψ , η , ϕ

$$[\phi]_{\phi} = \begin{bmatrix} \cos\phi & \sin\phi & 0 \\ -\sin\phi & \cos\phi & 0 \\ 0 & 0 & 1 \end{bmatrix} \quad (38)$$

The transformation from the reference coordinate system XYZ to the rigid body coordinate frame $X_v Y_v Z_v$ equals

$$\begin{bmatrix} X_v \\ Y_v \\ Z_v \end{bmatrix} = [\phi]_{\phi} [\phi]_{\eta} [\phi]_{\psi} \begin{bmatrix} X \\ Y \\ Z \end{bmatrix} \quad (39)$$

The rigid body rates ω_x , ω_y , and ω_z can be written in terms of the three Euler rates $\dot{\psi}$, $\dot{\eta}$, and $\dot{\phi}$ as follows

$$\begin{bmatrix} \omega_x \\ \omega_y \\ \omega_z \end{bmatrix} = [\phi]_{\phi} [\phi]_{\eta} [\phi]_{\psi} \begin{bmatrix} 0 \\ 0 \\ \dot{\psi} \end{bmatrix} + [\phi]_{\phi} [\phi]_{\eta} \begin{bmatrix} \dot{\eta} \\ 0 \\ 0 \end{bmatrix} + [\phi]_{\phi} \begin{bmatrix} 0 \\ 0 \\ \dot{\phi} \end{bmatrix} \quad (40)$$

Simplifying the above expression, ω_x , ω_y , and ω_z equal

$$\begin{bmatrix} \omega_x \\ \omega_y \\ \omega_z \end{bmatrix} = [\phi]_{\psi\eta\phi} \begin{bmatrix} \dot{\psi} \\ \dot{\eta} \\ \dot{\phi} \end{bmatrix} \quad (41)$$

where

$$[\phi]_{\psi\eta\phi} = \begin{bmatrix} \sin\eta\sin\phi & \cos\phi & 0 \\ \sin\eta\cos\phi & -\sin\phi & 0 \\ \cos\eta & 0 & 1 \end{bmatrix}$$

The Euler rates $\dot{\psi}$, $\dot{\eta}$, and $\dot{\phi}$ as a function of the body rates ω_x , ω_y , and ω_z equal

$$\begin{bmatrix} \dot{\psi} \\ \dot{\eta} \\ \dot{\phi} \end{bmatrix} = [\Phi]^{-1} \begin{bmatrix} \omega_x \\ \omega_y \\ \omega_z \end{bmatrix} \quad (42)$$

where $[\Phi]^{-1}$ is the inverse of $[\Phi]$.

The three Euler rotations ψ , η , and ϕ can be represented by three complex quaternions. The following quaternions \vec{q}_ψ , \vec{q}_η , and \vec{q}_ϕ correspond to the ψ , η , and ϕ Euler rotations, respectively.

$$\vec{q}_\psi = \cos \frac{\psi}{2} + \sin \frac{\psi}{2} \hat{k} \quad (43)$$

$$\vec{q}_\eta = \cos \frac{\eta}{2} + \sin \frac{\eta}{2} \hat{i} \quad (44)$$

$$\vec{q}_\phi = \cos \frac{\phi}{2} + \sin \frac{\phi}{2} \hat{k} \quad (45)$$

The quaternion \vec{q} that describes the final orientation of the rigid body as the results of the three Euler rotations ψ , η , and ϕ can be computed by performing the following quaternion multiplication.

$$\begin{aligned} \vec{q} &= q_1 + q_2 \hat{i} + q_3 \hat{j} + q_4 \hat{k} \\ &= (\cos \frac{\psi}{2} + \sin \frac{\psi}{2} \hat{k}) (\cos \frac{\eta}{2} + \sin \frac{\eta}{2} \hat{i}) (\cos \frac{\phi}{2} + \sin \frac{\phi}{2} \hat{k}) \end{aligned} \quad (46)$$

Note that

$$\begin{aligned} \hat{i}^2 &= \hat{j}^2 = \hat{k}^2 = -1 \\ \hat{i}\hat{j} &= -\hat{j}\hat{i} = \hat{k} \\ \hat{j}\hat{k} &= -\hat{k}\hat{j} = \hat{i} \\ \hat{k}\hat{i} &= -\hat{i}\hat{k} = \hat{j} \end{aligned}$$

The components of \vec{q} equal

$$q_1 = \cos \frac{\psi}{2} \cos \frac{\eta}{2} \cos \frac{\phi}{2} - \sin \frac{\psi}{2} \cos \frac{\eta}{2} \sin \frac{\phi}{2} \quad (47)$$

$$q_2 = \sin \frac{\psi}{2} \sin \frac{\eta}{2} \sin \frac{\phi}{2} + \cos \frac{\psi}{2} \sin \frac{\eta}{2} \cos \frac{\phi}{2} \quad (48)$$

$$q_3 = \sin \frac{\psi}{2} \sin \frac{\eta}{2} \cos \frac{\phi}{2} - \cos \frac{\psi}{2} \sin \frac{\eta}{2} \sin \frac{\phi}{2} \quad (49)$$

$$q_4 = \sin \frac{\psi}{2} \cos \frac{\eta}{2} \cos \frac{\phi}{2} + \cos \frac{\psi}{2} \cos \frac{\eta}{2} \sin \frac{\phi}{2} \quad (50)$$

The time derivatives of the above expressions for q_1 , q_2 , q_3 , and q_4 can be written as follows:

$$\dot{\vec{q}} = \begin{bmatrix} \dot{q}_1 \\ \dot{q}_2 \\ \dot{q}_3 \\ \dot{q}_4 \end{bmatrix} = \frac{1}{2} \begin{bmatrix} a_{1\dot{\psi}} & a_{1\dot{\eta}} & a_{1\dot{\phi}} \\ a_{2\dot{\psi}} & a_{2\dot{\eta}} & a_{2\dot{\phi}} \\ a_{3\dot{\psi}} & a_{3\dot{\eta}} & a_{3\dot{\phi}} \\ a_{4\dot{\psi}} & a_{4\dot{\eta}} & a_{4\dot{\phi}} \end{bmatrix} \begin{bmatrix} \omega_x \\ \omega_y \\ \omega_z \end{bmatrix} \quad (51)$$

where

$$a_{1\dot{\psi}} = -\sin \frac{\psi}{2} \cos \frac{\eta}{2} \cos \frac{\phi}{2} - \cos \frac{\psi}{2} \cos \frac{\eta}{2} \sin \frac{\phi}{2}$$

$$a_{1\dot{\eta}} = \sin \frac{\psi}{2} \sin \frac{\eta}{2} \sin \frac{\phi}{2} - \cos \frac{\psi}{2} \sin \frac{\eta}{2} \cos \frac{\phi}{2}$$

$$a_{1\dot{\phi}} = -\cos \frac{\psi}{2} \cos \frac{\eta}{2} \sin \frac{\phi}{2} - \sin \frac{\psi}{2} \cos \frac{\eta}{2} \cos \frac{\phi}{2}$$

$$a_{2\dot{\psi}} = \cos \frac{\psi}{2} \sin \frac{\eta}{2} \sin \frac{\phi}{2} - \sin \frac{\psi}{2} \sin \frac{\eta}{2} \cos \frac{\phi}{2}$$

$$a_{2\dot{\eta}} = \sin \frac{\psi}{2} \cos \frac{\eta}{2} \sin \frac{\phi}{2} + \cos \frac{\psi}{2} \cos \frac{\eta}{2} \cos \frac{\phi}{2}$$

$$a_{2\dot{\phi}} = \sin \frac{\psi}{2} \sin \frac{\eta}{2} \cos \frac{\phi}{2} - \cos \frac{\psi}{2} \sin \frac{\eta}{2} \sin \frac{\phi}{2}$$

$$a_{3\dot{\psi}} = \cos \frac{\psi}{2} \sin \frac{\eta}{2} \cos \frac{\phi}{2} + \sin \frac{\psi}{2} \sin \frac{\eta}{2} \sin \frac{\phi}{2}$$

$$a_{3\dot{\eta}} = \sin \frac{\psi}{2} \cos \frac{\eta}{2} \cos \frac{\phi}{2} - \cos \frac{\psi}{2} \cos \frac{\eta}{2} \sin \frac{\phi}{2}$$

$$a_{3\dot{\phi}} = -\sin \frac{\psi}{2} \sin \frac{\eta}{2} \sin \frac{\phi}{2} - \cos \frac{\psi}{2} \sin \frac{\eta}{2} \cos \frac{\phi}{2}$$

$$a_{4\dot{\psi}} = \cos \frac{\psi}{2} \cos \frac{\eta}{2} \cos \frac{\phi}{2} - \sin \frac{\psi}{2} \cos \frac{\eta}{2} \sin \frac{\phi}{2}$$

$$a_{4\eta} = -\sin \frac{\psi}{2} \sin \frac{\eta}{2} \cos \frac{\phi}{2} - \cos \frac{\psi}{2} \sin \frac{\eta}{2} \sin \frac{\phi}{2}$$

$$a_{4\phi} = \cos \frac{\psi}{2} \cos \frac{\eta}{2} \cos \frac{\phi}{2} - \sin \frac{\psi}{2} \cos \frac{\eta}{2} \sin \frac{\phi}{2}$$

By substituting equation 42 into 51 and then simplifying, $\dot{\vec{q}}$ in terms of the body rates ω_x , ω_y , and ω_z equals

$$\dot{\vec{q}} = \begin{bmatrix} \dot{q}_1 \\ \dot{q}_2 \\ \dot{q}_3 \\ \dot{q}_4 \end{bmatrix} = \frac{1}{2} \begin{bmatrix} -q_2 & -q_3 & -q_4 \\ q_1 & -q_4 & q_3 \\ q_4 & q_1 & -q_2 \\ -q_3 & q_2 & q_1 \end{bmatrix} \begin{bmatrix} \omega_x \\ \omega_y \\ \omega_z \end{bmatrix} \quad (52)$$

Using the above relationship, the quaternion rate $\dot{\vec{q}}$ is computed from the sensed body rates ω_x , ω_y , and ω_z . These computed quaternion rates $\dot{\vec{q}}$ are then integrated using a numerical integration technique to compute \vec{q} . Equation 52 and the equations used to perform this numerical integration are referred to as the quaternion strapdown equations. Assume that the numerical integration technique selected is trapezoidal integration. The resulting expressions for q_1 , q_2 , q_3 , and q_4 are:

$$q_1 = q_{1P} + 0.5(\dot{q}_{1P} + \dot{q}_1)\Delta t \quad (53)$$

$$q_2 = q_{2P} + 0.5(\dot{q}_{2P} + \dot{q}_2)\Delta t \quad (54)$$

$$q_3 = q_{3P} + 0.5(\dot{q}_{3P} + \dot{q}_3)\Delta t \quad (55)$$

$$q_4 = q_{4P} + 0.5(\dot{q}_{4P} + \dot{q}_4)\Delta t \quad (56)$$

q_{1P} , q_{2P} , q_{3P} , and q_{4P} are the previously computed quaternions while \dot{q}_{1P} , \dot{q}_{2P} , \dot{q}_{3P} , and \dot{q}_{4P} are their corresponding previously computed quaternion rates. Δt is the sample period in seconds between numerical integrations.

The sign of the quaternion parameter q_1 must remain plus or the rotational displacement θ will exceed π (180 degrees). After performing the integration indicated in equations 53 thru 56 over the period Δt , the sign of q_1 must be checked. If q_1 is negative, the signs of all the quaternions q_1 thru q_4 must be changed. In other words, if q_1 is less than zero as computed by equation 53,

$$q_1 = -q_1 \quad (57)$$

$$q_2 = -q_2 \quad (58)$$

$$q_3 = -q_3 \quad (59)$$

$$q_4 = -q_4 \quad (60)$$

where the q_1 thru q_4 on the right side of equations 57 thru 60 are those computed in equations 53 thru 56.

8.2.3 Quaternion Maneuver - Assume that one wants to maneuver the spacecraft to a new attitude described with respect to the reference frame XYZ by the following transformation $[\phi_D]$.

$$[\phi_D] = \begin{bmatrix} a_{11D} & a_{12D} & a_{13D} \\ a_{21D} & a_{22D} & a_{23D} \\ a_{31D} & a_{32D} & a_{33D} \end{bmatrix} \quad (61)$$

Using equations 32 through 35, the four quaternions q_{D1} , q_{D2} , q_{D3} , and q_{D4} describing the desired spacecraft attitude can be computed from the elements of $[\phi_D]$, a_{11D} , a_{12D} , ..., a_{33D} . q_{D1} , q_{D2} , q_{D3} , and q_{D4} equal

$$q_{D1} = \cos\left(\frac{\theta_D}{2}\right) \text{ where } \theta_D = \cos^{-1}[0.5(a_{11D} + a_{22D} + a_{33D} - 1)] \quad (62)$$

$$q_{D2} = \frac{a_{32D} - a_{23D}}{4q_{D1}} \quad (63)$$

$$q_{D3} = \frac{a_{13D} - a_{31D}}{4q_{D1}} \quad (64)$$

$$q_{D4} = \frac{a_{21D} - a_{12D}}{4q_{D1}} \quad (65)$$

The transformation $[\phi_{DV}]$ describing the desired vehicle orientation with respect to its present attitude equals

$$[\phi_{DV}] = [\phi_D][\phi]^{-1} \quad (66)$$

The corresponding quaternion \vec{q}_{DV} describing the desired maneuver defined by $[\phi_{DV}]$ equals

$$\vec{q}_{DV} = (q_1 - q_2\hat{i} - q_3\hat{j} - q_4\hat{k})(q_{D1} + q_{D2}\hat{i} + q_{D3}\hat{j} + q_{D4}\hat{k})$$

$$= \begin{bmatrix} q_{DV1} \\ q_{DV2} \\ q_{DV3} \\ q_{DV4} \end{bmatrix} = \begin{bmatrix} q_{D1} & q_{D2} & q_{D3} & q_{D4} \\ q_{D2} & -q_{D1} & -q_{D4} & q_{D3} \\ q_{D3} & q_{D4} & -q_{D1} & -q_{D2} \\ q_{D4} & -q_{D3} & q_{D2} & -q_{D1} \end{bmatrix} \begin{bmatrix} q_1 \\ q_2 \\ q_3 \\ q_4 \end{bmatrix} \quad (67)$$

The eigenaxis in vehicle coordinates about which the desired maneuver is to be performed is defined by the following three direction cosines $E_x^{(m)}$, $E_y^{(m)}$, and $E_z^{(m)}$.

$$E_x^{(m)} = \frac{q_{DV2}}{\sin(\frac{\theta_m}{2})} \quad (68)$$

$$E_y^{(m)} = \frac{q_{DV3}}{\sin(\frac{\theta_m}{2})} \quad (69)$$

$$E_z^{(m)} = \frac{q_{DV4}}{\sin(\frac{\theta_m}{2})} \quad (70)$$

where

$$\frac{\theta_m}{2} = \cos^{-1}(q_{DV1}) \quad 0^\circ \leq \frac{\theta_m}{2} \leq 90^\circ$$

This desired maneuver is performed by setting the vehicle attitude error $\Delta\vec{\theta}$ to zero (null vector) and by setting $\vec{\omega}_D$ equal to

$$\vec{\omega}_D = \omega_m \begin{bmatrix} E_x^{(m)} \\ E_y^{(m)} \\ E_z^{(m)} \end{bmatrix} \quad (71)$$

The maneuver rate ω_m is set equal to 1.745×10^{-3} radian per second (six degrees per minute) therefore, the individual maneuver rate about any single vehicle axis cannot exceed its limit of six degrees per minute. This maneuver rate command $\vec{\omega}_D$, equation 71, and the zeroed attitude error $\Delta\vec{\theta}$ is inputted to the vehicle control law until the quaternion q_{VD1} approaches unity indicating that the vehicle is close to its desired attitude. At this point, the maneuver has been completed and the desired vehicle rate $\vec{\omega}_D$ associated with the desired attitude is inputted to the vehicle control law along with the actual vehicle attitude error $\Delta\vec{\theta}$.

It should be noted that if the desired attitude is a local vertical attitude, the elements of the transformation $[\phi_D]$ are functions of time; and the magnitude of the desired vehicle rate $\vec{\omega}_D$ associated with this type of attitude equals ω_0 , the vehicle orbital rate. For an inertial attitude, the elements of $[\phi_D]$ are constant and the desired $\vec{\omega}_D$ equals zero.

8.2.4 Quaternion Vehicle Attitude Error - The quaternion \vec{q}_{DV} that describes the desired vehicle attitude with respect to its actual attitude equals

$$\vec{q}_{DV} = (q_1 - q_2 \hat{i} - q_3 \hat{j} - q_4 \hat{k}) (q_{D1} + q_{D2} \hat{i} + q_{D3} \hat{j} + q_{D4} \hat{k})$$

$$= \begin{bmatrix} q_{DV1} \\ q_{DV2} \\ q_{DV3} \\ q_{DV4} \end{bmatrix} = \begin{bmatrix} q_{D1} & q_{D2} & q_{D3} & q_{D4} \\ q_{D2} & -q_{D1} & -q_{D4} & q_{D3} \\ q_{D3} & q_{D4} & -q_{D1} & -q_{D2} \\ q_{D4} & -q_{D3} & q_{D2} & -q_{D1} \end{bmatrix} \begin{bmatrix} q_1 \\ q_2 \\ q_3 \\ q_4 \end{bmatrix} \quad (72)$$

The quaternions q_{DV1} , q_{DV2} , q_{DV3} , and q_{DV4} equal

$$q_{DV1} = \cos\left(\frac{\epsilon}{2}\right) \quad (73)$$

$$q_{DV2} = E_x^{(\epsilon)} \sin\left(\frac{\epsilon}{2}\right) \quad (74)$$

$$q_{DV3} = E_y^{(\epsilon)} \sin\left(\frac{\epsilon}{2}\right) \quad (75)$$

$$q_{DV4} = E_z^{(\epsilon)} \sin\left(\frac{\epsilon}{2}\right) \quad (76)$$

The vehicle attitude error $\Delta\vec{\theta}$ is completely defined by ϵ and the eigenaxis defined by the direction cosines $E_x^{(\epsilon)}$, $E_y^{(\epsilon)}$, and $E_z^{(\epsilon)}$. Because ϵ is normally small, the vehicle attitude error $\Delta\vec{\theta}$ can be approximated using the quaternions q_{DV2} , q_{DV3} , and q_{DV4} ($q_{DV2} = \frac{\epsilon}{2} E_x^{(\epsilon)}, \dots$).

$$\Delta\vec{\theta} = 2 \begin{bmatrix} q_{DV2} \\ q_{DV3} \\ q_{DV4} \end{bmatrix} \quad (77)$$

The above approximation of $\Delta\vec{\theta}$ is inputted to the vehicle control law in order to generate the appropriate CMG torque command \vec{T}_{COM} needed to correct for $\Delta\vec{\theta}$.

8.3 Direction Cosine Maneuver Control Law

8.3.1 Direction Cosine Definition - The orientation between two orthogonal coordinate systems can be described by specifying the projections between the various axes comprising the two coordinate frames. Figure 8.4 is a sketch of the vehicle coordinate frame $X_v Y_v Z_v$ and the reference frame XYZ . The direction cosines, the parameters $a_{11}, a_{12}, \dots, a_{33}$, are the projections between the axes comprising these two coordinate systems. For example, a_{11} is the projection of X_v onto X (or X onto X_v) and a_{12} is the projection of X_v onto Y (or Y onto X_v). The direction cosines $a_{11}, a_{12}, \dots, a_{33}$ are the cosines of the angles subtended between the corresponding axes shown in figure 8.4. The transformation $[\phi]$ describing the vehicle attitude $X_v Y_v Z_v$ with respect to XYZ

$$\begin{bmatrix} X_v \\ Y_v \\ Z_v \end{bmatrix} = [\phi] \begin{bmatrix} X \\ Y \\ Z \end{bmatrix} \quad (78)$$

equals

$$[\phi] = \begin{bmatrix} a_{11} & a_{12} & a_{13} \\ a_{21} & a_{22} & a_{23} \\ a_{31} & a_{32} & a_{33} \end{bmatrix} \quad (79)$$

8.3.2 Direction Cosine Strapdown Equations - Equations 18 thru 26 along with the quaternion strapdown equation, equation 52, are used to derive the corresponding direction cosine strapdown equations $\dot{a}_{11}, \dot{a}_{12}, \dots, \dot{a}_{33}$. From equation 18, a_{11} equals

$$a_{11} = q_1^2 + q_2^2 - q_3^2 - q_4^2 \quad (18)$$

The time rate of change of a_{11} equals

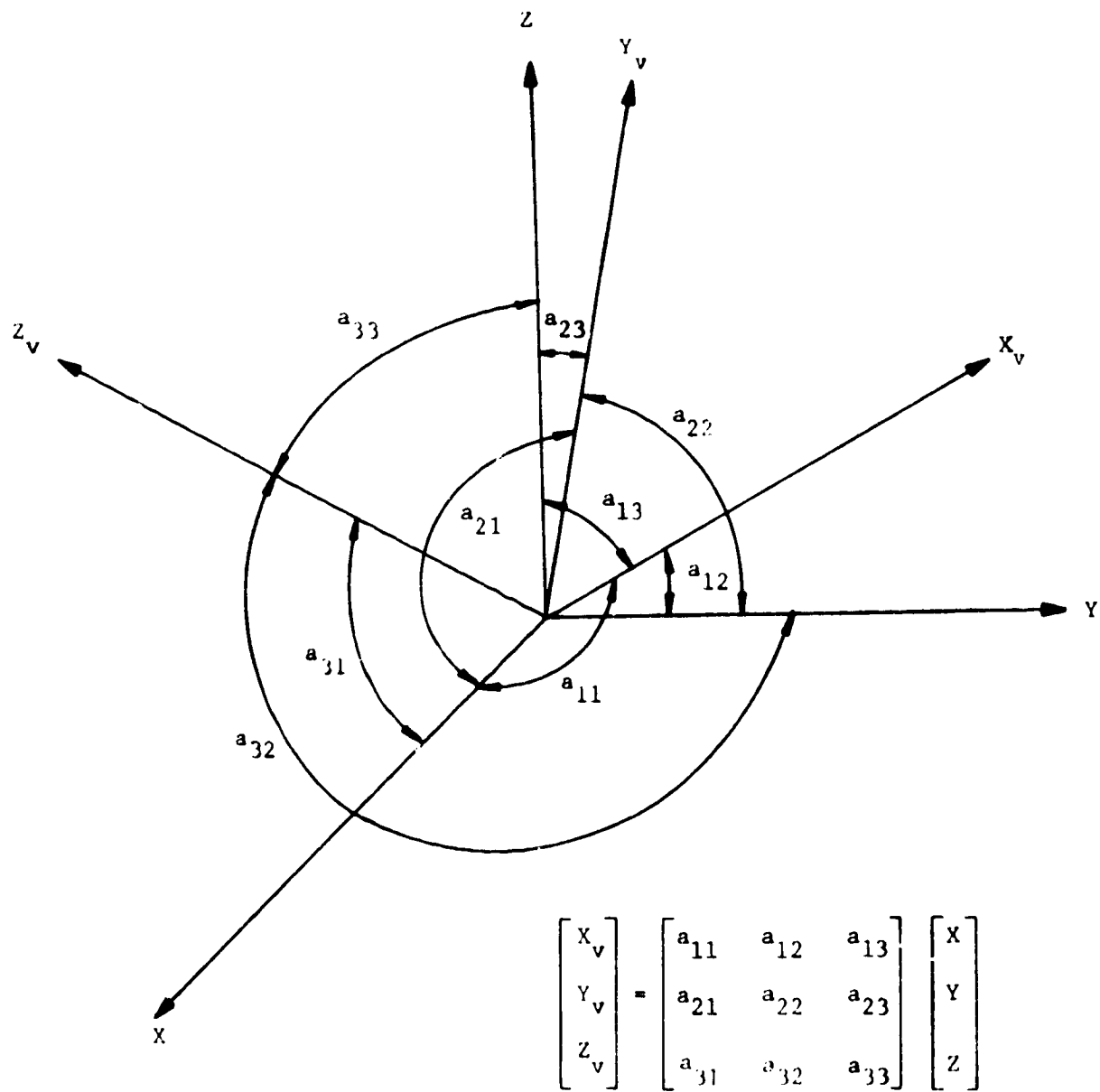


Figure 8.4 Direction Cosines Associated with Vehicle Frame $X_v Y_v Z_v$ and Reference Frame XYZ

$$\frac{da_{11}}{dt} = \dot{a}_{11} - 2q_1\dot{q}_1 + 2q_2\dot{q}_2 - 2q_3\dot{q}_3 - 2q_4\dot{q}_4 \quad (80)$$

Substituting the expressions for \dot{q}_1 , \dot{q}_2 , \dot{q}_3 , and \dot{q}_4 contained in equation 52 into equation 80, \dot{a}_{11} equals

$$\begin{aligned} \dot{a}_{11} = & q_1(-q_2\omega_x - q_3\omega_y - q_4\omega_z) + q_2(q_1\omega_x - q_4\omega_y + q_3\omega_z) \\ & - q_3(q_4\omega_x + q_1\omega_y - q_2\omega_z) - q_4(-q_3\omega_x + q_2\omega_y + q_1\omega_z) \end{aligned} \quad (81)$$

Simplifying and collecting terms of ω_x , ω_y , and ω_z , \dot{a}_{11} equals

$$\dot{a}_{11} = -2(q_2q_4 + q_1q_3)\omega_y + 2(q_2q_3 - q_1q_4)\omega_z \quad (82)$$

From equation 19 and 20, note that

$$a_{12} = 2(q_2q_3 - q_1q_4) \quad (19)$$

$$a_{13} = 2(q_2q_4 + q_1q_3) \quad (20)$$

Substituting equations 19 and 20 into equation 82, \dot{a}_{11} equals

$$\dot{a}_{11} = -a_{13}\omega_y + a_{12}\omega_z \quad (83)$$

Similarly, the time rate of change of a_{12} , a_{13} , ..., a_{33} can be computed. \dot{a}_{12} , \dot{a}_{13} , ..., \dot{a}_{33} equal

$$\dot{a}_{12} = a_{13}\omega_x - a_{11}\omega_z \quad (84)$$

$$\dot{a}_{13} = -a_{12}\omega_x + a_{11}\omega_y \quad (85)$$

$$\dot{a}_{21} = -a_{23}\omega_y + a_{22}\omega_z \quad (86)$$

$$\dot{a}_{22} = a_{23}\omega_x - a_{21}\omega_z \quad (87)$$

$$\dot{a}_{23} = -a_{22}\omega_x + a_{21}\omega_y \quad (88)$$

$$\dot{a}_{31} = -a_{33}\omega_y + a_{32}\omega_z \quad (89)$$

$$\dot{a}_{32} = a_{33}\omega_x - a_{31}\omega_z \quad (90)$$

$$\dot{a}_{33} = -a_{32}\omega_x + a_{31}\omega_y \quad (91)$$

From the above expressions, equations 83 through 91, the direction cosine rates \dot{a}_{11} , \dot{a}_{12} , ..., \dot{a}_{33} are computed using sensed body rates ω_x , ω_y , and ω_z . These direction cosine rates are then integrated using a numerical integration technique to compute the direction cosines a_{11} , a_{12} , ..., a_{33} . Equations 83 through 91 plus the equations used to perform this numerical integration are referred to as the direction cosine strapdown equations. Assume that trapezoidal integration is used. The resulting expressions for a_{11} , a_{12} , ..., a_{33} are:

$$a_{11} = a_{11P} + 0.5(\dot{a}_{11P} + \dot{a}_{11})\Delta t \quad (92)$$

$$a_{12} = a_{12P} + 0.5(\dot{a}_{12P} + \dot{a}_{12})\Delta t \quad (93)$$

$$a_{13} = a_{13P} + 0.5(\dot{a}_{13P} + \dot{a}_{13})\Delta t \quad (94)$$

$$a_{21} = a_{21P} + 0.5(\dot{a}_{21P} + \dot{a}_{21})\Delta t \quad (95)$$

$$a_{22} = a_{22P} + 0.5(\dot{a}_{22P} + \dot{a}_{22})\Delta t \quad (96)$$

$$a_{23} = a_{23P} + 0.5(\dot{a}_{23P} + \dot{a}_{23})\Delta t \quad (97)$$

$$a_{31} = a_{31P} + 0.5(\dot{a}_{31P} + \dot{a}_{31})\Delta t \quad (98)$$

$$a_{32} = a_{32P} + 0.5(\dot{a}_{32P} + \dot{a}_{32})\Delta t \quad (99)$$

$$a_{33} = a_{33P} + 0.5(\dot{a}_{33P} + \dot{a}_{33})\Delta t \quad (100)$$

a_{11P} , a_{12P} , ..., a_{33P} are the previously computed direction cosines a_{11} , a_{12} , ..., a_{33} , respectively while \dot{a}_{11P} , \dot{a}_{12P} , ..., \dot{a}_{33P} are their corresponding previously computed direction cosine rates \dot{a}_{11} , \dot{a}_{12} , ..., \dot{a}_{33} , respectively. Δt is the sample period in seconds between numerical integrations.

8.3.3 Direction Cosine Vehicle Attitude Error - Assume that the transformation $[\phi_D]$ describes the desired vehicle attitude with respect to the XYZ reference frame.

$$[\phi_D] = \begin{bmatrix} a_{11D} & a_{12D} & a_{13D} \\ a_{21D} & a_{22D} & a_{23D} \\ a_{31D} & a_{32D} & a_{33D} \end{bmatrix} \quad (101)$$

The corresponding transformation $[\Phi_{DV}]$ that defines the desired vehicle attitude with respect to its actual attitude equals

$$[\Phi_{DV}] = [\Phi_D][\Phi]^{-1} = \begin{bmatrix} a'_{11} & a'_{12} & a'_{13} \\ a'_{21} & a'_{22} & a'_{23} \\ a'_{31} & a'_{32} & a'_{33} \end{bmatrix} \quad (102)$$

Assume that the vehicle is displaced from its desired attitude by three small rotations ϵ_x , ϵ_y , and ϵ_z about the X_V , Y_V , and Z_V axes, respectively. The transformation $[\Phi_{DV}]$ can be approximated by the following small angle transformation.

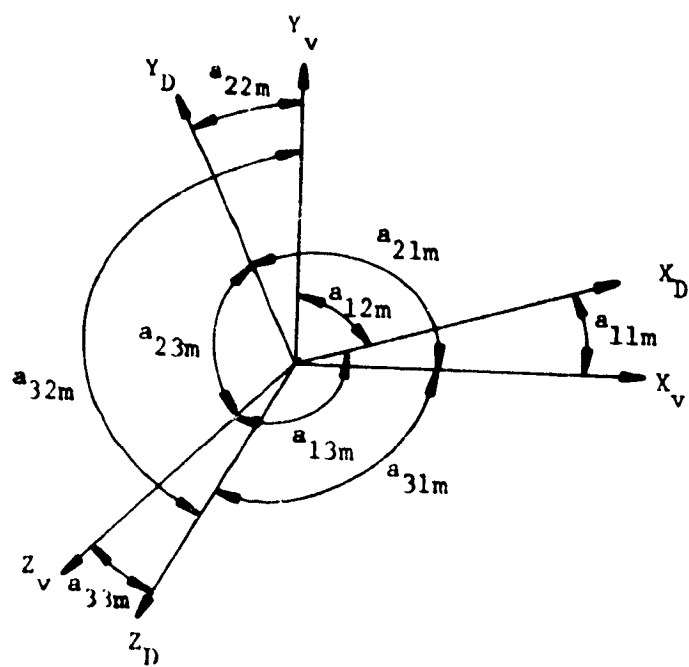
$$[\Phi_{DV}] \approx \begin{bmatrix} 1 & \epsilon_z & -\epsilon_y \\ -\epsilon_z & 1 & \epsilon_x \\ \epsilon_y & -\epsilon_x & 1 \end{bmatrix} \quad (103)$$

ϵ_x , ϵ_y , and ϵ_z are the vehicle attitude errors measured from vehicle to desired vehicle space. Matching terms in equation 102 and 103, the vehicle attitude error $\Delta\vec{\theta}$ can be approximated by

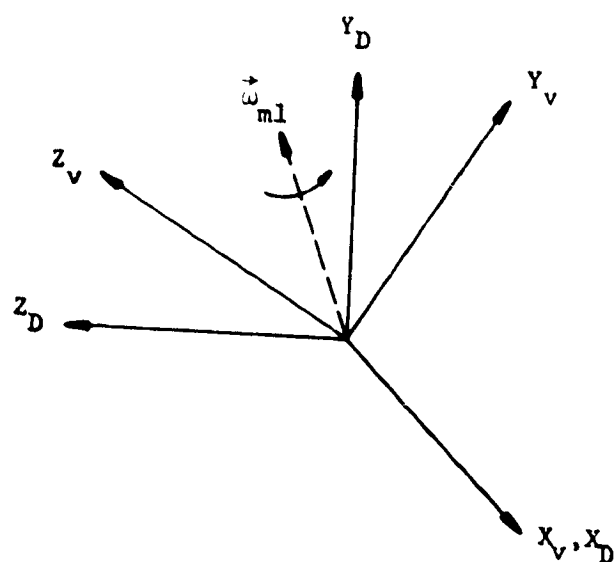
$$\Delta\vec{\theta} = \begin{bmatrix} \epsilon_x \\ \epsilon_y \\ \epsilon_z \end{bmatrix} \approx \begin{bmatrix} a'_{23} \\ a'_{31} \\ a'_{12} \end{bmatrix} \quad (104)$$

$\Delta\vec{\theta}$ is inputted to the vehicle control law in order to generate the appropriate CMG torque command \vec{T}_{COM} needed to correct for $\Delta\vec{\theta}$.

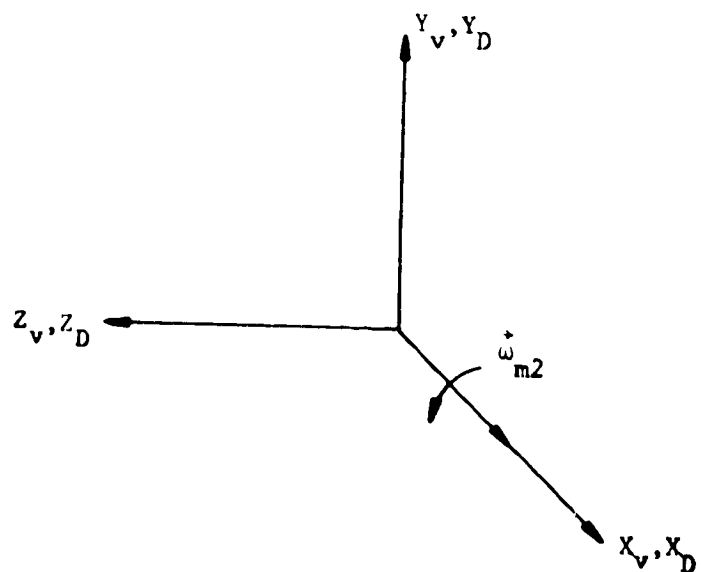
8.3.4 Direction Cosine Maneuver - The vehicle can be maneuvered to a new attitude described by the transformation $[\Phi_D]$ by two distinct rotations. The first rotation aligns one of the corresponding vehicle axes with its desired orientation and the second rotation about this axis aligns the remaining two vehicle axes with their desired orientations. A potential direction cosine rotational sequence is demonstrated in figure 8.5. Figure 8.5a defines the vehicle orientation, $X_V Y_V Z_V$, and its desired orientation, $X_D Y_D Z_D$, prior to any maneuver. Figure 8.5b illustrates the first rotation $\vec{\omega}_{m1}$ which



a). Orientation of X_D, Y_D, Z_D With Respect to X_v, Y_v, Z_v



b). First Rotation, Aligns X_v With X_D



c). Second Rotation, Aligns Y_v and Z_v With Y_D and Z_D Respectively

Figure 8.5 Sketch of Direction Cosine Maneuvers

aligns the vehicle X_v axis with its desired orientation X_D . This rotation is accomplished by maneuvering the vehicle about an axis lying in the $Y_v Z_v$ plane. Figure 8.5c illustrates the final rotation $\vec{\omega}_{m2}$ about the X_v axis which aligns the vehicle Y_v and Z_v axes with Y_D and Z_D , respectively.

The procedure for performing the maneuvers depicted in figure 8.5 is (1) to zero the vehicle attitude error $\Delta\vec{\theta}$ (null vector), (2) to compute maneuver rate $\vec{\omega}_{m1}$, (3) to perform the maneuver associated with $\vec{\omega}_{m1}$, (4) to generate the appropriate vehicle attitude error $\Delta\vec{\theta}$ that will keep the X_v axis aligned with X_D during the second maneuver, (5) to compute maneuver rate $\vec{\omega}_{m2}$, (6) to perform the maneuver associated with $\vec{\omega}_{m2}$, and (7) to reintroduce the vehicle attitude error $\Delta\vec{\theta}$ as given in equation 104. The transformation $[\phi_{DV}]$ describing the desired vehicle orientation with respect to its present attitude equals

$$[\phi_{DV}] = [\phi_D][\phi]^{-1} = \begin{bmatrix} a_{11m} & a_{12m} & a_{13m} \\ a_{21m} & a_{22m} & a_{23m} \\ a_{31m} & a_{32m} & a_{33m} \end{bmatrix} \quad (105)$$

The direction cosines $a_{11m}, a_{12m}, \dots, a_{33m}$ are defined in figure 4a. The unit vector \hat{i}_{DX} along the desired vehicle X_D axis described in vehicle space equals

$$\hat{i}_{DX} = a_{11m}\hat{i} + a_{12m}\hat{j} + a_{13m}\hat{k} \quad (106)$$

\hat{i} , \hat{j} , and \hat{k} are unit vectors along the X_v , Y_v , and Z_v axes, respectively. The maneuver rate $\vec{\omega}_{m1}$ equals

$$\vec{\omega}_{m1} = \frac{\omega_m (\hat{i} \times \hat{i}_{DX})}{|\hat{i} \times \hat{i}_{DX}|} = \frac{\omega_m (a_{12m}\hat{k} - a_{13m}\hat{j})}{(a_{12m}^2 + a_{13m}^2)^{1/2}} \quad (107)$$

The unit vector $\frac{(\hat{i} \times \hat{i}_{DX})}{|\hat{i} \times \hat{i}_{DX}|}$ defines the rotational axis and ω_m equals

1.745×10^{-3} radian per second (six degrees per minute), the maximum

maneuver rate allowed about any single vehicle axis. $\vec{\omega}_{m1}$ is inputted into the vehicle control law, equation 1, as $\vec{\omega}_D (\vec{\omega}_D = \vec{\omega}_{m1})$.

$$\vec{T}_{COM} = [K_r](\vec{\omega}_D - \vec{\omega}) + [K_p](\Delta\vec{\theta} + \vec{\epsilon}) \quad (1)$$

The vehicle is maneuvered at this rate $\vec{\omega}_{m1}$ until the direction cosine a_{11m} approaches unity indicating that X_v and X_D are aligned. $\vec{\omega}_{m1}$ is then zeroed. To keep the X_v vehicle axis aligned with X_D , the following vehicle attitude error $\Delta\vec{\theta}$ is fed to the vehicle control law.

$$\Delta\vec{\theta} = \begin{bmatrix} 0 \\ a'_{31} \\ a'_{12} \end{bmatrix} \quad (108)$$

The vehicle is then maneuvered about its X_v axis at a rate of $\vec{\omega}_{m2}$ until a_{22m} and a_{33m} approach unity indicating that the Y_v and Z_v axes are aligned with Y_D and Z_D , respectively. The unit vector \hat{j}_{DY} along the desired vehicle Y_D axis defined in vehicle space equals

$$\hat{j}_{DY} = a_{21m}\hat{i} + a_{22m}\hat{j} + a_{23m}\hat{k} \quad (109)$$

$\vec{\omega}_{m2}$ equals

$$\vec{\omega}_{m2} = \frac{\omega_m (\hat{j} \times \hat{j}_{DY})}{|\hat{j} \times \hat{j}_{DY}|} = \frac{\omega_m (a_{23m}\hat{i} - a_{21m}\hat{k})}{(a_{23m}^2 + a_{21m}^2)^{1/2}} \quad (110)$$

$\vec{\omega}_{m2}$ like $\vec{\omega}_{m1}$ is inputted into the vehicle control law as $\vec{\omega}_D (\vec{\omega}_D = \vec{\omega}_{m2})$. As soon as both a_{22m} and a_{33m} approach unity, $\vec{\omega}_{m2}$ is zeroed and the vehicle attitude error $\Delta\vec{\theta}$ as defined by equation 104 is reintroduced to the vehicle control law.

$$\Delta\vec{\theta} = \begin{bmatrix} a'_{23} \\ a'_{31} \\ a'_{12} \end{bmatrix} \quad (104)$$

Inputting $\Delta \vec{\theta}$ into the vehicle control law will zero out any residual maneuvering errors.

8.4 Euler Angle Maneuver Control Law

8.4.1 Euler Angle Definition - The transformation from one coordinate frame to a second one can be described by three separate rotations about three coordinate axes. These three rotations are referred to as the Euler angles. Figure 8.6 illustrates one of the various Euler angle sets that can be used. The order in which these three rotations ψ , η , and ϕ are performed are important. For the Euler angle set shown in figure 8.6, the first rotation ψ is about the X axis, the second rotation η is about the displaced Y_1 axis, and the third rotation ϕ is about the displaced Z_2 axis. The final orientation of this displaced coordinate frame is denoted as the vehicle coordinate system $X_v Y_v Z_v$. The vehicle attitude $X_v Y_v Z_v$ with respect to the reference frame XYZ can be described by the transformation $[\phi]$.

$$\begin{bmatrix} X_v \\ Y_v \\ Z_v \end{bmatrix} = [\phi] \begin{bmatrix} X \\ Y \\ Z \end{bmatrix} \quad (111)$$

$[\phi]$ is a function of the three Euler angles ψ , η , and ϕ . $[\phi]$ equals

$$[\phi] = [\phi_\phi][\phi_\eta][\phi_\psi] \quad (112)$$

where

$$[\phi_\psi] = \begin{bmatrix} 1 & 0 & 0 \\ 0 & \cos\psi & \sin\psi \\ 0 & -\sin\psi & \cos\psi \end{bmatrix} \quad (113)$$

$$[\phi_\eta] = \begin{bmatrix} \cos\eta & 0 & -\sin\eta \\ 0 & 1 & 0 \\ \sin\eta & 0 & \cos\eta \end{bmatrix} \quad (114)$$

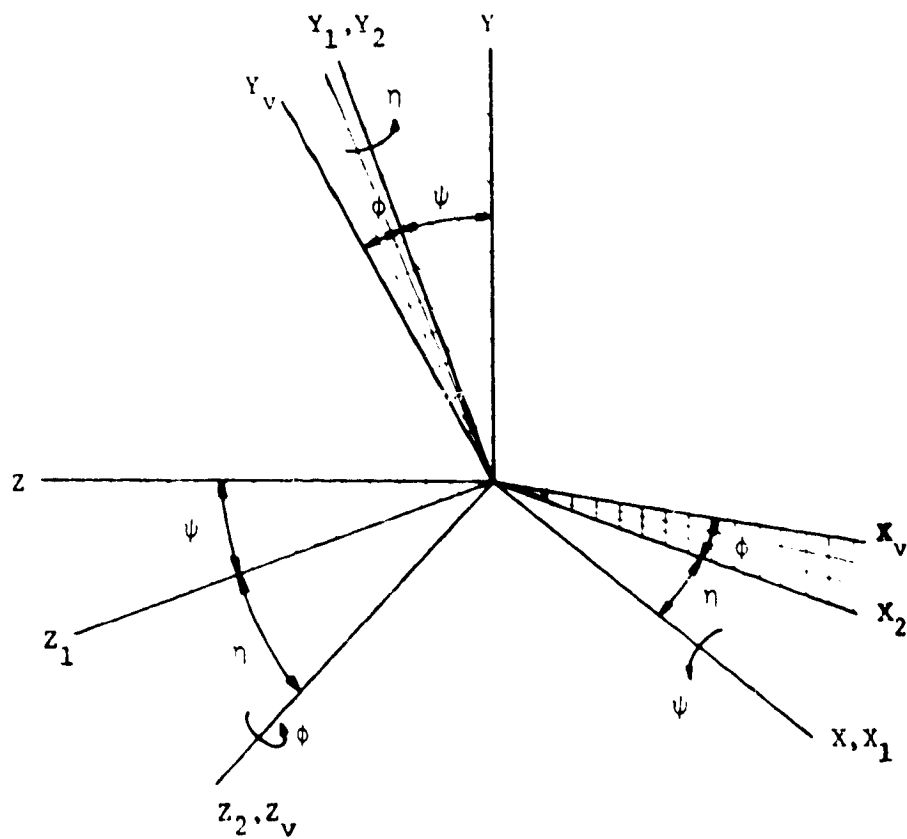


Figure 8.6 Euler Angles

$$[\phi_\phi] = \begin{bmatrix} \cos\phi & \sin\phi & 0 \\ -\sin\phi & \cos\phi & 0 \\ 0 & 0 & 1 \end{bmatrix} \quad (115)$$

Substituting the individual Euler transformation given in equations 113, 114, and 115 into equation 112, $[\phi]$ equals

$$[\phi] = \begin{bmatrix} a_{11} & a_{12} & a_{13} \\ a_{21} & a_{22} & a_{23} \\ a_{31} & a_{32} & a_{33} \end{bmatrix} \quad (116)$$

where

$$a_{11} = \cos\phi\cos\eta \quad (117)$$

$$a_{12} = \sin\eta\sin\psi\cos\phi + \sin\phi\cos\psi \quad (118)$$

$$a_{13} = \sin\phi\sin\psi - \sin\eta\cos\psi\cos\phi \quad (119)$$

$$a_{21} = -\sin\phi\cos\eta \quad (120)$$

$$a_{22} = \cos\phi\cos\psi - \sin\eta\sin\psi\sin\phi \quad (121)$$

$$a_{23} = \cos\phi\sin\psi + \sin\eta\cos\psi\sin\phi \quad (122)$$

$$a_{31} = \sin\eta \quad (123)$$

$$a_{32} = -\sin\psi\cos\eta \quad (124)$$

$$a_{33} = \cos\eta\cos\psi \quad (125)$$

8.4.2 Euler Angle Strapdown Equations - The Euler rates $\dot{\psi}$, $\dot{\eta}$, and $\dot{\phi}$ can be written as a function of vehicle body rates ω_x , ω_y , and ω_z . But first, let us write the body rates ω_x , ω_y , and ω_z in terms of their Euler rates $\dot{\psi}$, $\dot{\eta}$, and $\dot{\phi}$.

$$\begin{bmatrix} \omega_x \\ \omega_y \\ \omega_z \end{bmatrix} = [\phi_\phi][\phi_\eta][\phi_\psi] \begin{bmatrix} \dot{\psi} \\ 0 \\ 0 \end{bmatrix} + [\phi_\phi][\phi_\eta] \begin{bmatrix} 0 \\ \dot{\eta} \\ 0 \end{bmatrix} + [\phi_\phi] \begin{bmatrix} 0 \\ 0 \\ \dot{\phi} \end{bmatrix} \quad (126)$$

The transformations $[\phi_\psi]$, $[\phi_\eta]$, and $[\phi_\phi]$ are defined in equations 113 through 115. Substituting these transformations into equation 122, the body rates ω_x , ω_y , and ω_z equal

$$\begin{bmatrix} \omega_x \\ \omega_y \\ \omega_z \end{bmatrix} = \begin{bmatrix} \cos\phi\cos\eta & \sin\phi & 0 \\ -\sin\phi\cos\eta & \cos\phi & 0 \\ \sin\eta & 0 & 1 \end{bmatrix} \begin{bmatrix} \dot{\psi} \\ \dot{\eta} \\ \dot{\phi} \end{bmatrix} \quad (127)$$

By computing the inverse of the above matrix equation, the Euler rates $\dot{\psi}$, $\dot{\eta}$, and $\dot{\phi}$ in terms of the vehicle body rates ω_x , ω_y , and ω_z equal

$$\begin{bmatrix} \dot{\psi} \\ \dot{\eta} \\ \dot{\phi} \end{bmatrix} = \begin{bmatrix} \frac{\cos\phi}{\cos\eta} & \frac{-\sin\phi}{\cos\eta} & 0 \\ \sin\phi & \cos\phi & 0 \\ \frac{-\sin\eta\cos\phi}{\cos\eta} & \frac{\sin\phi\sin\eta}{\cos\eta} & 1 \end{bmatrix} \begin{bmatrix} \omega_x \\ \omega_y \\ \omega_z \end{bmatrix} \quad (128)$$

Note that when the Euler angle η equals

$$\eta = \frac{(2n+1)\pi}{2}$$

where n is an integer ($n=0, \pm 1, \pm 2, \dots$) the above Euler rate matrix equation is singular. For these values of n the Euler rates $\dot{\psi}$ and $\dot{\phi}$ "blow up." A similar singularity problem exists for all potential Euler angle rotational sequences. This singular problem is a major drawback of using an Euler angle implementation for tracking the angular motion of a vehicle.

The Euler rates $\dot{\psi}$, $\dot{\eta}$, and $\dot{\phi}$ are integrated numerically in order to compute the Euler angles ψ , η , and ϕ that describe the orientation of the vehicle with respect to the XYZ reference frame. Assume that trapezoidal integration is used. The resulting expressions for ψ , η , and ϕ are:

$$\psi = \psi_p + 0.5[\dot{\psi}_p + \dot{\psi}]\Delta t \quad (129)$$

$$\eta = \eta_p + 0.5[\dot{\eta}_p + \dot{\eta}]\Delta t \quad (130)$$

$$\phi = \phi_p + 0.5[\dot{\phi}_p + \dot{\phi}]\Delta t \quad (131)$$

ψ_p , η_p , and ϕ_p and $\dot{\psi}_p$, $\dot{\eta}_p$, and $\dot{\phi}_p$ are the previously computed Euler angles ψ , η , and ϕ and Euler rates $\dot{\psi}$, $\dot{\eta}$, and $\dot{\phi}$, respectively. Δt is the sample period in seconds between numerical integrations. Equations 128 through 131 are the Euler angle strapdown equations.

8.4.3 Euler Angle Vehicle Attitude Error - The transformation $[\phi_D]$ describes the desired vehicle attitude with respect to the XYZ reference frame.

$$[\phi_D] = \begin{bmatrix} a_{11D} & a_{12D} & a_{13D} \\ a_{21D} & a_{22D} & a_{23D} \\ a_{31D} & a_{32D} & a_{33D} \end{bmatrix} \quad (132)$$

where

$$a_{11D} = \cos\phi_D \cos\eta_D \quad (133)$$

$$a_{12D} = \sin\eta_D \sin\psi_D \cos\phi_D + \sin\phi_D \cos\psi_D \quad (134)$$

$$a_{13D} = \sin\phi_D \sin\psi_D - \sin\eta_D \cos\psi_D \cos\phi_D \quad (135)$$

$$a_{21D} = -\sin\phi_D \cos\eta_D \quad (136)$$

$$a_{22D} = \cos\phi_D \cos\psi_D - \sin\eta_D \sin\psi_D \sin\phi_D \quad (137)$$

$$a_{23D} = \cos\phi_D \sin\psi_D + \sin\eta_D \cos\psi_D \sin\phi_D \quad (138)$$

$$a_{31D} = \sin\eta_D \quad (139)$$

$$a_{32D} = -\sin\psi_D \cos\eta_D \quad (140)$$

$$a_{33D} = \cos\eta_D \cos\psi_D \quad (141)$$

ψ_D , η_D , and ϕ_D are the desired Euler angles that describe the desired vehicle attitude.

The transformation $[\phi_{DV}]$ describing the desired vehicle attitude with respect to actual attitude equals

$$[\phi_{DV}] = [\phi_D][\phi]^{-1} \quad (142)$$

where $[\phi]$ is the transformation describing the vehicle attitude with respect to reference, equation 116. Assume that the vehicle is displaced from its desired attitude by three small

rotations ϵ_x , ϵ_y , and ϵ_z about the X_V , Y_V , and Z_V axes, respectively. The transformation $[\Phi_{DV}]$ can be approximated by the following small angle transformation

$$[\Phi_{DV}] = \begin{bmatrix} 1 & \epsilon_z & -\epsilon_y \\ -\epsilon_z & 1 & \epsilon_x \\ \epsilon_y & -\epsilon_x & 1 \end{bmatrix} \quad (143)$$

ϵ_x , ϵ_y , and ϵ_z are the vehicle attitude errors measured from vehicle to desired vehicle space. Matching elements of equation 143 with those contained in equation 142, the three vehicle attitude errors ϵ_x , ϵ_y , and ϵ_z equal

$$\epsilon_x = a_{31}a_{21D} + a_{32}a_{22D} + a_{33}a_{23D} \quad (144)$$

$$\epsilon_y = a_{11}a_{31D} + a_{12}a_{32D} + a_{13}a_{33D} \quad (145)$$

$$\epsilon_z = a_{21}a_{11D} + a_{22}a_{12D} + a_{23}a_{13D}$$

Substituting the appropriate expressions for $a_{11}, a_{12}, \dots, a_{33}$, equations 117 thru 125, and $a_{11D}, a_{12D}, \dots, a_{33D}$, equations 133 thru 141, into the above equations, ϵ_x , ϵ_y , and ϵ_z equal

$$\begin{aligned} \epsilon_x = & 0.5 \sin \phi_D [1 + \cos(\psi_D - \psi)] \sin(\eta_D - \eta) \\ & - 0.5 \sin \phi_D [1 - \cos(\psi_D - \psi)] \sin(\eta_D + \eta) \\ & + \cos \eta \cos \phi_D \sin(\psi_D - \psi) \end{aligned} \quad (147)$$

$$\begin{aligned} \epsilon_y = & 0.5 \cos \phi [1 - \cos(\psi - \psi_D)] \sin(\eta_D + \eta) \\ & + 0.5 \cos \phi [1 + \cos(\psi - \psi_D)] \sin(\eta_D - \eta) \\ & - \sin \phi \cos \eta_D \sin(\psi_D - \psi) \end{aligned} \quad (148)$$

$$\begin{aligned}
\varepsilon_z = & -0.25\{[\cos(\psi_D - \psi) + 1]\cos(\eta_D - \eta) \\
& + [1 - \cos(\psi_D - \psi)]\cos(\eta_D + \eta) \\
& - 2\cos(\psi_D - \psi)\sin(\phi_D + \phi) \\
& + 0.25\{[\cos(\psi_D - \psi) + 1]\cos(\eta_D - \eta) \\
& + [1 - \cos(\psi_D - \psi)]\cos(\eta_D + \eta) \\
& + 2\cos(\psi_D - \psi)\sin(\phi_D - \phi) \\
& + 0.5\{(\sin\eta_D + \sin\eta)\cos(\phi_D - \phi) \\
& + (\sin\eta_D - \sin\eta)\cos(\phi_D + \phi)\sin(\psi_D - \psi)\}
\end{aligned} \tag{149}$$

Assume that the Euler angles ψ , η , and ϕ are approximately equal to their corresponding desired Euler angles ψ_D , η_D , and ϕ_D , respectively ($\psi \approx \psi_D$, $\eta \approx \eta_D$, $\phi \approx \phi_D$). The vehicle attitude errors can then be approximated by the following expressions.

$$\varepsilon_x \approx \Delta\eta \sin\phi_D + \Delta\psi \cos\phi_D \cos\eta_D \tag{150}$$

$$\varepsilon_y \approx \Delta\eta \cos\phi_D - \Delta\psi \sin\phi_D \cos\eta_D \tag{151}$$

$$\varepsilon_z \approx \Delta\phi + \Delta\psi \sin\eta_D \tag{152}$$

where $\Delta\psi$, $\Delta\eta$, and $\Delta\phi$ equal

$$\Delta\psi = \psi_D - \psi \tag{153}$$

$$\Delta\eta = \eta_D - \eta \tag{154}$$

$$\Delta\phi = \phi_D - \phi \tag{155}$$

The vehicle attitude error vector $\Delta\vec{\theta}$ equals

$$\Delta\vec{\theta} = \begin{bmatrix} \varepsilon_x \\ \varepsilon_y \\ \varepsilon_z \end{bmatrix} = \begin{bmatrix} \cos\phi_D \cos\eta_D & \sin\phi_D & 0 \\ -\sin\phi_D \cos\eta_D & \cos\phi_D & 0 \\ \sin\eta_D & 0 & 1 \end{bmatrix} \begin{bmatrix} \Delta\psi \\ \Delta\eta \\ \Delta\phi \end{bmatrix} \tag{156}$$

$\Delta\vec{\theta}$ is used by the vehicle control law to generate the appropriate CMG torque command \vec{T}_{COM} .

Note that in order to use this method for generating $\Delta\vec{\theta}$, one must be able to compute the Euler angles ψ_D , η_D , and ϕ_D given the transformation $[\phi_D]$. The Euler angles ψ_D , η_D , and ϕ_D describe three distinct maneuvers about the X, Y, and Z axes that will align the XYZ reference frame with the desired vehicle attitude $X_D Y_D Z_D$. The first rotation ψ_D about the X axis reorients the XYZ reference frame such that the Y axis is placed perpendicular to the desired Z_D axis. The Z axis can be aligned with Z_D by performing the second rotation η_D about the Y axis. And finally the third rotation ϕ_D about the Z axis aligns the X and Y axes with their corresponding desired axes X_D and Y_D .

The first rotation ψ_D places the Y axis perpendicular to Z_D , the desired orientation of the Z axis. After this rotation ψ_D , the transformation $[\phi'_D]$ relating the desired vehicle attitude with the displaced XYZ coordinate system denoted $X'Y'Z'$ equals

$$[\phi'_D] = \begin{bmatrix} a_{11}^{(\psi)} & a_{12}^{(\psi)} & a_{13}^{(\psi)} \\ a_{21}^{(\psi)} & a_{22}^{(\psi)} & a_{23}^{(\psi)} \\ a_{31}^{(\psi)} & a_{32}^{(\psi)} & a_{33}^{(\psi)} \end{bmatrix} = [\phi_D] \begin{bmatrix} 1 & 0 & 0 \\ 0 & \cos\psi_D & -\sin\psi_D \\ 0 & \sin\psi_D & \cos\psi_D \end{bmatrix} \quad (157)$$

The resultant element of $[\phi'_D]$, $a_{11}^{(\psi)}$, $a_{12}^{(\psi)}$, ..., $a_{33}^{(\psi)}$ equal

$$a_{11}^{(\psi)} = a_{11D} \quad (158)$$

$$a_{12}^{(\psi)} = a_{12D} \cos\psi_D + a_{13D} \sin\psi_D \quad (159)$$

$$a_{13}^{(\psi)} = -a_{12D} \sin\psi_D + a_{13D} \cos\psi_D \quad (160)$$

$$a_{21}^{(\psi)} = a_{21D} \quad (161)$$

$$a_{22}^{(\psi)} = a_{22D} \cos\psi_D + a_{23D} \sin\psi_D \quad (162)$$

$$a_{23}^{(\psi)} = -a_{22D} \sin\psi_D + a_{23D} \cos\psi_D \quad (163)$$

$$a_{31}^{(\psi)} = a_{31D} \quad (164)$$

$$a_{32}^{(\psi)} = a_{32D} \cos \psi_D + a_{33D} \sin \psi_D \quad (165)$$

$$a_{33D}^{(\psi)} = -a_{32D} \sin \psi_D + a_{33D} \cos \psi_D \quad (166)$$

The direction cosine elements of $[\phi_D]$ a_{11D} , a_{12D} , ..., a_{33D} are defined in equations 133 through 141. With the Y' axis perpendicular to Z_D , the direction cosine $a_{32}^{(\psi)}$ equals zero.

$$a_{32}^{(\psi)} = a_{32D} \cos \psi_D + a_{33D} \sin \psi_D = 0 \quad (167)$$

From equation 167, ψ_D equals

$$\psi_D = \tan^{-1} \left(\frac{-a_{32D}}{a_{33D}} \right) \quad (168)$$

There are two solutions for ψ_D , one where the magnitude of ψ_D is less than $\frac{\pi}{2}$ and one where its magnitude lies between $\frac{\pi}{2}$ and π . The former solution where

$$-\frac{\pi}{2} \leq \psi_D \leq \frac{\pi}{2} \quad (169)$$

is selected. The second rotation η_D aligns the Z' axis with Z_D . The resultant displaced $X'Y'Z'$ coordinate frame is denoted $X''Y''Z''$. The transformation $[\phi_D'']$ relating the desired vehicle attitude $X_D Y_D Z_D$ with respect to $X''Y''Z''$ equals

$$[\phi_D''] = \begin{bmatrix} a_{11}^{(\eta)} & a_{12}^{(\eta)} & a_{13}^{(\eta)} \\ a_{21}^{(\eta)} & a_{22}^{(\eta)} & a_{23}^{(\eta)} \\ a_{31}^{(\eta)} & a_{32}^{(\eta)} & a_{33}^{(\eta)} \end{bmatrix} = [\phi_D'] \begin{bmatrix} \cos \eta & 0 & \sin \eta \\ 0 & 1 & 0 \\ -\sin \eta & 0 & \cos \eta \end{bmatrix} \quad (170)$$

The resultant elements of $[\phi_D'']$, $a_{11}^{(\eta)}$, $a_{12}^{(\eta)}$, ..., $a_{33}^{(\eta)}$ equal

$$a_{11}^{(\eta)} = a_{11D} \cos \eta_D + (a_{12D} \sin \psi_D - a_{13D} \cos \psi_D) \sin \eta_D \quad (171)$$

$$a_{12}^{(\eta)} = a_{12D} \cos \psi_D + a_{13D} \sin \psi_D \quad (172)$$

$$a_{13}^{(\eta)} = a_{11D} \sin \eta_D + (a_{13D} \cos \psi_D - a_{12D} \sin \psi_D) \cos \eta_D \quad (173)$$

$$a_{21}^{(\eta)} = a_{21D} \cos \eta_D + (a_{22D} \sin \psi_D - a_{23D} \cos \psi_D) \sin \eta_D \quad (174)$$

$$a_{22}^{(\eta)} = a_{22D} \cos \psi_D + a_{23D} \sin \psi_D \quad (175)$$

$$a_{23}^{(\eta)} = a_{21D} \sin \eta_D + (a_{23D} \cos \psi_D - a_{22D} \sin \psi_D) \cos \eta_D \quad (176)$$

$$a_{31}^{(\eta)} = a_{31D} \cos \eta_D + (a_{32D} \sin \psi_D - a_{33D} \cos \psi_D) \sin \eta_D \quad (177)$$

$$a_{32}^{(\eta)} = a_{32D} \cos \psi_D + a_{33D} \sin \psi_D \quad (178)$$

$$a_{33}^{(\eta)} = a_{31D} \sin \eta_D + (a_{33D} \cos \psi_D - a_{32D} \sin \psi_D) \cos \eta_D \quad (179)$$

Note that if Z'' is aligned with Z_D ,

$$a_{33}^{(\eta)} = 1 \quad (180)$$

$$a_{13}^{(\eta)} = a_{23}^{(\eta)} = a_{31}^{(\eta)} = a_{32}^{(\eta)} = 0 \quad (181)$$

The definition of a_{31D} , equation 139, is

$$a_{31D} = \sin \eta_D \quad (182)$$

Solving equation 178 for η_D , η_D equals

$$\eta_D = \sin^{-1}(a_{31D}) \quad (183)$$

In the range from $-\pi$ to π , there are two solutions for η_D that satisfies equation 183. Only one of these solutions will align Z'' with Z_D . To determine which value of η_D is computed by setting the expression for $a_{13}^{(\eta)}$, equation 173, equal to zero. Solving for the cosine of η_D ,

$$\cos \eta_D = \frac{a_{11D} a_{31D}}{a_{12D} \sin \psi_D - a_{13D} \cos \psi_D} \quad (184)$$

Because the Euler angle ψ_D is known, equation 168, the $\cos \eta_D$ can be computed using the above expression. If the sign of cosine of η_D is positive, the desired value of η_D lies either in the first ($0 \leq \eta_D \leq \frac{\pi}{2}$) or the fourth ($-\frac{\pi}{2} \leq \eta_D \leq 0$) quadrant, but if it is negative η_D lies either in the second ($\frac{\pi}{2} \leq \eta_D \leq \pi$) or third ($-\pi \leq \eta_D \leq -\frac{\pi}{2}$) quadrant. In other words if the sign of $\cos \eta_D$ as computed in equation 184 is positive η_D equals

$$\eta_D = \sin^{-1}(a_{31D}) \quad (185)$$

where $\frac{\pi}{2} \geq \eta_D \geq -\frac{\pi}{2}$, but if the sign of $\cos \eta_D$ is negative

$$\eta_D = (\pi - |\eta_D|) \text{ sign}(\eta_D) \quad (186)$$

The value of η_D used in equation 186 is the value computed in equation 185. The third Euler angle ϕ_D can be computed using the definitions of a_{11D} and a_{21D} , and the computed value of $\cos \eta_D$. a_{11D} and a_{21D} equal

$$a_{11D} = \cos \phi_D \cos \eta_D \quad (187)$$

$$a_{21D} = -\sin \phi_D \cos \eta_D \quad (188)$$

The sine and cosine of ϕ_D equal

$$\cos \phi_D = \frac{a_{11D}}{\cos \eta_D} \quad (189)$$

$$\sin \phi_D = \frac{-a_{21D}}{\cos \eta_D} \quad (190)$$

If the sign of $\cos \phi_D$ is positive, ϕ_D equals

$$\phi_D = \sin^{-1} \left(\frac{-a_{21D}}{\cos \eta_D} \right) \quad (191)$$

where $\frac{\pi}{2} \geq \phi_D \geq -\frac{\pi}{2}$, but if the sign of $\cos \phi_D$ is negative, ϕ_D equals

$$\phi_D = (\pi - |\phi_D|) \text{ sign}(\phi_D) \quad (192)$$

The value of ϕ_D used in equation 188 is the value computed in equation 191

In summary, the Euler angles ψ_D , η_D , and ϕ_D can be computed using the following procedure:

1. Compute ψ_D ,

$$\psi_D = \tan^{-1} \left(\frac{-a_{32D}}{a_{33D}} \right)$$

where $-\frac{\pi}{2} \leq \psi_D \leq \frac{\pi}{2}$.

2. Compute $\cos \eta_D$,

$$\cos \eta_D = \frac{a_{11D} a_{31D}}{a_{12D} \sin \psi_D - a_{13D} \cos \psi_D}$$

3. Compute intermediate η_D , η'_D

$$\eta'_D = \sin^{-1}(a_{31D})$$

where $-\frac{\pi}{2} \leq \eta'_D \leq \frac{\pi}{2}$.

4. If the sign of $\cos \eta_D$ is positive,

$$\eta_D = \eta'_D$$

but if the sign of $\cos \eta_D$ is negative,

$$\eta_D = (\pi - |\eta'_D|) \text{ sign}(\eta'_D)$$

5. Compute $\cos \phi_D$.

$$\cos \phi_D = \frac{a_{11D}}{\cos \eta_D}$$

6. Compute intermediate ϕ_D , ϕ'_D

$$\phi'_D = \sin^{-1} \left(\frac{-a_{21D}}{\cos \eta_D} \right)$$

where $-\frac{\pi}{2} \leq \phi'_D \leq \frac{\pi}{2}$.

7. If the sign of $\cos \phi_D$ is positive,

$$\phi_D = \phi'_D$$

but if the sign of $\cos \phi_D$ is negative,

$$\phi_D = (\pi - |\phi'_D|) \text{ sign}(\phi'_D)$$

8.4.4 Euler Angle Maneuver - This maneuvering technique maneuvers the vehicle to its desired vehicle attitude defined by $[\phi_D]$ by computing the three corresponding Euler rotations ψ_m , η_m , and ϕ_m that will align the vehicle axes $X_V Y_V Z_V$ with their desired orientation $X_D Y_D Z_D$. The proper sequence in which these three maneuvers must be performed are: (1) a maneuver through an angle ψ_m about the X_V axis, (2) η_m about the displaced Y_V axis, and (3) ϕ_m about the displaced Z_V axis.

The transformation $[\phi_{DV}]$ that describes the desired vehicle attitude $X_D Y_D Z_D$ with respect to the present vehicle attitude $X_V Y_V Z_V$ equals

$$[\phi_{DV}] = [\phi_D] [\phi]^{-1} = \begin{bmatrix} a_{11m} & a_{12m} & a_{13m} \\ a_{21m} & a_{22m} & a_{23m} \\ a_{31m} & a_{32m} & a_{33m} \end{bmatrix} \quad (193)$$

The Euler angles ψ_m , η_m , and ϕ_m can be computed in the same manner as ψ_D , η_D , and ϕ_D are in section 8.4.3. The Euler angle ψ_m equals

$$\psi_m = \tan^{-1} \left(-\frac{a_{32m}}{a_{33m}} \right) \quad (194)$$

where $-\frac{\pi}{2} \leq \psi_m \leq \frac{\pi}{2}$. The Euler angle η_m equals

$$\eta_m = \sin^{-1}(a_{31m}) \quad (195)$$

Two possible solutions for η_m as given by equation 195 exists. For example, if a_{31m} equals +0.5, η_m can equal either $\frac{\pi}{6}$ or $\frac{5\pi}{6}$. Only one of these values is proper as can be determined by the sign of $\cos\eta_m$. If the sign of $\cos\eta_m$ is positive, η_m equals $\frac{\pi}{6}$, but, if the sign of $\cos\eta_m$ is negative, the proper value for η_m is $\frac{5\pi}{6}$. The cosine of η_m in terms of the elements of $[\phi_{DV}]$ equals

$$\cos\eta_m = \frac{a_{11m}a_{31m}}{a_{21m}\sin\psi_m - a_{13m}\cos\psi_m} \quad (196)$$

If the sign of $\cos\eta_m$ is positive, η_m lies within either the first ($0 \leq \eta_m \leq \frac{\pi}{2}$) or fourth ($-\frac{\pi}{2} \leq \eta_m \leq 0$) quadrants. But if the sign of $\cos\eta_m$ is negative, the proper value for η_m lies within the second ($\frac{\pi}{2} \leq \eta_m \leq \pi$) or third ($-\pi \leq \eta_m \leq -\frac{\pi}{2}$) quadrants. Equations 195 and 196 uniquely determine the proper value for η_m . The third Euler angle ϕ_m is determined in a similar manner. ϕ_m equals

$$\phi_m = \sin^{-1} \left(-\frac{a_{21m}}{\cos\eta_m} \right) \quad (197)$$

The cosine of ϕ_m equals

$$\cos\phi_m = \frac{a_{11m}}{\cos\eta_m} \quad (198)$$

If the cosine of ϕ_m is positive, ϕ_m lies within the first or fourth quadrant and if the cosine of ϕ_m is negative, ϕ_m lies within the second or third quadrant. Equations 197 and 198 uniquely determine the proper value for ϕ_m .

To perform the three maneuvers ψ_m , η_m , and ϕ_m , the vehicle attitude error $\Delta\theta$ is zeroed and each maneuver is performed in its proper sequence at the maximum allowable maneuver rate ω_m , 1.745×10^{-3} radian per second (six degrees per minute). The first vehicle maneuver rate command $\dot{\omega}_{m1}$ equals

$$\dot{\omega}_{m1} = \omega_m \text{sign}(\psi_m) \begin{bmatrix} 1 \\ 0 \\ 0 \end{bmatrix} \quad (199)$$

The sign of ψ_m in the above expression indicates which direction the vehicle is to be maneuvered about the X_v axis. This maneuver rate command $\dot{\omega}_{m1}$ is continued until the direction cosine a_{32m} approaches zero indicating that the Y_v axis is perpendicular to the desired Z_D axis. At this point $\dot{\omega}_{m1}$ is zeroed, and the second maneuver η_m about the Y_v axis commences. The vehicle rate command $\dot{\omega}_{m2}$ associated with this maneuver η_m equals

$$\dot{\omega}_{m2} = \omega_m \text{sign}(\eta_m) \begin{bmatrix} 0 \\ 1 \\ 0 \end{bmatrix} \quad (200)$$

This maneuver rate command $\dot{\omega}_{m2}$ is applied to the system until the direction cosine a_{33m} approaches unity indicating that the Z_v axis is aligned with the desired Z_D axis. $\dot{\omega}_{m2}$ is then zeroed and the third and final maneuver ϕ_m about the Z_v axis is performed. The vehicle rate commanded $\dot{\omega}_{m3}$ associated with this maneuver ϕ_m equals

$$\dot{\omega}_{m3} = \omega_m \text{sign}(\phi_m) \begin{bmatrix} 0 \\ 0 \\ 1 \end{bmatrix} \quad (201)$$

This maneuver rate command $\dot{\omega}_{m3}^+$ is applied to the system until the direction cosines a_{11m} and a_{22m} approach unity indicating that the vehicle X_v and Y_v axes are aligned with their corresponding desired orientations X_D and Y_D , respectively. These three vehicle maneuver rate commands are fed to the vehicle control law where they replace the desired vehicle rate $\dot{\omega}_D$. At the completion of the third maneuvers ϕ_m , the vehicle attitude error $\Delta\theta$ is reintroduced to the vehicle control law thus correcting for all residual vehicle maneuvering errors.

8.5 Strapdown Equation Initialization and Update - The strapdown equation implementations, the quaternions, the direction cosines, and the Euler angles, track the attitude of the vehicle by essentially integrating the vehicle body rates ω_x , ω_y , and ω_z . The numerical integrations associated with each of these implementations must be initialized and updated periodically. The periodic update corrects for computational errors and the accumulative effects of errors such as rate gyro drift contained in the measured vehicle rates ω_x , ω_y , and ω_z . For the quaternion initialization and update, the actual values of the four quaternion parameters q_1 , q_2 , q_3 , and q_4 are determined and then substituted for q_{1p} , q_{2p} , q_{3p} , and q_{4p} in the quaternion strapdown equations. The initialization and update of the direction cosine and Euler angle strapdown equations are performed in a similar manner except that the corresponding direction cosines a_{11p} , a_{12p} , ..., a_{33p} and Euler angles ψ_p , θ_p , and ϕ_p are determined.

To perform this initialization or update procedure, the transformation $[N]$ from reference space XYZ to vehicle space $X_v Y_v Z_v$ must be determined. This update or initialization procedure is normally performed using star trackers attached to the spacecraft. These star trackers are used to measure in vehicle coordinates the location of two reference stars whose coordinates in the XYZ reference frame are known. Assume that the locations of two reference stars in the XYZ reference frame are given by the two unit vectors S_1 and S_2 and that their corresponding vehicle coordinates as measured by the vehicle star trackers are described by the unit vectors S_1' and S_2' , respectively.

In order to compute $[\Phi]$, two additional unit vectors \vec{S}_{12} and \vec{S}_{12}' must be computed. \vec{S}_{12} and \vec{S}_{12}' are the unit vectors corresponding to the vector cross product of \vec{S}_1 and \vec{S}_2 and \vec{S}_1' and \vec{S}_2' , respectively.

$$\vec{S}_{12} = \frac{\vec{S}_1 \times \vec{S}_2}{||\vec{S}_1 \times \vec{S}_2||} \quad (202)$$

$$\vec{S}_{12}' = \frac{\vec{S}_1' \times \vec{S}_2'}{||\vec{S}_1' \times \vec{S}_2'||} \quad (203)$$

$||\vec{A}||$ represents the norm of the enclosed vector \vec{A} . \vec{S}_{12} and \vec{S}_{12}' are unit vectors that are perpendicular to the planes formed by \vec{S}_1 and \vec{S}_2 and \vec{S}_1' and \vec{S}_2' , respectively. These six unit vectors \vec{S}_1 , \vec{S}_2 , \vec{S}_{12} , \vec{S}_1' , \vec{S}_2' , and \vec{S}_{12}' completely specify the transformation $[\Phi]$. To compute $[\Phi]$, the following relationships must be satisfied.

$$\vec{S}_1 = [\Phi]\vec{S}_1' \quad (204)$$

$$\vec{S}_2 = [\Phi]\vec{S}_2' \quad (205)$$

$$\vec{S}_{12} = [\Phi]\vec{S}_{12}' \quad (206)$$

where

$$[\Phi] = \begin{bmatrix} a_{11} & a_{12} & a_{13} \\ a_{21} & a_{22} & a_{23} \\ a_{31} & a_{32} & a_{33} \end{bmatrix}$$

Assume that the unit vectors \vec{S}_1 , \vec{S}_1' , \vec{S}_2 , \vec{S}_2' , \vec{S}_{12} , and \vec{S}_{12}' are

$$\vec{s}_1 = \begin{bmatrix} c_{11} \\ c_{12} \\ c_{13} \end{bmatrix} \quad \vec{s}_1' = \begin{bmatrix} c_{21} \\ c_{22} \\ c_{23} \end{bmatrix}$$

$$\vec{s}_2 = \begin{bmatrix} d_{11} \\ d_{12} \\ d_{13} \end{bmatrix} \quad \vec{s}_2' = \begin{bmatrix} d_{21} \\ d_{22} \\ d_{23} \end{bmatrix}$$

$$\vec{s}_{12} = \begin{bmatrix} f_{11} \\ f_{12} \\ f_{13} \end{bmatrix} \quad \vec{s}_{12}' = \begin{bmatrix} f_{21} \\ f_{22} \\ f_{23} \end{bmatrix}$$

Substituting the above vectors into equations 204 thru 206.

$$\vec{s}_1 = [\phi] \vec{s}_1' = \begin{bmatrix} c_{11} \\ c_{12} \\ c_{13} \end{bmatrix} = \begin{bmatrix} a_{11} & a_{12} & a_{13} \\ a_{21} & a_{22} & a_{23} \\ a_{31} & a_{32} & a_{33} \end{bmatrix} \begin{bmatrix} c_{21} \\ c_{22} \\ c_{23} \end{bmatrix} \quad (207)$$

$$\vec{s}_2 = [\phi] \vec{s}_2' = \begin{bmatrix} d_{11} \\ d_{12} \\ d_{13} \end{bmatrix} = \begin{bmatrix} a_{11} & a_{12} & a_{13} \\ a_{21} & a_{22} & a_{23} \\ a_{31} & a_{32} & a_{33} \end{bmatrix} \begin{bmatrix} d_{21} \\ d_{22} \\ d_{23} \end{bmatrix} \quad (208)$$

$$\dot{S}_{12} = [\Phi] \dot{S}_{12}' = \begin{bmatrix} f_{11} \\ f_{12} \\ f_{13} \end{bmatrix} = \begin{bmatrix} a_{11} & a_{12} & a_{13} \\ a_{21} & a_{22} & a_{23} \\ a_{31} & a_{32} & a_{33} \end{bmatrix} \begin{bmatrix} f_{21} \\ f_{22} \\ f_{23} \end{bmatrix} \quad (209)$$

Equations 207 thru 209 can be rearranged into the following expressions.

$$\begin{bmatrix} c_{11} \\ d_{11} \\ f_{11} \end{bmatrix} = \begin{bmatrix} c_{21} & c_{22} & c_{23} \\ d_{21} & d_{22} & d_{23} \\ f_{21} & f_{22} & f_{23} \end{bmatrix} \begin{bmatrix} a_{11} \\ a_{12} \\ a_{13} \end{bmatrix} \quad (210)$$

$$\begin{bmatrix} c_{12} \\ d_{12} \\ f_{12} \end{bmatrix} = \begin{bmatrix} c_{21} & c_{22} & c_{23} \\ d_{21} & d_{22} & d_{23} \\ f_{21} & f_{22} & f_{23} \end{bmatrix} \begin{bmatrix} a_{21} \\ a_{22} \\ a_{23} \end{bmatrix} \quad (211)$$

$$\begin{bmatrix} c_{13} \\ d_{13} \\ f_{13} \end{bmatrix} = \begin{bmatrix} c_{21} & c_{22} & c_{23} \\ d_{21} & d_{22} & d_{23} \\ f_{21} & f_{22} & f_{23} \end{bmatrix} \begin{bmatrix} a_{31} \\ a_{32} \\ a_{33} \end{bmatrix} \quad (212)$$

Applying Cramer's rule for solving simultaneous algebraic equations, the elements of $[\Phi]$, a_{11} , a_{12} , ..., a_{33} , can be computed using equations 210 thru 212. Note that the 3 by 3 matrix appearing in each of these equations are identical. The symbol Δ is used to denote the determinant of this matrix. Δ equals

$$\Delta = \det \begin{bmatrix} c_{21} & c_{22} & c_{23} \\ d_{21} & d_{22} & d_{23} \\ f_{21} & f_{22} & f_{23} \end{bmatrix} = c_{21}(d_{22}f_{23} - d_{23}f_{22})$$

$$+ c_{22}(d_{23}f_{21} - d_{21}f_{23}) + c_{23}(d_{21}f_{22} - d_{22}f_{21}) \quad (213)$$

The nine elements of $[\Phi]$ in terms of the components of \vec{S}_1 , \vec{S}_2 , \vec{S}_{12} , \vec{S}_1' , \vec{S}_2' , and \vec{S}_{12}' equal

$$a_{11} = \frac{\det \begin{bmatrix} c_{11} & c_{22} & c_{23} \\ d_{11} & d_{22} & d_{23} \\ f_{11} & f_{22} & f_{23} \end{bmatrix}}{\Delta} = [c_{11}(d_{22}f_{23} - d_{23}f_{22})$$

$$+ c_{22}(d_{23}f_{11} - d_{11}f_{23}) + c_{23}(d_{11}f_{22} - d_{22}f_{11})]/\Delta \quad (214)$$

$$a_{12} = \frac{\det \begin{bmatrix} c_{21} & c_{11} & c_{23} \\ d_{21} & d_{11} & d_{23} \\ f_{21} & f_{11} & f_{23} \end{bmatrix}}{\Delta} = [c_{21}(d_{11}f_{23} - d_{23}f_{11})$$

$$+ c_{11}(d_{23}f_{21} - d_{21}f_{23}) + c_{23}(d_{21}f_{11} - d_{11}f_{21})]/\Delta \quad (215)$$

$$a_{13} = \frac{\det \begin{bmatrix} c_{21} & c_{22} & c_{11} \\ d_{21} & d_{22} & d_{11} \\ f_{21} & f_{22} & f_{11} \end{bmatrix}}{\Delta} = [c_{21}(d_{22}f_{11} - d_{11}f_{22})$$

$$+ c_{22}(d_{11}f_{21} - d_{21}f_{11}) + c_{11}(d_{21}f_{22} - d_{22}f_{21})]/\Delta \quad (216)$$

$$a_{21} = \frac{\det \begin{bmatrix} c_{12} & c_{22} & c_{23} \\ d_{12} & d_{22} & d_{23} \\ f_{12} & f_{22} & f_{23} \end{bmatrix}}{\Delta} = [c_{12}(d_{22}f_{23} - d_{23}f_{22})$$

$$+ c_{22}(d_{23}f_{12} - d_{12}f_{23}) + c_{23}(d_{12}f_{22} - d_{22}f_{12})]/\Delta \quad (217)$$

$$a_{22} = \frac{\det \begin{bmatrix} c_{21} & c_{12} & c_{23} \\ d_{21} & d_{12} & d_{23} \\ f_{21} & f_{12} & f_{23} \end{bmatrix}}{\Delta} = [c_{21}(d_{12}f_{23} - d_{23}f_{12})$$

$$+ c_{12}(d_{23}f_{21} - d_{21}f_{23}) + c_{23}(d_{21}f_{12} - d_{12}f_{21})]/\Delta \quad (218)$$

$$a_{23} = \frac{\det \begin{bmatrix} c_{21} & c_{22} & c_{12} \\ d_{21} & d_{22} & d_{12} \\ f_{21} & f_{22} & f_{12} \end{bmatrix}}{\Delta} = [c_{21}(d_{22}f_{12} - d_{12}f_{22})$$

$$+ c_{22}(d_{12}f_{21} - d_{21}f_{12}) + c_{12}(d_{21}f_{22} - d_{22}f_{21})]/\Delta \quad (219)$$

$$\begin{aligned}
 a_{31} = & \frac{\det \begin{bmatrix} c_{13} & c_{22} & c_{23} \\ d_{13} & d_{22} & d_{23} \\ f_{13} & f_{22} & f_{23} \end{bmatrix}}{\Delta} = [c_{13}(d_{22}f_{23} - d_{23}f_{22}) \\
 & + c_{22}(d_{23}f_{13} - d_{13}f_{23}) + c_{23}(d_{13}f_{22} - d_{22}f_{13})] / \Delta \quad (220)
 \end{aligned}$$

$$\begin{aligned}
 a_{32} = & \frac{\det \begin{bmatrix} c_{21} & c_{13} & c_{23} \\ d_{21} & d_{13} & d_{23} \\ f_{21} & f_{13} & f_{23} \end{bmatrix}}{\Delta} = [c_{21}(d_{13}f_{23} - d_{23}f_{13}) \\
 & + c_{13}(d_{23}f_{21} - d_{21}f_{23}) + c_{23}(d_{21}f_{13} - d_{13}f_{21})] / \Delta \quad (221)
 \end{aligned}$$

$$\begin{aligned}
 a_{33} = & \frac{\det \begin{bmatrix} c_{21} & c_{22} & c_{13} \\ d_{21} & d_{22} & d_{13} \\ f_{21} & f_{22} & f_{13} \end{bmatrix}}{\Delta} = [c_{21}(d_{22}f_{13} - d_{13}f_{22}) \\
 & + c_{22}(d_{13}f_{21} - d_{21}f_{13}) + c_{13}(d_{21}f_{22} - d_{22}f_{21})] / \Delta \quad (222)
 \end{aligned}$$

To update or to initialize the direction cosine strap-down equations, the above computed direction cosines a_{11} , a_{12} , ..., a_{33} are substituted for a_{11p} , a_{12p} , ..., a_{33p} . For the quaternion strapdown equations, the updated (or initial) values of q_{1p} , q_{2p} , q_{3p} , and q_{4p} are determined from the star tracker derived direction cosines. q_{1p} , q_{2p} , q_{3p} , and q_{4p} equal

$$q_{1P} = \cos\left(\frac{\theta}{2}\right) \quad (223)$$

where

$$\theta = \cos^{-1}[0.5(a_{11} + a_{22} + a_{33} - 1)]$$

$$q_{2P} = \frac{a_{21} - a_{12}}{4q_{1P}} \quad (224)$$

$$q_{3P} = \frac{a_{13} - a_{31}}{4q_{1P}} \quad (225)$$

$$q_{4P} = \frac{a_{21} - a_{12}}{4q_{1P}} \quad (226)$$

To update (or initialize) the Euler angle strapdown equations, the Euler angles ψ_p , η_p , and ϕ_p are also computed from these star tracker derived direction cosines. ψ_p equals

$$\psi_p = \tan^{-1} \left(-\frac{a_{32}}{a_{33}} \right) \quad (227)$$

where $-\frac{\pi}{2} \leq \psi_p \leq \frac{\pi}{2}$. The cosine of η_p equals

$$\cos \eta_p = \frac{a_{11}a_{31}}{a_{12}\sin \psi_p + a_{13}\cos \psi_p} \quad (228)$$

If the sign of $\cos \eta_p$ is positive, η_p equals

$$\eta_p = \sin^{-1}(a_{31}) \quad (229)$$

where $-\frac{\pi}{2} \leq \eta_p \leq \frac{\pi}{2}$, but if the sign of $\cos \eta_p$ is negative, η_p equals

$$\eta_p = (\pi - |\eta_p'|) \text{ sign } (\eta_p') \quad (230)$$

where the value of η_p' equals the value of η_p given by equation 229. The cosine of ϕ_p equals

$$\cos \phi_p = \frac{a_{11}}{\cos \eta_p} \quad (231)$$

If the sign of $\cos \phi_p$ is positive, ϕ_p equals

$$\phi_p = \sin^{-1} \left(- \frac{a_{21}}{\cos \eta_p} \right) \quad (232)$$

where $-\frac{\pi}{2} \leq \phi_p \leq \frac{\pi}{2}$, but if the sign of $\cos \phi_p$ is negative, ϕ_p equals

$$\phi_p = (\pi - |\phi_p'|) \text{sign}(\phi_p') \quad (233)$$

where the value of ϕ_p' equals the value of ϕ_p given by equation 232.

8.6 Comparison of Candidate Maneuver Control Laws - Three vehicle CMG maneuver control laws have been proposed. These three control laws are based on (1) quaternion, (2) direction cosine, and (3) Euler angle implementations. The vehicle strapdown equations of motion and associated maneuver equations were derived for each of these implementations. Listed in table 8.1 are the advantages and disadvantages of each of these three methods.

The chief advantages of the quaternion implementation are (1) the maneuver produced is optimal and (2) the associated strapdown and maneuver equations can be simply and readily computed. The maneuver is optimal because the vehicle is rotated about a single axis through the smallest angle required to generate the desired attitude change. The disadvantages of this quaternion control law are (1) updating the quaternion strapdown equations require computing the four quaternion parameters from the measured vehicle transformation $[\Phi]$, and (2) additional calculations are needed to derive the direction cosine matrix $[\hat{\Phi}]$ from the four quaternion parameters computed by the strapdown equations. These disadvantages are minor because (1) the additional computations needed to compute the updated quaternions are few and (2) it is not necessary to compute the direction cosine matrix $[\Phi]$ in order to implement this CMG maneuver control law. The reason one might want to compute the direction cosine matrix $[\Phi]$ is because one may be more familiar with this representation for describing the vehicle attitude than the corresponding quaternion representation.

Table 8.1. CMC Maneuver Control Laws

CONTROL LAW	ADVANTAGES	DISADVANTAGES
Quaternions	<p>Linear set of four linear differential equations - simple software implementation</p> <p>No singularities</p> <p>Optimal maneuver capability</p>	<p>Requires separate computation of direction cosine matrix $[\phi]$</p> <p>Requires addition computation to updated quaternion given vehicle transformation $[\phi]$</p>
Direction Cosines	<p>No singularities</p> <p>Direction cosine matrix always available</p> <p>No additional computations required to update strapdown equations given $[\phi]$</p>	<p>Requires the solution of nine linear differential equations</p> <p>Non optimal maneuver</p>
Euler Angles	<p>Solution of the smallest number of parameters, three</p>	<p>Singularity, $n = \frac{(2n+1)\pi}{2}$ $n=0, \pi, 2\pi, \dots$</p> <p>Solution of a non linear set of equations</p> <p>Non optimal maneuver</p> <p>Requires separate computation of direction cosine matrix $[\phi]$</p> <p>Requires additional computation to updated Euler angles given $[\phi]$</p>

The advantages of the direction cosine CMG maneuver control law are (1) the direction cosine matrix is always available and (2) no additional computations are required to update the direction cosine strapdown equations. The disadvantages are (1) nine linear differential equations must be solved as compared with only four for the quaternion CMG maneuver control law and (2) the resulting vehicle maneuver is non optimal. The maneuver is non optimal because in general two distinct rotations are needed to reorient the vehicle with its new desired attitude.

The single advantage of the Euler angle CMG maneuver control law is that only three parameters are needed to describe the vehicle attitude rather than four for the quaternion and nine for the direction cosine maneuver control laws. The disadvantages are (1) the strapdown equations are a set of non linear differential equations, (2) the strapdown equations are singular causing the Euler angles to "blow up" when the Euler angle η approaches $\frac{(2n+1)\pi}{2}$ ($n=0, \pm 1, \dots$), (3) updating the Euler angle strapdown equations require computing the three Euler angles from the measured vehicle transformation $[\phi]$, (4) additional computations are needed to derive the direction cosine matrix $[\phi]$ from the three computed Euler angles, and (5) the resulting vehicle maneuver is non optimal. To maneuver the vehicle to a new orientation, three separate rotations are required.

From a "pure" computational standpoint, either the Euler angle or quaternion control law are favored over the direction cosine law. For the Euler angle control law, only three parameters are needed to describe the vehicle attitude while for the quaternion implementation, four parameters are required. To describe the vehicle attitude using the direction cosine control law, nine parameters are needed. The major drawback with the Euler angle control law is that its strapdown equations of motion are singular. Because of this singularity problem, the Euler angle control law is eliminated from further considerations. The principal drawback of the direction cosine law besides its large computational requirements is that like the Euler angle control law the resultant vehicle maneuvers are non optimal. For the quaternion control law, the vehicle maneuvers are optimal.

The quaternion CMG maneuver control law is selected as baseline because (1) the computational requirements associated with the four linear quaternion strapdown equations are fewer than for the corresponding nine linear direction cosine equations

or the three nonlinear Euler angle strapdown equations, (2) there exists no singularity problem as in the case of the Euler angle strapdown equations, and (3) the resulting vehicle maneuver is optimal.

8.7 Selected CMG Maneuver Control Law Signal Flow Diagram -
 Figure 8.7 is a signal flow diagram describing the quaternion CMG maneuver control law logic flow. In box 1, the past vehicle quaternion rates \dot{q}_{1p} , \dot{q}_{2p} , \dot{q}_{3p} , and \dot{q}_{4p} are initialized. Boxes 2 and 3 represent the quaternion strapdown equations. In box 2, the quaternion rates \dot{q}_1 , \dot{q}_2 , \dot{q}_3 , and \dot{q}_4 are computed from the vehicle body rates ω_x , ω_y , and ω_z and are then integrated in box 3 to generate the vehicle quaternions q_1 , q_2 , q_3 , and q_4 . Box 4 represents the procedure for updating or initializing these strapdown equations. In box 5, the computed vehicle quaternions are normalized to insure that the sum of the squares of the quaternions equal unity. In box 6, the past quaternions q_{1p} , q_{2p} , q_{3p} , and q_{4p} and the quaternion rates \dot{q}_{1p} , \dot{q}_{2p} , \dot{q}_{3p} , and \dot{q}_{4p} are updated. These updated quaternion past values are needed to compute the strapdown equations during the next pass through the logic flow.

In boxes 7 thru 10, the vehicle attitude error $\Delta\vec{\theta}$ is computed. In box 7, the quaternions describing the desired vehicle attitude q_{D1} , q_{D2} , q_{D3} , and q_{D4} are computed from the transformation $\{\phi_D\}$ corresponding to the desired vehicle attitude.

In box 8, the determination whether a maneuver is being performed or not is made. If a maneuver is being performed, the control logic is routed to box 11 where the appropriate vehicle maneuver command is generated. If a maneuver is not in process, the logic flow moves on to box 9 where the quaternions describing the vehicle attitude with respect to the desired attitude q_{VD1} , q_{VD2} , q_{VD3} , and q_{VD4} are computed. In box 10, the vehicle attitude error $\Delta\vec{\theta}$ is computed; $\Delta\vec{\theta}$ and the appropriate vehicle rate $\vec{\omega}_D$ as specified by the transformation $\{\phi_D\}$ is routed to the vehicle control law. For an inertial attitude, $\vec{\omega}_D$ equals the null vector. The control logic transfers back to box 2.

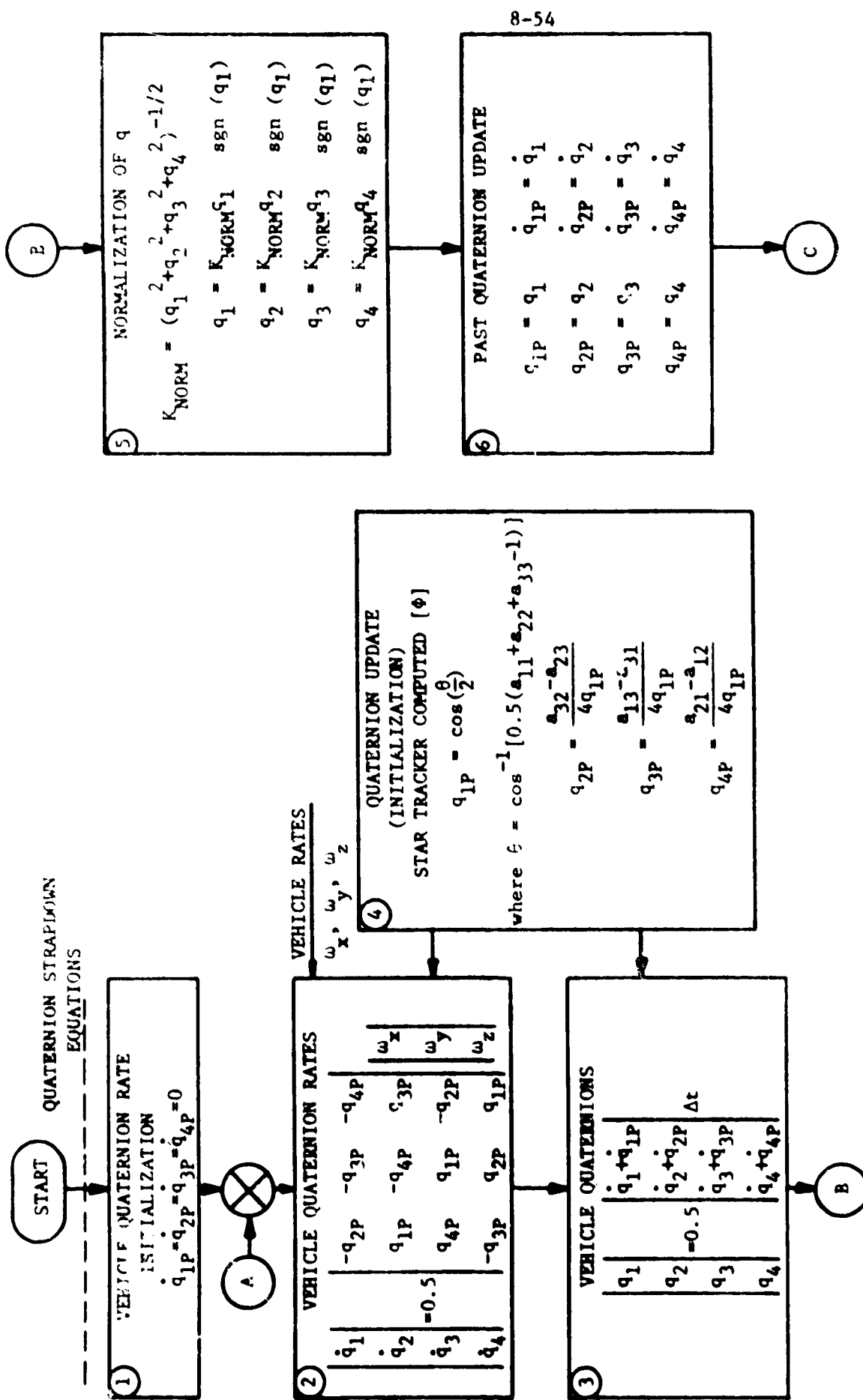


Figure 8.7 CMG Quaternion Maneuver Control Logic Flow Diagram (Sheet 1 of 3)

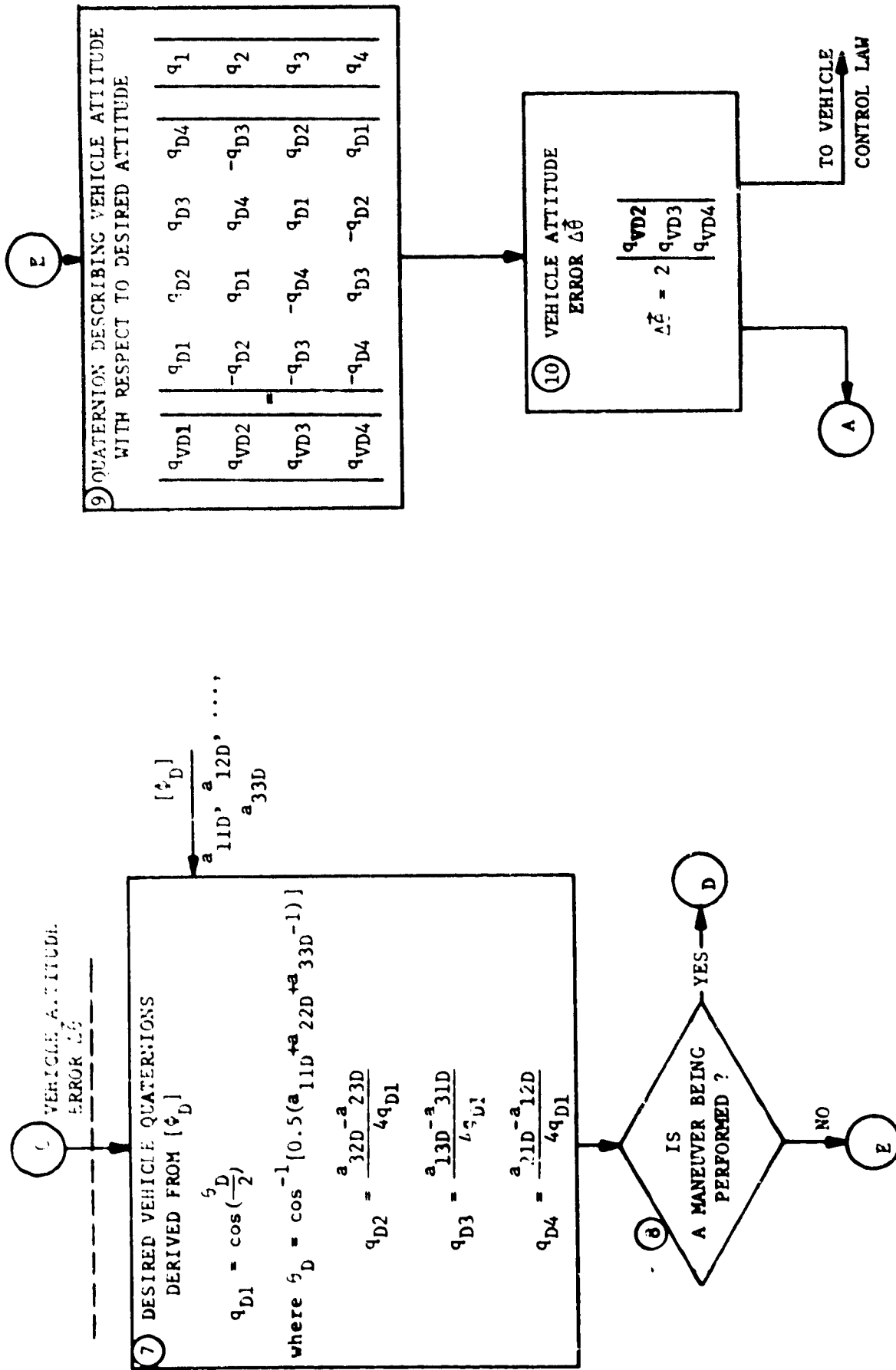


Figure 8.7 CMG Quaternion Maneuver Control Logic Flow Diagram (Sheet 2 of 3)

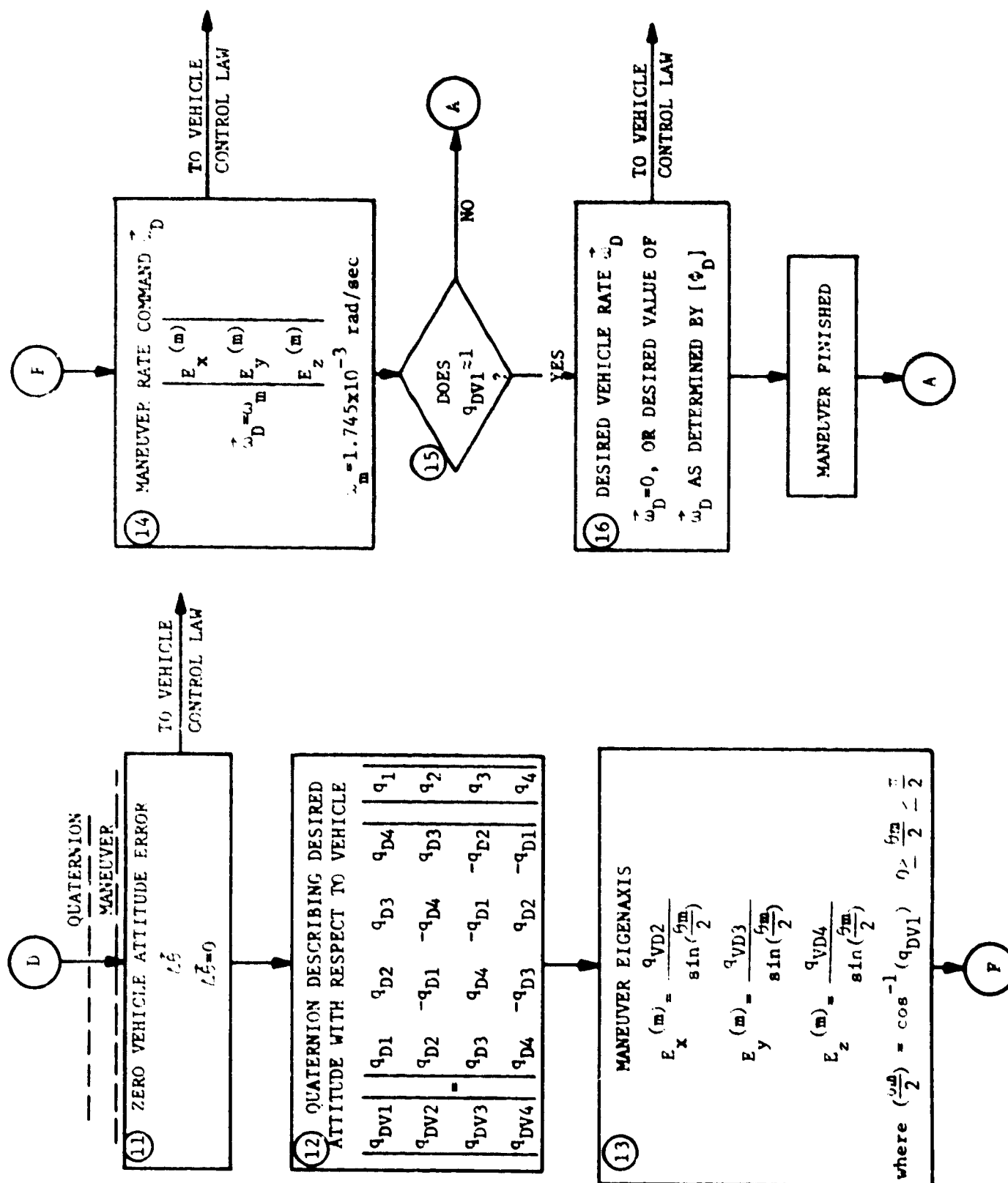


Figure 8.7 CMG Quaternion Maneuver Control Logic Flow Diagram (Sheet 3 of 3)

In boxes 11 thru 16, the appropriate vehicle maneuver command is generated. In box 11, the vehicle attitude error $\Delta\vec{\theta}$ is zeroed and is then routed to the vehicle control law. In box 12, the quaternions describing the desired attitude with respect to the vehicle q_{DV1} , q_{DV2} , q_{DV3} , and q_{DV4} are computed. In box 13, the maneuver axis is computed along with the total maneuver angle θ_m . The logic flow continues on to box 14 where the vehicle maneuver rate $\vec{\omega}_D$ is generated. The vehicle is maneuver about the computed maneuver axis at a rate ω_m of six degrees per minute; $\vec{\omega}_D$ is routed to the vehicle control law. In box 15, the quaternion q_{VD1} is compared with unity. If q_{VD1} is approximately equal to one, the maneuver is finished and the maneuver rate $\vec{\omega}_D$ is zeroed or set at its desired value as determined by the desired vehicle transformation $[\phi_D]$. If q_{VD1} does not equal unity, the logic flow is recycled back to box 2.

8.8 Notes

8.8.1 Symbols and Abbreviations

$a_{11}, a_{12}, \dots, a_{33}$	Direction cosine elements of transformation $[\phi]$
$\dot{a}_{11}, \dot{a}_{12}, \dots, \dot{a}_{33}$	Rate of change of direction cosine elements $a_{11}, a_{12}, \dots, a_{33}$
CMG	Control moment gyro
\vec{E}	Quaternion eigenaxis (unit vector)
E_x, E_y, E_z	Direction cosines describing \vec{E}
$[I]$	Vehicle inertia tensor
$\hat{i}, \hat{j}, \hat{k}$	Unit vectors along X, Y, and Z axes, respectively
$[K_p]$	Vehicle control law position gain matrix
$[K_r]$	Vehicle control law rate gain matrix
\vec{q}	Quaternion corresponding to transformation $[\phi]$
q_1, q_2, q_3, q_4	Elements of quaternion \vec{q}
$\dot{\vec{q}}$	Rate of change of quaternion \vec{q}
$\dot{q}_1, \dot{q}_2, \dot{q}_3, \dot{q}_4$	Elements of $\dot{\vec{q}}$

\vec{q}_{DV}	Quaternion corresponding to transformation $[\phi_{DV}]$
\vec{s}_1, \vec{s}_2	Unit vectors describing the locations of two reference stars in reference space
\vec{s}'_1, \vec{s}'_2	Unit vectors describing the locations of two reference stars in vehicle space
$\vec{s}_{12}, \vec{s}'_{12}$	Cross products of \vec{s}_1 and \vec{s}_2 and \vec{s}'_1 and \vec{s}'_2 , respectively
\vec{T}_{COM}	CMG torque command
Δt	Computational period (seconds)
α, β, γ	Direction cosine angles defining eigenaxis \vec{E}
\vec{e}	Vehicle offset angle
$\epsilon_x, \epsilon_y, \epsilon_z$	Components of vehicle attitude error $\Delta\vec{\theta}$
θ	Angular displacement about eigenaxis \vec{E}
$\Delta\vec{\theta}$	Vehicle attitude error
$[\phi]$	Transformation from reference to vehicle space
$[\phi_D]$	Transformation from reference to desired vehicle space
$[\phi_{DV}]$	Transformation from vehicle to desired vehicle attitude
ψ, η, ϕ	Euler angles corresponding to transformation $[\phi]$
$\dot{\psi}, \dot{\eta}, \dot{\phi}$	Euler angle rates
$\vec{\omega}$	Vehicle angular velocity
$\vec{\omega}_D$	Desired vehicle angular velocity
ω_m	Vehicle maneuver rate limit
$\omega_x, \omega_y, \omega_z$	Components of vehicle angular velocity $\vec{\omega}$

8.8.2 References

1. Goldstein, Herbert, Classical Mechanics, Addison-Wesley, 1959.
2. Whittaker, E. T., A Treatise on the Analytical Dynamics of Particles and Rigid Bodies, Cambridge University Press, 1961.

9. CMG CONTROL LAWS AND SINGULARITY AVOIDANCE TECHNIQUES

The function of the CMG control law is to generate an appropriate set of CMG gimbal rate commands that will generate the desired torque command \vec{T}_{COM} computed by the vehicle control law (section 7). The CMG control law is sometimes referred to as the CMG steering law. In order for the CMG control law to generate the desired torque command, \vec{T}_{COM} , the CMG system must avoid all singularity conditions. When a CMG system is in a singularity state, the CMG control system in general is physically unable to produce the desired torque \vec{T}_{COM} . The function of the singularity avoidance scheme is therefore to steer the CMG system away from all avoidable singularity conditions. A singularity avoidance law performs this task by distributing the CMG gimbal angles in such a manner as to avoid singularity but, without applying a net CMG torque to the vehicle. The separate gimbal rate commands generated by the CMG control and singularity avoidance laws are in general summed and sent to the appropriate CMG gimbal servomechanisms.

In this section, four CMG control laws, three singularity avoidance scheme, and a control function that attempts to combine the functions of the CMG control law and singularity avoidance scheme into a single law are developed. From these candidates, a preferred CMG control law and singularity avoidance scheme are selected.

9.1 CMG Configuration - The CMG control system selected in section 6 consists of six double gimbal CMGs (DGCs) with each CMG having an individual wheel momentum of 2,300 ft-lb-sec. These CMGs are similar to the Skylab ATM CMGs; the most significant difference is that unlike the ATM CMGs the proposed CMGs have no gimbal stops.

A possible CMG mounting configuration is shown in figure 9.1. Two CMGs are identically mounted along each of the three vehicle axes. The advantage of this configuration is that each axial CMG pair can be slaved together so that they act as a single CMG with a wheel momentum of 2H. This effective reduction in the number of CMGs from six to three reduces the computational complexity of the resultant CMG control laws and singularity avoidance schemes. The various control laws and singularity avoidance schemes derived in this report are formulated using this configuration. The computational requirements associated with these control laws and singularity avoidance schemes are determined for two operational modes: (1) when the CMGs are operated in slaved pairs as previously described and (2) when the CMGs are operated as six

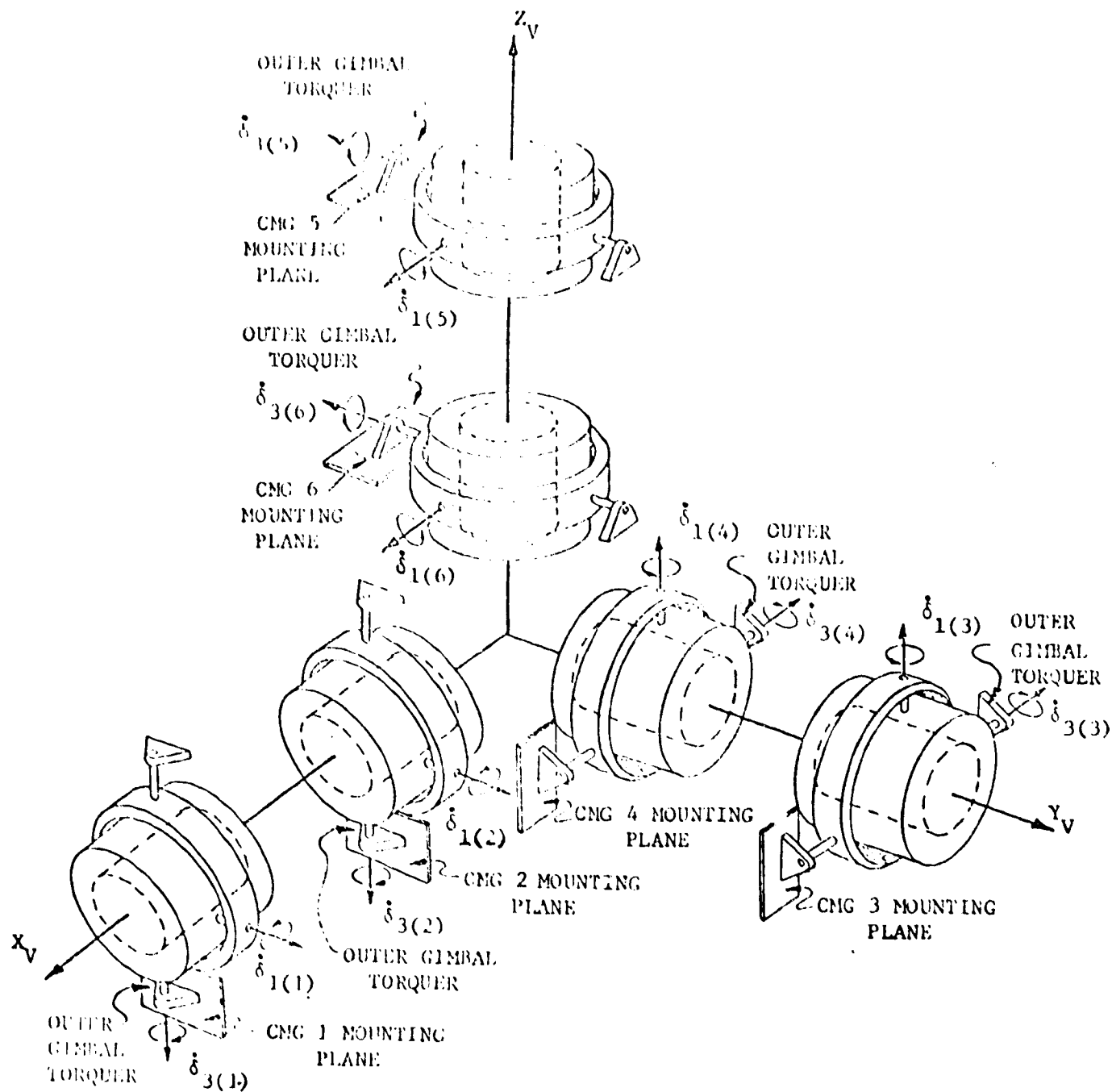


Figure 9.1. Proposed CMG Mounting Configuration

individual units. The CMG control laws and singularity avoidance schemes for both operational modes are formulated to handle the failure contingency of one or more CMGs.

9.2 CMG Torque Equations - The CMG torque equations are derived in this section and are used in later sections to derive the various CMG control laws. For the CMG configuration shown in figure 9.1, the resultant CMG output torque \vec{T}_{CMG} acting on the vehicle equals the summation of the output torque \vec{T}_{ci} of the six

individual CMGs ($\vec{T}_{CMG} = \sum_{i=1}^6 \vec{T}_{ci}$). \vec{T}_{ci} can be determined by (1)

computing the torque a CMG exerts on its base \vec{T}_{cb} and (2) transforming \vec{T}_{cb} from the i^{th} CMG base mounting orientation into vehicle space

$$\vec{T}_{ci} = [\phi]_{v \leftarrow bi} \vec{T}_{cb} \quad (1)$$

$[\phi]_{v \leftarrow bi}$ is the transformation from the i^{th} CMG base coordinate frame to vehicle space.

Figure 9.2 is a sketch of a CMG assembly showing the CMG wheel, inner gimbal, outer gimbal, and base. Three coordinate systems are defined: (1) an inner gimbal space $X_I Y_I Z_I$, (2) an outer gimbal space $X_O Y_O Z_O$, and (3) a CMG base space $X_b Y_b Z_b$. When the $X_I Y_I Z_I$ and $X_O Y_O Z_O$ frames are aligned, the inner gimbal angle δ_1 is defined to be zero; and when the $X_O Y_O Z_O$ and $X_b Y_b Z_b$ frames coincide, the outer gimbal angle δ_3 is defined to be zero. The transformation from base space $X_b Y_b Z_b$ to outer gimbal space $X_O Y_O Z_O$ equals

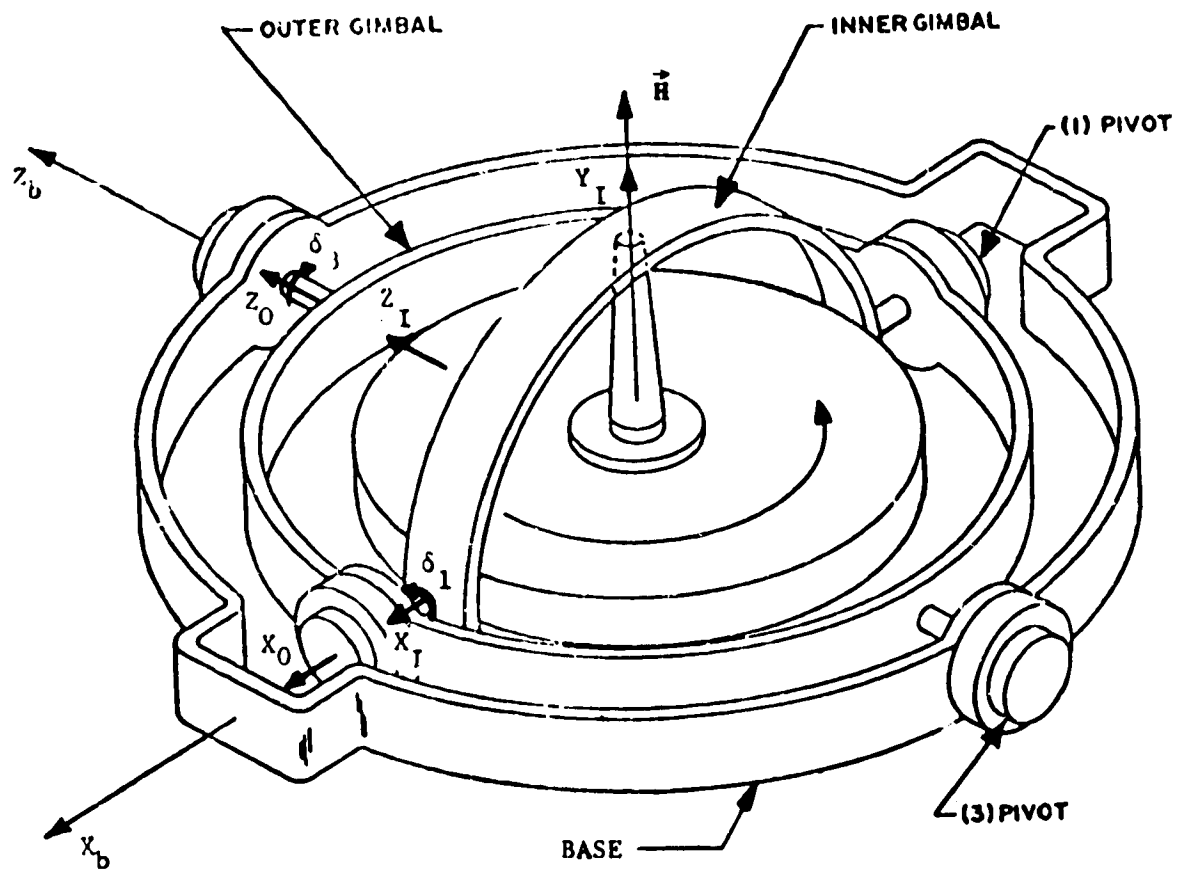


Figure 9.2. CMG Assembly

$$\begin{bmatrix} X_o \\ Y_o \\ Z_o \end{bmatrix} = [\phi]_{o+b} \begin{bmatrix} X_b \\ Y_b \\ Z_b \end{bmatrix} \quad (2)$$

where

$$[\phi]_{o+b} = \begin{bmatrix} \cos \delta_3 & \sin \delta_3 & 0 \\ -\sin \delta_3 & \cos \delta_3 & 0 \\ 0 & 0 & 1 \end{bmatrix} \quad (3)$$

The transformation from outer gimbal space to inner gimbal space X_I, Y_I, Z_I equals

$$\begin{bmatrix} X_I \\ Y_I \\ Z_I \end{bmatrix} = [\phi]_{I+o} \begin{bmatrix} X_o \\ Y_o \\ Z_o \end{bmatrix} \quad (4)$$

where

$$[\phi]_{I+o} = \begin{bmatrix} 1 & 0 & 0 \\ 0 & \cos \delta_1 & \sin \delta_1 \\ 0 & -\sin \delta_1 & \cos \delta_1 \end{bmatrix} \quad (5)$$

The torque exerted on the inner gimbal equals

$$\dot{\vec{H}} = \vec{\omega}_I \times \vec{H} + (\dot{\vec{H}})_r \quad (6)$$

$(\dot{\vec{H}})_r$ is the rate of change of \vec{H} with respect to the inner gimbal and $\vec{\omega}_I$ is the angular rate of change of the inner gimbal space $X_I Y_I Z_I$. The CMG's are assumed to have a constant wheel speed, $(\dot{H})_r$ is therefore zero, and

$$\dot{\vec{H}} = \vec{\omega}_I \times \vec{H} \quad (7)$$

From figure 9.2,

$$\vec{H} = \begin{bmatrix} 0 \\ H \\ 0 \end{bmatrix} \quad (8)$$

where the scalar H is the magnitude of the wheel momentum. Substituting equation 8 into 7,

$$\begin{aligned} \dot{\vec{H}} &= \begin{bmatrix} \hat{i} & \hat{j} & \hat{k} \\ \omega_{IX} & \omega_{IY} & \omega_{IZ} \\ 0 & H & 0 \end{bmatrix} \\ &= -H\omega_{IZ}\hat{i} + H\omega_{IX}\hat{k} \end{aligned} \quad (9)$$

ω_{IX} , ω_{IY} , and ω_{IZ} are the axial components of the inner gimbal rate $\vec{\omega}_I$. $\vec{\omega}_I$ can be written as a function of the inner gimbal rate $\dot{\delta}_1$, the outer gimbal rate $\dot{\delta}_2$, and the rotational rate of the CMG base $\vec{\omega}_0$. First using figure 9.2, let us write $\vec{\omega}_I$ in terms of $\dot{\delta}_1$ and $\vec{\omega}_0$, the outer gimbal rate.

$$\vec{\omega}_I = \begin{bmatrix} \dot{\delta}_1 \\ 0 \\ 0 \end{bmatrix} + [\Phi]_{I+0} \vec{\omega}_0 \quad (10)$$

$\vec{\omega}_o$ can be written in terms of $\dot{\delta}_3$ and $\vec{\omega}_b$.

$$\vec{\omega}_o = \begin{bmatrix} 0 \\ 0 \\ \dot{\delta}_3 \end{bmatrix} + [\phi]_{o+b} \vec{\omega}_b \quad (11)$$

Substituting expression 11 into 10

$$\vec{\omega}_I = \begin{bmatrix} \dot{\delta}_1 \\ 0 \\ 0 \end{bmatrix} + [\phi]_{I+o} \begin{bmatrix} 0 \\ 0 \\ \dot{\delta}_3 \end{bmatrix} + [\phi]_{I+o} [\phi]_{o+b} \vec{\omega}_b \quad (12)$$

Assume that $\vec{\omega}_b$ is small, $\vec{\omega}_I$ equals

$$\vec{\omega}_I = \begin{bmatrix} \dot{\delta}_1 \\ 0 \\ 0 \end{bmatrix} + \begin{bmatrix} 1 & 0 & 0 \\ 0 & \cos \delta_1 & \sin \delta_1 \\ 0 & -\sin \delta_1 & \cos \delta_1 \end{bmatrix} \begin{bmatrix} 0 \\ 0 \\ \dot{\delta}_3 \end{bmatrix} \quad (13)$$

The components of $\vec{\omega}_I$ are

$$\begin{aligned} \omega_{IX} &= \dot{\delta}_1 \\ \omega_{IY} &= \dot{\delta}_3 \sin \delta_1 \\ \omega_{IZ} &= \dot{\delta}_3 \cos \delta_1 \end{aligned} \quad (14)$$

Substituting equation 14 into 9,

$$\dot{\vec{H}} = \vec{H} \begin{bmatrix} -\dot{\delta}_3 \cos \delta_1 \\ 0 \\ \dot{\delta}_1 \end{bmatrix} \quad (15)$$

Note that it is the reaction torque that the inner gimbal applies to the outer gimbal equals $-\dot{\vec{H}}$ that gets transferred to the CMG base. \vec{T}_{cb} equals

$$\vec{T}_{cb} = [\phi]_{o+b}^{-1} [\phi]_{I+o}^{-1} (-\dot{\vec{H}}) \quad (16)$$

where $[\phi]_{o+b}^{-1}$ and $[\phi]_{I+o}^{-1}$ are the inverses of $[\phi]_{o+b}$ and $[\phi]_{I+o}$, respectively.

$$[\phi]_{o+b}^{-1} = \begin{bmatrix} \cos \delta_3 & -\sin \delta_3 & 0 \\ \sin \delta_3 & \cos \delta_3 & 0 \\ 0 & 0 & 1 \end{bmatrix} \quad (17)$$

$$[\phi]_{I+o}^{-1} = \begin{bmatrix} 1 & 0 & 0 \\ 0 & \cos \delta_1 & -\sin \delta_1 \\ 0 & \sin \delta_1 & \cos \delta_1 \end{bmatrix} \quad (18)$$

Substituting $[\phi]_{o+b}^{-1}$, $[\phi]_{I+o}^{-1}$, and equation 15 into 16,

$$\vec{T}_{cb} = H \begin{bmatrix} \dot{\delta}_{3(1)} \cos \delta_{1(1)} \cos \delta_{3(1)} - \dot{\delta}_{1(1)} \sin \delta_{1(1)} \sin \delta_{3(1)} \\ \dot{\delta}_{3(1)} \cos \delta_{1(1)} \sin \delta_{3(1)} + \dot{\delta}_{1(1)} \sin \delta_{1(1)} \cos \delta_{3(1)} \\ -\dot{\delta}_{1(1)} \cos \delta_{1(1)} \end{bmatrix} \quad (19)$$

For CMG No. 1 and 2 along the X_v axis,

$$[\phi]_{v+b1} = [\phi]_{v+b2} = \begin{bmatrix} 0 & 1 & 0 \\ 1 & 0 & 0 \\ 0 & 0 & -1 \end{bmatrix} \quad (20)$$

Substituting expressions 19 and 20 into 1,

$$\vec{T}_{c1} = H \begin{bmatrix} \dot{\delta}_{3(1)} \cos \delta_{1(1)} \sin \delta_{3(1)} + \dot{\delta}_{1(1)} \sin \delta_{1(1)} \cos \delta_{3(1)} \\ \dot{\delta}_{3(1)} \cos \delta_{1(1)} \cos \delta_{3(1)} - \dot{\delta}_{1(1)} \sin \delta_{1(1)} \sin \delta_{3(1)} \\ \dot{\delta}_{1(1)} \cos \delta_{1(1)} \end{bmatrix} \quad (21)$$

$$\vec{T}_{c2} = H \begin{bmatrix} \dot{\delta}_{3(2)} \cos \delta_{1(2)} \sin \delta_{3(2)} + \dot{\delta}_{1(2)} \sin \delta_{1(2)} \cos \delta_{3(2)} \\ \dot{\delta}_{3(2)} \cos \delta_{1(2)} \cos \delta_{3(2)} - \dot{\delta}_{1(2)} \sin \delta_{1(2)} \sin \delta_{3(2)} \\ \dot{\delta}_{1(2)} \cos \delta_{1(2)} \end{bmatrix} \quad (22)$$

The transformation $[\phi]_{v \rightarrow b1}$ corresponding to the other four CMGs are:

$$[\phi]_{v \rightarrow b3} = [\phi]_{v \rightarrow b4} = \begin{bmatrix} 0 & 0 & -1 \\ 0 & 1 & 0 \\ 1 & 0 & 0 \end{bmatrix} \quad (23)$$

$$[\phi]_{v \rightarrow b5} = [\phi]_{v \rightarrow b6} = \begin{bmatrix} 1 & 0 & 0 \\ 0 & 0 & -1 \\ 0 & 1 & 0 \end{bmatrix} \quad (24)$$

The corresponding individual CMG output torques \vec{T}_{ci} ($i=3, \dots, 6$) equal

$$\vec{T}_{c3} = H \begin{bmatrix} \dot{\delta}_{1(3)} \cos \delta_{1(3)} \\ \dot{\delta}_{3(3)} \cos \delta_{1(3)} \sin \delta_{3(3)} + \dot{\delta}_{1(3)} \sin \delta_{1(3)} \cos \delta_{3(3)} \\ \dot{\delta}_{3(3)} \cos \delta_{1(3)} \cos \delta_{3(3)} - \dot{\delta}_{1(3)} \sin \delta_{1(3)} \sin \delta_{3(3)} \end{bmatrix} \quad (25)$$

$$\vec{T}_{c4} = H \begin{bmatrix} \dot{\delta}_{1(4)} \cos \delta_{1(4)} \\ \dot{\delta}_{3(4)} \cos \delta_{1(4)} \sin \delta_{3(4)} + \dot{\delta}_{1(4)} \sin \delta_{1(4)} \cos \delta_{3(4)} \\ \dot{\delta}_{3(4)} \cos \delta_{1(4)} \cos \delta_{3(4)} - \dot{\delta}_{1(4)} \sin \delta_{1(4)} \sin \delta_{3(4)} \end{bmatrix} \quad (26)$$

$$\vec{T}_{c5} = H \begin{bmatrix} \dot{\delta}_{3(5)} \cos \delta_{1(5)} \cos \delta_{3(5)} - \dot{\delta}_{1(5)} \sin \delta_{1(5)} \sin \delta_{3(5)} \\ \dot{\delta}_{1(5)} \cos \delta_{1(5)} \\ \dot{\delta}_{3(5)} \cos \delta_{1(5)} \sin \delta_{3(5)} + \dot{\delta}_{1(5)} \sin \delta_{1(5)} \cos \delta_{3(5)} \end{bmatrix} \quad (27)$$

$$\vec{T}_{c6} = H \begin{bmatrix} \dot{\delta}_{3(6)} \cos \delta_{1(6)} \cos \delta_{3(6)} - \dot{\delta}_{1(6)} \sin \delta_{1(6)} \sin \delta_{3(6)} \\ \dot{\delta}_{1(6)} \cos \delta_{1(6)} \\ \dot{\delta}_{3(6)} \cos \delta_{1(6)} \sin \delta_{3(6)} + \dot{\delta}_{1(6)} \sin \delta_{1(6)} \cos \delta_{3(6)} \end{bmatrix} \quad (28)$$

The resultant output torque \vec{T}_{CMG} can be written as

$$\begin{aligned} \vec{T}_{CMG} &= \sum_{i=1}^6 \vec{T}_{ci} \\ &= H \{ [A] \dot{\delta}_1^{(1)} + [B] \dot{\delta}_3^{(1)} + [C] \dot{\delta}_1^{(2)} + [D] \dot{\delta}_3^{(2)} \} \end{aligned} \quad (29)$$

where

$$\dot{\delta}_1^{(1)} = \begin{bmatrix} \dot{\delta}_{1(1)} \\ \dot{\delta}_{1(3)} \\ \dot{\delta}_{1(5)} \end{bmatrix} \quad (30)$$

$$\dot{\delta}_3^{(1)} = \begin{bmatrix} \dot{\delta}_3(1) \\ \dot{\delta}_3(3) \\ \dot{\delta}_3(5) \end{bmatrix} \quad (31)$$

$$\dot{\delta}_1^{(2)} = \begin{bmatrix} \dot{\delta}_1(2) \\ \dot{\delta}_1(4) \\ \dot{\delta}_1(6) \end{bmatrix} \quad (32)$$

$$\dot{\delta}_3^{(2)} = \begin{bmatrix} \dot{\delta}_3(2) \\ \dot{\delta}_3(4) \\ \dot{\delta}_3(6) \end{bmatrix} \quad (33)$$

$$[A] = \begin{bmatrix} \sin \delta_1(1) \cos \delta_3(1) & \cos \delta_1(3) & -\sin \delta_1(5) \sin \delta_3(5) \\ -\sin \delta_1(1) \sin \delta_3(1) & \sin \delta_1(3) \cos \delta_3(3) & \cos \delta_1(5) \\ \cos \delta_1(1) & -\sin \delta_1(3) \sin \delta_3(3) & \sin \delta_1(5) \cos \delta_3(5) \end{bmatrix} \quad (34)$$

$$[B] = \begin{bmatrix} \cos \delta_1(1) \sin \delta_3(1) & 0 & \cos \delta_1(5) \cos \delta_3(5) \\ \cos \delta_1(1) \cos \delta_3(1) & \cos \delta_1(3) \sin \delta_3(3) & 0 \\ 0 & \cos \delta_1(3) \cos \delta_3(3) & \cos \delta_1(5) \sin \delta_3(5) \end{bmatrix} \quad (35)$$

$$[C] = \begin{bmatrix} \sin \delta_1(2) \cos \delta_3(2) & \cos \delta_1(4) & -\sin \delta_1(6) \sin \delta_3(6) \\ -\sin \delta_1(2) \sin \delta_3(2) & \sin \delta_1(4) \cos \delta_3(4) & \cos \delta_1(6) \\ \cos \delta_1(2) & -\sin \delta_1(4) \sin \delta_3(4) & \sin \delta_1(6) \cos \delta_3(6) \end{bmatrix} \quad (36)$$

$$[D] = \begin{bmatrix} \cos \delta_1(2) \sin \delta_3(2) & 0 & \cos \delta_1(6) \cos \delta_3(6) \\ \cos \delta_1(2) \cos \delta_3(2) & \cos \delta_1(4) \sin \delta_3(4) & 0 \\ 0 & \cos \delta_1(4) \cos \delta_3(4) & \cos \delta_1(6) \sin \delta_3(6) \end{bmatrix} \quad (37)$$

Equation 29 describes the CMG system output torque \vec{T}_{CMG} for a six CMG system for an inertially held vehicle ($\vec{\omega}_b = 0$). For a rotating vehicle, this expression for \vec{T}_{CMG} is not adequate; the rotational motion of the vehicle must be taken into account. The general expression for \vec{T}_{CMG} equals

$$\vec{T}_{CMG} = H \{ [A] \dot{\delta}_1^{(1)} + [B] \dot{\delta}_3^{(1)} + [C] \dot{\delta}_1^{(2)} + [D] \dot{\delta}_3^{(2)} \} + \vec{\omega} \times \vec{H}_{CMG} \quad (38)$$

where $\vec{\omega}$ and \vec{H}_{CMG} are the vehicle angular velocity and total CMG momentum imparted to the vehicle, respectively. For the six CMG configuration shown in figure 9.1, \vec{H}_{CMG} equals

$$\begin{aligned}
\vec{H}_{CMG} = & H \begin{bmatrix} -\cos \delta_{1(1)} & \cos \delta_{3(1)} \\ \cos \delta_{1(1)} & \sin \delta_{3(1)} \\ \sin \delta_{1(1)} & \end{bmatrix} + H \begin{bmatrix} -\cos \delta_{1(2)} & \cos \delta_{3(2)} \\ \cos \delta_{1(2)} & \sin \delta_{3(2)} \\ \sin \delta_{1(2)} & \end{bmatrix} \\
& + H \begin{bmatrix} \sin \delta_{1(3)} \\ -\cos \delta_{1(3)} & \cos \delta_{3(3)} \\ \cos \delta_{1(3)} & \sin \delta_{3(3)} \end{bmatrix} + H \begin{bmatrix} \sin \delta_{1(4)} \\ -\cos \delta_{1(4)} & \cos \delta_{3(4)} \\ \cos \delta_{1(4)} & \sin \delta_{3(4)} \end{bmatrix} \\
& + H \begin{bmatrix} \cos \delta_{1(5)} & \sin \delta_{3(5)} \\ \sin \delta_{1(5)} \\ -\cos \delta_{1(5)} & \cos \delta_{3(5)} \end{bmatrix} + H \begin{bmatrix} \cos \delta_{1(6)} & \sin \delta_{3(6)} \\ \sin \delta_{1(6)} \\ -\cos \delta_{1(6)} & \cos \delta_{3(6)} \end{bmatrix} \quad (39)
\end{aligned}$$

For the slaved CMG mode, let

$$\dot{\vec{\delta}}_1 = \begin{bmatrix} \dot{\delta}_{1x} \\ \dot{\delta}_{1y} \\ \dot{\delta}_{1z} \end{bmatrix} = \dot{\vec{\delta}}_1^{(1)} = \begin{bmatrix} \dot{\delta}_{1(1)} \\ \dot{\delta}_{1(3)} \\ \dot{\delta}_{1(5)} \end{bmatrix} = \dot{\vec{\delta}}_1^{(2)} = \begin{bmatrix} \dot{\delta}_{1(2)} \\ \dot{\delta}_{1(4)} \\ \dot{\delta}_{1(6)} \end{bmatrix} \quad (40)$$

$$\dot{\vec{\delta}}_3 = \begin{bmatrix} \dot{\delta}_{3x} \\ \dot{\delta}_{3y} \\ \dot{\delta}_{3z} \end{bmatrix} = \dot{\vec{\delta}}_3^{(1)} = \begin{bmatrix} \dot{\delta}_{3(1)} \\ \dot{\delta}_{3(3)} \\ \dot{\delta}_{3(5)} \end{bmatrix} = \dot{\vec{\delta}}_3^{(2)} = \begin{bmatrix} \dot{\delta}_{3(2)} \\ \dot{\delta}_{3(4)} \\ \dot{\delta}_{3(6)} \end{bmatrix} \quad (41)$$

The general expression of \vec{T}_{CMG} for the slaved CMG mode equals

$$\vec{T}_{CMG} = 2H\{[A']\dot{\delta}_1 + [B']\dot{\delta}_3\} + \vec{\omega} \times \vec{H}_{CMG} \quad (42)$$

where $[A']$, $[B']$, and \vec{H}_{CMG} are

$$[A'] = \begin{bmatrix} \sin\delta_{1x} \cos\delta_{3x} & \cos\delta_{1y} & -\sin\delta_{1z} \sin\delta_{3z} \\ -\sin\delta_{1x} \sin\delta_{3x} & \sin\delta_{1y} \cos\delta_{3y} & \cos\delta_{1z} \\ \cos\delta_{1x} & -\sin\delta_{1y} \sin\delta_{3y} & \sin\delta_{1z} \cos\delta_{3z} \end{bmatrix} \quad (43)$$

$$[B'] = \begin{bmatrix} \cos\delta_{1x} \sin\delta_{3x} & 0 & \cos\delta_{1z} \cos\delta_{3z} \\ \cos\delta_{1x} \cos\delta_{3x} & \cos\delta_{1y} \sin\delta_{3y} & 0 \\ 0 & \cos\delta_{1y} \cos\delta_{3y} & \cos\delta_{1z} \sin\delta_{3z} \end{bmatrix} \quad (44)$$

$$\begin{aligned} \vec{H}_{CMG} = H & \begin{bmatrix} -\cos\delta_{1x} \cos\delta_{3x} \\ \cos\delta_{1x} \sin\delta_{3x} \\ \sin\delta_{1x} \end{bmatrix} + H \begin{bmatrix} \sin\delta_{1y} \\ -\cos\delta_{1y} \cos\delta_{3y} \\ \cos\delta_{1y} \sin\delta_{3y} \end{bmatrix} \\ & + H \begin{bmatrix} \cos\delta_{1z} \sin\delta_{3z} \\ \sin\delta_{1z} \\ -\cos\delta_{1z} \cos\delta_{3z} \end{bmatrix} \end{aligned} \quad (45)$$

9.3 CMG Control Laws and Singularity Avoidance - The attitude of a CMG stabilized spacecraft is controlled by commanding an appropriate set of gimbal rates $\dot{\delta}_{1(i)}$ and $\dot{\delta}_{3(i)}$ that results in a control torque \vec{T}_{CMG} that equals or approximates the command torque \vec{T}_{COM} . The ability of a CMG system to generate \vec{T}_{COM} is a function of the CMG gimbal angles $\delta_{1(i)}$ and $\delta_{3(i)}$. Note from equation 7,

$$\dot{\vec{H}} = \vec{\omega}_I \times \vec{H} \quad (7)$$

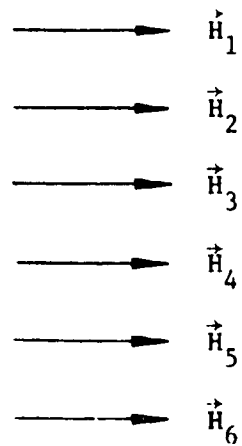
the torque that an individual CMG can generate is constrained to lie in the plane perpendicular to its wheel momentum \vec{H} . This plane is referred to as the CMG's torque plane. If all of the individual CMG torque planes coincide, the only CMG control torque \vec{T}_{CMG} that can be generated lies in this single common plane. The CMG system is incapable of three axis control and is said to be singular.

Figure 9.3 illustrates the two types of singularity that a double gimbal CMG system can exhibit. Figure 9.3.a shows all of the momentum vectors \vec{H}_i pointed in the same direction. This singularity condition corresponds to saturation and the CMG system must be desaturated in order to re-establish three axis control. In figure 9.3.b, the momentum vectors are all aligned, but with some of the momentum vectors \vec{H}_i pointed in opposite directions. This singularity condition is referred to as the anti-parallel condition that must be avoided in order to insure three axis control. With three or more DGCMS, this anti-parallel condition can always be avoided without degrading system performance by commanding appropriate CMG gimbal rates $\dot{\delta}_{1(i)}$ and $\dot{\delta}_{3(i)}$. For three or more DGCMS, the number of degrees-of-freedom, the number of independent CMG gimbals, exceeds the three degrees-of-freedom needed to generate \vec{T}_{COM} . The remaining degrees-of-freedom can be used to redistribute the CMG gimbal angles in such a manner as to avoid the various anti-parallel conditions. This redistribution can be performed without exerting any additional net torque on the vehicle. The form of the resultant CMG gimbal rate commands are in general:

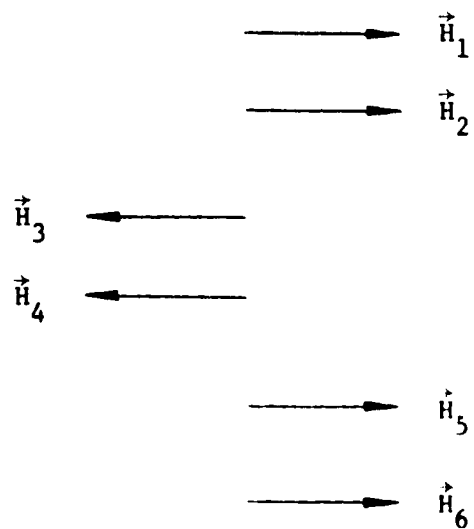
$$\dot{\delta}_{1(i)} = \dot{\delta}_{1(i)}^{(CL)} + K_{SA} \dot{\delta}_{1(i)}^{(SA)} \quad (46)$$

$$\dot{\delta}_{3(i)} = \dot{\delta}_{3(i)}^{(CL)} + K_{SA} \dot{\delta}_{3(i)}^{(SA)} \quad (47)$$

$\dot{\delta}_{1(i)}^{(CL)}$ and $\dot{\delta}_{3(i)}^{(CL)}$ are the inner and outer CMG gimbal rate commands that are generated by the CMG control law logic. $\dot{\delta}_{1(i)}^{(SA)}$ and $\dot{\delta}_{3(i)}^{(SA)}$ are the gimbal rate commands that are used by the singularity avoidance scheme to redistribute the CMG gimbals. The resultant



(a) Saturation



(b) Anti-Parallel Singularity

Figure 9.3. Singularity Conditions for a Double Gimbal CMG System

torque generated by the gimbal rate commands $\dot{\delta}_{1(i)}^{(SA)}$ and $\dot{\delta}_{3(i)}^{(SA)}$ is zero therefore, in general any singularity avoidance scheme can be used with any CMG control law. The gain K_{SA} is sized so that the combined CMG gimbal rate commands $\dot{\delta}_{1(i)}$ and $\dot{\delta}_{3(i)}$ will not exceed the CMG gimbal rate limits due to $\dot{\delta}_{1(i)}^{(SA)}$ and $\dot{\delta}_{3(i)}^{(SA)}$.

9.4 CMG Control Laws - In this report, the following four CMG control laws are derived:

- a. Cross Product CMG Control Law
- b. H-Vector CMG Control Law
- c. Decoupled Scissored Pair CMG Control Law
- d. Decoupled Pseudo-Inverse CMG Control Law

Each of the above control laws are derived for both proposed CMG operational modes: (1) when the CMGs are operated in slaved pairs and (2) when the CMGs are operated as six individual actuators.

9.4.1 Cross Product CMG Control Law - The Cross Product CMG Control Law is an open-loop, nonideal control law. This control law is developed for an inertially held vehicle and is then modified to handle the case of a rotating vehicle. This control law is nonideal because the resultant control torque \vec{T}_{CMG} in general does not equal the torque command \vec{T}_{COM} . As illustrated in figure 9.4, \vec{T}_{CMG} consists of two components: (1) \vec{T}_{cp} , an undesirable component perpendicular to \vec{T}_{COM} and (2) \vec{T}'_{CMG} , a component along the desired torque \vec{T}_{COM} . Figure 9.5 is a block diagram of the corresponding vehicle control loop. Note that because the CMG control law is open-loop, the unwanted torque \vec{T}_{cp} gets applied directly to the vehicle as a disturbance torque and thus degrades system performance. \vec{T}_{cp} is driven towards zero by the action of the control loop being closed through the vehicle dynamics. The torque component \vec{T}'_{CMG} acting along \vec{T}_{COM} does not in general equal \vec{T}_{COM} , its magnitude is a function of the CMG gimbal angles. The

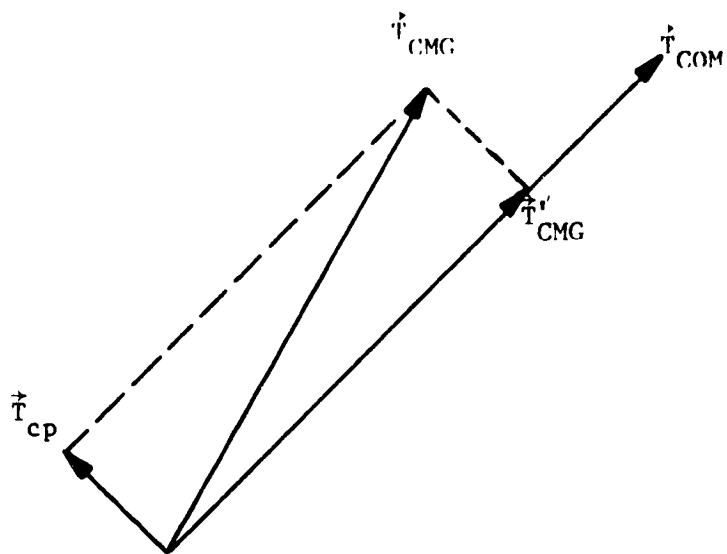


Figure 9.4. Relationship Between Cross Product
CMG Control Torque \vec{T}_{CMG} and \vec{T}_{COM}

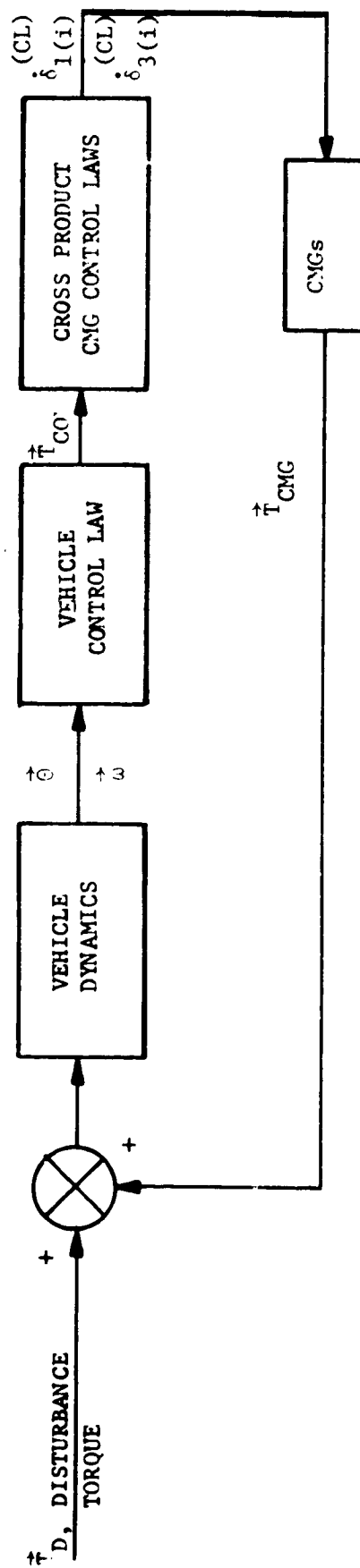


Figure 9.5. Cross Product CMG Control Law Vehicle Control Loops

open-loop CMG control law gain $\frac{\dot{\vec{T}}_{CMG}}{\vec{T}_{COM}}$ is a function of the CMG gimbal

angles and therefore, the bandwidth of the vehicle control loop is also a function of the CMG gimbal angles. The chief advantage of this CMG control law is that it can be implemented in an analog manner, thus not requiring a digital computer.

A DCCMG with a constant wheel speed ($\dot{(\vec{H})}_r = 0$) can generate a torque only in the plane perpendicular to its wheel momentum \vec{H} . The Cross Product CMG Control Law commands each individual CMG to generate a control torque \vec{T}_{ci} that is proportional to the component of the command torque \vec{T}_{COM} perpendicular to \vec{H} . The resultant CMG control torque \vec{T}_{CMG} equals the summation of the individual CMG torque \vec{T}_{ci} ($\vec{T}_{CMG} = \sum_{i=1}^n \vec{T}_{ci}$). To understand the operation of the Cross Product CMG Control Law, the CMG gimbal rate commands $\dot{\delta}_{1(i)}^{(CL)}$ and $\dot{\delta}_{3(i)}^{(CL)}$ are computed for the i^{th} CMG and the results are applied to the specific CMG configuration shown in figure 9.1.

For the i^{th} CMG, the torque that is exerted on the inner gimbal \vec{H}_{Ii} equals

$$\dot{\vec{H}}_{Ii} = \vec{\omega}_{Ii} \times \vec{H}_{Ii} \quad (48)$$

where $\vec{\omega}_{Ii}$ is the rotational rate of the i^{th} CMG inner gimbal. To minimize the magnitude of $\dot{\vec{H}}_{Ii}$, $\vec{\omega}_{Ii}$ is constrained to lie in the plane perpendicular to \vec{H} and therefore $\dot{\vec{H}}_{Ii}$ is also perpendicular to \vec{H}_{Ii} as illustrated in figure 9.6. \vec{H}_{Ii} as a function of the torque command \vec{T}_{COM} can be written as

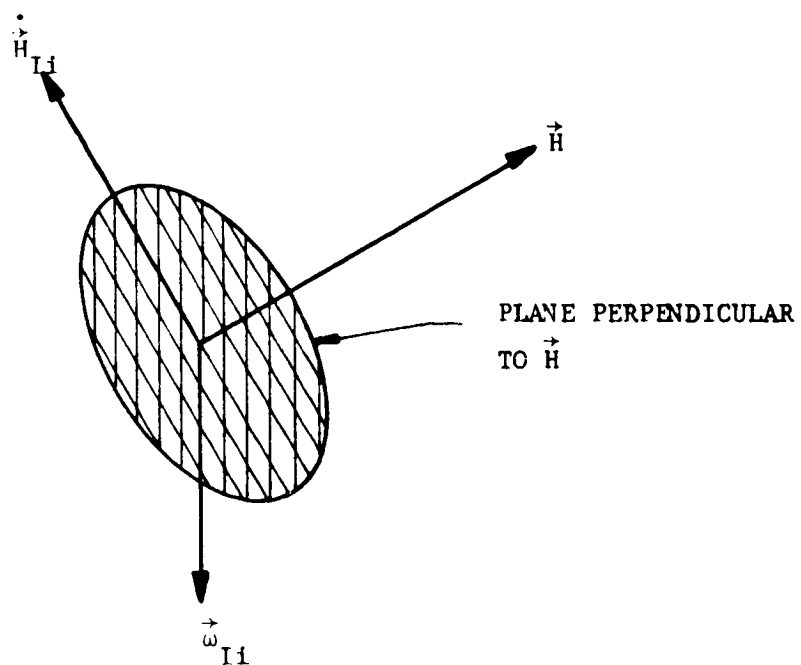


Figure 9.6. Relative Orientations of $\vec{\omega}_{I1}$, $\dot{\vec{H}}_{I1}$, and \vec{H}

$$\dot{\vec{H}}_{I1} = (\hat{i}_H \times K_1 \vec{T}_{COM1}) \times \hat{i}_H \quad (49)$$

\hat{i}_H is a unit vector along the CMG wheel momentum \vec{H} in inner gimbal space ($\hat{i}_H = \frac{\vec{H}}{|\vec{H}|}$), K_1 is a control law gain associated with the i^{th}

CMG, and \vec{T}_{COM1} equals $-\vec{T}_{COM}$ transformed into the i^{th} CMG inner gimbal space. \vec{T}_{COM1} equals the negative of \vec{T}_{COM} transformed into inner gimbal space because it is the reaction torque $-\dot{\vec{H}}_{I1}$ that gets transferred to the vehicle. \vec{T}_{COM1} equals

$$\vec{T}_{COM1} = -[\phi]_{I+O} [\phi]_{O+B} [\phi]_{V+BI}^{-1} \vec{T}_{COM} \quad (50)$$

At this point, the Cross Product CMG Control Law can be corrected for any rotational motion of the vehicle by replacing \vec{T}_{COM} in equation 50 with $\vec{T}_{COM} - \vec{\omega} \times \vec{H}_{CMG}$. \vec{H}_{CMG} is the total CMG system momentum imparted to the vehicle. Correcting for the rotational motion of the vehicle, \vec{T}_{COM1} equals

$$\vec{T}_{COM1} = -[\phi]_{I+O} [\phi]_{O+B} [\phi]_{V+BI}^{-1} (\vec{T}_{COM} - \vec{\omega} \times \vec{H}_{CMG}) \quad (51)$$

From figure 9.6, the magnitude of $\vec{\omega}_{I1}$ equals

$$|\vec{\omega}_{I1}| = \frac{|\dot{\vec{H}}_{I1}|}{|\vec{H}|} \quad (52)$$

$\vec{\omega}_{I1}$ can be written as the following vector cross product

$$\vec{\omega}_{I1} = |\vec{\omega}_{I1}| (\hat{i}_H \times \frac{\dot{\vec{H}}_{I1}}{|\dot{\vec{H}}_{I1}|}) = \frac{1}{|\vec{H}|^2} (\vec{H} \times \dot{\vec{H}}_{I1}) \quad (53)$$

Substituting equation 49 into 53, $\vec{\omega}_{I1}$ becomes

$$\begin{aligned}\vec{\omega}_{I1} &= \frac{1}{|\vec{H}|^2} \{ \vec{H} \times [(\hat{i}_H \times K_1 \vec{T}_{COM1}) \times \hat{i}_H] \} \\ &= \frac{1}{|\vec{H}|^2} \{ \vec{H} \times K_1 \vec{T}_{COM1} \}\end{aligned}\quad (54)$$

Since \vec{H} is $(0, H, 0)$, $\vec{\omega}_{I1}$ equals

$$\vec{\omega}_{I1} = \frac{K_1}{H} (T_{COM1z} \hat{i} - T_{COM1x} \hat{k}) \quad (55)$$

where T_{COM1x} and T_{COM1z} are the X and Z components of \vec{T}_{COM1} , respectively. Using equation 14, the corresponding inner and outer gimbal rate commands $\dot{\delta}_{1(1)}^{(CL)}$ and $\dot{\delta}_{3(1)}^{(CL)}$ needed to generate $\vec{\omega}_{I1}$ are:

$$\dot{\delta}_{1(1)}^{(CL)} = \omega_{I1x} = -\frac{K_1}{H} T_{COM1z} \quad (56)$$

$$\dot{\delta}_{3(1)}^{(CL)} = \frac{\omega_{I1z}}{\cos \delta_{1(1)}} = -\frac{K_1 \sec \delta_{1(1)}}{H} T_{COM1x} \quad (57)$$

ω_{I1x} and ω_{I1z} are the X and Z components of $\vec{\omega}_{I1}$, respectively.

The gimbal rate commands $\dot{\delta}_{1(1)}^{(CL)}$ and $\dot{\delta}_{3(1)}^{(CL)}$ can be computed for both CMG operational modes, the slaved mode and the six individual CMG modes, by solving equations 51, 56, and 57.

Slaved CMG Mode - Substitute the following slaved CMG gimbal angles $\vec{\delta}_1$ and $\vec{\delta}_3$ for the individual CMG gimbal angles $\delta_{1(1)}$ and $\delta_{3(1)}$.

$$\vec{\delta}_1 = \begin{bmatrix} \delta_{1x} \\ \delta_{1y} \\ \delta_{1z} \end{bmatrix} = \begin{bmatrix} \frac{k_1 \delta_{1(1)} + k_2 \delta_{1(2)}}{k_1 + k_2} \\ \frac{k_3 \delta_{1(3)} + k_4 \delta_{1(4)}}{k_3 + k_4} \\ \frac{k_5 \delta_{1(5)} + k_6 \delta_{1(6)}}{k_5 + k_6} \end{bmatrix} \quad (58)$$

$$\vec{\delta}_3 = \begin{bmatrix} \delta_{3x} \\ \delta_{3y} \\ \delta_{3z} \end{bmatrix} = \begin{bmatrix} \frac{k_1 \delta_{3(1)} + k_2 \delta_{3(2)}}{k_1 + k_2} \\ \frac{k_3 \delta_{3(3)} + k_4 \delta_{3(4)}}{k_3 + k_4} \\ \frac{k_5 \delta_{3(5)} + k_6 \delta_{3(6)}}{k_5 + k_6} \end{bmatrix} \quad (59)$$

The gains k_i ($i=1, \dots, 6$) describe the status of the CMG system,

$$k_i = 1 \quad (60)$$

when the i^{th} CMG is operational and

$$k_i = 0 \quad (61)$$

when the i^{th} CMG is inoperative. The gains k_i should not be confused with the control law gains K_i . By initially neglecting the CMG control law gains K_i , equations 51, 56, and 57 can be solved for an intermediate set of gimbal rate commands $\dot{\delta}_1^I$ and $\dot{\delta}_3^I$.

$$\dot{\delta}_1^I = \begin{bmatrix} \dot{\delta}_{1x}^I \\ \dot{\delta}_{1y}^I \\ \dot{\delta}_{1z}^I \end{bmatrix} = \frac{1}{H} [A']^T (\vec{T}_{\text{COM}} - \vec{\omega} \times \vec{H}_{\text{CMG}}) \quad (62)$$

$$\dot{\delta}_3^I = \begin{bmatrix} \dot{\delta}_{3x}^I \\ \dot{\delta}_{3y}^I \\ \dot{\delta}_{3z}^I \end{bmatrix} = \frac{1}{H} [S^2] [B']^T (\vec{T}_{\text{COM}} - \vec{\omega} \times \vec{H}_{\text{CMG}}) \quad (63)$$

where

$$[S^2] = \begin{bmatrix} \sec^2 \delta_{1x} & 0 & 0 \\ 0 & \sec^2 \delta_{1y} & 0 \\ 0 & 0 & \sec^2 \delta_{1z} \end{bmatrix} \quad (64)$$

[A'] and [B'] were previously defined in equations 43 and 44 respectively. \vec{H}_{CMG} is defined in equation 45. The resultant CMG gimbal rate commands $\dot{\delta}_{1(i)}^{(CL)}$ and $\dot{\delta}_{3(i)}^{(CL)}$ equal

$$\dot{\delta}_1^{(1)(CL)} = \begin{bmatrix} \dot{\delta}_{1(1)}^{(CL)} \\ \dot{\delta}_{1(3)}^{(CL)} \\ \dot{\delta}_{1(5)}^{(CL)} \end{bmatrix} = -[K^{(1)}] \dot{\delta}_1^I \quad (65)$$

$$\dot{\delta}_3^{(1)(CL)} = \begin{bmatrix} \dot{\delta}_{3(1)}^{(CL)} \\ \dot{\delta}_{3(3)}^{(CL)} \\ \dot{\delta}_{3(5)}^{(CL)} \end{bmatrix} = -[K^{(1)}] \dot{\delta}_3^I \quad (66)$$

$$\dot{\delta}_1^{(2)(CL)} = \begin{bmatrix} \dot{\delta}_{1(2)}^{(CL)} \\ \dot{\delta}_{1(4)}^{(CL)} \\ \dot{\delta}_{1(6)}^{(CL)} \end{bmatrix} = -[K^{(2)}] \dot{\delta}_1^I \quad (67)$$

$$\dot{\delta}_3^{(2)(CL)} = \begin{bmatrix} \dot{\delta}_{3(2)}^{(CL)} \\ \dot{\delta}_{3(4)}^{(CL)} \\ \dot{\delta}_{3(6)}^{(CL)} \end{bmatrix} = -[K^{(2)}] \dot{\delta}_3^I \quad (68)$$

where

$$[K^{(1)}] = \begin{bmatrix} k_1 K_1 & 0 & 0 \\ 0 & k_3 K_3 & 0 \\ 0 & 0 & k_5 K_5 \end{bmatrix} \quad (69)$$

$$[K^{(2)}] = \begin{bmatrix} k_2 K_2 & 0 & 0 \\ 0 & k_4 K_4 & 0 \\ 0 & 0 & k_6 K_6 \end{bmatrix} \quad (70)$$

Six Individual CMG Mode - Solving equations 51, 56, and 57,

the resultant CMG gimbal rate commands $\dot{\delta}_1^{(1)}(CL)$, $\dot{\delta}_3^{(1)}(CL)$, $\dot{\delta}_1^{(2)}(CL)$, and $\dot{\delta}_3^{(2)}(CL)$ for this operational mode are:

$$\dot{\delta}_1^{(1)}(CL) = \frac{1}{H} [K^{(1)}] [A]^T (\vec{T}_{COM} - \vec{\omega} \times \vec{H}_{CMG}) \quad (71)$$

$$\dot{\delta}_3^{(1)}(CL) = \frac{1}{H} [K^{(1)}] [S^{2(1)}] [B]^T (\vec{T}_{COM} - \vec{\omega} \times \vec{H}_{CMG}) \quad (72)$$

$$\dot{\delta}_1^{(2)}(CL) = \frac{1}{H} [K^{(2)}] [C]^T (\vec{T}_{COM} - \vec{\omega} \times \vec{H}_{CMG}) \quad (73)$$

$$\dot{\delta}_3^{(2)}(CL) = \frac{1}{H} [K^{(2)}] [S^{2(2)}] [D]^T (\vec{T}_{COM} - \vec{\omega} \times \vec{H}_{CMG}) \quad (74)$$

where

$$[S^{2(1)}] = \begin{bmatrix} \sec^2 \delta_{1(1)} & 0 & 0 \\ 0 & \sec^2 \delta_{1(3)} & 0 \\ 0 & 0 & \sec^2 \delta_{1(5)} \end{bmatrix} \quad (75)$$

$$[S^{2(2)}] = \begin{bmatrix} \sec^2 \delta_{1(2)} & 0 & 0 \\ 0 & \sec^2 \delta_{1(4)} & 0 \\ 0 & 0 & \sec^2 \delta_{1(6)} \end{bmatrix} \quad (76)$$

[A], [B], [C], and [D] are defined in equations 34, 35, 36, and 37, respectively. \vec{H}_{CMG} for this individual CMG mode is defined in equation 39.

Control Law Gain K_i selection - The control law gains K_i are

determined on the basis of system stability and response characteristics. One method of selecting these gains K_i is to choose them so that for the zero CMG gimbal condition ($\delta_{1(i)} = \delta_{3(i)} = 0$), the resultant CMG control torque \vec{T}_{CMG} equals the command torque \vec{T}_{COM} . For the zero gimbal condition, the individual CMG torques \vec{T}_{ci} are:

$$\vec{T}_{c1} = K_1 (T_{COMy} \hat{j} + T_{COMz} \hat{k}) \quad (77)$$

$$\vec{T}_{c2} = K_2 (T_{COMy} \hat{j} + T_{COMz} \hat{k}) \quad (78)$$

$$\vec{T}_{c3} = K_3 (T_{COMx} \hat{i} + T_{COMz} \hat{k}) \quad (79)$$

$$\vec{T}_{c4} = K_4 (T_{COMx} \hat{i} + T_{COMz} \hat{k}) \quad (80)$$

$$\vec{T}_{c5} = K_5 (T_{COMx} \hat{i} + T_{COMy} \hat{j}) \quad (81)$$

$$\vec{T}_{c6} = K_6 (T_{COMx} \hat{i} + T_{COMy} \hat{j}) \quad (82)$$

Note that \vec{T}_{ci} is proportional to the portion of \vec{T}_{COM} that is perpendicular to its corresponding i^{th} wheel momentum \vec{H}_i .

The resultant CMG control torque \vec{T}_{CMG} equals:

$$\begin{aligned} \vec{T}_{CMG} = \sum_{i=1}^6 \vec{T}_{ci} &= (K_3 + K_4 + K_5 + K_6) T_{COMx} \hat{i} \\ &+ (K_1 + K_2 + K_5 + K_6) T_{COMy} \hat{j} + (K_1 + K_2 + K_3 + K_4) T_{COMz} \hat{k} \end{aligned} \quad (83)$$

By selecting

$$K_i = 0.25 \quad (84)$$

The control torque \vec{T}_{CMG} equals \vec{T}_{COM} . Depending on the orientation of the CMGs, \vec{T}_{CMG} the component of \vec{T}_{CMG} along \vec{T}_{COM} can exceed the desired torque command \vec{T}_{COM} . When the individual CMG momentum vectors \vec{H}_i are perpendicular to the desired torque \vec{T}_{COM} , \vec{T}_{CMG} is a maximum and equals $1.5 \vec{T}_{COM}$. For this orientation, \vec{T}_{cp} is zero.

Another method of selecting the control law gains K_i is to note that \vec{T}_{ci} , the torque produced by the i^{th} CMG, equals

$$\vec{T}_{ci} = K_i (\vec{T}_{COM} - \vec{T}_{COM} \cdot \hat{i}_{Hi}) \quad (85)$$

where \hat{i}_{Hi} is a unit vector in vehicle space along the i^{th} CMG wheel momentum \vec{H}_i .

$$\hat{i}_{Hi} = \frac{\vec{H}_i}{H} \quad (86)$$

The total CMG control torque \vec{T}_{CMG} equals

$$\vec{T}_{CMG} = \sum_{i=1}^6 K_i (\vec{T}_{COM} - \vec{T}_{COM} \cdot \hat{i}_{Hi}) \quad (87)$$

By selecting

$$K_i = 0.167 \quad (88)$$

\vec{T}_{CMG} equals \vec{T}_{COM} plus an undesired torque

$$- \sum_{i=1}^6 K_i \vec{T}_{COM} \cdot \hat{i}_{Hi} \quad (89)$$

It should be noted that the above undesired torque component does not correspond to the previously unwanted torque \vec{T}_{cp} . This undesired torque given in equation 89 in general will have a component that is in the opposite direction of \vec{T}_{COM} . Only when the individual CMG momentum vectors \vec{H}_i are all perpendicular to \vec{T}_{COM} will \vec{T}_{CMG} and \vec{T}_{COM} equal \vec{T}_{COM} .

9.4.2 H-Vector CMG Control Law - The H-vector CMG Control Law is a modification of the previously defined Cross Product CMG Control Law. Figure 9.7 is a block diagram of the corresponding H-vector vehicle control loop. A feedback path is added from the output of the CMG cluster to the input of the Cross Product Control Law. This feedback path compares the momentum state of the CMGs with a desired momentum state \vec{H}_{COM} . \vec{H}_{COM} is computed

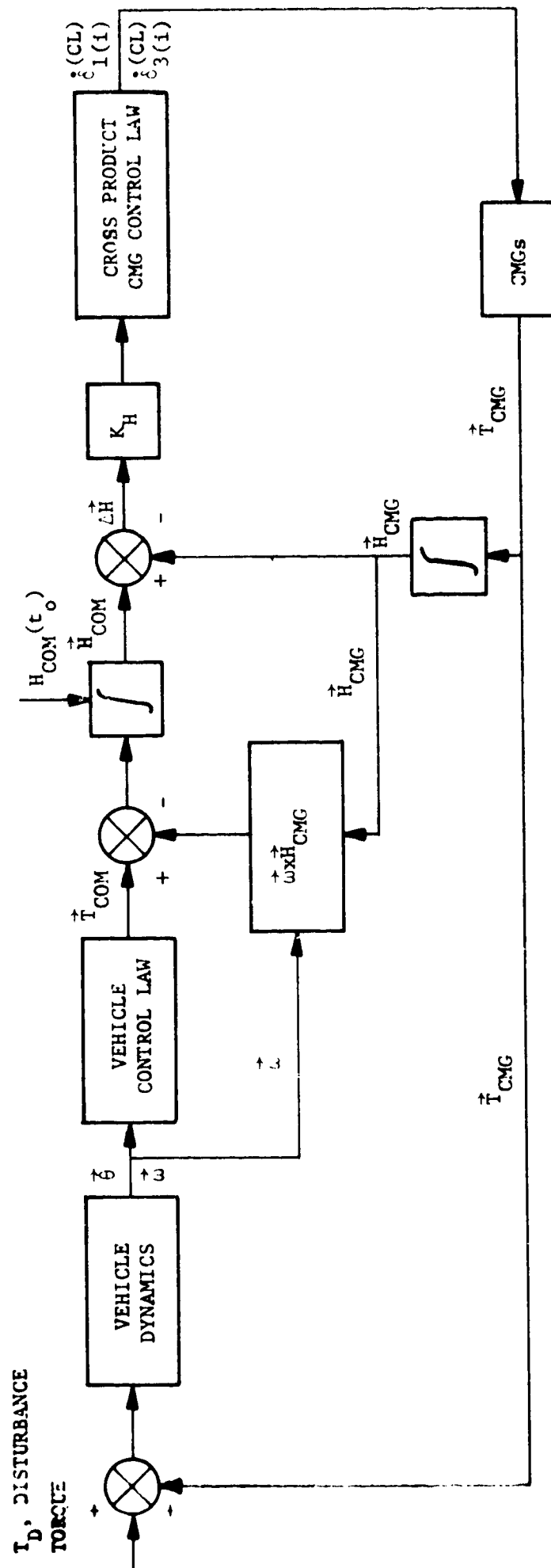


Figure 9.7. H-Vector CMG Control Law Vehicle Control Loop

by integrating with respect to time the torque command \vec{T}_{COM} generated by the vehicle control law. A signal $\Delta\vec{H}$ proportional to the difference between \vec{H}_{COM} and \vec{H}_{CMG} is fed to the Cross Product Control Law as a torque command. The $\vec{\omega} \times \vec{H}_{CMG}$ term shown in figure 9.7 is used to compensate for any rotational motion of the vehicle. The advantage of instrumenting the Cross Product Control Law in this manner is that by selecting an appropriate value for the gain K_H shown in figure 9.7 the response of the inner loop can be made to be much faster than that of the outer vehicle control loop. This faster inner loop tends to compensate for the undesirable cross product torque \vec{T}_{cp} before it can adversely affect the outer vehicle loop thus, improving vehicle performance. The H-Vector CMG Control Law like the Cross Product CMG Control Law can also be instrumented in an analog fashion.

The CMG momentum \vec{H}_{CMG} is the angular momentum that the CMG system transfers to the vehicle. \vec{H}_{CMG} is computed using the outputs of the CMG gimbal resolver trains. \vec{H}_{CMG} equals

$$\vec{H}_{CMG} = \sum_{i=1}^6 k_i [\phi]_{v+bi} [\phi]_{o+b}^{-1} [\phi]_{i+o}^{-1} (-\vec{H}) \quad (90)$$

where k_i are the operational status gains defined in equation 60 and 61. For the slaved CMG mode,

$$\begin{aligned} \vec{H}_{CMG} = & k_x H \begin{bmatrix} -\cos \delta_{1x} & \cos \delta_{3x} \\ \cos \delta_{1x} & \sin \delta_{3x} \\ \sin \delta_{1x} & \end{bmatrix} + k_y H \begin{bmatrix} \sin \delta_{1y} \\ -\cos \delta_{1y} & \cos \delta_{3y} \\ \cos \delta_{1y} & \sin \delta_{3y} \end{bmatrix} \\ & + k_z H \begin{bmatrix} \cos \delta_{1z} & \sin \delta_{3z} \\ \sin \delta_{1z} \\ -\cos \delta_{1z} & \cos \delta_{3z} \end{bmatrix} \quad (91) \end{aligned}$$

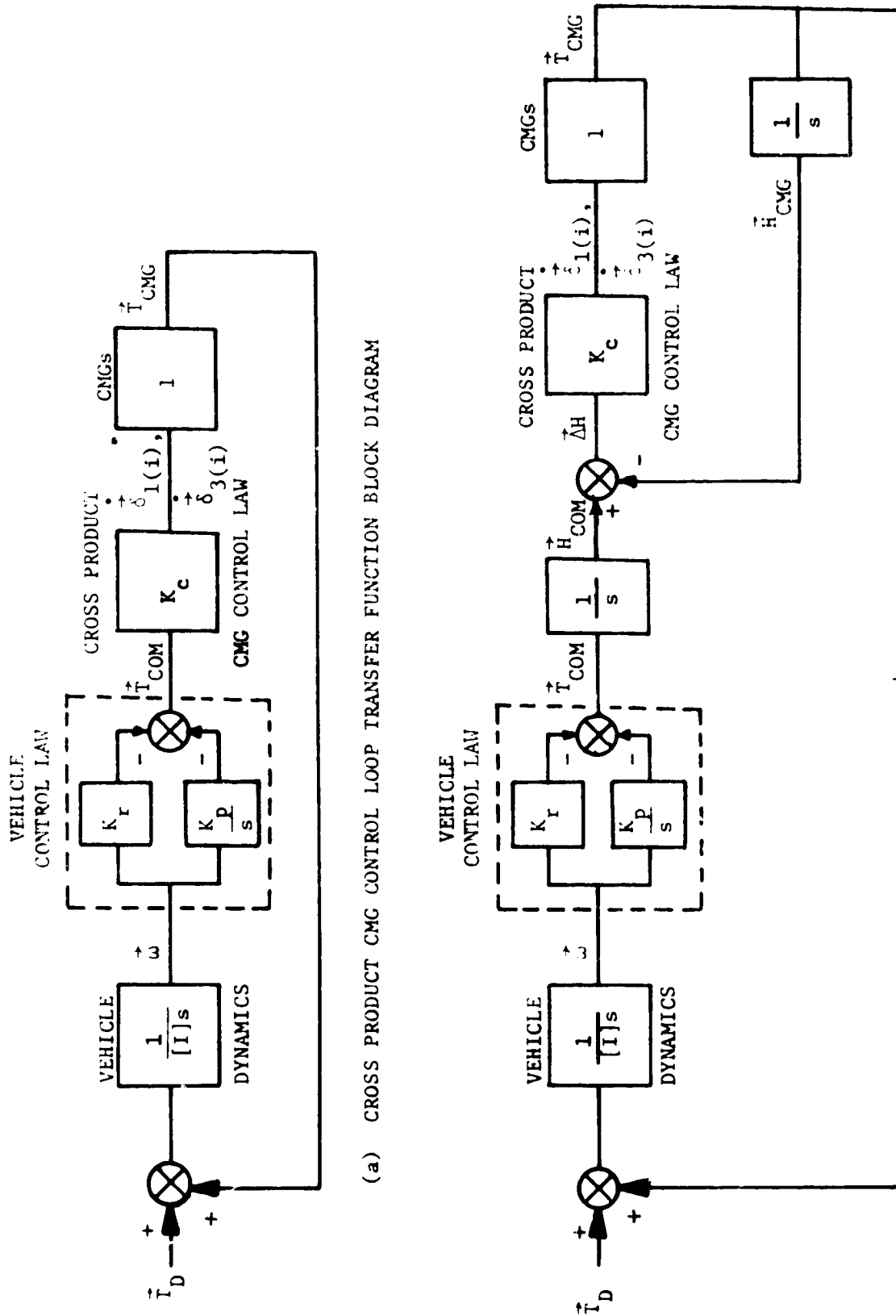
where

$$\begin{aligned} k_x &= k_1 + k_2 \\ k_y &= k_3 + k_4 \\ k_z &= k_5 + k_6 \end{aligned} \quad (92)$$

For the six individual CMG mode,

$$\begin{aligned} \vec{H}_{CMG} &= k_1 H \begin{bmatrix} -\cos\delta_{1(1)} \cos\delta_{3(1)} \\ \cos\delta_{1(1)} \sin\delta_{3(1)} \\ \sin\delta_{1(1)} \end{bmatrix} + k_2 H \begin{bmatrix} -\cos\delta_{1(2)} \cos\delta_{3(2)} \\ \cos\delta_{1(2)} \sin\delta_{3(2)} \\ \sin\delta_{1(2)} \end{bmatrix} \\ &+ k_3 H \begin{bmatrix} \sin\delta_{1(3)} \\ -\cos\delta_{1(3)} \cos\delta_{3(3)} \\ \cos\delta_{1(3)} \sin\delta_{3(3)} \end{bmatrix} + k_4 H \begin{bmatrix} \sin\delta_{1(4)} \\ -\cos\delta_{1(4)} \cos\delta_{3(4)} \\ \cos\delta_{1(4)} \sin\delta_{3(4)} \end{bmatrix} \\ &+ k_5 H \begin{bmatrix} \cos\delta_{1(5)} \sin\delta_{3(5)} \\ \sin\delta_{1(5)} \\ -\cos\delta_{1(6)} \cos\delta_{3(5)} \end{bmatrix} + k_6 H \begin{bmatrix} \cos\delta_{1(6)} \sin\delta_{3(6)} \\ \sin\delta_{1(6)} \\ -\cos\delta_{1(6)} \cos\delta_{3(6)} \end{bmatrix} \end{aligned} \quad (93)$$

The addition of this H-vector path around the Cross Product CMG Control Law can result in a low gain system instability. For the following analysis assume that the vehicle is being held in an inertial attitude; the $\vec{\omega} \times \vec{H}_{CMG}$ term is zero. Figure 9.8 contains the transfer function block diagrams of the vehicle control loops with and without this feedback path. The gain K_c represents the Cross Product CMG Control Law; this gain K_c varies as a function of the direction of \vec{T}_{COM} relative to the orientations of the individual CMG wheel momentum vectors \vec{H}_i . For the H-vector CMG control loop, the gain K_H is included in K_c .



(a) CROSS PRODUCT CMG CONTROL LOOP TRANSFER FUNCTION BLOCK DIAGRAM

(b) H-VECTOR CMG CONTROL LOOP TRANSFER FUNCTION BLOCK DIAGRAM

Figure 9.8. Cross Product and H-Vector CMG Control Law Block Diagrams

For the Cross Product CMG control loop, figure 9.8.a, the transfer function $\frac{\vec{T}_{CMG}}{\vec{T}_D}$ equals

$$\frac{\vec{T}_{CMG}}{\vec{T}_D} = \frac{\frac{K_c K_r}{I} (s + \frac{K_p}{K_r})}{s^2 + \frac{K_c K_r}{I} s + \frac{K_c K_p}{I}} \quad (94)$$

The system's characteristic equation is

$$s^2 + \frac{K_c K_r}{I} s + \frac{K_c K_p}{I} = 0 \quad (95)$$

Using Routh's stability criteria, the range of K_c for which the system is stable can be computed; the corresponding Routh array is

$$\begin{array}{c|cc} s^2 & 1 & \frac{K_c K_r}{I} \\ s^1 & \frac{K_c K_p}{I} & \\ s^0 & \frac{K_c K_r}{I} & \end{array}$$

Routh's criterion states: The number of roots of the characteristic equation with positive real parts is equal to the number of changes of sign of the coefficients in the first column.¹ If there are no sign changes in the first column, there are no characteristic roots with positive real parts and the system is stable. Noting that the vehicle control law gains $K_r K_p$ and the vehicle inertia I are positive quantities, the cross product CMG control system is stable as long as the control law gain K_c is also positive; all of the coefficients in the first column are positive. Because it is physically impossible for K_c to go negative, the system will not go unstable due to a change in K_c .

¹ D'Azzo and Houpis, Feedback Control System Analysis and Synthesis, second edition, McGraw-Hill, 1966, p. 123.

For the H-vector CMG control loop, figure 9.8.b, the transfer function $\frac{\vec{T}_{CMG}}{\vec{T}_D}$ equals

$$\frac{\vec{T}_{CMG}}{\vec{T}_D} = \frac{\frac{K_c K_r}{I} (s + \frac{K_p}{K_r})}{s^3 + K_c s^2 + \frac{K_c K_r}{I} s + \frac{K_c K_p}{I}} \quad (96)$$

The system's characteristic equation is

$$s^3 + K_c s^2 + \frac{K_c K_r}{I} s + \frac{K_c K_p}{I} = 0 \quad (97)$$

The corresponding Routh array is

$$\begin{array}{l|ll} s^3 & 1 & \frac{K_c K_r}{I} \\ \textcircled{1} s^2 & K_c & \frac{K_c K_p}{I} \\ \textcircled{2} s^1 & \frac{K_c K_r - K_p}{I} & \\ \textcircled{3} s^0 & \frac{K_c K_p}{I} & \end{array}$$

From the Routh stability conditions $\textcircled{1}$ and $\textcircled{3}$, the control law gain K_c must be greater than zero ($K_c > 0$). From stability condition

$\textcircled{2}$,

$$\frac{K_c K_r - K_p}{I} > 0$$

or

$$K_c > \frac{K_p}{K_r} \quad (98)$$

From section 7, the ratio $\frac{K_p}{K_r}$ equals 0.121 which means that in order for the H-vector CMG control loop to be stable K_c must exceed 0.121. Normally, this gain K_c will be considerably larger than the above limit. K_c will only approach this value when the CMGs approach saturation or approach the undesired anti-parallel condition. Since both of these conditions must be avoided for all double gimbal CMG systems, this low gain instability of the H-vector CMG control loop is not a very important trade consideration.

9.4.3 Decoupled Scissored Pair CMG Control Law - The Decoupled Scissored Pair CMG Control Law is a digital law requiring a digital computer. This control law is decoupled meaning that the resultant CMG control torque \vec{T}_{CMG} equals the torque command \vec{T}_{COM} assuming that the actual CMG gimbal rates equal the gimbal rate commands $\dot{\delta}_{1(i)}$ and $\dot{\delta}_{3(i)}$. Figure 9.9 is the corresponding vehicle control loop block diagram showing the required analog to digital (A/D) and digital to analog (D/A) digital computer interfaces.

The Decoupled Scissored Pair CMG Control Law groups the CMGs into pairs; each CMG is paired with the remaining CMGs. For example, a three CMG system (e.g., the slaved CMG operational mode) has three CMG pairs and a six CMG system (e.g., the individual CMG operational mode) has fifteen CMG pair combinations. The control law commands each CMG pair to generate a portion of the torque command \vec{T}_{COM} based on the pair's remaining momentum storage capability.

To understand how the Decoupled Scissored Pair CMG Control Law operates assume that CMG 1 and 2 form a CMG pair. Figure 9.10 is a sketch of the CMG reaction momentum ($-\vec{H}$) vectors \vec{H}_1 and \vec{H}_2 in vehicle space corresponding to CMG 1 and 2, respectively. \vec{H}_{12} is the vector sum of \vec{H}_1 and \vec{H}_2 . A torque \vec{T}_{12r} perpendicular to \vec{H}_{12} can be produced by rotating the vector sum \vec{H}_{12} at an angular rate ω_{12r} .

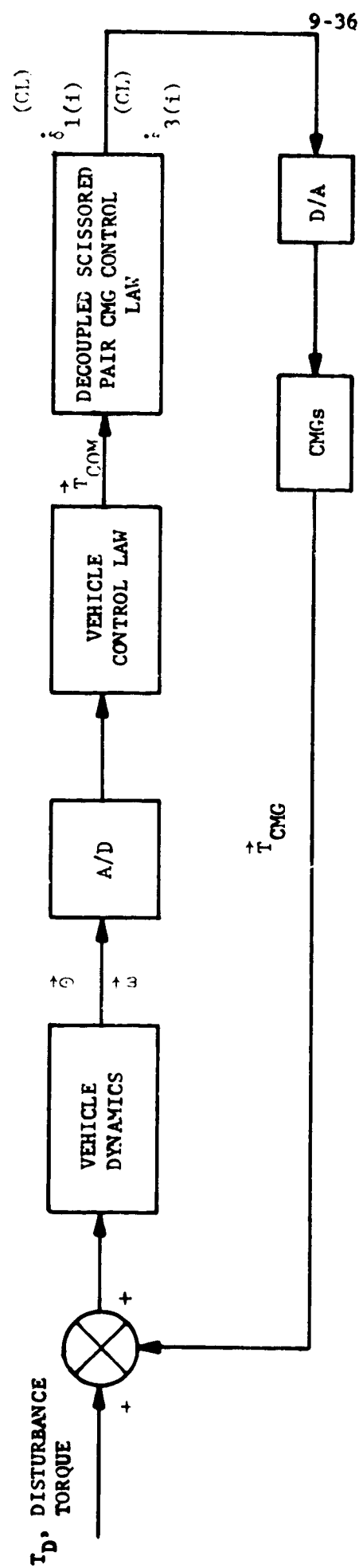
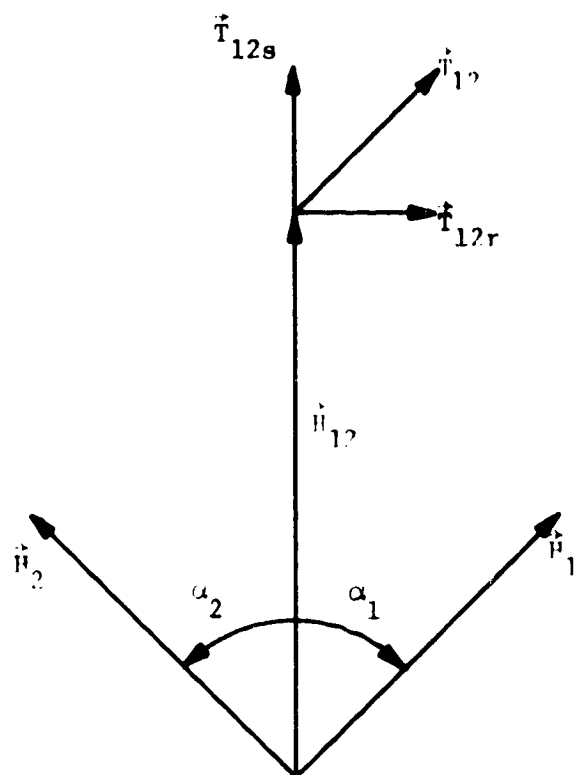


Figure 9.9. Decoupled Scissored Pair CMG Control Law Vehicle Control Loop



Note: A counterclockwise rotation is assumed to be positive.

Figure 9.10. CMG Scissored Pair 1, 2

$$\vec{T}_{12r} = \vec{\omega}_{12r} \times \vec{H}_{12} \quad (99)$$

\vec{T}_{12r} and $\vec{\omega}_{12r}$ are orthogonal and lie in a plane perpendicular to \vec{H}_{12} . \vec{T}_{12r} as a function of the torque command \vec{T}_{COM} equals

$$\vec{T}_{12r} = \left[\frac{\vec{H}_{12}}{|\vec{H}_{12}|} \times K_{12} \vec{T}_{COM} \right] \times \frac{\vec{H}_{12}}{|\vec{H}_{12}|} \quad (100)$$

K_{12} is a fractional gain ($K_{12} < 1$) indicating the portion of \vec{T}_{COM} that the CMG pair is to generate. K_{12} is based on the remaining momentum storage capability of the CMG pair along \vec{H}_{12} . $\vec{\omega}_{12r}$ equals

$$\vec{\omega}_{12r} = \frac{\vec{H}_{12}}{|\vec{H}_{12}|} \times K_{12} \vec{T}_{COM} \quad (101)$$

The remaining component of $K_{12} \vec{T}_{COM}$ along \vec{H}_{12} is generated by the scissoring action of \vec{H}_1 and \vec{H}_2 . By closing the scissored pair, the magnitude of \vec{H}_{12} increases producing a torque directed along \vec{H}_{12} . By spreading the scissored pair, the magnitude of \vec{H}_{12} decreases creating a torque directed in the opposite direction of \vec{H}_{12} . The resultant torque generated by the scissoring action is denoted by \vec{T}_{12s} . Using figure 9.10, the magnitude of \vec{H}_{12} is

$$|\vec{H}_{12}| = |\vec{H}_1| \cos \alpha_1 + |\vec{H}_2| \cos \alpha_2 \quad (102)$$

The angles α_1 and α_2 are defined in figure 9.10. The sum of the projection of \vec{H}_1 and \vec{H}_2 perpendicular to \vec{H}_{12} is zero.

$$|\vec{H}_1| \sin \alpha_1 + |\vec{H}_2| \sin \alpha_2 = 0 \quad (103)$$

Differentiating equations 101 and 102 with respect to time,

$$-|\dot{\vec{H}}_1| \dot{\alpha}_1 \sin \alpha_1 - |\dot{\vec{H}}_2| \dot{\alpha}_2 \sin \alpha_2 = |\dot{\vec{H}}_{12}| = |\dot{\vec{T}}_{12s}| \quad (104)$$

$$|\dot{\vec{H}}_1| \dot{\alpha}_1 \cos \alpha_1 + |\dot{\vec{H}}_2| \dot{\alpha}_2 \cos \alpha_2 = 0 \quad (105)$$

Solving equations 104 and 105 for $\dot{\alpha}_1$ and $\dot{\alpha}_2$,

$$\dot{\alpha}_1 = (|\dot{\vec{H}}_2| |\dot{\vec{T}}_{12s}| \cos \alpha_2) / \Delta \quad (106)$$

$$\dot{\alpha}_2 = (|\dot{\vec{H}}_1| |\dot{\vec{T}}_{12s}| \cos \alpha_1) / \Delta \quad (107)$$

where

$$\begin{aligned} \Delta &= |\dot{\vec{H}}_1| |\dot{\vec{H}}_2| (\cos \alpha_1 \sin \alpha_2 - \sin \alpha_1 \cos \alpha_2) \\ &= |\dot{\vec{H}}_1| |\dot{\vec{H}}_2| \sin (\alpha_2 - \alpha_1) = |\dot{\vec{H}}_1 \times \dot{\vec{H}}_2| \end{aligned} \quad (108)$$

The rotational rate $\dot{\omega}_{1s}^{(12)}$ and $\dot{\omega}_{2s}^{(12)}$ associated with $\dot{\alpha}_1$ and $\dot{\alpha}_2$ that result in the desired scissoring action equal

$$\dot{\omega}_{1s}^{(12)} = \dot{\alpha}_1 \frac{(\dot{\vec{H}}_1 \times \dot{\vec{H}}_2)}{|\dot{\vec{H}}_1 \times \dot{\vec{H}}_2|} \frac{\dot{\vec{H}}_{12} \cdot \dot{\vec{T}}_{COM}}{|\dot{\vec{H}}_{12} \cdot \dot{\vec{T}}_{COM}|} \quad (109)$$

$$\dot{\omega}_{2s}^{(12)} = \dot{\alpha}_2 \frac{(\dot{\vec{H}}_1 \times \dot{\vec{H}}_2)}{|\dot{\vec{H}}_1 \times \dot{\vec{H}}_2|} \frac{\dot{\vec{H}}_{12} \cdot \dot{\vec{T}}_{COM}}{|\dot{\vec{H}}_{12} \cdot \dot{\vec{T}}_{COM}|} \quad (110)$$

The cross product term $\frac{(\vec{H}_1 \times \vec{H}_2)}{|\vec{H}_1 \times \vec{H}_2|}$ defines the rotational

axis of $\vec{\omega}_{1s}^{(12)}$ and $\vec{\omega}_{2s}^{(12)}$ perpendicular to the plane containing both \vec{H}_1 and \vec{H}_2 . The dot product term $\frac{\vec{H}_{12} \cdot \vec{T}_{COM}}{|\vec{H}_{12} \cdot \vec{T}_{COM}|}$ indicates whether the

desired scissor torque \vec{T}_{12s} is directed along \vec{H}_{12} or in the opposite direction. Note that $|\vec{H}_{12} \cdot \vec{T}_{COM}|$ equals

$$|\vec{H}_{12} \cdot \vec{T}_{COM}| = \frac{|\vec{H}_{12}| |\vec{T}_{12s}|}{K_{12}} \quad (111)$$

The trigometric functions $\cos \alpha_1$ and $\cos \alpha_2$ in terms of \vec{H}_1 , \vec{H}_2 , and \vec{H}_{12} equal

$$\cos \alpha_1 = \frac{\vec{H}_1 \cdot \vec{H}_{12}}{|\vec{H}_1| |\vec{H}_{12}|} = \frac{|\vec{H}_1|^2 + \vec{H}_1 \cdot \vec{H}_2}{|\vec{H}_1| |\vec{H}_{12}|} \quad (112)$$

$$\cos \alpha_2 = \frac{\vec{H}_2 \cdot \vec{H}_{12}}{|\vec{H}_2| |\vec{H}_{12}|} = \frac{|\vec{H}_2|^2 + \vec{H}_1 \cdot \vec{H}_2}{|\vec{H}_2| |\vec{H}_{12}|} \quad (113)$$

Appropriately combining equation 106 thru 113, $\vec{\omega}_{1s}^{(12)}$ and $\vec{\omega}_{2s}^{(12)}$ equal

$$\vec{\omega}_{1s}^{(12)} = \frac{K_{12} (|\vec{H}_2|^2 + \vec{H}_1 \cdot \vec{H}_2) (\vec{H}_1 \times \vec{H}_2) (\vec{H}_{12} \cdot \vec{T}_{COM})}{|\vec{H}_{12}|^2 |\vec{H}_1 \times \vec{H}_2|^2} \quad (114)$$

$$\vec{\omega}_{2s}^{(12)} = \frac{-K_{12}(|\vec{H}_1|^2 + \vec{H}_1 \cdot \vec{H}_2)(\vec{H}_1 \times \vec{H}_2)(\vec{H}_{12} \cdot \vec{T}_{COM})}{|\vec{H}_{12}|^2 |\vec{H}_1 \times \vec{H}_2|^2} \quad (115)$$

\vec{T}_{12s} equals

$$\vec{T}_{12s} = (\vec{\omega}_{1s}^{(12)} \times \vec{H}_1) + (\vec{\omega}_{2s}^{(12)} \times \vec{H}_2) \quad (116)$$

The desired control torque $K_{12} \vec{T}_{COM}$ equals the sum of \vec{T}_{12r} and \vec{T}_{12s} .

$$\begin{aligned} K_{12} \vec{T}_{COM} &= \vec{T}_{12r} + \vec{T}_{12s} \\ &= (\vec{\omega}_{12r} + \vec{\omega}_{1s}^{(12)}) \times \vec{H}_1 + (\vec{\omega}_{12r} + \vec{\omega}_{2s}^{(12)}) \times \vec{H}_2 \end{aligned} \quad (117)$$

To compute the CMG gimbal rate commands $\dot{\delta}_1(1)$, $\dot{\delta}_3(1)$, $\dot{\delta}_1(2)$, and $\dot{\delta}_3(2)$ needed to generate $K_{12} \vec{T}_{COM}$, the negative of the following CMG rates are transformed from vehicle space to the appropriate CMG gimbal space; the negative sign is needed because it is the reaction torque $-\dot{\vec{H}}$ that is transferred to the vehicle.

$$\text{CMG 1: } \vec{\omega}_1^{(12)} = \vec{\omega}_{12r} + \vec{\omega}_{1s}^{(12)} - \vec{\omega} \quad (118)$$

$$\text{CMG 2: } \vec{\omega}_2^{(12)} = \vec{\omega}_{12r} + \vec{\omega}_{2s}^{(12)} - \vec{\omega} \quad (119)$$

The vehicle angular rate $\vec{\omega}$ is subtracted from the above rates because $\vec{\omega}_{12r}$, $\vec{\omega}_{1s}^{(12)}$, and $\vec{\omega}_{2s}^{(12)}$ are computed with respect to an inertial space. Subtracting $\vec{\omega}$ from $\vec{\omega}_1^{(12)}$ and $\vec{\omega}_2^{(12)}$ is equivalent to subtracting $\vec{\omega} \times \vec{H}_{CMG}$ from the torque command \vec{T}_{COM} . The inner gimbal rotational rates $\vec{\omega}_{I1}$ and $\vec{\omega}_{I2}$ needed to generate $K_{12} \vec{T}_{COM}$ are:

$$\vec{\omega}_{I1} = -[\phi(1)]_{I \leftarrow a} [\phi(1)]_{o \leftarrow b} [\phi(1)]_{v \leftarrow b}^{-1} \vec{\omega}_1^{(12)} \quad (120)$$

$$\vec{\omega}_{I2} = -[\phi_{(2)}]_{I \leftarrow o} [\phi_{(2)}]_{o \leftarrow b} [\phi_{(2)}]_{v \leftarrow b}^{-1} \vec{\omega}_2^{(12)} \quad (121)$$

Using equation 14, the gimbal rate commands $\dot{\delta}_{1(1)}^{(CL)}$, $\dot{\delta}_{3(1)}^{(CL)}$,

$\dot{\delta}_{1(2)}^{(CL)}$ and $\dot{\delta}_{3(2)}^{(CL)}$ are

$$\dot{\delta}_{1(1)}^{(CL)} = \omega_{11X} \quad (122)$$

$$\dot{\delta}_{3(1)}^{(CL)} = \frac{\omega_{11Z}}{\cos \delta_{1(1)}} \quad (123)$$

$$\dot{\delta}_{1(2)}^{(CL)} = \omega_{12X} \quad (124)$$

$$\dot{\delta}_{3(2)}^{(CL)} = \frac{\omega_{12Z}}{\cos \delta_{1(2)}} \quad (125)$$

ω_{11X} and ω_{11Z} and ω_{12X} and ω_{12Z} are the X and Z components of $\vec{\omega}_{I1}$ and $\vec{\omega}_{I2}$, respectively.

Using the above derivation of the Decoupled Scissored Pair CMG

Control Law, the CMG gimbal rate commands $\dot{\delta}_{1(1)}^{(CL)}$ and $\dot{\delta}_{3(1)}^{(CL)}$ for

both operational modes are formulated in the following paragraphs.

Slaved CMG Mode - For this mode of operation, there are effectively only three CMGs. The two CMGs mounted along each vehicle axis can be represented by a single CMG with a momentum equal to the sum of the two individual CMG momentums. The effective CMG momentums

\vec{H}_x , \vec{H}_y , and \vec{H}_z corresponding to the three vehicle axes are:

$$\vec{H}_x = (k_1 + k_2) [\phi_{(x)}]_{v \leftarrow b} [\phi_{(x)}]_{o \leftarrow b}^{-1} [\phi_{(x)}]_{I \leftarrow o}^{-1} (-\vec{H}) \quad (126)$$

$$\vec{H}_y = (k_3 + k_4) [\phi_{(y)}]_{v \leftarrow b} [\phi_{(y)}]_{o \leftarrow b}^{-1} [\phi_{(y)}]_{I \leftarrow o}^{-1} (-\vec{H}) \quad (127)$$

$$\vec{H}_z = (k_5 + k_6) [\phi_{(z)}]_{v \leftarrow b} [\phi_{(z)}]_{o \leftarrow b}^{-1} [\phi_{(z)}]_{I \leftarrow o}^{-1} (-\vec{H}) \quad (128)$$

The transportations $[\phi]_{v \leftarrow b}$, $[\phi]_{o \leftarrow b}$, and $[\phi]_{I \leftarrow o}$ are defined using the appropriate CMG gimbal angles δ_{1x} , δ_{3x} , δ_{1y} , δ_{3y} , δ_{1z} , and δ_{3z} . The gains k_i describe the operational status of the six individual CMGs as defined in equations 60 and 61.

For the slaved CMG mode, three CMG scissored pairs exist: (X,Y), (Y,Z), and (Z,X). The following scissored pair parameters are defined to simplify the computational requirements of the re-

sultant CMG gimbal commands $\delta_{1(i)}^{(Cl)}$ and $\delta_{3(i)}^{(Cl)}$.

Scissored Pair Sum:

$$\begin{aligned}\vec{H}_{xy} &= \vec{H}_x + \vec{H}_y \\ \vec{H}_{yz} &= \vec{H}_y + \vec{H}_z \\ \vec{H}_{zx} &= \vec{H}_z + \vec{H}_x\end{aligned}\tag{129}$$

Scissored Pair Dot Products:

$$\begin{aligned}H_{xdy} &= \vec{H}_x \cdot \vec{H}_y \\ H_{ydz} &= \vec{H}_y \cdot \vec{H}_z \\ H_{zdx} &= \vec{H}_z \cdot \vec{H}_x\end{aligned}\tag{130}$$

Scissored Pair Cross Products:

$$\begin{aligned}\vec{H}_{xcy} &= \vec{H}_x \times \vec{H}_y \\ \vec{H}_{ycz} &= \vec{H}_y \times \vec{H}_z \\ \vec{H}_{zcx} &= \vec{H}_z \times \vec{H}_x\end{aligned}\tag{131}$$

The portion of the torque command \vec{T}_{COM} that each CMG pair is to generate is determined by the scissored pair control law gains K_{xy} , K_{yz} , and K_{zx} . These gains are based on each pair's remaining momentum capability along its momentum sum. To illustrate, figure 9.11 is a sketch of the XY CMG pair momentum vectors \vec{H}_x , \vec{H}_y , and \vec{H}_{xy} . Note that the cross product $\vec{H}_x \times \vec{H}_y$ is proportional to the area of the parallelogram formed by \vec{H}_x , \vec{H}_y , and \vec{H}_{xy} . This cross product $\vec{H}_x \times \vec{H}_y$ is used as a measure of the pair's remaining momentum capability along \vec{H}_{xy} . The gain K_{xy} is chosen to equal

$$K_{xy} = \frac{|\vec{H}_{xcy}|^2}{\sum |\vec{H}_c|^2} \quad (132)$$

where

$$\sum |\vec{H}_c|^2 = |\vec{H}_{xcy}|^2 + |\vec{H}_{ycz}|^2 + |\vec{H}_{zcx}|^2 \quad (133)$$

The control law gains K_{yz} and K_{zx} similarly equal

$$K_{yz} = \frac{|\vec{H}_{ycz}|^2}{\sum |\vec{H}_c|^2} \quad (134)$$

$$K_{zx} = \frac{|\vec{H}_{zcx}|^2}{\sum |\vec{H}_c|^2} \quad (135)$$

The sum of K_{xy} , K_{yz} , and K_{zx} equals unity ($K_{xy} + K_{yz} + K_{zx} = 1$).

The control torque \vec{T}_{CMG} is generated by applying a rotational rate $\vec{\omega}_r$ to each of the individual CMG momentum pairs (\vec{H}_{xy} , \vec{H}_{yz} , \vec{H}_{zx}) and a scissoring rate $\vec{\omega}_s$ to each of the individual CMG momentum vectors (\vec{H}_x , \vec{H}_y , \vec{H}_z). These rates $\vec{\omega}_s$ and $\vec{\omega}_r$ for each CMG pair are computed using equations 101, 114, and 115.

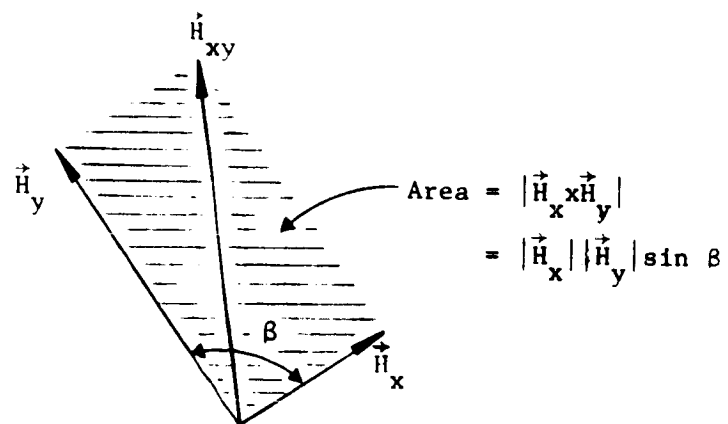


Figure 9.11. Sketch of \vec{H}_x , \vec{H}_y , and \vec{H}_{xy}

XY CMG Scissored Pair:

$$\vec{\omega}_{xyr} = \frac{\vec{H}_{xy}}{|\vec{H}_{xy}|} \times K_{xy} \vec{T}_{COM} \quad (136)$$

$$\vec{\omega}_{xs}^{(XY)} = \frac{K_{xy} (|\vec{H}_y|^2 + H_{xdy}) \vec{H}_{xcy} (\vec{H}_{xy} \cdot \vec{T}_{COM})}{|\vec{H}_{xy}|^2 |\vec{H}_{xcy}|^2} \quad (137)$$

$$\vec{\omega}_{ys}^{(XY)} = - \frac{K_{xy} (|\vec{H}_x|^2 + H_{xdy}) \vec{H}_{xcy} (\vec{H}_{xy} \cdot \vec{T}_{COM})}{|\vec{H}_{xy}|^2 |\vec{H}_{xcy}|^2} \quad (138)$$

YZ CMG Scissored Pair

$$\vec{\omega}_{yzt} = \frac{\vec{H}_{yz}}{|\vec{H}_{yz}|} \times K_{yz} \vec{T}_{COM} \quad (139)$$

$$\vec{\omega}_{ys}^{(YZ)} = \frac{K_{yz} (|\vec{H}_z|^2 + H_{ydz}) \vec{H}_{ycz} (\vec{H}_{yz} \cdot \vec{T}_{COM})}{|\vec{H}_{yz}|^2 |\vec{H}_{ycz}|^2} \quad (140)$$

$$\vec{\omega}_{zs}^{(YZ)} = - \frac{K_{yz} (|\vec{H}_y|^2 + H_{ydz}) \vec{H}_{ycz} (\vec{H}_{yz} \cdot \vec{T}_{COM})}{|\vec{H}_{yz}|^2 |\vec{H}_{ycz}|^2} \quad (141)$$

ZX CMG Scissored Pair

$$\vec{\omega}_{zxt} = \frac{\vec{H}_{zx}}{|\vec{H}_{zx}|} \times K_{zx} \vec{T}_{COM} \quad (142)$$

$$\vec{\omega}_{zs}^{(ZX)} = \frac{K_{zx} (|\vec{H}_x|^2 + H_{zdx}) \vec{H}_{zcx} (\vec{H}_{zx} \cdot \vec{T}_{COM})}{|\vec{H}_{zx}|^2 |\vec{H}_{zcx}|^2} \quad (143)$$

$$\vec{\omega}_{xs}^{(ZX)} = - \frac{K_{zx} (|\vec{H}_z|^2 + H_z dx) \vec{H}_{zcx} (\vec{H}_{zx} \cdot \vec{T}_{COM})}{|\vec{H}_{zx}|^2 |\vec{H}_{zcx}|^2} \quad (144)$$

The resultant individual CMG rate commands are:

$$\vec{\omega}_{(x)} = \vec{\omega}_{xyr} + \vec{\omega}_{xs}^{(XY)} + \vec{\omega}_{zxr} + \vec{\omega}_{xs}^{(ZX)} - \vec{\omega} \quad (145)$$

$$\vec{\omega}_{(y)} = \vec{\omega}_{xyr} + \vec{\omega}_{ys}^{(XY)} + \vec{\omega}_{yxr} + \vec{\omega}_{ys}^{(YZ)} - \vec{\omega} \quad (146)$$

$$\vec{\omega}_{(z)} = \vec{\omega}_{yxr} + \vec{\omega}_{zs}^{(YZ)} + \vec{\omega}_{zxr} + \vec{\omega}_{zx}^{(ZX)} - \vec{\omega} \quad (147)$$

$\vec{\omega}$ is the vehicle rotational rate. Transforming the above CMG rates into the appropriate CMG inner gimbal space,

$$\vec{\omega}_{I(x)} = -[\Phi_{(x)}]_{I \leftarrow o} [\Phi_{(x)}]_{o \leftarrow b} [\Phi_{(x)}]_{v \leftarrow b}^{-1} \vec{\omega}_{(x)} \quad (148)$$

$$\vec{\omega}_{I(y)} = -[\Phi_{(y)}]_{I \leftarrow o} [\Phi_{(y)}]_{o \leftarrow b} [\Phi_{(y)}]_{o \leftarrow b}^{-1} \vec{\omega}_{(y)} \quad (149)$$

$$\vec{\omega}_{I(z)} = -[\Phi_{(z)}]_{I \leftarrow o} [\Phi_{(z)}]_{o \leftarrow b} [\Phi_{(z)}]_{o \leftarrow b}^{-1} \vec{\omega}_{(z)} \quad (150)$$

Using equation 14, the gimbal rate commands $\dot{\delta}_{1x}^{(CL)}$, $\dot{\delta}_{3x}^{(CL)}$,

$\dot{\delta}_{1y}^{(CL)}$, $\dot{\delta}_{3y}^{(CL)}$, $\dot{\delta}_{1z}^{(CL)}$, and $\dot{\delta}_{3z}^{(CL)}$ are:

$$\dot{\delta}_{1x}^{(CL)} = \omega_{I(x)x} \quad (151)$$

$$\dot{\delta}_{3x}^{(CL)} = \frac{\omega_{I(x)z}}{\cos \delta_{1x}} \quad (152)$$

$$\dot{\delta}_{1y}^{(CL)} = \omega_{I(y)x} \quad (153)$$

$$\dot{\delta}_{3y}^{(CL)} = \frac{\omega_{I(y)z}}{\cos \delta_{1y}} \quad (154)$$

$$\dot{\delta}_{1z}^{(CL)} = \omega_{I(z)x} \quad (155)$$

$$\dot{\delta}_{3z}^{(CL)} = \frac{\omega_{I(z)z}}{\cos \delta_{1z}} \quad (156)$$

$\omega_{I(x)x}$ and $\omega_{I(x)z}$, $\omega_{I(x)x}$ and $\omega_{I(y)z}$, and $\omega_{I(z)x}$ and $\omega_{I(z)z}$ are the X and Z components of $\vec{\omega}_{I(x)}$, $\vec{\omega}_{I(y)}$, and $\vec{\omega}_{I(z)}$, respectively. The individual CMG gimbal rates $\dot{\delta}_{1(i)}$ and $\dot{\delta}_{3(i)}$ equal:

$$\begin{bmatrix} \dot{\delta}_{1(1)}^{(CL)} \\ \dot{\delta}_{1(3)}^{(CL)} \\ \dot{\delta}_{1(5)}^{(CL)} \end{bmatrix} = \begin{bmatrix} k_1 & 0 & 0 \\ 0 & k_2 & 0 \\ 0 & 0 & k_5 \end{bmatrix} \begin{bmatrix} \dot{\delta}_{1x}^{(CL)} \\ \dot{\delta}_{1y}^{(CL)} \\ \dot{\delta}_{1z}^{(CL)} \end{bmatrix} \quad (157)$$

$$\begin{bmatrix} \dot{\delta}_{3(1)}^{(CL)} \\ \dot{\delta}_{3(3)}^{(CL)} \\ \dot{\delta}_{3(5)}^{(CL)} \end{bmatrix} = \begin{bmatrix} k_1 & 0 & 0 \\ 0 & k_3 & 0 \\ 0 & 0 & k_5 \end{bmatrix} \begin{bmatrix} \dot{\delta}_{3x}^{(CL)} \\ \dot{\delta}_{3y}^{(CL)} \\ \dot{\delta}_{3z}^{(CL)} \end{bmatrix} \quad (158)$$

$$\begin{bmatrix} \dot{\delta}_{1(2)}^{(CL)} \\ \dot{\delta}_{1(4)}^{(CL)} \\ \dot{\delta}_{1(6)}^{(CL)} \end{bmatrix} = \begin{bmatrix} k_2 & 0 & 0 \\ 0 & k_4 & 0 \\ 0 & 0 & k_6 \end{bmatrix} \begin{bmatrix} \dot{\delta}_{1x}^{(CL)} \\ \dot{\delta}_{1y}^{(CL)} \\ \dot{\delta}_{1z}^{(CL)} \end{bmatrix} \quad (159)$$

$$\begin{bmatrix} \delta_{3(2)}^{(CL)} \\ \delta_{3(4)}^{(CL)} \\ \delta_{3(6)}^{(CL)} \end{bmatrix} = \begin{bmatrix} k_2 & 0 & 0 \\ 0 & k_4 & 0 \\ 0 & 0 & k_6 \end{bmatrix} \begin{bmatrix} \delta_{3x}^{(CL)} \\ \delta_{3y}^{(CL)} \\ \delta_{3z}^{(CL)} \end{bmatrix} \quad (160)$$

Six Individual CMG Mode - The six individual CMG reaction momentums $\vec{H}_i (i=1, \dots, 6)$ in vehicle coordinate are:

$$\begin{aligned} \vec{H}_1 &= k_1 [\phi_{(1)}]_{v \leftarrow b} [\phi_{(1)}]_{o \leftarrow b}^{-1} [\phi_{(1)}]_{I \leftarrow o}^{-1} (-\vec{H}) \\ &\vdots \\ \vec{H}_i &= k_i [\phi_{(i)}]_{v \leftarrow b} [\phi_{(i)}]_{o \leftarrow b}^{-1} [\phi_{(i)}]_{I \leftarrow o}^{-1} (-\vec{H}) \\ &\vdots \\ \vec{H}_6 &= k_6 [\phi_{(6)}]_{v \leftarrow b} [\phi_{(6)}]_{o \leftarrow b}^{-1} [\phi_{(6)}]_{I \leftarrow o}^{-1} (-\vec{H}) \end{aligned} \quad (161)$$

For this mode of operation, there are 15 scissored CMG pairs (1,j): (1,2), (1,3), (1,4), (1,5), (1,6), (2,3), (2,4), (2,5), (2,6), (3,4), (3,5), (3,6), (4,5), (4,6), and (5,6). The resultant CMG scissored pair sums, dot products, and cross products are:

Scissored Pair Sums:

$$\begin{aligned} \vec{H}_{12} &= \vec{H}_1 + \vec{H}_2 \\ &\vdots \\ \vec{H}_{ij} &= \vec{H}_i + \vec{H}_j \\ &\vdots \\ \vec{H}_{56} &= \vec{H}_5 + \vec{H}_6 \end{aligned} \quad (162)$$

Scissored Pair Dot Products:

$$\begin{aligned}
 H_{1d2} &= \vec{H}_1 \cdot \vec{H}_2 \\
 &\vdots \\
 H_{1dj} &= \vec{H}_1 \cdot \vec{H}_j \\
 &\vdots \\
 H_{5d6} &= \vec{H}_5 \cdot \vec{H}_6
 \end{aligned} \tag{163}$$

Scissored Pair Cross Products:

$$\begin{aligned}
 \vec{H}_{1c2} &= \vec{H}_1 \times \vec{H}_2 \\
 &\vdots \\
 \vec{H}_{1cj} &= \vec{H}_1 \times \vec{H}_j \\
 &\vdots \\
 \vec{H}_{5c6} &= \vec{H}_5 \times \vec{H}_6
 \end{aligned} \tag{164}$$

The scissored pair control gains K_{ij} equal

$$\begin{aligned}
 K_{12} &= \frac{|\vec{H}_{1c2}|^2}{|\vec{H}_c|^2} \\
 &\vdots \\
 K_{1j} &= \frac{|\vec{H}_{1cj}|^2}{|\vec{H}_c|^2} \\
 &\vdots \\
 K_{56} &= \frac{|\vec{H}_{5c6}|^2}{|\vec{H}_c|^2}
 \end{aligned} \tag{165}$$

where

$$|\vec{H}_c|^2 = |\vec{H}_{1c2}|^2 + \dots + |\vec{H}_{icj}|^2 + \dots + |\vec{H}_{5c6}|^2 \quad (166)$$

For each scissored pair (i,j), one rotation rate $\vec{\omega}_r$ and two scissoring rates $\vec{\omega}_s$ are computed. For scissored pair (i,j), the rotational rate $\vec{\omega}_{ijr}$ and scissoring rates $\vec{\omega}_{is}^{(ij)}$ and $\vec{\omega}_{js}^{(ij)}$ are

$$\vec{\omega}_{ijr} = \frac{|\vec{H}_{ij}|}{|\vec{H}_{ij}|^2} \times K_{ij} \vec{T}_{COM} \quad (167)$$

$$\vec{\omega}_{is}^{(ij)} = \frac{K_{ij} (|\vec{H}_j|^2 + H_{idj}) \vec{H}_{icj} (\vec{H}_{ij} \cdot \vec{T}_{COM})}{|\vec{H}_{ij}|^2 |\vec{H}_{icj}|^2} \quad (168)$$

$$\vec{\omega}_{js}^{(ij)} = - \frac{K_{ij} (|\vec{H}_i|^2 + H_{idj}) \vec{H}_{icj} (\vec{H}_{ij} \cdot \vec{T}_{COM})}{|\vec{H}_{ij}|^2 |\vec{H}_{icj}|^2} \quad (169)$$

To compute the resultant individual CMG rate commands $\vec{\omega}_i$ ($i=1, \dots, 6$), all of the above rotational rate $\vec{\omega}_{ijr}$ and scissoring rates $\vec{\omega}_{is}^{()}$, with subscripts that correspond to the i^{th} CMG are summed with $-\vec{\omega}$, the rotational rate of the vehicle. As an example, $\vec{\omega}_1$ which corresponds to CMG 1 equals

$$\begin{aligned} \vec{\omega}_1 = & \vec{\omega}_{12r} + \vec{\omega}_{13r} + \vec{\omega}_{14r} + \vec{\omega}_{15r} + \vec{\omega}_{16r} + \vec{\omega}_{1s}^{(12)} \\ & + \vec{\omega}_{1s}^{(13)} + \vec{\omega}_{1s}^{(14)} + \vec{\omega}_{1s}^{(15)} + \vec{\omega}_{1s}^{(16)} - \vec{\omega} \end{aligned} \quad (170)$$

Similarly the five remaining CMGs have similar CMG rate commands $\vec{\omega}_i$. The negative of these rates $-\vec{\omega}_i$ are then transformed into the appropriate CMG inner gimbal space as follows:

$$\vec{\omega}_{Ii} = -[\Phi_{(i)}]_{I \cdot O} [\Phi_{(i)}]_{O \cdot b} [\Phi_{(i)}]_{v \cdot b}^{-1} \vec{\omega}_i \quad (171)$$

The corresponding CMG gimbal rate commands $\dot{\delta}_{1(i)}^{(CL)}$ and $\dot{\delta}_{3(i)}^{(CL)}$ equal:

$$\dot{\delta}_{1(i)}^{(CL)} = \omega_{I1x} \quad (172)$$

$$\dot{\delta}_{3(i)}^{(CL)} = \frac{\omega_{I1z}}{\cos \delta_{1(i)}} \quad (173)$$

ω_{I1x} and ω_{I1z} are the X and Z components of $\vec{\omega}_{I1}$.

Note that increasing the number of independent CMGs increases the number of CMG scissored pairs and thus significantly increases the computational requirements associated with this decoupled, digital CMG control law.

9.4.4 Decoupled Pseudo-Inverse CMG Control Law - The Pseudo-Inverse CMG Control Law is an optimal, digital, decoupled CMG control law. The CMG gimbal rate commands $\dot{\delta}_{1(i)}^{(CL)}$ and $\dot{\delta}_{3(i)}^{(CL)}$ are computed by optimizing a performance index P with the constraint that the CMG control torque \vec{T}_{CMG} equals the command torque \vec{T}_{COM} . The optimization method used is the Lagrange multiplier technique. The selected performance index P minimizes the sum of the squares of the gimbal rate commands $\dot{\delta}_{1(i)}^{(CL)}$ and $\dot{\delta}_{3(i)}^{(CL)}$. P equals

$$P = (\dot{\delta}_{1(i)}^{(CL)}, \dot{\delta}_{3(i)}^{(CL)}) = \frac{1}{2} \sum_{i=1}^6 \{ (\dot{\delta}_{1(i)}^{(CL)})^2 + (\dot{\delta}_{3(i)}^{(CL)})^2 \} \quad (174)$$

The constraint equation associated with the performance index P is

$$\vec{T}_{CMG} - \vec{T}_{COM} = 0 \quad (175)$$

Figure 9.12 is a block diagram of the corresponding vehicle control loop.

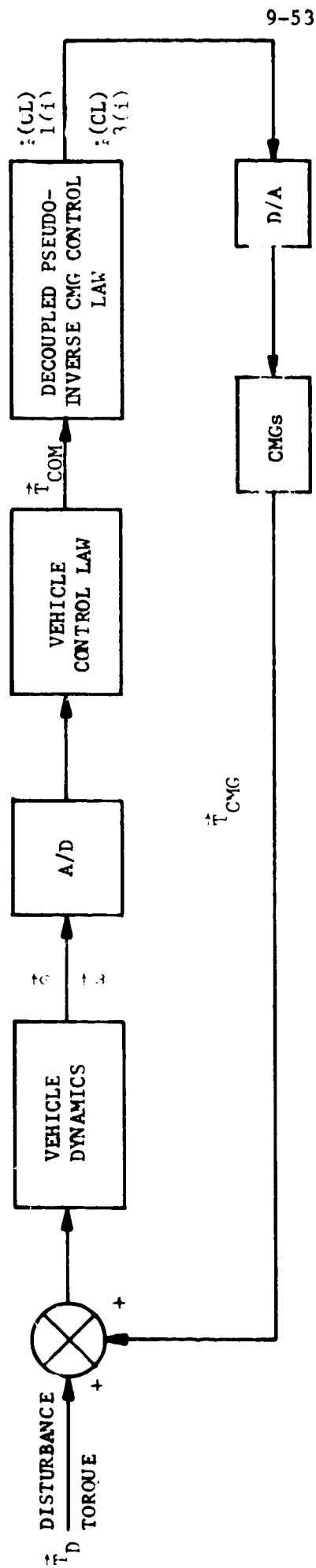


Figure 9.12. Decoupled Pseudo-Inverse CMG Control Law Control Loop

Slaved CMG Mode - The performance index P with provisions for CMG failures equals

$$P = \frac{1}{2} \{ \dot{\delta}_1^T [k_{(1)}^2]^{-1} \dot{\delta}_1 + \dot{\delta}_3^T [k_{(1)}^2]^{-1} \dot{\delta}_3 \} \quad (176)$$

where

$$\dot{\delta}_1 = \begin{bmatrix} \dot{\delta}_{1x}^{(CL)} \\ \dot{\delta}_{1y}^{(CL)} \\ \dot{\delta}_{1z}^{(CL)} \end{bmatrix} \quad (177)$$

$$\dot{\delta}_3 = \begin{bmatrix} \dot{\delta}_{3x}^{(CL)} \\ \dot{\delta}_{3y}^{(CL)} \\ \dot{\delta}_{3z}^{(CL)} \end{bmatrix} \quad (178)$$

$$[k_{(1)}^2] = \begin{bmatrix} (k_1+k_2)^2 & 0 & 0 \\ 0 & (k_3+k_4)^2 & 0 \\ 0 & 0 & (k_5+k_6)^2 \end{bmatrix} \quad (179)$$

The corresponding constraint placed on the performance index P is

$$H\{[k_{(1)}][A']\dot{\delta}_1 + [k_{(1)}][B']\dot{\delta}_3 + \vec{\omega} \times \vec{H}_{CMG} - \vec{T}_{COM}\} = 0 \quad (180)$$

[A'] and [B'] are defined in equation 43 and 44, respectively.
[k₍₁₎] equals

$$[k_{(1)}] = \begin{bmatrix} (k_1+k_2) & 0 & 0 \\ 0 & (k_3+k_4) & 0 \\ 0 & 0 & (k_5+k_6) \end{bmatrix} \quad (181)$$

The Lagrange adjoin equation formed from equations 176 and 180 equals

$$L = \frac{1}{2} \{ \dot{\delta}_1^T [k_{(1)}^2]^{-1} \dot{\delta}_1 + \dot{\delta}_3^T [k_{(1)}^2]^{-1} \dot{\delta}_3 \} - \lambda^T \{ H([k_{(1)}]) [A'] \dot{\delta}_1 + [k_{(1)}] [B'] \dot{\delta}_3 \} + \omega \times \vec{H}_{CMG} - \vec{T}_{COM} \quad (182)$$

where λ is the Lagrange multiplier

$$\lambda = \begin{bmatrix} \lambda_1 \\ \lambda_2 \\ \lambda_3 \end{bmatrix} \quad (183)$$

To minimize L , the partial derivatives $\frac{dL}{d\dot{\delta}_1}$, $\frac{dL}{d\dot{\delta}_3}$, and $\frac{dL}{d\lambda}$ are set equal to zero.

$$\frac{dL}{d\dot{\delta}_1} = ([k_{(1)}^2]^{-1} \dot{\delta}_1 - H([k_{(1)}]) [A'])^T \lambda = 0 \quad (184)$$

$$\frac{dL}{d\dot{\delta}_3} = ([k_{(1)}^2]^{-1} \dot{\delta}_3 - H([k_{(1)}]) [B'])^T \lambda = 0 \quad (185)$$

$$\frac{dL}{d\lambda} = -H([k_{(1)}]) [A'] \dot{\delta}_1 + [k_{(1)}] [B'] \dot{\delta}_3 - \omega \times \vec{H}_{CMG} + \vec{T}_{COM} = 0 \quad (186)$$

Solving equations 184 and 185 for $\dot{\delta}_1$ and $\dot{\delta}_3$,

$$\dot{\delta}_1 = H[k_{(1)}^2] ([k_{(1)}] [A'])^T \lambda \quad (187)$$

$$\dot{\delta}_3 = H[k_{(1)}^2] ([k_{(1)}] [B'])^T \lambda \quad (188)$$

Substituting equations 187 and 188 into 186

$$H^2[G] \lambda = \vec{T}_{COM} - \omega \times \vec{H}_{CMG} \quad (189)$$

where

$$[G] = [k_{(1)}][A'] [k_{(1)}^2] ([k_{(1)}][A'])^T + [k_{(1)}][B'] [k_{(1)}^2] ([k_{(1)}][B'])^T \quad (190)$$

From equation 189,

$$\lambda = \frac{1}{H^2} [G]^{-1} (\vec{T}_{COM} - \vec{\omega} \times \vec{H}_{CMG}) \quad (191)$$

Substituting equation 191 into equations 187 and 188, the CMG gimbal rate commands $\dot{\delta}_1$ and $\dot{\delta}_3$ equal

$$\dot{\delta}_1 = \frac{1}{H} [k_{(1)}^2] ([k_{(1)}][A'])^T [G]^{-1} (\vec{T}_{COM} - \vec{\omega} \times \vec{H}_{CMG}) \quad (192)$$

$$\dot{\delta}_3 = \frac{1}{H} [k_{(1)}^2] ([k_{(1)}][B'])^T [G]^{-1} (\vec{T}_{COM} - \vec{\omega} \times \vec{H}_{CMG}) \quad (193)$$

The individual CMG gimbal rate commands $\dot{\delta}_{1(i)}^{(CL)}$ and $\dot{\delta}_{3(i)}^{(CL)}$ equal

$$\begin{bmatrix} \dot{\delta}_{1(1)}^{(CL)} \\ \dot{\delta}_{1(3)}^{(CL)} \\ \dot{\delta}_{1(5)}^{(CL)} \end{bmatrix} = [k_{(2)}] \dot{\delta}_1 \quad (194)$$

$$\begin{bmatrix} \dot{\delta}_{3(1)}^{(CL)} \\ \dot{\delta}_{3(3)}^{(CL)} \\ \dot{\delta}_{3(5)}^{(CL)} \end{bmatrix} = [k_{(2)}] \dot{\delta}_3 \quad (195)$$

$$\begin{bmatrix} \text{(CL)} \\ \dot{\delta}_{1(2)} \\ \text{(CL)} \\ \dot{\delta}_{1(4)} \\ \text{(CL)} \\ \dot{\delta}_{1(6)} \end{bmatrix} = [k_{(3)}] \dot{\delta}_1 \quad (196)$$

$$\begin{bmatrix} \text{(CL)} \\ \dot{\delta}_{3(2)} \\ \text{(CL)} \\ \dot{\delta}_{3(4)} \\ \text{(CL)} \\ \dot{\delta}_{3(6)} \end{bmatrix} = [k_{(3)}] \dot{\delta}_3 \quad (197)$$

where

$$[k_{(2)}] = \begin{bmatrix} k_1 & 0 & 0 \\ 0 & k_3 & 0 \\ 0 & 0 & k_5 \end{bmatrix} \quad (198)$$

$$[k_{(3)}] = \begin{bmatrix} k_2 & 0 & 0 \\ 0 & k_4 & 0 \\ 0 & 0 & k_6 \end{bmatrix} \quad (199)$$

Six Individual CMG Mode - The performance index P equals

$$P = \frac{1}{2} \{ \dot{\delta}_1^{(1)T} [k_{(2)}^2]^{-1} \dot{\delta}_1^{(1)} + \dot{\delta}_3^{(1)T} [k_{(2)}^2]^{-1} \dot{\delta}_3^{(1)} + \dot{\delta}_1^{(2)T} [k_{(3)}^2]^{-1} \dot{\delta}_1^{(2)} + \dot{\delta}_3^{(2)T} [k_{(3)}^2]^{-1} \dot{\delta}_3^{(2)} \} \quad (200)$$

where

$$\dot{\delta}_1^{(1)} = \begin{bmatrix} (CL) \\ \dot{\delta}_{1(1)} \\ (CL) \\ \dot{\delta}_{1(3)} \\ (CL) \\ \dot{\delta}_{1(5)} \end{bmatrix} \quad (201)$$

$$\dot{\delta}_3^{(1)} = \begin{bmatrix} (CL) \\ \dot{\delta}_{3(1)} \\ (CL) \\ \dot{\delta}_{3(3)} \\ (CL) \\ \dot{\delta}_{3(5)} \end{bmatrix} \quad (202)$$

$$\dot{\delta}_1^{(2)} = \begin{bmatrix} (CL) \\ \dot{\delta}_{1(2)} \\ (CL) \\ \dot{\delta}_{1(4)} \\ (CL) \\ \dot{\delta}_{1(6)} \end{bmatrix} \quad (203)$$

$$\dot{\delta}_3^{(2)} = \begin{bmatrix} (CL) \\ \dot{\delta}_{3(2)} \\ (CL) \\ \dot{\delta}_{3(4)} \\ (CL) \\ \dot{\delta}_{3(6)} \end{bmatrix} \quad (204)$$

$$[k_{(2)}^2] = \begin{bmatrix} k_1^2 & 0 & 0 \\ 0 & k_3^2 & 0 \\ 0 & 0 & k_5^2 \end{bmatrix} \quad (205)$$

$$[k_{(3)}^2] = \begin{bmatrix} k_2^2 & 0 & 0 \\ 0 & k_4^2 & 0 \\ 0 & 0 & k_6^2 \end{bmatrix} \quad (206)$$

The constraint associated with performance index P is

$$\begin{aligned} & H\{[k_{(2)}][A]\dot{\delta}_1^{(1)} + [k_{(2)}][B]\dot{\delta}_3^{(1)} + [k_{(3)}][C]\dot{\delta}_1^{(2)} \\ & + [k_{(3)}][D]\dot{\delta}_3^{(2)}\} + \vec{\omega}_x \vec{H}_{CMG} - \vec{T}_{COM} = 0 \end{aligned} \quad (207)$$

The adjoint equation L equals

$$\begin{aligned} L = & \frac{1}{2} \{ \dot{\delta}_1^{(1)T} [k_{(2)}^2]^{-1} \dot{\delta}_1^{(1)} + \dot{\delta}_3^{(1)T} [k_{(2)}^2]^{-1} \dot{\delta}_3^{(1)} + \dot{\delta}_1^{(2)T} [k_{(3)}^2]^{-1} \dot{\delta}_1^{(2)} \\ & + \dot{\delta}_3^{(2)T} [k_{(3)}^2]^{-1} \dot{\delta}_3^{(2)} \} - \lambda^T \{ H\{[k_{(2)}][A]\dot{\delta}_1^{(1)} + [k_{(2)}][B]\dot{\delta}_3^{(1)} \\ & + [k_{(3)}][C]\dot{\delta}_1^{(2)} + [k_{(3)}][D]\dot{\delta}_3^{(2)}\} + \vec{\omega}_x \vec{H}_{CMG} - \vec{T}_{COM} \} = 0 \end{aligned} \quad (208)$$

To minimize L, the partial derivatives $\frac{dL}{d\dot{\delta}_1^{(1)}}$, $\frac{dL}{d\dot{\delta}_3^{(1)}}$, $\frac{dL}{d\dot{\delta}_1^{(2)}}$, $\frac{dL}{d\dot{\delta}_3^{(2)}}$, and $\frac{dL}{d\lambda}$ are set equal to zero.

$$\frac{dL}{d\dot{\delta}_1^{(1)}} = [k_{(2)}^2]^{-1} \dot{\delta}_1^{(1)} - H([k_{(2)}][A])^T \lambda = 0 \quad (209)$$

$$\frac{dL}{d\dot{\delta}_3^{(1)}} = [k_{(2)}^2]^{-1} \dot{\delta}_3^{(1)} - H([k_{(2)}][B])^T \lambda = 0 \quad (210)$$

$$\frac{dL}{d\dot{\delta}_1^{(2)}} = [k_{(3)}^2]^{-1} \dot{\delta}_1^{(2)} - H([k_{(3)}][C])^T \lambda = 0 \quad (211)$$

$$\frac{dL}{d\dot{\delta}_3^{(2)}} = [k_{(3)}^2]^{-1} \dot{\delta}_3^{(2)} - H([k_{(3)}][D])^T \lambda = 0 \quad (212)$$

$$\begin{aligned} \frac{dL}{d\lambda} = & -H([k_{(2)}][A])\dot{\delta}_1^{(1)} + [k_{(2)}][B]\dot{\delta}_3^{(1)} + [k_{(3)}][C]\dot{\delta}_1^{(2)} \\ & + [k_{(3)}][D]\dot{\delta}_3^{(2)} - \vec{\omega} \times \vec{H}_{CMG} + \vec{T}_{COM} = 0 \end{aligned} \quad (213)$$

Solving equations 209 thru 212 for $\dot{\delta}_1^{(1)}$, $\dot{\delta}_3^{(1)}$, $\dot{\delta}_1^{(2)}$, and $\dot{\delta}_3^{(2)}$,

$$\dot{\delta}_1^{(1)} = H[k_{(2)}^2]([k_{(2)}][A])^T \lambda \quad (214)$$

$$\dot{\delta}_3^{(1)} = H[k_{(2)}^2]([k_{(2)}][B])^T \lambda \quad (215)$$

$$\dot{\delta}_1^{(2)} = H[k_{(3)}^2]([k_{(3)}][C])^T \lambda \quad (216)$$

$$\dot{\delta}_3^{(2)} = H[k_{(3)}^2]([k_{(3)}][D])^T \lambda \quad (217)$$

Substituting equations 213 thru 216 into 212.

$$H^2[G]\lambda = \vec{T}_{COM} - \vec{\omega} \times \vec{H}_{CMG} \quad (218)$$

where

$$\begin{aligned} [G] = & [k_{(2)}][A][k_{(2)}^2]([k_{(2)}][A])^T \\ & + [k_{(2)}][B][k_{(2)}^2]([k_{(2)}][B])^T \\ & + [k_{(3)}][C][k_{(3)}^2]([k_{(3)}][C])^T \\ & + [k_{(3)}][D][k_{(3)}^2]([k_{(3)}][D])^T \end{aligned} \quad (219)$$

From equation 218,

$$\lambda = \frac{1}{H^2}[G]^{-1}(\vec{T}_{COM} - \vec{\omega} \times \vec{H}_{CMG}) \quad (220)$$

Substituting equation 220 into equations 214 thru 217,

$\dot{\delta}_1^{(1)}$, $\dot{\delta}_3^{(1)}$, $\dot{\delta}_1^{(2)}$, and $\dot{\delta}_3^{(2)}$ equal

$$\dot{\delta}_1^{(1)} = \frac{1}{H}[k_{(2)}^2]([k_{(2)}][A])^T[G]^{-1}(\vec{T}_{COM} - \vec{\omega} \times \vec{H}_{CMG}) \quad (221)$$

$$\dot{\delta}_3^{(1)} = \frac{1}{H}[k_{(2)}^2]([k_{(2)}][B])^T[G]^{-1}(\vec{T}_{COM} - \vec{\omega} \times \vec{H}_{CMG}) \quad (222)$$

$$\dot{\delta}_1^{(2)} = \frac{1}{H}[k_{(3)}^2]([k_{(3)}][C])^T[G]^{-1}(\vec{T}_{COM} - \vec{\omega} \times \vec{H}_{CMG}) \quad (223)$$

$$\dot{\delta}_3^{(2)} = \frac{1}{H}[k_{(3)}^2]([k_{(3)}][D])^T[G]^{-1}(\vec{T}_{COM} - \vec{\omega} \times \vec{H}_{CMG}) \quad (224)$$

9.5 CMG Singularity Avoidance Laws - The following three candidate CMG singularity avoidance laws are presented in this report:

- a. Arbitrary Torquing of CMGs Away From Singularity
- b. Isogonal CMG Distribution Law
- c. Optimal CMG Distribution Law

Each singularity avoidance scheme distributes the CMG momentum vectors \vec{H}_i so as to avoid the anti-parallel singularity condition. The momentum vectors \vec{H}_i are distributed in such a manner that no net torque is applied to the vehicle due to these singularity avoidance schemes.

9.5.1 Arbitrary Torquing of CMGs Away From Singularity -

This singularity avoidance scheme remains inoperative until two CMGs are detected approaching an anti-parallel condition. Before this anti-parallel condition occurs, a threshold detector is triggered causing the two CMG momentum vectors \vec{H}_1 to be scissored towards one another thus avoiding a potential CMG pair anti-parallel condition. A CMG pair anti-parallel condition occurs when the momentum vectors \vec{H}_1 of any two CMGs are pointed in opposite directions. The above scissoring action of the two momentum vectors \vec{H}_1 is continued until their relative orientations are deemed close enough not to represent a potentially dangerous CMG pair anti-parallel condition. The torque resulting from this scissoring action is absorbed by the total CMG system by modifying the torque command \vec{T}_{COM} .

It should be noted that because two CMGs are anti-parallel, it does not necessarily follow that the total CMG system is singular. But if the total CMG system is both singular and anti-parallel, it does follow that at least one CMG pair is anti-parallel. By preventing all possible CMG pairs from becoming anti-parallel, the anti-parallel singularity condition associated with the total CMG system is also avoided. The proposed singularity avoidance scheme described in this section uses this technique to prevent the total CMG system from becoming singular.

To illustrate how this technique operates assume that CMGs 1 and 2 are approaching an anti-parallel condition as shown in figure 9.13. \hat{l}_{H1} and \hat{l}_{H2} are unit vectors along \vec{H}_1 and \vec{H}_2 , respectively. Let CMG 1 be denoted as the "test" CMG. The "test" CMG checks the remaining CMGs to see if any of them are approaching an anti-parallel condition with the "test" CMG. The designation of "test" CMG sequences through the complete set of CMGs so that every CMG in a prescribed order receives the designation of "test" CMG.

If the projection of \hat{l}_{H2} onto \hat{l}_{H1} is less than the preset threshold limit $\cos \gamma_0$, the CMG pair 1, 2 is said to be approaching an anti-parallel condition.

$$\hat{l}_{H1} \cdot \hat{l}_{H2} < \cos \gamma_0 \quad (225)$$

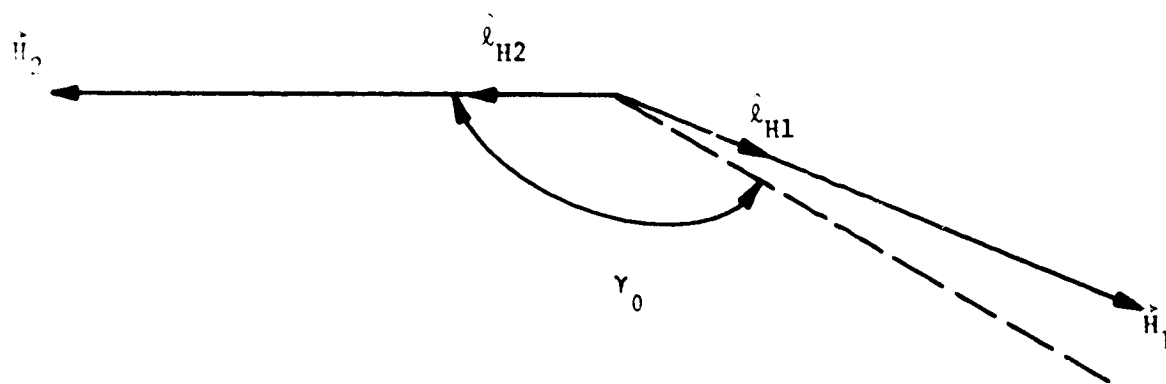


Figure 9.13. Detection of \vec{H}_1 and \vec{H}_2 Approaching
Anti-Parallel Condition

Once the threshold detector is triggered, \vec{H}_2 is rotated towards \vec{H}_1 at the following rate $\vec{\omega}_2^{(12)}$.

$$\vec{\omega}_2^{(12)} = \omega_{SA} \frac{\hat{\ell}_{H2} \times \hat{\ell}_{H1}}{|\hat{\ell}_{H2} \times \hat{\ell}_{H1}|} \quad (226)$$

ω_{SA} is a scalar constant. $\vec{\omega}_2^{(12)}$ is converted into the appropriate gimbal rate commands $\dot{\delta}_1^{(12)}$ and $\dot{\delta}_3^{(12)}$. The appropriate inner gimbal rate command $\vec{\omega}_{12}^{(12)}$ equals

$$\vec{\omega}_{12}^{(12)} = -[\phi_{(2)}]_{I \leftarrow O} [\phi_{(2)}]_{O \leftarrow b} [\phi_{(2)}]_{v \leftarrow b}^{-1} \vec{\omega}_2^{(12)} \quad (227)$$

Using equation 14, the gimbal rate commands $\dot{\delta}_1^{(12)}$ and $\dot{\delta}_3^{(12)}$ are

$$\dot{\delta}_1^{(12)} = \omega_{12x}^{(12)} \quad (228)$$

$$\dot{\delta}_3^{(12)} = \frac{\omega_{12z}^{(12)}}{\cos \delta_1^{(12)}} \quad (229)$$

$\omega_{12x}^{(12)}$ and $\omega_{12z}^{(12)}$ are the X and Z components of $\vec{\omega}_{12}^{(12)}$, respectively.

The torque exerted on the vehicle due to $\dot{\delta}_1^{(12)}$ and $\dot{\delta}_3^{(12)}$ is

$$\vec{T}_{SA}^{(12)} = \omega_2^{(12)} \times \vec{H}_2 \quad (230)$$

To compensate for $\vec{T}_{SA}^{(12)}$, the CMG torque command \vec{T}_{COM} is modified by subtracting $\vec{T}_{SA}^{(12)}$ for \vec{T}_{COM} .

$$\vec{T}_{COM}' = \vec{T}_{COM} - \vec{T}_{SA}^{(12)} \quad (231)$$

The CMG gimbal rate commands $\dot{\delta}_1^{(12)}$, $\dot{\delta}_3^{(12)}$, and the resultant modification of \vec{T}_{COM} are applied to the system until CMG pair (1, 2) are checked again. If this second time CMG pair (1, 2) passes

the threshold test, the gimbal rate commands $\dot{\delta}_{1(2)}^{(12)}$, $\dot{\delta}_{3(2)}^{(12)}$, and the CMG torque command modification $\vec{T}_{SA}^{(12)}$ are zeroed; if the pair does not pass the threshold test, new values of $\dot{\delta}_{1(2)}^{(12)}$, $\dot{\delta}_{3(2)}^{(12)}$, and $\vec{T}_{SA}^{(12)}$ are computed. Figure 9.14 is a block diagram of this singularity avoidance system.

Slaved CMG Mode - For this slaved CMG mode, the unit vectors \hat{l}_{HX} , \hat{l}_{HY} , and \hat{l}_{HZ} are

$$\hat{l}_{HX} = \begin{bmatrix} -\cos \delta_{1x} & \cos \delta_{3x} \\ \cos \delta_{1x} & \sin \delta_{3x} \\ & \sin \delta_{1x} \end{bmatrix} \quad (232)$$

$$\hat{l}_{HY} = \begin{bmatrix} & \sin \delta_{1y} \\ -\cos \delta_{1y} & \cos \delta_{3y} \\ \cos \delta_{1y} & \sin \delta_{3y} \end{bmatrix} \quad (233)$$

$$\hat{l}_{HZ} = \begin{bmatrix} \cos \delta_{1z} & \sin \delta_{3z} \\ & \sin \delta_{1z} \\ -\cos \delta_{1z} & \cos \delta_{3z} \end{bmatrix} \quad (234)$$

The slaved CMG momentum vectors \vec{H}_x , \vec{H}_y , and \vec{H}_z equal

$$\vec{H}_x = k_x H \hat{l}_{Hx} \quad (235)$$

$$\vec{H}_y = k_y H \hat{l}_{Hy} \quad (236)$$

$$\vec{H}_z = k_z H \hat{l}_{Hz} \quad (237)$$

Figure 9.15 is the corresponding signal flow logic diagram associated with this proposed singularity avoidance scheme and CMG mode of operation. The subscripts i and j used in this signal flow logic diagram correspond to the "test" CMG and the CMG being tested, respectively. Let the subscripts i and j take on the following significance:

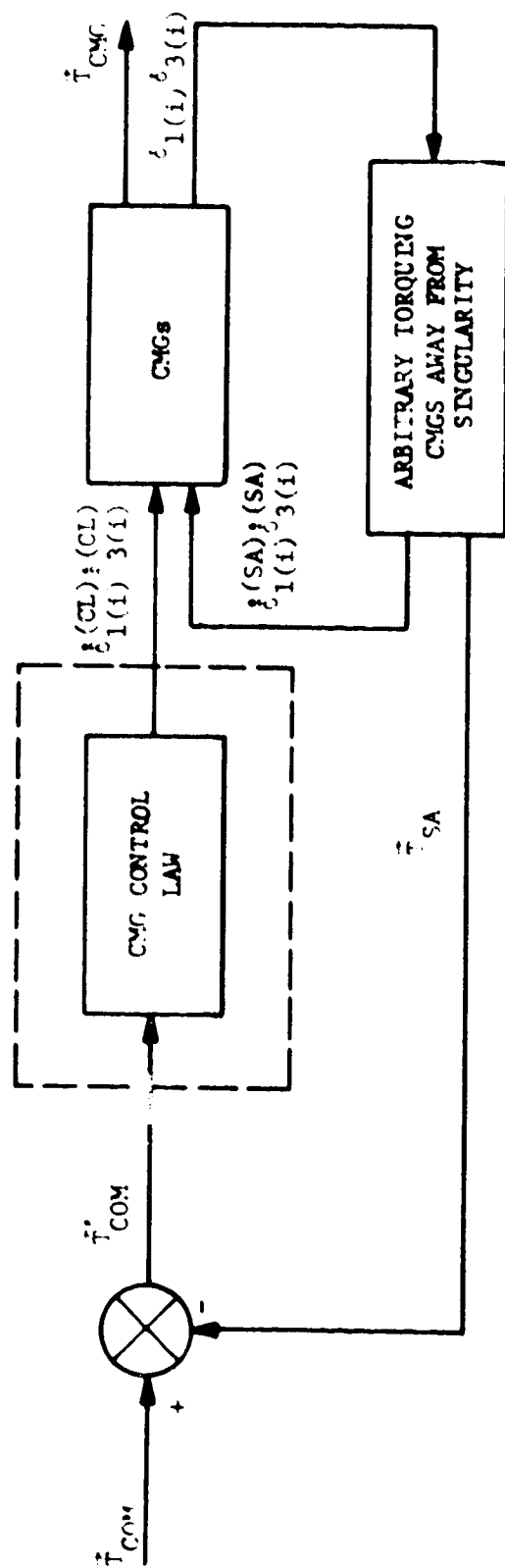


Figure 9.14. Block Diagram of Arbitrary Torquing CMGs Away From Singularity Scheme

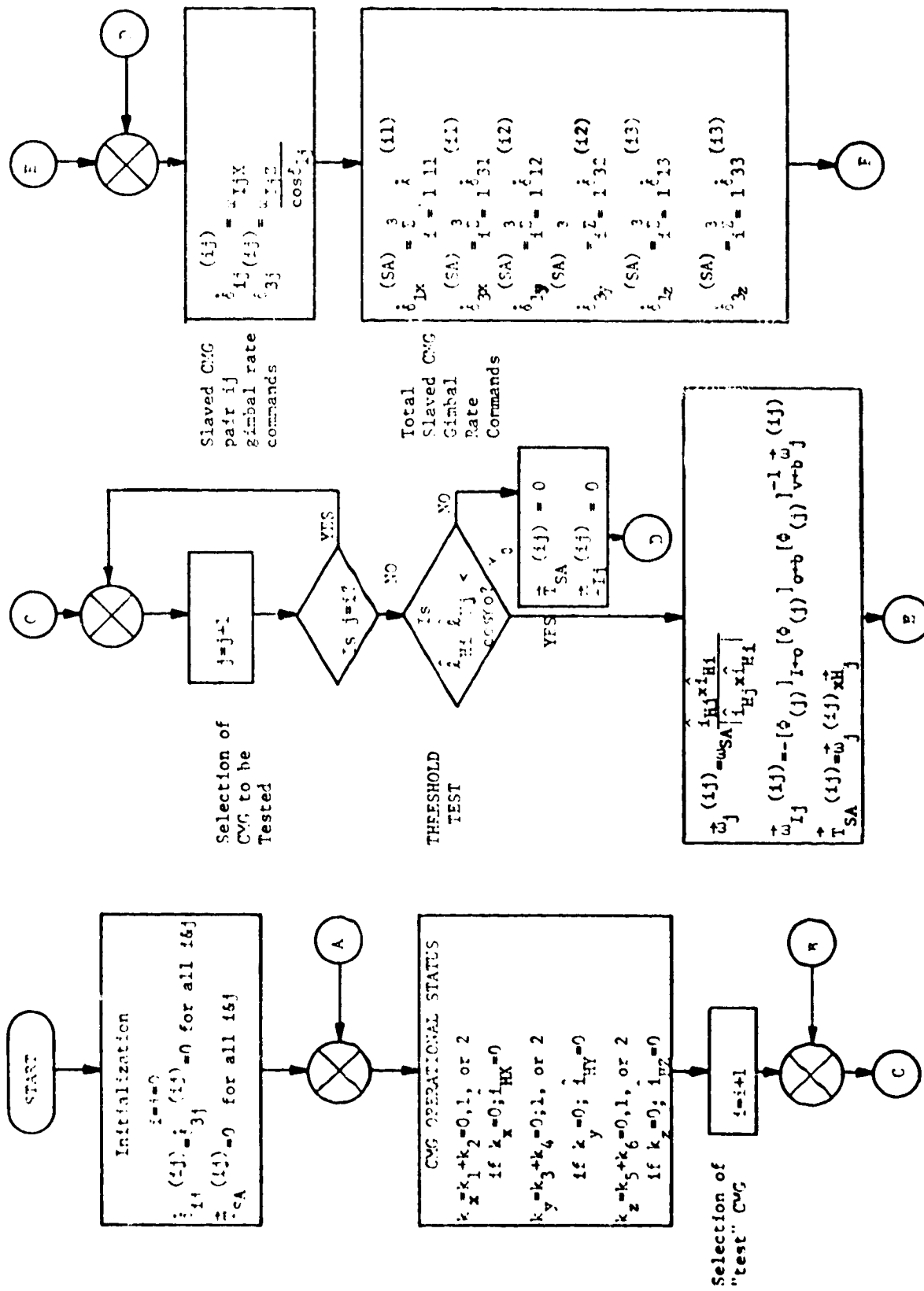


Figure 9.15. Signal Flow Logic Diagram for Arbitrary Torquing of CMGs Away From Singularity (Slaved CMG Mode of Operation) (Sheet 1 of 2)

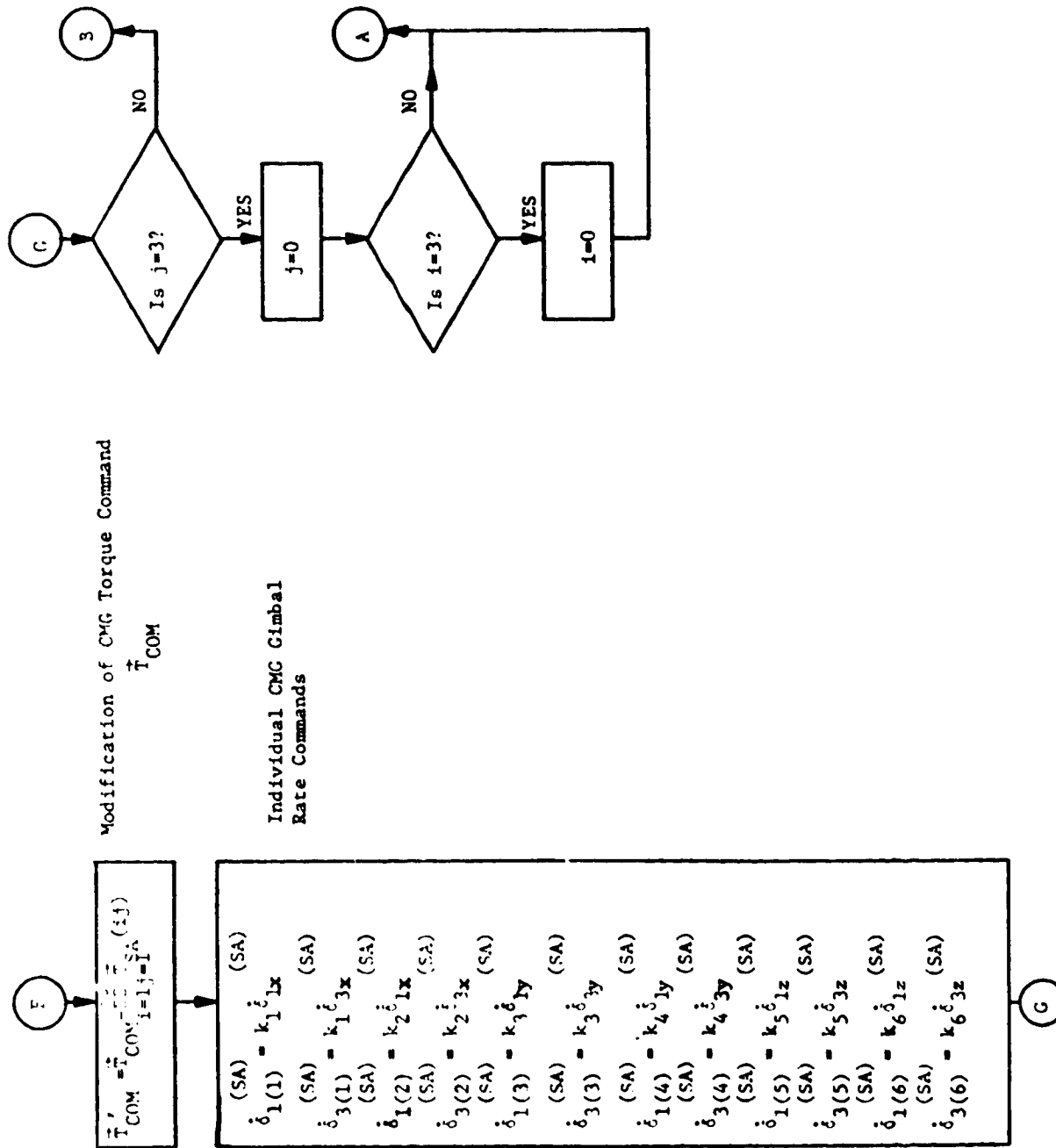


Figure 9.15. Signal Flow Logic Diagram for Arbitrary Torquing of CMGs Away From Singularity (Slaved CMG Mode of Operation) (Sheet 2 of 2)

$i=1$, i corresponds to x

$j=1$, j corresponds to x

$i=2$, i corresponds to y

$j=2$, j corresponds to y

$i=3$, i corresponds to z

$i=3$, i corresponds to z

For example if i equals 1 and j equals 2, the CMG gimbal angles δ_{1i} , δ_{3i} , δ_{1j} , and δ_{3j} correspond to δ_{1x} , δ_{3x} , δ_{1y} , and δ_{3y} , respectively.

Six Individual CMG Mode - The unit vectors \hat{l}_{H1} , \hat{l}_{H2} , \hat{l}_{H3} , \hat{l}_{H4} , \hat{l}_{H5} , and \hat{l}_{H6} equal

$$\hat{l}_{H1} = \begin{bmatrix} -\cos \delta_{1(1)} & \cos \delta_{3(1)} \\ \cos \delta_{1(1)} & \sin \delta_{3(1)} \\ & \sin \delta_{1(1)} \end{bmatrix} \quad (238)$$

$$\hat{l}_{H2} = \begin{bmatrix} -\cos \delta_{1(2)} & \cos \delta_{3(2)} \\ \cos \delta_{1(2)} & \sin \delta_{3(2)} \\ & \sin \delta_{1(2)} \end{bmatrix} \quad (239)$$

$$\hat{l}_{H3} = \begin{bmatrix} & \sin \delta_{1(2)} \\ -\cos \delta_{1(3)} & \cos \delta_{3(3)} \\ \cos \delta_{1(3)} & \sin \delta_{3(3)} \end{bmatrix} \quad (240)$$

$$\hat{\ell}_{H4} = \begin{bmatrix} \sin \delta_{1(4)} \\ -\cos \delta_{1(4)} \cos \delta_{3(4)} \\ \cos \delta_{1(4)} \sin \delta_{3(4)} \end{bmatrix} \quad (241)$$

$$\hat{\ell}_{H5} = \begin{bmatrix} \cos \delta_{1(5)} \sin \delta_{3(5)} \\ \sin \delta_{1(5)} \\ -\cos \delta_{1(5)} \cos \delta_{3(5)} \end{bmatrix} \quad (242)$$

$$\hat{\ell}_{H6} = \begin{bmatrix} \cos \delta_{1(6)} \sin \delta_{3(6)} \\ \sin \delta_{1(6)} \\ -\cos \delta_{1(6)} \cos \delta_{3(6)} \end{bmatrix} \quad (243)$$

The individual CMG momentum vectors \vec{H}_i ($i=1, \dots, 6$) are

$$\vec{H}_1 = k_1 H \hat{\ell}_{H1} \quad (244)$$

$$\vec{H}_2 = k_2 H \hat{\ell}_{H2} \quad (245)$$

$$\vec{H}_3 = k_3 H \hat{\ell}_{H3} \quad (246)$$

$$\vec{H}_4 = k_4 H \hat{\ell}_{H4} \quad (247)$$

$$\vec{H}_5 = k_5 H \hat{\ell}_{H5} \quad (248)$$

$$\vec{H}_6 = k_6 H \hat{\ell}_{H6} \quad (249)$$

For this CMG mode of operation, figure 9.16 is the corresponding signal flow logic diagram associated with this singularity avoidance scheme.

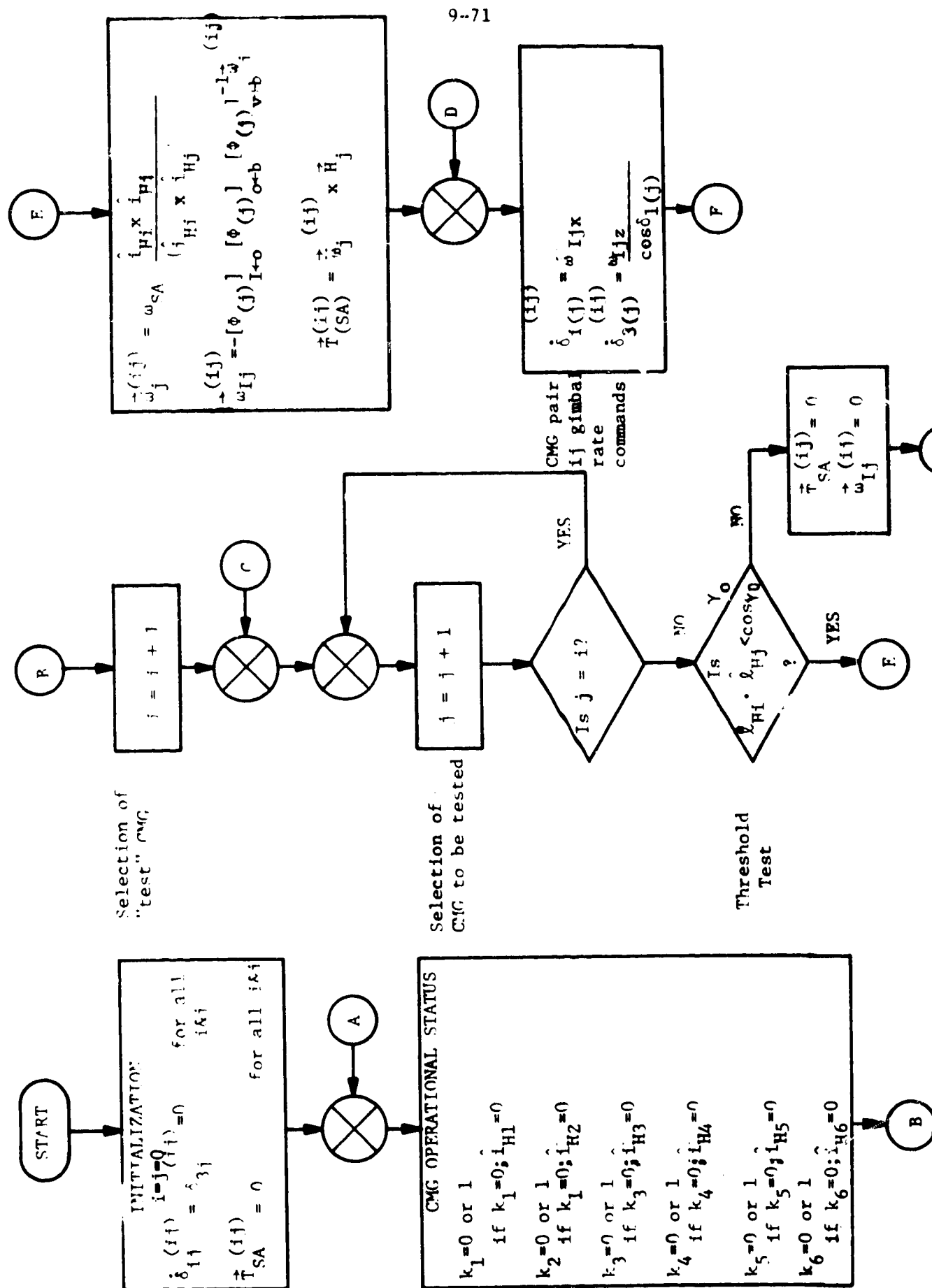


Figure 9.16. Signal Flow Logic Diagram for Arbitrary Torquing of CMGs Away From Singularity (Six Individual CMG Mode) (Sheet 1 of 2)

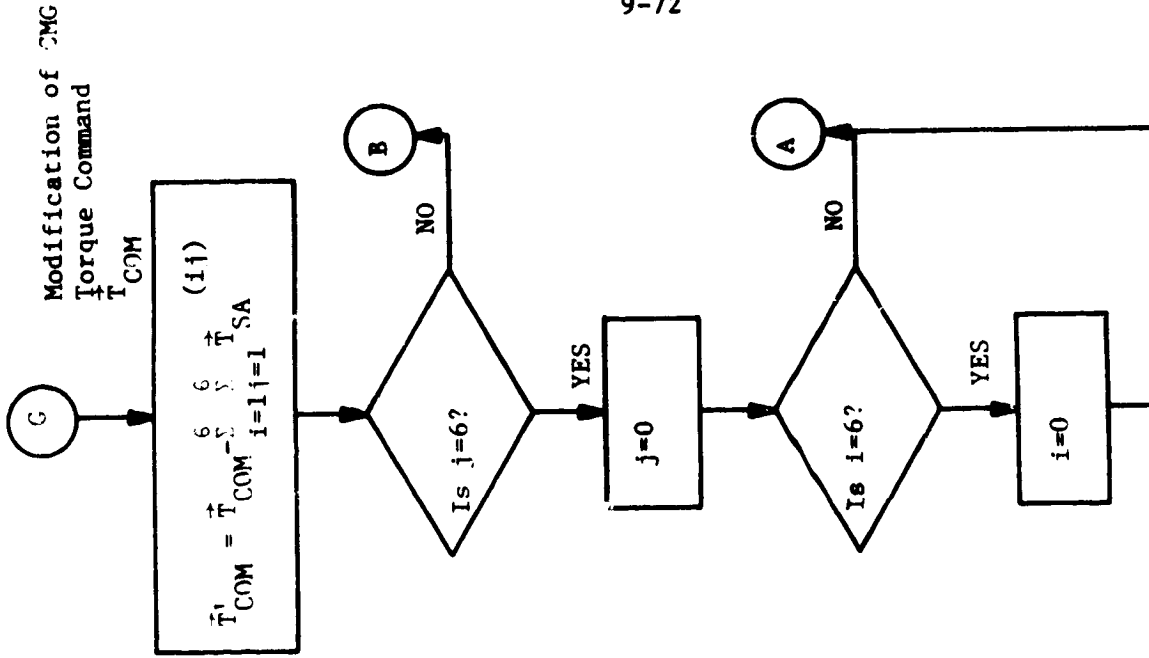
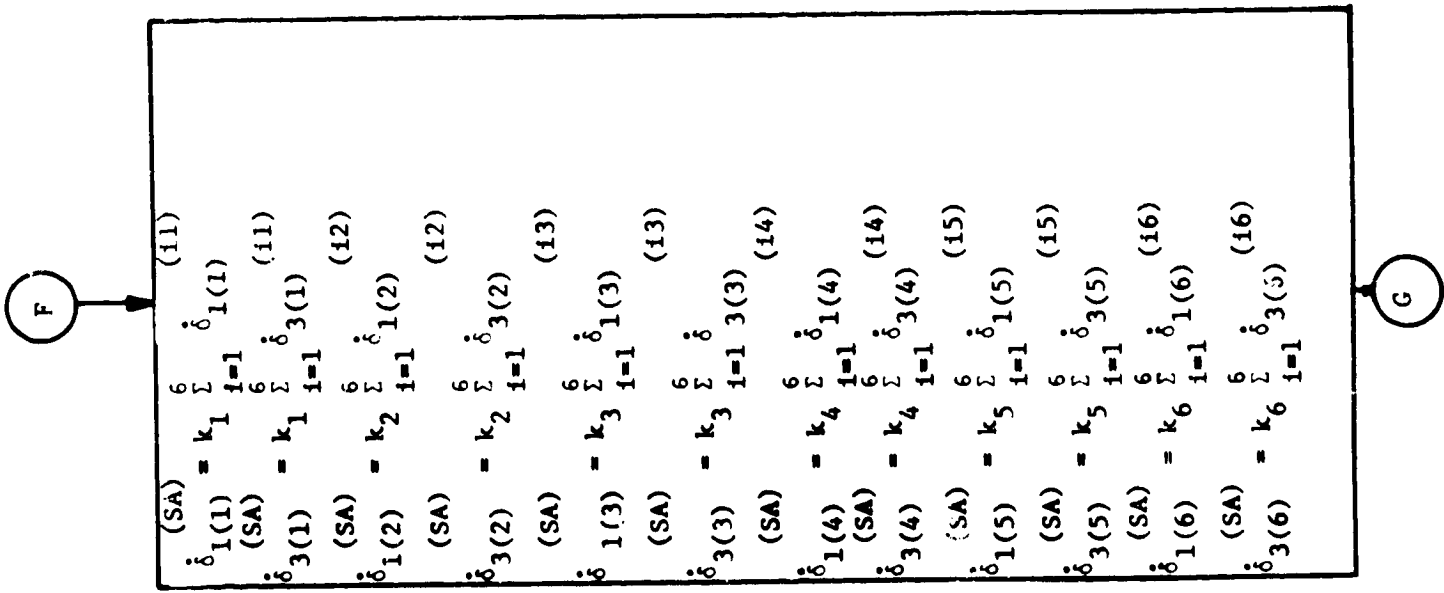


Figure 9.16. Signal Flow Logic Diagram for Arbitrary Torquing CMGs Away From Singularity (Six Individual CMG Mode) (Sheet 2 of 2)



9.5.2 Isogonal CMG Distribution Law - This singularity avoidance scheme distributes the individual CMG momentum vectors \vec{H}_i such that each CMG contributes an equal portion to the total CMG momentum vector \vec{H}_{CMG} . As shown in figure 9.17 the individual momentum vectors \vec{H}_i form a cone about \vec{H}_{CMG} . Because each CMG momentum vector \vec{H}_i has a component that is along \vec{H}_{CMG} , the anti-parallel singularity condition is prevented.

Like the decoupled scissored pair CMG control law, the CMGs are grouped into pairs. Let figure 9.18 represent CMG pair (1,2). \hat{l}_{H1} and \hat{l}_{H2} are unit vectors along \vec{H}_1 and \vec{H}_2 , respectively. The CMG momentum vectors \vec{H}_1 and \vec{H}_2 are distributed by rotating the CMG pair about its vector sum \vec{H}_{12} at a rate $\vec{\omega}_{12}$. Because $\vec{\omega}_{12}$ and \vec{H}_{12} are parallel, no net torque is exerted on the vehicle.

$$\vec{\omega}_{12} \times \vec{H}_{12} = \vec{\omega}_{12} \times \vec{H}_1 + \vec{\omega}_{12} \times \vec{H}_2 = 0 \quad (250)$$

or

$$\vec{\omega}_{12} \times \hat{l}_{H1} + \vec{\omega}_{12} \times \hat{l}_{H2} = 0 \quad (251)$$

$\vec{\omega}_{12} \times \hat{l}_{H1}$ and $\vec{\omega}_{12} \times \hat{l}_{H2}$ are normalized torque commands associated with CMGs 1 and 2, respectively. Let

$$\dot{\hat{l}}_{H1} = \vec{\omega}_{12} \times \hat{l}_{H1} \quad (252)$$

$$\dot{\hat{l}}_{H2} = \vec{\omega}_{12} \times \hat{l}_{H2} \quad (253)$$

where $\dot{\hat{l}}_{H1}$ and $\dot{\hat{l}}_{H2}$ are rate of change of the normalized momentum vectors \hat{l}_{H1} and \hat{l}_{H2} . Since $\vec{\omega}_{12}$ lies along \vec{H}_{12} , $\vec{\omega}_{12}$ can be written as

$$\vec{\omega}_{12} = \epsilon_{12} (\dot{\hat{l}}_{H1} + \dot{\hat{l}}_{H2}) \quad (254)$$

where ϵ_{12} is a scalar error function corresponding to CMG pair (1,2). ϵ_{12} is proportional to the difference between the projections of \hat{l}_{H1} and \hat{l}_{H2} onto the normalized total CMG momentum

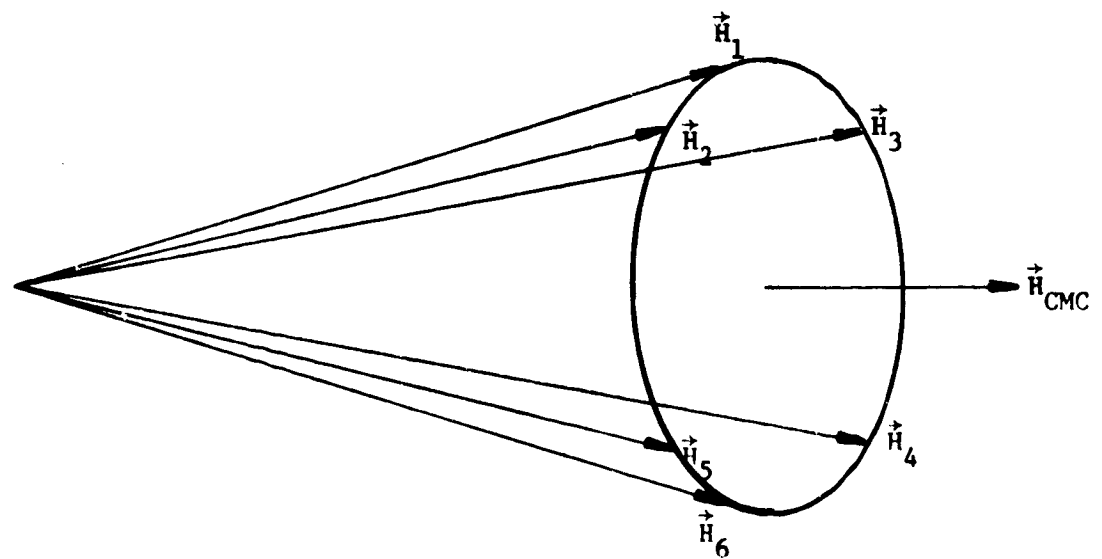


Figure 9.17. Sketch of an Isogonal CMC Distribution

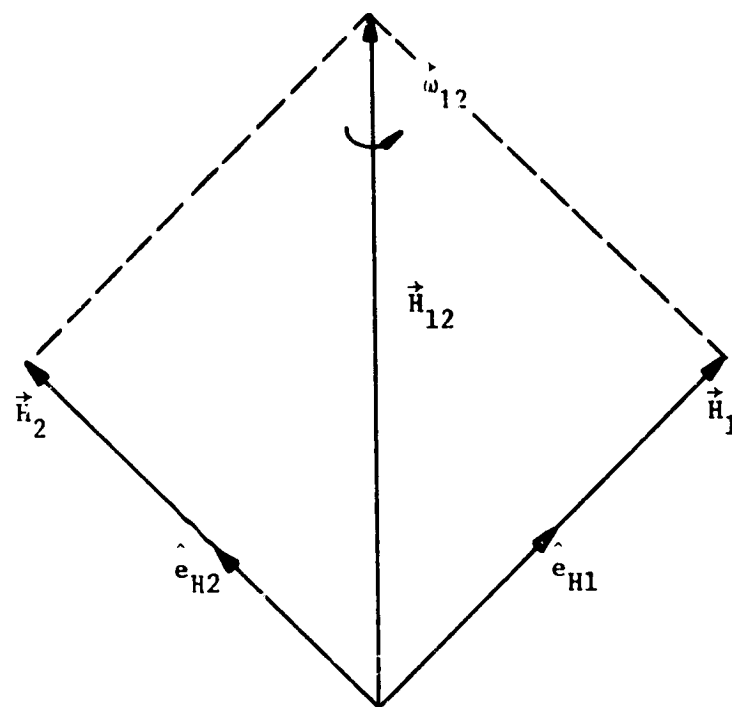


Figure 9.18. CMG Pair 1, 2

vector \hat{l}_T ($\hat{l}_T = \frac{\vec{H}_{CMG}}{|\vec{H}_{CMG}|}$). ϵ_{12} equals

$$\epsilon_{12} = k_c (\hat{l}_{H1} \cdot \hat{l}_T - \hat{l}_{H2} \cdot \hat{l}_T) \quad (255)$$

Substituting equations 254 and 255 into 252 and 253, the normalized CMG torque commands $\dot{\hat{l}}_{H1}$ and $\dot{\hat{l}}_{H2}$ equal

$$\dot{\hat{l}}_{H1} = k_c (\hat{l}_{H1} \cdot \hat{l}_T - \hat{l}_{H2} \cdot \hat{l}_T) (\hat{l}_{H2} \times \hat{l}_{H1}) \quad (256)$$

$$\dot{\hat{l}}_{H2} = k_c (\hat{l}_{H1} \cdot \hat{l}_T - \hat{l}_{H2} \cdot \hat{l}_T) (\hat{l}_{H1} \times \hat{l}_{H2}) \quad (257)$$

These normalized torque commands can be converted into the appropriate CMG gimbal commands $\delta_{1(1)}^{(SA)}$, $\delta_{3(1)}^{(SA)}$, $\delta_{1(2)}^{(SA)}$, and $\delta_{3(2)}^{(SA)}$ by recognizing that

$$\dot{\hat{l}}_{H1} = \omega_1^{(12)} \times \hat{l}_{H1} \quad (258)$$

$$\dot{\hat{l}}_{H2} = \omega_2^{(12)} \times \hat{l}_{H2} \quad (259)$$

From equations 256 and 257, $\omega_1^{(12)}$ and $\omega_2^{(12)}$ equal

$$\omega_1^{(12)} = k_c (\hat{l}_{H1} \cdot \hat{l}_T - \hat{l}_{H2} \cdot \hat{l}_T) \hat{l}_{H2} \quad (260)$$

$$\omega_2^{(12)} = k_c (\hat{l}_{H1} \cdot \hat{l}_T - \hat{l}_{H2} \cdot \hat{l}_T) \hat{l}_{H1} \quad (261)$$

Transforming $\omega_1^{(12)}$ and $\omega_2^{(12)}$ into the appropriate inner gimbal rate commands $\omega_{I1}^{(12)}$ and $\omega_{I2}^{(12)}$,

$$\omega_{I1}^{(12)} = -[\phi_{(1)}]_{I \rightarrow o} [\phi_{(1)}]_{o \rightarrow b} [\phi_{(1)}]_{v \rightarrow b}^{-1} \omega_1^{(12)} \quad (262)$$

$$\omega_{I2}^{(12)} = -[\phi_{(2)}]_{I \rightarrow o} [\phi_{(2)}]_{o \rightarrow b} [\phi_{(2)}]_{v \rightarrow b}^{-1} \omega_2^{(12)} \quad (263)$$

From equation 14, the singularity avoidance gimbal rate commands

$\delta_{1(1)}^{(SA)}$, $\delta_{3(1)}^{(SA)}$, $\delta_{1(2)}^{(SA)}$, and $\delta_{3(2)}^{(SA)}$ are:

$$\delta_{1(1)}^{(SA)} = \omega_{11X}^{(12)} \quad (264)$$

$$\delta_{3(1)}^{(SA)} = \frac{\omega_{11Z}^{(12)}}{\cos \delta_{1(1)}} \quad (265)$$

$$\delta_{1(2)}^{(SA)} = \omega_{12X}^{(12)} \quad (266)$$

$$\delta_{3(2)}^{(SA)} = \frac{\omega_{12Z}^{(12)}}{\cos \delta_{1(2)}} \quad (267)$$

$\omega_{11X}^{(12)}$ and $\omega_{11Z}^{(12)}$ and $\omega_{12X}^{(12)}$ and $\omega_{12Z}^{(12)}$ are the X and Z components of $\vec{\omega}_{I1}^{(12)}$ and $\vec{\omega}_{I2}^{(12)}$, respectively.

Figure 9.19 is a functional block diagram showing the relationship between the isogonal CMG distribution law and CMG control law.

Slaved CMG Mode - For the slaved CMG mode, there are three CMG pairs: (X,Y), (Y,Z), and (X,Z). The unit vectors \hat{l}_{HX} , \hat{l}_{HY} , and \hat{l}_{HZ} along the slaved CMG momentum vectors \vec{H}_x , \vec{H}_y , and \vec{H}_z are:

$$\hat{l}_{HX} = \begin{bmatrix} -\cos \delta_{1x} & \cos \delta_{3x} \\ \cos \delta_{1x} & \sin \delta_{3x} \\ & \sin \delta_{1x} \end{bmatrix} \quad (268)$$

$$\hat{l}_{HY} = \begin{bmatrix} & \sin \delta_{1y} \\ -\cos \delta_{1y} & \cos \delta_{3y} \\ \cos \delta_{1y} & \sin \delta_{3y} \end{bmatrix} \quad (269)$$

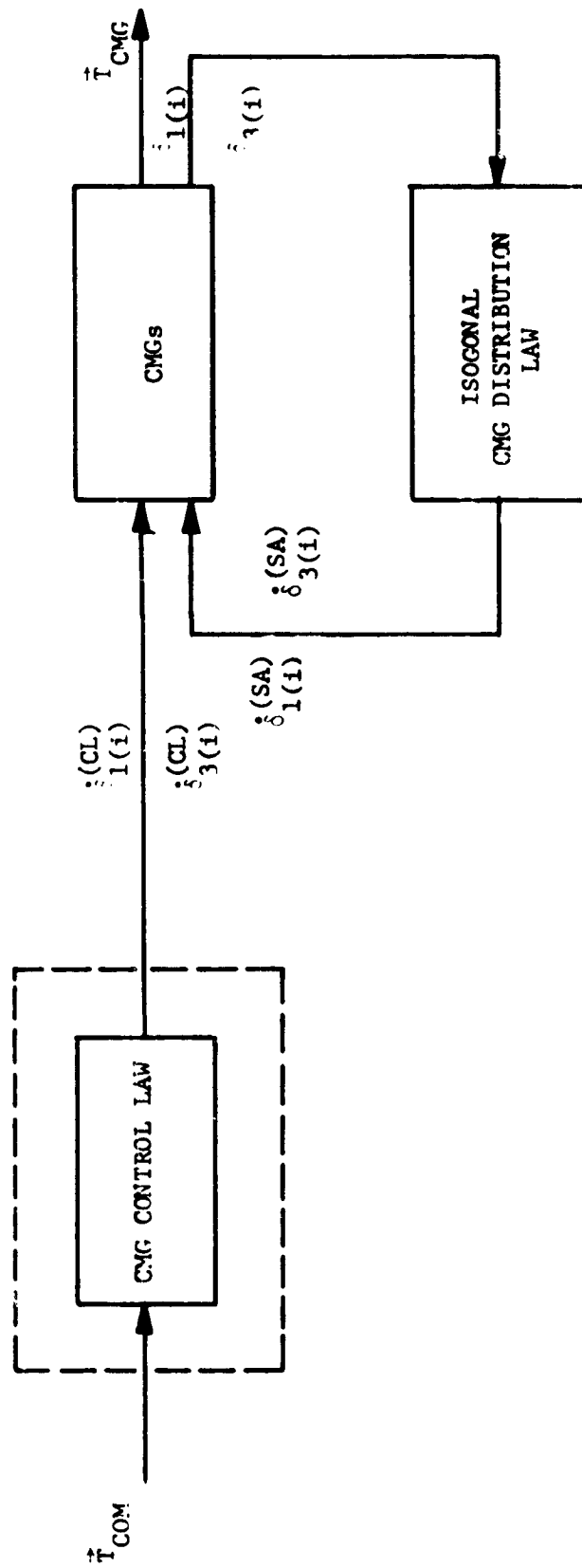


Figure 9.19. Functional Block Diagram of Isogonal CMG Distribution Law

$$\hat{\ell}_{HZ} = \begin{bmatrix} \cos \delta_{1z} & \sin \delta_{3z} \\ & \sin \delta_{1z} \\ -\cos \delta_{1z} & \cos \delta_{3z} \end{bmatrix} \quad (270)$$

For CMG pair (X,Y), the normalized CMG torque commands $\dot{\ell}_{HX}^{(XY)}$ and $\dot{\ell}_{HY}^{(XY)}$ equal

$$\dot{\ell}_{HX}^{(XY)} = \omega_{XY} x k_x \hat{\ell}_{HX} \quad (271)$$

$$\dot{\ell}_{HY}^{(XY)} = \omega_{XY} y k_y \hat{\ell}_{HY} \quad (272)$$

k_x and k_y are the slaved CMG operational status gains previously defined. ω_{XY} equal

$$\omega_{XY} = \epsilon_{XY} [k_x \hat{\ell}_{HX} + k_y \hat{\ell}_{HY}] \quad (273)$$

where

$$\epsilon_{XY} = k_c [\hat{\ell}_{HX} \cdot \hat{\ell}_T - \hat{\ell}_{HY} \cdot \hat{\ell}_T] \quad (274)$$

Substituting equation 273 into 271 and 272, $\dot{\ell}_{HX}^{(XY)}$ and $\dot{\ell}_{HY}^{(XY)}$ equal

$$\dot{\ell}_{HX}^{(XY)} = \epsilon_{XY} k_y k_x (\hat{\ell}_{HY} \times \hat{\ell}_{HX}) \quad (275)$$

$$\dot{\ell}_{HY}^{(XY)} = \epsilon_{XY} k_x k_y (\hat{\ell}_{HX} \times \hat{\ell}_{HY}) \quad (276)$$

For CMG pair (Y,Z), the normalized CMG torque commands $\dot{\ell}_{HY}^{(YZ)}$ and $\dot{\ell}_{HZ}^{(YZ)}$ equal

$$\dot{\ell}_{HY}^{(YZ)} = \epsilon_{YZ} k_y k_z (\hat{\ell}_{HZ} \times \hat{\ell}_{HY}) \quad (277)$$

$$\dot{\ell}_{HZ}^{(YZ)} = \epsilon_{YZ} k_y k_z (\hat{\ell}_{HY} \times \hat{\ell}_{HZ}) \quad (278)$$

where

$$\epsilon_{YZ} = k_c [\hat{l}_{HY} \cdot \hat{l}_T - \hat{l}_{HZ} \cdot \hat{l}_T] \quad (279)$$

For CMG pair (Z,X), $\dot{\hat{l}}_{HZ}^{(ZX)}$ and $\dot{\hat{l}}_{HX}^{(ZX)}$ equal

$$\dot{\hat{l}}_{HZ}^{(ZX)} = \epsilon_{ZX} k_x k_z (\hat{l}_{HX} \times \hat{l}_{HZ}) \quad (280)$$

$$\dot{\hat{l}}_{HX}^{(ZX)} = \epsilon_{ZX} k_z k_x (\hat{l}_{HZ} \times \hat{l}_{HX}) \quad (281)$$

where

$$\epsilon_{ZX} = k_c [\hat{l}_{HZ} \cdot \hat{l}_T - \hat{l}_{HX} \cdot \hat{l}_T] \quad (282)$$

The combined normalized torque commands $\dot{\hat{l}}_{HX}$, $\dot{\hat{l}}_{HY}$, and $\dot{\hat{l}}_{HZ}$ associated with each slaved CMG pair equals

$$\begin{aligned} \dot{\hat{l}}_{HX} &= \dot{\hat{l}}_{HX}^{(XY)} + \dot{\hat{l}}_{HX}^{(ZX)} \\ &= \omega_X^{(SA)} \times \hat{l}_{HX} \end{aligned} \quad (283)$$

$$\begin{aligned} \dot{\hat{l}}_{HY} &= \dot{\hat{l}}_{HY}^{(XY)} + \dot{\hat{l}}_{HY}^{(YZ)} \\ &= \omega_Y^{(SA)} \times \hat{l}_{HY} \end{aligned} \quad (284)$$

$$\begin{aligned} \dot{\hat{l}}_{HZ} &= \dot{\hat{l}}_{HZ}^{(YZ)} + \dot{\hat{l}}_{HZ}^{(ZX)} \\ &= \omega_Z^{(SA)} \times \hat{l}_{HZ} \end{aligned} \quad (285)$$

where

$$\dot{\omega}_X^{(SA)} = k_x (k_y \epsilon_{XY} \hat{l}_{HY} + k_z \epsilon_{ZX} \hat{l}_{HZ}) \quad (286)$$

$$\dot{\omega}_Y^{(SA)} = k_y (k_x \epsilon_{XY} \hat{l}_{HX} + k_z \epsilon_{YZ} \hat{l}_{HZ}) \quad (287)$$

$$\dot{\omega}_Z^{(SA)} = k_z (k_y \epsilon_{YZ} \hat{l}_{HY} + k_x \epsilon_{ZX} \hat{l}_{HX}) \quad (288)$$

The CMG rates $\dot{\omega}_X^{(SA)}$, $\dot{\omega}_Y^{(SA)}$, and $\dot{\omega}_Z^{(SA)}$ are transformed into the following inner gimbal rate commands $\dot{\omega}_{IX}^{(SA)}$, $\dot{\omega}_{IY}^{(SA)}$, and $\dot{\omega}_{IZ}^{(SA)}$.

$$\dot{\omega}_{IX}^{(SA)} = -[\phi_{(x)}]_{I \leftarrow o} [\phi_{(x)}]_{o \leftarrow b} [\phi_{(x)}]_{v \leftarrow b}^{-1} \dot{\omega}_X^{(SA)} \quad (289)$$

$$\dot{\omega}_{IY}^{(SA)} = -[\phi_{(y)}]_{I \leftarrow o} [\phi_{(y)}]_{o \leftarrow b} [\phi_{(y)}]_{v \leftarrow b}^{-1} \dot{\omega}_Y^{(SA)} \quad (290)$$

$$\dot{\omega}_{IZ}^{(SA)} = -[\phi_{(z)}]_{I \leftarrow o} [\phi_{(z)}]_{o \leftarrow b} [\phi_{(z)}]_{v \leftarrow b}^{-1} \dot{\omega}_Z^{(SA)} \quad (291)$$

Using equation 14, the above rates are converted into the appropriate slaved CMG gimbal rate commands:

$$\dot{\delta}_{1x}^{(SA)} = \dot{\omega}_{IX}^{(SA)} \quad (292)$$

$$\dot{\delta}_{3x}^{(SA)} = \frac{\dot{\omega}_{IXZ}^{(SA)}}{\cos \delta_{1x}} \quad (293)$$

$$\dot{\delta}_{1y}^{(SA)} = \dot{\omega}_{IYX}^{(SA)} \quad (294)$$

$$\dot{\delta}_{3y}^{(SA)} = \frac{\dot{\omega}_{IYZ}^{(SA)}}{\cos \delta_{1y}} \quad (295)$$

$$\dot{\delta}_{1z}^{(SA)} = \dot{\omega}_{IZX}^{(SA)} \quad (296)$$

$$\dot{\delta}_{3z}^{(SA)} = \frac{\omega_{IZZ}^{(SA)}}{\cos \delta_{1z}} \quad (297)$$

$\omega_{1XX}^{(SA)}$, $\omega_{1XZ}^{(SA)}$, $\omega_{1YX}^{(SA)}$, . . . , etc., are the X and Z components of $\vec{\omega}_{IX}^{(SA)}$, $\vec{\omega}_{IY}^{(SA)}$, and $\vec{\omega}_{IZ}^{(SA)}$, respectively. The individual CMG gimbal rate $\dot{\delta}_{1(i)}^{(SA)}$ and $\dot{\delta}_{3(i)}^{(SA)}$ are:

$$\begin{bmatrix} \dot{\delta}_{1(1)}^{(SA)} \\ \dot{\delta}_{1(3)}^{(SA)} \\ \dot{\delta}_{1(5)}^{(SA)} \end{bmatrix} = \begin{bmatrix} k_1 & 0 & 0 \\ 0 & k_3 & 0 \\ 0 & 0 & k_5 \end{bmatrix} \begin{bmatrix} \dot{\delta}_{1x}^{(SA)} \\ \dot{\delta}_{1y}^{(SA)} \\ \dot{\delta}_{1z}^{(SA)} \end{bmatrix} \quad (298)$$

$$\begin{bmatrix} \dot{\delta}_{3(1)}^{(SA)} \\ \dot{\delta}_{3(3)}^{(SA)} \\ \dot{\delta}_{3(5)}^{(SA)} \end{bmatrix} = \begin{bmatrix} k_1 & 0 & 0 \\ 0 & k_3 & 0 \\ 0 & 0 & k_5 \end{bmatrix} \begin{bmatrix} \dot{\delta}_{3x}^{(SA)} \\ \dot{\delta}_{3y}^{(SA)} \\ \dot{\delta}_{3z}^{(SA)} \end{bmatrix} \quad (299)$$

$$\begin{bmatrix} \dot{\delta}_{1(2)}^{(SA)} \\ \dot{\delta}_{1(4)}^{(SA)} \\ \dot{\delta}_{1(6)}^{(SA)} \end{bmatrix} = \begin{bmatrix} k_2 & 0 & 0 \\ 0 & k_4 & 0 \\ 0 & 0 & k_6 \end{bmatrix} \begin{bmatrix} \dot{\delta}_{1x}^{(SA)} \\ \dot{\delta}_{1y}^{(SA)} \\ \dot{\delta}_{1z}^{(SA)} \end{bmatrix} \quad (300)$$

$$\begin{bmatrix} \dot{\delta}_{3(2)}^{(SA)} \\ \dot{\delta}_{3(4)}^{(SA)} \\ \dot{\delta}_{3(6)}^{(SA)} \end{bmatrix} = \begin{bmatrix} k_2 & 0 & 0 \\ 0 & k_4 & 0 \\ 0 & 0 & k_6 \end{bmatrix} \begin{bmatrix} \dot{\delta}_{3x}^{(SA)} \\ \dot{\delta}_{3y}^{(SA)} \\ \dot{\delta}_{3z}^{(SA)} \end{bmatrix} \quad (301)$$

Six Individual CMG Mode - For this mode of operation, there are 15 CMG pairs: (1,2), (1,3), (1,4), (1,5), (1,6), (2,3), (2,4), (2,5), (2,6), (3,4), (3,5), (3,6), (4,5), (4,6), and (5,6). The unit vectors \hat{l}_{H1} , \hat{l}_{H2} , \hat{l}_{H3} , \hat{l}_{H4} , \hat{l}_{H5} , and \hat{l}_{H6} are:

$$\hat{l}_{H1} = \begin{bmatrix} -\cos \delta_{1(1)} & \cos \delta_{3(1)} \\ \cos \delta_{1(1)} & \sin \delta_{3(1)} \\ & \sin \delta_{1(1)} \end{bmatrix} \quad (302)$$

$$\hat{l}_{H2} = \begin{bmatrix} -\cos \delta_{1(2)} & \sin \delta_{3(2)} \\ \cos \delta_{1(2)} & \sin \delta_{3(2)} \\ & \sin \delta_{1(2)} \end{bmatrix} \quad (303)$$

$$\hat{l}_{H3} = \begin{bmatrix} & \sin \delta_{1(3)} \\ -\cos \delta_{1(3)} & \cos \delta_{3(3)} \\ \cos \delta_{1(3)} & \sin \delta_{3(3)} \end{bmatrix} \quad (304)$$

$$\hat{l}_{H4} = \begin{bmatrix} & \sin \delta_{1(4)} \\ -\cos \delta_{1(4)} & \cos \delta_{3(4)} \\ \cos \delta_{1(4)} & \sin \delta_{3(4)} \end{bmatrix} \quad (305)$$

$$\hat{l}_{H5} = \begin{bmatrix} \cos \delta_{1(5)} & \sin \delta_{3(5)} \\ \sin \delta_{1(5)} & \\ -\cos \delta_{1(5)} & \cos \delta_{3(5)} \end{bmatrix} \quad (306)$$

$$\hat{\ell}_{H6} = \begin{bmatrix} \cos \delta_{1(6)} & \sin \delta_{3(6)} \\ \sin \delta_{1(6)} \\ -\cos \delta_{1(6)} & \cos \delta_{3(6)} \end{bmatrix} \quad (307)$$

The normalized torque commands $\dot{\hat{\ell}}_{H1}^{(ij)}$ and $\dot{\hat{\ell}}_{Hj}^{(ij)}$ for the general CMG pair (i,j) are:

$$\dot{\hat{\ell}}_{H1}^{(ij)} = \epsilon_{ij} k_j k_i (\hat{\ell}_{Hj} \times \hat{\ell}_{H1}) \quad (308)$$

$$\dot{\hat{\ell}}_{Hj}^{(ij)} = \epsilon_{ij} k_i k_j (\hat{\ell}_{H1} \times \hat{\ell}_{Hj}) \quad (309)$$

where

$$\epsilon_{ij} = k_c [\hat{\ell}_{H1} \cdot \hat{\ell}_T - \hat{\ell}_{Hj} \cdot \hat{\ell}_T] \quad (310)$$

Summing all the normalized torque commands associated with the i^{th} CMG, the total i^{th} CMG torque command equals

$$\dot{\hat{\ell}}_{Hi} = \sum \dot{\hat{\ell}}_{Hi}^{(ij)} = \omega_i^{(SA)} \times \hat{\ell}_{Hi} \quad (311)$$

The negative of $\omega_i^{(SA)}$ is transformed into the i^{th} CMG inner gimbal space to compute the CMG inner gimbal rate command $\omega_{Ii}^{(SA)}$.

$$\omega_{Ii}^{(SA)} = -[\phi_{(i)}]_{I \leftarrow O} [\phi_{(i)}]_{O \leftarrow B} [\phi_{(i)}]_{B \leftarrow V}^{-1} \omega_i^{(SA)} \quad (312)$$

Using equation 14, the appropriate i^{th} CMG gimbal rate commands $\dot{\delta}_{1(i)}^{(SA)}$ and $\dot{\delta}_{3(i)}^{(SA)}$ are computed.

$$\dot{\delta}_{1(i)}^{(SA)} = \omega_{Iix}^{(SA)} \quad (313)$$

$$\dot{\delta}_{3(i)}^{(SA)} = \frac{\omega_{Iiz}^{(SA)}}{\cos \delta_{1(i)}} \quad (314)$$

The above procedure is repeated to compute the other five sets of gimbal rate commands.

9.5.3 Optimal CMG Distribution Law - This singularity avoidance scheme attempts to further optimize the Pseudo-Inverse CMG Control Law described in section 9.4.4. The Pseudo-Inverse CMG Control Law minimizes the sum of the square of the gimbal rate

commands $\dot{\delta}_{1(i)}^{(CL)}$ and $\dot{\delta}_{3(i)}^{(CL)}$ needed to generate the torque command \vec{T}_{COM} . The solution of this control problem takes the following form:

$$\dot{\delta}_{1(i)}^{(CL)} = \frac{1}{H} [A]^T [G]^{-1} (\vec{T}_{COM} - \vec{\omega} \times \vec{H}_{CMG}) \quad (315)$$

$$\dot{\delta}_{3(i)}^{(CL)} = \frac{1}{H} [B]^T [G]^{-1} (\vec{T}_{COM} - \vec{\omega} \times \vec{H}_{CMG}) \quad (316)$$

The inverse of $[G]$ is inversely proportional to the determinant of $[G]$, $\det [G]$. When $\det [G]$ approaches zero, the resultant

gimbal rate commands $\dot{\delta}_{1(i)}^{(CL)}$ and $\dot{\delta}_{3(i)}^{(CL)}$ tend to "blow-up" indicating

that the system is approaching either saturation or an anti-parallel singularity condition. This optimal CMG singularity avoidance scheme avoids the anti-parallel singularity condition by distributing the CMG gimbal angles $\delta_{1(i)}$ and $\delta_{3(i)}$ in such a manner as to maximize the magnitude of $\det [G]$. By maximizing the magnitude of

$\det [G]$, the resultant gimbal rate commands $\dot{\delta}_{1(i)}^{(CL)}$ and $\dot{\delta}_{3(i)}^{(CL)}$ are

also minimized thus further optimizing the Pseudo-Inverse CMG Control Law. The reason for maximizing the magnitude of $\det [G]$ rather than just $\det [G]$ is that if $\det [G]$ is negative and one tried to maximize just $\det [G]$, its value would be driven through zero, an anti-parallel singularity condition, towards its maximum positive value. Since the purpose of a singularity avoidance scheme is to avoid singularity, the magnitude of $\det [G]$ is maximized instead of $\det [G]$. Now if $\det [G]$ is negative, $\det [G]$ is driven towards its largest negative value away from zero thus, avoiding singularity. Figure 9.20 is a functional block diagram of this singularity avoidance system.

Slaved CMG Mode - First, a designation between the CMG gimbal rate commands that are generated by the CMG control law and singularity avoidance scheme must be made. Let $\dot{\delta}_{1C}$ and $\dot{\delta}_{3C}$ and $\dot{\delta}_{1D}$ and $\dot{\delta}_{3D}$ represent the CMG gimbal rate commands that result from the CMG control law and singularity avoidance scheme, respectively.

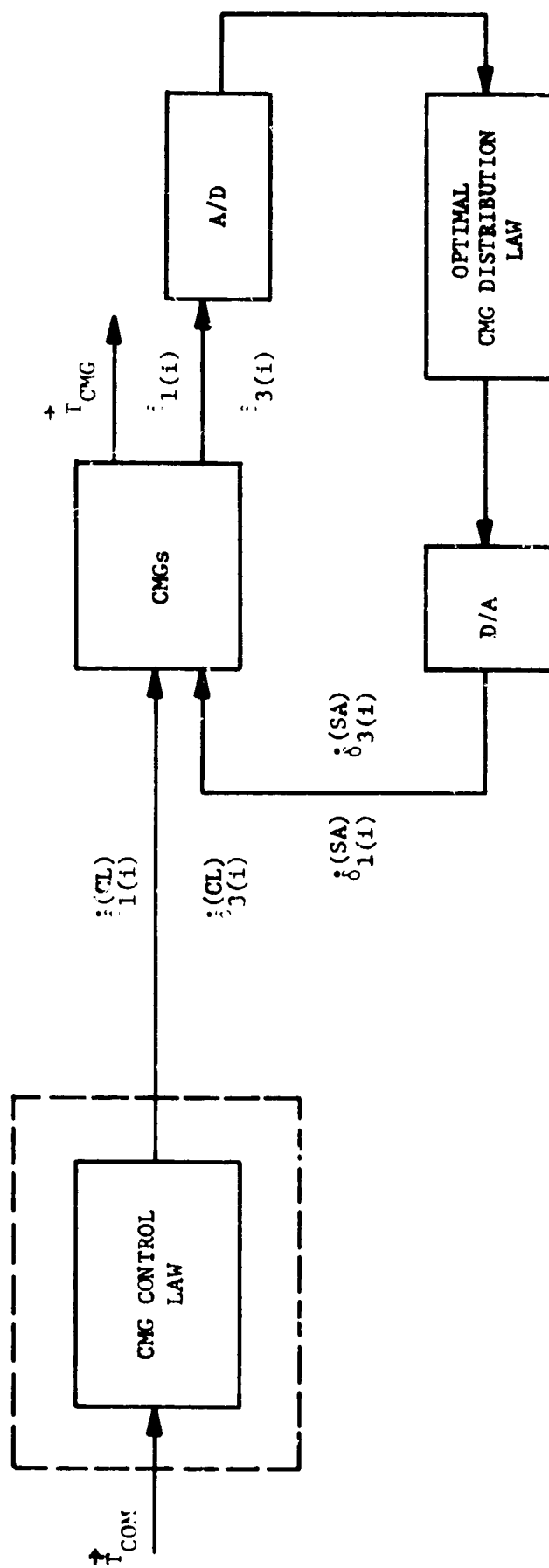


Figure 9.20. Block Diagram of Optimal CMG Distribution Law

The performance index P is the same one used in the development of the Decoupled Pseudo-Inverse CMG Control Law except that $\dot{\delta}_{1D}$ and $\dot{\delta}_{3D}$ replace $\dot{\delta}_{1C}$ and $\dot{\delta}_{3C}$, respectively.

$$P = \frac{1}{2} \{ \dot{\delta}_{1D}^T [k_{(1)}^2]^{-1} \dot{\delta}_{1D} + \dot{\delta}_{3D}^T [k_{(1)}^2] \dot{\delta}_{3D} \} \quad (317)$$

The objective of this distribution law is to maximize the magnitude of $\det [G]$ without exerting a net torque on the vehicle due to this redistribution of CMG gimbal angles. Let

$$f(\delta_1, \delta_3) = \det [G] \quad (318)$$

δ_1 and δ_3 are the actual CMG gimbal angles as measured by the CMG gimbal resolver trains. To maximize $f(\delta_1, \delta_3)$, the derivative of $\frac{df}{dt}$ times sign of f must be positive.

$$\text{sgn}(f) \frac{df}{dt} = \text{sgn}(f) \{ \nabla f_1 \cdot \dot{\delta}_{1D} + \nabla f_3 \cdot \dot{\delta}_{3D} \} = \gamma > 0 \quad (319)$$

∇f is the gradient of f and the function $\text{sgn}(\)$ has the magnitude of unity with the same sign as the quantity enclosed within the parentheses. ∇f_1 and ∇f_3 equal

$$\nabla f_1 = \begin{bmatrix} \frac{df}{d\delta_{1x}} \\ \frac{df}{d\delta_{1y}} \\ \frac{df}{d\delta_{1z}} \end{bmatrix} \quad (320)$$

$$\nabla f_3 = \begin{bmatrix} \frac{df}{d\delta_{3x}} \\ \frac{df}{d\delta_{3y}} \\ \frac{df}{d\delta_{3z}} \end{bmatrix} \quad (321)$$

The other constraint equation states that the net torque acting on the vehicle is zero.

$$[k_{(1)}][A']\dot{\delta}_{1D} + [k_{(1)}][B']\dot{\delta}_{3D} = 0 \quad (322)$$

The Lagrange adjoin equation formed from equations 317, 319, and 322 equals

$$L = \frac{1}{2} \{ \dot{\delta}_{1D}^T [k_{(1)}^2]^{-1} \dot{\delta}_{1D} + \dot{\delta}_{3D}^T [k_{(1)}^2]^{-1} \dot{\delta}_{3D} \} - \lambda^T \{ [A'_{(1)}]\dot{\delta}_{1D} + [B'_{(1)}]\dot{\delta}_{3D} - \gamma \operatorname{sgn}(f) \hat{e} \} \quad (323)$$

where

$$[A'_{(1)}] = \begin{bmatrix} [k_{(1)}][A'] \\ \frac{df}{d\delta_{1x}} & \frac{df}{d\delta_{1y}} & \frac{df}{d\delta_{1z}} \end{bmatrix} \quad (324)$$

$$[B'_{(1)}] = \begin{bmatrix} [k_{(1)}][B'] \\ \frac{df}{d\delta_{3x}} & \frac{df}{d\delta_{3y}} & \frac{df}{d\delta_{3z}} \end{bmatrix} \quad (325)$$

$$\hat{e} = \begin{bmatrix} 0 \\ 0 \\ 0 \\ 1 \end{bmatrix} \quad (326)$$

Note that $[A'_{(1)}]$ and $[B'_{(1)}]$ are 3 by 4 matrices. To minimize L , the partial derivatives $\frac{dL}{d\dot{\delta}_{1D}}$, $\frac{dL}{d\dot{\delta}_{3D}}$, and $\frac{dL}{d\lambda}$ are set equal to zero.

$$\frac{dL}{d\dot{\delta}_{1D}} = [k^2_{(1)}]^{-1} \dot{\delta}_{1D} - [A'_{(1)}]^T \lambda = 0 \quad (327)$$

$$\frac{dL}{d\dot{\delta}_{3D}} = [k^2_{(1)}]^{-1} \dot{\delta}_{3D} - [B'_{(1)}]^T \lambda = 0 \quad (328)$$

$$\frac{dL}{d\lambda} = -\{[A'_{(1)}] \dot{\delta}_{1D} + [B'_{(1)}] \dot{\delta}_{3D} - \gamma \operatorname{sgn}(\bar{z}) \hat{e}\} = 0 \quad (329)$$

Solving equations 327 and 328 for $\dot{\delta}_{1D}$ and $\dot{\delta}_{3D}$,

$$\dot{\delta}_{1D} = [k_{(1)}^2] [A'_{(1)}]^T \lambda \quad (330)$$

$$\dot{\delta}_{3D} = [k_{(1)}^2] [B'_{(1)}]^T \lambda \quad (331)$$

Substituting equations 330 and 331 into 329,

$$[J] \lambda = \gamma \operatorname{sgn}(f) \hat{e} \quad (332)$$

where

$$[J] = [A'_{(1)}] [k_{(1)}^2] [A'_{(1)}]^T + [B'_{(1)}] [k_{(1)}^2] [B'_{(1)}]^T \quad (333)$$

λ equals

$$\lambda = [J]^{-1} \gamma \operatorname{sgn}(f) \hat{e} \quad (334)$$

Substituting equation 334 into equations 330 and 331, the gimbal rate commands $\dot{\delta}_{1D}$ and $\dot{\delta}_{3D}$ equal

$$\dot{\delta}_{1D} = \operatorname{sgn}(f) [k_{(1)}^2] [A'_{(1)}]^T [J]^{-1} \gamma \hat{e} \quad (335)$$

$$\dot{\delta}_{3D} = \operatorname{sgn}(f) [k_{(1)}^2] [B'_{(1)}]^T [J]^{-1} \gamma \hat{e} \quad (336)$$

The only remaining task is to select the positive scalar γ . But note that as the magnitude of the det [G] approaches its maximum, gradient of f , ∇f_1 and ∇f_3 , approach zero. Under these conditions, the gimbal rate commands $\dot{\delta}_{1D}$ and $\dot{\delta}_{3D}$ as defined by equations 335 and 336, respectively can be excessive even for very small values of γ . Because each CMG has a physical gimbal rate limit, these potentially excessive CMG gimbal rate limits must be avoided.

One method of solving the above problem is to normalize $\dot{\delta}_{1D}$ and $\dot{\delta}_{3D}$ and then limit their magnitude so that the total gimbal rate command due to both the CMG control law and singularity avoidance scheme is limited to an acceptable value α_{max} . $\dot{\delta}_{1D}$ and $\dot{\delta}_{3D}$ can be normalized as follows:

$$\dot{\delta}_{1D}^{(n)} = \frac{\dot{\delta}_{1D}'}{\dot{\delta}_{norm}} \quad (337)$$

$$\dot{\delta}_{3D}^{(n)} = \frac{\dot{\delta}_{3D}'}{\dot{\delta}_{norm}} \quad (338)$$

where

$$\dot{\delta}_{1D}' = \text{sgn}(f) [k_{(1)}^2] [A']^T [J]^{-1} \hat{e} \quad (339)$$

$$\dot{\delta}_{3D}' = \text{sgn}(f) [k_{(1)}^2] [B']^T [J]^{-1} \hat{e} \quad (340)$$

$$\dot{\delta}_{norm} = (\dot{\delta}_{1D}'^2 + \dot{\delta}_{3D}'^2)^{1/2} \quad (341)$$

Note that normalized values of $\dot{\delta}_{1D}$ and $\dot{\delta}_{3D}$, $\dot{\delta}_{1D}^{(n)}$ and $\dot{\delta}_{3D}^{(n)}$ are no longer a function of γ . The normalized vector quantities $\dot{\delta}_{1D}^{(n)}$ and $\dot{\delta}_{3D}^{(n)}$ describe only the relative magnitudes and directions of $\dot{\delta}_{1D}$ and $\dot{\delta}_{3D}$ but, not their actual magnitudes. To compute $\dot{\delta}_{1D}$ and $\dot{\delta}_{3D}$, define the following parameter.

$$\alpha_{max}^{(D)} = (\alpha_{max}^2 - \dot{\delta}_{norm}^2)^{1/2} \quad (342)$$

If $\alpha_{\max}^{(D)}$ is negative, the CMG distribution gimbal rate commands $\dot{\delta}_{1D}$ and $\dot{\delta}_{3D}$ are set equal to zero. This condition indicates that the combined magnitudes of $\dot{\delta}_{1C}$ and $\dot{\delta}_{3C}$ exceed α_{\max} . This condition may occur occasionally for very short time intervals due to either a very large disturbance torque or a CMG vehicle maneuver. If the combined magnitudes of $\dot{\delta}_{1C}$ and $\dot{\delta}_{3C}$ exceed α_{\max} too often, the value of α_{\max} should be reviewed and increased if possible, or more stringent limits placed on the magnitude of $\dot{\delta}_{1C}$ and $\dot{\delta}_{3C}$. For the general case where $\alpha_{\max}^{(D)}$ is positive, the gimbal rate commands $\dot{\delta}_{1D}$ and $\dot{\delta}_{3D}$ equal

$$\dot{\delta}_{1D} = \alpha_{\max}^{(D)} \dot{\delta}_{1C} \quad (343)$$

$$\dot{\delta}_{3D} = \alpha_{\max}^{(D)} \dot{\delta}_{3C} \quad (344)$$

The components of $\dot{\delta}_{1D}$ and $\dot{\delta}_{3D}$ are

$$\dot{\delta}_{1D} = \begin{bmatrix} \dot{\delta}_{1x}^{(SA)} \\ \dot{\delta}_{1y}^{(SA)} \\ \dot{\delta}_{1z}^{(SA)} \end{bmatrix} \quad (345)$$

$$\dot{\delta}_{3D} = \begin{bmatrix} \dot{\delta}_{3x}^{(SA)} \\ \dot{\delta}_{3y}^{(SA)} \\ \dot{\delta}_{3z}^{(SA)} \end{bmatrix} \quad (346)$$

The combined resultant CMG gimbal rate commands $\dot{\delta}_1$ and $\dot{\delta}_3$ equal

$$\dot{\delta}_1 = \dot{\delta}_{1C} + \dot{\delta}_{1D} \quad (347)$$

$$\dot{\delta}_3 = \dot{\delta}_{3C} + \dot{\delta}_{3D} \quad (348)$$

The individual CMG gimbal rate commands $\dot{\delta}_{1(1)}$ and $\dot{\delta}_{3(1)}$ equal

$$\begin{bmatrix} \dot{\delta}_{1(1)} \\ \dot{\delta}_{1(3)} \\ \dot{\delta}_{1(5)} \end{bmatrix} = \begin{bmatrix} k_1 & 0 & 0 \\ 0 & k_3 & 0 \\ 0 & 0 & k_5 \end{bmatrix} \begin{bmatrix} \dot{\delta}_{1x}^{(CL)} + \dot{\delta}_{1x}^{(SA)} \\ \dot{\delta}_{1y}^{(CL)} + \dot{\delta}_{1y}^{(SA)} \\ \dot{\delta}_{1z}^{(CL)} + \dot{\delta}_{1z}^{(SA)} \end{bmatrix} \quad (349)$$

$$\begin{bmatrix} \dot{\delta}_{1(2)} \\ \dot{\delta}_{1(4)} \\ \dot{\delta}_{1(6)} \end{bmatrix} = \begin{bmatrix} k_2 & 0 & 0 \\ 0 & k_4 & 0 \\ 0 & 0 & k_6 \end{bmatrix} \begin{bmatrix} \dot{\delta}_{1x}^{(CL)} + \dot{\delta}_{1x}^{(SA)} \\ \dot{\delta}_{1y}^{(CL)} + \dot{\delta}_{1y}^{(SA)} \\ \dot{\delta}_{1z}^{(CL)} + \dot{\delta}_{1z}^{(SA)} \end{bmatrix} \quad (350)$$

$$\begin{bmatrix} \dot{\delta}_{3(1)} \\ \dot{\delta}_{3(3)} \\ \dot{\delta}_{3(5)} \end{bmatrix} = \begin{bmatrix} k_1 & 0 & 0 \\ 0 & k_3 & 0 \\ 0 & 0 & k_5 \end{bmatrix} \begin{bmatrix} \dot{\delta}_{3x}^{(CL)} + \dot{\delta}_{3x}^{(SA)} \\ \dot{\delta}_{3y}^{(CL)} + \dot{\delta}_{3y}^{(SA)} \\ \dot{\delta}_{3z}^{(CL)} + \dot{\delta}_{3z}^{(SA)} \end{bmatrix} \quad (351)$$

$$\begin{bmatrix} \dot{\delta}_{3(2)} \\ \dot{\delta}_{3(4)} \\ \dot{\delta}_{3(6)} \end{bmatrix} = \begin{bmatrix} k_2 & 0 & 0 \\ 0 & k_4 & 0 \\ 0 & 0 & k_6 \end{bmatrix} \begin{bmatrix} \dot{\delta}_{3x}^{(CL)} + \dot{\delta}_{3x}^{(SA)} \\ \dot{\delta}_{3y}^{(CL)} + \dot{\delta}_{3y}^{(SA)} \\ \dot{\delta}_{3z}^{(CL)} + \dot{\delta}_{3z}^{(SA)} \end{bmatrix} \quad (352)$$

Six Individual CMG Mode - The performance index P is

$$P = \frac{1}{2} \{ \dot{\delta}_{1D}^{(1)T} [k_{(2)}^2]^{-1} \dot{\delta}_{1D}^{(1)} + \dot{\delta}_{3D}^{(1)T} [k_{(2)}^2]^{-1} \dot{\delta}_{3D}^{(1)} + \dot{\delta}_{1D}^{(2)T} [k_{(3)}^2]^{-1} \dot{\delta}_{1D}^{(2)} + \dot{\delta}_{3D}^{(2)T} [k_{(3)}^2]^{-1} \dot{\delta}_{3D}^{(2)} \} \quad (353)$$

where $\dot{\delta}_{1D}^{(1)}$, $\dot{\delta}_{3D}^{(1)}$, $\dot{\delta}_{1D}^{(2)}$, and $\dot{\delta}_{3D}^{(2)}$ are defined as follows:

$$\dot{\delta}_{1D}^{(1)} = \begin{bmatrix} \dot{\delta}_{1(1)}^{(SA)} \\ \dot{\delta}_{1(3)}^{(SA)} \\ \dot{\delta}_{1(5)}^{(SA)} \end{bmatrix} \quad (354)$$

$$\dot{\delta}_{3D}^{(1)} = \begin{bmatrix} \dot{\delta}_{3(1)}^{(SA)} \\ \dot{\delta}_{3(3)}^{(SA)} \\ \dot{\delta}_{3(5)}^{(SA)} \end{bmatrix} \quad (355)$$

$$\dot{\delta}_{1D}^{(2)} = \begin{bmatrix} \dot{\delta}_{1(2)}^{(SA)} \\ \dot{\delta}_{1(4)}^{(SA)} \\ \dot{\delta}_{1(6)}^{(SA)} \end{bmatrix} \quad (356)$$

$$\dot{\delta}_{3D}^{(2)} = \begin{bmatrix} \dot{\delta}_{3(2)}^{(SA)} \\ \dot{\delta}_{3(4)}^{(SA)} \\ \dot{\delta}_{3(6)}^{(SA)} \end{bmatrix} \quad (357)$$

The two constraints associated with the performance index P given in equation 353 are:

$$\begin{aligned} \text{sgn}(f) \frac{df}{dt} = & \text{sgn}(f) \{ \nabla f_{1(1)} \cdot \dot{\delta}_{1D}^{(1)} + \nabla f_{3(1)} \cdot \dot{\delta}_{3D}^{(1)} \\ & + \nabla f_{1(2)} \cdot \dot{\delta}_{1D}^{(2)} + \nabla f_{3(2)} \cdot \dot{\delta}_{3D}^{(2)} \} = \gamma > 0 \end{aligned} \quad (358)$$

$$[A] \dot{\delta}_{1D}^{(1)} + [B] \dot{\delta}_{3D}^{(1)} + [C] \dot{\delta}_{1D}^{(2)} + [D] \dot{\delta}_{3D}^{(2)} = 0 \quad (359)$$

where

$$\nabla f_{1(1)} = \begin{bmatrix} \frac{df}{d\delta_{1(1)}} \\ \frac{df}{d\delta_{1(3)}} \\ \frac{df}{d\delta_{1(5)}} \end{bmatrix} \quad (360)$$

$$\nabla f_{3(1)} = \begin{bmatrix} \frac{df}{d\delta_{3(1)}} \\ \frac{df}{d\delta_{3(3)}} \\ \frac{df}{d\delta_{3(5)}} \end{bmatrix} \quad (361)$$

$$\nabla f_{1(2)} = \begin{bmatrix} \frac{df}{d\delta_{1(2)}} \\ \frac{df}{d\delta_{1(4)}} \\ \frac{df}{d\delta_{1(6)}} \end{bmatrix} \quad (362)$$

$$\nabla f_{3(2)} = \begin{bmatrix} \frac{df}{d\delta_{3(2)}} \\ \frac{df}{d\delta_{3(4)}} \\ \frac{df}{d\delta_{3(6)}} \end{bmatrix} \quad (363)$$

The two constraints given in equations 358 and 359 can be combined into the following constraint equation.

$$[A_{(1)}] \dot{\delta}_{1D}^{(1)} + [B_{(1)}] \dot{\delta}_{3D}^{(1)} + [C_{(1)}] \dot{\delta}_{1D}^{(2)} + [n_{(1)}] \dot{\delta}_{3D}^{(2)} - \gamma \operatorname{sgn}(f) \hat{e} = 0 \quad (364)$$

where

$$[A_{(1)}] = \begin{bmatrix} [k_{(2)}][A] \\ \frac{df}{d\delta_{1(1)}} \quad \frac{df}{d\delta_{1(3)}} \quad \frac{df}{d\delta_{1(5)}} \end{bmatrix} \quad (365)$$

$$[B_{(1)}] = \begin{bmatrix} [k_{(2)}][B] \\ \frac{df}{d\delta_{3(1)}} \quad \frac{df}{d\delta_{3(3)}} \quad \frac{df}{d\delta_{3(5)}} \end{bmatrix} \quad (366)$$

$$[C_{(1)}] = \begin{bmatrix} [k_{(3)}][C] \\ \hline \frac{df}{d\delta_{1(2)}} & \frac{df}{d\delta_{1(4)}} & \frac{df}{d\delta_{1(6)}} \end{bmatrix} \quad (367)$$

$$[D_{(1)}] = \begin{bmatrix} [k_{(3)}][D] \\ \hline \frac{df}{d\delta_{3(2)}} & \frac{df}{d\delta_{3(4)}} & \frac{df}{d\delta_{3(6)}} \end{bmatrix} \quad (368)$$

The adjoint equation L equals

$$\begin{aligned} L = & \frac{1}{2} \{ \dot{\delta}_{1D}^{(1)T} [k_{(2)}^2]^{-1} \dot{\delta}_{1D}^{(1)} + \dot{\delta}_{3D}^{(1)T} [k_{(2)}^2]^{-1} \dot{\delta}_{3D}^{(1)} \\ & + \dot{\delta}_{1D}^{(2)T} [k_{(3)}^2]^{-1} \dot{\delta}_{1D}^{(2)} + \dot{\delta}_{3D}^{(2)T} [k_{(3)}^2]^{-1} \dot{\delta}_{3D}^{(2)} \} \\ & - \lambda^T \{ [A_{(1)}] \dot{\delta}_{1D}^{(1)} + [B_{(1)}] \dot{\delta}_{3D}^{(1)} + [C_{(1)}] \dot{\delta}_{1D}^{(2)} \\ & + [D_{(1)}] \dot{\delta}_{3D}^{(2)} - \gamma \operatorname{sgn}(f) \hat{e} \} \end{aligned} \quad (369)$$

Setting the partial derivatives $\frac{dL}{d\dot{\delta}_{1D}^{(1)}}$, $\frac{dL}{d\dot{\delta}_{3D}^{(1)}}$, $\frac{dL}{d\dot{\delta}_{1D}^{(2)}}$, $\frac{dL}{d\dot{\delta}_{3D}^{(2)}}$,

and $\frac{dL}{d\lambda}$ equal to zero,

$$\frac{dL}{d\dot{\delta}_{1D}^{(1)}} = [k_{(2)}^2]^{-1} \dot{\delta}_{1D}^{(1)} - [A_{(1)}]^T \lambda = 0 \quad (370)$$

$$\frac{dL}{d\dot{\delta}_{3D}^{(1)}} = [k_{(2)}^2]^{-1} \dot{\delta}_{3D}^{(1)} - [B_{(1)}]^T \lambda = 0 \quad (371)$$

$$\frac{dL}{d\dot{\delta}_{1D}^{(2)}} = [k_{(3)}^2]^{-1} \dot{\delta}_{1D}^{(2)} - [C_{(1)}]^T \lambda = 0 \quad (372)$$

$$\frac{dL}{d\dot{\delta}_{3D}^{(2)}} = [k_{(3)}^2]^{-1} \dot{\delta}_{3D}^{(2)} - [D_{(1)}]^T \lambda = 0 \quad (373)$$

$$\begin{aligned} \frac{dL}{d\lambda} = & -\{[A_{(1)}] \dot{\delta}_{1D}^{(1)} + [B_{(1)}] \dot{\delta}_{3D}^{(1)} + [C_{(1)}] \dot{\delta}_{1D}^{(2)} \\ & + [D_{(1)}] \dot{\delta}_{3D}^{(2)} - \gamma \operatorname{sgn}(f) \hat{e}\} = 0 \end{aligned} \quad (374)$$

Solving equations 370, 371, 372, and 373 for $\dot{\delta}_{1D}^{(1)}$, $\dot{\delta}_{3D}^{(1)}$, $\dot{\delta}_{1D}^{(2)}$, and $\dot{\delta}_{3D}^{(2)}$,

$$\dot{\delta}_{1D}^{(1)} = [k_{(2)}^2] [A_{(1)}]^T \lambda \quad (375)$$

$$\dot{\delta}_{3D}^{(1)} = [k_{(2)}^2] [B_{(1)}]^T \lambda \quad (376)$$

$$\dot{\delta}_{1D}^{(2)} = [k_{(3)}^2] [C_{(1)}]^T \lambda \quad (377)$$

$$\dot{\delta}_{3D}^{(2)} = [k_{(3)}^2] [D_{(1)}]^T \lambda \quad (378)$$

Substituting equations 375 thru 378 into 374,

$$[J] \lambda - \gamma \operatorname{sgn}(f) \hat{e} \quad (379)$$

where

$$\begin{aligned}
 [J] = & [A_{(1)}] [k_{(2)}^2] [A_{(1)}]^T + [B_{(1)}] [k_{(2)}^2] [B_{(1)}]^T \\
 & + [C_{(1)}] [k_{(3)}^2] [C_{(1)}]^T + [D_{(1)}] [k_{(3)}^2] [D_{(1)}]^T
 \end{aligned} \quad (380)$$

λ equals

$$\lambda = [J]^{-1} \operatorname{sgn}(f) \gamma \hat{e} \quad (381)$$

Substituting equation 381 into equations 375 thru 378, the gimbal rate commands $\dot{\delta}_{1D}^{(1)}$, $\dot{\delta}_{3D}^{(1)}$, $\dot{\delta}_{1D}^{(2)}$, and $\dot{\delta}_{3D}^{(2)}$ are:

$$\dot{\delta}_{1D}^{(1)} = \operatorname{sgn}(f) [k_{(2)}^2] [A_{(1)}]^T [J]^{-1} \gamma \hat{e} \quad (382)$$

$$\dot{\delta}_{3D}^{(1)} = \operatorname{sgn}(f) [k_{(2)}^2] [B_{(1)}]^T [J]^{-1} \gamma \hat{e} \quad (383)$$

$$\dot{\delta}_{1D}^{(2)} = \operatorname{sgn}(f) [k_{(3)}^2] [C_{(1)}]^T [J]^{-1} \gamma \hat{e} \quad (384)$$

$$\dot{\delta}_{3D}^{(2)} = \operatorname{sgn}(f) [k_{(3)}^2] [D_{(1)}]^T [J]^{-1} \gamma \hat{e} \quad (385)$$

Normalizing the above CMG gimbal rate commands,

$$\dot{\delta}_{1D}^{(1)n} = \frac{\dot{\delta}_{1D}^{(1)'}}{\dot{\delta}_{norm}} \quad (386)$$

$$\dot{\delta}_{3D}^{(1)n} = \frac{\dot{\delta}_{3D}^{(1)'}}{\dot{\delta}_{norm}} \quad (387)$$

$$\dot{\delta}_{1D}^{(2)n} = \frac{\dot{\delta}_{1D}^{(2)'}}{\dot{\delta}_{norm}} \quad (388)$$

$$\dot{\delta}_{3D}^{(2)n} = \frac{\dot{\delta}_{3D}^{(2)'}}{\dot{\delta}_{norm}} \quad (389)$$

where

$$\dot{\delta}_{1D}^{(1)'} = \text{sgn}(f) [k_{(2)}^2] [A_{(1)}]^T [J]^{-1} \hat{e} \quad (390)$$

$$\dot{\delta}_{3D}^{(1)'} = \text{sgn}(f) [k_{(2)}^2] [B_{(1)}]^T [J]^{-1} \hat{e} \quad (391)$$

$$\dot{\delta}_{1D}^{(2)'} = \text{sgn}(f) [k_{(3)}^2] [C_{(1)}]^T [J]^{-1} \hat{e} \quad (392)$$

$$\dot{\delta}_{3D}^{(2)'} = \text{sgn}(f) [k_{(3)}^2] [D_{(1)}]^T [J]^{-1} \hat{e} \quad (393)$$

$$\dot{\delta}_{norm} = (\dot{\delta}_{1D}^{(1)'}{}^T \dot{\delta}_{1D}^{(1)'} + \dot{\delta}_{3D}^{(1)'}{}^T \dot{\delta}_{3D}^{(1)'} + \dot{\delta}_{1D}^{(2)'}{}^T \dot{\delta}_{1D}^{(2)'} + \dot{\delta}_{3D}^{(2)'}{}^T \dot{\delta}_{3D}^{(2)'})^{1/2} \quad (394)$$

$\alpha_{max}^{(D)}$ equals

$$\alpha_{max}^{(D)} = (\alpha_{max}^2 - \dot{\delta}_{norm}^2)^{1/2} \quad (395)$$

If $\alpha_{\max}^{(D)}$ is negative, the CMG distribution gimbal rate commands $\dot{\delta}_{1D}^{(1)}$, $\dot{\delta}_{3D}^{(1)}$, $\dot{\delta}_{1D}^{(2)}$, and $\dot{\delta}_{3D}^{(2)}$ equal

$$\dot{\delta}_{1D}^{(1)} = \dot{\delta}_{3D}^{(1)} = \dot{\delta}_{1D}^{(2)} = \dot{\delta}_{3D}^{(2)} = 0 \quad (396)$$

For $\alpha_{\max}^{(D)}$ greater than zero,

$$\dot{\delta}_{1D}^{(1)} = \alpha_{\max}^{(D)} \dot{\delta}_{1D}^{(1)n} \quad (397)$$

$$\dot{\delta}_{3D}^{(1)} = \alpha_{\max}^{(D)} \dot{\delta}_{3D}^{(1)n} \quad (398)$$

$$\dot{\delta}_{1D}^{(2)} = \alpha_{\max}^{(D)} \dot{\delta}_{1D}^{(2)n} \quad (399)$$

$$\dot{\delta}_{3D}^{(2)} = \alpha_{\max}^{(D)} \dot{\delta}_{3D}^{(2)n} \quad (400)$$

The combined resultant CMG gimbal rate commands $\dot{\delta}_1^{(1)}$, $\dot{\delta}_3^{(1)}$, $\dot{\delta}_1^{(2)}$, and $\dot{\delta}_3^{(2)}$ equal

$$\dot{\delta}_1^{(1)} = \dot{\delta}_{1C}^{(1)} + \dot{\delta}_{1D}^{(1)} \quad (401)$$

$$\dot{\delta}_3^{(1)} = \dot{\delta}_{3C}^{(1)} + \dot{\delta}_{3D}^{(1)} \quad (402)$$

$$\dot{\delta}_1^{(2)} = \dot{\delta}_{1C}^{(2)} + \dot{\delta}_{1D}^{(2)} \quad (403)$$

$$\dot{\delta}_3^{(2)} = \dot{\delta}_{3C}^{(2)} + \dot{\delta}_{3D}^{(2)} \quad (404)$$

9.6 Combined CMG Gimbal Rate Command Law - The combined CMG law described in this section is an attempt to combine into a single law the Decoupled Pseudo-Inverse CMG Control and the Optimal CMG Distribution laws developed in sections 9.4.4 and 9.5.3, respectively. This combined CMG law is developed using the Lagrange multiplier optimization technique used to derive both the Decoupled Pseudo-Inverse CMG Control Law and the Optimal CMG Distribution Law.

The performance index P equals

$$P(\dot{\delta}_{1(i)}, \dot{\delta}_{3(i)}) = \frac{1}{2} \sum_{i=1}^6 \{ (\dot{\delta}_{1(i)})^2 + (\dot{\delta}_{3(i)})^2 \} + K \frac{d}{dt} \left[\frac{\text{sgn}(f)}{f} \right] \quad (405)$$

The first term on the right side of equation 405 is the performance index associated with both the Decoupled Pseudo-Inverse CMG Control Law and the Optimal CMG Distribution Law. The remaining term of this performance index P is an attempt to drive the CMG system away from singularity in the same manner as the Optimal CMG Distribution Law does. The two objectives of P are: (1) to minimize the sum of the squares of the CMG gimbal rate commands $\dot{\delta}_{1(i)}$ and $\dot{\delta}_{3(i)}$ ($i=1, \dots, 6$) and (2) to drive the CMG system away from the anti-parallel singularity condition. The scalar constant K is a weighting function that weighs the relative importance of the two terms comprising the performance index P.

The constraint equation associated with the performance index given in equation 405 is

$$\vec{T}_{\text{CMG}} - \vec{T}_{\text{COM}} = 0 \quad (406)$$

This constraint states that this combined CMG law is decoupled or in other words, the torque \vec{T}_{CMG} generated by the CMG control system equals the CMG command torque \vec{T}_{COM} .

Slaved CMG Mode - For the slaved CMG mode, the performance index P is

$$P = \frac{1}{2} \{ \dot{\delta}_1^T [k_{(1)}^2]^{-1} \dot{\delta}_1 + \dot{\delta}_3^T [k_{(1)}^2]^{-1} \dot{\delta}_3 \} + K \frac{d}{dt} \left[\frac{\text{sgn}(f)}{f} \right] \quad (407)$$

f is the singularity function used as a measure of how close the CMG system is to singularity. The CMG anti-parallel singularity condition is avoided by maximizing the magnitude of f. f equals

$$f(\vec{\delta}_1, \vec{\delta}_3) = \text{determinant of } [G], \det [G] \quad (408)$$

where

$$[G] = [k_{(1)}][A'] [k_{(1)}^2] ([k_{(1)}][A'])^T + [k_{(1)}][B'] [k_{(1)}^2] ([k_{(1)}][B'])^T \quad (409)$$

The performance index P term $\frac{d}{dt}[\frac{\text{sgn}(f)}{f}]$ can be written in the following more convenient form

$$\frac{d}{dt}[\frac{\text{sgn}(f)}{f}] = -\frac{\text{sgn}(f)}{f^2} (\nabla f_1 \cdot \dot{\delta}_1 + \nabla f_3 \cdot \dot{\delta}_3) \quad (410)$$

∇f_1 and ∇f_3 are defined in equations 320 and 321, respectively. Substituting equation 410 into 407, the performance index P equals

$$P = \frac{1}{2} \{ \dot{\delta}_1^T [k_{(1)}^2]^{-1} \dot{\delta}_1 + \dot{\delta}_3^T [k_{(1)}^2]^{-1} \dot{\delta}_3 \} - \frac{K \text{sgn}(f)}{f^2} (\nabla f_1 \cdot \dot{\delta}_1 + \nabla f_3 \cdot \dot{\delta}_3) \quad (411)$$

The Lagrange multiplier optimization technique attempts to minimize this performance index P. Minimizing P tends to cause the term $\frac{d}{dt}[\frac{\text{sgn}(f)}{f}]$ to be negative, thus maximizing the magnitude of f and driving the CMG system away from singularity.

The constraint associated with this performance index P is that the output torque of the CMG system \vec{T}_{CMG} equals the command torque \vec{T}_{COM} .

$$\vec{T}_{CMG} - \vec{T}_{COM} = 0 \quad (412)$$

Substituting the appropriate expression for \vec{T}_{CMG} into the above constraint equation,

$$H\{[k_{(1)}] [A'] \dot{\delta}_1 + [k_{(1)}] [B'] \dot{\delta}_3\} + \vec{\omega} \times \vec{H}_{CMG} - \vec{T}_{COM} = 0 \quad (413)$$

$\vec{\omega}$ is the vehicle angular rate and \vec{H}_{CMG} is the CMG momentum imparted to the vehicle defined by equation 91.

The Lagrange multiplier adjoin equation equals

$$\begin{aligned} L = & P - \lambda^T (\vec{T}_{CMG} - \vec{T}_{COM}) \\ = & \frac{1}{2} \{ \dot{\delta}_1^T [k_{(1)}^2]^{-1} \dot{\delta}_1 + \dot{\delta}_3^T [k_{(1)}^2]^{-1} \dot{\delta}_3 \} \\ & - \frac{K \text{sgn}(f)}{f^2} (\nabla f_1 \cdot \dot{\delta}_1 + \nabla f_3 \cdot \dot{\delta}_3) \\ & - \lambda^T \{ H[k_{(1)}] [A'] \dot{\delta}_1 + H[k_{(1)}] [B'] \dot{\delta}_3 + \vec{\omega} \times \vec{H}_{CMG} - \vec{T}_{COM} \} \end{aligned} \quad (414)$$

λ is the Lagrange multiplier. To minimize the adjoint equation, the partial derivatives $\frac{dL}{d\dot{\delta}_1}$, $\frac{dL}{d\dot{\delta}_3}$, and $\frac{dL}{d\lambda}$ are set equal to zero.

$$\begin{aligned} \frac{dL}{d\dot{\delta}_1} &= [k_{(1)}^2]^{-1} \dot{\delta}_1 - K \frac{\text{sgn}(f)}{f^2} \nabla f_1 \\ &\quad - H([k_{(1)}][A'])^T \lambda = 0 \end{aligned} \quad (415)$$

$$\begin{aligned} \frac{dL}{d\dot{\delta}_3} &= [k_{(1)}^2]^{-1} \dot{\delta}_3 - K \frac{\text{sgn}(f)}{f^2} \nabla f_3 \\ &\quad - H([k_{(1)}][B'])^T \lambda = 0 \end{aligned} \quad (416)$$

$$\frac{dL}{d\lambda} = -\{H[k_{(1)}][A']\dot{\delta}_1 + H[k_{(1)}][B']\dot{\delta}_3 + \vec{\omega} \times \vec{H}_{CMG} - \vec{T}_{COM}\} = 0 \quad (417)$$

Solving equations 415 and 416 for $\dot{\delta}_1$ and $\dot{\delta}_3$,

$$\dot{\delta}_1 = K \frac{\text{sgn}(f)}{f^2} [k_{(1)}^2] \nabla f_1 + H[k_{(1)}]([k_{(1)}][A'])^T \lambda \quad (418)$$

$$\dot{\delta}_3 = K \frac{\text{sgn}(f)}{f^2} [k_{(1)}^2] \nabla f_3 + H[k_{(1)}]([k_{(1)}][B'])^T \lambda \quad (419)$$

Substituting equations 418 and 419 into 417 and solving for λ ,

$$\begin{aligned} \lambda &= \frac{1}{H^2} [G]^{-1} (\vec{T}_{COM} - \vec{\omega} \times \vec{H}_{CMG}) \\ &\quad - \frac{K}{H} \frac{\text{sgn}(f)}{f^2} [G]^{-1} [k_{(1)}][A'] [k_{(1)}^2] \nabla f_1 \\ &\quad - \frac{K}{H} \frac{\text{sgn}(f)}{f^2} [G]^{-1} [k_{(1)}][B'] [k_{(1)}^2] \nabla f_2 \end{aligned} \quad (420)$$

Substituting the above expressions for λ into equations 418 and 419, $\dot{\delta}_1$ and $\dot{\delta}_3$ equal

$$\begin{aligned}
\dot{\delta}_1 = & \frac{1}{H} [k_{(1)}^2] ([k_{(1)}] [A'])^T [G]^{-1} (\dot{T}_{COM} - \vec{\omega} \times \vec{H}_{CMG}) \\
& + K \frac{\text{sgn}(f)}{f^2} [k_{(1)}^2] \nabla f_1 + [B'] [k_{(1)}^2] \nabla f_3 \\
& - K \frac{\text{sgn}(f)}{f^2} [k_{(1)}^2] ([k_{(1)}] [A'])^T [G]^{-1} [k_{(1)}] ([A'] [k_{(1)}^2]) \nabla f_1 \quad (421)
\end{aligned}$$

$$\begin{aligned}
\dot{\delta}_3 = & \frac{1}{H} [k_{(1)}^2] ([k_{(1)}] [B'])^T [G]^{-1} (\dot{T}_{COM} - \vec{\omega} \times \vec{H}_{CMG}) \\
& + K \frac{\text{sgn}(f)}{f^2} [k_{(1)}^2] \nabla f_3 + [B'] [k_{(1)}^2] \nabla f_3 \\
& - K \frac{\text{sgn}(f)}{f^2} [k_{(1)}^2] ([k_{(1)}] [B'])^T [G]^{-1} [k_{(1)}] ([A'] [k_{(1)}^2]) \nabla f_1 \quad (422)
\end{aligned}$$

Six Individual CMG Mode - For this mode of operation, the performance index P equals

$$\begin{aligned}
P = & \frac{1}{2} \{ \dot{\delta}_1^{(1)T} [k_{(2)}^2]^{-1} \dot{\delta}_1^{(1)} + \dot{\delta}_3^{(1)T} [k_{(2)}^2]^{-1} \dot{\delta}_3^{(1)} \\
& + \dot{\delta}_1^{(2)T} [k_{(3)}^2]^{-1} \dot{\delta}_1^{(2)} + \dot{\delta}_3^{(2)T} [k_{(3)}^2]^{-1} \dot{\delta}_3^{(2)} \} \\
& + K \frac{d}{dt} \left[\frac{\text{sgn}(f)}{f} \right] \quad (423)
\end{aligned}$$

f equals

$$f(\dot{\delta}_1^{(1)}, \dot{\delta}_3^{(1)}, \dot{\delta}_1^{(2)}, \dot{\delta}_3^{(2)}) = \det [G] \quad (424)$$

where

$$\begin{aligned}
[G] = & [k_{(2)}] [A] [k_{(2)}^2] ([k_{(2)}] [A])^T \\
& + [k_{(2)}] [B] [k_{(2)}^2] ([k_{(2)}] [B])^T \\
& + [k_{(3)}] [C] [k_{(3)}^2] ([k_{(3)}] [C])^T \\
& + [k_{(3)}] [D] [k_{(3)}^2] ([k_{(3)}] [D])^T \quad (425)
\end{aligned}$$

The term $K \frac{d}{dt} \left[\frac{\text{sgn}(f)}{f} \right]$ equals

$$K \frac{d}{dt} \left[\frac{\text{sgn}(f)}{f} \right] = -K \frac{\text{sgn}(f)}{f^2} (\nabla f_{1(1)} \cdot \dot{\delta}_1^{(1)} + \nabla f_{3(1)} \cdot \dot{\delta}_3^{(1)} + \nabla f_{1(2)} \cdot \dot{\delta}_1^{(2)} + \nabla f_{3(2)} \cdot \dot{\delta}_3^{(2)}) \quad (426)$$

$\nabla f_{1(1)}$, $\nabla f_{3(1)}$, $\nabla f_{1(2)}$, and $\nabla f_{3(2)}$ are defined in equations 360 thru 363. Substituting equation 426 into 423, the performance index P is

$$P = \frac{1}{2} \{ \dot{\delta}_1^{(1)T} [k_{(2)}^2]^{-1} \dot{\delta}_1^{(1)} + \dot{\delta}_3^{(1)T} [k_{(2)}^2]^{-1} \dot{\delta}_3^{(1)} + \dot{\delta}_1^{(2)T} [k_{(3)}^2]^{-1} \dot{\delta}_1^{(2)} + \dot{\delta}_3^{(2)T} [k_{(3)}^2]^{-1} \dot{\delta}_3^{(2)} - K \frac{\text{sgn}(f)}{f^2} (\nabla f_{1(1)} \cdot \dot{\delta}_1^{(1)} + \nabla f_{3(1)} \cdot \dot{\delta}_3^{(1)} + \nabla f_{1(2)} \cdot \dot{\delta}_1^{(2)} + \nabla f_{3(2)} \cdot \dot{\delta}_3^{(2)}) \} \quad (427)$$

The corresponding constraint equation associated with the above performance index is

$$\vec{T}_{\text{CMG}} - \vec{T}_{\text{COM}} = 0$$

or

$$H \{ [k_{(2)}] [A] \dot{\delta}_1^{(1)} + [k_{(2)}] [B] \dot{\delta}_3^{(1)} + [k_{(3)}] [C] \dot{\delta}_1^{(2)} + [k_{(3)}] [D] \dot{\delta}_3^{(2)} \} + \omega \times \vec{H}_{\text{CMG}} - \vec{T}_{\text{COM}} = 0 \quad (428)$$

The CMG angular momentum \vec{H}_{CMG} is defined in equation 93. The Lagrange adjoin equation formed from equations 427 and 428 equals

$$\begin{aligned}
L = & \frac{1}{2} \{ \dot{\delta}_1^{(1)T} [k_{(2)}^2]^{-1} \dot{\delta}_1^{(1)} + \dot{\delta}_3^{(1)T} [k_{(2)}^2]^{-1} \dot{\delta}_3^{(1)} \\
& + \dot{\delta}_1^{(2)T} [k_{(3)}^2]^{-1} \dot{\delta}_1^{(2)} + \dot{\delta}_3^{(2)T} [k_{(3)}^2]^{-1} \dot{\delta}_3^{(2)} \} \\
& - K \frac{\text{sgn}(f)}{f^2} (\nabla f_{1(1)} \cdot \dot{\delta}_1^{(1)} + \nabla f_{3(1)} \cdot \dot{\delta}_3^{(1)} + \nabla f_{1(2)} \cdot \dot{\delta}_1^{(2)} \\
& + \nabla f_{3(2)} \cdot \dot{\delta}_3^{(2)}) - \lambda^T \{ H[k_{(2)}] [A] \dot{\delta}_1^{(1)} \\
& + H[k_{(2)}] [B] \dot{\delta}_3^{(1)} + H[k_{(3)}] [C] \dot{\delta}_1^{(2)} + H[k_{(3)}] [D] \dot{\delta}_3^{(2)} \\
& + \vec{\omega} \times \vec{H}_{\text{CMG}} - \vec{T}_{\text{COM}} \}
\end{aligned} \tag{429}$$

To minimize L , the following partial derivatives $\frac{dL}{d\dot{\delta}_1^{(1)}}$, $\frac{dL}{d\dot{\delta}_3^{(1)}}$,

$\frac{dL}{d\dot{\delta}_1^{(2)}}$, $\frac{dL}{d\dot{\delta}_3^{(2)}}$, and $\frac{dL}{d\lambda}$ are set equal to zero.

$$\frac{dL}{d\dot{\delta}_1^{(1)}} = [k_{(2)}^2]^{-1} \dot{\delta}_1^{(1)} - K \frac{\text{sgn}(f)}{f^2} \nabla f_{1(1)} - H([k_{(2)}] [A])^T \lambda = 0 \tag{430}$$

$$\frac{dL}{d\dot{\delta}_3^{(1)}} = [k_{(2)}^2]^{-1} \dot{\delta}_3^{(1)} - K \frac{\text{sgn}(f)}{f^2} \nabla f_{3(1)} - H([k_{(2)}] [B])^T \lambda = 0 \tag{431}$$

$$\frac{dL}{d\dot{\delta}_1^{(2)}} = [k_{(3)}^2]^{-1} \dot{\delta}_1^{(2)} - K \frac{\text{sgn}(f)}{f^2} \nabla f_{1(2)} - H([k_{(3)}] [C])^T \lambda = 0 \tag{432}$$

$$\frac{dL}{d\dot{\delta}_3^{(2)}} = [k_{(3)}^2]^{-1} \dot{\delta}_3^{(2)} - K \frac{\text{sgn}(f)}{f^2} \nabla f_{3(2)} - H([k_{(3)}] [D])^T \lambda = 0 \tag{433}$$

$$\begin{aligned}
\frac{dL}{d\lambda} = & - \{ H[k_{(2)}] [A] \dot{\delta}_1^{(1)} + H[k_{(2)}] [B] \dot{\delta}_3^{(1)} + H[k_{(3)}] [C] \dot{\delta}_1^{(2)} \\
& + H[k_{(3)}] [D] \dot{\delta}_3^{(2)} + \vec{\omega} \times \vec{H}_{\text{CMG}} - \vec{T}_{\text{COM}} \} = 0
\end{aligned} \tag{434}$$

Solving equations 430 thru 433 for $\dot{\delta}_1^{(1)}$, $\dot{\delta}_3^{(1)}$, $\dot{\delta}_1^{(2)}$, and $\dot{\delta}_3^{(2)}$,

$$\dot{\delta}_1^{(1)} = K \frac{\text{sgn}(f)}{f^2} [k_{(2)}^2] \nabla f_{1(1)} + H[k_{(2)}^2] ([k_{(2)}] [A])^T \lambda \quad (435)$$

$$\dot{\delta}_3^{(1)} = K \frac{\text{sgn}(f)}{f^2} [k_{(2)}^2] \nabla f_{3(1)} + H[k_{(2)}^2] ([k_{(2)}] [B])^T \lambda \quad (436)$$

$$\dot{\delta}_1^{(2)} = K \frac{\text{sgn}(f)}{f^2} [k_{(3)}^2] \nabla f_{1(2)} + H[k_{(3)}^2] ([k_{(3)}] [C])^T \lambda \quad (437)$$

$$\dot{\delta}_3^{(2)} = K \frac{\text{sgn}(f)}{f^2} [k_{(3)}^2] \nabla f_{3(2)} + H[k_{(3)}^2] ([k_{(3)}] [D])^T \lambda \quad (438)$$

Substituting equations 435 thru 438 into 434 and solving for λ , λ equals

$$\begin{aligned} \lambda = & \frac{1}{H^2} [G]^{-1} (\ddot{T}_{\text{COM}} - \ddot{\omega} \times \ddot{H}_{\text{CMG}}) \\ & - \frac{K}{H} \frac{\text{sgn}(f)}{f^2} [G]^{-1} [k_{(2)}] [A] [k_{(2)}^2] \nabla f_{1(1)} \\ & - \frac{K}{H} \frac{\text{sgn}(f)}{f^2} [G]^{-1} [k_{(2)}] [B] [k_{(2)}^2] \nabla f_{3(1)} \\ & - \frac{K}{H} \frac{\text{sgn}(f)}{f^2} [G]^{-1} [k_{(3)}] [C] [k_{(3)}^2] \nabla f_{1(2)} \\ & - \frac{K}{H} \frac{\text{sgn}(f)}{f^2} [G]^{-1} [k_{(3)}] [D] [k_{(3)}^2] \nabla f_{3(2)} \end{aligned} \quad (439)$$

Substituting the above expression for λ into equations 435 thru 438, $\dot{\delta}_1^{(1)}$, $\dot{\delta}_3^{(1)}$, $\dot{\delta}_1^{(2)}$, and $\dot{\delta}_3^{(2)}$ equal

$$\begin{aligned}
\dot{\delta}_1^{(1)} = & \frac{1}{H} [k_{(2)}^2] ([k_{(2)}] [A])^T [G]^{-1} (\dot{T}_{COM} - \vec{\omega} \times \vec{H}_{CMG}) \\
& + K \frac{\text{sgn}(f)}{f^2} [k_{(2)}^2] \nabla f_{1(1)} \\
& - K \frac{\text{sgn}(f)}{f^2} [k_{(2)}^2] ([k_{(2)}] [A])^T [G]^{-1} \{ [k_{(2)}] [A] [k_{(2)}^2] \nabla f_{1(1)} \\
& + [k_{(2)}] [B] [k_{(2)}^2] \nabla f_{3(1)} + [k_{(3)}] [C] [k_{(3)}^2] \nabla f_{1(2)} \\
& + [k_{(3)}] [D] [k_{(3)}^2] \nabla f_{3(2)} \}
\end{aligned} \tag{440}$$

$$\begin{aligned}
\dot{\delta}_3^{(1)} = & \frac{1}{H} [k_{(2)}^2] ([k_{(2)}] [B])^T [G]^{-1} (\dot{T}_{COM} - \vec{\omega} \times \vec{H}_{CMG}) \\
& + K \frac{\text{sgn}(f)}{f^2} [k_{(2)}^2] \nabla f_{3(1)} \\
& - K \frac{\text{sgn}(f)}{f^2} [k_{(2)}^2] ([k_{(2)}] [B])^T [G]^{-1} \{ [k_{(2)}] [A] [k_{(2)}^2] \nabla f_{1(1)} \\
& + [k_{(2)}] [B] [k_{(2)}^2] \nabla f_{3(1)} + [k_{(3)}] [C] [k_{(3)}^2] \nabla f_{1(2)} \\
& + [k_{(3)}] [D] [k_{(3)}^2] \nabla f_{3(2)} \}
\end{aligned} \tag{441}$$

$$\begin{aligned}
\dot{\delta}_1^{(2)} = & \frac{1}{H} [k_{(3)}^2] ([k_{(3)}] [C])^T [G]^{-1} (\dot{T}_{COM} - \vec{\omega} \times \vec{H}_{CMG}) \\
& + K \frac{\text{sgn}(f)}{f^2} [k_{(3)}^2] \nabla f_{1(2)} \\
& - K \frac{\text{sgn}(f)}{f^2} [k_{(3)}^2] ([k_{(3)}] [C])^T [G]^{-1} \{ [k_{(2)}] [A] [k_{(2)}^2] \nabla f_{1(1)} \\
& + [k_{(2)}] [B] [k_{(2)}^2] \nabla f_{3(1)} + [k_{(3)}] [C] [k_{(3)}^2] \nabla f_{1(2)} \\
& + [k_{(3)}] [D] [k_{(3)}^2] \nabla f_{3(2)} \}
\end{aligned} \tag{442}$$

$$\begin{aligned}
\dot{\delta}_3^{(2)} = & \frac{1}{H} [k_{(3)}^2] ([k_{(3)}] [D])^T [G]^{-1} (\dot{T}_{COM} - \dot{\omega} x \dot{H}_{CMG}) \\
& + K \frac{\text{sgn}(f)}{f^2} [k_{(3)}^2] \nabla f_{3(2)} \\
& - K \frac{\text{sgn}(f)}{f^2} [k_{(3)}^2] ([k_{(3)}] [D])^T [G]^{-1} \{ [k_{(2)}] [A] [k_{(2)}^2] \nabla f_{1(1)} \\
& + [k_{(2)}] [B] [k_{(2)}^2] \nabla f_{3(1)} + [k_{(3)}] [C] [k_{(3)}^2] \nabla f_{1(2)} \\
& + [k_{(3)}] [D] [k_{(3)}^2] \nabla f_{3(2)} \}
\end{aligned} \tag{443}$$

The above Combined CMG Gimbal Rate Command Law and the Decoupled Pseudo-Inverse CMG Control and the Optimal CMG Distribution laws are examples of laws derived using the Lagrange multiplier optimization technique. The derivation of additional laws is possible using this method; all one needs to do is define a new performance index P along with the appropriate system constraints.

9.7 Selection of CMG Control Law and Singularity Avoidance Scheme - Four candidate CMG control laws, three candidate CMG singularity avoidance scheme, and one combined CMG gimbal rate command law were derived. The combined CMG gimbal rate command law combines the functions of the CMG control law and the singularity avoidance scheme into a single law. The four candidate CMG control laws are:

- a. Cross Product CMG Control Law (section 9.4.1)
- b. H-Vector CMG Control Law (section 9.4.2)
- c. Scissored Pair CMG Control Law (section 9.4.3)
- d. Pseudo-Inverse CMG Control Law (section 9.4.4)

The three derived CMG singularity avoidance schemes are:

- a. Arbitrary Torquing of CMGs Away From Singularity (section 9.5.1)
- b. Isogonal CMG Distribution Law (section 9.5.2)
- c. Optimal CMG Distribution Law (section 9.5.3)

In section 9.6, the combined CMG gimbal rate command law is derived; this law combines the Pseudo-Inverse CMG Control Law and the Optimal CMG Distribution Law into a single control function. This control function or law computes a single set of CMG gimbal rate commands that generate the desired CMG output torque and also drives the CMG gimbals away from singularity. All of these laws were formulated for a nominal and a failed CMG mode plus, the two operational modes, slaved and individual modes described in this report.

The first two candidate CMG control laws listed above, a and b, can be implemented in an analog fashion whereas control laws c and d require a digital processor or computer. It should be noted that although control laws a and b are normally instrumented in an analog fashion, they can also be instrumented digitally using a digital computer. CMG control laws c and d are decoupled laws meaning that the resultant CMG output torque \vec{T}_{CMG} equals the command torque \vec{T}_{COM} generated by the vehicle control law. On the other hand, the two analog laws, a and b, are coupled laws because the CMG output torque \vec{T}_{CMG} only approximates \vec{T}_{COM} . Because control laws c and d are decoupled, their corresponding vehicle attitude control systems can exhibit slightly better performance characteristics than their coupled counterparts, control laws a and b. Vehicle stabilization capability is not a major trade consideration because all four CMG control laws are expected to be able to meet pointing stability within one arc minute. The chief trade between these four control laws is a hardware one. Implementing either control law a or b in analog fashion requires the addition of a number of analog components to the system. Because of the availability of a digital computer, a digital control law is preferred. Although all four of the control laws can be implemented digitally, the two decoupled control laws c and d are preferred because of the additional system performance that these two control laws afford can be obtained with no or little cost to the system. Of these two laws, the Pseudo-Inverse CMG Control Law, candidate d, is recommended because it is an optimal law that minimizes CMG gimbal rate commands.

The three singularity avoidance laws listed above are companion laws to the CMG control laws; they insure that the CMG gimbal angles are distributed in such a manner that the CMG control system can generate the desired torque command \vec{T}_{COM} . For a DGCMG system, there are two singularity conditions. The first one corresponds to when all of the individual wheel momentums \vec{H}_i are pointed in the same

direction; this corresponds to the CMG system being saturated and the system must therefore be desaturated. The second singularity condition corresponds to a gimbal state where all of the wheel momentums \vec{H}_1 are aligned, but with some of them pointing in opposite directions. It is this anti-parallel singularity condition that these singularity avoidance laws are designed to avoid. The singularity avoidance control law a, Arbitrary Torquing of CMGs Away From Singularity, remains inoperative until the CMG system is detected approaching a potential anti-parallel singularity condition then, the CMGs are torqued away from this potential singularity condition by redistributing the CMG gimbal angles. The Isogonal CMG Distribution Law, candidate b, distributes the individual CMG momentum vector \vec{H}_1 in such a manner that each CMG contributes an equal share to the total CMG momentum vector \vec{H}_{CMG} . Because each CMG momentum vector \vec{H}_1 has a component that is along \vec{H}_{CMG} , the anti-parallel singularity condition is avoided. The Optimal CMG Distribution Law, c, is a further optimization of the Pseudo-Inverse CMG Control Law. This Optimal CMG Distribution Law distributes the gimbal angles as a function of the total CMG momentum \vec{H}_{CMG} in an optimal manner so that the gimbal rates for an arbitrary torque command \vec{T}_{COM} can be further minimized. By distributing the CMG gimbal angles in this way, the anti-parallel singularity condition is avoided.

Arbitrary Torquing of CMGs Away From Singularity, candidate a, is mathematically the simplest of the three singularity avoidance schemes, but it does not attempt to distribute the CMG gimbal angles in either an optimal or sub-optimal manner. The Isogonal CMG Distribution Law orients the CMGs in a manner that could be classified as sub-optimal, but at the expense of being mathematically more complex than candidate a. The Optimal CMG Distribution Law distributes the CMG gimbal angles in an optimum fashion as prescribed by its performance index and constraint equations. Although this law is normally as complex as the Isogonal CMG Distribution Law, its computational requirements can be reduced if the CMG control used is the Pseudo-Inverse CMG Control Law. For this reason, the Optimal CMG Distribution Law is preferred.

Because the development of the recommended Pseudo-Inverse CMG Control Law and Optimal CMG Distribution Law are very similar, an attempt was made to combine these two laws into a single CMG law. The obvious advantage of combining these two laws is that

their functions can be accomplished using a single control expression. The result is the Combined CMG Gimbal Rate Command Law described in section 9.6. For this combined CMG law, the resultant expressions for the CMG gimbal rate commands $\dot{\delta}_1$ and $\dot{\delta}_3$ are more complex than those for the Pseudo-Inverse CMG Control Law and the Optimal CMG Distribution Law. Because of the apparent control logic complexity associated with this combined law, no advantage from either a software or a performance standpoint exists for this combined CMG law. The recommended method for generating the CMG gimbal rate commands $\dot{\delta}_1$ and $\dot{\delta}_3$ remains utilizing two laws, the Pseudo-Inverse CMG Control Law and the Optimal CMG Distribution Law.

The CMG control laws and singularity avoidance techniques were formulated for both a slaved and a six individual CMG operational mode. Operating the CMGs in the slaved mode reduces the computational requirements associated with the CMG control and singularity avoidance laws. The advantage of operating the CMGs in the individual CMG operational mode is that the CMG gimbal angles associated with the six individual CMGs can be distributed in a more optimal manner than for the slaved CMG mode. Unless digital computer size becomes critical, the preferred operational mode is the six individual CMG mode.

9.8 Logic Flow Diagram for Recommended CMG Control Law and Singularity Avoidance System - Figure 9.21 is the logic flow diagram for the recommended Pseudo-Inverse CMG Control Law and Optimal CMG Distribution Law. In box 1 of figure 9.21, the CMG operational status gain matrices are computed; these gain matrices describe the operational status of each CMG. In box 2, the CMG output torque matrices [A], [B], [C], and [D] are computed using the CMG gimbal angles $\delta_{1(i)}$ and $\delta_{3(i)}$ ($i=1, \dots, 6$) measured by the CMG gimbal resolver trains. These output torque matrices are used by both the Pseudo-Inverse CMG Control Law and the Optimal CMG Distribution Law to generate the appropriate CMG gimbal rate commands $\dot{\delta}_1^{(1)}$, $\dot{\delta}_3^{(1)}$, $\dot{\delta}_1^{(2)}$, and $\dot{\delta}_3^{(2)}$.

In boxes 3 thru 5, the Pseudo-Inverse CMG Control Law gimbal rate commands $\dot{\delta}_{1C}^{(1)}$, $\dot{\delta}_{3C}^{(1)}$, $\dot{\delta}_{1C}^{(2)}$, and $\dot{\delta}_{3C}^{(2)}$ are generated. In box 3, the matrix [G] is computed; the inverse of [G] must be determined in order to generate the appropriate control law gimbal rate commands. In box 4, appropriate CMG gimbal rate commands

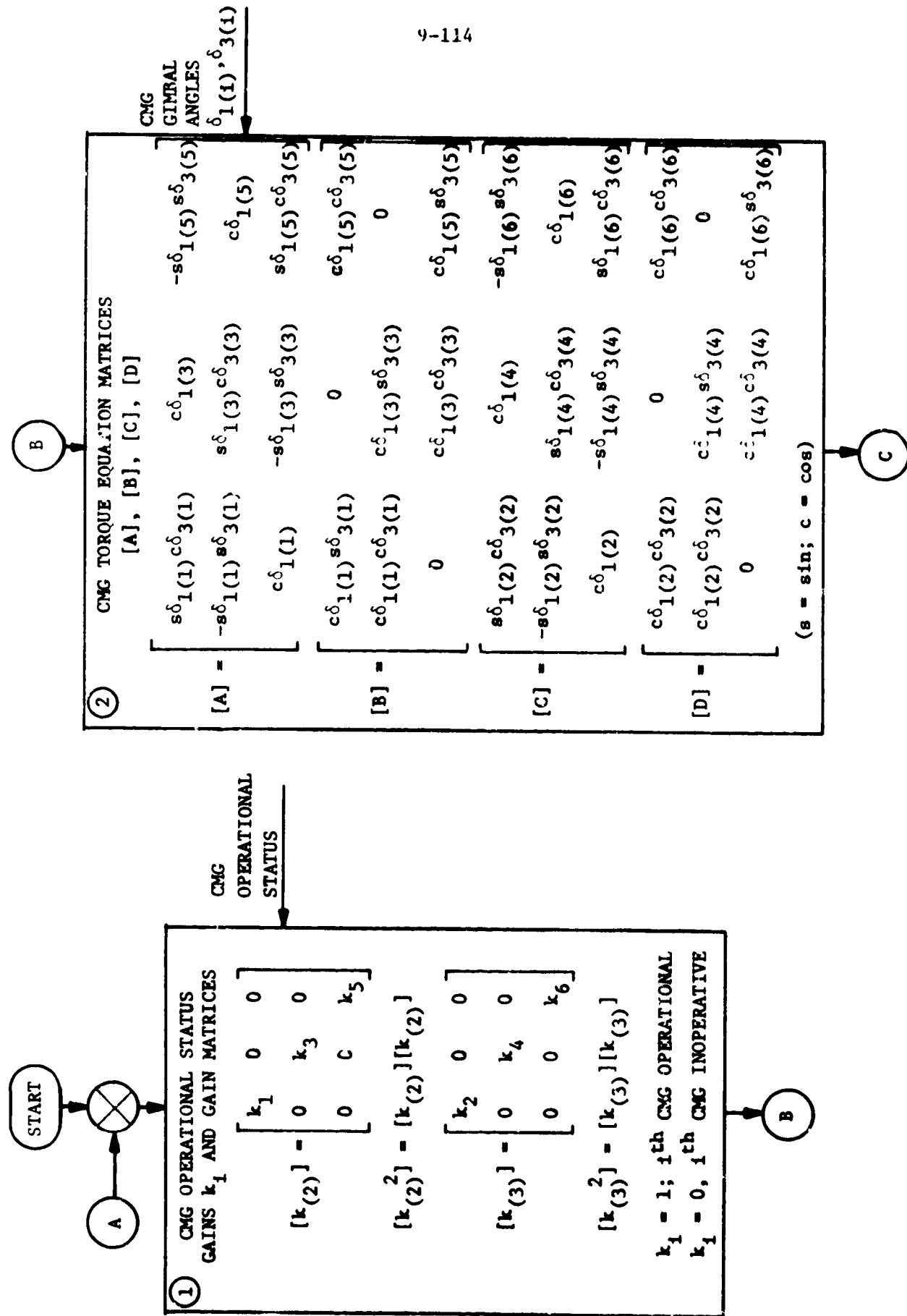


Figure 9.21. Pseudo-Inverse CMG Control Law and Optimal CMG Distribution Law Logic Flow Diagram (Sheet 1 of 5)

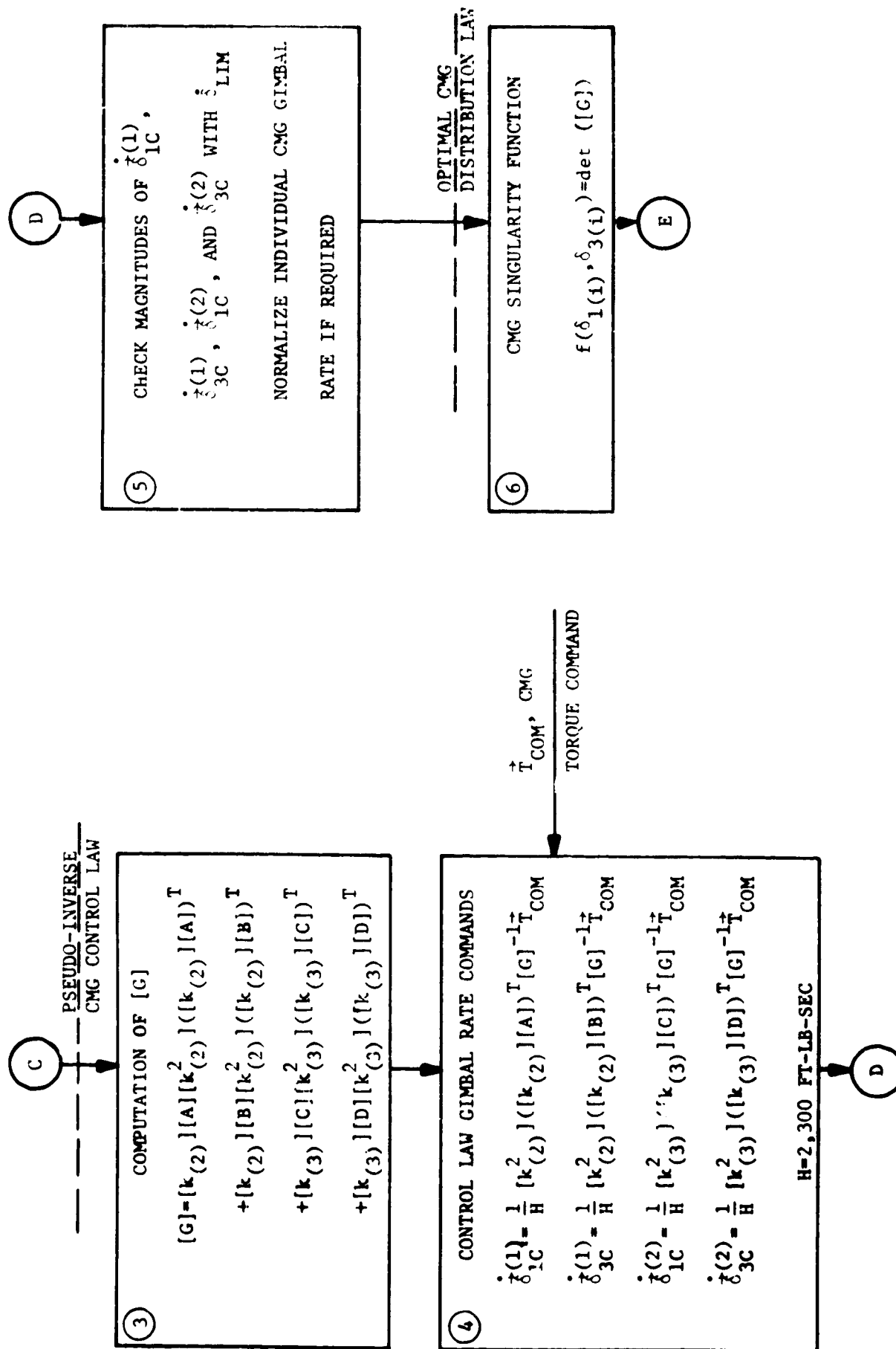


Figure 9.21. Pseudo-Inverse CMG Control Law and Optimal CMG Distribution Law Logic Flow Diagram (Sheet 2 of 5)

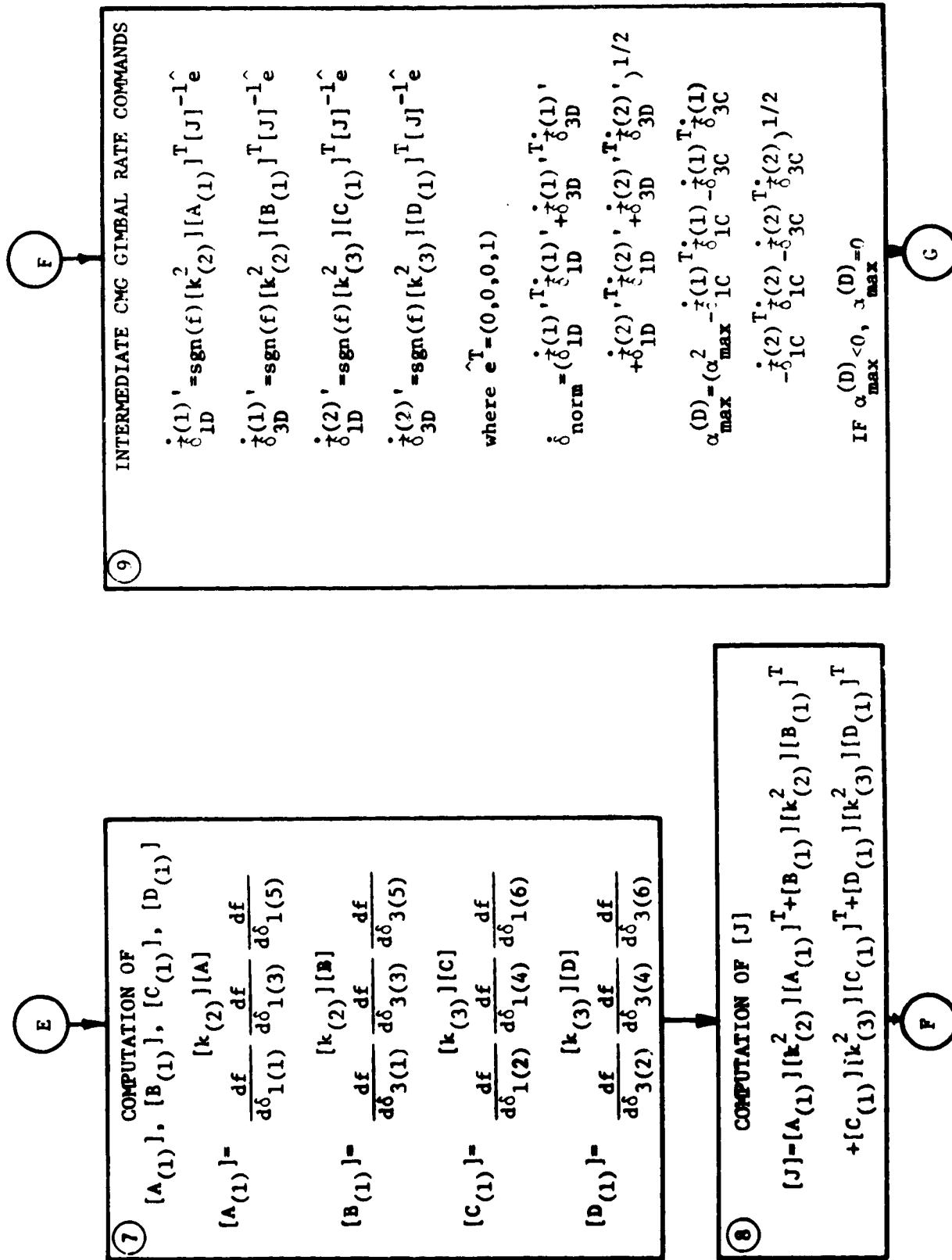


Figure 9.21. Pseudo-Inverse CMG Control Law and Optimal CMG Distribution Law Logic Flow Diagram (Sheet 3 of 5)

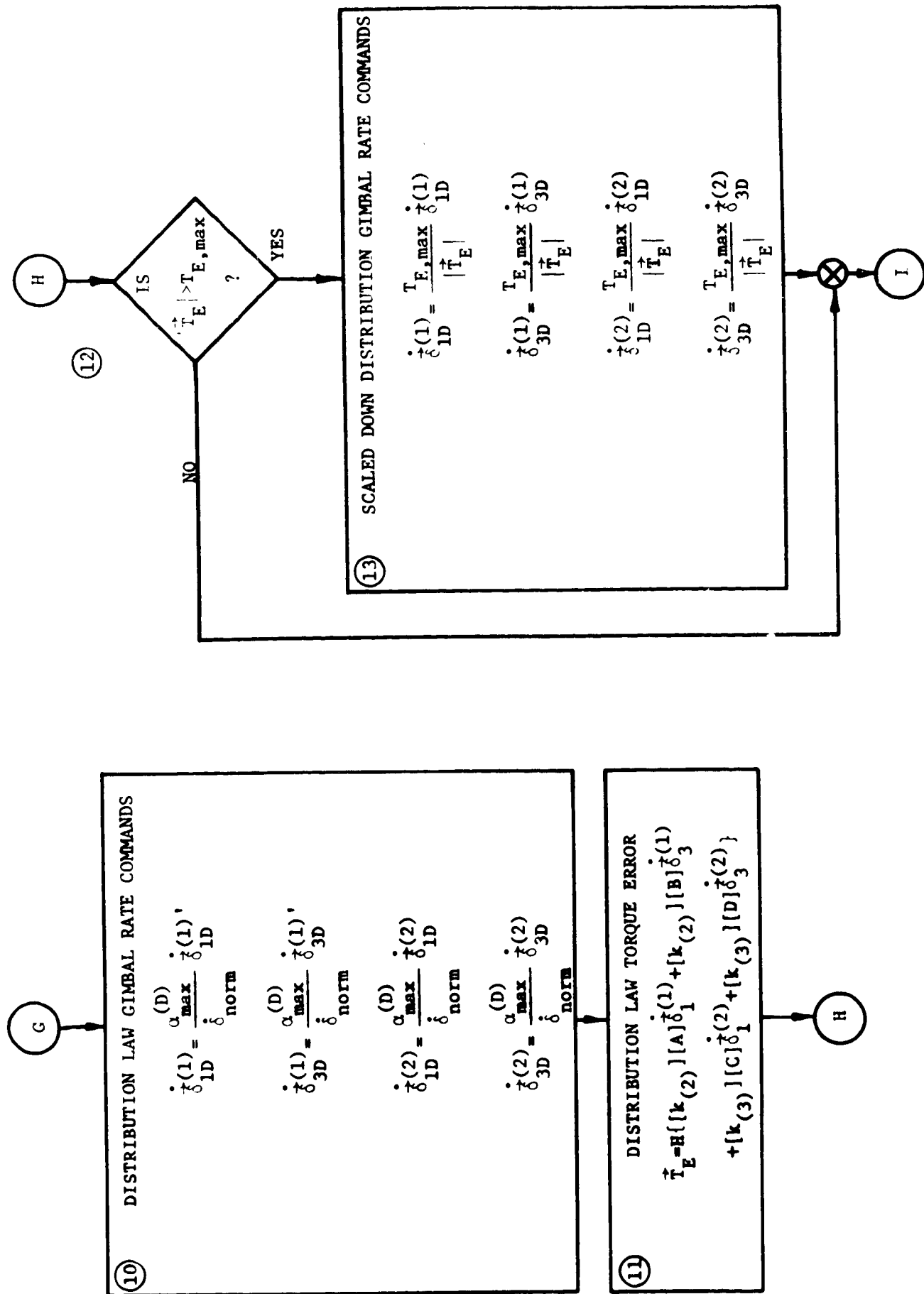


Figure 9.21. Pseudo-Inverse CMG Control Law and Optimal CMG Distribution
Law Logic Flow Diagram (Sheet 4 of 5)

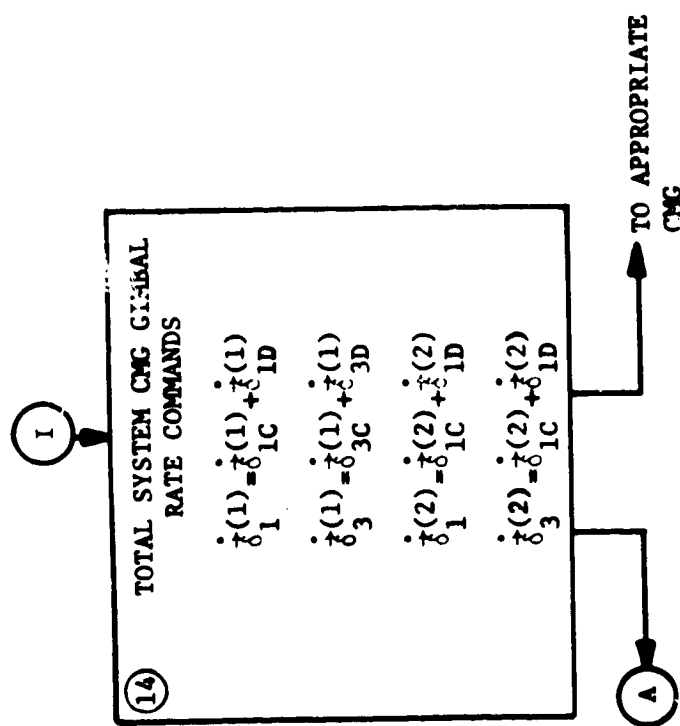


Figure 9.21. Pseudo-Inverse CMG Control Law and Optimal CMG Distribution Law Logic Flow Diagram (Sheet 5 of 5)

$\dot{\delta}_{1C}^{(1)}$, $\dot{\delta}_{3C}^{(1)}$, $\dot{\delta}_{1C}^{(2)}$, and $\dot{\delta}_{3C}^{(2)}$ are computed that will generate the CMG torque command \vec{T}_{COM} generated by the vehicle control law. The individual CMG gimbal rate commands comprising $\dot{\delta}_{1C}^{(1)}$, $\dot{\delta}_{3C}^{(1)}$, $\dot{\delta}_{1C}^{(2)}$, and $\dot{\delta}_{3C}^{(2)}$ are compared with a gimbal rate limit $\dot{\delta}_{LIM}$ in box 5. If one of the individual gimbal rate commands exceeds $\dot{\delta}_{LIM}$, the gimbal rate commands are all scaled down so that none of the individual rate commands exceed $\dot{\delta}_{LIM}$.

In boxes 6 thru 13, the Optimal CMG Distribution Law gimbal rate commands $\dot{\delta}_{1D}^{(1)}$, $\dot{\delta}_{3D}^{(1)}$, $\dot{\delta}_{1D}^{(2)}$, and $\dot{\delta}_{3D}^{(2)}$ are generated. In box 6, the CMG singularity function f that measures the distance the CMG system is away from singularity in CMG gimbal space is computed. In boxes 7 and 8, the control matrices $[A_{(1)}]$, $[B_{(1)}]$, $[C_{(1)}]$, $[D_{(1)}]$, and $[J]$ are computed. In box 9, a set of intermediate CMG gimbal rate commands $\dot{\delta}_{1D}'^{(1)}$, $\dot{\delta}_{3D}'^{(1)}$, $\dot{\delta}_{1D}'^{(2)}$, and $\dot{\delta}_{3D}'^{(2)}$ are generated along with a CMG distribution gimbal rate limit $\alpha_{max}^{(D)}$. Using these intermediate gimbal rate commands and rate limit, the CMG distribution gimbal rate commands $\dot{\delta}_{1D}^{(1)}$, $\dot{\delta}_{3D}^{(1)}$, $\dot{\delta}_{1D}^{(2)}$, and $\dot{\delta}_{3D}^{(2)}$ are computed in box 10. In box 11, a CMG distribution torque error \vec{T}_E due to $\dot{\delta}_{1D}^{(1)}$, $\dot{\delta}_{3D}^{(1)}$, $\dot{\delta}_{1D}^{(2)}$, and $\dot{\delta}_{3D}^{(2)}$ is computed. Ideally, \vec{T}_E should be zero. But due to computational errors, \vec{T}_E can be appreciable. In box 12, the magnitude of \vec{T}_E is checked with a torque limit $T_{E,max}$. If the magnitude of \vec{T}_E exceeds $T_{E,max}$, the control logic proceeds onto box 13 where the distribution gimbal rate commands $\dot{\delta}_{1D}^{(1)}$, $\dot{\delta}_{3D}^{(1)}$, $\dot{\delta}_{1D}^{(2)}$, and $\dot{\delta}_{3D}^{(2)}$ are scaled down so that the magnitude of \vec{T}_E does not exceed $T_{E,max}$.

In box 14, the Pseudo-Inverse CMG Control Law gimbal rate commands $\dot{\delta}_{1C}^{(1)}$, $\dot{\delta}_{3C}^{(1)}$, $\dot{\delta}_{1C}^{(2)}$, and $\dot{\delta}_{3C}^{(2)}$ are added to the appropriate Optimal CMG Distribution Law gimbal rate commands $\dot{\delta}_{1D}^{(1)}$, $\dot{\delta}_{3D}^{(1)}$, $\dot{\delta}_{1D}^{(2)}$, and $\dot{\delta}_{3D}^{(2)}$. The total system CMG gimbal rate commands $\dot{\delta}_1^{(1)}$, $\dot{\delta}_3^{(1)}$, $\dot{\delta}_1^{(2)}$, and $\dot{\delta}_3^{(2)}$ are routed to the appropriate CMG gimbal actuators. The logic flow then recycles back to box 1.

9.9 Notes9.9.1 Abbreviations and Symbols

ATM	Apollo Telescope Mount
$[A],[B],[C],[D]$	Individual mode CMG system output torque matrices
$[A'],[B']$	Slaved mode CMG system output torque matrices
$[A_{(1)}],[B_{(1)}],[C_{(1)}],$ $[D_{(1)}],[J]$	CMG distribution law control matrices (individual mode)
$[A'_{(1)}],[B'_{(1)}],[J]$	CMG distribution law control matrices (slaved mode)
CMG	Control moment gyro
DGCMG	Double gimbal control moment gyro
f	CMG distribution law function
∇f	Gradient of f
H	CMG wheel momentum
\vec{H}_{CMG}	CMG system momentum imparted to the vehicle
\vec{H}_{COM}	H vector control law momentum command
K_p	Vehicle control law position gain
K_r	Vehicle control law rate gain
L	Lagrange adjoint equation
P	Performance index
\vec{T}_{Cb}	Individual CMG output torque in base space
\vec{T}_{Ci}	Individual CMG output torque in vehicle coordinates ($i=1,\dots,6$)
\vec{T}_{CMC}	CMG system output torque in vehicle coordinates
\vec{T}_{COM}	CMG system torque command
\vec{T}_D	Vehicle disturbance torque
$X_b Y_b Z_b$	CMG base space
$X_I Y_I Z_I$	CMG inner gimbal space
$X_o Y_o Z_o$	CMG outer gimbal space
$\alpha^{(D)}$	CMG distribution gimbal rate command limit
δ_{max}	
δ_{LIM}	CMG control law gimbal rate command limit

$\dot{\phi}_1^{(1)}, \dot{\phi}_3^{(1)}, \dot{\phi}_1^{(2)}, \dot{\phi}_3^{(2)}$	Total CMG system gimbal rate commands
$[\phi]_{I \rightarrow o}$	Transformation from CMG outer to inner gimbal space
$[\phi]_{o \rightarrow b}$	Transformation from CMG base to outer gimbal space
$[\phi]_{v \rightarrow b1}$	Transformation from i^{th} CMG base to vehicle coordinates ($i=1, \dots, 6$)
ϵ	Vehicle angular velocity
ϵ_o	CMG base angular velocity
ϵ_b	CMG inner gimbal angular velocity
ϵ_1	Vehicle orbital rate
ϵ_o	

9.9.2 References

1. Kennel, Hans F., A Control Law For Double-Gimbaled Control Moment Gyros Used For Space Vehicle Attitude Control, NASA TM X-64536, George C. Marshall Space Flight Center, Marshall Space Flight Center, Alabama, August 7, 1970.
2. Powell, Barry K., etc., Synthesis Of Double Gimbal Control Moment Gyro Systems For Spacecraft Attitude Control, AIAA Guidance, Control and Flight Mechanics Conference, Hofstra University, Hempsted, New York, August 16-18, 1971.
3. Mayo, Ronald A., Redistribution and Singularity Avoidance For An n Single-Gimbal Control Moment Gyro Torque Actuator, MT-2313, The Bendix Corporation, Navigation and Control Division, Denver Operations, Denver, Colorado, January 24, 1971.
4. D'Azzo and Houpis, Feedback Control System Analysis and Synthesis, second edition, McGraw-Hill, 1966.

10. CMG SYSTEM MOMENTUM MANAGEMENT

A CMG control system has a finite momentum storage capability and therefore, the momentum that must be stored in the CMG system must be bounded. The objective of a CMG momentum management system is to keep the CMG system momentum storage requirement within the physical limits of the CMG system. Two mechanisms are described in this section for accomplishing this task. The first mechanism is a momentum desaturation system. The function of a CMG momentum desaturation system is to reduce the momentum stored in the CMG system by applying a torque to the vehicle such that the magnitude of the resultant momentum stored in the CMG system is reduced. Two basic types of CMG desaturation control laws are derived in this section; they are: (1) reaction control system (RCS) laws and (2) gravity gradient desaturation laws. The RCS desaturation control laws utilize the baseline Shuttle RCS described in section 3.2 to generate the required CMG desaturation torque and the CMG gravity gradient desaturation laws use the natural gravity gradient torques acting on the vehicle to desaturate the CMG system. The second mechanism described in this section is a Pseudo-Axis Alignment Control Law. The function of the Pseudo-Axis Alignment Control Law is to minimize the CMG momentum that must be desaturated by reducing the momentum build-up due to vehicle principal and control axis misalignments.

10.1 Shuttle and Baseline RCS Models - The baseline Shuttle RCS and vehicle dynamic characteristics used in this study are given in section 3. For convenience, the baseline RCS and vehicle characteristics are summarized in table 10.1.

10.2 Prediction of CMG Momentum Profile - A CMG desaturation system should be capable of predicting the near future momentum profile to be encountered by the CMG system. This projected momentum profile is used to alert the desaturation system to potential CMG saturation conditions. These momentum profiles can be used by mission planning to schedule momentum "dumps" so that their impact on mission objectives such as experimentation can be minimized.

In this section, a method for predicting the momentum stored in the CMG system is devised. The following assumptions are made:

- a. The vehicle is constrained to the following ideal Shuttle attitudes: (1) X-POP inertial, (2) X-IOP inertial, (3) X-POP Z-LV, and (4) X-IOP Z-LV.
- b. The only disturbance torques acting on the vehicle are gravity gradient torques.
- c. The orbit is circular.

Table 10.1. Assumed Shuttle RCS and Vehicle Characteristics

RCS Characteristics

Thrust level, F : 400 lbf.

Minimum pulse duration, t_f : 0.1 sec.

Minimum attitude deadband, θ_o : ± 0.5 deg.

Fuel: Monopropellant hydrazine with a specific impulse I_{sp} of 200 sec.

Roll moment arm, ℓ_x : 20.7 ft.

Pitch moment arm, ℓ_y : 100 ft.

Yaw moment arm, ℓ_z : 100 ft.

Vehicle Inertia Characteristics

$$I_{xx} = 1.04 \times 10^6 \text{ slug ft}^2$$

$$I_{yy} = 8.21 \times 10^6 \text{ slug ft}^2$$

$$I_{zz} = 8.55 \times 10^6 \text{ slug ft}^2$$

$$I_{xy} = I_{xz} = I_{yz} = 0$$

- d. The vehicle cross products of inertia I_{xy} , I_{xz} , and I_{yz} are zero.
- e. The CMG mounting configuration is shown in figure 10.1. (This is the CMG configuration recommended in section 6.)

The torque acting on the vehicle as observed in vehicle space,

$\left(\frac{d\vec{H}}{dt}\right)_v$ equals

$$\left(\frac{d\vec{H}}{dt}\right)_v = \vec{T}_{gg} + \left(\frac{d\vec{H}_{CMG}}{dt}\right)_v + \vec{\omega} \times \vec{H}_{CMG} - \vec{\omega} \times \vec{H}_v \quad (1)$$

\vec{T}_{gg} is the gravity gradient torque acting on the vehicle in vehicle space. \vec{H}_{CMG} is the CMG angular momentum imparted to the vehicle in vehicle space. \vec{H}_v is the vehicle angular momentum and equals

$$\vec{H}_v = [I]\vec{\omega} \quad (2)$$

where $[I]$ is the vehicle inertia tensor and $\vec{\omega}$ is the vehicle angular velocity.

$$[I] = \begin{bmatrix} I_{xx} & 0 & 0 \\ 0 & I_{yy} & 0 \\ 0 & 0 & I_{zz} \end{bmatrix} \quad (3)$$

$$\vec{\omega} = \begin{bmatrix} \omega_x \\ \omega_y \\ \omega_z \end{bmatrix} \quad (4)$$

Rearranging equation 1, the rate of change of the CMG momentum \vec{H}_{CMG} in vehicle coordinates equals

$$\left(\frac{d\vec{H}_{CMG}}{dt}\right)_v = \left(\frac{d\vec{H}_v}{dt}\right)_v + \vec{\omega} \times [I]\vec{\omega} - \vec{\omega} \times \vec{H}_{CMG} - \vec{T}_{gg} \quad (5)$$

Assume that the vehicle is in a steady state condition meaning that

$\vec{\omega}$ is either zero or a constant vector quantity. Then, $\left(\frac{d\vec{H}_v}{dt}\right)_v$ equals

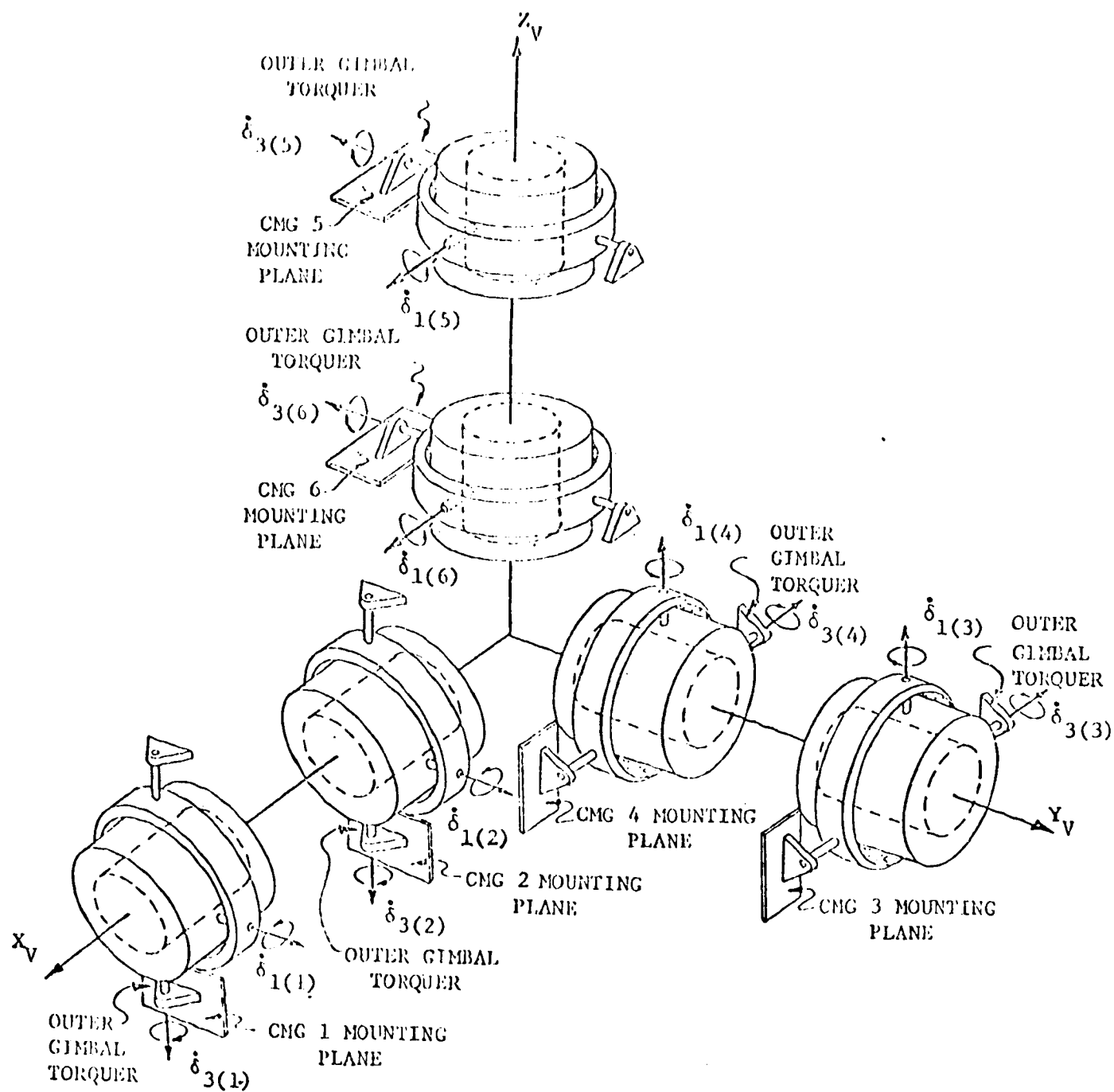


Figure 10.1. Recommended CMG Mounting Configuration

$$\left(\frac{d\vec{H}_v}{dt}\right)_v = [I]\dot{\vec{\omega}} = 0 \quad (6)$$

In steady state, $\left(\frac{d\vec{H}_{CMG}}{dt}\right)_v$ equals

$$\left(\frac{d\vec{H}_{CMG}}{dt}\right)_v = \vec{\omega} \times [I]\vec{\omega} - \vec{\omega} \times \vec{H}_{CMG} - \vec{T}_{gg} \quad (7)$$

For an inertially held vehicle, $\vec{\omega}$ is zero and $\left(\frac{d\vec{H}_{CMG}}{dt}\right)_v$ reduces to

$$\left(\frac{d\vec{H}_{CMG}}{dt}\right)_v = -\vec{T}_{gg} \quad (8)$$

Integrating equation 8, $\vec{H}_{CMG}(t)$ equals

$$\vec{H}_{CMG}(t) = \vec{H}_{CMG}(t_0) - \int_{t_0}^t \vec{T}_{gg} dt \quad (9)$$

$\vec{H}_{CMG}(t_0)$ is the CMG momentum state measured at time t_0 . $\vec{H}_{CMG}(t_0)$ can be computed as follows using the CMG gimbal angles $\delta_{1(i)}$ and $\delta_{3(i)}$, $i=1, \dots, 6$.

$$\begin{aligned} \vec{H}_{CMG}(t_0) = & \begin{bmatrix} H_{CMGx}(t_0) \\ H_{CMGy}(t_0) \\ H_{CMGz}(t_0) \end{bmatrix} = k_1 H \begin{bmatrix} -\cos \delta_{1(1)} \cos \delta_{3(1)} \\ \cos \delta_{1(1)} \sin \delta_{3(1)} \\ \sin \delta_{1(1)} \end{bmatrix} \\ & + k_2 H \begin{bmatrix} -\cos \delta_{1(2)} \cos \delta_{3(2)} \\ \cos \delta_{1(2)} \sin \delta_{3(2)} \\ \sin \delta_{1(2)} \end{bmatrix} + k_3 H \begin{bmatrix} \sin \delta_{1(3)} \\ -\cos \delta_{1(3)} \cos \delta_{3(3)} \\ \cos \delta_{1(3)} \sin \delta_{3(3)} \end{bmatrix} \\ & + k_4 H \begin{bmatrix} \sin \delta_{1(4)} \\ -\cos \delta_{1(4)} \cos \delta_{3(4)} \\ \cos \delta_{1(4)} \sin \delta_{3(4)} \end{bmatrix} + k_5 H \begin{bmatrix} \cos \delta_{1(5)} \sin \delta_{3(5)} \\ \sin \delta_{1(5)} \\ -\cos \delta_{1(5)} \cos \delta_{3(5)} \end{bmatrix} \\ & + k_6 H \begin{bmatrix} \cos \delta_{1(6)} \sin \delta_{3(6)} \\ \sin \delta_{1(6)} \\ -\cos \delta_{1(6)} \cos \delta_{3(6)} \end{bmatrix} \quad (10) \end{aligned}$$

The gains k_i , $i=1, \dots, 6$, are the CMG operational status gains described in section 9.2.

$$k_i = 1 \quad (11)$$

when the i^{th} CMG is operational and

$$k_i = 0 \quad (12)$$

when the i^{th} CMG is inoperative. H is the magnitude of the individual CMG wheel momentum.

The gravity gradient torque \vec{T}_{gg} equals

$$\vec{T}_{gg} = 3\omega_o^2 (\hat{a} \times [I] \hat{a}) \quad (13)$$

\hat{a} is a unit vector in vehicle coordinates along the local vertical directed from the center of the Earth towards the vehicle center of mass. ω_o is the orbital rate; ω_o^2 equals

$$\omega_o^2 = \frac{gR^2}{r^3} \quad (14)$$

where g is the gravitational acceleration of the Earth (32.2 ft/sec^2), R is the mean radius of the Earth in feet, and r is the distance from the center of the Earth to the vehicle center of mass. Expanding equation 13, \vec{T}_{gg} equals

$$\vec{T}_{gg}(t) = \begin{bmatrix} T_{gx}(t) \\ T_{gy}(t) \\ T_{gz}(t) \end{bmatrix} = 3\omega_o^2 \begin{bmatrix} a_y a_z (I_{zz} - I_{yy}) \\ a_x a_z (I_{xx} - I_{zz}) \\ a_x a_y (I_{yy} - I_{xx}) \end{bmatrix} \quad (15)$$

a_x , a_y , and a_z are the X, Y, and Z components of the local vertical vector \hat{a} .

To demonstrate how equations 9 and 15 can be used to predict the CMG momentum $\vec{H}_{CMG}(t)$ for an inertially held vehicle, assume the vehicle is in the inertial X-IOP attitude shown in figure 10.2. The local vertical vector \hat{a} equals

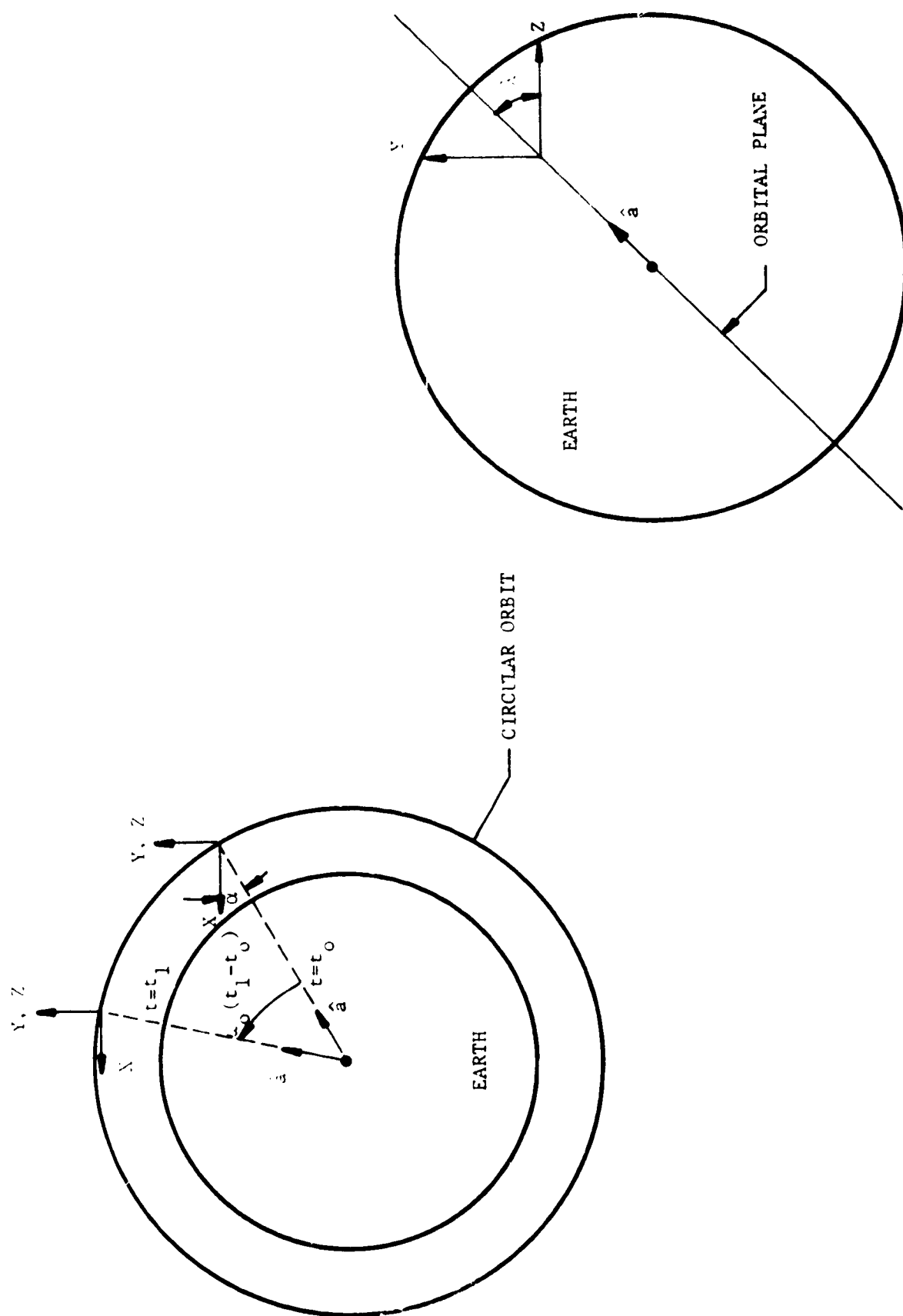


Figure 10.2. Sketch of Inertial X-IOP Attitude

$$\hat{a} = \begin{bmatrix} a_x \\ a_y \\ a_z \end{bmatrix} = \begin{bmatrix} -\cos(\omega_o t + \alpha) \\ \sin \lambda \sin(\omega_o t + \alpha) \\ \cos \lambda \sin(\omega_o t + \alpha) \end{bmatrix} \quad (16)$$

The resultant gravity gradient torque equations T_{gx} , T_{gy} , and T_{gz} are:

$$T_{gx}(t) = \frac{3\omega_o^2}{2} (I_{zz} - I_{yy}) \sin \lambda \cos \lambda \{1 - \cos 2[\omega_o(t - t_o) + \alpha]\} \quad (17)$$

$$T_{gy}(t) = \frac{3\omega_o^2}{2} (I_{zz} - I_{xx}) \cos \lambda \sin 2[\omega_o(t - t_o) + \alpha] \quad (18)$$

$$T_{gz}(t) = \frac{-3\omega_o^2}{2} (I_{yy} - I_{xx}) \sin \lambda \sin 2[\omega_o(t - t_o) + \alpha] \quad (19)$$

The projected axial components of the CMG momentum vector are:

$$H_{CMGx}(t) = H_{CMGx}(t_o) - \int_{t_o}^t T_{gx}(t) dt \quad (20)$$

$$H_{CMGy}(t) = H_{CMGy}(t_o) - \int_{t_o}^t T_{gy}(t) dt \quad (21)$$

$$H_{CMGz}(t) = H_{CMGz}(t_o) - \int_{t_o}^t T_{gz}(t) dt \quad (22)$$

$H_{CMGx}(t_o)$, $H_{CMGy}(t_o)$, and $H_{CMGz}(t_o)$ are the initial X, Y, and Z components of the CMG momentum vector $\vec{H}_{CMG}(t)$ computed using equation 10. For the example X-IOP attitude illustrated in figure 10.2, $H_{CMGx}(t)$, $H_{CMGy}(t)$, and $H_{CMGz}(t)$ equal

$$\begin{aligned} H_{CMGx}(t) = & H_{CMGx}(t_o) - \frac{3\omega_o}{4} (I_{zz} - I_{yy}) \sin \lambda \cos \lambda \\ & \{2\omega_o(t - t_o) - \sin 2[\omega_o(t - t_o) + \alpha] \\ & + \sin 2\alpha\} \end{aligned} \quad (23)$$

$$H_{CMGy}(t) = H_{CMGy}(t_0) + \frac{3\omega_0}{4}(I_{zz} - I_{xx}) \cos \lambda \{\cos 2[\omega_0(t-t_0) + \alpha] - \cos 2\alpha\} \quad (24)$$

$$H_{CMGz}(t) = H_{CMGz}(t_0) - \frac{3\omega_0}{4}(I_{yy} - I_{xx}) \sin \lambda \{\cos 2[\omega_0(t-t_0) + \alpha] - \cos 2\alpha\} \quad (25)$$

Note that for our example, H_{CMGx} is the only component of \vec{H}_{CMG} that has a term whose magnitude increases with time. It is this type of an unbounded momentum term

$$-\left\{\frac{3\omega_0^2}{2}(I_{zz} - I_{yy}) \sin \lambda \cos \lambda\right\}(t-t_0) \quad (26)$$

that causes the CMG system to become saturated. All of the remaining momentum terms are sinusoidal and are therefore bounded.

For a Z-local vertical attitude, the vehicle is spinning at the orbital rate ($\vec{\omega} \neq 0$) and the gravity gradient torque \vec{T}_{gg} acting on the vehicle is ideally zero ($\vec{T}_{gg} = 0$) because the local vertical vector \hat{a} has only a single nonzero component a_z ($a_x = 0$, $a_y = 0$, $a_z = -1$). One can confirm that \vec{T}_{gg} is zero for an ideal Z-LV attitude by looking at the gravity gradient torque equation, equation 15. The vehicle dynamic torque term $\vec{\omega} \times [I]\vec{\omega}$ for the two allowable Z-LV attitudes, X-POP Z-LV and X-IOP Z-LV, is also zero because the vehicle is spinning about a principal axis. Spinning the vehicle about a principal axis means that $\vec{\omega}$ and the vehicle momentum $[I]\vec{\omega}$ are co-linear and therefore their vector cross product is zero. For any other Z-LV attitude, this dynamic torque term is not zero because $\vec{\omega}$ and $[I]\vec{\omega}$ are not co-linear. For the two ideal Z-LV attitudes, X-POP Z-LV and X-IOP Z-LV, the rate of change of \vec{H}_{CMG} in vehicle

space, $\left(\frac{d\vec{H}_{CMG}}{dt}\right)_v$, as given by equation 7 reduces to

$$\left(\frac{d\vec{H}_{CMG}}{dt} \right)_v = -\vec{\omega} \times \vec{H}_{CMG} \quad (27)$$

Equation 27 can be solved for \vec{H}_{CMG} by using state space analysis.

Let \dot{H}_{CMGx} , \dot{H}_{CMGy} , and \dot{H}_{CMGz} denote the components of $\left(\frac{d\vec{H}_{CMG}}{dt} \right)_v$. Equation 27 can be expanded as follows

$$\begin{bmatrix} \dot{H}_{CMGx} \\ \dot{H}_{CMGy} \\ \dot{H}_{CMGz} \end{bmatrix} = \begin{bmatrix} 0 & \omega_z & -\omega_y \\ -\omega_z & 0 & \omega_x \\ \omega_y & -\omega_x & 0 \end{bmatrix} \begin{bmatrix} H_{CMGx} \\ H_{CMGy} \\ H_{CMGz} \end{bmatrix} \quad (28)$$

Let the above 3 by 3 matrix be denoted by A. To determine $\vec{H}_{CMG}(t)$, the state transition matrix $\Phi(t, t_0)$ must be computed. $\vec{H}_{CMG}(t)$ equals

$$\vec{H}_{CMG}(t) = \Phi(t, t_0) \vec{H}_{CMG}(t_0) \quad (29)$$

where $\vec{H}_{CMG}(t_0)$ is the initial CMG momentum at time t_0 . The first step in computing $\Phi(t, t_0)$ is to determine (SI-A) where I is the identity matrix and S is the Laplace transform operator.

$$I = \begin{bmatrix} 1 & 0 & 0 \\ 0 & 1 & 0 \\ 0 & 0 & 1 \end{bmatrix} \quad (30)$$

$\Phi(t, t_0)$ equals

$$\Phi(t, t_0) = \mathcal{L}^{-1} (SI-A)^{-1} \quad (31)$$

where \mathcal{L}^{-1} is the inverse Laplace transform of the inverse of (SI-A). The inverse of (SI-A) equals

$$(SI-A)^{-1} = \frac{1}{s(s^2 + \omega_0^2)} \begin{bmatrix} s^2 + \omega_x^2 & \omega_x \omega_y - s\omega_z & \omega_x \omega_z + s\omega_y \\ \omega_x \omega_y + s\omega_z & s^2 + \omega_y^2 & \omega_y \omega_z - s\omega_x \\ \omega_x \omega_z - s\omega_y & \omega_y \omega_z + s\omega_x & s^2 + \omega_z^2 \end{bmatrix} \quad (32)$$

To demonstrate how equations 29, 31, and 32 can be used to predict the CMG momentum profile given the CMG momentum state at time t_o , assume the vehicle is in the X-POP Z-LV attitude where ω_y and ω_z are zero and ω_x equals the orbital rate ω_o . $(SI-A)^{-1}$ reduces to

$$(SI-A)^{-1} = \begin{bmatrix} \frac{1}{s} & 0 & 0 \\ 0 & \frac{s}{s^2 + \omega_o^2} & -\frac{\omega_o}{s^2 + \omega_o^2} \\ 0 & \frac{\omega_o}{s^2 + \omega_o^2} & \frac{s}{s^2 + \omega_o^2} \end{bmatrix} \quad (33)$$

The state transition matrix $\phi(t, t_o)$ equals

$$\phi(t, t_o) = \begin{bmatrix} 1 & 0 & 0 \\ 0 & \cos \omega_o(t-t_o) & -\sin \omega_o(t-t_o) \\ 0 & \sin \omega_o(t-t_o) & \cos \omega_o(t-t_o) \end{bmatrix} \quad (34)$$

and $\vec{H}_{CMG}(t)$ equals

$$\vec{H}_{CMG}(t) = \begin{bmatrix} 1 & 0 & 0 \\ 0 & \cos \omega_o(t-t_o) & -\sin \omega_o(t-t_o) \\ 0 & \sin \omega_o(t-t_o) & \cos \omega_o(t-t_o) \end{bmatrix} \begin{bmatrix} H_{CMGx}(t_o) \\ H_{CMGy}(t_o) \\ H_{CMGz}(t_o) \end{bmatrix} \quad (35)$$

It should be noted that the magnitude of $\vec{H}_{CMG}(t)$ is always constant. The only reason that $\vec{H}_{CMG}(t)$ is time varying is because it is being measured in the rotating vehicle frame. If $\vec{H}_{CMG}(t)$ is transformed into an inertial coordinate system, $(\vec{H}_{CMG}(t))_I$ would be time invariant. Ideally, if the vehicle is held in one of the two Shuttle Z-LV attitudes, X-POP Z-LV or X-IOP Z-LV, the magnitude of the CMG momentum would remain constant.

Figure 10.3 is a computational flow diagram for predicting the CMG momentum for m future orbits based on the above analysis. This CMG momentum prediction scheme is good for only the inertial X-POP and X-IOP Shuttle attitudes. No prediction scheme is needed for

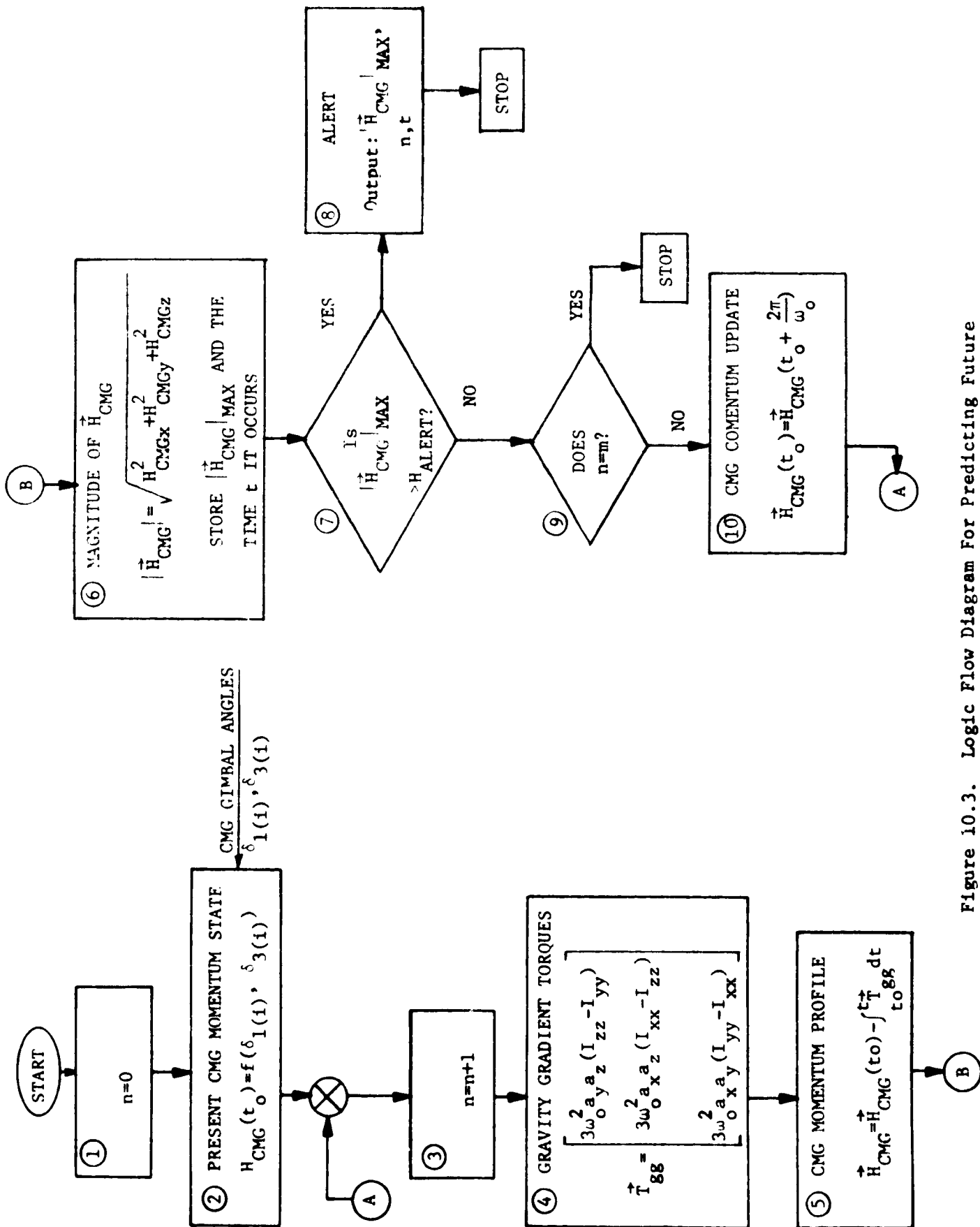


Figure 10.3. Logic Flow Diagram For Predicting Future CMG Momentum Profiles

the ideal X-POP Z-LV and X-IOP Z-LV attitudes since the CMG momentum viewed from an inertial frame is constant. The only way the magnitude of the CMG momentum can change is if the Shuttle is perturbed away from these two ideal Z-LV attitudes.

Box 1 of figure 10.3 initializes the orbit counter to zero. In box 2, the present CMG momentum state $\vec{H}_{CMG}(t_0)$ is computed using the CMG gimbal angles $\delta_{1(i)}$ and $\delta_{3(i)}$, $i=1, \dots, 6$. For the CMG mounting configuration shown in figure 10.1, $\vec{H}_{CMG}(t_0)$ is given by equation 10. Box 3 is the orbit counter indicating which orbit the following momentum profile corresponds. In box 4, the gravity gradient torque \vec{T}_{gg} acting on the vehicle is computed, equation 15. In box 5, the projected momentum profile for the n^{th} orbit is determined by integrating the negative of the gravity gradient torque $-\vec{T}_{gg}$ as illustrated in equations 20 thru 22.

In box 6, the magnitude of $\vec{H}_{CMG}(t)$, $|\vec{H}_{CMG}(t)|$, is computed. The maximum value of $|\vec{H}_{CMG}(t)|$ is stored for the n^{th} orbit along with time t at which this maximum value is projected to occur. In box 7, the maximum value of $|\vec{H}_{CMG}(t)|$ is compared with a preset momentum alert threshold H_{ALERT} . A reasonable criteria for setting this threshold is to let it correspond to ninety percent of saturation. For an operational six CMG system, H_{ALERT} equals

$$H_{ALERT} = 0.9(6H) = 5.4H \quad (36)$$

If the maximum value of $|\vec{H}_{CMG}(t)|$ computed in box 6 equals or exceeds H_{ALERT} , an alert is given as illustrated in box 8. The orbit n , the time t , and the projected value of $|\vec{H}_{CMG}(t)|$ is given. At this point, the momentum prediction scheme is terminated.

If the maximum value of $|\vec{H}_{CMG}(t)|$ computed in box 6 is less than H_{ALERT} , the prediction scheme proceeds to box 9 which checks to see if the n^{th} orbit corresponds to the last orbit m for which a projected momentum profile is to be computed. If n equals m , the prediction scheme is terminated with no alert given. If n is less than m , the initial CMG momentum vector $\vec{H}_{CMG}(t_0)$ is updated

using the value of \vec{H}_{CMG} computed in box 5 that corresponds to the end of the n^{th} orbit ($t=t_0 + \frac{2\pi}{\omega_0}$). This momentum prediction scheme continues by proceeding back to box 3 where the momentum profile corresponding to the next orbit is computed.

10.3 Reaction Control System (RCS) CMG Desaturation Systems. - Two RCS CMG desaturation systems are proposed; they are:

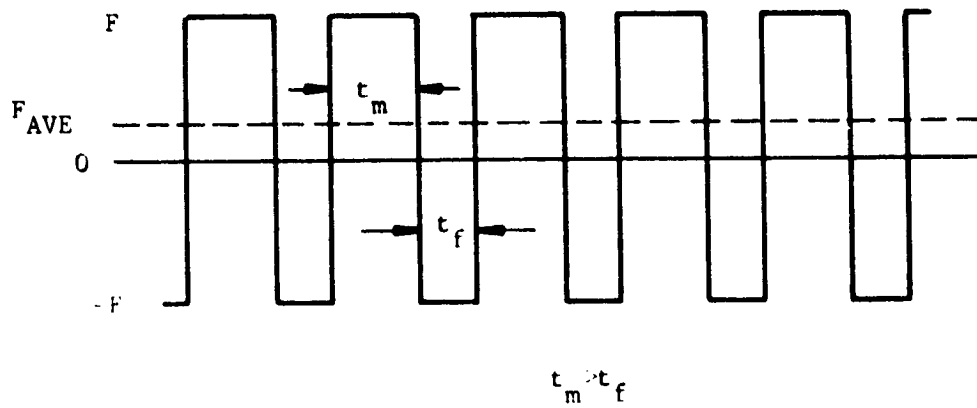
System 1: Reaction jets attached to the vehicle are fired in such a manner as to desaturate the CMGs while the CMGs continue to control the vehicle attitude.

System 2: The CMG system is commanded to a new momentum state with a reaction control system (RCS) assuming attitude control. The RCS absorbs the resultant CMG torque applied to the vehicle due to the change in CMG momentum.

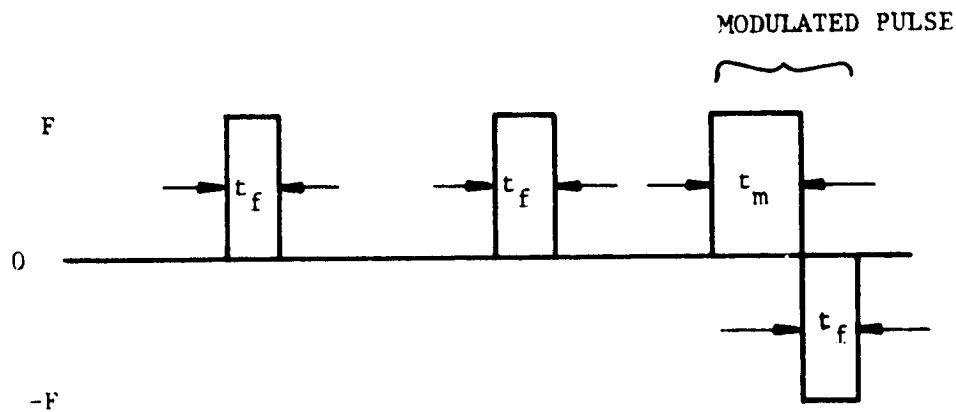
10.3.1 System 1: CMG Attitude Control - The CMG system is desaturated by firing reaction jets attached to the vehicle in such a manner that the resultant counteracting CMG torques will desaturate the CMG system besides counteracting the RCS torques generated. The reason for attempting to hold vehicle attitude with the CMG system during desaturation is in the hope that the resultant vehicle stabilization will permit experimentation during this interval. For the RCS and CMG systems used in this study, the major problem with this type of RCS desaturation is that the control authority of the baseline RCS described in table 10.1 is larger than that of the proposed CMG system. The minimum torque that the baseline RCS can generate about its three control axes is 8280 ft-lb about the X axis and 40000 ft-lb about both the Y and Z axes. The torque capability of the selected CMG system along each vehicle axis is 200 ft-lb, section 5. This large difference in torque capabilities makes this type of a RCS desaturation system difficult to implement. Two possible ways of implementing this system are illustrated in figure 10.4; they are:

Case A: As illustrated in figure 10.4a, the baseline RCS is time modulated so that its average torque T_{AVE} is less than the torque capability of the CMG system. This average RCS torque T_{AVE} is used to desaturate the CMG system.

Case B: As shown in figure 10.4b, a series of minimum RCS impulses are fired and the resultant momentum is absorbed by the CMG system. The time between pulses should be large



a). MODULATED RCS SYSTEM



b). PULSED RCS SYSTEM

Figure 10.4. Potential Implementations of RCS Desaturation System, System 1

enough to allow all CMG transients caused by the previous impulse to die out before the next impulse is fired. Any residual momentum left in the CMG system is removed by the modulated pulse shown in figure 10.4b. By varying the pulse duration t_m the amount of momentum imparted to the vehicle can be precisely controlled. By firing a sufficient number of minimum RCS impulses and a final modulated pulse, the CMG momentum state can be changed to any desired state.

Case A: Modulated RCS Desaturation System - The problem with this modulation system is that (1) the fuel consumed by this system is high because the RCS is on all of the time, (2) the contamination resulting from this large fuel consumption will prevent most if not all experiments from being performed during desaturation thus, defeating the purpose of accurately stabilizing the vehicle during this interval, (3) the modulated pulse duration t_m must be accurately controlled, and (4) the capability of obtaining high vehicle stabilization is questionable because of the transients generated by the continuous RCS alternating impulse train.

Assume that a change in CMG momentum along the Y axis of 13 000 ft-lb-sec is desired and that the average RCS torque T_{AVE} is 150 ft-lb. The time t_D required to produce this change in momentum is

$$t_D = \frac{\Delta H}{T_{AVE}} = \frac{13\ 000}{150} = 86.7 \text{ seconds} \quad (37)$$

The fuel consumption W.O.F., weight of fuel, required to produce this desired change in CMG momentum equals

$$W.O.F. = \frac{2Ft_D}{I_{sp}} = 346.8 \text{ lb} \quad (38)$$

This required fuel consumption is extremely high.

To compute the modulated pulse duration t_m needed, note that

$$T_{AVE} = \frac{F\ell_y(t_m - t_f)}{t_m + t_f} \quad (39)$$

Solving equation 39 for t_m ,

$$t_m = \frac{(F\ell_y + T_{AVE})}{F\ell_y - T_{AVE}} t_f \quad (40)$$

Substituting the appropriate values of T_{AVE} , F , ℓ_y , and t_f into equation 40, t_m equals

$$t_m = \frac{(40\ 150)(0.1)}{(39\ 850)} = 100.75 \text{ milliseconds} \quad (41)$$

The difference between t_m and the system's minimum pulse duration t_f is so small, less than one millisecond, that it is highly impractical to require the baseline RCS to have this fine a pulse regulation capability. The feasibility of a large RCS, the size of the baseline system, having this small a pulse regulation capability is highly questionable.

This modulated RCS desaturation system, Case A, is eliminated as a potential CMG desaturation system on the basis of its large fuel requirements and its impractical pulse modulation requirements.

Case B: Pulsed RCS Desaturation System - To demonstrate how this pulsed RCS desaturation system operates, assume that a change in the CMG momentum state of 13 000 ft-lb-sec along the vehicle Y axis is desired. The minimum momentum impulse bit (MIB) that the baseline RCS can impart to the Y axis equals

$$(MIB)_y = F\ell_y t_f = 4\ 000 \text{ ft-lb-sec} \quad (42)$$

As shown in figure 10.4b, the first RCS impulse Ft_f will result in a change in momentum of 4 000 ft-lb-sec along the Y axis. By firing these minimum impulses, a change of $3(MIB)_y$ or 12 000 ft-lb-sec along the Y axis will result leaving a residual momentum of 1 000 ft-lb-sec. To remove this residual momentum, a modulated pulse like the one shown in figure 10.4b is generated. The momentum imparted to the vehicle Y axis due to this modulated pulse equals

$$H_{MOD,Y} = F\ell_y (t_m - t_f) \quad (43)$$

From equation 43, the desired modulated pulse duration t_m equals

$$t_m = \frac{H_{MOD,Y} + F\ell_y t_f}{F\ell_y} \quad (44)$$

Substituting the appropriate values of $H_{MOD,Y}$ (1 000 ft-lb-sec), F , ℓ_y , and t_f into equation 44, t_m equals

$$t_m = 125 \text{ milliseconds} \quad (45)$$

This modulated pulse using the above value of t_m results in the desired change of 1 000 ft-lb-sec along the Y axis thus completing the desired CMG desaturation along this axis. Desaturation along the remaining vehicle axes is accomplished in an identical manner.

The RCS fuel required to perform this desired desaturation along the Y axis equals

$$W.O.F. = \frac{2F[(n_y + 1)t_f + t_m]}{I_{sp}} \quad (46)$$

where n_y is number of minimum impulses Ft_f required, $n_y = 3$. Substituting the appropriate values of n_y , F , t_f , t_m , and I_{sp} in equation 46, W.O.F. equals

$$W.O.F. = 2.1 \text{ lb} \quad (47)$$

This above fuel consumption is considerably less than that for the previous system, Case A.

As noted earlier, the minimum torque capability of the baseline RCS along each vehicle axis is much smaller than the maximum torque capability of the CMG system. This large difference in torque capabilities means that the CMG system cannot instantaneously absorb the momentum generated by a single RCS impulse thus causing an attitude error. To compute the magnitude of this error, the following assumptions are made.

- a. The CMG system is approaching saturation along one of the vehicle control axes as shown in figure 10.5a.
- b. The CMG system has reached ninety-five percent of saturation.
- c. The CMGs are arranged in an isogonal distribution. An isogonal distribution is one in which each CMG contributes an equal share to the total CMG momentum vector \vec{H}_{CMG} .
- d. The CMG system is desaturated along the affected vehicle control axis shown in figure 10.5a by firing the appropriate RCS thruster pair for its minimum pulse duration t_f .

Because the CMGs are arranged in an isogonal distribution, the magnitude of the CMG momentum vector \vec{H}_{CMG} equals

$$|\vec{H}_{CMG}| = 6H \cos \theta_I \quad (48)$$

where θ_I is the angle between the individual CMG wheel momentums and \vec{H}_{CMG} as illustrated in figure 10.5a. For a ninety-five percent saturated system,

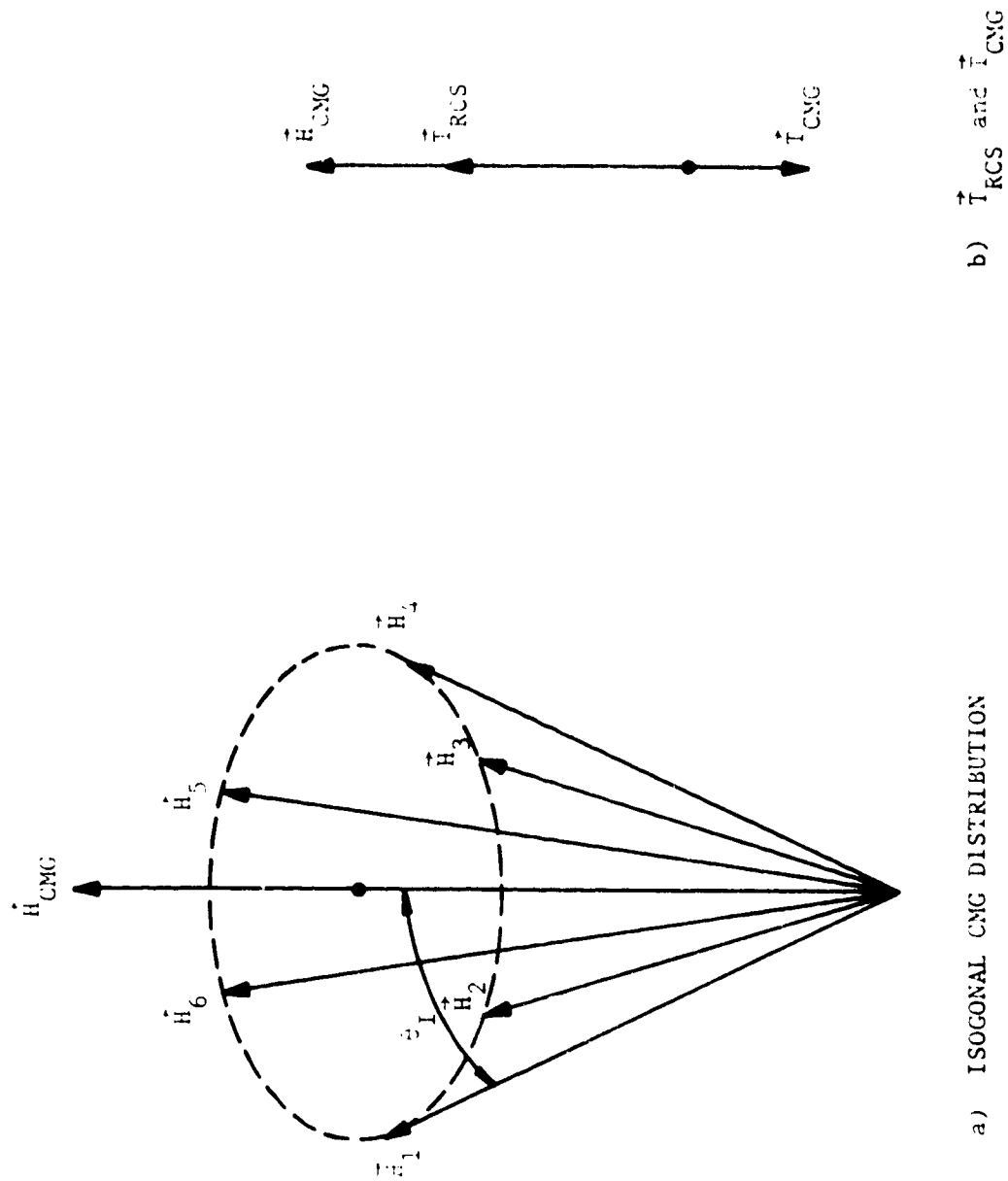


Figure 10.5. Sketches of CMG Isogonal Distribution and RCS Desaturation Torque \vec{T}_{RCS} and Resultant CMG Torque \vec{T}_{CMG}

$$\cos\theta_I = 0.95$$

or

$$\theta_I = 18 \text{ degrees} \quad (49)$$

As illustrated in figure 10.5b, a RCS desaturation torque \vec{T}_{RCS} along the vehicle control axis is generated causing the CMG system to produce a counteracting torque \vec{T}_{CMG} in the opposite direction. Note that a double gimbal CMG can generate a torque only in the plane perpendicular to its wheel momentum \vec{H} . For the isogonal CMG orientation shown in figure 10.5a, the maximum magnitude of \vec{T}_{CMG} that can be generated along or opposite the affected control axis equals

$$|\vec{T}_{CMG}|_{\max} = 6T_{\max} \sin\theta_I \quad (50)$$

where T_{\max} is the maximum torque that an individual CMG can generate in the plane perpendicular to its rotor \vec{H} . The maximum torque capability T_{\max} for the CMGs selected in section 6 is 122 ft-lb thus, the corresponding value of $|\vec{T}_{CMG}|_{\max}$ equals

$$|\vec{T}_{CMG}|_{\max} = 6(122)\sin(18^\circ) = 226 \text{ ft-lb} \quad (51)$$

The above value of $|\vec{T}_{CMG}|_{\max}$ will increase as the CMG system is desaturated because the angle θ_I will increase. For this analysis, the magnitude of the CMG torque \vec{T}_{CMG} generated due to the RCS desaturation torque \vec{T}_{RCS} is assumed to be constant and equal to the above value of $|\vec{T}_{CMG}|_{\max}$ given in equation 50.

Contained in figure 10.6 are sketches of the RCS desaturation torque profile \vec{T}_{RCS} , the resultant CMG torque profile \vec{T}_{CMG} , and the corresponding vehicle angular acceleration α , velocity ω , and position θ time histories generated by these torque profiles. The equations of motion governing α , ω , and θ are:

$$\vec{\alpha} = \frac{(\vec{T}_{RCS} + \vec{T}_{CMG})}{[I]} \quad (52)$$

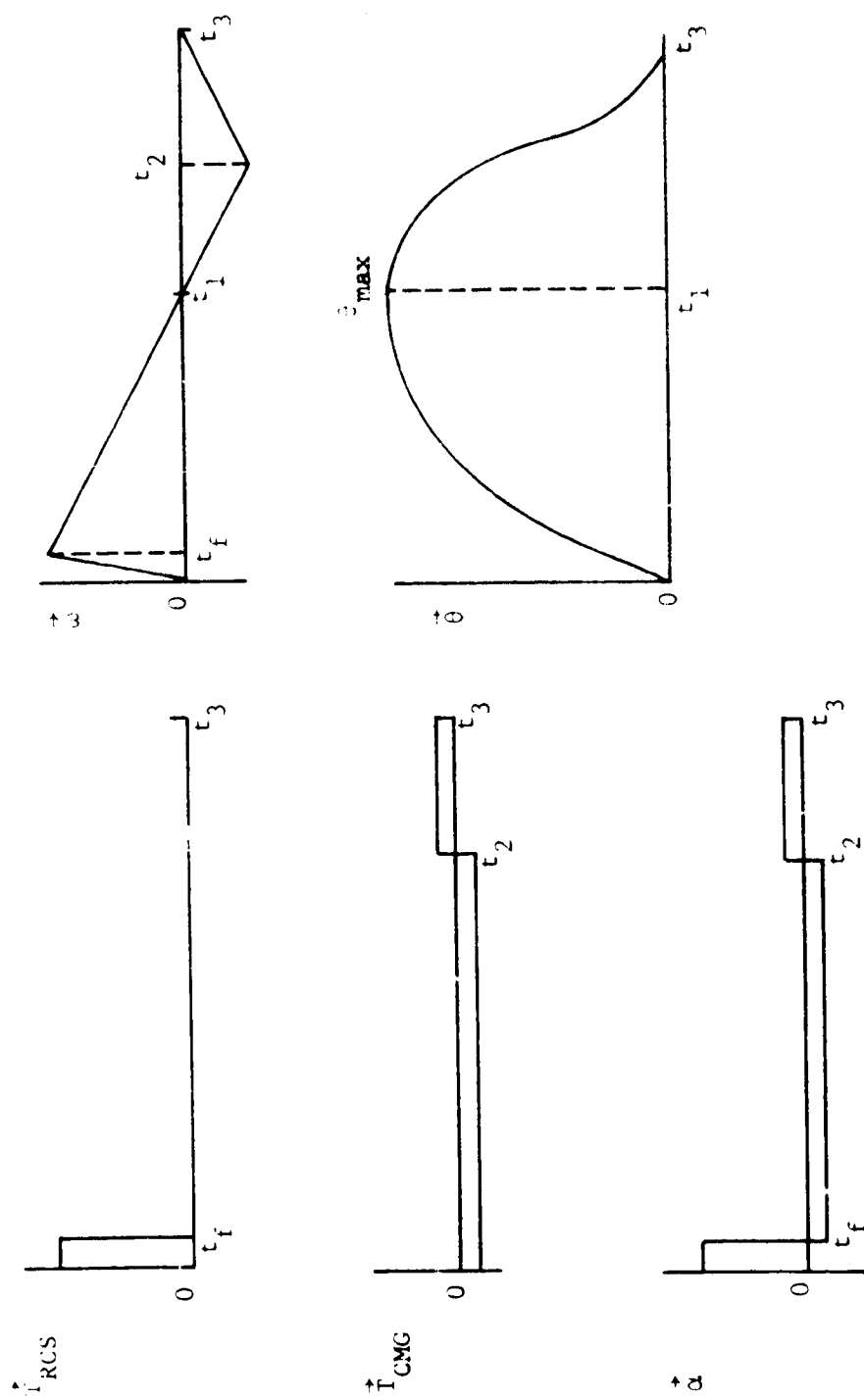


Figure 10.6. Sketches of \dot{T}_{RCS} , \dot{T}_{CMG} , $\dot{\alpha}$, $\dot{\omega}$, and $\dot{\delta}$

$$\vec{\omega} = \int_0^t \vec{\alpha} dt = \frac{1}{[I]} \int_0^t (\vec{T}_{RCS} + \vec{T}_{CMG}) dt \quad (53)$$

$$\vec{\theta} = \int_0^t \vec{\omega} dt = \frac{1}{[I]} \int_0^t \int_0^t (\vec{T}_{RCS} + \vec{T}_{CMG}) dt dt \quad (54)$$

where $[I]$ is the vehicle inertia tensor.

Assume that the CMG system is approaching saturation along the X axis. At time t_1 , the angular velocity ω_x goes through zero and θ , the axial angular displacement, is a maximum θ_{max} . From equations 53, time t_1 , can be computed by solving the following relationship.

$$\omega_x = \frac{1}{I_{xx}} \left\{ \int_0^{t_f} T_{RCS,x} dt - \int_0^{t_1} |\vec{T}_{CMG}|_{max} dt \right\} = 0 \quad (55)$$

$T_{RCS,x}$ is the torque generated due to firing the X axis RCS thruster pair; $T_{RCS,x}$ equals

$$T_{RCS,x} = F \ell_x = 8\,280 \text{ ft-lb} \quad (56)$$

Substituting the appropriate values of I_{xx} , t_f , $T_{RCS,x}$, and $|\vec{T}_{CMG}|_{max}$ into equation 55, time t_1 equals

$$t_1 = 3.67 \text{ seconds} \quad (57)$$

The maximum angular displacement of the X axis occurs at t_1 and equals

$$\begin{aligned} \theta_{max,x} &= \frac{1}{I_{xx}} \left[\int_0^{t_1} (\vec{T}_{RCS} + \vec{T}_{CMG}) dt dt \right] \\ &= 1.42 \times 10^{-3} \text{ radian or } 4.9 \text{ arc-minutes} \end{aligned} \quad (58)$$

At time t_2 , θ_x equals $0.5 \theta_{max,x}$. Utilizing equation 54, t_2 equals

$$\begin{aligned} 0.5 \theta_{max,x} &= \frac{1}{I_{xx}} \left[\int_0^{t_2} (\vec{T}_{RCS} + \vec{T}_{CMG}) dt dt \right] \\ t_2 &= 7.29 \text{ seconds} \end{aligned} \quad (59)$$

At time t_3 , the transient is assumed to have been damped out and θ_x equals zero. Using equation 54, t_3 equals

$$\frac{1}{I_{xx}} \left[\int_0^{t_3} (\vec{T}_{RCS} + \vec{T}_{CMG}) dt \right] = 0$$

$$t_3 = 10.91 \text{ seconds} \quad (60)$$

Performing the above analysis for the Y and Z axes, the corresponding values of t_1 , t_2 , t_3 , and θ_{\max} equal

Y axis: $t_1 = 17.6$ seconds
 $t_2 = 35.2$ seconds
 $t_3 = 52.8$ seconds
 $\theta_{\max, y} = 4.25 \times 10^{-3}$ rad or 14.6°

Z axis: $t_1 = 17.6$ seconds
 $t_2 = 35.2$ seconds
 $t_3 = 52.8$ seconds
 $\theta_{\max, z} = 4.08 \times 10^{-3}$ rad or 14.0°

This analysis corresponds to a worst case analysis since the CMG system is desaturated along the direction of smallest CMG torque capability, the direction of \vec{H}_{CMG} . From this analysis, the maximum attitude errors generated by firing the appropriate RCS thruster pair for a minimum pulse duration are less than a 0.1 degree for the X axis and approximately 0.25 degrees for both the Y and Z axes. For all experiments that have a relatively high stabilization requirement, these attitude errors would be excessive and would prevent experimentation during this desaturation interval. A major problem with this system is that firing a minimum RCS impulse causes the CMG system to be turned hard on in an attempt to compensate for the resultant large RCS torques produced. This turning the CMGs hard on could result in excessive CMG wear particularly to the individual CMG gear trains. Because this RCS desaturation system cannot meet the high degree of vehicle stabilization desired and because of the excessive CMG wear that can result, this system is not recommended.

Alternative to the RCS Desaturation Systems, Cases

A and B - An additional low torque RCS system could be added to the vehicle for the purpose of desaturating the CMG system. The control authority of this RCS system would have to be less than that of the CMG system. This system would be turned on and off gradually as shown in figure 10.7 in order to minimize attitude errors due to transients introduced by this RCS system. A thruster pair would remain on until the desired change in CMG momentum along its control axis has been reached. A representative value for the maximum torque capability of this RCS system would be approximately 100 ft-lb. Most of the high stabilization requirements imposed on the vehicle by its experiments could be met while this RCS desaturation system is operating. The major drawback to this system is that an additional system is added to the vehicle with only one function that of desaturating the CMG system.

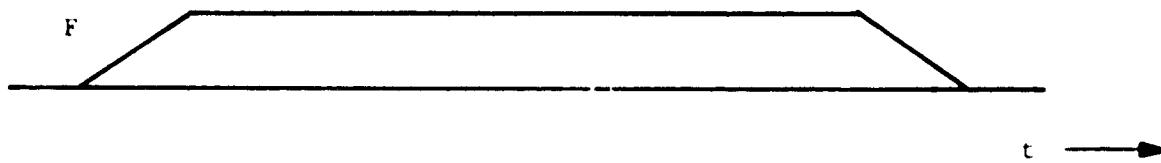
10.3.2 System 2: RCS Attitude Control - This RCS desaturation system transfers attitude control from the CMG system to the baseline RCS system. With the baseline RCS controlling vehicle attitude, the CMG system is commanded to its desired momentum state. Because the baseline RCS stabilization capability is much less than that of the CMG system, this system precludes the possibility of performing any experimentation during the desaturation interval that requires a high degree of stabilization. This loss in experimentation capability during the desaturation interval is not a major drawback since neither of the two previously described RCS desaturation systems utilizing the baseline RCS would permit experimentation during this period either.

To demonstrate how this system operates, assume that a change in CMG momentum of 13 000 ft-lb-sec along the vehicle Y axis is desired. Assume that the rate of change of the Y axis CMG momentum state T_{CMG} is 150 ft-lb. To produce the desired momentum change along the Y axis ΔH_y , this CMG torque T_{CMG} must last for t_D seconds where t_D equals

$$t_D = \frac{\Delta H_y}{T_{CMG}} = \frac{13\,000}{150} = 86.67 \text{ seconds} \quad (61)$$

After t_D seconds, the CMG system will be in its desired momentum state.

A RCS thruster pair is commanded to fire when the i^{th} vehicle axis impinges on one of the attitude deadband limits. Assume that the RCS firing logic is governed by the following rate plus position law.



F, MAXIMUM RCS THRUST LEVEL.

Figure 10.7. Alternative Implementation RCS
Desaturation System, System 1

$$|K_{Ri} \omega_i + K_{Pi} \theta_i| = E \quad (i=x, y, z) \quad (62)$$

E is a positive constant scalar that corresponds to the RCS attitude deadband limit. For the Y axis, assume that K_R , K_P and E have the following values.

$$K_{Ry} = 1 \text{ second} \quad (63)$$

$$K_{Py} = 1 \quad (64)$$

$$E = 0.5 \text{ degree} \quad (65)$$

These values of E, K_{Ry} , and K_{Py} correspond to a ± 0.5 degree RCS attitude deadband.

At time t equal to zero, the transfer from CMG to RCS attitude control has been accomplished and the CMG torque T_{CMG} is applied to the Y axis. Assume that initial Y axis angular rate $\omega_y(0)$ and position $\theta_y(0)$ at t equal to zero are:

$$\omega_y(0) = 0 \quad (66)$$

$$\theta_y(0) = 0 \quad (67)$$

The CMG torque T_{CMG} will accelerate the vehicle Y axis towards one of its attitude deadband limits defined by equation 62. Assume that the sign of T_{CMG} is positive; the resultant Y axis angular acceleration α_y equals

$$\alpha_y = \frac{T_{CMG}}{I_{yy}} (57.3 \text{ deg/rad}) = 1.047 \times 10^{-3} \text{ deg/sec}^2 \quad (68)$$

As the Y axis is accelerated towards its upper attitude deadband, $\omega_y(t)$ and $\theta_y(t)$ equal

$$\omega_y(t) = \alpha_y t + \omega_y(0) \text{ deg/sec} \quad (69)$$

$$\theta_y(t) = \frac{\alpha_y t^2}{2} + \omega_y(0)t + \theta_y(0) \text{ deg} \quad (70)$$

At time t_1 , the RCS firing logic equation, equation 62, will be satisfied and an appropriate RCS thruster pair will be fired

accelerating the Y axis away from the deadband limit. Substituting the above expressions for $\omega_y(t_1)$ and $\theta_y(t_1)$ and the appropriate values of K_{Ry} , K_{Py} , and E into equation 62,

$$|\omega_y(t_1) + \theta_y(t_1)| = 0.5$$

or

$$1.047 \times 10^{-3} t_1 + 0.5235 \times 10^{-3} t_1^2 - 0.5 = 0 \quad (71)$$

Solving for t_1 , t_1 equals

$$t_1 = 29.92 \text{ seconds} \quad (72)$$

Substituting the above value of t_1 into equation 69 and 70, $\omega_y(t_1)$ and $\theta_y(t_1)$ equal

$$\omega_y(t_1) = 0.0313 \text{ deg/sec} \quad (73)$$

$$\theta_y(t_1) = 0.4687 \text{ degree} \quad (74)$$

Assume that the momentum produced by firing the appropriate RCS thruster pair is instantaneously applied to the vehicle and results in a change of axial velocity ω_y . This change in velocity $\Delta\omega_y$ due to firing the RCS pair for its minimum time duration t_f equals

$$\Delta\omega_y = \frac{F l_y t_f}{I_{yy}} (57.3 \text{ deg/rad}) = 0.0279 \text{ deg/sec} \quad (75)$$

At time t_1^- , just after the appropriate RCS thruster pair has been fired, $\omega(t_1^-)$ and $\theta(t_1^-)$ equal

$$\omega(t_1^-) = \omega(t_1) - \Delta\omega_y = 0.0034 \text{ deg/sec} \quad (76)$$

$$\theta(t_1^-) = \theta(t_1) = 0.4687 \text{ degree} \quad (77)$$

Note that angular rate $\omega_y(t_1^-)$ is still positive meaning that the minimum momentum impulse bit (MIB)_y was not large enough to change the sign of ω_y . The CMG torque T_{CMG} will continue to accelerate the Y axis towards its upper deadband limit, $+\theta_0$. $\omega_y(t)$ and $\theta_y(t)$ equal

$$\omega_y(t) = \alpha_y(t-t_1) + \omega_y(t_1^-) \text{ for } t > t_1 \quad (78)$$

$$\theta_y(t) = \frac{\alpha_y(t-t_1)^2}{2} + \omega_y(t_1^-)(t-t_1) + \theta_y(t_1^-) \text{ for } t > t_1 \quad (79)$$

At time t_2 , the RCS firing logic equation will be satisfied once more and an appropriate RCS thruster pair will be fired again accelerating the Y axis away from its attitude deadband. Substituting $\omega_y(t_2)$ and $\theta_y(t_2)$ into equation 62,

$$|\omega_y(t_2) + \theta_y(t_2)| = 0.5$$

or

$$0.5235 \times 10^{-3}(t_2 - t_1)^2 + 4.455 \times 10^{-3}(t_2 - t_1) - 27.92 \times 10^{-3} = 0 \quad (80)$$

Solving equation 80, $(t_2 - t_1)$ equals

$$t_2 - t_1 = 4.20 \text{ seconds} \quad (81)$$

Time t_2 equals

$$t_2 = t_1 + 4.20 = 34.12 \text{ seconds} \quad (82)$$

Substituting t_2 into equations 78 and 79, $\omega_y(t_2)$ and $\theta_y(t_2)$ equal

$$\omega_y(t_2) = +0.0078 \text{ deg/sec} \quad (83)$$

$$\theta_y(t_2) = 0.4922 \text{ degree} \quad (84)$$

At time t_2^- , the appropriate RCS thruster pair has been fired and $\omega_y(t_2^-)$ and $\theta_y(t_2^-)$ equal

$$\omega_y(t_2^-) = \omega_y(t_2) - \Delta\omega_y = -0.0201 \text{ deg/sec} \quad (85)$$

$$\theta_y(t_2^-) = \theta_y(t_2) = 0.4922 \text{ degree} \quad (86)$$

For t greater than t_2 , $\omega_y(t)$ and $\theta_y(t)$ equal

$$\omega_y(t) = \alpha_y(t-t_2) + \omega_y(t_2^-) \text{ for } t > t_2 \quad (87)$$

$$\theta_y(t) = \frac{\alpha_y(t-t_2)^2}{2} + \omega_y(t_2^-)(t-t_2) + \theta_y(t_2^-) \text{ for } t > t_2 \quad (88)$$

At time t_2^- , ω_y is negative indicating that the Y axis is moving away from the upper deadband limit $+\theta_o$. The CMG torque T_{CMG} acting on the Y axis decelerates this motion and at time t_3 , the Y axis starts back towards its upper attitude deadband limit. At time t_3 , the Y axis velocity ω_y is zero. Substituting t_3 for t into equation 87 and setting the resulting expression to zero

$$\alpha_y(t_3-t_2) + \omega_y(t_2^-) = 0 \quad (89)$$

or

$$1.047 \times 10^{-3}(t_3-t_2) - 0.0201 = 0 \quad (90)$$

Solving for t_3-t_2 ,

$$t_3-t_2 = 19.21 \text{ seconds} \quad (91)$$

t_3 equals

$$t_3 = t_2 + 19.21 = 53.33 \text{ seconds} \quad (92)$$

From equation 88, the corresponding value of $\theta_y(t_3)$ equals

$$\theta_y(t_3) = 0.2990 \text{ degree} \quad (93)$$

At time t_4 , the state of the Y axis (ω_y, θ_y) will once again satisfy the RCS firing logic and another minimum RCS impulse will result sending the Y axis away from its upper deadband limit. Substituting $\omega_y(t_4)$ and $\theta_y(t_4)$ into equation 62, the RCS firing logic equals

$$|\omega_y(t_4) + \theta_y(t_4)| - 0.5 = 0$$

or

$$0.5235(t_4-t_2)^2 - 19.1 \times 10^{-3}(t_4-t_2) - 27.9 \times 10^{-3} = 0 \quad (94)$$

Solving for t_4 ,

$$t_4-t_2 = 37.88 \text{ seconds}$$

or

$$t_4 = t_2 + 37.88 = 72.00 \text{ seconds} \quad (95)$$

Substituting t_4 into equations 87 and 88, $\omega_y(t_4)$ and $\theta_y(t_4)$ equal

$$\omega_y(t_4) = 0.0195 \text{ deg/sec} \quad (96)$$

$$\theta_y(t_4) = 0.4805 \text{ degree} \quad (97)$$

At time t_4^- , $\omega_y(t_4^-)$ and $\theta_y(t_4^-)$ equal

$$\omega_y(t_4^-) = \omega_y(t_4) - \Delta\omega_y = -0.0084 \text{ deg/sec} \quad (98)$$

$$\theta_y(t_4^-) = \theta_y(t_4) = 0.4805 \text{ degree} \quad (99)$$

For t greater than t_4 , $\omega_y(t)$ and $\theta_y(t)$ equal

$$\omega_y(t) = \alpha_y(t - t_4) + \omega_y(t_4^-) \text{ for } t > t_4 \quad (100)$$

$$\theta_y(t) = \frac{\alpha_y(t - t_4)^2}{2} + \omega_y(t_4^-)(t - t_4) + \theta_y(t_4^-) \text{ for } t > t_4 \quad (101)$$

At time t_4^- , ω_y is again negative meaning that the Y axis is traveling away from the upper deadband limit $+\theta_o$. At time t_5 , the Y axis velocity ω_y is zero and the Y axis starts moving back towards $+\theta_o$. Substituting t_5 for t and setting equation 100 equal to zero, t_5 equals

$$1.047 \times 10^{-3}(t_5 - t_4) - 0.0084 = 0$$

$$(t_5 - t_4) = 8.04 \text{ seconds}$$

$$t_5 = t_4 + 8.04 = 80.04 \text{ seconds} \quad (102)$$

Substituting t_5 into equation 101, $\theta_y(t_5)$ equals

$$\theta_y(t_5) = 0.4467 \text{ degree} \quad (103)$$

Note that at t equal to 86.67 seconds, T_{CMG} becomes zero and the CMG system is at its desired momentum state. Substituting t equal to 86.67 seconds into equation 100 and 101, θ_y and ω_y equal

$$\omega_y(86.67)=0.0070 \text{ deg/sec} \quad (104)$$

$$\theta_y(86.67)=0.4700 \text{ degree} \quad (105)$$

For t greater than 86.67 seconds, T_{CMG} is zero and will no longer accelerate the Y axis towards its upper RCS deadband limit $+\theta_o$. But since ω_y at this time has a positive sign, the Y axis will continue to travel towards $+\theta_o$; when it reaches $+\theta_o$, the RCS will fire a minimum impulse sending the Y axis away from $+\theta_o$. For time t greater than 86.67 seconds, $\omega_y(t)$ and $\theta_y(t)$ equal

$$\omega_y(t)=\omega_y(86.67) \text{ for } t > 86.67 \text{ seconds} \quad (106)$$

$$\theta_y(t)=[\omega_y(86.67)](t-86.67)+\theta_y(86.67) \text{ for } t > 86.67 \text{ sec} \quad (107)$$

At time t_6 , the state of the Y axis satisfies the RCS firing logic, equation 62. Using equations 106 and 107, substitute $\omega_y(t_6)$ and $\theta_y(t_6)$ into equation 62.

$$|\omega_y(t_6)+\theta_y(t_6)|-0.5=0 \quad (108)$$

Solving equation 108 for t_6 ,

$$t_6=89.96 \text{ seconds} \quad (109)$$

$\omega_y(t_6)$ and $\theta_y(t_6)$ equal

$$\omega_y(t_6)=0.0070 \text{ deg/sec} \quad (110)$$

$$\theta_y(t_6)=0.4930 \text{ degree} \quad (111)$$

At time t_6^- , the RCS has fired sending the Y axis away from $+\theta_o$ at a constant rate $\omega_y(t_6^-)$. $\omega_y(t_6^-)$ and $\theta_y(t_6^-)$ equal

$$\omega_y(t_6^-)=\omega_y(t_6)-\Delta\omega_y=-0.0209 \text{ deg/second} \quad (112)$$

$$\theta_y(t_6^-)=\theta_y(t_6)=0.4930 \text{ degree} \quad (113)$$

For time t greater than t_6 , $\omega_y(t)$ and $\theta_y(t)$ equal

$$\omega_y(t) = \omega_y(t_6^-) \text{ deg/sec for } t < t_6 \quad (114)$$

$$\theta_y(t) = [\omega_y(t_6^-)](t - t_6) + \theta_y(t_6^-) \text{ degree for } t > t_6 \quad (115)$$

The baseline RCS has fired four minimum impulses Ft_f introducing four minimum momentum impulse bits $(MIB)_y$ to the system. Four $(MIB)_y$'s correspond to a momentum of 16 000 ft-lb-sec; this value of momentum exceeds the desired change in momentum of 13 000 ft-lb-sec by 3 000 ft-lb-sec. This additional momentum, 3 000 ft-lb-sec, must be removed from the system. As the Y axis passes through an angular displacement θ_y of zero, a modulated pulse, like the one described for system 1, Case B, is fired absorbing this additional momentum. Figure 10.8 is a sketch of this modulated pulse. Firing this modulated pulse causes the net change in momentum along the Y axis to equal the desired change of 13 000 ft-lb-sec. The modulated pulse duration t_m is computed using equation 44 where $H_{MOD,y}$ equals 3 000 ft-lb-sec, t_m equals

$$t_m = \frac{H_{MOD,y} + F\ell_y t_f}{F\ell_y} = 175 \text{ milliseconds} \quad (116)$$

At time t_7 , θ_y passes through zero and the modulated pulse is fired. Substituting t_7 for t and setting equation 115 equal to zero, t_7 equals

$$[\omega_y(t_6^-)](t_7 - t_6) + \theta_y(t_6^-) = 0$$

$$(t_7 - t_6) = 23.59$$

$$t_7 = t_6 + 23.59 = 113.55 \text{ seconds} \quad (117)$$

At time t_7^- , just after the modulated pulse has been fired, $\omega_y(t_7^-)$ and $\theta_y(t_7^-)$ equal

$$\omega_y(t_7^-) = 0 \text{ for } t > t_7 \quad (118)$$

$$\theta_y(t_7^-) = 0 \text{ for } t > t_7 \quad (119)$$

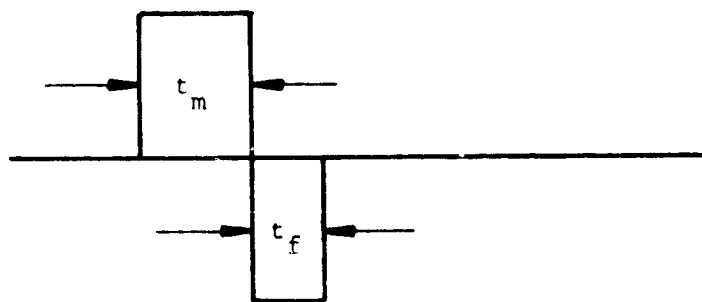


Figure 10.8. Sketch of RCS Desaturation System,
System 2 Modulated Pulse

The desired desaturation along the Y axis is completed and it takes slightly less than two minutes to perform. Figure 10.9 is the corresponding phase plane describing the time history of $\omega_y(t)$ versus $\theta_y(t)$ during these two minutes.

The amount of fuel W.O.F. required to perform this desired 13 000 ft-lb-sec change in the CMG momentum state along the Y axis is given by equation 46 where n_y , the number of minimum impulse firings, equals four. W.O.F. equals

$$\text{W.O.F.} = \frac{2F[(n_y+1)t_f + t_m]}{I_{sp}} = 2.7 \text{ lb} \quad (120)$$

This RCS desaturation system, system 2, expends 0.6 pounds more fuel than system 1, Case B for the same change in CMG momentum, but unlike system 1, Case B it performs the desired desaturation without resulting in excessive CMG wear.

10.3.3 Comparison of RCS CMG Desaturation Systems - Three RCS CMG desaturation systems utilizing the Shuttle baseline RCS system have been proposed. The systems are denoted as system 1 Case A and Case B and system 2. Both system 1 Cases A and B attempt to hold the attitude of the vehicle using the CMG system. The rationale behind this method is that by accurately stabilizing the vehicle with the CMG system during desaturation, experimentation can presumably continue during this interval. Both systems, Cases A and B fire the baseline RCS in such a manner that the resultant RCS torques generated will desaturate the CMG system. Case A attempts to time modulate a RCS pulse train of both positive and negative pulses in such a fashion that the average resultant RCS torque generated is less than the torque capability of the CMG system. Case B desaturates the CMG system by imparting a number of minimum RCS impulses to the vehicle and then allowing the CMG system to absorb the resultant momentum produced. System 2 transfers attitude control from the CMG system to the baseline RCS and then commands the CMGs to the desired CMG momentum state. The resultant CMG torques that are generated due to the change in CMG momentum state are absorbed by the RCS. The use of system 2 precludes the continuation of most experiments with relatively high vehicle stabilization requirements during desaturation since the vehicle stabilization capability is limited to that attainable by the baseline RCS.

Listed in table 10.2 are the advantages and disadvantages of the three proposed systems. The major disadvantage of system 1 Case A is that its fuel consumption is extremely large and is a

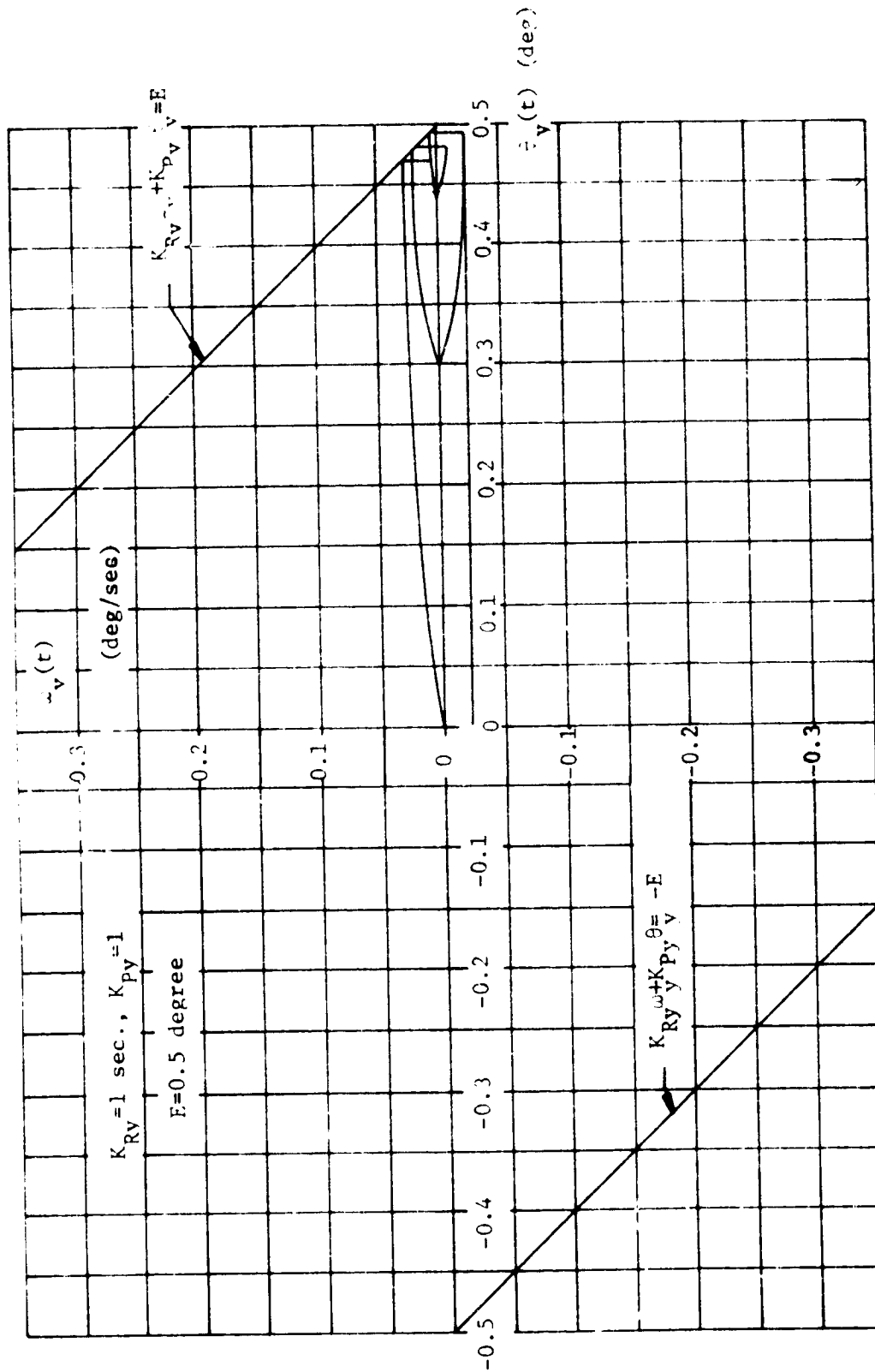
Figure 10.9. System 2: Phase Plane $\omega_y(t)$ Versus $\theta_y(t)$

Table 10.2. Advantages and Disadvantages of RCS Desaturation Systems
System 1 and 2

SYSTEM	ADVANTAGES	DISADVANTAGES
System 1: Case A Modulated RCS System		1). Desired vehicle stabilization is doubtful 2). Large fuel consumption - severe source of experiment contamination 3). Modulation control of pulse duration too extreme
System 1: Case B Pulsed RCS System	1). Requires much less fuel than System 1: Case A	1). Desired vehicle stabilization not feasible 2). Excessive CMG wear
System 2: RCS Attitude Control System	1). Fuel requirements approximately the same as System 1: Case B 2). No excessive CMG wear problem 3). Easily implemented	1). Precludes attaining high vehicle stabilization during desaturation

severe source of experiment contamination. The major problem with system 1 Case B is that firing a minimum RCS impulse produces such a large torque that it saturates the CMG system from a torque standpoint causing excessive CMG wear particularly to the individual CMG gear trains. Meeting the experiment vehicle stabilization requirements during desaturation with either Case A or B is extremely doubtful since the control authority of the baseline RCS is much larger than that of the CMG system. System 2 does not attempt to accurately stabilize the vehicle during desaturation, but neither can system 1 Cases A or B. It does not have the CMG wear problem of Case B and its RCS fuel consumption rate is relatively low unlike Case A. System 2 can also be easily implemented. The recommended RCS desaturation system is system 2.

10.3.4 Recommended RCS CMG Desaturation Signal Flow Diagram - Figure 10.10 is a signal flow diagram corresponding to the recommended RCS desaturation system, system 2. This CMG desaturation system can be initiated by either a manual, a programmed, or an automatic command. The CMG system is automatically desaturated whenever the magnitude of the CMG momentum vector \vec{H}_{CMG} exceeds a preset value H_{MAX} . A reasonable value for H_{MAX} is ninety-five percent of saturation. For an operational six CMG system, H_{MAX} using the above criteria equals

$$H_{MAX} = 0.95(6H) = 5.7H \quad (121)$$

where H is the magnitude of the individual CMG wheel momentum.

In box 1 of the signal flow diagram, the CMG momentum vector \vec{H}_{CMG} is computed using the CMG gimbal angles $\delta_{1(i)}$ and $\delta_{3(i)}$. The system then goes onto box 2 where the magnitude of \vec{H}_{CMG} is computed. In box 3, the magnitude of \vec{H}_{CMG} is compared with H_{MAX} . If the magnitude of \vec{H}_{CMG} is less than H_{MAX} , the system recycles back to box 1. If the magnitude of \vec{H}_{CMG} equals or exceeds H_{MAX} , the CMG system is approaching saturation and the logic flow proceeds to box 4 where the process of desaturating the CMGs is started.

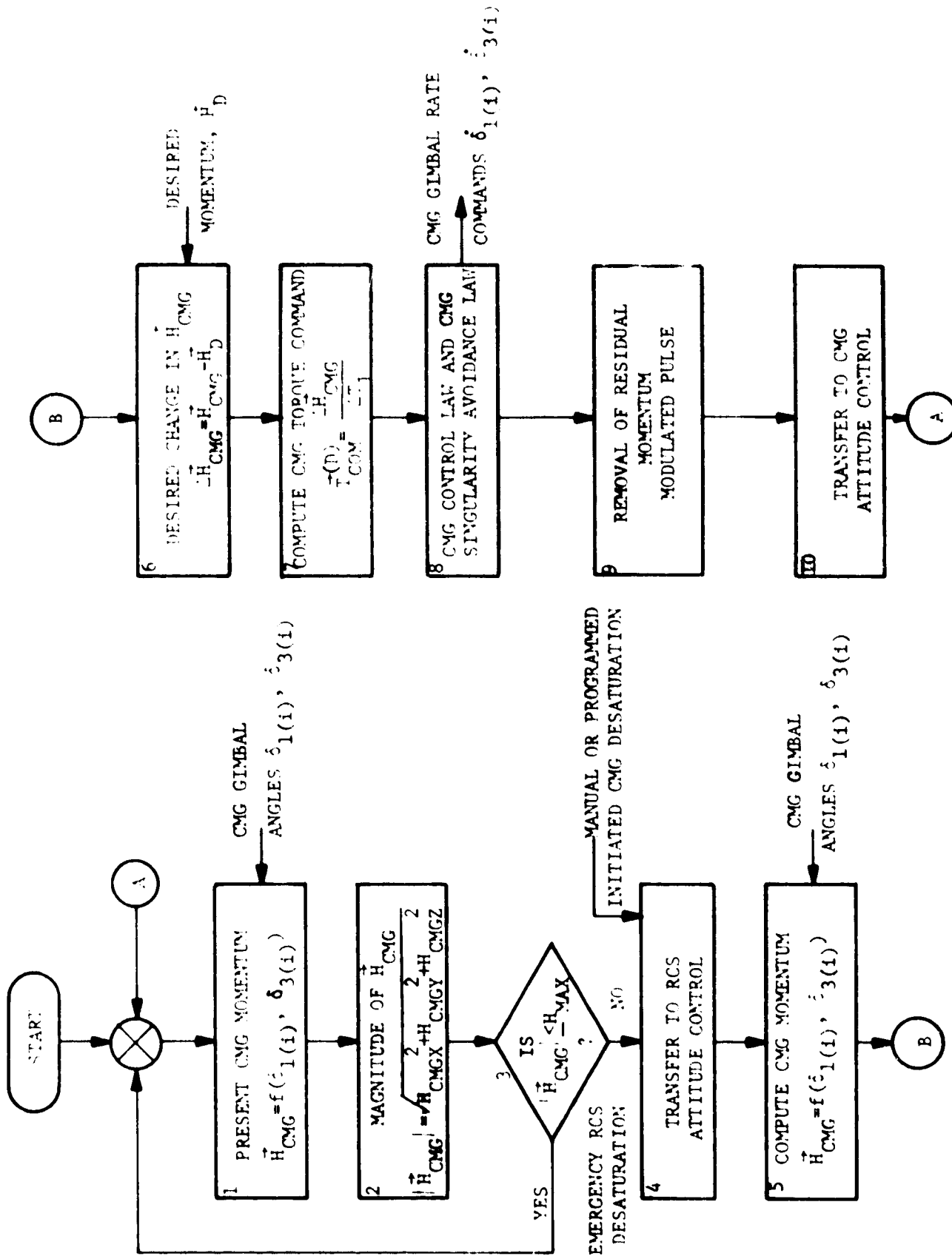


Figure 10.10. Logic Signal Flow Diagram for Recommended RCS CMG Desaturation System

At box 4, CMG desaturation is initiated either automatically as described above or by a manual or programmed CMG desaturation command. In box 4, vehicle attitude control is transferred from CMG control to the baseline RCS control system. The CMG torque command \vec{T}_{COM} generated by the CMG vehicle control law is zeroed. After this transfer has been completed, the desaturation system proceeds onto box 5 where the CMG momentum vector \vec{H}_{CMG} is recomputed.

In box 6, the desired change in the CMG momentum state $\Delta \vec{H}_{CMG}$ is computed. The system then proceeds onto box 7 where the CMG torque command $\vec{T}_{COM}^{(D)}$ that will produce the desired change in \vec{H}_{CMG} is computed. $\vec{T}_{COM}^{(D)}$ equals

$$\vec{T}_{COM}^{(D)} = \frac{\Delta \vec{H}_{CMG}}{\Delta T_1} \quad (122)$$

where ΔT_1 is a preset time interval corresponding to the length of time the torque command $\vec{T}_{COM}^{(D)}$ is to be applied to the CMG system. The value of ΔT_1 should be picked so that the magnitude of $\vec{T}_{COM}^{(D)}$ does not exceed the CMG system torque capability along $\vec{T}_{COM}^{(D)}$. This torque command $\vec{T}_{COM}^{(D)}$ is inputted to box 8 of the logic flow where the appropriate CMG gimbal rate commands $\dot{\delta}_{1(i)}$ and $\dot{\delta}_{3(i)}$ are generated in accordance with the CMG control law and singularity avoidance scheme. After ΔT_1 seconds, the torque command $\vec{T}_{COM}^{(D)}$ is zeroed and the system proceeds onto box 9. In box 9, the modulated RCS pulse commands that will remove any residual momentum left in the system as the affected control axes pass through their zero angular displacement are generated. The system then proceeds onto box 10 where the transfer from RCS to CMG attitude control is reinitiated. After CMG attitude control is re-established, the logic flow recycles back to box 1.

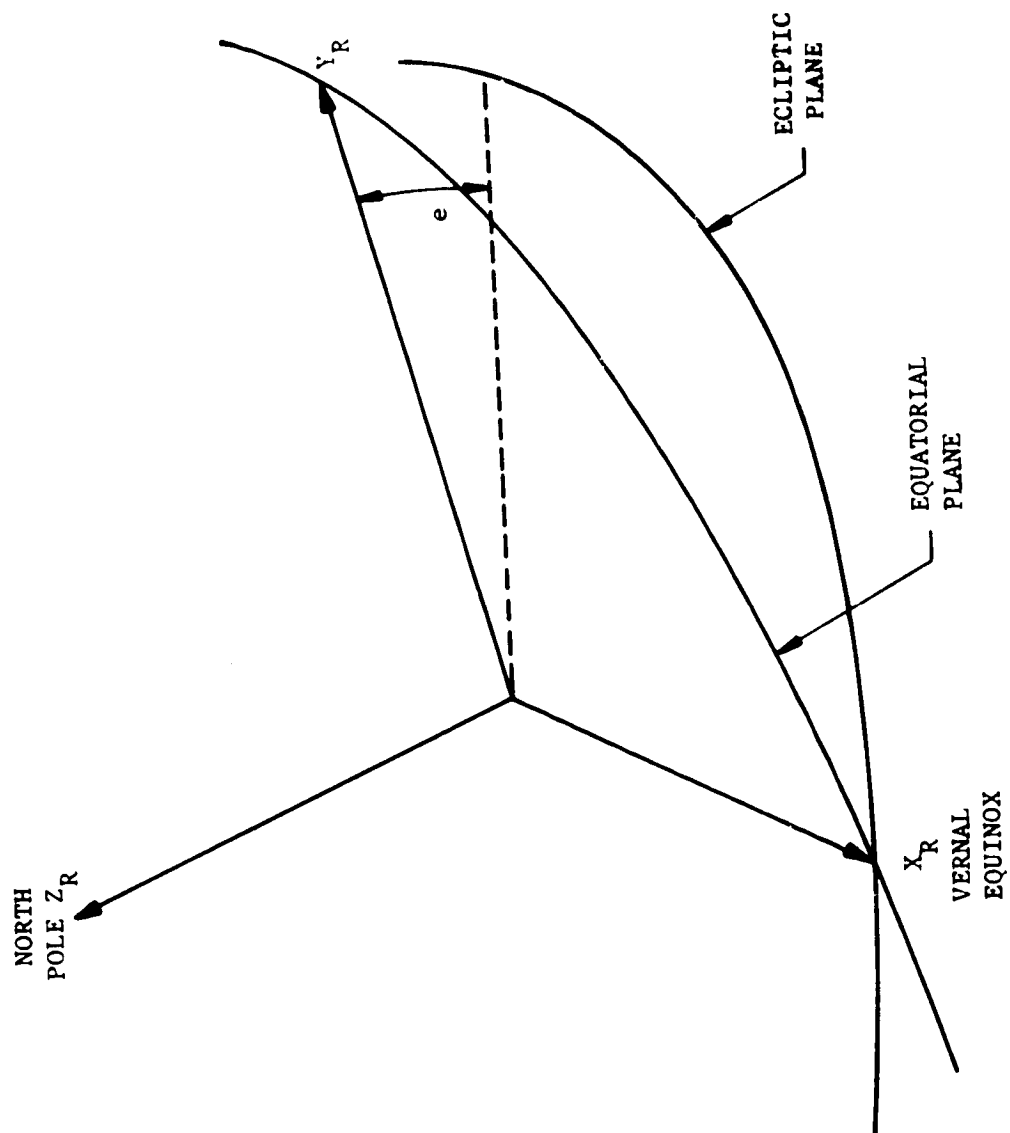
Instead of computing a CMG torque command $\vec{T}_{COM}^{(D)}$, an alternative method of implementing this RCS desaturation system is to drive the CMG gimbals to a predetermined CMG gimbal orientation

$\delta_{1(i)}$ and $\delta_{3(i)}$. This alternative method would by-pass the CMG control law and singularity avoidance scheme; it would command each gimbal to move at its maximum safe rate until its desired CMG gimbal angle had been achieved. The previous method described that of computing a CMG torque command $\vec{T}_{COM}^{(D)}$ has the advantage that the CMG system can be driven to any particular momentum state by just changing the desired CMG momentum state \vec{H}_D . To transfer to a new CMG momentum state using this alternative method a new set of gimbal angles must be computed of which there are an infinite number for each new \vec{H}_D .

10.4 Gravity Gradient CMG Desaturation Systems - Gravity gradient CMG desaturation systems desaturate the CMG system by maneuvering the vehicle to a favorable orientation where the natural gravity gradient torques acting on the vehicle will result in the desired change in the CMG system momentum state. Four representative gravity gradient desaturation laws are developed in the following sections; they are: (1) a small angle maneuver desaturation law (i.e., less than 15°), (2) a law requiring a large maneuver about one vehicle axis, (3) a reflexive law requiring large multiaxis maneuvers, and (4) a gravity tracking law also requiring large multiaxis maneuvers. Laws 2 and 3 also require additional small angle maneuvers during the desaturation interval in order to control small momentum accumulations due to finite maneuver times and aerodynamic torques. The gravity tracking law, law 4, involves a continuous multiaxis rotation about the orbit normal after the initial desaturation attitude is established in order to track the local gravity force vector. These four gravity gradient CMG desaturation laws 1 thru 4 are derived in sections 10.4.2 thru 10.4.5, respectively, for an inertially held vehicle. In section 10.4.7, the problem of desaturating the CMG system from a Z-LV attitude will be discussed and an appropriate gravity gradient desaturation law developed.

10.4.1 Orbit, Coordinate Frames, and Coordinate Transformations - The vehicle is assumed to be in an ideal low attitude circular Earth orbit. The position of the vehicle in this orbit can therefore be given in terms of the orbital rate ω_o and the elapsed time t measured from some orbit reference position ($\theta_t = \omega_o t$).

The reference coordinate frame used in this study is designated by the subscript R and is illustrated in figure 10.11. The $X_R Y_R$

Figure 10.11. Vehicle Reference Frame $X_R Y_R Z_R$

plane coincides with the Earth's equatorial plane, the X_R axis is directed towards the vernal equinox, and the Z_R axis towards the north pole. The Y_R axis completes the right handed coordinate system shown in figure 10.11.

A quasi-inertial orbital reference frame $X_O Y_O Z_O$ is shown in figure 10.12 along with its relationship to the $X_R Y_R Z_R$ frame and is defined by the longitude of the ascending node α (rotation about Z_R) and the orbital inclination i (rotation about X_O). The transformation from the vehicle reference frame to the orbital reference frame is given by:

$$\begin{bmatrix} X_O \\ Y_O \\ Z_O \end{bmatrix} = \begin{bmatrix} 1 & 0 & 0 \\ 0 & \cos i & \sin i \\ 0 & -\sin i & \cos i \end{bmatrix} \begin{bmatrix} \cos \alpha & \sin \alpha & 0 \\ -\sin \alpha & \cos \alpha & 0 \\ 0 & 0 & 1 \end{bmatrix} \begin{bmatrix} X_R \\ Y_R \\ Z_R \end{bmatrix}$$

$$= \begin{bmatrix} \cos \alpha & \sin \alpha & 0 \\ -\cos i \sin \alpha & \cos i \cos \alpha & \sin i \\ \sin i \sin \alpha & -\sin i \cos \alpha & \cos i \end{bmatrix} \begin{bmatrix} X_R \\ Y_R \\ Z_R \end{bmatrix} \quad (123)$$

The frame is quasi-inertial due to the precession of the orbit about the X_R axis which will cause a systematic variation in α . The variation (which depends primarily on i) is slow and α can be assumed constant over each orbit, thus justifying the quasi-inertial nature of the frame.

Certain of the control laws to be considered are derived with respect to a quasi-inertial frame in which one of the axes (usually Z) is directed toward a point on the celestial sphere which is normally the point of observation. This point can be given in terms of the right ascension and declination (designated ρ and δ) but more usefully in terms of an angle ψ measured from the orbital plane and a second angle locating the point in the orbital plane from which ψ is measured. Figure 10.13 shows the relation of these angles with respect to the R and O frames.

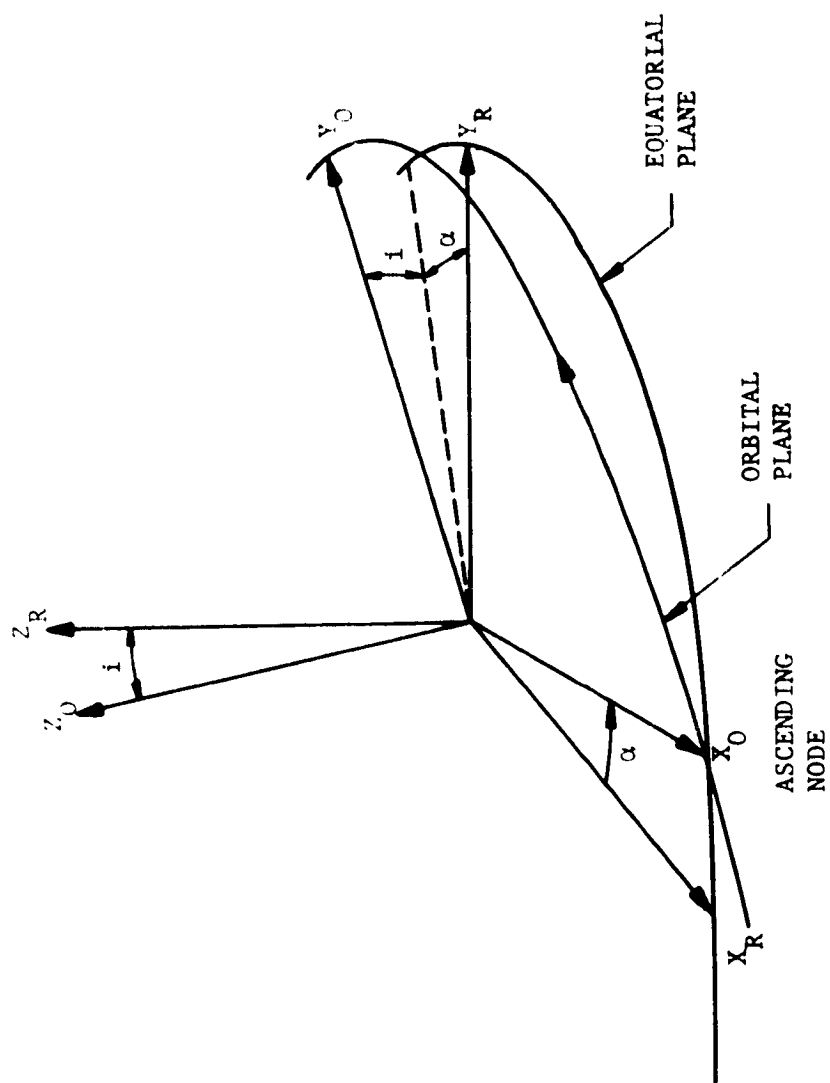


Figure 10.12. Orbital Reference Frame $X_0 Y_0 Z_0$

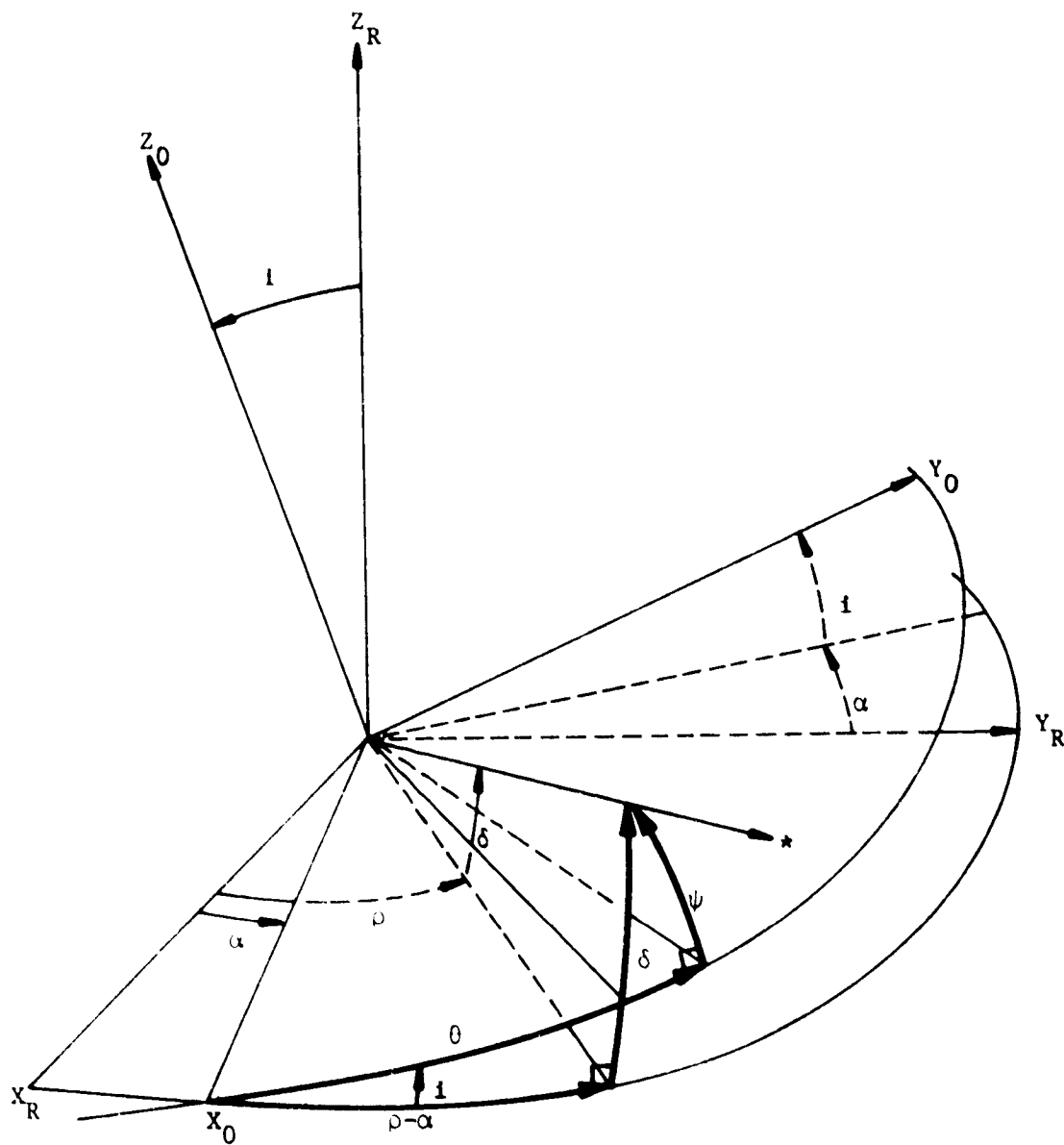


Figure 10.13. Relation of a Vector (Axis) Directed Toward a Celestial Target with Respect to the $X_R Y_R Z_R$ Frame

Details of the usage will be left for the particular sections involved, as will needed details of the transformations. It should be noted that for celestial targets the frame is very nearly inertial, being affected only by the very minute precession of the equinoxes. In the case of solar pointing the target point varies slowly due to the revolution of the Earth in its orbit and a frame based on the solar target is quasi-inertial and the angles can be considered as constant only for a limited time period.

Other subsidiary coordinate frames will be introduced only as they are required along with the necessary transformations.

10.4.2 Small Angle CMG Desaturation Law - A small angle CMG desaturation law is ideal where (1) the primary CMG momentum accumulation is along the vehicle axis corresponding to the minimum moment of inertia or where the accumulation along the other two axes are small and (2) the two large moments of inertia are approximately equal. All of these requirements are fulfilled by the Shuttle and its candidate attitudes, X-POP and X-IOP. The principal advantage of this type of desaturation law is that CMG momentum "dump" can be accomplished using only small maneuvers thus, minimizing maneuvering resources such as time and momentum expended maneuvering the vehicle to and back from its desaturation orientation. Its chief disadvantage is that it cannot be used to desaturate the CMG system of an "all attitude" vehicle like the proposed Large Space Telescope (LST) spacecraft. For the proposed Shuttle CMG control system, this apparent drawback has no significance since the Shuttle is not assumed to be an "all attitude" vehicle and its candidate attitudes are compatible with this type of desaturation law.

Derivation of Small Angle Gravity Gradient CMG Desaturation Law - The gravity gradient torque \vec{T}_{gg} acting on the vehicle was given in equation 15. This expression for \vec{T}_{gg} is reproduced below for convenience.

$$\vec{T}_{gg}(t) = \begin{bmatrix} T_{gx}(t) \\ T_{gy}(t) \\ T_{gz}(t) \end{bmatrix} = 3\omega_o^2 \begin{bmatrix} a_y a_z (I_{zz} - I_{yy}) \\ a_x a_z (I_{xx} - I_{zz}) \\ a_x a_y (I_{yy} - I_{xx}) \end{bmatrix} \quad (124)$$

a_x , a_y , and a_z are the X, Y, and Z components of the local vertical vector a in vehicle coordinates, respectively. This local vertical

vector \hat{a} can readily be written in the quasi-inertial orbital reference frame shown in figure 10.12 independent of vehicle attitude as follows:

$$\hat{a}_O = \begin{bmatrix} \cos \omega_o t \\ \sin \omega_o t \\ 0 \end{bmatrix} \quad (125)$$

where time t is zero when the orbital position of the vehicle is coincident with the positive X_o axis. \hat{a} in vehicle coordinates equals

$$\hat{a} = [\phi_{v \rightarrow o}] \hat{a}_O \quad (126)$$

where $[\phi_{v \rightarrow o}]$ is the transformation from the orbital reference frame to the desired vehicle attitude. $[\phi_{v \rightarrow o}]$ equals

$$[\phi_{v \rightarrow o}] = [\phi_D][\phi_o]^{-1} \quad (127)$$

where $[\phi_D]$ and $[\phi_o]$ are the transformations from the reference frame $X_R Y_R Z_R$ to the desired vehicle attitude and from $X_R Y_R Z_R$ to the orbital reference frame $X_o Y_o Z_o$, respectively. $[\phi_o]$ is defined in equation 123, $[\phi_o]$ equals

$$[\phi_o] = \begin{bmatrix} \cos \alpha & \sin \alpha & 0 \\ -\cos i \sin \alpha & \cos i \cos \alpha & \sin i \\ \sin i \sin \alpha & -\sin i \cos \alpha & \cos i \end{bmatrix} \quad (128)$$

Let the transformation $[\phi_{v \rightarrow o}]$ equal

$$[\phi_{v \rightarrow o}] = \begin{bmatrix} a_{11D} & a_{12D} & a_{13D} \\ a_{21D} & a_{22D} & a_{23D} \\ a_{31D} & a_{32D} & a_{33D} \end{bmatrix} \quad (129)$$

The local vertical vector \hat{a} in vehicle coordinates then equals

$$\hat{a} = \begin{bmatrix} a_x \\ a_y \\ a_z \end{bmatrix} = [\phi_{v \rightarrow o}] \hat{a}_o = \begin{bmatrix} a_{11D} \cos \omega_o t + a_{12D} \sin \omega_o t \\ a_{21D} \cos \omega_o t + a_{22D} \sin \omega_o t \\ a_{31D} \cos \omega_o t + a_{32D} \sin \omega_o t \end{bmatrix} \quad (130)$$

Assume that the vehicle is maneuvered through a small angle $\vec{\epsilon}$ where ϵ_x , ϵ_y , and ϵ_z are the X, Y, and Z components of $\vec{\epsilon}$, respectively. The resultant local vertical vector \hat{a} equals

$$\begin{aligned} \hat{a}_D = \begin{bmatrix} a_{xD} \\ a_{yD} \\ a_{zD} \end{bmatrix} &= \begin{bmatrix} 1 & \epsilon_z & -\epsilon_y \\ -\epsilon_z & 1 & \epsilon_x \\ \epsilon_y & -\epsilon_x & 1 \end{bmatrix} \begin{bmatrix} a_x \\ a_y \\ a_z \end{bmatrix} \\ &= \begin{bmatrix} a_x - a_z \epsilon_y + a_y \epsilon_z \\ a_y + a_z \epsilon_x - a_x \epsilon_z \\ a_z - a_y \epsilon_x + a_x \epsilon_y \end{bmatrix} \end{aligned} \quad (131)$$

Substituting the components of \hat{a}_D into the gravity gradient torque equation, equation 124, and neglecting all second order terms of ϵ_i , $i=x,y,z$, the gravity gradient torque \vec{T}'_{gg} equals

$$\vec{T}'_{gg} = 3\omega_o^2 \begin{bmatrix} [a_y a_z + (a_z^2 - a_y^2) \epsilon_x + a_x a_y \epsilon_y - a_x a_z \epsilon_z] \Delta I_x \\ [a_x a_z - a_x a_y \epsilon_x + (a_x^2 - a_z^2) \epsilon_y + a_y a_z \epsilon_z] \Delta I_y \\ [a_x a_y + a_x a_z \epsilon_x - a_y a_z \epsilon_y + (a_y^2 - a_x^2) \epsilon_z] \Delta I_z \end{bmatrix} \quad (132)$$

where

$$\Delta I_x = I_{zz} - I_{yy} \quad (133)$$

$$\Delta I_y = I_{xx} - I_{zz} \quad (134)$$

$$\Delta I_z = I_{yy} - I_{xx} \quad (135)$$

Transforming \vec{T}'_{gg} back into the desired vehicle attitude, where the CMG momentum was accumulated, $\vec{T}^{(D)}_{gg}$ equals

$$\vec{T}^{(D)}_{gg} = \begin{bmatrix} 1 & -\epsilon_z & \epsilon_y \\ \epsilon_z & 1 & -\epsilon_x \\ -\epsilon_y & \epsilon_x & 1 \end{bmatrix} \vec{T}'_{gg} \quad (136)$$

Neglecting second order terms of ϵ_1 , $\vec{T}^{(D)}_{gg}$ equals

$$\vec{T}^{(D)}_{gg} = 3\omega_o^2 \begin{bmatrix} a_y a_z \Delta I_x \\ a_x a_z \Delta I_y \\ a_x a_y \Delta I_z \end{bmatrix} + 3\omega_o^2 \begin{bmatrix} A_{11} & A_{12} & A_{13} \\ A_{21} & A_{22} & A_{23} \\ A_{31} & A_{32} & A_{33} \end{bmatrix} \begin{bmatrix} \Delta I_x \epsilon_x \\ \Delta I_y \epsilon_y \\ \Delta I_z \epsilon_z \end{bmatrix} \quad (137)$$

where

$$A_{11} = a_z^2 - a_y^2 \quad (138)$$

$$A_{12} = -A_{21} = -a_x a_y \quad (139)$$

$$A_{13} = -A_{31} = a_x a_z \quad (140)$$

$$A_{22} = a_x^2 - a_z^2 \quad (141)$$

$$A_{23} = -A_{32} = -a_y a_z \quad (142)$$

$$A_{33} = a_y^2 - a_x^2 \quad (143)$$

Note that the first term in equation 137 is just the gravity gradient torque \vec{T}_{gg} given in equation 124 without small angle maneuvers ϵ_1 . The second term is the additional gravity gradient torque acting on the vehicle due to the small angle desaturation maneuvers ϵ_1 . This additional torque \vec{T}_{gc} is used to desaturate the CMG system; \vec{T}_{gc} equals

$$\vec{T}_{gc} = 3\omega_o^2 [A] [\Delta I] \vec{\epsilon} \quad (144)$$

where

$$[A] = \begin{bmatrix} A_{11} & A_{12} & A_{13} \\ A_{21} & A_{22} & A_{23} \\ A_{31} & A_{32} & A_{33} \end{bmatrix} \quad (145)$$

$$[\Delta I] = \begin{bmatrix} \Delta I_x & 0 & 0 \\ 0 & \Delta I_y & 0 \\ 0 & 0 & \Delta I_z \end{bmatrix} \quad (146)$$

$$\vec{\epsilon} = \begin{bmatrix} \epsilon_x \\ \epsilon_y \\ \epsilon_z \end{bmatrix} \quad (147)$$

Integrating \vec{T}_{gc} over the desaturation interval from t_o to t_f results in the change in CMG momentum $\Delta \vec{H}_{CMG}$ due to the desaturation maneuver $\vec{\epsilon}$. $\Delta \vec{H}_{CMG}$ equals

$$\Delta \vec{H}_{CMG} = 3\omega_o^2 \int_{t_o}^{t_f} [A] dt [\Delta I] \vec{\epsilon} \quad (148)$$

Note that $\Delta \vec{H}_{CMG}$ is the change in CMG momentum imparted to the vehicle or the negative of the change in CMG momentum stored in the CMG system.

Two methods of computing the desaturation maneuver $\vec{\epsilon}$ are described in the following paragraphs. The first method computes a constant time invariant vehicle maneuver $\vec{\epsilon}$ that the vehicle holds throughout the desaturation interval. The second method or option described is to compute $\vec{\epsilon}$ based on some performance index P . The performance index P used is the sum of the squares of the individual desaturation maneuvers ϵ_i . This method is an attempt to optimize $\vec{\epsilon}$ by minimizing the above performance index P . In general, $\vec{\epsilon}$ will be time varying.

Option 1: Constant Small Angle CMG Desaturation Maneuvers -
 Let $\Delta \vec{H}_{CMG}$ equal

$$\Delta \vec{H}_{CMG} = \begin{bmatrix} H_{Dx} \\ H_{Dy} \\ H_{Dz} \end{bmatrix} \quad (149)$$

where H_{Dx} , H_{Dy} , and H_{Dz} are the desired changes in CMG momentum imparted to the vehicle measured in vehicle space. H_{Dx} , H_{Dy} , and H_{Dz} are computed from actual CMG momentum samples made during the observation portion of the orbit. Performing the integration indicated in equation 148, let $[B]$ equal

$$[B] = \int_{t_o}^{t_f} [A] dt = \begin{bmatrix} B_{11} & B_{12} & B_{13} \\ B_{21} & B_{22} & B_{23} \\ B_{31} & B_{32} & B_{33} \end{bmatrix} \quad (150)$$

where

$$B_{11} = \int_{t_o}^{t_f} A_{11} dt \quad (151)$$

$$B_{12} = -B_{21} = \int_{t_o}^{t_f} A_{12} dt \quad (152)$$

$$B_{13} = -B_{31} = \int_{t_o}^{t_f} A_{13} dt \quad (153)$$

$$B_{22} = \int_{t_o}^{t_f} A_{22} dt \quad (154)$$

$$B_{23} = -B_{32} = \int_{t_0}^{t_f} A_{23} dt \quad (155)$$

$$B_{33} = \int_{t_0}^{t_f} A_{33} dt \quad (156)$$

Substituting equations 149 and 150 into equation 148, $\Delta \vec{H}_{CMG}$ equals

$$\Delta \vec{H}_{CMG} = \begin{bmatrix} H_{Dx} \\ H_{Dy} \\ H_{Dz} \end{bmatrix} = 3\omega_o^2 \begin{bmatrix} B_{11}\Delta I_x & B_{12}\Delta I_y & B_{13}\Delta I_z \\ -B_{12}\Delta I_x & B_{22}\Delta I_y & B_{23}\Delta I_z \\ -B_{13}\Delta I_x & -B_{23}\Delta I_y & B_{33}\Delta I_z \end{bmatrix} \begin{bmatrix} \epsilon_x \\ \epsilon_y \\ \epsilon_z \end{bmatrix} \quad (157)$$

Using Cramer's method to solve the three simultaneous algebraic equations given in equation 157, ϵ_x , ϵ_y , and ϵ_z equal

$$\epsilon_x = [H_{Dx}(B_{22}B_{33} + B_{23}^2) - H_{Dy}(B_{13}B_{23} + B_{12}B_{33}) + H_{Dz}(B_{12}B_{23} - B_{13}B_{22})] / 3\omega_o^2 \Delta I_x \Delta' \quad (158)$$

$$\epsilon_y = [-H_{Dx}(B_{13}^2 + B_{11}B_{33}) + H_{Dy}(B_{11}B_{33} + B_{13}^2) + H_{Dz}(B_{12}B_{13} - B_{11}B_{23})] / 3\omega_o^2 \Delta I_y \Delta' \quad (159)$$

$$\epsilon_z = [H_{Dx}(B_{13}B_{22} - B_{12}B_{23}) - H_{Dy}(B_{12}B_{13} + B_{11}B_{23}) + H_{Dz}(B_{11}B_{22} + B_{12}^2)] / 3\omega_o^2 \Delta I_z \Delta' \quad (160)$$

where

$$\Delta' = B_{11}B_{22}B_{33} + B_{11}B_{23}^2 + B_{22}B_{13}^2 + B_{33}B_{12}^2 \quad (161)$$

At time t_0 , the vehicle is maneuvered through the small angle $\vec{\epsilon}$. This new attitude offset from its original attitude by the small angle $\vec{\epsilon}$ is held until time t_f when the vehicle is maneuvered back to its desired attitude.

Option 2: Optimal Small Angle CMG Desaturation Maneuvers - This method of computing the desaturation maneuvers ϵ_1 attempts to optimize these maneuvers by minimizing the sum of the squares of ϵ_1 . This problem is treated as a Lagrange multiplier optimization problem with an equality constraint. The performance index P used equals

$$P = \frac{1}{2} \vec{\epsilon}^T \vec{\epsilon} \quad (162)$$

with the following equality constraint.

$$3\omega_o^2 [A] [\Delta I] \vec{\epsilon} - \vec{T}_{gc} = 0 \quad (163)$$

Note that integrating the above constraint equation over the desaturation interval t_o to t_f results in the following relationship:

$$3\omega_o^2 \int_{t_o}^{t_f} [A] [\Delta I] \vec{\epsilon} dt = \Delta \vec{H}_{CMG} \quad (164)$$

where $\Delta \vec{H}_{CMG}$ is the desired change in CMG momentum.

The Lagrange adjoin equation L is formed by combining the performance index P , equation 162, and its constraint equation, equation 163, as follows:

$$L = \frac{1}{2} \vec{\epsilon}^T \vec{\epsilon} - \lambda^T \{ [A] [\Delta I] \vec{\epsilon} - \vec{T}_{gc} / 3\omega_o^2 \} \quad (165)$$

λ is the Lagrange multiplier.

$$\lambda = \begin{bmatrix} \lambda_1 \\ \lambda_2 \\ \lambda_3 \end{bmatrix} \quad (166)$$

To minimize L , the derivative of L as a function $\vec{\epsilon}$ is set equal to zero.

$$\frac{dL}{d\vec{\epsilon}} = \vec{\epsilon} - \{[A][\Delta I]\}^T \lambda = 0 \quad (167)$$

Solving equation 167 for ϵ ,

$$\epsilon = [A']^T \lambda \quad (168)$$

where

$$[A'] = [A][\Delta I] \quad (169)$$

Assume that the Lagrange multiplier λ is a constant vector quantity. Multiplying equation 168 by $3\omega_o^2 [A']$ and then integrating the resultant expression over the desaturation interval from time t_o to t_f ,

$$3\omega_o^2 \int_{t_o}^{t_f} [A'] \vec{\epsilon} dt = 3\omega_o^2 \int_{t_o}^{t_f} [A'] [A']^T dt \lambda \quad (170)$$

Note that the expression on the left side of equation 170 is just $\Delta \vec{H}_{CMG}$. Let the integral expression of $[A'] [A']^T$ equal the constant matrix $[C]$.

$$[C] = \int_{t_o}^{t_f} [A'] [A']^T dt \quad (171)$$

Making the above substitutions into equation 170,

$$\Delta \vec{H}_{CMG} = 3\omega_o^2 [C] \lambda \quad (172)$$

Solving equation 172 for λ , λ equals

$$\lambda = \frac{1}{3\omega_o^2} [C]^{-1} \Delta \vec{H}_{CMG} \quad (173)$$

Substituting the above expression for λ into equation 168, the maneuver command $\vec{\epsilon}$ equals

$$\vec{\epsilon} = \frac{1}{3\omega_o^2} [A']^T [C]^{-1} \Delta \vec{H}_{CMG} \quad (174)$$

Note that because $[A']$ is time varying, and therefore the desaturation maneuver $\vec{\epsilon}$ is also time varying during the desaturation interval.

The small angle gravity gradient desaturation maneuver $\vec{\epsilon}$ computed using either option 1 or 2 is implemented by inputting $\vec{\epsilon}$ into the vehicle control law described in section 7.1 as a small vehicle offset angle.

10.4.3 A Single Axis Large Angle Desaturation Control Law -
In general, a small angle formulation of a desaturation control law is possible as long as the primary momentum buildup is along the axis of minimum inertia. For vehicle attitudes in which the minimum axis of inertia is constrained in or near the orbital plane this requirement is satisfied. If, however, the minimum axis of inertia is to be the pointed axis during observation periods, the above requirement clearly is violated except for the extremely restricted case of observation of targets lying in or very near the orbital plane. In this case at least one large angular maneuver will be required to control the momentum accumulated during the observation period. This technique, which is taken from reference 6, requires a single large maneuver which essentially leaves the pointed vehicle axis in a position -2ψ degrees from the directed orientation (i.e., reflected in the orbital plane) and subsequent small angle trim maneuvers about this new orientation.

Determination of the Large Angle Maneuver - For this development the quasi-inertial reference system $X_s Y_s Z_s$ will be defined with X_s directed toward the sun, Y_s in the orbital plane and Z_s above the orbital plane. During observation the vehicle axes will coincide with the reference axes. The orbital position θ_t ($\theta_t = \omega_o t$) is measured from the quadrature point on the sunrise side of the orbit. The assumption of solar pointing is made in this case although a general celestial target could be considered with minimal modification.

The general format calls for initial large Y_v axis maneuvers followed by complex simultaneous maneuvers about two vehicle axes at a multiplicity of orbital positions as shown in figure 10.14. For the case of instantaneous maneuvers in an environment without aerodynamics, only a large Y_v axis maneuver at the dark side terminator ($\theta_t = 180^\circ$) would be required. Even in the case of finite maneuvers at an inclination of less than 45 degrees, it is conceptually possible to desaturate the primary momentum accumulation, as the maximum desaturation torque is larger than the accumulation bias torque for this case.

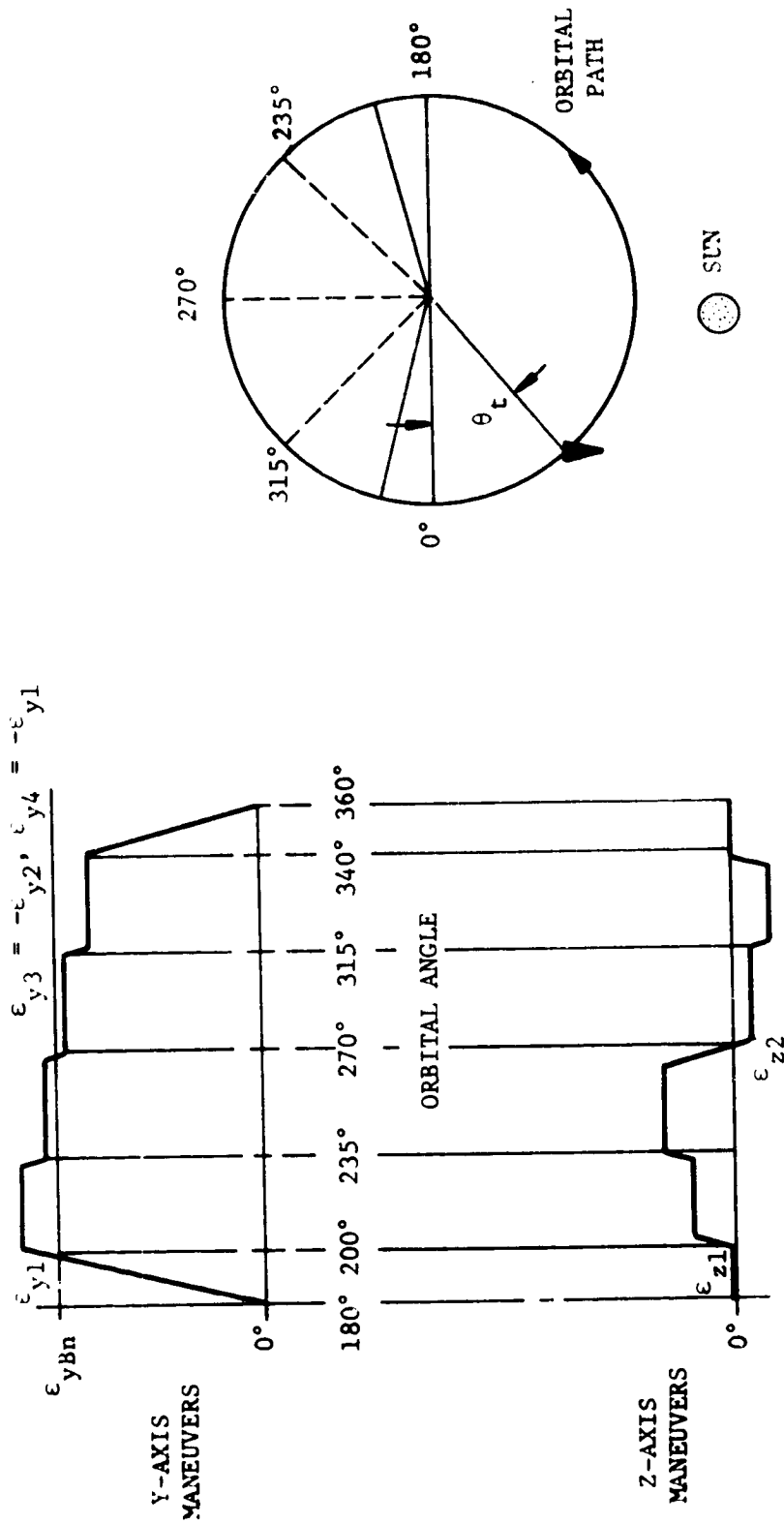


Figure 10.14. Vehicle Desaturation Maneuvers for the Single Axis Large Angle Law

In an actual vehicle, the maneuvers require a finite amount of time. Furthermore, there may be a resultant accumulation due to gravity about the other vehicle axes in the course of performing a large vehicle maneuver. It is also desirable to employ more than 50 percent of the orbital plane for experimental purposes. These restrictions would render the desaturation problem insoluble unless maneuvers are performed about orthogonal vehicle axes which resolve the gravity torque into these vehicle axes. These maneuvers are restricted to small values to easily de-manuever to the solar orientation.

If large angle maneuvers are employed they are basically dependent upon the daytime average accumulated value of Y_v axis momentum, the allowable percentage of orbital desaturation, and the previous or initial large maneuver value. The initial value is generally chosen to be in the vicinity of an equilibrium value which depends upon the orbital to ecliptic inclination. For example, the large initial maneuver might be

$$\epsilon_{yBo} = -\left(\frac{\pi}{4}\right) \text{sgn}(\psi + \psi) \quad (175)$$

where ψ is the inclination angle. In subsequent orbits ϵ_{yB} is recursively defined and once equilibrium has been achieved, it is only necessary to repeat the large maneuver from one orbit to the next.

The torque due to gravity gradient is normally defined in the vehicle coordinate system. However, the direction of the gravity forces is conveniently specified in the orbital plane by the vector \hat{a}_0 . Hence, it is necessary to first resolve the components of \hat{a}_0 into vehicle space to develop the torque equations in that space. Subsequent to this, it is necessary to resolve these torque components into the intermediate coordinate system where they are used for control law development.

The relationship between the vehicle body axes and intermediate XYZ system obtained after a large Y_v axis rotation and small rotations $(\epsilon_x, \epsilon_y, \epsilon_z)^T$ about the vehicle axes is given by:

$$\begin{bmatrix} X_v \\ Y_v \\ Z_v \end{bmatrix} = \begin{bmatrix} 1 & \epsilon_z & -\epsilon_y \\ -\epsilon_z & 1 & \epsilon_x \\ \epsilon_y & -\epsilon_x & 1 \end{bmatrix} \begin{bmatrix} X \\ Y \\ Z \end{bmatrix} \quad (176)$$

The coordinates of \hat{a}_0 in XYZ space are defined from figures 10.14 and 10.15 as follows:

$$\begin{aligned} a_x &= \sin\theta_t \cos\eta \\ a_y &= -\cos\theta_t \\ a_z &= -\sin\theta_t \sin\eta \end{aligned} \quad (177)$$

where η includes the effect of the large angular rotation about the Y_v axis.

Since the gravity torques are conveniently given in vehicle coordinates, the coordinates of \hat{a}_0 are resolved into that space with the above transform. The resulting torque equations in the intermediate space are obtained by substituting the components given in equations 177 as transformed by equation 176 into equation 15 then transforming the result by the inverse of equation 176, ignoring all products $\epsilon_i \epsilon_j$. The resulting torque \vec{T}_{gg} in the intermediate space is:

$$\vec{T}_{gg} = \frac{3}{2} \omega_o^2 \frac{1}{2} \begin{bmatrix} \Delta I_x \sin 2\theta_t \sin \eta \\ \Delta I_y (\cos 2\theta_t - 1) \sin 2\eta \\ -\Delta I_z \sin 2\theta_t \cos \eta \end{bmatrix} + \frac{3}{2} \omega_o^2 \begin{bmatrix} B_{11} & B_{12} & B_{13} \\ -B_{12} & B_{22} & B_{23} \\ -B_{13} & -B_{23} & B_{33} \end{bmatrix} \begin{bmatrix} \Delta I_x \epsilon_x \\ \Delta I_y \epsilon_y \\ \Delta I_z \epsilon_z \end{bmatrix} \quad (178)$$

$$\text{where: } B_{11} = \frac{1}{2} (1 - \cos 2\theta_t)(1 - \cos 2\eta) - (1 + \cos 2\theta_t)$$

$$B_{12} = \sin 2\theta_t \cos \eta$$

$$B_{13} = \frac{1}{2} (\cos 2\theta_t - 1) \sin 2\eta \quad (179)$$

$$B_{22} = (1 - \cos 2\theta_t) \cos 2\eta$$

$$B_{23} = -\sin 2\theta_t \sin \eta$$

$$B_{33} = (1 + \cos 2\theta_t) - (1 - \cos 2\theta_t)(1 + \cos 2\eta)$$

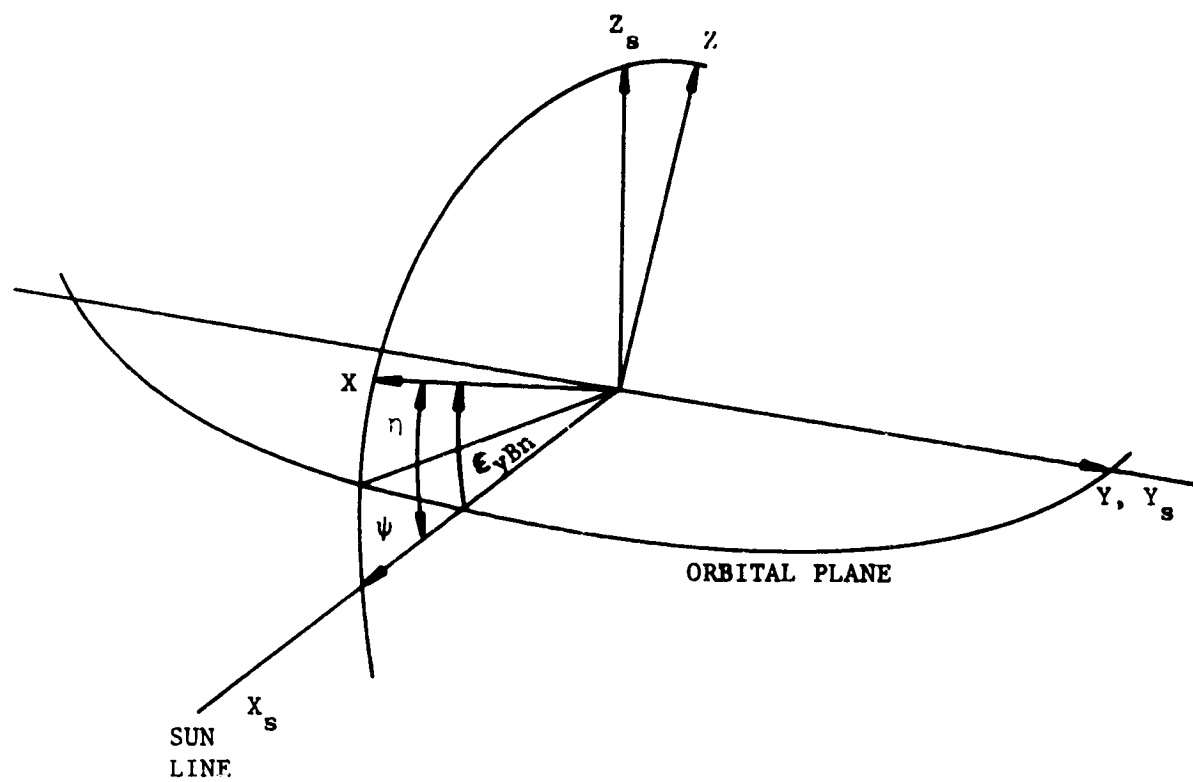


Figure 10.15. Orientation of the Intermediate Coordinates

In order to define the desaturation period, which in this case can be less than half an orbit, an angle θ_d is defined with respect to orbital midnight such that $|\theta_d| \leq \frac{\pi}{2}$. Desaturation thus begins when $\theta_t = 3\pi/2 - \theta_d$ and ends at $\theta_t = 3\pi/2 + \theta_d$. Since ψ is the orbital to ecliptic inclination and η is the angle between the orbital plane and the intermediate system obtained by the large angle maneuver for the n th orbit ϵ_{yBn} , then with all angles defined positive when ccw about Y:

$$\eta = \psi - \epsilon_{yBn}$$

The angle ϵ_{yBn} can be obtained by requiring that the maneuver be defined such that no differential maneuvers are required for Y axis desaturation in an ideal situation. It is also desirable to base the present command on past history. If H_{Myn} is defined as the aggregate of the weighted change in average momentum from one orbit to the next and the total of all weighted changes in average Y_v axis on a per orbit basis as determined by appropriate sampling, such a maneuver angle is:

$$\epsilon_{yBn} = \epsilon_{yBn-1} + \frac{2H_{Myn}}{3\omega_o \Delta I_x (2\theta_d + \sin\theta_d)} \quad (180)$$

where the incremental term of equation 180 can be obtained by integrating the first term of equation 179 between $3\pi/2 - \theta_d$ and $3\pi/2 + \theta_d$, i.e., it is the approximate amount of residual momentum about the Y axis in the intermediate system. In order to complete the recursive definition the initial value ϵ_{yB0} must be specified, for example as given by equation 175.

Derivation of the Trim Maneuvers - The strategy to be used in determining the trim maneuvers is to compute the components of torque which can be generated during the desaturation period by small angle maneuvers by integrating the second term of equation 178. This torque must then desaturate the residual momentum about all axes and inversion of the integrated equation will yield the small angle commands.

Because the Y and Z vehicle axes moments of inertia I_{yy} and I_{zz} are approximately equal, ΔI_x is small compared to ΔI_y and ΔI_z . Therefore, a small angle maneuver ϵ_x about the X_v axis will result in only a small change in CMG momentum as compared with the same size rotation about either the Y_v or Z_v axes. For this reason, ϵ_x is constrained to be zero and the residual CMG momentum will be "dumped" using only small angle maneuvers ϵ_y and ϵ_z about the vehicle Y and Z axes, respectively. In addition, it will be required that these small trim maneuvers be piecewise constant. The resulting trim torque which can be generated by the trim maneuvers ϵ_y and ϵ_z can be written with reference to equation 178 as:

$$\vec{T}_r = \begin{bmatrix} B_{12} & B_{13} \\ B_{22} & B_{23} \\ -B_{23} & B_{33} \end{bmatrix} \begin{bmatrix} \Delta I_y \epsilon_y \\ \Delta I_z \epsilon_z \end{bmatrix} \quad (181)$$

Referring to equations 179 it can be seen that B_{12} and B_{23} are odd functions with respect to midnight ($\theta_t = \frac{3\pi}{2}$), while B_{13} , B_{22} and B_{33} are even. In addition the latter three coefficients contain terms of the form $\pm 2\cos\theta_t$ which change sign at $\theta_t = 5\pi/4$ and $\theta_t = 7\pi/4$, and these positions become possible switching points.

If the possible switching points for ϵ_y and ϵ_z are denoted as $\theta_t = 3\pi/2 + \theta_d$, $3\pi/2 + \theta_s$ and $3\pi/2$, the momentum resulting from the trim maneuvers in intermediate space is given by integration of equation 181 over the appropriate intervals:

$$\vec{H} = \frac{1}{\omega_o} \left[\int_{\frac{3\pi}{2} - \theta_d}^{\frac{3\pi}{2} - \theta_s} \vec{T}_r d\theta_t + \int_{\frac{3\pi}{2} - \theta_s}^{\frac{3\pi}{2}} \vec{T}_r d\theta_t + \int_{\frac{3\pi}{2}}^{\frac{3\pi}{2} + \theta_s} \vec{T}_r d\theta_t + \int_{\frac{3\pi}{2} + \theta_s}^{\frac{3\pi}{2} + \theta_d} \vec{T}_r d\theta_t \right] \quad (182)$$

The intervals are numbered 1 thru 4 reading from left to right and the commands during each interval are:

$$\epsilon_{y1}, \epsilon_{z1} \text{ for } 3\pi/2 - \theta_d \leq \theta_t < 3\pi/2 - \theta_s$$

$$\epsilon_{y2}, \epsilon_{z2} \text{ for } 3\pi/2 - \theta_s \leq \theta_t < 3\pi/2$$

$$\epsilon_{y3}, \epsilon_{z3} \text{ for } 3\pi/2 \leq \theta_t < 3\pi/2 + \theta_s$$

$$\epsilon_{y4}, \epsilon_{z4} \text{ for } 3\pi/2 + \theta_s \leq \theta_t < 3\pi/2 + \theta_d$$

Defining the following integrals, using the even and odd characteristics of the B_{ij} :

$$g_{11} \stackrel{\Delta}{=} 2 \int_{\frac{3\pi}{2} - \theta_d}^{\frac{3\pi}{2} - \theta_s} B_{12} d\theta_t = -2 \int_{\frac{3\pi}{2} + \theta_s}^{\frac{3\pi}{2} + \theta_d} B_{12} d\theta_t \quad (183a)$$

$$g_{12} \stackrel{\Delta}{=} 2 \int_{\frac{3\pi}{2} - \theta_s}^{\frac{3\pi}{2}} B_{12} d\theta_t = -2 \int_{\frac{3\pi}{2}}^{\frac{3\pi}{2} - \theta_s} B_{12} d\theta_t \quad (183b)$$

$$c_{11} \stackrel{\Delta}{=} 2 \int_{\frac{3\pi}{2} - \theta_d}^{\frac{3\pi}{2} - \theta_s} B_{13} d\theta_t = 2 \int_{\frac{3\pi}{2} + \theta_s}^{\frac{3\pi}{2} + \theta_d} B_{13} d\theta_t \quad (183c)$$

$$c_{12} \stackrel{\Delta}{=} 2 \int_{\frac{3\pi}{2} - \theta_s}^{\frac{3\pi}{2}} B_{13} d\theta_t = 2 \int_{\frac{3\pi}{2}}^{\frac{3\pi}{2} + \theta_s} B_{13} d\theta_t \quad (183d)$$

$$d_{11} \stackrel{\Delta}{=} 2 \int_{\frac{3\pi}{2} - \theta_d}^{\frac{3\pi}{2} - \theta_s} B_{22} d\theta_t = 2 \int_{\frac{3\pi}{2} + \theta_s}^{\frac{3\pi}{2} + \theta_d} B_{22} d\theta_t \quad (183e)$$

$$d_{12} \stackrel{\Delta}{=} 2 \int_{\frac{3\pi}{2} - \theta_s}^{\frac{3\pi}{2}} B_{22} d\theta_t = 2 \int_{\frac{3\pi}{2}}^{\frac{3\pi}{2} + \theta_s} B_{22} d\theta_t \quad (183f)$$

$$e_{11} \stackrel{\Delta}{=} 2 \int_{\frac{3\pi}{2} - \theta_d}^{\frac{3\pi}{2} - \theta_s} B_{23} d\theta_t = -2 \int_{\frac{3\pi}{2} + \theta_s}^{\frac{3\pi}{2} + \theta_d} B_{23} d\theta_t \quad (183g)$$

$$e_{12} \Delta^2 \int_{\frac{3\pi}{2} - \theta_s}^{\frac{3\pi}{2}} B_{23} d\theta_t = -2 \int_{\frac{3\pi}{2}}^{\frac{3\pi}{2} + \theta_s} B_{23} d\theta_t \quad (183h)$$

$$f_{11} \Delta^2 \int_{\frac{3\pi}{2} - \theta_d}^{\frac{3\pi}{2} - \theta_s} B_{33} d\theta_t = 2 \int_{\frac{3\pi}{2} + \theta_d}^{\frac{3\pi}{2} + \theta_s} B_{33} d\theta_t \quad (183i)$$

$$f_{12} \Delta^2 \int_{\frac{3\pi}{2} - \theta_s}^{\frac{3\pi}{2}} B_{33} d\theta_t = 2 \int_{\frac{3\pi}{2}}^{\frac{3\pi}{2} + \theta_s} B_{33} d\theta_t \quad (183j)$$

and equation 181 can be rewritten over the appropriate intervals in the following form:

$$\vec{H}_1 = \frac{3}{4} \omega_0 \begin{bmatrix} g_{11} & c_{11} \\ d_{11} & e_{11} \\ -e_{11} & f_{11} \end{bmatrix} \begin{bmatrix} \Delta I_y \epsilon_{y1} \\ \Delta I_z \epsilon_{z1} \end{bmatrix} \quad (184a)$$

$$\vec{H}_2 = \frac{3}{4} \omega_0 \begin{bmatrix} g_{12} & c_{12} \\ d_{12} & e_{12} \\ -e_{12} & f_{12} \end{bmatrix} \begin{bmatrix} \Delta I_y \epsilon_{y2} \\ \Delta I_z \epsilon_{z2} \end{bmatrix} \quad (184b)$$

$$\vec{H}_3 = \frac{3}{4} \omega_0 \begin{bmatrix} -g_{12} & c_{12} \\ d_{12} & -e_{12} \\ e_{12} & f_{12} \end{bmatrix} \begin{bmatrix} \Delta I_y \epsilon_{y3} \\ \Delta I_z \epsilon_{z3} \end{bmatrix} \quad (184c)$$

$$\vec{H}_4 = \frac{3}{4} \omega_0 \begin{bmatrix} -g_{11} & c_{11} \\ d_{11} & -e_{11} \\ e_{11} & f_{11} \end{bmatrix} \begin{bmatrix} \Delta I_y \epsilon_{y4} \\ \Delta I_y \epsilon_{z4} \end{bmatrix} \quad (184d)$$

In order to maintain a zero average value for the small angle ϵ_y commands about the large angle command define:

$$\epsilon_{y4} = -\epsilon_{y1} \quad (185)$$

$$\epsilon_{y3} = -\epsilon_{y2}$$

Since \vec{H} is the sum of equations 184, substituting equation 185 into equations 184a thru 184d, \vec{H} equals

$$\vec{H} = \begin{bmatrix} 0 & g_{11} & c_{11} \\ e_{11} & 0 & 0 \\ 0 & -e_{11} & f_{11} \end{bmatrix} \begin{bmatrix} \Delta I_z (\epsilon_{z1} - \epsilon_{z4}) \\ 2\Delta I_y \epsilon_{y1} \\ \Delta I_z (\epsilon_{z1} + \epsilon_{z4}) \end{bmatrix} + \begin{bmatrix} 0 & g_{12} & c_{12} \\ e_{12} & 0 & 0 \\ 0 & -e_{12} & f_{12} \end{bmatrix} \begin{bmatrix} \Delta I_z (\epsilon_{z2} - \epsilon_{z3}) \\ 2\Delta I_y \epsilon_{y2} \\ \Delta I_z (\epsilon_{z2} + \epsilon_{z3}) \end{bmatrix} \quad (186)$$

or, more simply when $3\pi/2 - \theta_d \leq \theta_t < 3\pi/2 - \theta_s$ or $3\pi/2 + \theta_s \leq \theta_t < 3\pi/2 + \theta_d$:

$$\vec{H} = \frac{3}{4} \omega_0 \begin{bmatrix} 0 & b_{12} & b_{13} \\ -b_{23} & 0 & 0 \\ 0 & b_{23} & b_{33} \end{bmatrix} \begin{bmatrix} \Delta I_z (\epsilon_{z1} - \epsilon_{z4}) \\ 2\Delta I_y \epsilon_{y1} \\ \Delta I_z (\epsilon_{z1} + \epsilon_{z4}) \end{bmatrix} \quad (187a)$$

and for $3\pi/2 - \theta_s \leq \theta_t < 3\pi/2 + \theta_s$,

$$\vec{H} = \frac{3}{4} \omega_0 \begin{bmatrix} 0 & b_{12} & b_{13} \\ -b_{23} & 0 & 0 \\ 0 & b_{23} & b_{33} \end{bmatrix} \begin{bmatrix} \Delta I_z (\epsilon_{z2} - \epsilon_{z3}) \\ 2\Delta I_y \epsilon_{y2} \\ \Delta I_z (\epsilon_{z2} + \epsilon_{z3}) \end{bmatrix} \quad (187b)$$

$$b_{ij} = 2 \int B_{ij} d\theta_t \quad (187c)$$

where the integral of equation 187c is evaluated over the proper interval.

The momentum equations given above thus represents the momentum resulting from the small angle commands about the Y_v and Z_v axes in the intermediate system. It is thus necessary to specify these commands in such a way that the residual momentum is desaturated. The momentum accumulation is obtained during the daylight portion of the orbit by some sampling scheme and is of course obtained in the quasi-inertial $X_s Y_s Z_s$ coordinate system and defined as:

$$\vec{H}_D = (H_{Dx}, H_{Dy}, H_{Dz})^T \quad (188)$$

In order to perform the operations on the momentum in the intermediate space, the components of equation 188 must be resolved according to the transformation involving the previously defined large angle maneuver ϵ_{yBn} . Thus, in the intermediate space:

$$\vec{H}'_D = \begin{bmatrix} H'_{Dx} \\ H'_{Dy} \\ H'_{Dz} \end{bmatrix} = \begin{bmatrix} H_{Dx} \cos \epsilon_{yBn} + H_{Dz} \sin \epsilon_{yBn} \\ H_{Dy} \\ -H_{Dx} \sin \epsilon_{yBn} + H_{Dz} \cos \epsilon_{yBn} \end{bmatrix} \quad (189)$$

The trim commands can now be obtained by inverting the equations in \vec{H} , after replacing \vec{H} with $-\vec{H}'_D$. Considering that four intervals are available for command definition, all approximately equal in length, the additional definition will be made requiring one quarter of the residual momentum be desaturated during each interval. Consider equation 187a only over the interval $3\pi/2 - \theta_d \leq \theta_t < 3\pi/2 - \theta_s$ and setting $\vec{H} = -\frac{1}{4} \vec{H}'_D$. The inverse can be given as:

$$\begin{bmatrix} \Delta I_z (\epsilon_{z1} - \epsilon_{z4}) \\ 2\Delta I_y \epsilon_{y1} \\ \Delta I_z (\epsilon_{z1} + \epsilon_{z4}) \end{bmatrix} = \frac{1}{3\omega_0} \begin{bmatrix} 0 & b_{12} & b_{13} \\ -b_{23} & 0 & 0 \\ 0 & b_{23} & b_{33} \end{bmatrix}^{-1} \begin{bmatrix} -H'_{Dx} \\ -H'_{Dy} \\ -H'_{Dz} \end{bmatrix}$$

$$= -\frac{1}{3\omega_0 D'_1} \begin{bmatrix} 0 & b_{13}b_{23} - b_{12}b_{23} & 0 \\ b_{23}b_{33} & 0 & -b_{13}b_{23} \\ -\frac{2}{b_{23}} & 0 & b_{12}b_{23} \end{bmatrix} \begin{bmatrix} H'_{Dx} \\ H'_{Dy} \\ H'_{Dz} \end{bmatrix} \quad (190)$$

$$\text{where: } D'_1 = b_{23}(b_{12}b_{33} - b_{13}b_{23}) \quad (191)$$

$$\text{Thus: } \epsilon_{y1} = -\frac{b_{33}H'_{Dx} - b_{13}H'_{Dz}}{6\omega_0 \Delta I_y (b_{12}b_{33} - b_{13}b_{23})} \quad (192)$$

$$\epsilon_{z1} - \epsilon_{z4} = \frac{H'_{Dy}}{3\omega_0 \Delta I_z b_{23}} \quad (193)$$

$$\epsilon_{z1} + \epsilon_{z4} = \frac{b_{23}H'_{Dx} - b_{12}H'_{Dz}}{3\omega_0 \Delta I_z (b_{12}b_{33} - b_{13}b_{23})} \quad (194)$$

Over the interval under consideration the b_{ij} can be expressed in terms of the equations 183 as:

$$b_{12} = g_{11}, \quad b_{13} = c_{11}, \quad b_{23} = e_{11}, \quad b_{33} = f_{11} \quad (195)$$

Making the above notation change and solving explicitly for ϵ_{z1} and ϵ_{z4} , letting $D_1 = D'_1 / e_{11}$:

$$\epsilon_{y1} = \frac{c_{11}H'_{Dz} - f_{11}H'_{Dx}}{6\omega_0 \Delta I_y D_1} \quad (196)$$

$$\epsilon_{z1} = \frac{e_{11}^2 H'_{Dx} + D_1 H'_{Dy} - g_{11} e_{11} H'_{Dz}}{6\omega_0 \Delta I_z e_{11} D_1} \quad (197)$$

$$e_{z4} = \frac{e_{11}^2 H'_1 - D_1 H'_1 - g_{11} e_{11} H'_1 D_z}{6\omega_0 \Delta I_z e_{11} D_1} \quad (198)$$

Finally, substituting from equation 199:

$$e_{y1} = A_1 (C_{11} H_{Dx} + C_{13} H_{Dz}) \quad (199)$$

$$e_{y4} = -e_{y1} \quad (200)$$

$$e_{z1} = A_2 (C_{21} H_{Dx} + C_{22} H_{Dy} + C_{23} H_{Dz}) \quad (201)$$

$$e_{z4} = A_2 (C_{21} H_{Dx} - C_{22} H_{Dy} + C_{23} H_{Dz}) \quad (202)$$

$$\text{where: } A_1 = \frac{1}{6\omega_0 \Delta I_y} \quad (203a)$$

$$A_2 = \frac{1}{6\omega_0 \Delta I_z} \quad (203b)$$

$$C_{11} = -\frac{c_{11}}{D_1} \sin e_{yBn} - \frac{f_{11}}{D_1} \cos e_{yBn} \quad (203c)$$

$$C_{13} = \frac{c_{11}}{D_1} \cos e_{yBn} - \frac{f_{11}}{D_1} \sin e_{yBn} \quad (203d)$$

$$C_{21} = -\frac{e_{11}}{D_1} \sin e_{yBn} - \frac{g_{11}}{D_1} \cos e_{yBn} \quad (203e)$$

$$C_{22} = \frac{1}{e_{11}} \quad (203f)$$

$$C_{23} = \frac{e_{11}}{D_1} \cos e_{yBn} - \frac{g_{11}}{D_1} \sin e_{yBn} \quad (203g)$$

$$D_1 = g_{11} f_{11} - c_{11} e_{11} \quad (204)$$

Proceeding in a parallel development from equation 183b:

$$e_{y2} = A_1 (E_{11} H_{Dx} + E_{13} H_{Dz}) \quad (205)$$

$$e_{y3} = -e_{y2} \quad (206)$$

$$e_{z2} = A_2 (E_{21} H_{Dx} + E_{22} H_{Dy} + E_{23} H_{Dz}) \quad (207)$$

$$e_{z3} = A_2 (E_{21} H_{Dx} - E_{22} H_{Dy} + E_{23} H_{Dz}) \quad (208)$$

$$\text{where: } E_{11} = -\frac{c_{12}}{D_2} \sin \epsilon_{yBn} - \frac{f_{12}}{D_2} \cos \epsilon_{yBn} \quad (209a)$$

$$E_{13} = \frac{c_{12}}{D_2} \cos \epsilon_{yBn} - \frac{f_{12}}{D_2} \sin \epsilon_{yBn} \quad (209b)$$

$$E_{21} = -\frac{e_{12}}{D_2} \sin \epsilon_{yBn} - \frac{g_{12}}{D_2} \cos \epsilon_{yBn} \quad (209c)$$

$$E_{22} = \frac{1}{e_{12}} \quad (209d)$$

$$E_{23} = \frac{e_{12}}{D_2} \cos \epsilon_{yBn} - \frac{g_{12}}{D_2} \sin \epsilon_{yBn} \quad (209e)$$

$$D_2 = g_{12} f_{12} - c_{12} e_{12} \quad (210)$$

Thus equations 199 thru 209 along with the integrals of equations 183 give the trim maneuver angles about the large angle maneuver as a function of the residual momentum to be desaturated.

Logic and Maneuvering Summary - The implementation of the desaturation control law derived above involves the determination of the large angle and trim maneuvers as given explicitly in the preceding two sections. It should be noted that all the maneuvers for a given orbit depend only on constants for that orbit and momentum samples taken during the daylight portion of the orbit, thus all commands can be computed as soon as momentum information is available and prior to the first maneuver, then issued to the maneuver and vehicle control laws as indicated in the subsequent outline. Since a large angle maneuver is required it is necessary to provide the direction cosine matrix with respect to the vehicle reference system of the desired orientation for processing by the quaternion maneuvering law. The maneuver is made with respect to the quasi-inertial $X_s Y_s Z_s$ coordinate system described previously which is related to the orbital $X_o Y_o Z_o$ system by a rotation θ about Z_o followed by a rotation ψ about $Y_o' = Y_s$. The transformation from $X_s Y_s Z_s$ to $X_o Y_o Z_o$ can then be given as:

$$\begin{bmatrix} X_o \\ Y_o \\ Z_o \end{bmatrix} = \begin{bmatrix} \cos \psi \cos \theta & -\sin \theta & \sin \psi \cos \theta \\ \cos \psi \sin \theta & \cos \theta & \sin \psi \sin \theta \\ -\sin \psi & 0 & \cos \psi \end{bmatrix} \begin{bmatrix} X_s \\ Y_s \\ Z_s \end{bmatrix} \quad (211)$$

The transformation from $X_o Y_o Z_o$ to the $X_R Y_R Z_R$ reference system is given by the inverse of equation 123. The matrix of ϵ_{yBn} with respect to $X_s Y_s Z_s$ is:

$$[\epsilon_s] = \begin{bmatrix} \cos \epsilon_{yBn} & 0 & -\sin \epsilon_{yBn} \\ 0 & 1 & 0 \\ \sin \epsilon_{yBn} & 0 & \cos \epsilon_{yBn} \end{bmatrix} \quad (212)$$

The desired matrix to be passed to the maneuver law is thus given by the product:

$$\begin{bmatrix} \cos \alpha & -\cos i \sin \alpha & \sin i \sin \alpha \\ \sin \alpha & \cos i \cos \alpha & -\sin i \cos \alpha \\ 0 & -\sin i \cos \alpha & \cos i \end{bmatrix} [\phi_{so}][\epsilon_s] \quad (213)$$

where $[\phi_{so}]$ is the matrix from equation 211 and $[\epsilon_s]$ is defined by equation 212. The idealized logic for a cycle of the large axis desaturation control law is outlined below starting at the sunrise quadrature point:

- a. During daylight operation sample the CMG gimbal angles at discrete times to be specified and compute the primary momentum to be dumped H_{Myn} and the residual momentum \vec{H}_D .
- b. Compute the large angle maneuver ϵ_{yBn} from equation 180 and calculate the direction cosine matrix elements from equation 213. Compute the trim maneuvers from equations 199 thru 202 and 205 thru 208.
- c. At $\theta_t = 3\pi/2 - \theta_d$ pass the large angle matrix to the maneuver control law and upon completion of the maneuver set $\epsilon_{yc} = \epsilon_{y1}$ and $\epsilon_{zc} = \epsilon_{z1}$.
- d. At $\theta_t = 3\pi/2 - \theta_s$ set $\epsilon_{yc} = \epsilon_{y2}$ and $\epsilon_{zc} = \epsilon_{z2}$.

- e. At $t = 3\pi/2$ set $\epsilon_{yc} = \epsilon_{y3}$ and $\epsilon_{zc} = \epsilon_{z3}$.
- f. At $t = 3\pi/2 + 0_s$ set $\epsilon_{yc} = \epsilon_{y4}$ and $\epsilon_{zc} = \epsilon_{z4}$.
- g. At $t = 3\pi/2 + 0_d$ set $\epsilon_{yc} = \epsilon_{zc} = 0$, then command return to observation attitude by passing the inverse of equation 213 as modified for variation in the angles to the maneuver control law.

Reference 6 contains considerable discussion of this type of a control and includes some qualitative simulation results which can be utilized in evaluation of this technique. Reference 7 contains the derivation of a similar desaturation law requiring trim maneuvers about only one axis.

10.4.4 A Reflexive Control Law for Desaturation From An Arbitrary Attitude - While each of the techniques considered above will accomplish CMG system desaturation by means of gravity gradient torques, they share the common characteristic of assuming a particular vehicle orientation during that portion of the orbit used for experimental operation. For missions in which the observing attitude cannot be constrained due to multiple targeting requirements and due to secondary limitations on the attitude of the axes which are not pointed, a more general desaturation law is required. As in most applications, a penalty results from generality and in this case it is an increase in the complexity of the equations involved and also a requirement for large multi-axis maneuvers exists which was not present in the simpler laws considered in the previous sections. The desaturation control law derived below assumes that the vehicle orientation will be determined in flight by experimental and secondary requirements and does not depend on any a-priori knowledge of vehicle attitude. This method is one conceived by S. C. Rybak of The Bendix Corporation, Navigation and Control Division.

Determination of The Large Angle Maneuvers - It can be shown that the torque acting on an arbitrarily oriented vehicle in a circular orbit over half an orbit can be exactly reversed by maneuvering to a reflexive or mirror image orientation for the remaining half of the orbit. This property forms the basis for the reflexive control law large angle maneuvers.

The procedure to be followed is initially the same as that of the previous laws, i.e., to obtain the idealized torque exerted on the vehicle during the observation period. From figure 10.12, the local vertical vector in the quasi-inertial orbital frame $X_o Y_o Z_o$ is simply:

$$\begin{bmatrix} a_{xo} \\ a_{yo} \\ a_{zo} \end{bmatrix} = \begin{bmatrix} \cos \omega_o t \\ \sin \omega_o t \\ 0 \end{bmatrix} \quad (214)$$

where the orbital position is defined with respect to ascending node. The transformation from orbital coordinates to vehicle coordinates is taken to be completely arbitrary and defined by the transformation:

$$\begin{bmatrix} X_v \\ Y_v \\ Z_v \end{bmatrix} = \begin{bmatrix} a_{11} & a_{12} & a_{13} \\ a_{21} & a_{22} & a_{23} \\ a_{31} & a_{32} & a_{33} \end{bmatrix} \begin{bmatrix} X_o \\ Y_o \\ Z_o \end{bmatrix} \quad (215)$$

where the matrix with elements a_{ij} is the orthogonal rotation matrix taking any vector expressed in the orbital coordinates into its vehicle coordinate components. The local vertical vector a_o thus is resolved in vehicle coordinates as:

$$\begin{bmatrix} a_{xv} \\ a_{yv} \\ a_{zv} \end{bmatrix} = \begin{bmatrix} a_{11} & a_{12} & a_{13} \\ a_{21} & a_{22} & a_{23} \\ a_{31} & a_{32} & a_{33} \end{bmatrix} \begin{bmatrix} \cos \omega_o t \\ \sin \omega_o t \\ 0 \end{bmatrix} = \begin{bmatrix} a_{11} \cos \omega_o t + a_{12} \sin \omega_o t \\ a_{21} \cos \omega_o t + a_{22} \sin \omega_o t \\ a_{31} \cos \omega_o t + a_{32} \sin \omega_o t \end{bmatrix} \quad (216)$$

Substituting the components from equation 216 into equation 15, the torques acting on the vehicle due to gravity gradient are:

$$\begin{aligned} T_{xv} = \frac{3}{2} \omega_o^2 [a_{21}a_{31} + a_{22}a_{32} + (a_{21}a_{31} - a_{22}a_{32}) \cos 2\omega_o t \\ + (a_{21}a_{32} + a_{22}a_{31}) \sin 2\omega_o t] \Delta I_x \end{aligned} \quad (217a)$$

$$T_{yv} = \frac{3}{2} \omega_o^2 [a_{11}a_{31} + a_{12}a_{32} + (a_{11}a_{31} - a_{12}a_{32})\cos 2\omega_o t + (a_{11}a_{32} + a_{12}a_{31})\sin 2\omega_o t] \Delta I_y \quad (217b)$$

$$T_{zv} = \frac{3}{2} \omega_o^2 [a_{11}a_{21} + a_{12}a_{22} + (a_{11}a_{21} - a_{12}a_{22})\cos 2\omega_o t + (a_{11}a_{22} + a_{12}a_{21})\sin 2\omega_o t] \Delta I_z \quad (217c)$$

Examination of equation 217 reveals that the average torque over any half orbit does not involve the orbital position due to the terms $\sin 2\omega_o t$ and $\cos 2\omega_o t$. The average torque is thus:

$$\begin{bmatrix} \bar{T}_{xv} \\ \bar{T}_{yv} \\ \bar{T}_{zv} \end{bmatrix} = \frac{3}{2} \omega_o^2 \begin{bmatrix} (a_{21}a_{31} + a_{22}a_{32})\Delta I_x \\ (a_{11}a_{31} + a_{12}a_{32})\Delta I_y \\ (a_{11}a_{21} + a_{12}a_{22})\Delta I_z \end{bmatrix} \quad (218)$$

Transforming the half orbit average torque back into orbital coordinates, using the inverse (transpose) of the transformation 215:

$$\begin{bmatrix} \bar{T}_{xo} \\ \bar{T}_{yo} \\ \bar{T}_{zo} \end{bmatrix} = \begin{bmatrix} a_{11} & a_{21} & a_{31} \\ a_{12} & a_{22} & a_{32} \\ a_{13} & a_{23} & a_{33} \end{bmatrix} \begin{bmatrix} \bar{T}_{xv} \\ \bar{T}_{yv} \\ \bar{T}_{zv} \end{bmatrix}$$

$$\bar{T}_{xo} = \frac{3}{2} \omega_o^2 [a_{11}(a_{21}a_{31} + a_{22}a_{32})\Delta I_x + a_{21}(a_{11}a_{31} + a_{12}a_{32})\Delta I_y + a_{31}(a_{11}a_{21} + a_{12}a_{22})\Delta I_z] \quad (219a)$$

$$\bar{T}_{yo} = \frac{3}{2} \omega_o^2 [a_{12}(a_{21}a_{31} + a_{22}a_{32})\Delta I_x + a_{22}(a_{11}a_{31} + a_{12}a_{32})\Delta I_y + a_{32}(a_{11}a_{21} + a_{12}a_{22})\Delta I_z] \quad (219b)$$

$$\bar{T}_{zo} = \frac{3}{2} \omega_o^2 [a_{13}(a_{21}a_{31} + a_{22}a_{32})\Delta I_x + a_{23}(a_{11}a_{31} + a_{12}a_{32})\Delta I_y + a_{33}(a_{11}a_{21} + a_{12}a_{22})\Delta I_z] \quad (219c)$$

Expanding equations 219a and 219b gives, noting $\Delta I_x + \Delta I_y + \Delta I_z = 0$:

$$\bar{T}_{x0} = \frac{3}{2} \omega_o^2 (a_{11}a_{22}a_{32}\Delta I_x + a_{12}a_{21}a_{32}\Delta I_y + a_{12}a_{22}a_{31}\Delta I_z) \quad (220a)$$

$$\bar{T}_{y0} = \frac{3}{2} \omega_o^2 (a_{12}a_{21}a_{31}\Delta I_x + a_{11}a_{22}a_{31}\Delta I_y + a_{11}a_{21}a_{32}\Delta I_z) \quad (220b)$$

Since the transformation matrix of equation 215 is by definition orthogonal, the product of the matrix and its transpose is the 3x3 unit matrix, and further since it represents a proper rotation its determinant is unity. Expansion of the product results in the following relations between the elements a_{ij} :

$$a_{11}^2 + a_{12}^2 + a_{13}^2 = 1$$

$$a_{11}a_{21} + a_{12}a_{22} + a_{13}a_{23} = 0$$

$$a_{11}a_{31} + a_{12}a_{32} + a_{13}a_{33} = 0$$

$$a_{21}^2 + a_{22}^2 + a_{23}^2 = 1$$

$$a_{21}a_{31} + a_{22}a_{32} + a_{23}a_{33} = 0$$

$$a_{31}^2 + a_{32}^2 + a_{33}^2 = 1$$

Substituting the 2nd, 3rd and 5th of the above expressions into equation 219c gives:

$$\begin{aligned} \bar{T}_{z0} &= \frac{3}{2} \omega_o^2 (-a_{13}a_{23}a_{33}\Delta I_x - a_{13}a_{23}a_{33}\Delta I_y - a_{13}a_{23}a_{33}\Delta I_z) \\ &= -\frac{3}{2} \omega_o^2 a_{13}a_{23}a_{33}(\Delta I_x + \Delta I_y + \Delta I_z) = 0 \end{aligned} \quad (220c)$$

Thus, there is no net average torque acting about the orbit normal when the torque is resolved in the orbital frame regardless of vehicle orientation. For total desaturation during the remaining half orbit assuming instantaneous maneuvers and no disturbance torques it is necessary to assume an orientation in which the average torque is exactly reversed, that is we need an attitude transformation b_{ij} given by:

$$\begin{bmatrix} X_v' \\ Y_v' \\ Z_v' \end{bmatrix} = \begin{bmatrix} b_{11} & b_{12} & b_{13} \\ b_{21} & b_{22} & b_{23} \\ b_{31} & b_{32} & b_{33} \end{bmatrix} \begin{bmatrix} X_o \\ Y_o \\ Z_o \end{bmatrix} \quad (221)$$

such that $\bar{T}_{xv}' = -\bar{T}_{xv}$ and $\bar{T}_{yv}' = -\bar{T}_{yv}$. From the above development, the average torque over half an orbit in the desaturation attitude is:

$$\bar{T}_{xo}' = \frac{3}{2} \omega_o^2 (b_{11}b_{22}b_{32}\Delta I_x + b_{12}b_{21}b_{32}\Delta I_y + b_{12}b_{22}b_{31}\Delta I_z) \quad (222a)$$

$$\bar{T}_{yo}' = \frac{3}{2} \omega_o^2 (b_{12}b_{21}b_{31}\Delta I_x + b_{11}b_{22}b_{31}\Delta I_y + b_{11}b_{21}b_{32}\Delta I_z) \quad (222b)$$

$$\bar{T}_{zo}' = 0 \quad (222c)$$

The selection of the b_{ij} is made to reverse the average X and Y torque components given by equations 220a and 220b while satisfying all orthogonality constraints and can be given as:

$$\begin{array}{lll} b_{11} = -a_{11} & b_{12} = a_{12} & b_{13} = -a_{13} \\ b_{21} = a_{21} & b_{22} = a_{22} & b_{23} = -a_{23} \\ b_{31} = -a_{31} & b_{32} = -a_{32} & b_{33} = a_{33} \end{array} \quad (223)$$

Substitution into equations 222 will verify that this selection is sufficient. Further inspection of equation 221 reveals after some thought that the desaturation attitude as defined by equation 223 is the reflection of the observing attitude in the orbital plane, hence the desaturation attitude will be designated as the "mirror image" orientation related to the orbital coordinate system by:

$$\begin{bmatrix} X_{MI} \\ Y_{MI} \\ Z_{MI} \end{bmatrix} = \begin{bmatrix} a_{11} & a_{12} & -a_{13} \\ a_{21} & a_{22} & -a_{23} \\ -a_{31} & -a_{32} & a_{33} \end{bmatrix} \begin{bmatrix} X_o \\ Y_o \\ Z_o \end{bmatrix} \quad (224)$$

Equation 224 thus defines the desaturation attitude which will in general require large rotations about all vehicle axes to be reached from the observing attitude. The total maneuver from observation to desaturation attitudes is thus:

$$\begin{bmatrix} X_{MI} \\ Y_{MI} \\ Z_{MI} \end{bmatrix} = \begin{bmatrix} a_{11} & a_{12} & -a_{13} \\ 1 & a_{22} & -a_{23} \\ -a_{31} & -a_{32} & a_{33} \end{bmatrix} \begin{bmatrix} a_{11} & a_{21} & a_{31} \\ a_{12} & a_{22} & a_{32} \\ a_{13} & a_{23} & a_{33} \end{bmatrix} \begin{bmatrix} X_v \\ Y_v \\ Z_v \end{bmatrix} \quad (225)$$

and in general the maneuver will involve large angle rotations about all vehicle axes. Since the maneuvering control law is based on the quaternion formulation this will present no difficulty.

Derivation of The Trim Maneuvers - Since finite maneuver times, nongravity gradient disturbance torques and a non-ideal gravity field are all to be present in a real mission, the above derived mirror image maneuver cannot reverse all the actual momentum buildup during the desaturation period. It is thus necessary to formulate a series of trim maneuvers ϵ_x , ϵ_y and ϵ_z about the mirror image orientation in order to dump the residual momentum not desaturated by the large maneuvers.

The unit vector along the local vertical in vehicle resolved components after the trim maneuvers are made about the mirror image orientation is given by:

$$\begin{aligned} \hat{a}_t = \begin{bmatrix} a_{xvt} \\ a_{yvt} \\ a_{zvt} \end{bmatrix} &= \begin{bmatrix} 1 & \epsilon_z & -\epsilon_y \\ -\epsilon_z & 1 & \epsilon_x \\ \epsilon_y & -\epsilon_x & 1 \end{bmatrix} \begin{bmatrix} b_{11} & b_{12} & b_{13} \\ b_{21} & b_{22} & b_{23} \\ b_{31} & b_{32} & b_{33} \end{bmatrix} \begin{bmatrix} \cos \omega_0 t \\ \sin \omega_0 t \\ 0 \end{bmatrix} \\ &= \begin{bmatrix} 1 & \epsilon_z & -\epsilon_y \\ -\epsilon_z & 1 & \epsilon_x \\ \epsilon_y & -\epsilon_x & 1 \end{bmatrix} \begin{bmatrix} k_1 \\ k_2 \\ k_3 \end{bmatrix} \end{aligned} \quad (226)$$

$$\text{where: } k_1 = b_{11} \cos \omega_0 t + b_{12} \sin \omega_0 t \quad (227a)$$

$$k_2 = b_{21} \cos \omega_0 t + b_{22} \sin \omega_0 t \quad (227b)$$

$$k_3 = b_{31} \cos \omega_0 t + b_{32} \sin \omega_0 t \quad (227c)$$

Thus,

$$\begin{bmatrix} a_{xvt} \\ a_{yvt} \\ a_{zvt} \end{bmatrix} = \begin{bmatrix} k_1 + \epsilon_z k_2 - \epsilon_y k_3 \\ k_2 - \epsilon_z k_1 + \epsilon_x k_3 \\ k_3 + \epsilon_y k_1 - \epsilon_x k_2 \end{bmatrix} \quad (228)$$

The torque in vehicle space is given by substituting equation 228 into equation 15 and neglecting products of the ϵ 's gives:

$$\begin{bmatrix} T_{xvt} \\ T_{yvt} \\ T_{zvt} \end{bmatrix} = 3\omega_0^2 \begin{bmatrix} [k_2 k_3 + \epsilon_x (k_3^2 - k_2^2) + \epsilon_y k_1 k_2 - \epsilon_z k_1 k_3] \Delta I_x \\ [k_1 k_3 - \epsilon_x k_1 k_2 + \epsilon_y (k_1^2 - k_3^2) + \epsilon_z k_2 k_3] \Delta I_y \\ [k_1 k_2 + \epsilon_x k_1 k_3 - \epsilon_y k_2 k_3 + \epsilon_z (k_2^2 - k_1^2)] \Delta I_z \end{bmatrix} \quad (229)$$

Transforming back into the mirror image coordinate frame:

$$\begin{bmatrix} T_{xMI} \\ T_{yMI} \\ T_{zMI} \end{bmatrix} = \begin{bmatrix} 1 & -\epsilon_z & \epsilon_y \\ \epsilon_z & 1 & -\epsilon_x \\ -\epsilon_y & \epsilon_x & 1 \end{bmatrix} \begin{bmatrix} T_{xvt} \\ T_{yvt} \\ T_{zvt} \end{bmatrix}$$

$$\begin{bmatrix} T_{xMI} \\ T_{yMI} \\ T_{zMI} \end{bmatrix} = 3\omega_0^2 \begin{bmatrix} [k_1 k_2 \Delta I_x + \epsilon_x (k_3^2 - k_2^2) \Delta I_x - \epsilon_y k_1 k_2 \Delta I_y + \epsilon_z k_1 k_3 \Delta I_z] \\ [k_1 k_3 \Delta I_y + \epsilon_x k_1 k_3 \Delta I_x + \epsilon_y (k_1^2 - k_3^2) \Delta I_y - \epsilon_z k_2 k_3 \Delta I_z] \\ [k_1 k_2 \Delta I_z - \epsilon_x k_1 k_3 \Delta I_x + \epsilon_y k_2 k_3 \Delta I_y + \epsilon_z (k_2^2 - k_1^2) \Delta I_z] \end{bmatrix} \quad (230)$$

where use of the relations $\Delta I_x + \Delta I_y = -\Delta I_z$, $\Delta I_y + \Delta I_z = -\Delta I_x$, $\Delta I_z + \Delta I_x = -\Delta I_y$ has been made. Substituting from equations 227 for the k_i and simplifying the torque equations become:

$$\begin{aligned} T_{xMI} = & 3\omega_o^2 k_2 k_3 \Delta I_x + \frac{3}{2} \omega_o^2 [\epsilon_x (\alpha_1 + \alpha_2 \cos 2\omega_o t + \alpha_3 \sin 2\omega_o t) \Delta I_x \\ & - \epsilon_y (\alpha_4 + \alpha_5 \cos 2\omega_o t + \alpha_6 \sin 2\omega_o t) \Delta I_y \\ & + \epsilon_z (\alpha_7 + \alpha_8 \cos 2\omega_o t + \alpha_9 \sin 2\omega_o t) \Delta I_z] \end{aligned} \quad (231a)$$

$$\begin{aligned} T_{yMI} = & 3\omega_o^2 k_1 k_3 \Delta I_y + \frac{3}{2} \omega_o^2 [\epsilon_x (\alpha_4 + \alpha_5 \cos 2\omega_o t + \alpha_6 \sin 2\omega_o t) \Delta I_x \\ & + \epsilon_y (\alpha_{10} + \alpha_{11} \cos 2\omega_o t + \alpha_{12} \sin 2\omega_o t) \Delta I_y \\ & - \epsilon_z (\alpha_{13} + \alpha_{14} \cos 2\omega_o t + \alpha_{15} \sin 2\omega_o t) \Delta I_z] \end{aligned} \quad (231b)$$

$$\begin{aligned} T_{zMI} = & 3\omega_o^2 k_1 k_2 \Delta I_z + \frac{3}{2} \omega_o^2 [-\epsilon_x (\alpha_7 + \alpha_8 \cos 2\omega_o t + \alpha_9 \sin 2\omega_o t) \Delta I_x \\ & + \epsilon_y (\alpha_{13} + \alpha_{14} \cos 2\omega_o t + \alpha_{15} \sin 2\omega_o t) \Delta I_z \\ & + \epsilon_z (\alpha_{16} + \alpha_{17} \cos 2\omega_o t + \alpha_{18} \sin 2\omega_o t) \Delta I_z] \end{aligned} \quad (231c)$$

$$\text{where: } \alpha_1 = b_{31}^2 + b_{32}^2 - b_{21}^2 - b_{22}^2 \quad (232a)$$

$$\alpha_2 = b_{31}^2 - b_{32}^2 - b_{21}^2 + b_{22}^2 \quad (232b)$$

$$\alpha_3 = 2(b_{31} b_{32} - b_{21} b_{22}) \quad (232c)$$

$$\alpha_4 = b_{11} b_{21} + b_{12} b_{22} \quad (232d)$$

$$\alpha_5 = b_{11} b_{21} - b_{12} b_{22} \quad (232e)$$

$$\alpha_6 = b_{11} b_{22} + b_{12} b_{21} \quad (232f)$$

$$\alpha_7 = b_{11}b_{31} + b_{12}b_{32} \quad (232g)$$

$$\alpha_8 = b_{11}b_{31} - b_{12}b_{32} \quad (232h)$$

$$\alpha_9 = b_{11}b_{32} + b_{12}b_{31} \quad (232i)$$

$$\alpha_{10} = b_{11}^2 + b_{12}^2 - b_{31}^2 - b_{32}^2 \quad (232j)$$

$$\alpha_{11} = b_{11}^2 - b_{12}^2 - b_{31}^2 + b_{32}^2 \quad (232k)$$

$$\alpha_{12} = 2(b_{11}b_{12} - b_{31}b_{32}) \quad (232l)$$

$$\alpha_{13} = b_{21}b_{31} + b_{22}b_{32} \quad (232m)$$

$$\alpha_{14} = b_{21}b_{31} - b_{22}b_{32} \quad (232n)$$

$$\alpha_{15} = b_{21}b_{32} + b_{22}b_{31} \quad (232o)$$

$$\alpha_{16} = b_{21}^2 + b_{22}^2 - b_{11}^2 - b_{12}^2 \quad (232p)$$

$$\alpha_{17} = b_{21}^2 - b_{22}^2 - b_{11}^2 + b_{12}^2 \quad (232q)$$

$$\alpha_{18} = 2(b_{21}b_{22} - b_{11}b_{12}) \quad (232r)$$

Since ΔI_x is some 20 times smaller than ΔI_y and ΔI_z , maneuvers about X_v can produce relatively little torque compared to Y_v and Z_v rotations. Therefore ϵ_x will be set to zero, and the trim maneuvers ϵ_y and ϵ_z will be used. The torque available by trim maneuvering equals:

$$T_{xMI} = 3\omega_o^2 k_2 k_3 \Delta I_x + \frac{3}{2} \omega_o^2 [-\epsilon_y (\alpha_4 + \alpha_5 \cos 2\omega_o t + \alpha_6 \sin 2\omega_o t) \Delta I_y + \epsilon_z (\alpha_7 + \alpha_8 \cos 2\omega_o t + \alpha_9 \sin 2\omega_o t) \Delta I_z] \quad (233a)$$

$$T_{yMI} = 3\omega_o^2 k_1 k_3 \Delta I_y + \frac{3}{2} \omega_o^2 [\epsilon_y (\alpha_{10} + \alpha_{11} \cos 2\omega_o t + \alpha_{12} \sin 2\omega_o t) \Delta I_y - \epsilon_z (\alpha_{13} + \alpha_{14} \cos 2\omega_o t + \alpha_{15} \sin 2\omega_o t) \Delta I_z] \quad (233b)$$

$$T_{zMI} = 3\omega_o^2 k_1 k_2 \Delta I_z + \frac{3}{2} \omega_o^2 [\epsilon_y (\alpha_{13} + \alpha_{14} \cos 2\omega_o t + \alpha_{15} \sin 2\omega_o t) \Delta I_y + \epsilon_z (\alpha_{16} + \alpha_{17} \cos 2\omega_o t + \alpha_{18} \sin 2\omega_o t) \Delta I_z] \quad (233c)$$

One approach to determine the trim maneuvers is to express them as some dynamic function of the residual angular momentum as expressed in mirror image coordinates, thus:

$$\begin{bmatrix} \epsilon_y \\ \epsilon_z \end{bmatrix} = \begin{bmatrix} A & B & C \\ D & E & F \end{bmatrix} \begin{bmatrix} -H_{xRMI} \\ -H_{yRMI} \\ -H_{zRMI} \end{bmatrix} \quad (234)$$

where $\vec{H}_{RMI} = (H_{xRMI}, H_{yRMI}, H_{zRMI})^T$ is the residual angular momentum to be dumped expressed in the mirror image coordinates, and A through F are function or operations yet to be determined. The residual momentum can be computed by sampling the stored momentum (through reading out CMG gimbal angles) just after desaturation is completed and the samples as taken during an observation orientation must be transformed by equation 225 to express it in mirror image coordinates. In addition prior studies have indicated that time history dependence can be important so the form chosen for \vec{H}_{MRI} will be:

$$\vec{H}_{MRI} = \vec{H}_s - \vec{H}_a + k_M (\vec{H}_{MRIp} - \vec{H}_s) \quad (235)$$

Where \vec{H}_s is the sampled momentum, \vec{H}_a is some reference or desired momentum state, \vec{H}_{MRIp} is the residual momentum from the previous orbit and k_M is some constant gain which can best be determined from simulation studies.

In order to define the functions A through F required for residual desaturation equation 234 is substituted into the equations 233 yielding:

$$\begin{aligned}
T_{xMI} = & 3\omega_o^2 k_2 k_3 \Delta I_x + \frac{3}{2} \omega_o^2 H_{xRMI} [A \Delta I_y (\alpha_4 + \alpha_5 \cos 2\omega_o t + \alpha_6 \sin 2\omega_o t) \\
& - D \Delta I_z (\alpha_7 + \alpha_8 \cos 2\omega_o t + \alpha_9 \sin 2\omega_o t)] \\
& + \frac{3}{2} \omega_o^2 H_{yRMI} [B \Delta I_y (\alpha_4 + \alpha_5 \cos 2\omega_o t + \alpha_6 \sin 2\omega_o t) \\
& - E \Delta I_z (\alpha_7 + \alpha_8 \cos 2\omega_o t + \alpha_9 \sin 2\omega_o t)] \\
& + \frac{3}{2} \omega_o^2 H_{zRMI} [C \Delta I_y (\alpha_4 + \alpha_5 \cos 2\omega_o t + \alpha_6 \sin 2\omega_o t) \\
& - F \Delta I_z (\alpha_7 + \alpha_8 \cos 2\omega_o t + \alpha_9 \sin 2\omega_o t)] \quad (236a)
\end{aligned}$$

$$\begin{aligned}
T_{yMI} = & 3\omega_o^2 k_1 k_3 \Delta I_y - \frac{3}{2} \omega_o^2 H_{xRMI} [A \Delta I_y (\alpha_{10} + \alpha_{11} \cos 2\omega_o t + \alpha_{12} \sin 2\omega_o t) \\
& - D \Delta I_z (\alpha_{13} + \alpha_{14} \cos 2\omega_o t + \alpha_{15} \sin 2\omega_o t)] \\
& - \frac{3}{2} \omega_o^2 H_{yRMI} [B \Delta I_y (\alpha_{10} + \alpha_{11} \cos 2\omega_o t + \alpha_{12} \sin 2\omega_o t) \\
& - E \Delta I_z (\alpha_{13} + \alpha_{14} \cos 2\omega_o t + \alpha_{15} \sin 2\omega_o t)] \\
& - \frac{3}{2} \omega_o^2 H_{zRMI} [C \Delta I_y (\alpha_{10} + \alpha_{11} \cos 2\omega_o t + \alpha_{12} \sin 2\omega_o t) \\
& - F \Delta I_z (\alpha_{13} + \alpha_{14} \cos 2\omega_o t + \alpha_{15} \sin 2\omega_o t)] \quad (236b)
\end{aligned}$$

$$\begin{aligned}
T_{zMI} = & 3\omega_o^2 k_1 k_2 \Delta I_z - \frac{3}{2} \omega_o^2 H_{xRMI} [A \Delta I_y (\alpha_{13} + \alpha_{14} \cos 2\omega_o t + \alpha_{15} \sin 2\omega_o t) \\
& + D \Delta I_z (\alpha_{16} + \alpha_{17} \cos 2\omega_o t + \alpha_{18} \sin 2\omega_o t)] \\
& - \frac{3}{2} \omega_o^2 H_{yRMI} [B \Delta I_y (\alpha_{13} + \alpha_{14} \cos 2\omega_o t + \alpha_{15} \sin 2\omega_o t) \\
& + E \Delta I_z (\alpha_{16} + \alpha_{17} \cos 2\omega_o t + \alpha_{18} \sin 2\omega_o t)] \\
& - \frac{3}{2} \omega_o^2 H_{zRMI} [C \Delta I_y (\alpha_{13} + \alpha_{14} \cos 2\omega_o t + \alpha_{15} \sin 2\omega_o t) \\
& + F \Delta I_z (\alpha_{16} + \alpha_{17} \cos 2\omega_o t + \alpha_{18} \sin 2\omega_o t)] \quad (236c)
\end{aligned}$$

If all momentum is to be removed in a half orbit ($\Delta t = \pi/\omega_0$), the integrals of the above equations must equal the negative of the accumulated momentum. The first term in each equation reverses the primary momentum accumulation by the development of the previous section, thus the integrals of the remaining terms must reverse the residual accumulation \vec{H}_{RMI} . Defining the final three terms of each equation as T_{xRMI} , T_{yRMI} , and T_{zRMI} respectively:

$$\int_t^{t+\frac{\pi}{\omega_0}} \vec{T}_{RMI} d\tau = -\vec{H}_{RMI} \quad (237)$$

This can be accomplished without any cross coupling by requiring:

$$\begin{aligned} & \frac{3}{2} \omega_0^2 \Delta I_y \int_t^{t+\frac{\pi}{\omega_0}} A(\alpha_4 + \alpha_5 \cos 2\omega_0 \tau + \alpha_6 \sin 2\omega_0 \tau) d\tau \\ & - \frac{3}{2} \omega_0^2 \Delta I_z \int_t^{t+\frac{\pi}{\omega_0}} D(\alpha_7 + \alpha_8 \cos 2\omega_0 \tau + \alpha_9 \sin 2\omega_0 \tau) d\tau = -1 \end{aligned} \quad (238a)$$

$$\begin{aligned} & \frac{3}{2} \omega_0^2 \Delta I_y \int_t^{t+\frac{\pi}{\omega_0}} B(\alpha_4 + \alpha_5 \cos 2\omega_0 \tau + \alpha_6 \sin 2\omega_0 \tau) d\tau \\ & - \frac{3}{2} \omega_0^2 \Delta I_z \int_t^{t+\frac{\pi}{\omega_0}} E(\alpha_7 + \alpha_8 \cos 2\omega_0 \tau + \alpha_9 \sin 2\omega_0 \tau) d\tau = 0 \end{aligned} \quad (238b)$$

$$\begin{aligned} & \frac{3}{2} \omega_0^2 \Delta I_y \int_t^{t+\frac{\pi}{\omega_0}} C(\alpha_4 + \alpha_5 \cos 2\omega_0 \tau + \alpha_6 \sin 2\omega_0 \tau) d\tau \\ & - \frac{3}{2} \omega_0^2 \Delta I_z \int_t^{t+\frac{\pi}{\omega_0}} F(\alpha_7 + \alpha_8 \cos 2\omega_0 \tau + \alpha_9 \sin 2\omega_0 \tau) d\tau = 0 \end{aligned} \quad (238c)$$

$$\begin{aligned}
& \frac{3}{2} \omega_o^2 \Delta I_y \int_t^{t+\frac{\pi}{\omega_o}} A(\alpha_{10} + \alpha_{11} \cos 2\omega_o \tau + \alpha_{12} \sin 2\omega_o \tau) d\tau \\
& - \frac{3}{2} \omega_o^2 \Delta I_z \int_t^{t+\frac{\pi}{\omega_o}} D(\alpha_{13} + \alpha_{14} \cos 2\omega_o \tau + \alpha_{15} \sin 2\omega_o \tau) d\tau = 0
\end{aligned} \quad (238d)$$

$$\begin{aligned}
& \frac{3}{2} \omega_o^2 \Delta I_y \int_t^{t+\frac{\pi}{\omega_o}} B(\alpha_{10} + \alpha_{11} \cos 2\omega_o \tau + \alpha_{12} \sin 2\omega_o \tau) d\tau \\
& - \frac{3}{2} \omega_o^2 \Delta I_z \int_t^{t+\frac{\pi}{\omega_o}} E(\alpha_{13} + \alpha_{14} \cos 2\omega_o \tau + \alpha_{15} \sin 2\omega_o \tau) d\tau = 1
\end{aligned} \quad (238e)$$

$$\begin{aligned}
& \frac{3}{2} \omega_o^2 \Delta I_y \int_t^{t+\frac{\pi}{\omega_o}} C(\alpha_{10} + \alpha_{11} \cos 2\omega_o \tau + \alpha_{12} \sin 2\omega_o \tau) d\tau \\
& - \frac{3}{2} \omega_o^2 \Delta I_z \int_t^{t+\frac{\pi}{\omega_o}} F(\alpha_{13} + \alpha_{14} \cos 2\omega_o \tau + \alpha_{15} \sin 2\omega_o \tau) d\tau = 0
\end{aligned} \quad (238f)$$

$$\begin{aligned}
& \frac{3}{2} \omega_o^2 \Delta I_y \int_t^{t+\frac{\pi}{\omega_o}} A(\alpha_{13} + \alpha_{14} \cos 2\omega_o \tau + \alpha_{15} \sin 2\omega_o \tau) d\tau \\
& + \frac{3}{2} \omega_o^2 \Delta I_z \int_t^{t+\frac{\pi}{\omega_o}} D(\alpha_{16} + \alpha_{17} \cos 2\omega_o \tau + \alpha_{18} \sin 2\omega_o \tau) d\tau = 0
\end{aligned} \quad (238g)$$

$$\begin{aligned}
& \frac{3}{2} \omega_o^2 \Delta I_y \int_t^{t+\frac{\pi}{\omega_o}} B(\alpha_{13} + \alpha_{14} \cos 2\omega_o \tau + \alpha_{15} \sin 2\omega_o \tau) d\tau \\
& + \frac{3}{2} \omega_o^2 \Delta I_z \int_t^{t+\frac{\pi}{\omega_o}} F(\alpha_{16} + \alpha_{17} \cos 2\omega_o \tau + \alpha_{18} \sin 2\omega_o \tau) d\tau = 0
\end{aligned} \quad (238h)$$

$$\begin{aligned}
& \frac{3}{2} \omega_o^2 \Delta I_y \int_t^{t+\frac{\pi}{\omega_o}} C(\alpha_{13} + \alpha_{14} \cos 2\omega_o \tau + \alpha_{15} \sin 2\omega_o \tau) d\tau \\
& + \frac{3}{2} \omega_o^2 \Delta I_z \int_t^{t+\frac{\pi}{\omega_o}} F(\alpha_{16} + \alpha_{17} \cos 2\omega_o \tau + \alpha_{18} \sin 2\omega_o \tau) d\tau = 1 \quad (238i)
\end{aligned}$$

After examination of the equations 238 select A through F as follows:

$$A \triangleq a_1 \operatorname{sgn}\{\sin 2\omega_o t\} + a_2 \operatorname{sgn}\{\cos 2\omega_o t\} \quad (239a)$$

$$B \triangleq b_1 \operatorname{sgn}\{\sin 2\omega_o t\} + b_2 \operatorname{sgn}\{\cos 2\omega_o t\} \quad (239b)$$

$$C \triangleq c_1 \operatorname{sgn}\{\sin 2\omega_o t\} + c_2 \operatorname{sgn}\{\cos 2\omega_o t\} \quad (239c)$$

$$D \triangleq d \operatorname{sgn}\{\sin 2\omega_o t\} \quad (239d)$$

$$E \triangleq e \operatorname{sgn}\{\cos 2\omega_o t\} \quad (239e)$$

$$F \triangleq f \operatorname{sgn}\{\cos 2\omega_o t\} \quad (239f)$$

Also, note that:

$$\int_t^{t+\frac{\pi}{\omega_o}} \operatorname{sgn}\{\sin 2\omega_o \tau\} \sin 2\omega_o \tau d\tau = \int_t^{t+\frac{\pi}{\omega_o}} \operatorname{sgn}\{\cos 2\omega_o \tau\} \cos 2\omega_o \tau d\tau = \frac{2}{\omega_o} \quad (240)$$

$$\int_t^{t+\frac{\pi}{\omega_o}} \operatorname{sgn}\{\sin 2\omega_o \tau\} \cos 2\omega_o \tau d\tau = \int_t^{t+\frac{\pi}{\omega_o}} \operatorname{sgn}\{\cos 2\omega_o \tau\} \sin 2\omega_o \tau d\tau = 0 \quad (241)$$

Substituting equations 239a and 239d into equations 238a, 238d, and 238g and using equations 240 and 241 then gives the following simultaneous equations in a_1 , a_2 and d :

$$\alpha_6 \Delta I_y a_1 + \alpha_5 \Delta I_y a_2 - \alpha_9 \Delta I_z d = -\frac{1}{3\omega_o} \quad (242)$$

$$\alpha_{12} \Delta I_y a_1 + \alpha_{11} \Delta I_y a_2 - \alpha_{15} \Delta I_z d = 0 \quad (243)$$

$$\alpha_{15} \Delta I_y a_1 + \alpha_{14} \Delta I_y a_2 + \alpha_{18} \Delta I_z d = 0 \quad (244)$$

Solving for a_1 , a_2 and d by Cramer's Rule gives.

$$a_1 = \frac{\Delta I_y \Delta I_z}{3\omega_o \Delta_{a,d}} (\alpha_{11}\alpha_{18} + \alpha_{14}\alpha_{15}) \quad (245)$$

$$a_2 = -\frac{\Delta I_y \Delta I_z}{3\omega_o \Delta_{a,d}} (\alpha_{15}^2 + \alpha_{12}\alpha_{18}) \quad (246)$$

$$d = \frac{\Delta I_y^2}{3\omega_o \Delta_{a,d}} (\alpha_{12}\alpha_{14} - \alpha_{11}\alpha_{15}) \quad (247)$$

$$\text{where: } \Delta_{a,d} = \Delta I_y^2 \Delta I_z (\alpha_5 \alpha_{15}^2 + \alpha_5 \alpha_{12} \alpha_{18} + \alpha_9 \alpha_{12} \alpha_{14} - \alpha_6 \alpha_{11} \alpha_{18} - \alpha_6 \alpha_{14} \alpha_{15} - \alpha_9 \alpha_{11} \alpha_{15}) \quad (248)$$

Following the same procedure with the other equations, the remaining constants are found to be:

$$b_1 = \frac{\Delta I_y \Delta I_z}{3\omega_o \Delta_{b,e}} (\alpha_5 \alpha_{17} + \alpha_8 \alpha_{14}) \quad (249)$$

$$b_2 = -\frac{\Delta I_y \Delta I_z}{3\omega_o \Delta_{b,e}} (\alpha_6 \alpha_{17} + \alpha_8 \alpha_{15}) \quad (250)$$

$$e = \frac{\Delta I_y^2}{3\omega_o \Delta_{b,e}} (\alpha_6 \alpha_{14} - \alpha_5 \alpha_{15}) \quad (251)$$

$$\Delta_{b,e} = \Delta I_y^2 \Delta I_z (\alpha_5 \alpha_{14} \alpha_{15} + \alpha_5 \alpha_{12} \alpha_{17} + \alpha_8 \alpha_{12} \alpha_{14} - \alpha_6 \alpha_{11} \alpha_{17} - \alpha_6 \alpha_{14}^2 - \alpha_8 \alpha_{11} \alpha_{15}) \quad (252)$$

$$\text{and, } c_1 = \frac{\Delta I_y \Delta I_z}{3\omega_o \Delta_{c,f}} (\alpha_5 \alpha_{14} - \alpha_8 \alpha_{11}) \quad (253)$$

$$c_2 = -\frac{\Delta I_y \Delta I_z}{3\omega_o \Delta_{c,f}} (\alpha_6 \alpha_{14} - \alpha_8 \alpha_{12}) \quad (254)$$

$$f = \frac{\Delta I_y^2}{3\omega_o \Delta_{c,f}} (\alpha_5 \alpha_{12} - \alpha_6 \alpha_{11}) \quad (255)$$

$$\Delta_{c,f} = \Delta I_y^2 \Delta I_z (\alpha_5 \alpha_{14} \alpha_{15} + \alpha_5 \alpha_{12} \alpha_{17} + \alpha_8 \alpha_{12} \alpha_{14} - \alpha_6 \alpha_{11} \alpha_{17} - \alpha_6 \alpha_{14}^2 - \alpha_8 \alpha_{11} \alpha_{15}) \quad (256)$$

The trim maneuvers are defined by equation 234 along with the equations 239, 245 thru 256 and 232. Examination of the equations 239 reveals that the maneuvers are piecewise constant about the mirror image orientation switching as $\sin 2\omega_o t$ or $\cos 2\omega_o t$ change sign. Like the large maneuver, the trim maneuvers are dependent on the observation orientation, but they are influenced directly by the residual momentum as obtained by sampling the stored momentum.

Logic and Maneuvering Summary - As in the previous developments, the large angle maneuvers will be accomplished by passing the direction cosine matrix of the desired orientation to the quaternion maneuver law. The transformation from orbital coordinates to the mirror image desaturation attitude is given by equation 224 in terms of the direction cosine coefficients of the observation attitude. The relation between orbital and reference coordinates is given by the inverse of equation 123. The matrix to be supplied to the maneuver law to move to the desaturation attitude is thus:

$$\begin{bmatrix} a_{11} & a_{12} & -a_{13} \\ a_{21} & a_{22} & -a_{23} \\ -a_{31} & -a_{32} & a_{33} \end{bmatrix} \begin{bmatrix} \cos \alpha & -\cos i \sin \alpha & \sin i \sin \alpha \\ \sin \alpha & \cos i \cos \alpha & -\sin i \cos \alpha \\ 0 & \sin i & \cos i \end{bmatrix} \quad (257)$$

In performing the maneuver back to the same observation attitude at the end of the desaturation period the matrix is:

$$\begin{bmatrix} a_{11} & a_{12} & a_{13} \\ a_{21} & a_{22} & a_{23} \\ a_{31} & a_{32} & a_{33} \end{bmatrix} \begin{bmatrix} \cos \alpha & -\cos i \sin \alpha & \sin i \sin \alpha \\ \sin \alpha & \cos i \cos \alpha & -\sin i \cos \alpha \\ 0 & \sin i & \cos i \end{bmatrix} \quad (258)$$

The basic operation of over one orbit measured from target reacquisition thus can be outlined as follows:

- a. When demaneuver to observation attitude is complete sample the stored momentum and compute \vec{H}_{RMI} to determine trim maneuvers during the desaturation period.
- b. During the observation period monitor the momentum accumulation to determine the total accumulated momentum \vec{H}_D .
- c. Just prior to the initiation of desaturation compare the magnitude of \vec{H}_D with the gross desaturation capability of the trim maneuvers \vec{H}_R . If $|\vec{H}_D| < |\vec{H}_R|$ set $\vec{H}_{MRI} = \vec{H}_D$ and go directly to the trim maneuvers (step e) without performing the mirror image maneuver.
- d. If $|\vec{H}_D| > |\vec{H}_R|$ move to the mirror image orientation by passing the matrix 257 to the maneuver control law.
- e. Begin the trim maneuver sequence about vehicle axes as defined by equation 234.
- f. At the end of the desaturation period set the trim commands to zero, and if step d was performed, demaneuver to the observation attitude by passing the matrix 258 to the maneuver control law.

During the above procedure, the angle α will require periodic update as the orbit precesses. In addition if a new target is to be acquired the demaneuver at step f will be to that new target and the start of the next desaturation period will be altered depending on the relation between the old and new target points.

10.4.5 A Gravity Tracking Control Law For Desaturation From an Arbitrary Attitude - The gravity tracking technique consists of large angle maneuvers about at least two vehicle axes selected to place the minimum axis of inertia in the vicinity of the local vertical vector for maximum torque regulation about all axes. The rationale for this can be understood by recalling that gravity torques tend to align the minimum axis of inertia with the local vertical and maximal torques may thus be developed by bringing this axis close to the vertical in an orientation determined by the accumulation of angular momentum in the CMG

system. The method is thus more complex than the single axis large angle law presented in section 10.4.3 since in general at least two large angle maneuvers are required. Like the law of the previous section, desaturation can be accomplished from an arbitrary attitude, however this method requires continuous maneuvering during desaturation to maintain the desired relationship between the vehicle minimum axis of inertia and the local vertical vector, i.e., to track the gravity vector, and the tacit assumption is made that observation will be along the vehicle X axis.

The basic gravity tracking method was presented in reference 4 and variations are given in references 5 and 6 from which the following development is made.

Determination of the Maneuver Format - For a vehicle having an inertia distribution approximating a cylinder, the gravity torques tend to align the minimum axis of inertia with the gravity vector. Thus, the torque vector is always perpendicular to the plane formed by the minimum axis and the gravity vector. The magnitude of this torque is proportional to the angle between the minimum axis and the gravity vector and, in particular, is related according to the sine of twice that angle. A torque plane is formed, as shown in figure 10.16, by rotation of the vehicle about the gravity vector through a specified angle $\Delta\gamma$. This torque plane is always normal to the local vertical, i.e., tangent to the orbital path of a circular orbit when viewed perpendicular to the orbital plane.

As the vehicle center of mass moves in orbit, the torque vector moves as shown in figure 10.17. The object is to maneuver the vehicle during the desaturation cycle in such a manner that the resolved components in the inertial frame are favorable for desaturation. Visualization of the torque in this manner allows a design that accomplishes momentum control about all axes. Since the torque vector is in a plane tangent to the orbital plane, it is often desirable to maneuver such that the torque component in the orbital plane changes the sign of a specific component. Thus, maneuvers are often performed at points which yield the additional necessary control.

Before considering the desaturation maneuvering sequence, it is worthwhile to justify the preceding remarks concerning the general gravity torque behavior. If it is assumed that the vehicle orientation is arbitrary, then the relation between the orbital coordinates $X_0 Y_0 Z_0$ and vehicle coordinates may be represented by an arbitrary direction cosine matrix as in equation 215. To

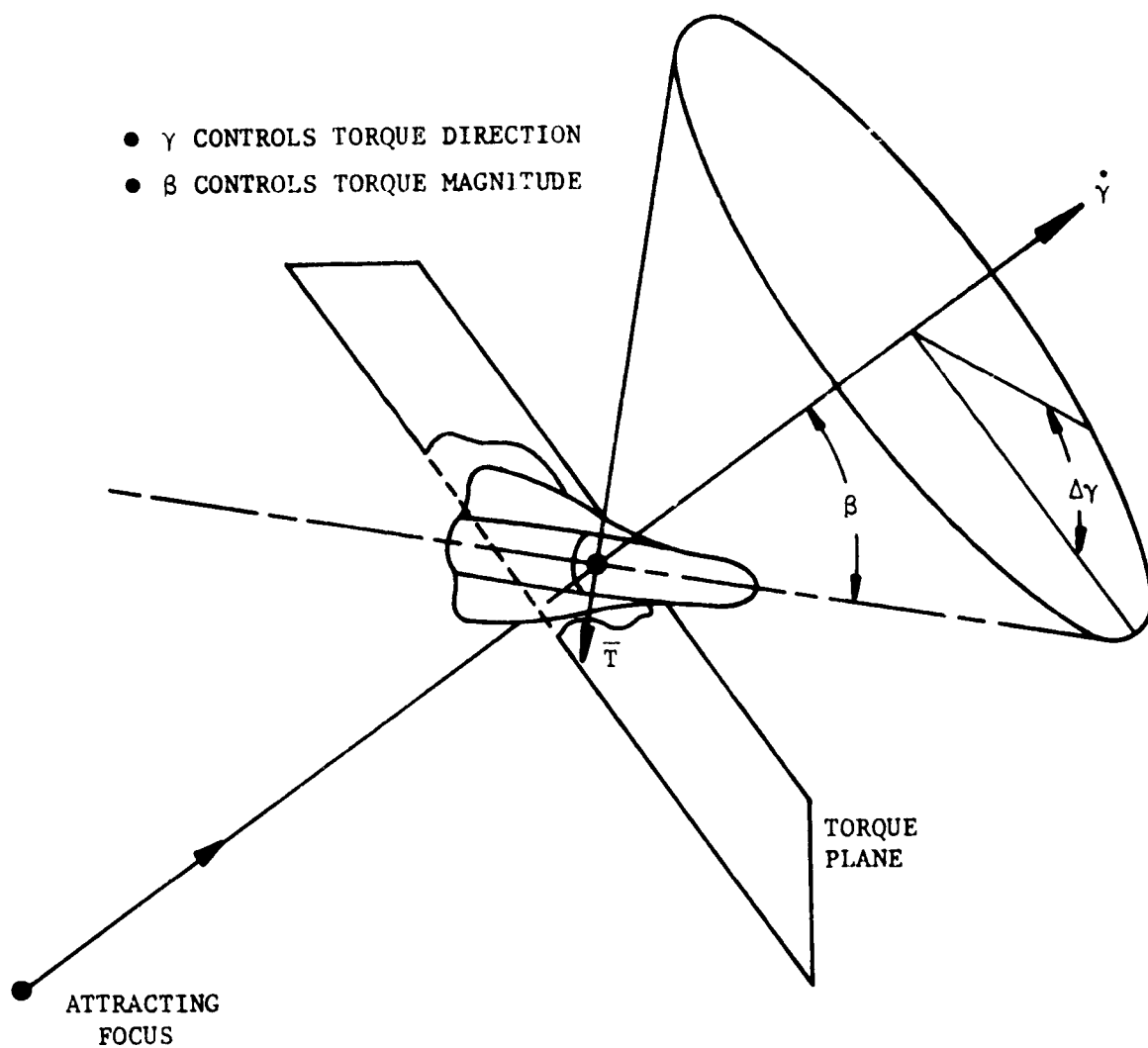


Figure 10.16. The Gravity Torque Plane

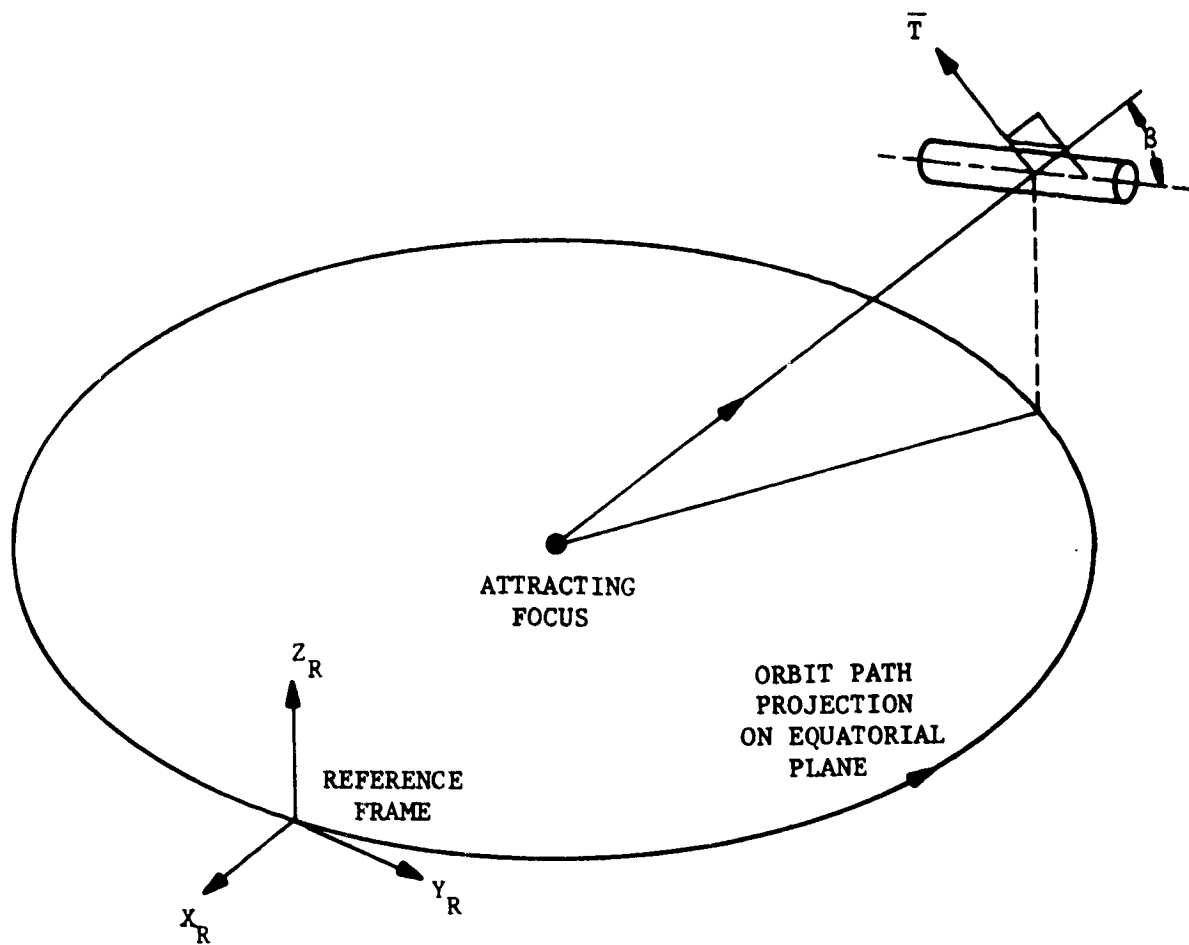


Figure 10.17. Torque Vector Orientation

verify the existence of the torque plane it is necessary to resolve the torque into a coordinate system in which the X axis is directed along the local vertical. The Y axis will be confined to the orbital plane and Z will thus be normal to the orbit plane and is taken to be directed above it. The relation between the vehicle coordinates and this system is thus:

$$\begin{bmatrix} X_v \\ Y_v \\ Z_v \end{bmatrix} = \begin{bmatrix} a_{11} & a_{12} & a_{13} \\ a_{21} & a_{22} & a_{23} \\ a_{31} & a_{32} & a_{33} \end{bmatrix} \begin{bmatrix} \cos \omega_o t & \sin \omega_o t & 0 \\ -\sin \omega_o t & \cos \omega_o t & 0 \\ 0 & 0 & 1 \end{bmatrix} \begin{bmatrix} X \\ Y \\ Z \end{bmatrix}$$

$$= \begin{bmatrix} P_{11} & P_{12} & P_{13} \\ P_{21} & P_{22} & P_{23} \\ P_{31} & P_{32} & P_{33} \end{bmatrix} \begin{bmatrix} X \\ Y \\ Z \end{bmatrix} \quad (259)$$

denoting the matrix product of equation 259 as P with elements P_{ij} and noting that the local vertical unit vector in XYZ coordinates is simply $(1,0,0)^T$, gives the local vertical vector in vehicle coordinates as:

$$\hat{a} = \begin{bmatrix} P_{11} \\ P_{21} \\ P_{31} \end{bmatrix} \quad (260)$$

Substituting into equation 15, the gravity gradient torque in vehicle space is:

$$\vec{T}_v = 3\omega_o^2 \begin{bmatrix} P_{21}P_{31}\Delta I_x \\ P_{11}P_{31}\Delta I_y \\ P_{11}P_{21}\Delta I_z \end{bmatrix} \quad (261)$$

Since P is the product of two orthogonal matrices it is also orthogonal and the torque resolved into the XYZ system is thus:

$$\vec{T} = 3\omega_o^2 \begin{bmatrix} P_{11} & P_{21} & P_{31} \\ P_{12} & P_{22} & P_{32} \\ P_{13} & P_{23} & P_{33} \end{bmatrix} \begin{bmatrix} P_{21} P_{31} \Delta I_x \\ P_{11} P_{31} \Delta I_y \\ P_{11} P_{21} \Delta I_z \end{bmatrix}$$

$$\vec{T} = 3\omega_o^2 \begin{bmatrix} P_{11} P_{21} P_{31} (\Delta I_x + \Delta I_y + \Delta I_z) \\ P_{12} P_{21} P_{31} \Delta I_x + P_{11} P_{22} P_{31} \Delta I_y + P_{11} P_{21} P_{32} \Delta I_z \\ P_{13} P_{21} P_{31} \Delta I_x + P_{11} P_{23} P_{31} \Delta I_y + P_{11} P_{21} P_{33} \Delta I_z \end{bmatrix} \quad (262)$$

Since the sum of the ΔI_i is identically zero, there is no torque in the X direction, that is about the local vertical, thus the gravity gradient torque is always in a plane normal to the local vertical regardless of vehicle inertia distribution or orientation and the existence of the torque plane is confirmed.

The actual torque resolved into the XYZ system can be obtained by substitution of the P_{ij} from equation 259 into 262, using the orthogonality of the a_{ij} giving:

$$T_x = 0 \quad (263)$$

$$T_y = 3\omega_o^2 [(a_{12} a_{21} a_{31} \cos \omega_o t + a_{11} a_{22} a_{32} \sin \omega_o t) \Delta I_x \\ + (a_{11} a_{22} a_{31} \cos \omega_o t + a_{12} a_{21} a_{32} \sin \omega_o t) \Delta I_y \\ + (a_{11} a_{21} a_{32} \cos \omega_o t + a_{12} a_{22} a_{31} \sin \omega_o t) \Delta I_z] \quad (264)$$

$$T_z = \frac{3}{2} \omega_o^2 \{ [a_{13} (a_{21} a_{31} - a_{22} a_{32}) \cos 2\omega_o t - a_{13} (a_{21} a_{32} + a_{22} a_{31}) \sin 2\omega_o t] \Delta I_x \\ + [a_{23} (a_{11} a_{31} - a_{12} a_{32}) \cos 2\omega_o t - a_{23} (a_{11} a_{32} + a_{12} a_{31}) \sin 2\omega_o t] \Delta I_y \\ + [a_{33} (a_{11} a_{21} - a_{12} a_{22}) \cos 2\omega_o t - a_{33} (a_{11} a_{22} + a_{12} a_{21}) \sin 2\omega_o t] \Delta I_z \} \quad (265)$$

The equations 263, 264, and 265 yield the gravity torques on an arbitrarily oriented vehicle resolved into the local vertical coordinate system XYZ.

In general, large rotations about any two vehicle axes will be sufficient to place the X_v axis near the local vertical when maneuvering from an arbitrary orientation. Consider an orbital frame X_o, Y_o, Z_o , with X_o directed along the target line projected in the orbital plane and Y_o , leading X_o , by $\pi/2$ in the orbit plane. The orbital position θ_t is measured from the post desaturation quadrature point (i.e., the $-Y_o$ axis). From this system a rotation of $\omega_o t - \pi/2$ about the Z_o axis will place the X_v axis along the local vertical. A rotation about the Y axis of μ_y will develop the angle θ , while small maneuvers ϵ_x and ϵ_z can generate the angle $\Delta\gamma$ thus setting up the general orientation of figure 10.15. The total maneuver with respect to the X_o, Y_o, Z_o frame can be represented by:

$$\begin{bmatrix} X_{Dv} \\ Y_{Dv} \\ Z_{Dv} \end{bmatrix} = \begin{bmatrix} \cos\mu_y & 0 & -\sin\mu_y \\ 0 & 1 & 0 \\ \sin\mu_y & 0 & \cos\mu_y \end{bmatrix} \begin{bmatrix} 1 & \epsilon_z & 0 \\ -\epsilon_z & 1 & 0 \\ 0 & 0 & 1 \end{bmatrix} \begin{bmatrix} -\sin\omega_o t & \cos\omega_o t & 0 \\ -\cos\omega_o t & -\sin\omega_o t & 0 \\ 0 & 0 & 1 \end{bmatrix} \begin{bmatrix} 1 & 0 & 0 \\ 0 & 1 & \epsilon_x \\ 0 & -\epsilon_x & 1 \end{bmatrix} \begin{bmatrix} X_o \\ Y_o \\ Z_o \end{bmatrix} \quad (266)$$

where the X_o, Y_o, Z_o system is related to the $X_o Y_o Z_o$ system of figures 10.12 and 10.13 by a rotation of θ degrees about the Z_o axis.

The sequence of rotations is relatively unimportant since the maneuver will ultimately be generated by the quaternion maneuver law and will be about an eigenaxis. The order shown in equation 261 involves a small roll ϵ_x to initialize the position for the $\Delta\gamma$ maneuver followed by the yaw of $\omega_o t - \pi/2$ to place the X axis near the vertical, then additional yaw of ϵ_x to develop $\Delta\gamma$ followed by pitch of μ_y to complete the maneuver. The total transformation from observation to desaturation attitudes is given by the combination of equation 215, a rotation about Z_o by θ , and equation 266.

Derivation of the Required Maneuvers - The first step in determining the desaturation maneuvers is the determination of the gravity torques in the desaturation attitude. Resolving the local vertical vector $\hat{a}_o = (\sin\omega_o t, -\cos\omega_o t, 0)^T$ into the vehicle desaturation attitude coordinates using equation 266 gives:

$$\begin{bmatrix} a_{xv} \\ a_{yv} \\ a_{zv} \end{bmatrix} = \begin{bmatrix} -\cos\mu_y - \epsilon_x \sin\mu_y \cos\omega_o t \\ \epsilon_z \\ -\sin\mu_y + \epsilon_x \cos\mu_y \cos\omega_o t \end{bmatrix} \quad (267)$$

Substituting into the torque equation 15 gives:

$$\begin{bmatrix} T_{dxv} \\ T_{dyv} \\ T_{dzv} \end{bmatrix} = 3\omega_o^2 \begin{bmatrix} -\epsilon_z \sin\mu_y \Delta I_x \\ (\frac{1}{2} \sin 2\mu_y - \epsilon_x \cos 2\mu_y \cos\omega_o t) \Delta I_y \\ -\epsilon_z \cos\mu_y \Delta I_z \end{bmatrix} \quad (268)$$

Transforming back to orbital coordinates using the inverse of equation 266:

$$\begin{bmatrix} T_{dxo'} \\ T_{dyo'} \\ T_{dzo'} \end{bmatrix} = 3\omega_o^2 \begin{bmatrix} (\epsilon_x \cos 2\mu_y \cos\omega_o t - \frac{1}{2} \sin 2\mu_y) \cos\omega_o t \Delta I_y \\ (\epsilon_x \cos 2\mu_y \cos\omega_o t - \frac{1}{2} \sin 2\mu_y) \sin\omega_o t \Delta I_y \\ \epsilon_z \Delta I_x + (\epsilon_z \cos^2 \mu_y - \frac{1}{2} \epsilon_x \sin 2\mu_y \sin\alpha) \Delta I_y \end{bmatrix} \quad (269)$$

where all products of the small maneuvers have been neglected. Further since ϵ_z is by definition small and ΔI_x is an order of magnitude smaller than ΔI_y , the product $\epsilon_z \Delta I_x$ can be neglected in the Z component of 269 leaving:

$$\begin{bmatrix} T_{dxo'} \\ T_{dyo'} \\ T_{dzo'} \end{bmatrix} = 3\omega_o^2 \Delta I_y \begin{bmatrix} (\epsilon_x \cos 2\mu_y \cos\omega_o t - \frac{1}{2} \sin 2\mu_y) \cos\omega_o t \\ (\epsilon_x \cos 2\mu_y \cos\omega_o t - \frac{1}{2} \sin 2\mu_y) \sin\omega_o t \\ \frac{1}{2} (\epsilon_z + \epsilon_z \cos 2\mu_y - \epsilon_x \sin 2\mu_y \sin\omega_o t) \end{bmatrix} \quad (270)$$

The momentum components generated during occultation are obtained by integrating the torque components of equation 270 over the interval $\theta_1 < \theta < \theta_2$ where:

$$\theta_t = \omega_o t \quad (271)$$

$$\theta_1 = 3\pi/2 + \epsilon_\theta - \Delta\mu_z \quad (272)$$

$$\theta_2 = 3\pi/2 + \epsilon_\theta + \Delta\mu_z \quad (273)$$

As shown in figure 10.18, ϵ_θ represents a shift of mid-desaturation with respect to mid-occultation, the significance of which will be apparent upon examination of the momentum equations. The angle between $3\pi/2 + \epsilon_\theta \pm \Delta\mu_z$ is the range of orbital positions beginning after all maneuvers placing the X_v axis near the local vertical and ending just prior to the demaneuver to observing attitude. The nominal vehicle orientation will be constant with respect to local vertical for $\theta_1 < \omega_o t < \theta_2$. The momentum equations in orbital coordinates are thus:

$$\vec{H}_{do} = \int_{t_1}^{t_2} \vec{T}_{do} dt = \frac{1}{\omega_o} \int_{\theta_1}^{\theta_2} \vec{T}_{do} d(\omega_o t) \quad (274)$$

Performing the indicated integration yields:

$$H_{dxo} = \frac{3}{2} \omega_o \Delta I_y [\epsilon_x \cos 2\mu_y (\theta_2 - \theta_1) + \frac{1}{2} \epsilon_x \cos 2\mu_y (\sin 2\theta_2 - \sin 2\theta_1) - \sin 2\mu_y (\sin \theta_2 - \sin \theta_1)]$$

$$H_{dyo} = \frac{3}{2} \omega_o \Delta I_y [\sin 2\mu_y (\cos \theta_2 - \cos \theta_1) - \frac{1}{2} \epsilon_x \cos 2\mu_y (\cos 2\theta_2 - \cos 2\theta_1)]$$

$$H_{dzo} = \frac{3}{2} \omega_o \Delta I_y [(\epsilon_z + \epsilon_z \cos 2\mu_y) (\theta_2 - \theta_1) + \epsilon_x \sin 2\mu_y (\cos \theta_2 - \cos \theta_1)]$$

Assuming μ_x and $2\epsilon_\theta$ are sufficiently small that their product is negligible and the sine of either equals the angle (cosine ≈ 1). Then the momentum equations become:

$$\begin{bmatrix} H_{dxo} \\ H_{dyo} \\ H_{dzo} \end{bmatrix} = 3\omega_o \Delta I_y \begin{bmatrix} \frac{1}{2} \epsilon_x \cos 2\mu_y (2\Delta\mu_z - \sin 2\Delta\mu_z) - \epsilon_\theta \sin 2\mu_y \sin \Delta\mu_z \\ \sin 2\mu_y \sin \Delta\mu_z \\ \epsilon_x \sin 2\mu_y \sin \Delta\mu_z + \epsilon_z \Delta\mu_z (1 + \cos 2\mu_y) \end{bmatrix} \quad (275)$$

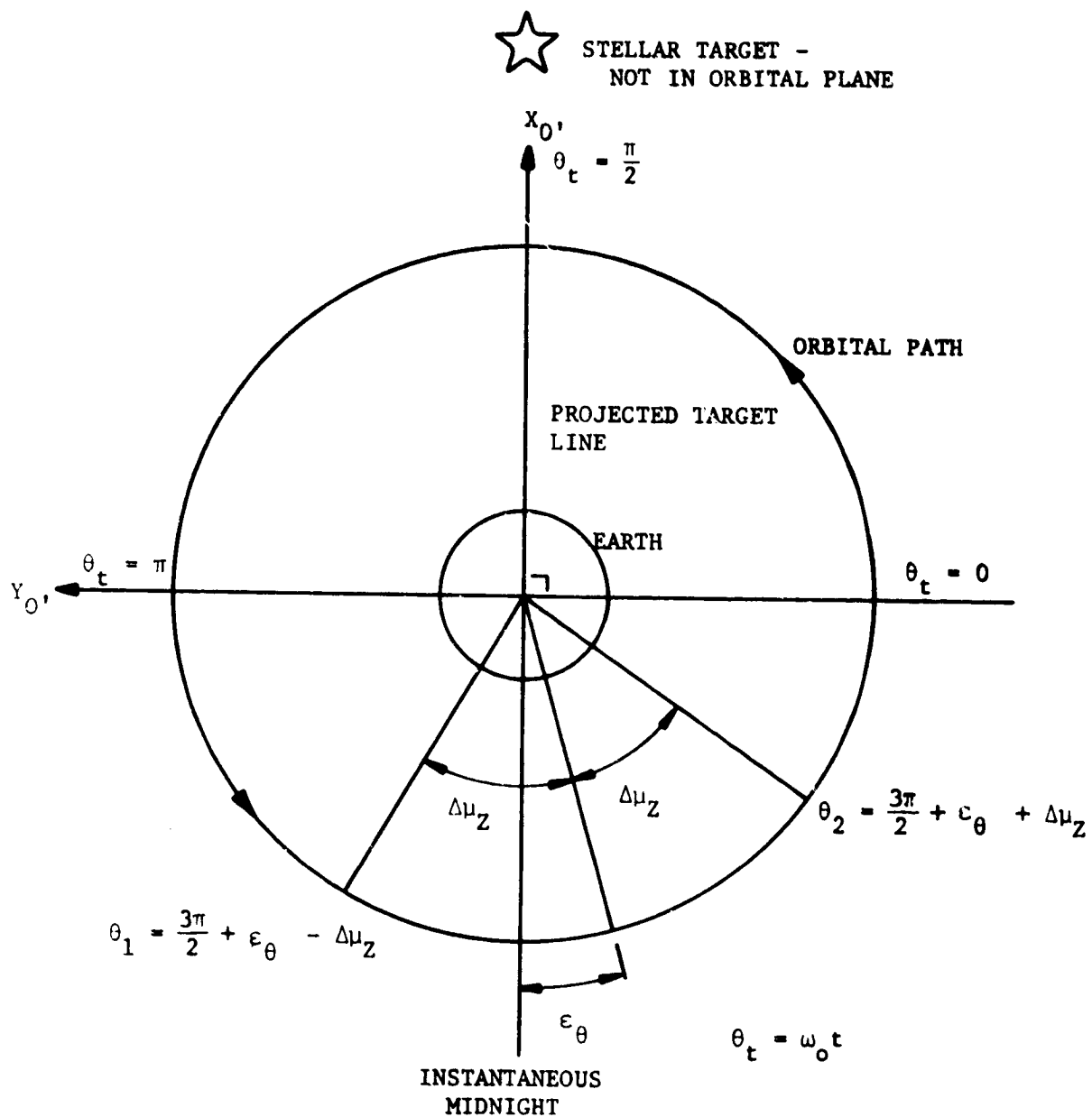


Figure 10.18. Control Switching for the Gravity Tracking Method

Denoting the momentum to be desaturated as $\vec{H}_D = (H_{xD}, H_{yD}, H_{zD})^T$, determined from appropriate sampling during observation, it is necessary that $\vec{H}_{do} = -\vec{H}_D$. With the substitution of the momentum to be dumped into equation 275, it is necessary to in some sense invert the equation and solve for the five unknowns ϵ_x , μ_y , ϵ_z , $\Delta\mu_z$ and ϵ_θ . The expressions will be chosen in a manner similar to that of reference 4. As can be verified by substitution, the equation in H_{xD} is completely satisfied if:

$$\epsilon_\theta = \frac{H_{xD}}{3\omega_o \Delta I_y} \frac{\sin 2\mu_y}{\sin \Delta\mu_z} \quad (276)$$

$$\epsilon_x = - \frac{H_{xD}}{3\omega_o \Delta I_y} \frac{2\cos 2\mu_y}{(2\Delta\mu_z - \sin 2\Delta\mu_z)} \quad (277)$$

An expression for ϵ_z can be obtained from the H_{zD} as:

$$\epsilon_z = - \frac{\frac{H_{zD}}{3\omega_o \Delta I_y} + \epsilon_x \sin 2\mu_y \sin \Delta\mu_z}{\Delta\mu_z (1 + \cos 2\mu_y)} \quad (278)$$

An expression for μ_y is obtained basically from the following reasoning. Since principal momentum accumulation is about Y_v and is proportional to $\sin 2\psi$, an initial maneuver about Y_v of -2ψ would tend to compensate for the primary accumulation. In any case, after having chosen an initial value, subsequent values should be updated to account for variations in primary momentum accumulation ΔH_{yD} . Thus, a recursion in μ_y develops as:

$$\mu_{yn} = \mu_{yp} + K_{yy} \Delta H_{yD} \quad (279)$$

where p denotes the previous orbit and K_{yy} is to be determined. From the previous equation, K_{yy} is related to the differential relationship between μ_y and H_{yD} . Such a differential relationship is obtainable from the equation in H_{yD} . Thus, from that equation:

$$d(\sin 2\mu_y) = - \frac{1}{3\omega_o \Delta I_y} d(H_{yD} / \sin \Delta\mu_z) \quad (280)$$

Or, since $\Delta\mu_z$ is a constant angle when once determined:

$$2\cos 2\mu_y d\mu_y = \frac{dH_{yD}}{3\omega_o \Delta I_y \sin \Delta\mu_z} \quad (281)$$

A change in μ_y is thus approximately:

$$\Delta\mu_y \approx d\mu_y = \frac{\Delta H_{yD}}{6\omega_o \Delta I_y \sin \Delta\mu_z \cos 2\mu_y} \quad (282)$$

Thus,

$$K_{yy} = \frac{\Delta\mu_y}{\Delta H_{yD}} = \frac{1}{6\Delta I_y \omega_o \sin \Delta\mu_z \cos 2\mu_y} \quad (283)$$

The expression for $\Delta\mu_z$ is obtained directly from consideration of the allowed desaturation angle θ_ℓ and the angular maneuvers required to move to the initial desaturation attitude. In particular if the total eigenangle required to maneuver from observation attitude to initial desaturation attitude is ϕ and the maximum maneuver rate is $\dot{\phi}_\ell$, then:

$$\Delta\mu_z = \theta_\ell - K_\epsilon |\phi| \quad (284)$$

where:

$$K_\epsilon = \omega_o / \dot{\phi}_\ell \quad (285)$$

Logic and Maneuvering Summary - The equations required to generate the desaturation maneuvers may be summarized as follows where the subscript p is used to denote the previous orbit:

$$\mu_y = \mu_{yp} + K_{yy} \Delta H_y \quad (286)$$

$$K_{yy} = (6\Delta I_y \omega_o \sin \Delta\mu_{zp} \cos 2\mu_{yp})^{-1} \quad (287)$$

$$\epsilon_x = \epsilon_{xp} + K_{xx} \Delta H_x \quad (288)$$

$$K_{xx} = \frac{2\cos 2\mu_{yp}}{3\Delta I_y \omega_o (\sin 2\Delta\mu_{zp} - 2\Delta\mu_{zp})} \quad (289)$$

$$\epsilon_z = \epsilon_{zp} + K_{zz} \Delta H_z + K_{zx} \epsilon_x \quad (290)$$

$$K_{zz} = -(6\Delta I_y \omega_o \Delta\mu_{zp} \cos^2 \mu_{yp})^{-1} \quad (291)$$

$$K_{xz} = -\frac{\sin 2\mu_{yp} \sin \Delta\mu_{zp}}{2\Delta\mu_{zp} \cos^2 \mu_{yp}} \quad (292)$$

$$\epsilon_\theta = \epsilon_{\theta p} + K_\theta \Delta H_x \quad (293)$$

$$K_\theta = \frac{\sin 2\mu_{yp}}{3\Delta I_y \omega_o \sin \Delta\mu_{zp}} \quad (294)$$

$$\Delta\mu_z = \theta_\ell - K_\epsilon |\phi| \quad (295)$$

$$K_\epsilon = \omega_o / \dot{\phi}_\ell \quad (296)$$

where:

$$\begin{bmatrix} \Delta H_x \\ \Delta H_y \\ \Delta H_z \end{bmatrix} = \begin{bmatrix} H_{xD} - H_{xDp} \\ H_{yD} + H_{yDp} \\ H_{zD} + H_{zDp} \end{bmatrix} \quad (297)$$

The basic operation is thus to sample the momentum during observation, then generate the above angles and gains prior to desaturation maneuvering. The matrix of the maneuver is generated from these parameters along with knowledge of the relation between the observing attitude and the target oriented orbital plane. Once the primary maneuver has been completed the vehicle rates $\dot{\epsilon}_x = -\omega_o \sin \mu_y$ and $\dot{\epsilon}_z = \omega_o \cos \mu_y$ must be commanded in order to track the gravity vector. At the end of the desaturation period demaneuver to the observing attitude is accomplished by generating the corresponding demaneuver direction cosine matrix after updating the parameters dependent on the time varying orbital elements. If demaneuver is to be to a new target additional computation is required to generate the maneuver matrix and update the history values accordingly so the subsequent desaturation attitude is valid.

10.4.6 Gravity Gradient CMG Desaturation Law Comparison -

In sections 10.4.2 thru 10.4.5, four representative gravity gradient desaturation laws were developed for an inertially held vehicle. The four laws are: (1) a small angle multiaxis maneuver law, (2) a large single axis maneuver law, (3) a reflexive law requiring large multiaxis maneuvers, and (4) a gravity tracking law also requiring large multiaxis maneuvers. All of these laws involve maneuvering the vehicle at the start of the desaturation period to a favorable orientation where the gravity gradient torques acting on the vehicle will cause the magnitude of the CMG momentum to decrease.

The first two laws (1) and (2) place constraints on possible vehicle attitudes for which these desaturation laws will operate. For the candidate vehicle attitudes specified in sections 4 and 5, these vehicle attitude requirements are automatically met. Desaturation laws (3) and (4) are "all attitude" gravity gradient desaturation laws which means there are no constraints placed on possible vehicle attitudes. In other words, these desaturation laws can be used independent of the inertial attitude of the vehicle. Because of the vehicle attitude constraints already imposed on the system, there is no particular advantages in having an "all attitude" desaturation law such as laws (3) and (4) over the attitude restrictive laws (1) and (2).

Of the four gravity gradient desaturation laws derived in this study, the small angle multiaxis CMG desaturation law, law (1), was selected because of the following reasons: (1) the computational requirements associated with this law are fewer than those associated with the other laws and (2) the resultant small angle desaturation maneuvers can be performed by the CMG control system. This latter reason is important because the other candidate desaturation laws require at least a single large angle maneuver. To perform these large angle maneuvers, the baseline reaction control system (RCS) would probably have to be used in order to generate the large torque and momentum required to perform these maneuvers in a reasonable period of time. Firing the baseline RCS to perform these large angular maneuvers tends to defeat the principal purpose for adding a CMG control system to a vehicle like the Shuttle that of reducing RCS contamination.

For the computer verification task documented in section 12, this small angle multiaxis CMG desaturation law is simulated using option 2 for computing $\vec{\epsilon}$.

10.4.7 Small Angle Gravity Gradient Z-LV Desaturation Law -

In section 10.4.6, the four gravity gradient CMG desaturation laws

for an inertially held vehicle derived in sections 10.4.2 thru 10.4.5 were compared. For this particular application, the small angle gravity gradient CMG desaturation law, section 10.4.2, was selected. In this section, a small angle desaturation law is derived for desaturating the CMG system from a Z-LV attitude. This law is basically identical to the small angle desaturation law derived in section 10.4.2 for an inertially held vehicle. The torques acting on the rotating vehicle are resolved into an inertial reference frame where the appropriate small angle desaturation maneuvers are determined. For an inertially held vehicle, the desaturation maneuvers are computed in vehicle coordinate because this coordinate frame is inertial. But for a Z-LV attitude, the vehicle coordinate frame is not inertial, but rotating. This is the only significant difference between these two desaturation laws.

For a vehicle held in an ideal Z-LV attitude, the vector sum of the vehicle momentum \vec{H}_v and CMG momentum \vec{H}_{CMG} imparted to the vehicle as viewed from an inertial frame is a constant \vec{H}_c .

$$\vec{H}_v + \vec{H}_{CMG}^{(I)} = \vec{H}_c \quad (298)$$

The vehicle momentum \vec{H}_v equals

$$\vec{H}_v = [I]\vec{\omega} \quad (299)$$

where $[I]$ is the vehicle inertia tensor and $\vec{\omega}$ is the vehicle angular velocity. For an ideal Z-LV attitude, $\vec{\omega}$ is constrained to be perpendicular to the orbital plane and therefore $\vec{\omega}$ has at most only two components, ω_x and ω_y .

$$\vec{\omega} = \begin{bmatrix} \omega_x \\ \omega_y \\ 0 \end{bmatrix} \quad (300)$$

In order to keep the Z axis pointed along the local vertical, the norm of $\vec{\omega}$ must equal the orbital rate ω_o .

Assume that at time t_o the vehicle is maneuvered instantaneously through a small angle $\vec{\epsilon}$ where ϵ_x , ϵ_y , and ϵ_z , are the X,

Y, and Z angular components of $\vec{\epsilon}$, respectively. Also assume the vehicle is constrained at all times to rotate about the axis perpendicular to the orbital plane at approximately the orbital rate ω_0 . As a result of the small maneuver $\vec{\epsilon}$, the vehicle angular velocity $\vec{\omega}$ equals

$$\vec{\omega}(\epsilon_1) = \begin{bmatrix} 1 & \epsilon_z & -\epsilon_y \\ -\epsilon_z & 1 & \epsilon_x \\ \epsilon_y & -\epsilon_x & 1 \end{bmatrix} \begin{bmatrix} \omega_x \\ \omega_y \\ 0 \end{bmatrix} = \begin{bmatrix} \omega_x + \epsilon_z \omega_y \\ \omega_y - \epsilon_z \omega_x \\ \epsilon_y \omega_x - \epsilon_x \omega_y \end{bmatrix} \quad (i=x,y,z) \quad (301)$$

The vehicle momentum $\vec{H}_v(\epsilon_1)$ due to this instantaneous maneuver $\vec{\epsilon}$ now equals

$$\begin{aligned} \vec{H}_v(\epsilon_1) &= [I] \vec{\omega}(\epsilon_1) \\ &= \begin{bmatrix} I_{xx} & 0 & 0 \\ 0 & I_{yy} & 0 \\ 0 & 0 & I_{zz} \end{bmatrix} \begin{bmatrix} \omega_x + \epsilon_z \omega_y \\ \omega_y - \epsilon_z \omega_x \\ \epsilon_y \omega_x - \epsilon_x \omega_y \end{bmatrix} = \begin{bmatrix} I_{xx}(\omega_x + \epsilon_z \omega_y) \\ I_{yy}(\omega_y - \epsilon_z \omega_x) \\ I_{zz}(\epsilon_y \omega_x - \epsilon_x \omega_y) \end{bmatrix} \end{aligned} \quad (302)$$

The change in \vec{H}_v due to the maneuver $\vec{\epsilon}$ equals

$$\Delta \vec{H}_v(\epsilon_1) = \vec{H}_v(\epsilon_1) - \vec{H}_v(t_0^-) = \begin{bmatrix} I_{xx} \epsilon_z \omega_y \\ -I_{yy} \epsilon_z \omega_x \\ I_{zz}(\epsilon_y \omega_x - \epsilon_x \omega_y) \end{bmatrix} \quad (303)$$

$\vec{H}_v(t_0^-)$ is the vehicle momentum just prior to the maneuver $\vec{\epsilon}$. $\vec{H}_v(t_0^-)$ is equal to \vec{H}_v computed in equation 299, $\vec{H}_v(\epsilon_1)$ equals

$$\vec{H}_v(\epsilon_1) = \vec{H}_v(t_0^-) + \Delta \vec{H}_v(\epsilon_1) \quad (304)$$

During the maneuver $\vec{\epsilon}$, the total system momentum \vec{H}_c is conserved. Substituting equation 304 into equation 298,

$$\vec{H}_v(t_0^-) + \Delta \vec{H}_v(\epsilon_1) + \vec{H}_{CMG}^{(I)}(t_0^+) = \vec{H}_c \quad (305)$$

where $\vec{H}_{CMG}^{(1)}(t_o^+)$ is the CMG momentum just after the instantaneous maneuver ϵ . Note that in order for the above expression to hold, the CMG momentum $\vec{H}_{CMG}^{(I)}$ must also change instantaneously.

$$\vec{H}_{CMG}^{(1)}(t_o^+) = \vec{H}_{CMG}^{(I)}(t_o^-) + \Delta\vec{H}_{CMG}^{(I)}(\epsilon_1) \quad (306)$$

where

$$\Delta\vec{H}_{CMG}^{(I)}(\epsilon_1) = -\vec{H}_v(\epsilon_1) \quad (307)$$

Due to the small maneuver ϵ , the vehicle Z principal axis is slightly misaligned from the local vertical resulting in a non zero gravity gradient torque \vec{T}_{gg} to act on the vehicle. The resultant gravity gradient momentum imparted to the vehicle must therefore be absorbed in order to keep \vec{H}_c constant. \vec{H}_v is completely determined by the vehicle attitude therefore, this gravity gradient momentum must be absorbed by the CMG control system. The constant momentum \vec{H}_c for time t greater than t_o^+ equals

$$\begin{aligned} \vec{H}_c = & \vec{H}_v(t_o^-) + \Delta\vec{H}_c(\epsilon_1) + \vec{H}_{CMG}^{(I)}(t_o^-) + \Delta\vec{H}_{CMG}^{(I)}(\epsilon_1) \\ & + \Delta\vec{H}_{CMG}^{(I)}(t) + \int_{t_o}^t (\vec{T}_{gg})_I dt \quad \text{for } t > t_o^+ \end{aligned} \quad (308)$$

$(\vec{T}_{gg})_I$ is the gravity gradient torque acting on the vehicle as measured in an inertial coordinate frame. At time t_f , assume the vehicle is instantaneously maneuvered back to the initial Z-LV attitude. The instantaneous change in vehicle momentum \vec{H}_v and \vec{H}_{CMG} at t_f as measured in the inertial reference frame equals

$$\Delta\vec{H}_v(t_f^+) = -\Delta\vec{H}_v(\epsilon_1) \quad (309)$$

$$\Delta\vec{H}_{CMG}^{(I)}(t_f^+) = -\Delta\vec{H}_{CMG}^{(I)}(\epsilon_1) \quad (310)$$

Adding these instantaneous changes to equation 308, \vec{H}_c at time t greater than t_f equals

$$\vec{H}_c = \vec{H}_v(t_o^-) + \vec{H}_{CMG}^{(I)}(t_o^-) + \Delta\vec{H}_{CMG}^{(I)} + \int_{t_o}^{t_f} (\vec{T}_{gg})_I dt \quad (311)$$

Because the total momentum \vec{H}_c must be conserved, the net change in the inertial momentum $\Delta \vec{H}_{CMG}^{(I)}(t)$ during the desaturation interval, t_o to t_f , equals the negative of the gravity gradient momentum measured in the same inertial frame.

$$\Delta \vec{H}_{CMG}^{(I)}(t) = - \int_{t_o}^{t_f} (\vec{T}_{gg})_I dt \quad (312)$$

From the above expression, one can see that the only torque acting on the vehicle that can be used for desaturating the CMG system is the gravity gradient torque due to the small maneuver $\vec{\epsilon}$.

The gravity gradient torque acting on the vehicle \vec{T}_{gg} in vehicle coordinate equals

$$\vec{T}_{gg} = 3\omega_o^2 (\hat{a} \times [I] \hat{a}) \quad (313)$$

where \hat{a} is the unit local vertical vector. For an ideal Z-LV attitude \hat{a} equals

$$\hat{a} = \begin{bmatrix} 0 \\ 0 \\ -1 \end{bmatrix} \quad (314)$$

During the desaturation interval from time t_o to t_f , the local vertical vector \hat{a} equals

$$\hat{a}(\epsilon_1) = \begin{bmatrix} 1 & \epsilon_z & -\epsilon_y \\ -\epsilon_z & 1 & \epsilon_x \\ \epsilon_y & -\epsilon_x & 1 \end{bmatrix} \begin{bmatrix} 0 \\ 0 \\ -1 \end{bmatrix} = \begin{bmatrix} \epsilon_y \\ -\epsilon_x \\ -1 \end{bmatrix} \quad (315)$$

Substituting $\hat{a}(\epsilon_1)$ into equation 313 and neglecting all second order terms of ϵ_1 , \vec{T}_{gg} equals

$$\vec{T}_{gg} = 3\omega_o^2 \begin{bmatrix} \epsilon_x (I_{zz} - I_{yy}) \\ -\epsilon_y (I_{xx} - I_{zz}) \\ 0 \end{bmatrix} \quad (316)$$

In order to compute the change in CMG momentum $\vec{H}_{CMG}^{(I)}$, \vec{T}_{gg} as observed in vehicle coordinates must be transformed into some inertial frame. Let

$$(\vec{T}_{gg})_I = [\phi_{O \leftarrow V}^{(m)}(t)] \vec{T}_{gg} \quad (317)$$

where $[\phi_{O \leftarrow V}^{(m)}(t)]$ is the time varying transformation from vehicle space to some inertial orbital reference frame. Because there are only two candidate Z-LV attitudes, X-POP Z-LV and X-IOP Z-LV, two inertial orbital frames are defined, one for each attitude, in order to simplify the problem. These two orbital reference frames are defined in figure 10.19. For an X-POP Z-LV attitude, assume the inertial orbital reference frame $X_O'Y_O'Z_O'$ is defined as shown in figure 10.19a. The Y_O' and Z_O' axes are constrained to lie in the orbital plane. At time t equal zero, the vehicle X, Y, and Z axes are aligned with the X_O' , Y_O' , and Z_O' axes, respectively. The corresponding transformation $[\phi_{O \leftarrow V}^{(m)}(t)]$ for a X-POP Z-LV attitude equals

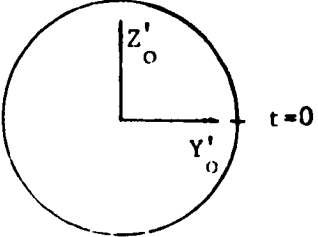
$$[\phi_{O \leftarrow V}^{(m)}(t)]_{\text{X-POP}} = \begin{bmatrix} 1 & 0 & 0 \\ 0 & \cos \omega_o t & -\sin \omega_o t \\ 0 & \sin \omega_o t & \cos \omega_o t \end{bmatrix} \quad (318)$$

For a X-IOP Z-LV attitude, assume the orbital reference frame $X_O'Y_O'Z_O'$ is defined as shown in figure 10.19b. The X_O' and Z_O' axes are constrained to the orbital plane. The transformation $[\phi_{O \leftarrow V}^{(m)}(t)]$ for a X-IOP Z-LV attitude equals

$$[\phi_{O \leftarrow V}^{(m)}(t)]_{\text{X-IOP}} = \begin{bmatrix} \cos \omega_o t & 0 & \sin \omega_o t \\ 0 & 1 & 0 \\ -\sin \omega_o t & 0 & \cos \omega_o t \end{bmatrix} \quad (319)$$

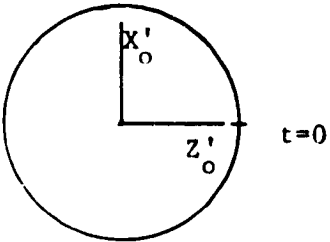
From equation 312, the change in CMG momentum state $\Delta \vec{H}_{CMG}^{(I)}$ equals

$$\Delta \vec{H}_{CMG}^{(I)} = - \int_{t_o}^{t_f} [\phi_{O \leftarrow V}^{(m)}(t)] \vec{T}_{gg} dt \quad (320)$$



$$\left[\begin{matrix} \phi_{O \rightarrow V}^{(m)}(t) \\ \text{X-POP} \end{matrix} \right] = \begin{bmatrix} 1 & 0 & 0 \\ 0 & \cos \omega_o t & -\sin \omega_o t \\ 0 & \sin \omega_o t & \cos \omega_o t \end{bmatrix}$$

(a) X-POP Z-LV INERTIAL ORBITAL REFERENCE FRAME



$$\left[\begin{matrix} \phi_{O \rightarrow V}^{(m)}(t) \\ \text{X-IOP} \end{matrix} \right] = \begin{bmatrix} \cos \omega_o t & 0 & \sin \omega_o t \\ 0 & 1 & 0 \\ -\sin \omega_o t & 0 & \cos \omega_o t \end{bmatrix}$$

(b) X-IOP Z-LV INERTIAL ORBITAL REFERENCE FRAME

NOTE: X'_0, Y'_0, Z'_0 , AXES ALIGNED WITH VEHICLE XYZ AXES AT TIME $t=0$

Figure 10.19. Z-LV Inertial Orbital Reference Frames

$\Delta \vec{H}_{CMG}^{(I)}$ is the desired change in CMG momentum state $\vec{H}_{CMG}^{(I)}$ as observed in the appropriate orbital reference frame. $\Delta \vec{H}_{CMG}^{(I)}$ can be computed by sampling the CMG system momentum imparted to the vehicle \vec{H}_{CMG} as measured in vehicle space. Note that the CMG momentum imparted to the vehicle is the negative of the CMG momentum stored in the CMG system. $\Delta \vec{H}_{CMG}^{(I)}$ equals

$$\Delta \vec{H}_{CMG}^{(I)} = \{ \vec{H}_D^{(I)} - [\phi_{o+v}^{(m)}(t_s)] \vec{H}_{CMG}(t_s) \} \quad (321)$$

$\vec{H}_D^{(I)}$ is the desired CMG momentum state as observed from the appropriate orbital reference frame. The time t_s is the sample time when \vec{H}_{CMG} is measured. t_s can correspond to any time during the observation portion of the orbit although the most logical time to sample \vec{H}_{CMG} is just prior to desaturation. $\Delta \vec{H}_{CMG}^{(I)}$ is the CMG momentum "dump" command used to compute $\vec{\epsilon}$, the desaturation maneuver command. Let the components of $\Delta \vec{H}_{CMG}^{(I)}$ be described as follows:

$$\Delta \vec{H}_{CMG}^{(I)} = \begin{bmatrix} H_{Ex} \\ H_{Ey} \\ H_{Ez} \end{bmatrix} \quad (322)$$

X-POP Z-LV Desaturation Case - For a X-POP Z-LV attitude,

$(\vec{T}_{gg})_I$ equals

$$\begin{aligned} (\vec{T}_{gg})_I &= [\phi_{o+v}^{(m)}(t)] \vec{T}_{gg}^{X-POP} \\ &= 3\omega_o^2 \begin{bmatrix} 1 & 0 & 0 \\ 0 & \cos \omega_o t & -\sin \omega_o t \\ 0 & \sin \omega_o t & \cos \omega_o t \end{bmatrix} \begin{bmatrix} \epsilon_x(I_{zz} - I_{yy}) \\ -\epsilon_y(I_{xx} - I_{zz}) \\ 0 \end{bmatrix} \\ &= 3\omega_o^2 \begin{bmatrix} \epsilon_x(I_{zz} - I_{yy}) \\ -\epsilon_y(I_{xx} - I_{zz}) \cos \omega_o t \\ -\epsilon_y(I_{yy} - I_{xx}) \sin \omega_o t \end{bmatrix} \end{aligned} \quad (323)$$

Note from equation 322 that the X axis component of $(\vec{T}_{gg})_I$ is decoupled from the Y and Z components of $(\vec{T}_{gg})_I$. The small maneuver ϵ_x can be used to desaturate the X-axis, the axis normal to the orbital plane, but it will not result in any change in the CMG momentum state $\vec{H}_{CMG}^{(I)}$ in the orbital plane. The desired maneuver ϵ_x can be readily computed using equation 320.

$$H_{Ex} = - \int_{t_0}^{t_f} 3\omega_o^2 \epsilon_x (I_{zz} - I_{yy}) dt \quad (324)$$

Assume that ϵ_x is a constant offset maneuver. Solving equation 324 for ϵ_x ,

$$\epsilon_x = - \frac{H_{Ex}}{3\omega_o^2 (I_{zz} - I_{yy}) (t_f - t_0)} \quad (325)$$

Also assume that the desaturation interval corresponds to a half orbit, $\omega_o (t_f - t_0)$ equals π , and ϵ_x equals

$$\epsilon_x = - \frac{H_{Ex}}{3\pi\omega_o (I_{zz} - I_{yy})} \quad (326)$$

The maneuver ϵ_y must desaturate both the Y and Z axes and therefore ϵ_y must be a function of both H_{Ey} and H_{Ez} , the desired changes in $\vec{H}_{CMG}^{(I)}$ along the Y and Z axes. Let ϵ_y have the following form.

$$\epsilon_y = A H_{Ey} + B H_{Ez} \quad (327)$$

There are a number of possible solutions for the coefficient A and B. One possible solution is

$$A = a \operatorname{sgn} (\cos \omega_o t)$$

$$B = b \operatorname{sgn} (\sin \omega_o t)$$

where $\operatorname{sgn} ()$ corresponds to the algebraic sign of the quantity enclosed within the parentheses. ϵ_y therefore equals

$$\epsilon_y = a H_{Ey} \operatorname{sgn}(\cos \omega_o t) + b H_{Ez} \operatorname{sgn}(\sin \omega_o t)$$

From equation 320,

$$H_{Ey} = \int_{t_o}^{t_f} 3\omega_o^2 \epsilon_y (I_{xx} - I_{zz}) \cos \omega_o t \, dt \quad (331)$$

$$H_{Ez} = \int_{t_o}^{t_f} 3\omega_o^2 \epsilon_y (I_{xx} - I_{zz}) \sin \omega_o t \, dt \quad (332)$$

Substituting ϵ_y given in equation 330 into equations 331 and 332,

$$\begin{aligned} H_{Ey} &= 3\omega_o^2 (I_{xx} - I_{zz}) \int_{t_o}^{t_f} [a H_{Ey} \operatorname{sgn}(\cos \omega_o t) \\ &+ b H_{Ez} \operatorname{sgn}(\sin \omega_o t)] \cos \omega_o t \, dt \end{aligned} \quad (333)$$

$$\begin{aligned} H_{Ez} &= 3\omega_o^2 (I_{xx} - I_{zz}) \int_{t_o}^{t_f} [a H_{Ey} \operatorname{sgn}(\cos \omega_o t) \\ &+ b H_{Ez} \operatorname{sgn}(\sin \omega_o t)] \sin \omega_o t \, dt \end{aligned} \quad (334)$$

Integrating the above equations over half an orbit,

$$H_{Ey} = 6\omega_o^2 a (I_{xx} - I_{zz}) H_{Ey} \quad (335)$$

$$H_{Ez} = 6\omega_o^2 b (I_{xx} - I_{zz}) H_{Ez} \quad (336)$$

Noting that

$$\int \operatorname{sgn}(\sin \omega_o t) \cos \omega_o t \, dt = 0 \quad (337)$$

$$\int \operatorname{sgn}(\cos \omega_o t) \sin \omega_o t \, dt = 0 \quad (338)$$

when integrated over a half orbit. Solving equations 335 and 336 for a and b ,

$$a = b = \frac{1}{6\omega_o^2 (I_{xx} - I_{zz})} \quad (339)$$

Substituting the above expression for a and b into equation 330, ϵ_y equals

$$\epsilon_y = \frac{[H_{Ey} \operatorname{sgn}(\cos \omega_o t) + H_{Ez} \operatorname{sgn}(\sin \omega_o t)]}{6\omega_o^2 (I_{xx} - I_{zz})} \quad (340)$$

Note that ϵ_y has two discontinuities, one when $\sin \omega_o t$ switches sign and another when $\cos \omega_o t$ switches sign. The CMG momentum state $\vec{H}_{CMG}^{(I)}$ will change instantaneously at these switching points due to the instantaneous changes in vehicle momentum \vec{H}_V . But as long as the vehicle returns to the same Z-LV attitude it had prior to desaturation and therefore to the same momentum state $\vec{H}_V(t_o^-)$, the net change in CMG momentum $\Delta \vec{H}_{CMG}^{(I)}$ is due only to the gravity gradient torques acting on the vehicle.

The only remaining task is to compute the desired vehicle rate command $\vec{\omega}_D$ that will keep the vehicle spinning at the orbital rate ω_o about an axis normal to the orbital plane during desaturation. For an ideal X-POP Z-LV attitude, the vehicle angular velocity $\vec{\omega}$ equals

$$\vec{\omega} = \begin{bmatrix} \omega_o \\ 0 \\ 0 \end{bmatrix} \quad (341)$$

During the desaturation interval, $\vec{\omega}_D$ equals

$$\vec{\omega}_D = \begin{bmatrix} 1 & 0 & -\epsilon_y \\ 0 & 1 & \epsilon_x \\ \epsilon_y & -\epsilon_x & 1 \end{bmatrix} \begin{bmatrix} \omega_o \\ 0 \\ 0 \end{bmatrix} = \begin{bmatrix} \omega_o \\ 0 \\ \epsilon_y \omega_o \end{bmatrix} \quad (342)$$

Also note that whenever ϵ_y has a discontinuity so does $\vec{\omega}_D$. The desaturation offset maneuver ϵ_x and ϵ_y given in equations 326 and 340, respectively, and the above vehicle rate command $\vec{\omega}_D$ are implemented by the vehicle control law defined in section 7. Another thing that should be noted is that there are no maneuver ϵ_z about

the Z axis. A maneuver ϵ_z about the Z axis produces only a very small second order gravity gradient torque, a torque that is too small to effectively desaturate the CMG system.

X-IOP Z-LV Desaturation Case - For a X-IOP Z-LV attitude,

$(\vec{T}_{gg})_I$ equals

$$\begin{aligned}
 (\vec{T}_{gg})_I &= [\phi_{O \leftarrow V}^{(m)}(t)] \vec{T}_{gg} \\
 &\quad \text{X-IOP} \\
 &= 3\omega_o^2 \begin{bmatrix} \cos\omega_o t & 0 & \sin\omega_o t \\ 0 & 1 & 0 \\ -\sin\omega_o t & 0 & \cos\omega_o t \end{bmatrix} \begin{bmatrix} \epsilon_x (I_{zz} - I_{yy}) \\ -\epsilon_y (I_{xx} - I_{zz}) \\ 0 \end{bmatrix} \\
 &= 3\omega_o^2 \begin{bmatrix} \epsilon_x (I_{zz} - I_{yy}) \cos\omega_o t \\ -\epsilon_y (I_{xx} - I_{zz}) \\ -\epsilon_x (I_{zz} - I_{yy}) \sin\omega_o t \end{bmatrix} \quad (343)
 \end{aligned}$$

The procedure for computing ϵ_x and ϵ_y for this X-IOP Z-LV attitude is identical to the method previously described for the X-POP Z-LV case and therefore the derivation of ϵ_x and ϵ_y for this X-IOP Z-LV case is dispensed with. The resultant expression for ϵ_x and ϵ_y derived from equations 320 and 343 are:

$$\epsilon_x = \frac{[H_{Ez} \operatorname{sgn}(\sin\omega_o t) - H_{Ex} \operatorname{sgn}(\cos\omega_o t)]}{6\omega_o^2 (I_{zz} - I_{yy})} \quad (344)$$

$$\epsilon_y = \frac{H_{Ey}}{3\pi\omega_o (I_{xx} - I_{zz})} \quad (345)$$

For an ideal X-IOP Z-LV attitude, the vehicle angular velocity $\vec{\omega}$ equals

$$\vec{\omega} = \begin{bmatrix} 0 \\ \omega_o \\ 0 \end{bmatrix} \quad (346)$$

During desaturation, the desired vehicle rate command $\vec{\omega}_D$ equals

$$\vec{\omega}_D = \begin{bmatrix} 1 & 0 & -\epsilon_y \\ 0 & 1 & \epsilon_x \\ \epsilon_y & -\epsilon_x & 1 \end{bmatrix} \begin{bmatrix} 0 \\ \omega_o \\ 0 \end{bmatrix} = \begin{bmatrix} 0 \\ \omega_o \\ -\epsilon_x \omega_o \end{bmatrix} \quad (347)$$

Both the X-POP and X-IOP Z-LV desaturation laws utilize half an orbit to desaturate the CMG system.

Other Potential Solutions for ϵ_x and ϵ_y - The solutions given above for both the X-POP and X-IOP Z-LV attitudes are not unique. For the X-POP Z-LV attitude, the form of ϵ_y was assumed to be

$$\epsilon_y = a H_{Ey} \operatorname{sgn}(\cos \omega_o t) + b H_{Ez} \operatorname{sgn}(\sin \omega_o t) \quad (348)$$

Another possible form of ϵ_y that would also work is

$$\epsilon_y = c H_{Ey} \cos \omega_o t + d H_{Ez} \sin \omega_o t \quad (349)$$

where c and d are constants. A similar form for ϵ_x in the X-IOP Z-LV case could also be used.

10.4.8 Gravity Gradient CMG Desaturation Law Signal Flow Diagrams - Figures 10.20 and 10.21 are the logic signal flow diagrams for the recommended inertial and Z-LV small angle gravity gradient CMG desaturation laws, respectively.

Figure 10.20 is the signal flow diagram for the recommended gravity gradient CMG desaturation law derived in section 10.4.2. In box 1 of figure 10.20, the CMG momentum desaturation command $\Delta \vec{H}_{CMG}$ is computed. There are a number of methods of determining $\Delta \vec{H}_{CMG}$. The one used in box 1 is to compute the average CMG momentum state using N equally spaced CMG momentum samples over a half orbit during the CMG observation interval and then comparing this average value with a desired average momentum state \vec{H}_D . In box 2, the desaturation control matrices $[A']$ and $[C]$ are computed. $[A']$ and $[C]$ are defined in section 10.4.2. In box 3, using the momentum desaturation command $\Delta \vec{H}_{CMG}$ and the control matrices $[A']$ and $[C]$, the gravity gradient offset maneuver command $\vec{\epsilon}$ is computed. $\vec{\epsilon}$ is then sent to the vehicle control law where this maneuver $\vec{\epsilon}$ is implemented.

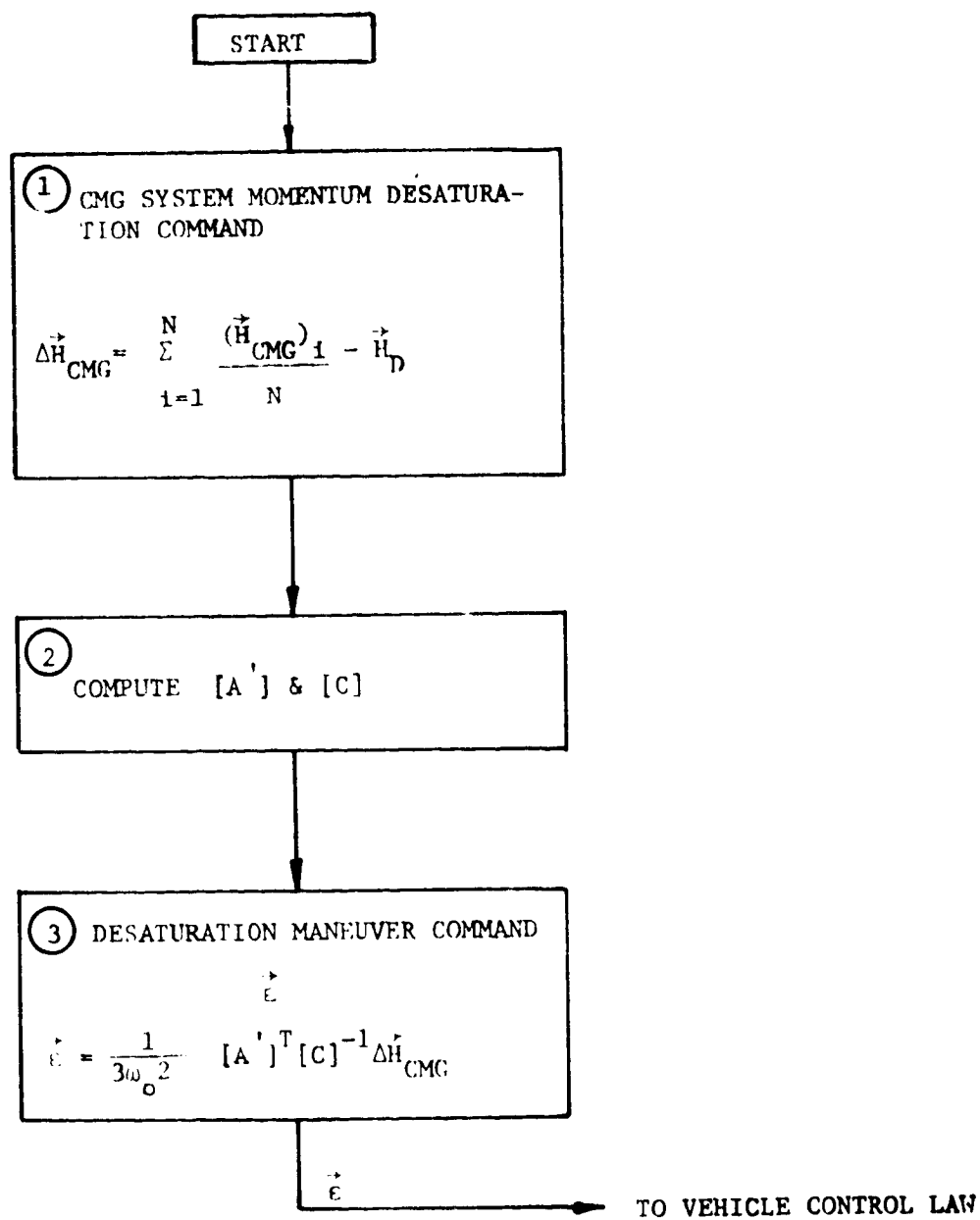


Figure 10.20. Internal Small Angle Gravity Gradient Desaturation Law Logic Flow Diagram

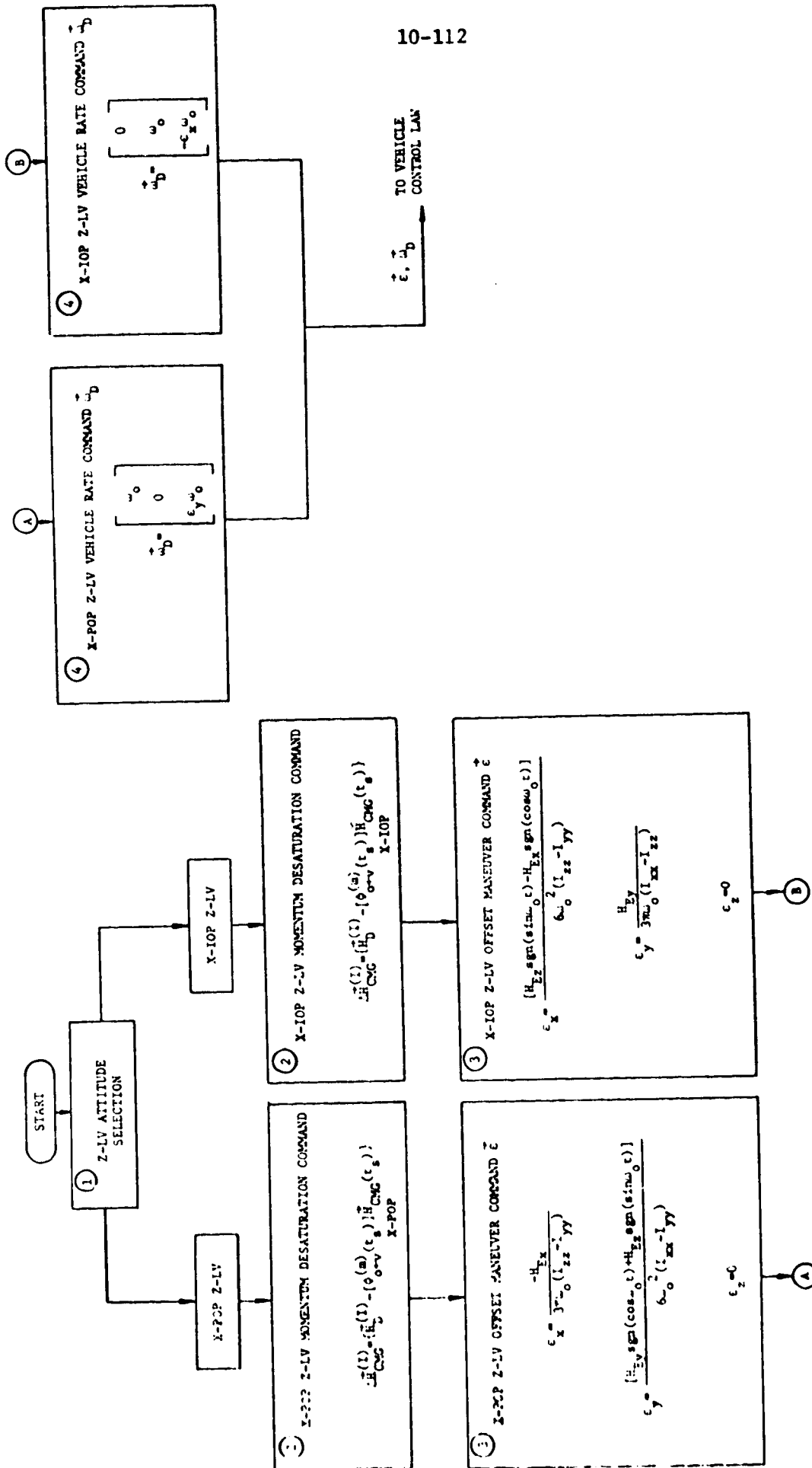


Figure 10.21. Z-LV Small Angle Gravity Gradient CMG Desaturation Law Logic Flow Diagram

Figure 10.21 is the signal flow diagram for the Z-LV gravity gradient CMG desaturation law derived in section 10.4.7. In box 1 of figure 10.21, the appropriate Z-LV attitude is determined. Depending on the vehicle Z-LV attitude, the momentum desaturation command $\Delta \vec{H}_{CMG}^{(1)}$ is computed in box 2. In box 3, the appropriate maneuver command \vec{e} is determined. The logic flow then proceeds onto box 4 where the desired vehicle rate command $\vec{\omega}_D$ is computed. The desaturation maneuver command \vec{e} and vehicle rate command $\vec{\omega}_D$ are sent to the vehicle control law. Note that this Z-LV desaturation law utilizes a full half orbit.

10.5 Selection of Baseline CMG Desaturation System - Two basic types of CMG desaturation systems have been described in this report; they are: (1) a RCS system that utilizes the vehicle baseline RCS and (2) a gravity gradient system. A RCS CMG desaturation system is more versatile than a corresponding gravity gradient system in that it can develop large desaturation torques in any direction thus desaturating the CMG system in a very short time. On the other hand, a gravity gradient CMG desaturation system requires on the average a significant portion of each orbit to desaturate the CMG system because (1) the gravity gradient torque \vec{T}_{gg} produced is orders of magnitude smaller than that generated by the baseline RCS and (2) the gravity gradient torque generated is constrained to the plane perpendicular to the local vertical vector \hat{a} ($\vec{T}_{gg} = 3\omega_o^2 [\hat{a} \times [I] \hat{a}]$). Because of this second constraint, the vehicle must be maneuvered away from its desired observation attitude in order to orient the vehicle into a favorable attitude where the gravity gradient torque will result in the desired desaturation.

The chief advantage of a RCS CMG desaturation system is that it can quickly desaturate the CMG system from any arbitrary momentum state in a very short period of time thus maximizing the time available per orbit for experimentation. Its major drawback is that it expells mass during desaturation that can be a severe source of experiment contamination. A gravity gradient desaturation system requires on the average that a significant portion of each orbit be set aside for desaturating the CMG system, thus greatly limiting the available experimentation time. The major advantage of a gravity gradient CMG system over a RCS one is that it is a contamination free system in that it expells no matter. Because the principal reason for adding a CMG system to the Shuttle is to minimize RCS contaminants, the use of a RCS CMG desaturation system would tend to defeat this purpose. Therefore, the preferred

baseline CMG desaturation system is the recommended small angle gravity gradient desaturation system documented in sections 10.4.2 and 10.4.7 for an inertial and a Z-LV held vehicle, respectively. The recommended RCS desaturation system described in section 10.3.2 is retained as a backup CMG desaturation system in order to give the system an emergency CMG desaturation capability.

10.6 Pseudo-Axis Alignment Scheme - Up to this point, the only momentum management system that has been discussed has been CMG desaturation systems. In this section, a pseudo-axis alignment control law is described that attempts to minimize the average momentum that is stored in the CMG system for the X-POP and X-IOP inertial vehicle attitudes. By minimizing the momentum stored in the CMG system, the momentum that the CMG desaturation system must "dump" on a per orbit basis is also minimized.

It has been assumed that the vehicle principal and control axes have been aligned. In general this is not the case; the vehicle control and principal axes are normally slightly misaligned. The result of this misalignment is that the vehicle cross products of inertia I_{xy} , I_{xz} , and I_{yz} are not zero. The general expression for the components of the gravity gradient torque \vec{T}_{gg} acting on a vehicle with non zero cross products of inertia are:

$$\begin{aligned} T_{gx} = 3\omega_o^2 \{ & a_y a_z (I_{zz} - I_{yy}) + a_x a_z I_{xy} \\ & - a_x a_y I_{xz} + (a_z^2 - a_y^2) I_{yz} \} \end{aligned} \quad (350)$$

$$\begin{aligned} T_{gy} = 3\omega_o^2 \{ & a_x a_z (I_{xx} - I_{zz}) + a_x a_y I_{yz} \\ & - a_x a_z I_{xy} + (a_x^2 - a_z^2) I_{xz} \} \end{aligned} \quad (351)$$

$$\begin{aligned} T_{gz} = 3\omega_o^2 \{ & a_x a_y (I_{yy} - I_{xx}) + a_y a_z I_{xz} \\ & - a_x a_z I_{yz} + (a_y^2 - a_x^2) I_{xy} \} \end{aligned} \quad (352)$$

Because the vehicle principal and control axes are assumed to be only slightly misaligned, the vehicle's cross products of inertia can be approximated by

$$I_{xy} = \epsilon_{oz} (I_{yy} - I_{xx}) \quad (353)$$

$$I_{xz} = \epsilon_{oy} (I_{xx} - I_{zz}) \quad (354)$$

$$I_{yz} = \epsilon_{ox} (I_{zz} - I_{yy}) \quad (355)$$

where ϵ_{ox} , ϵ_{oy} , and ϵ_{oz} are the misalignments between the X, Y, and Z principal and control axis, respectively. It is the above cross products of inertia resulting from these misalignments ϵ_{ox} , ϵ_{oy} , and ϵ_{oz} that increases the magnitude of the gravity gradient torque acting on the vehicle and therefore the magnitude of the resultant gravity gradient momentum that the CMG system must store.

The basic idea behind the pseudo-axis alignment scheme is to compensate for the small axial misalignments ϵ_{ox} , ϵ_{oy} , and ϵ_{oz} by performing small offset maneuvers about the vehicle control axes that minimize the CMG system momentum requirement for a particular vehicle attitude. Compensating for ϵ_{ox} , ϵ_{oy} , and ϵ_{oz} effectively reduces the vehicle cross products of inertia I_{xy} , I_{xz} , and I_{yz} to zero. For an inertial X-POP attitude, the pseudo-axis alignment scheme performs small offset maneuvers about the vehicle's Y and Z control axes in an attempt to keep the vehicle's X principal axis perpendicular to the orbital plane. By keeping the vehicle's X principal axis perpendicular to the orbital plane, the vehicle cross products of inertia are effectively reduced to zero thus minimizing the gravity gradient momentum stored in the CMG system. For an inertia X-IOP attitude, the vehicle's principal X axis is kept in the orbital plane by performing a small offset maneuver about the Z control axis.

10.6.1 Derivation of Inertial X-POP Pseudo-Axis Alignment Control Law - Assume that the unit local vertical vector \hat{a} in vehicle coordinate equals

$$\hat{a} = \begin{bmatrix} 0 \\ \cos \omega_o t \\ \sin \omega_o t \end{bmatrix} \quad (356)$$

After the pseudo-axis alignment maneuvers ϵ_{ya} and ϵ_{za} are performed about the vehicle Y and Z control axes, respectively, \hat{a} equals

$$\hat{a}' = \begin{bmatrix} a'_x \\ a'_y \\ a'_z \end{bmatrix} = \begin{bmatrix} 1 & \epsilon_{za} & -\epsilon_{ya} \\ -\epsilon_{za} & 1 & 0 \\ \epsilon_{ya} & 0 & 1 \end{bmatrix} \begin{bmatrix} 0 \\ \cos \omega_o t \\ \sin \omega_o t \end{bmatrix}$$

$$= \begin{bmatrix} \epsilon_{za} \cos \omega_o t - \epsilon_{ya} \sin \omega_o t \\ \cos \omega_o t \\ \sin \omega_o t \end{bmatrix} \quad (357)$$

Computing the averages of $a'_y a'_z$, $a'_x a'_z$, $a'_x a'_y$, $(a'_x)^2$, $(a'_y)^2$, and $(a'_z)^2$ neglecting all terms containing products or squares of ϵ_{ya} and ϵ_{za} ,

$$\overline{a'_y a'_z} = 0 \quad (358)$$

$$\overline{a'_x a'_z} = 0 \quad (359)$$

$$\overline{a'_x a'_y} = \frac{\epsilon_{za}}{2} \quad (360)$$

$$\overline{(a'_x)^2} = 0 \quad (361)$$

$$\overline{(a'_y)^2} = 1/2 \quad (362)$$

$$\overline{(a'_z)^2} = 1/2 \quad (363)$$

Substituting equations 358 thru 363 into equations 350 thru 352, the average gravity gradient torques acting on the vehicle are:

$$\overline{T}_{gx} = \frac{-3\omega_o^2}{2} [\epsilon_{ya} I_{xy} + \epsilon_{za} I_{xz}] \quad (364)$$

$$\overline{T}_{gy} = \frac{-3\omega_o^2}{2} [\epsilon_{ya} (I_{xx} - I_{zz}) - \epsilon_{ya} I_{yz} + I_{xz}] \quad (365)$$

$$\overline{T}_{gz} = \frac{-3\omega_o^2}{2} [\epsilon_{za} (I_{yy} - I_{xx}) + \epsilon_{ya} I_{yz} + I_{xy}] \quad (366)$$

By integrating the above average gravity gradient torques over one orbit, the resultant average gravity gradient angular momentum equals

$$\bar{H}_{gx} = -3\pi\omega_o [\epsilon_{ya} I_{xy} + \epsilon_{za} I_{xz}] \quad (367)$$

$$\bar{H}_{gy} = -3\pi\omega_o [\epsilon_{ya} (I_{xx} - I_{zz}) - \epsilon_{za} I_{yz} + I_{xz}] \quad (368)$$

$$\bar{H}_{gz} = 3\pi\omega_o [\epsilon_{za} (I_{yy} - I_{xx}) + \epsilon_{ya} I_{yz} + I_{xy}] \quad (369)$$

By judiciously substituting the approximations for I_{xy} , I_{xz} , and I_{yz} given in equations 353 thru 355 into equations 367 thru 369, the gravity gradient momentum equations are:

$$\bar{H}_{gx} = 0 \quad (370)$$

$$\bar{H}_{gy} = -3\pi\omega_o [\epsilon_{ya} (I_{xx} - I_{zz}) + I_{xz}] \quad (371)$$

$$\bar{H}_{gz} = -3\pi\omega_o [\epsilon_{za} (I_{yy} - I_{xx}) + I_{xy}] \quad (372)$$

If ϵ_{ya} and ϵ_{za} are zero, the momentum that the CMG system will accumulate during one orbit equals

$$\bar{H}_{x \text{ CMG}} = 0 \quad (373)$$

$$\bar{H}_{y \text{ CMG}} = -3\pi\omega_o I_{xy} \quad (374)$$

$$\bar{H}_{z \text{ CMG}} = -3\pi\omega_o I_{xy} \quad (375)$$

Equations 370 thru 372 can be written as

$$\bar{H}_{gx} = 0 \quad (376)$$

$$\bar{H}_{gy} = k_1 \epsilon_{ya} + \bar{H}_{y \text{ CMG}} \quad (377)$$

$$\bar{H}_{gz} = k_2 \epsilon_{za} + \bar{H}_{z \text{ CMG}} \quad (378)$$

where

$$k_1 = 3\pi\omega_o (I_{zz} - I_{xx}) \quad (379)$$

$$k_2 = 3\pi\omega_o (I_{yy} - I_{xx}) \quad (380)$$

If this pseudo-axis misalignment scheme operates properly \bar{H}_{gy} and \bar{H}_{gz} will equal zero.

$$\bar{H}_{gy} = k_1 \epsilon_{ya} + \bar{H}_{y \text{ CMG}} = 0 \quad (381)$$

$$\bar{H}_{gz} = k_2 \epsilon_{za} + \bar{H}_{z \text{ CMG}} = 0 \quad (382)$$

Solving equations 381 and 382 for the pseudo-axis alignment maneuvers ϵ_{ya} and ϵ_{za} ,

$$\epsilon_{ya} = \frac{-\bar{H}_{y \text{ CMG}}}{k_1} \quad (383)$$

$$\epsilon_{za} = \frac{-\bar{H}_{z \text{ CMG}}}{k_2} \quad (384)$$

The average momentum stored in the CMG system $\bar{H}_{y \text{ CMG}}$ and $\bar{H}_{z \text{ CMG}}$ can be determined by sampling the momentum stored in the CMG system. The above offset maneuvers ϵ_{ya} and ϵ_{za} correspond to offsets from the previously held vehicle attitude. The total vehicle offset commands $\epsilon_{ya}^{(T)}$ and $\epsilon_{za}^{(T)}$ equal

$$\epsilon_{ya}^{(T)} = \epsilon_{ya}^{(P)} + \epsilon_{ya} \quad (385)$$

$$\epsilon_{za}^{(T)} = \epsilon_{za}^{(P)} + \epsilon_{za} \quad (386)$$

where $\epsilon_{ya}^{(P)}$ and $\epsilon_{za}^{(P)}$ are the previous orbit offset commands $\epsilon_{ya}^{(T)}$ and $\epsilon_{za}^{(T)}$. Assuming that the CMG system is desaturated once an orbit these offset maneuvers $\epsilon_{ya}^{(T)}$ and $\epsilon_{za}^{(T)}$ are performed at the end of each desaturation interval.

10.6.2 Derivation of Inertial X-IOP Pseudo-Axis Alignment Control Law - Assume that \hat{a} in vehicle coordinates equal

$$\hat{a} = \begin{bmatrix} -\cos \omega_o t \\ \sin \lambda \sin \omega_o t \\ \cos \lambda \sin \omega_o t \end{bmatrix} \quad (387)$$

After the pseudo-axis alignment maneuver ϵ_{za} is performed about the vehicle Z control axis, \hat{a} equals

$$\begin{aligned} \hat{a}' &= \begin{bmatrix} a'_x \\ a'_y \\ a'_z \end{bmatrix} = \begin{bmatrix} 1 & \epsilon_{za} & 0 \\ -\epsilon_{za} & 1 & 0 \\ 0 & 0 & 1 \end{bmatrix} \begin{bmatrix} -\cos \omega_o t \\ \sin \lambda \sin \omega_o t \\ \cos \lambda \sin \omega_o t \end{bmatrix} \\ &= \begin{bmatrix} -\cos \omega_o t + \epsilon_{za} \sin \lambda \sin \omega_o t \\ \epsilon_{za} \cos \omega_o t + \sin \lambda \sin \omega_o t \\ \cos \lambda \sin \omega_o t \end{bmatrix} \end{aligned} \quad (388)$$

Computing the averages of $a'_y a'_z$, $a'_x a'_z$, $a'_x a'_y$, $(a'_x)^2$, $(a'_y)^2$, and $(a'_z)^2$ and neglecting all terms containing squares of ϵ_{za} ,

$$\overline{a'_y a'_z} = \frac{\sin 2\lambda}{4} \quad (389)$$

$$\overline{a'_x a'_z} = \frac{\epsilon_{za} \sin 2\lambda}{4} \quad (390)$$

$$\overline{a'_x a'_y} = -\frac{\epsilon_{za} \cos^2 \lambda}{2} \quad (391)$$

$$\overline{(a'_x)^2} = 1/2 \quad (392)$$

$$\overline{(a'_y)^2} = \frac{\sin^2 \lambda}{2} \quad (393)$$

$$\overline{(a'_z)^2} = \frac{\cos^2 \lambda}{2} \quad (394)$$

Substituting the above expressions and the approximations for I_{xy} , I_{xz} , and I_{yz} given in equations 353 thru 355 into the gravity gradient torque equations and neglecting all products of ϵ_{za} , ϵ_{ox} , ϵ_{oy} , and ϵ_{oz} , the average gravity gradient torques acting on the inertial X-IOP vehicle are:

$$\bar{T}_{gx} = \frac{3\omega_o^2}{4} \{ (I_{zz} - I_{yy}) \sin 2\lambda + 2(\cos 2\lambda) I_{yz} \} \quad (395)$$

$$\bar{T}_{gy} = \frac{3\omega_o^2}{4} \{ (I_{xx} - I_{zz}) \epsilon_{za} \sin 2\lambda + (\sin 2\lambda) I_{xy} + 2(\sin^2 \lambda) I_{xz} \} \quad (396)$$

$$\bar{T}_{gz} = \frac{3\omega_o^2}{4} \{ -2(I_{yy} - I_{xx}) \epsilon_{za} \cos^2 \lambda + (\sin 2\lambda) I_{xz} - 2(\cos^2 \lambda) I_{xy} \} \quad (397)$$

Integrating the above average gravity gradient torques over one orbit, the resultant average gravity gradient angular momentum equals

$$\bar{H}_{gx} = \frac{3\pi\omega_o}{2} \{ (I_{zz} - I_{yy}) \sin 2\lambda + 2(\cos 2\lambda) I_{yz} \} \quad (398)$$

$$\bar{H}_{gy} = \frac{3\pi\omega_o}{2} \{ (I_{xx} - I_{zz}) \epsilon_{za} \sin 2\lambda + (\sin 2\lambda) I_{xy} + 2(\sin^2 \lambda) I_{xz} \} \quad (399)$$

$$\bar{H}_{gz} = \frac{3\pi\omega_o}{2} \{ -2(I_{yy} - I_{xx}) \epsilon_{za} \cos^2 \lambda + (\sin 2\lambda) I_{xz} - 2(\cos^2 \lambda) I_{xy} \} \quad (400)$$

If ϵ_{za} is zero, the momentum that the CMG system will accumulate during one orbit equals

$$\bar{H}_{x \text{ CMG}} = \bar{H}_{gx} \quad (401)$$

$$\bar{H}_{y \text{ CMG}} = \frac{3\pi\omega_o}{2} \{ (\sin 2\lambda) I_{xy} + 2(\sin^2 \lambda) I_{xz} \} \quad (402)$$

$$\bar{H}_{z \text{ CMG}} = \frac{3\pi\omega_o}{2} \{ (\sin 2\lambda) I_{xz} - 2(\cos^2 \lambda) I_{xy} \} \quad (403)$$

Equations 398 thru 400 can be written as

$$\bar{H}_{gx} = \bar{H}_x \text{ CMG} \quad (404)$$

$$\bar{H}_{gy} = k_1 \epsilon_{za} + \bar{H}_y \text{ CMG} \quad (405)$$

$$\bar{H}_{gz} = k_2 \epsilon_{za} + \bar{H}_z \text{ CMG} \quad (406)$$

where

$$k_1 = \frac{3\pi\omega_0}{2} (I_{xx} - I_{zz}) \sin 2\lambda \quad (407)$$

$$k_2 = -3\pi\omega_0 (I_{yy} - I_{xx}) \cos^2 \lambda \quad (408)$$

If this pseudo-axis misalignment scheme operates properly \bar{H}_{gy} and \bar{H}_{gz} will equal zero.

$$\bar{H}_{gy} = k_1 \epsilon_{za} + \bar{H}_y \text{ CMG} = 0 \quad (409)$$

$$\bar{H}_{gz} = k_2 \epsilon_{za} + \bar{H}_z \text{ CMG} = 0 \quad (410)$$

Solving equations 409 and 410 for ϵ_{za} , ϵ_{za} equals

$$\epsilon_{za} = \frac{-\bar{H}_y \text{ CMG}}{k_1} \quad (411)$$

$$\epsilon_{za} = \frac{-\bar{H}_z \text{ CMG}}{k_2} \quad (412)$$

From equations 411 and 412 there appears to be two possible solutions for ϵ_{za} . But if the vehicle moments of inertia I_{yy} and I_{zz} are approximately equal, the two values of ϵ_{za} computed above are also approximately equal; this can be shown by substituting the appropriate expressions of $\bar{H}_y \text{ CMG}$, $\bar{H}_z \text{ CMG}$, k_1 , and k_2 into the above equations. Since for the vehicle used in this study, section 3, I_{yy} and I_{zz} are approximately equal, either of the two above expressions can be used to compute ϵ_{za} . The average momentum stored in

the CMG system \bar{H}_y CMG and \bar{H}_z CMG can be computed by sampling the momentum stored in the CMG system. As in the X-POP case, $\epsilon_{za}^{(P)}$ corresponds to an update of the total offset angle $\epsilon_{za}^{(T)}$ from the previous orbit. The new updated value of $\epsilon_{za}^{(P)}$, $\epsilon_{za}^{(T)}$ equals

$$\epsilon_{za}^{(T)} = \epsilon_{za}^{(P)} + \epsilon_{za} \quad (413)$$

Assuming that the CMG system is desaturated once an orbit this offset maneuver $\epsilon_{za}^{(T)}$ is performed at the end of each desaturation interval.

If a gravity gradient desaturation system is used to desaturate the CMG system, the effects of the pseudo-axis alignment offset maneuvers for both the X-POP and X-IOP cases must be accounted for in the desaturation law.

10.7 Notes

10.7.1 Symbols and Abbreviations

\hat{a}	Unit local vertical vector in vehicle coordinates
\hat{a}_0	Unit local vertical vector in orbital reference frame
CMG	Control moment gyro
g	Gravitational acceleration of the Earth (32.2 ft/sec ²)
H	Magnitude of CMG wheel momentum
\vec{H}_c	Total system momentum measured in Z-LV inertial reference frame
\vec{H}_{CMG}	CMG system momentum imparted to the vehicle
$\vec{H}_{CMG}^{(I)}$	CMG momentum state measured in Z-LV inertial reference frame
$\vec{H}_D^{(I)}$	Desired Z-LV CMG momentum state
\vec{H}_v	Vehicle momentum
$\Delta \vec{H}_{CMG}$	CMG momentum desaturation command (inertial case)
$\Delta \vec{H}_{CMG}^{(I)}$	CMG momentum desaturation command (Z-LV case)

$\Delta \vec{H}_v$	Change in vehicle momentum
I	Identity matrix
I_{ii}	Vehicle moments of inertia ($i=x,y,z$)
I_{ij}	Vehicle cross products of inertia ($i=x,y,z$, $j=x,y,z, i \neq j$)
I_{sp}	RCS fuel specific impulse
[I]	Vehicle inertia tensor
L	Lagrange adjoint equation
ℓ_i	RCS moment arms ($i=x,y,z$)
min	Arc minute
P	Performance index
R	Mean radius of the Earth
r	Distance from the center of the Earth to vehicle center of mass
RCS	Reaction control system
s	Laplace operator
t	Time in seconds
\vec{T}_{gg}	Gravity gradient torque
$(\vec{T}_{gg})_I$	Z-LV gravity gradient torque observed in Z-LV inertial reference frame
W.O.F.	Weight of fuel
X-IOP	X axis in the orbital plane
X-POP	X axis perpendicular to the orbital plane
Z-LV	Z axis along local vertical
$\delta_{1(i)}$	Inner CMG gimbal angle ($i=1,\dots,6$)
$\delta_{3(i)}$	Outer CMG gimbal angle ($i=1,\dots,6$)
$\dot{\delta}_{1(i)}$	Inner CMG gimbal rate ($i=1,\dots,6$)
$\dot{\delta}_{3(i)}$	Outer CMG gimbal rate ($i=1,\dots,6$)
ϵ	Vehicle offset maneuver
ϵ_{oi}	Vehicle principal and control axis misalignment ($i=x,y,z$)
$\epsilon_{ya}, \epsilon_{za}$	Pseudo-axis alignment maneuver
θ_o	RCS attitude deadband limit
$[\Phi_{v \rightarrow o}]$	Transformation from orbital to vehicle coordinate frame
$[\Phi_D]$	Transformation from reference to desired vehicle attitude
λ	Lagrange multiplier
$\vec{\omega}$	Vehicle angular velocity
$\vec{\omega}_D$	Desired vehicle rate command
ω_o	Vehicle orbital rate

10.7.2 References

1. Frik, Martin A., Desaturation of the ATM Control System By Gravity Gradient Torques, Marshall Space Flight Center, NASA TM-X53783, August 23, 1968.
2. Ingwerson, D. R., CMG Momentum Dumping During ATM Operation, Lockheed Missiles and Space Company, Sunnyvale, California, Enclosure (1) to LMSC/A842116, February 7, 1967.
3. Kennel, H. F., Large Angle Method for Space Vehicle Angular Momentum Desaturation Using Gravity Torques, Marshall Space Flight Center, NASA TM X-53748, May 27, 1968.
4. Kennel, H. F., Large Angle Method for Space Vehicle Angular Momentum Desaturation Using Gravity Torques, Marshall Space Flight Center, NASA TM X-53958, October 14, 1969.
5. Powell, B. K., CMG Desaturation for the RAM Using Gravity Tracking, The Bendix Corporation, Research Laboratories, Southfield, Michigan, Letter No. 7613-E71-6, August 17, 1971.
6. Powell, B. K., Gravity Gradient Momentum Management of a Solar Oriented Space Vehicle, The Bendix Corporation, Research Laboratories, Southfield, Michigan, Report 5315, October 1970.
7. Rybak, C., Gravity Gradient Momentum Dump of the CSM/LM/ATM Vehicle Configuration, The Bendix Corporation, Navigation and Control Division, Denver, Colorado, MT-1617, February 22, 1968.

11. REVIEW OF SELECTED CMG CONTROL LOGIC

The CMG control logic selected in sections 8 thru 10 are:

CMG Maneuver Control Law

- Quaternion CMG Maneuver Control Law (section 8.2)

CMG Gimbal Rate Command Law

- Pseudo-Inverse CMG Control Law (section 9.4.4)
- Optimal CMG Distribution Law (section 9.5.3)
- Operational Mode: six individual CMG operating mode

CMG Momentum Management

- Primary CMG Desaturation Law: Small Angle Gravity Gradient CMG Desaturation Law (inertial, section 10.4.2; Z-LV, section 10.4.7)
- Back-Up CMG Desaturation Law: RCS Attitude Control CMG Desaturation Law (section 10.3.2)
- Pseudo-Axis CMG Alignment Control Law (section 10.6)

12. COMPUTER VERIFICATION

The purpose of this section is to document the hybrid computer simulation study used to verify proper operation of the selected CMG attitude control system described in section 11.

12.1 Simulated CMG Control System - The selected CMG control system consists of six Skylab ATM type double gimbal CMGs. Each CMG has a wheel momentum of 2,300 ft-lb-sec. Therefore, the total CMG system momentum storage capability is 13,800 ft-lb-sec. The assumed CMG mounting configuration is shown in figure 12.1. Two CMGs are identically mounted along each of the three vehicle principal axes as shown in this figure. The CMG system was operated as six individual actuators rather than the slaved CMG operational mode also described in this report.

The vehicle was assumed to be a rigid body. The vehicle dynamic equations of motion along with the assumed vehicle inertia matrix $[I]$ are contained in section 3. Gravity gradient torque was assumed to be the principal vehicle torque environment. The gravity gradient torque equation used is contained in section 5.2.1.

The vehicle control law employed was the standard rate plus position law described in section 7.1. The function of the vehicle control law is to generate an appropriate CMG torque command \vec{T}_{COM} .

The vehicle control law was

$$\vec{T}_{COM} = [K_r](\vec{\omega}_D - \vec{\omega}_s) + [K_p](\vec{\phi}_E + \vec{\epsilon})$$

where $\vec{\omega}_D$, $\vec{\omega}_s$, $\vec{\phi}_E$, and $\vec{\epsilon}$ are the desired vehicle angular velocity, sensed body angular velocity, vehicle attitude error, and gravity gradient CMG desaturation command, respectively. $[K_r]$ and $[K_p]$ are the vehicle control law rate and position gain matrices, respectively. The gain matrices used in this simulation are computed in section 7.

The control logic associated with a CMG attitude control system consists of four basic elements: (1) a CMG maneuver control law, (2) a CMG control law, (3) a CMG singularity avoidance scheme, and (4) a CMG desaturation law. Listed below is the selected CMG control logic corresponding to these elements along with the sections in this report where these control laws are derived.

CMG Maneuver Control Law: Quaternion Maneuver
Control Law (section 8.2)

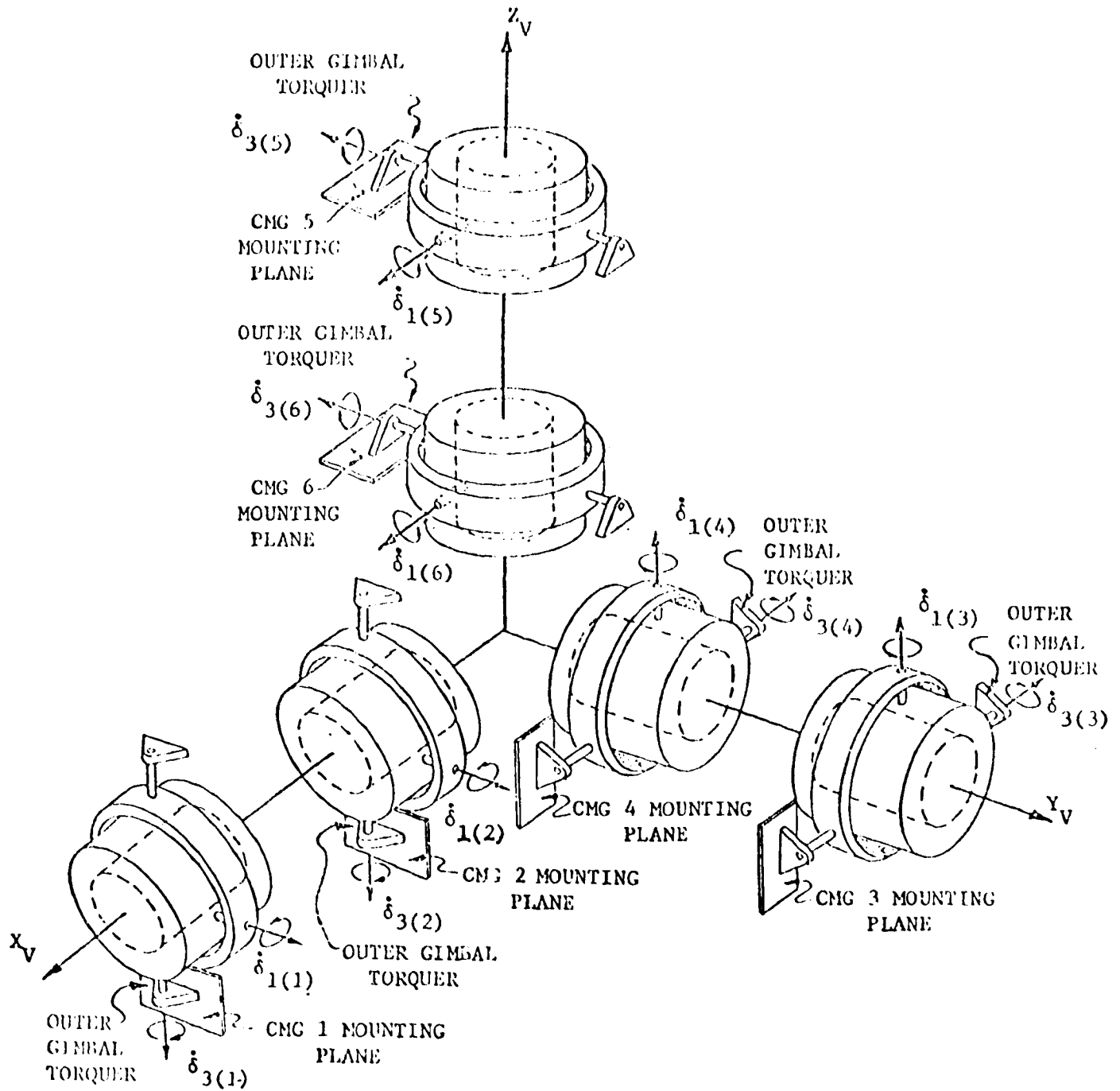


Figure 12.1. Selected CMG Mounting Configuration

CMG Control Law: Pseudo-Inverse CMG Control Law
(section 9.4.4)

CMG Singularity Avoidance Scheme: Optimal CMG
Distribution Law (section 9.5.3)

CMG Desaturation Law: Small Angle Gravity Gradient
CMG Desaturation Law (inertial case: option 2,
section 10.4.2, Z-LV case: section 10.4.7)

Figure 12.2 is a block diagram of the CMG attitude control system as implemented on the hybrid computer. Inasmuch as open loop integration on an analog computer over long periods of time is inaccurate, the vehicle orbital position and quaternion were computed on the digital computer. The gravity gradient torque was also computed on the digital computer since it is a slowly varying quantity, having a rate of change equal to twice the vehicle orbital rate of 0.001108 rad/sec as compared to the digital computer sample time of 0.7 second. To reduce the analog computer errors due to torque scaling (maximum CMG torque is an order of magnitude larger than maximum gravity gradient torque), the vehicle dynamic equations were implemented on the analog in momentum form, i.e.,

$$\begin{aligned}\vec{H}_T &= \vec{H}_{CMG} + [I] \vec{\omega} \\ \Delta \vec{H}_T &= \int_{t_1}^t (\vec{T}_g - \vec{\omega} \times \vec{H}_T) dt \\ \vec{H}_V &= \vec{H}_{T1} + \Delta \vec{H}_T - \vec{H}_{CMG} \\ \vec{\omega} &= [I]^{-1} \vec{H}_V\end{aligned}$$

12.2 Computer Study Results - The results of the computer study are given in figures 12.3 thru 12.15. The quantities shown on each of these figures are as follows:

- θ_{oc} - calculated vehicle orbital position (deg)
- $||\dot{\delta}_g||$ - Euclidean norm of the unlimited Pseudo-Inverse Steering Law gimbal rate vector (rad/sec)
- $||\dot{\delta}_s||$ - Euclidean norm of the limited ($||\dot{\delta}_s||_{max} = 0.05$ rad/sec) Pseudo-Inverse Steering Law gimbal rate vector used to control vehicle attitude (rad/sec)
- $||\nabla f||$ - Euclidean norm of the gradient of f (dimensionless)

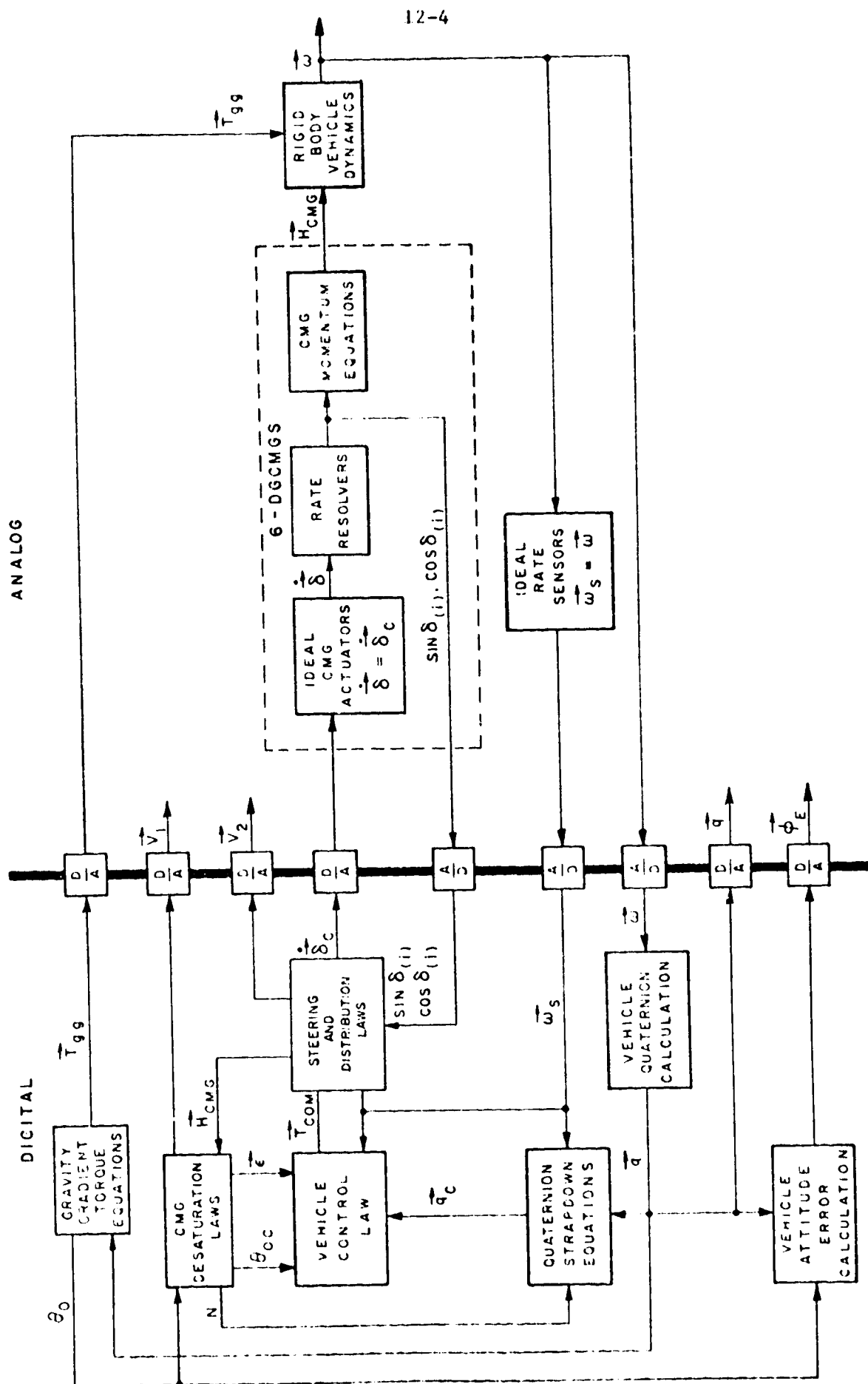


Figure 12.2. CMG Attitude Control System Block Diagram.

- $||\vec{T}_E||$ - Euclidean norm of the CMG torque that would be generated by the unlimited Singularity Avoidance Distribution Law gimbal rate vector. Since theoretically this quantity is zero, it is an error. (ft-lb)
- T_{gx} - vehicle X principal axis gravity gradient torque (ft-lb)
- T_{gy} - vehicle Y principal axis gravity gradient torque (ft-lb)
- T_{gz} - vehicle Z principal axis gravity gradient torque (ft-lb)
- $||\dot{\delta}_D||$ - Euclidean norm of the limited $(H||([A]+[B]+[C]+[D])\dot{\delta}_D||)_{\max} = ||\vec{T}_E||_{\max} = 10.0$ ft-lb Singularity Avoidance Distribution Law gimbal rate vector (rad/sec)
- f - determinant of $[A][A]^T + [B][B]^T + [C][C]^T + [D][D]^T$ defined in section 9.4.4 (dimensionless)
- $||\vec{\epsilon}||$ - Euclidean norm of the CMG Desaturation Law small angle gravity gradient CMG desaturation maneuver (deg)
- $||\vec{H}_{CMG}||$ - Euclidean norm of the total CMG momentum vector (ft-lb-sec)
- ω_x - vehicle X principal axis rate (rad/sec)
- ω_y - vehicle Y principal axis rate (rad/sec)
- ω_z - vehicle Z principal axis rate (rad/sec)
- q_1 - first component of the vehicle quaternion vector (dimensionless)
- q_2 - second component of the vehicle quaternion vector (dimensionless)
- q_3 - third component of the vehicle quaternion vector (dimensionless)
- q_4 - fourth component of the vehicle quaternion vector (dimensionless)
- ϕ_{Ex} - vehicle X principal axis attitude error (desired attitude minus achieved attitude) (arc-min)
- ϕ_{Ey} - vehicle Y principal axis attitude error (arc-min)

ϕ_{Ez} - vehicle Z principal axis attitude error (arc-min)

Computer runs were made to determine the response of the CMG attitude control system, to determine the ability of the distribution law to avoid CMG singularity, and to determine the ability of the desaturation law to avoid CMG saturation.

12.2.1 System Response Runs - Figure 12.3 shows the system response to impulses and steps in gravity gradient torque. These runs were performed for a vehicle orientation with the X axis perpendicular to the orbital plane (X-POP) and the vehicle Z axis pointing toward an inertially fixed target (Z-TT). The vehicle was initialized at an orbital position of 45° from mid-occultation ($\theta_{oc} = 45^\circ$). The CMGs were initialized with their inner gimbal angles at zero and their outer gimbal angles at 45 degrees, which gives zero total momentum and also satisfies the distribution law, i.e., $V_f = 0$.

The distribution law was initially allowed to bring f to its maximum value of 64. This took approximately 700 seconds. Then a step input of 0.00005 rad/sec was added to all three vehicle rate components. The position errors were allowed to settle out. Then the steps were removed and the system allowed to settle out again. The procedure was then repeated for vehicle rate steps in the opposite direction. The system response to gravity gradient torque step inputs of 20 ft-lb in the three axes was investigated in the same way. The system took approximately 30 seconds to settle out in both cases of vehicle disturbances.

12.2.2 Singularity Avoidance Runs - Figure 12.4 shows the results of the singularity avoidance runs with X-POP and Z-TT. The initial vehicle orbital position was the same as for the response runs. The initial CMG gimbal angles were selected to put four CMG momentum vectors along the Y axis, two in each direction, and the other two momentum vectors along the X axis, one in each direction. The initial gimbal angles used were:

$$\delta_{1(1)i} = 0, \delta_{3(1)i} = \frac{\pi}{2}, \delta_{1(2)i} = 0, \delta_{3(2)i} = 0, \delta_{1(3)i} = 0,$$

$$\delta_{3(3)i} = 0, \delta_{1(4)i} = 0, \delta_{3(4)i} = 0, \delta_{1(5)i} = \frac{\pi}{2}, \delta_{3(5)i} = 0,$$

$$\delta_{1(6)i} = 0, \delta_{3(6)i} = \frac{\pi}{2}.$$

A disturbance torque of 3 ft-lb was added to the Y axis gravity gradient torque to force the X axis momentum vectors toward the singular configuration with all vectors along the Y axis, four positive and two negative. Three values for maximum distribution law torque error $||\vec{T}_E||_{\max}$ were used: zero, which corresponds to having no singularity avoidance scheme; one ft-lb; and ten ft-lb, which was found to be the strongest law obtainable without causing significant vehicle attitude errors. The results show the necessity and effectiveness of the distribution law in avoiding singular momentum configurations. Without a distribution law, f comes close to zero about halfway through the run. Thus, the steering law rates become large at this point in the run. With a strong distribution law, f is quickly driven to its maximum value of 64 and held there throughout the run so that the steering law rates do not become large.

12.2.3 Orbital Runs - Figures 12.5 thru 12.15 show the results of the orbital runs. Each run shows four orbits. The calculated vehicle orbital position and quaternion were updated once per orbit at the beginning of the orbit. The CMGs were initialized in the same way as for the system response runs. With no desaturation law active, the four orbit run was started immediately. With the desaturation law active, the four orbit run was started when the CMG momentum settled into steady state.

Figures 12.5 thru 12.10 show the results of the inertial runs with the vehicle Z-axis pointing toward an inertially fixed target (Z-TT). In the runs corresponding to figures 12.5 thru 12.7, the vehicle X axis is in the orbital plane (X-IOP) and the target is 45 degrees above the orbital plane. In figures 12.8 thru 12.10, the X axis is perpendicular to the orbital plane (X-POP). The vehicle orbital position for all inertial runs was initialized to be 45 degrees from mid-occultation ($\theta_{oc} = 45^\circ$) in order to minimize CMG momentum buildup.

In figure 12.5, (X-IOP, Z-TT) no desaturation law was used. It is seen that the CMG momentum as measured by $||\vec{H}_{CMG}||$ builds up. The primary momentum accumulation occurs on the X axis because of a bias term in the X component of gravity gradient torque.

Figure 12.6 shows the results of repeating the run of figure 12.5, except that the CMG desaturation law was active about mid-occultation for half an orbit. It is seen that the law is effective in holding the momentum to below 8,000 ft-lb-sec with a maneuver angle of six degrees as measured by $||\vec{\epsilon}||$.

In figure 12.7 the vehicle principal axes were each offset 1/2 degree from the nominal orientation (Z-TT, X-IOP). This was done in order to show the effect on momentum buildup and subsequent desaturation maneuvers of misalignment between vehicle axes and vehicle principal axes. For this orientation, no significant effect resulted.

Figures 12.8 thru 12.10 show the results of repeating the runs of figures 12.5 thru 12.7, respectively, except that the X-POP orientation was used. In figure 12.8, no desaturation law was used. The heavy part of the trace of $||\delta_D||$ occurring on sheet 2 of figure 12.8 is due to the distribution law turning on when f drops below 64 and off when f reaches 64. Theoretically, there should be no CMG momentum buildup. The momentum buildup seen on this sheet is due to analog computer inaccuracy. In the absence of a desaturation law, CMG momentum is open loop. Therefore, any bias in the analog computer gravity gradient torque due to inaccuracies causes a CMG momentum buildup. For instance, a one percent bias in the maximum scaled value of gravity gradient torque of 0.2 ft-lb would result in a momentum buildup of approximately 1,000 ft-lb-sec per orbit. The computer inaccuracy momentum buildup does not invalidate the orbital runs since it can be considered due to some small vehicle disturbance torque.

From figure 12.9, which repeats the run of figure 12.8 with the desaturation law active when the vehicle is behind the earth from the target (136°), it is seen that the momentum is held to below 2,000 ft-lb-sec with a maneuver angle of 6° .

Figure 12.10 shows the results obtained with a 1/2 degree offset of each vehicle principal axis from the nominal orientation of Z-TT and X-POP. A much larger momentum buildup resulted with a 9° maneuver angle required for desaturation.

Figures 12.11 thru 12.15 show the results of the Earth pointing runs with the vehicle Z-axis pointing toward the local vertical vector (Z-LV). In the runs corresponding to figures 12.11 thru 12.13, the vehicle was in the X-IOP orientation. The runs of figures 12.14 and 12.15 are for the X-POP orientation. For all Z-LV orbital runs, the vehicle orbital position was initialized at zero ($\theta_{oc} = 0^\circ$). The vehicle rate for the axis about which the vehicle turned $_{oc}$ was initialized at the orbital rate.

Figure 12.11 corresponds to the run with X-IOP, Z-LV and no desaturation law present. Theoretically, no momentum buildup

should occur. The observed buildup is due to analog computer inaccuracy as explained above. Figure 12.12 repeats the run of the previous figure with the desaturation law active for half an orbit every other orbit. As can be seen, computer inaccuracy momentum buildup was not the same for each orbit. An average maneuver angle of 1° was required for desaturation.

In figure 12.13 with $1/2$ degree vehicle offset of each axis from the nominal X-IOP and Z-LV, much larger momentum buildups are observed. Furthermore, they are the same from orbit to orbit. This is because the momentum accumulation is mainly due to induced vehicle position errors and not to analog computer inaccuracy. A maneuver angle of 1.5° was required to desaturate 3,000 ft-lb-sec of momentum.

The results of the X-POP, Z-LV run with the CMG desaturation law are shown in figure 12.14. No momentum buildup occurred when this run was made. Therefore, although present, the desaturation law was not required.

Similarly, referring to figure 12.15 when the vehicle was offset $1/2$ degree on each axis from the nominal X-POP and Z-LV orientation, only cyclical momentum buildup occurred so that desaturation was not necessary.

LIST OF SYMBOLS

<u>SYMBOL</u>	<u>DESCRIPTION</u>
ΔQ	Finite change in the quantity Q
$\delta_{1(j)}$	Inner gimbal angle of the jth CMG; $\delta_{1(j)} = \delta_{(2j-1)}$ (j=1,...,6)
$\delta_{3(j)}$	Outer gimbal angle of the jth CMG; $\delta_{3(j)} = \delta_{(2j)}$ (j=1,...,6)
$\dot{\delta}_D$	Limited Singularity Avoidance Distribution Law gimbal rate vector
$\dot{\delta}_S$	Limited Psuedo - Inverse Steering Law gimbal rate vector
$\dot{\delta}_s$	Unlimited Psuedo - Inverse Steering Law gimbal rate vector
$\vec{\epsilon}$	Gravity Gradient Desaturation Law small angle maneuver vector
Δ	Determinant of $[A][A]^T + [B][B]^T + [C][C]^T + [D][D]^T$ defined in section 9.4.4.
$\vec{\phi}_E$	Vehicle principal axes attitude error vector
H	CMG wheel momentum
\vec{H}_{CMG}	Total CMG momentum vector
\vec{H}_T	Total (CMG plus vehicle) momentum vector
\vec{H}_V	Vehicle momentum vector
[I]	Vehicle principal axes inertia matrix
$[K_p]$	Vehicle Control Law position gain matrix

<u>SYMBOL</u>	<u>DESCRIPTION</u>
$[K_Y]$	Vehicle Control Law rate gain matrix
Q_i	Initial value of the quantity Q
Q_{\max}	Maximum value of the quantity Q
q_l	lth component of vehicle quaternion vector ($l=1, \dots, 4$).
t	time
\vec{T}_{COM}	CMG torque command
\vec{T}_E	Unlimited Distribution Law torque error vector
\vec{T}_g	Gravity gradient torque vector
θ_{oc}	Calculated vehicle orbital position
V_k	Vehicle principal axes kth component of the vector \vec{V} ($k=x, y, z$)
X-IOP	Orientation with vehicle X principal axis in orbital plane.
X-POP	Orientation with vehicle X principal axis perpendicular to orbital plane
Z-LV	Orientation with vehicle Z principal axis pointing toward the earth
Z-TT	Orientation with vehicle Z principal axis pointing toward an inertial target
$\vec{\omega}$	Vehicle angular velocity vector
$\vec{\omega}_D$	Desired vehicle angular velocity vector
$\vec{\omega}_s$	Sensed vehicle angular velocity vector
∇f	Gradient of the quantity f with respect to CMG gimbal angles
\dot{Q}	Time derivative of the quantity Q .
$ \vec{V} $	Euclidean norm of the vector \vec{V}

10 SECOND TIME MARKS

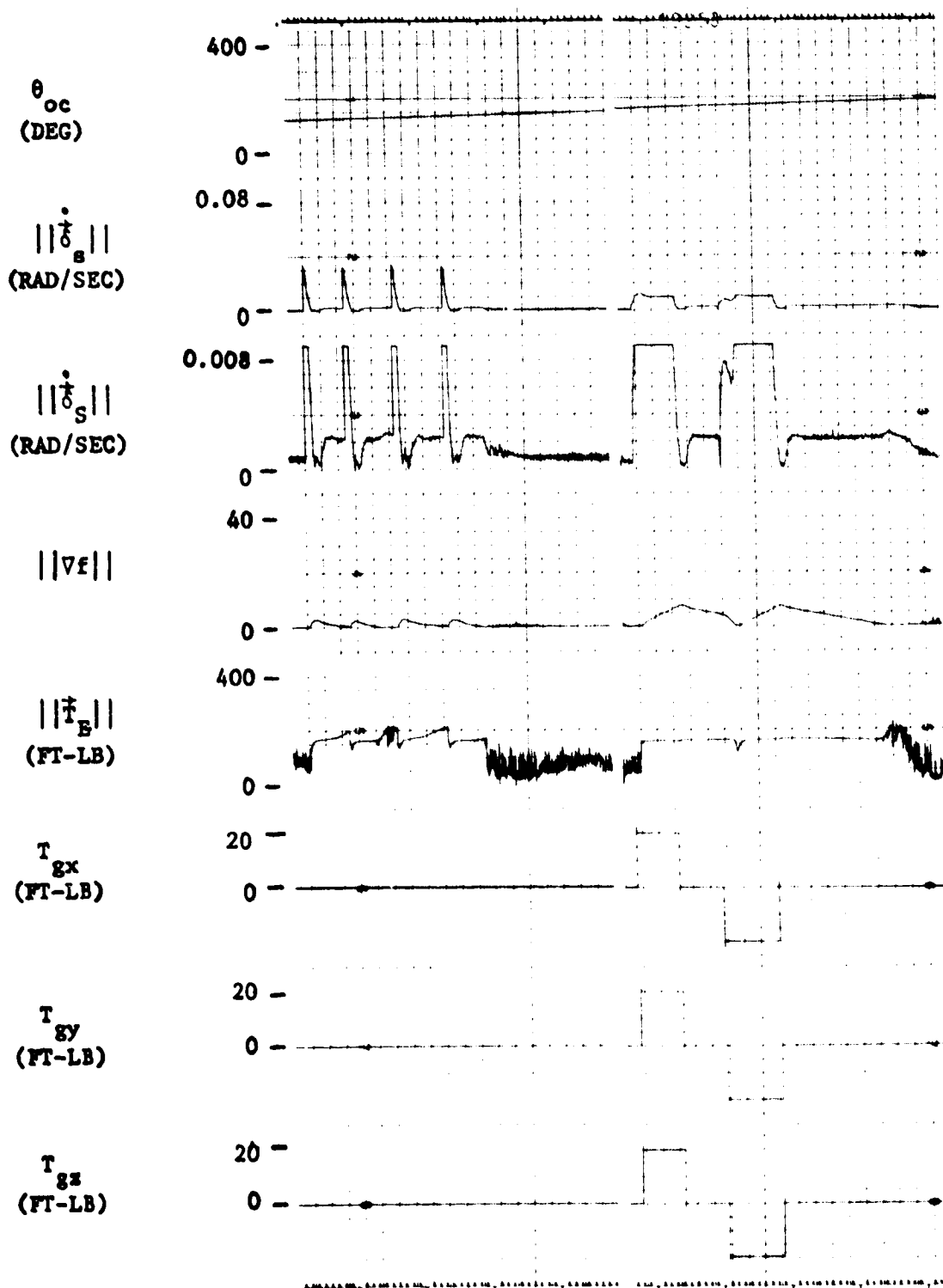


Figure 12.3 Impulse and Step Response Runs With X-POP, Z-TT (Sheet 1 of 3)

10 SECOND TIME MARKS

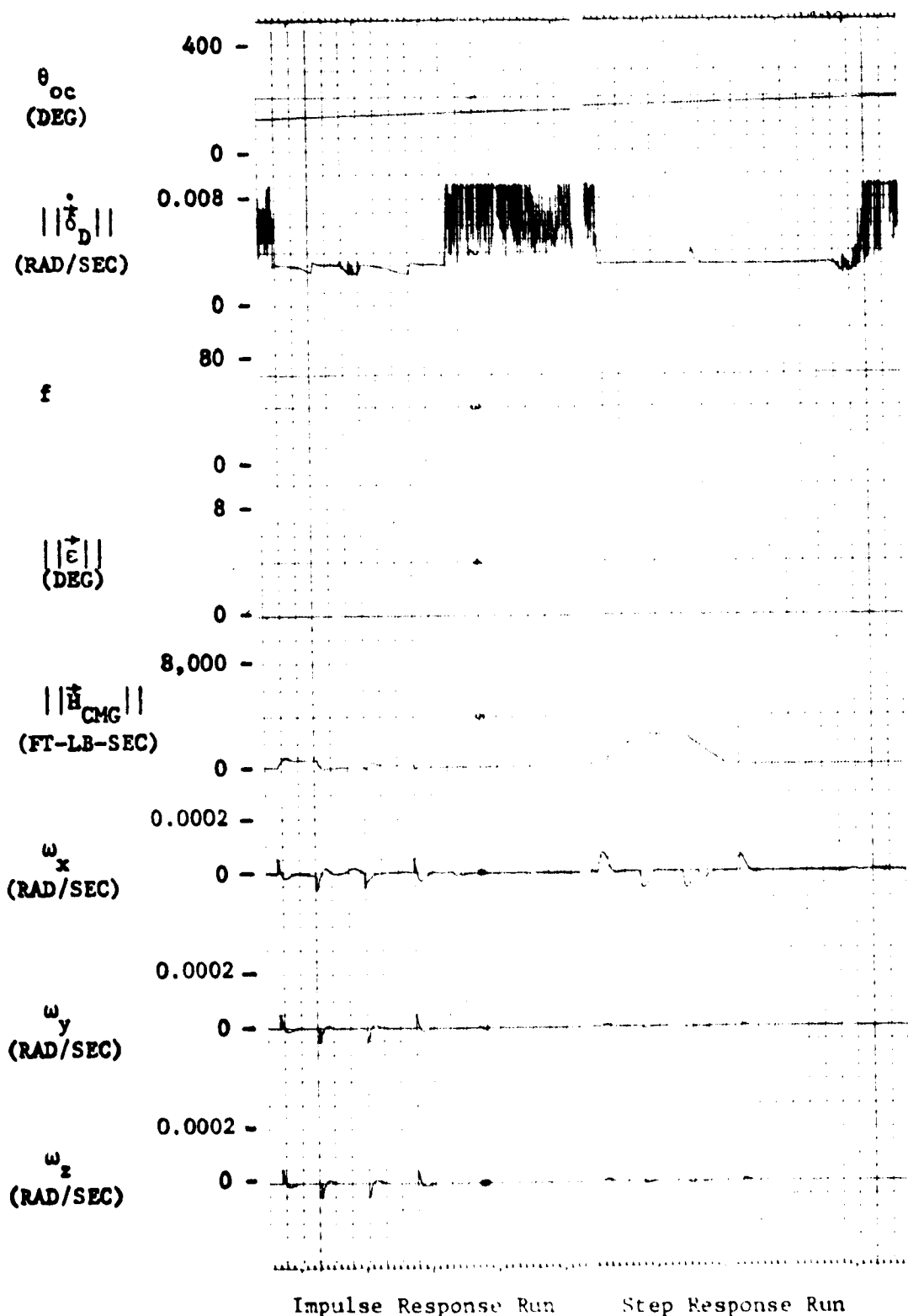


Figure 12.3 Impulse and Step Response Runs With X-POP, Z-TT (Sheet 2 of 3)

10 SECOND TIME MARKS

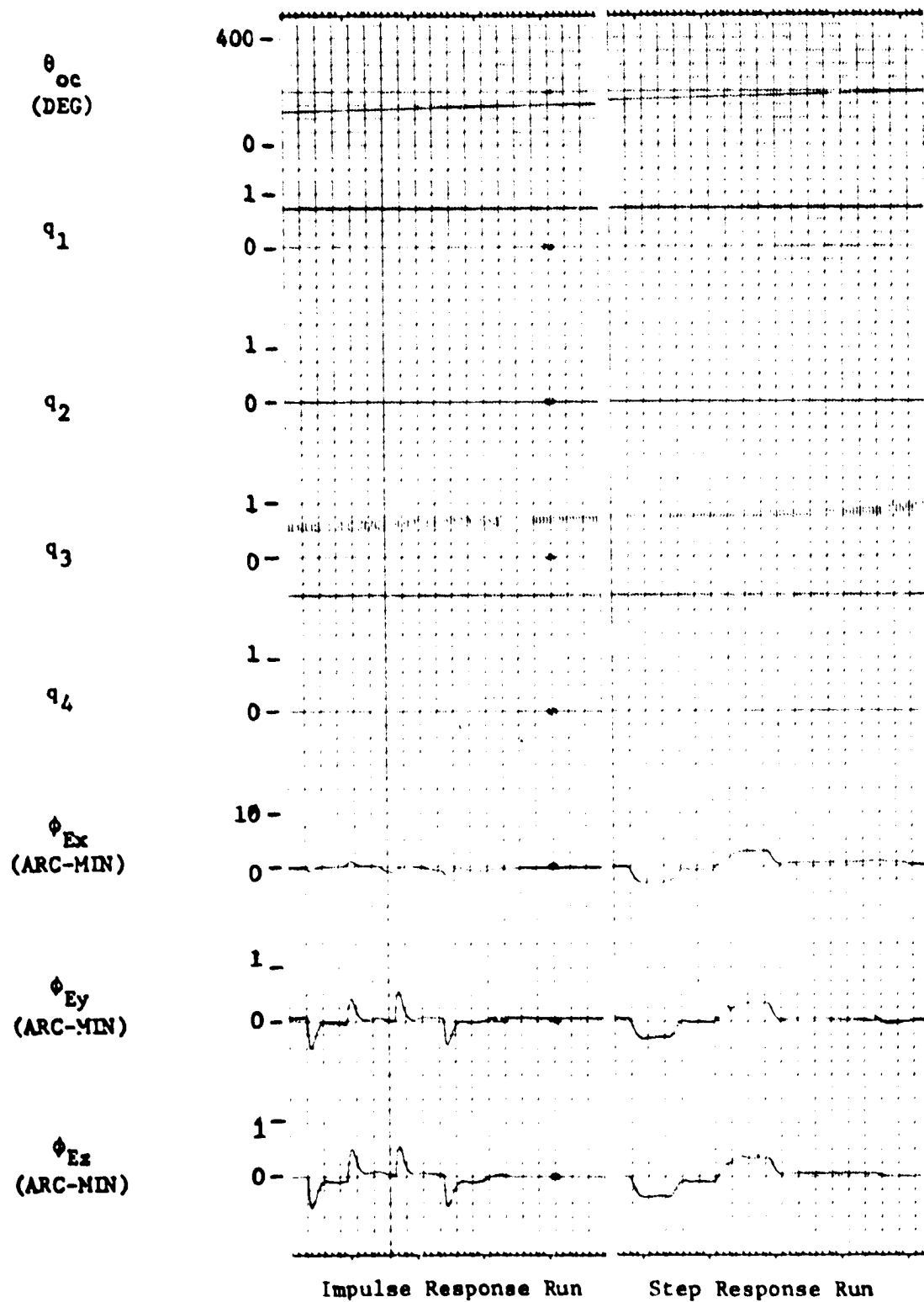


Figure 12.3 Impulse and Step Response Runs With X-POP, Z-TT (Sheet 3 of 3)

100 SECOND TIME MARKS

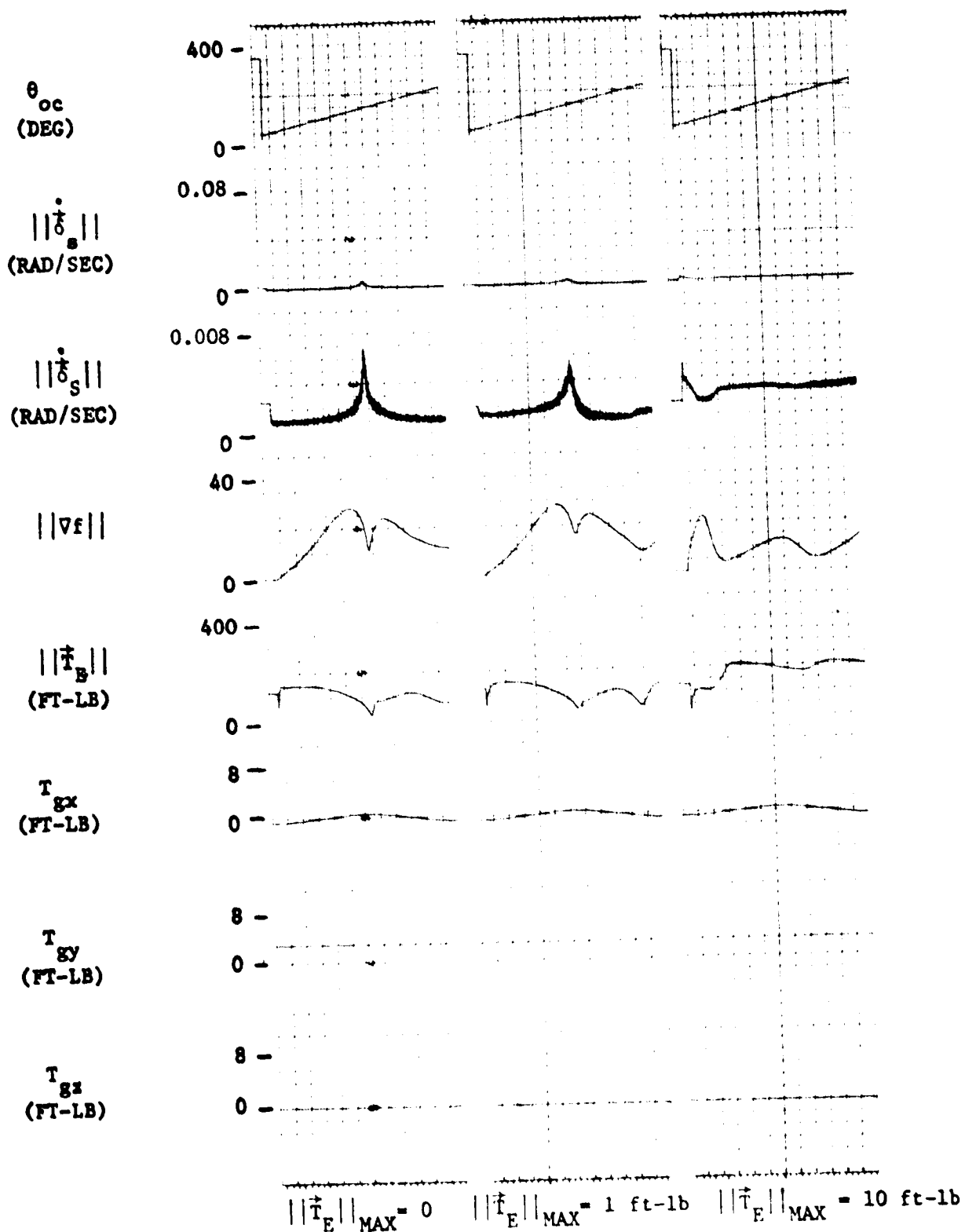


Figure 12.4 Singularity Avoidance Runs With X-POP, Z-TT (Sheet 1 of 3)

100 SECOND TIME MARKS

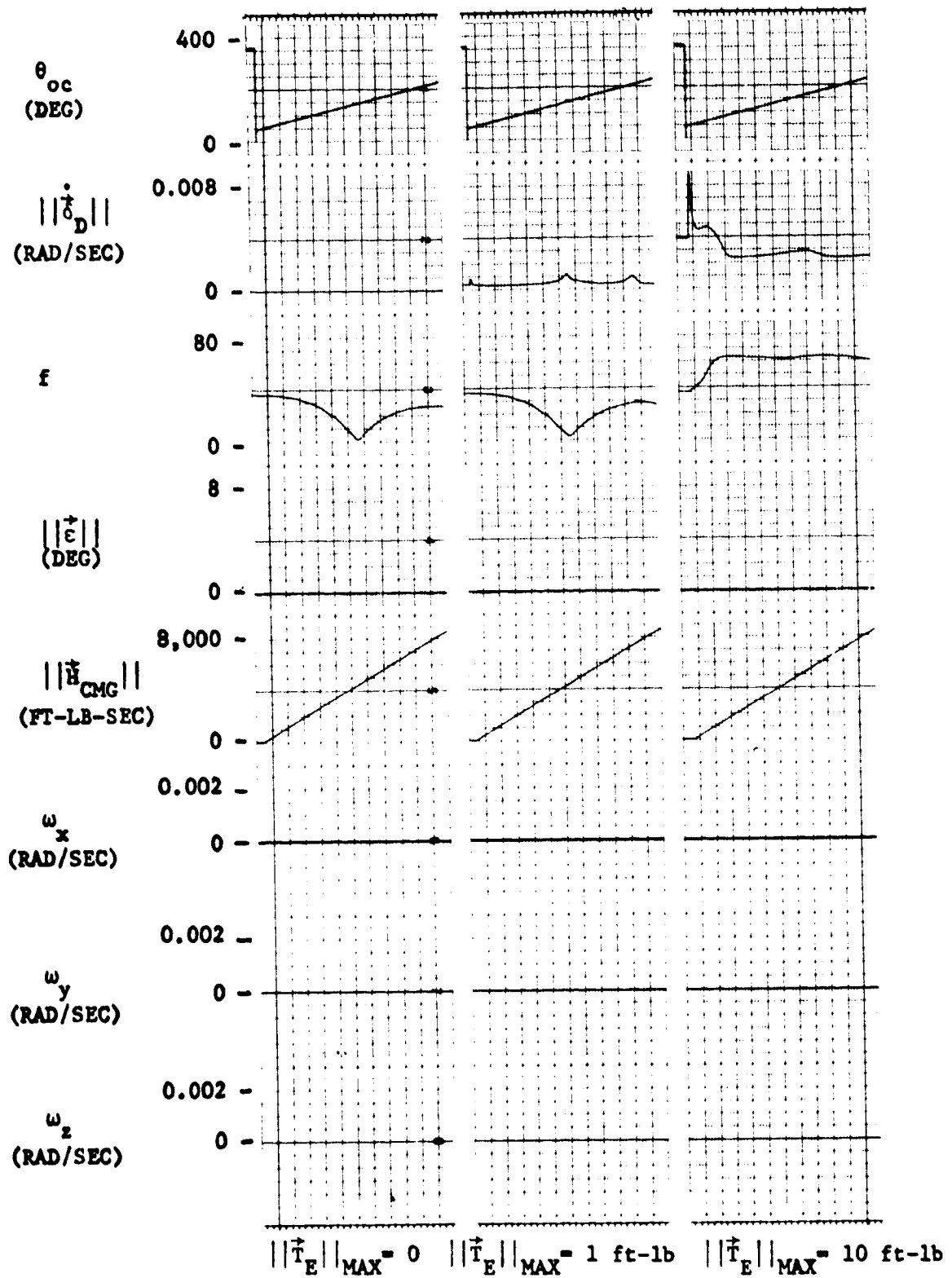


Figure 12.4 Singularity Avoidance Runs With X-POP, Z-TT (Sheet 2 of 3)

100 SECOND TIME MARKS

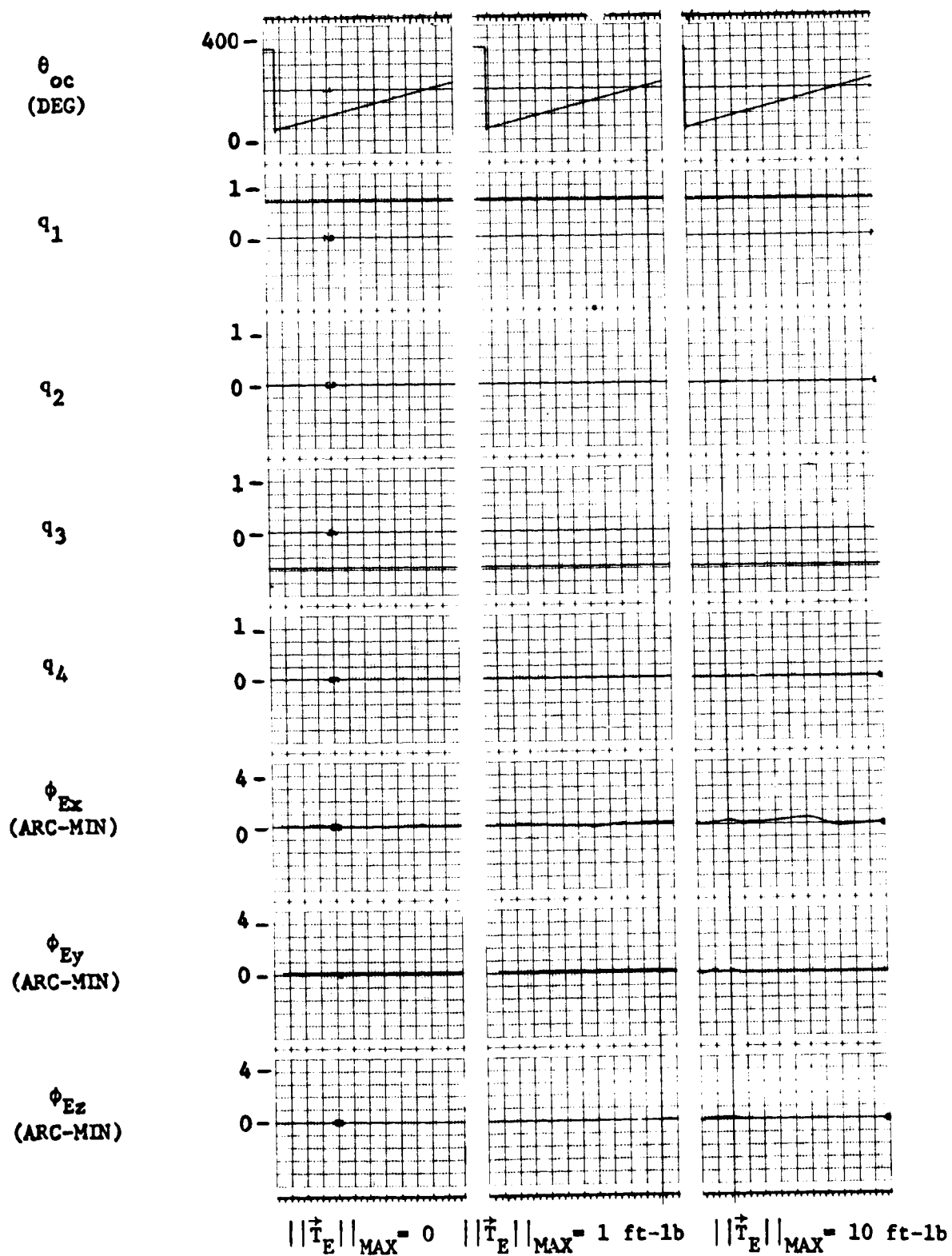


Figure 12.4 Singularity Avoidance Runs With X-POP, Z-TT (Sheet 3 of 3)

100 SECOND TIME MARKS

θ_{oc}
(DEG)

$\dot{\theta}_s$
(RAD/SEC)

$\dot{\theta}_s$
(RAD/SEC)

$||\nabla f||$

$||\dot{T}_E||$
(FT-LB)

T_{gx}
(FT-LB)

T_{gy}
(FT-LB)

T_{gz}
(FT-LB)

FOLDOUT FR

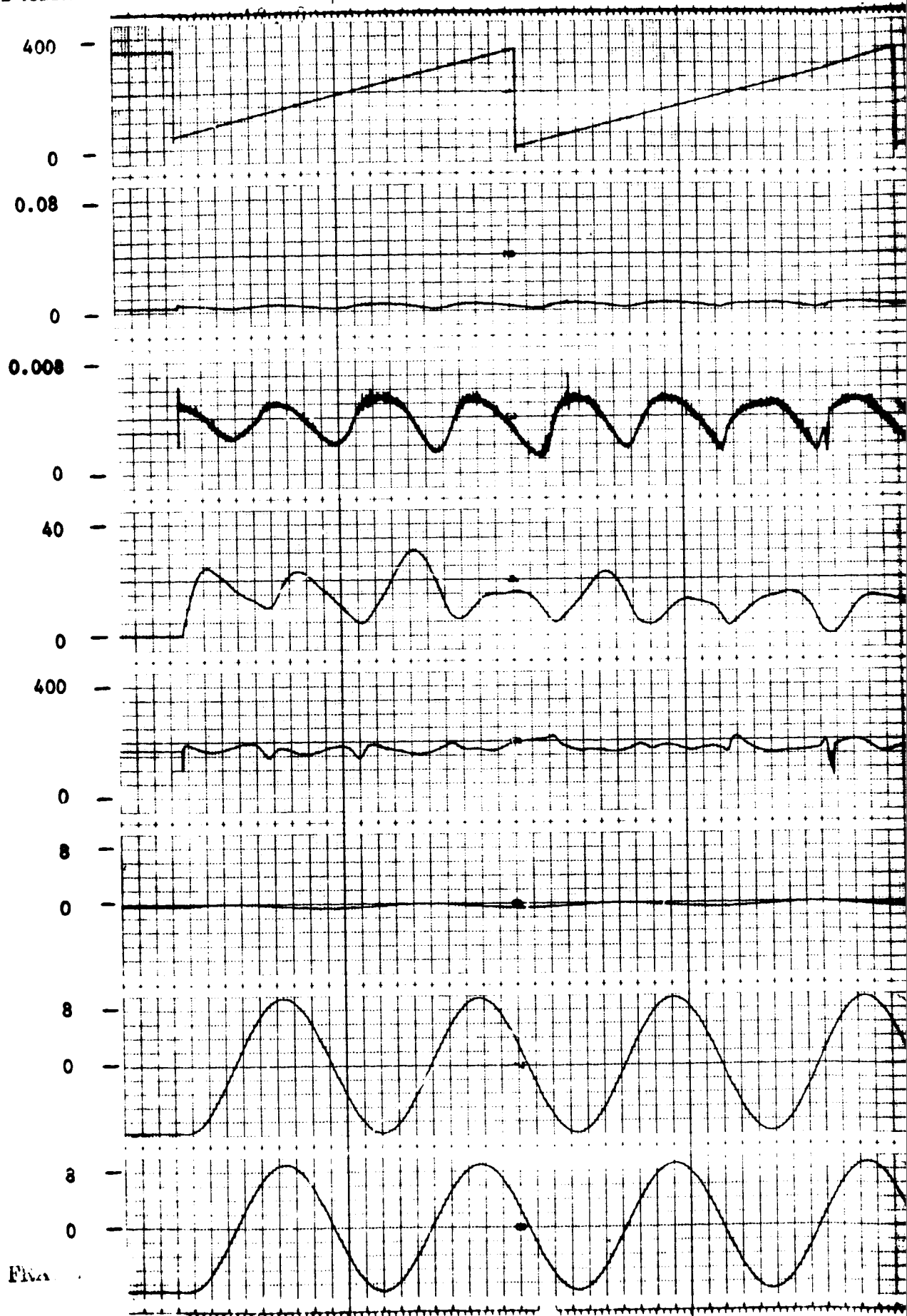
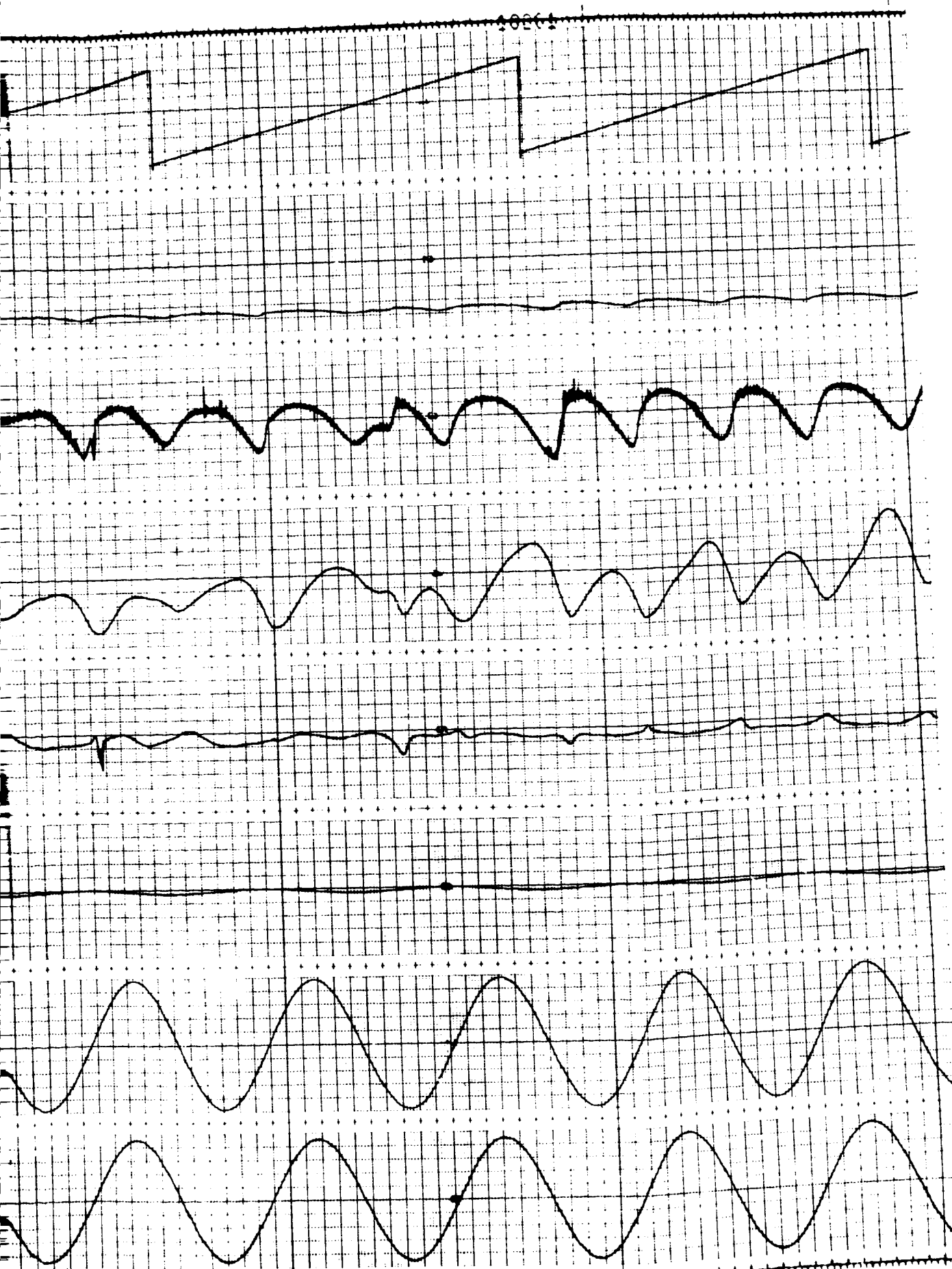


Figure 12.5. Inertial Orbital Run with X-IOP and



100 SECOND TIME MARKS

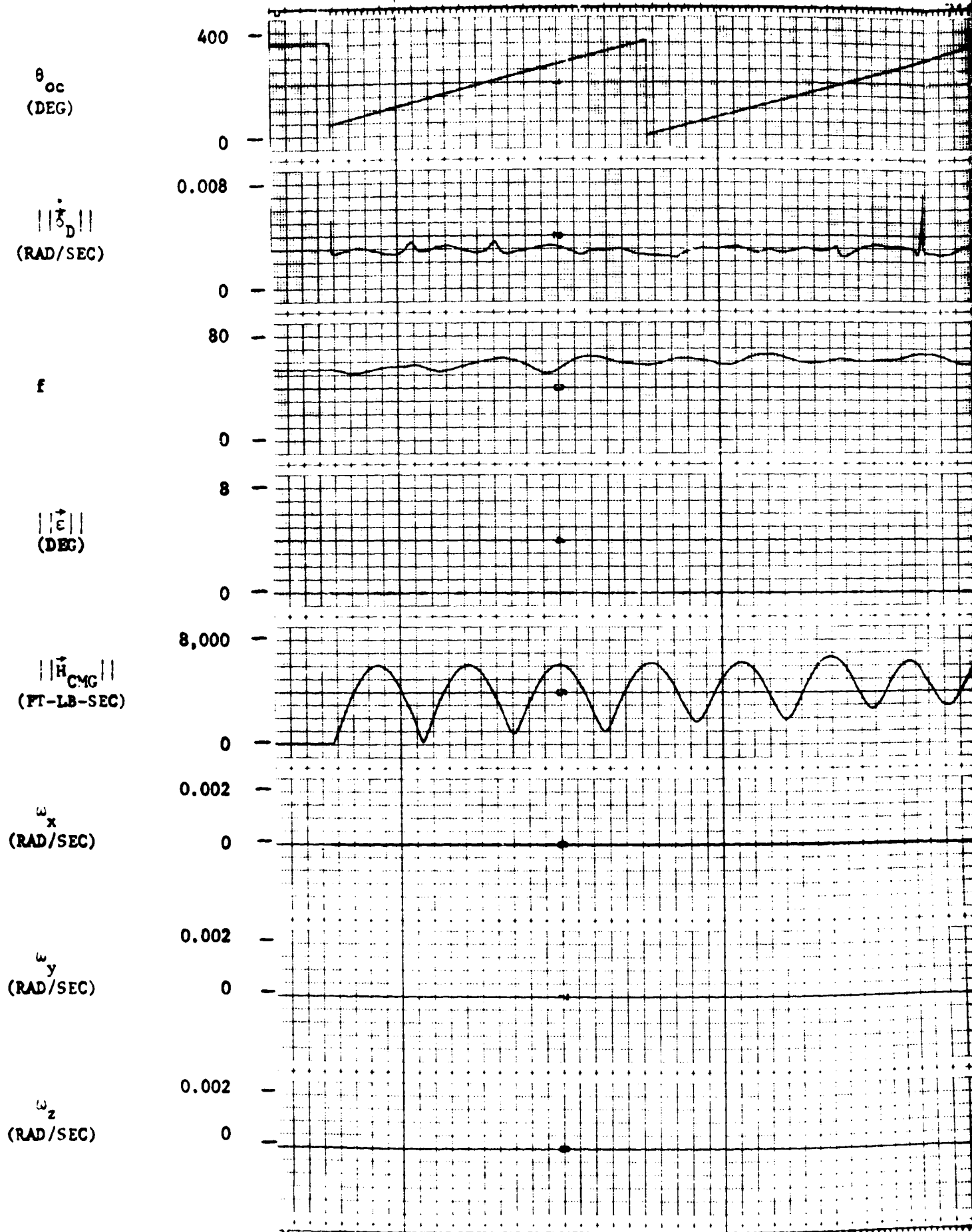


Figure 12.5. Inertial Orbital Run with X-



100 SECOND TIME MARKS

θ_{oc}
(DEG)

400 —

0 —

q_1

1 —

0 —

q_2

1 —

0 —

q_3

1 —

0 —

q_4

1 —

0 —

ϕ_{Ex}
(ARC-MIN)

4 —

0 —

ϕ_{Ey}
(ARC-MIN)

4 —

0 —

ϕ_{Ez}
(ARC-MIN)

4 —

0 —

FOLDOUT FRAME

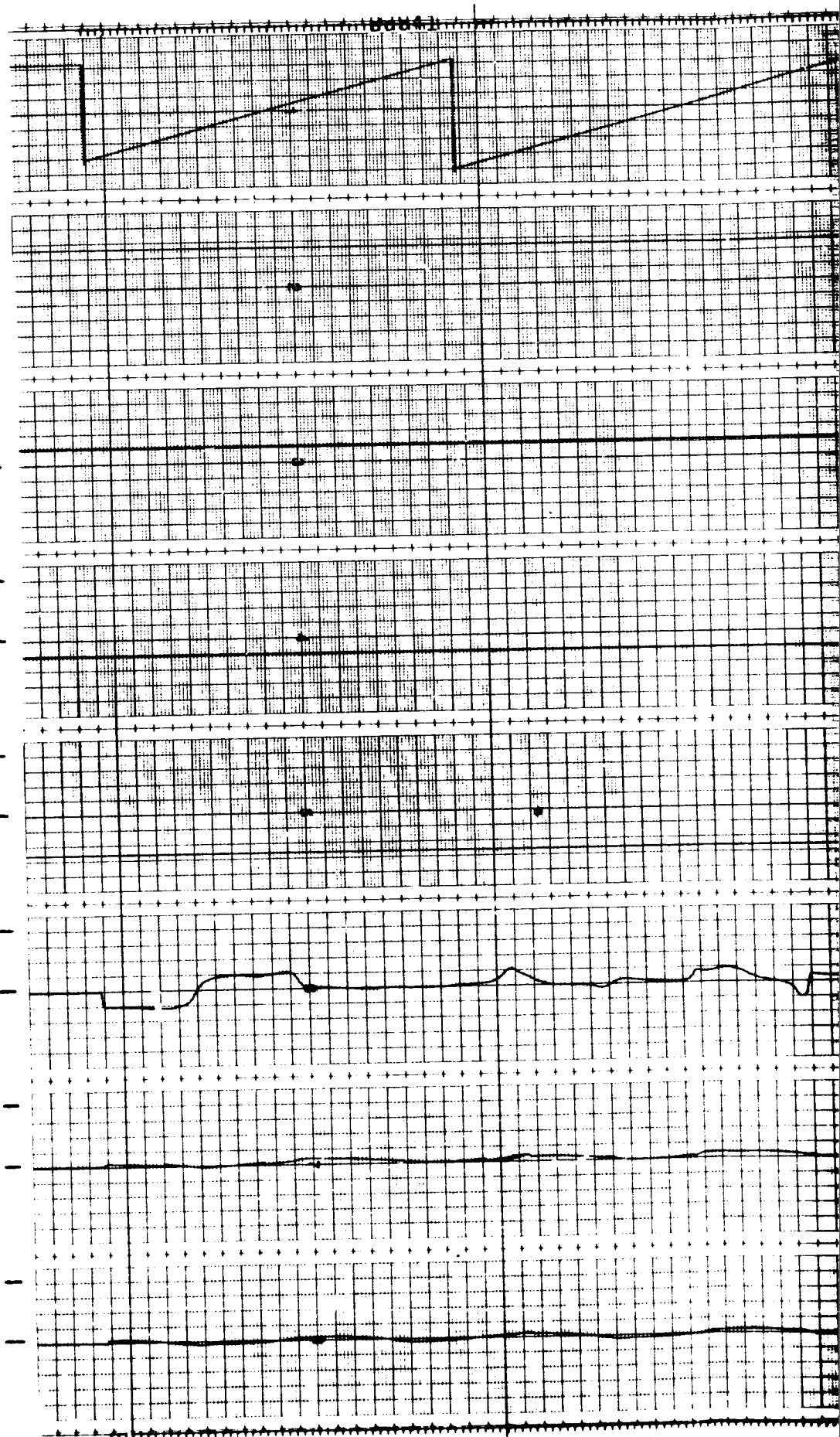
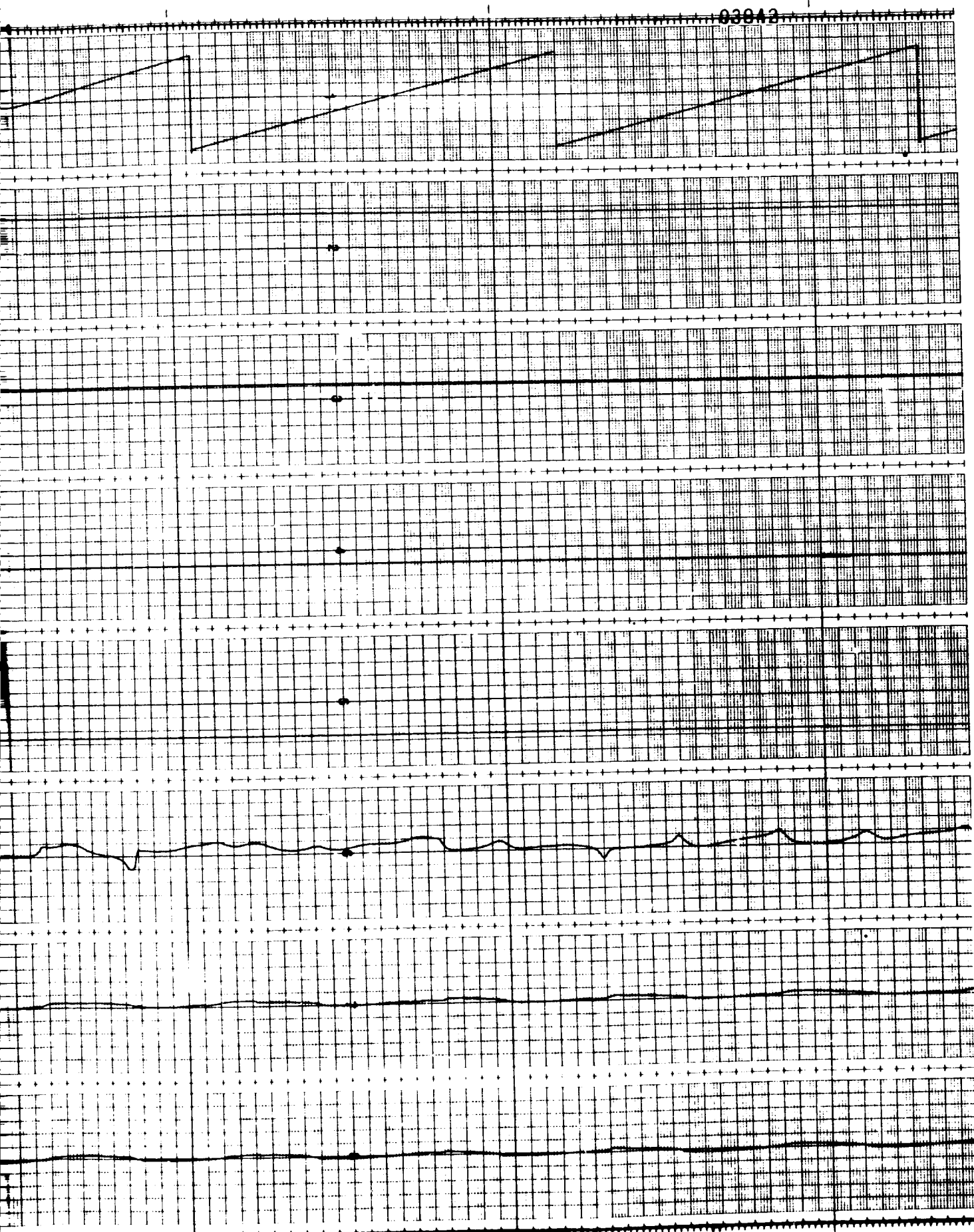


Figure 12.5. Inertial Orbital Run with



100 SECOND TIME MARKS

θ_{oc}
(DEG)

$||\dot{\delta}_s||$
(RAD/SEC)

$||\dot{\delta}_s||$
(RAD/SEC)

$||\nabla f||$

$||\dot{T}_E||$
(FT-LB)

T_{gx}
(FT-LB)

T_{gy}
(FT-LB)

T_{gz}
(FT-LB)

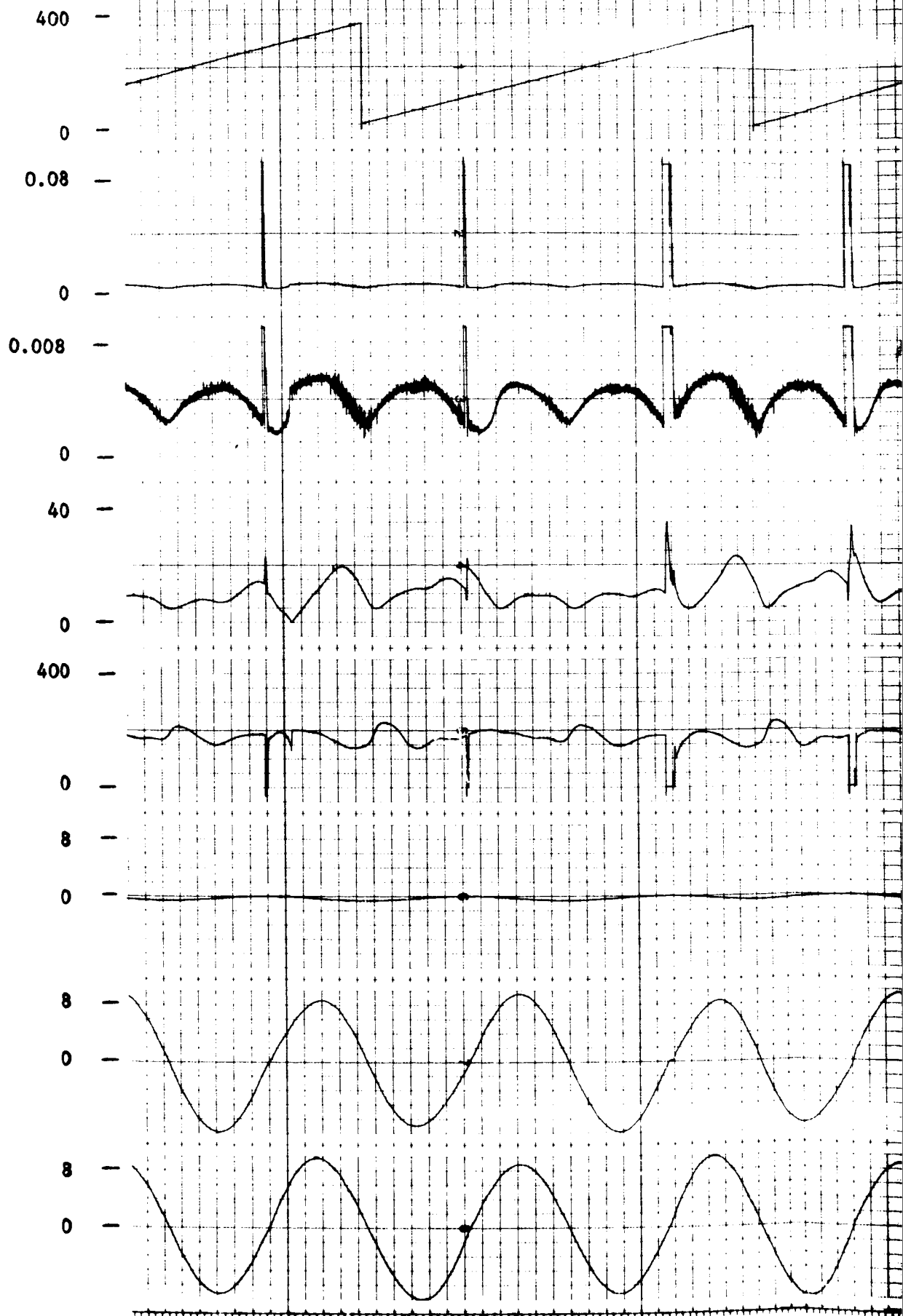
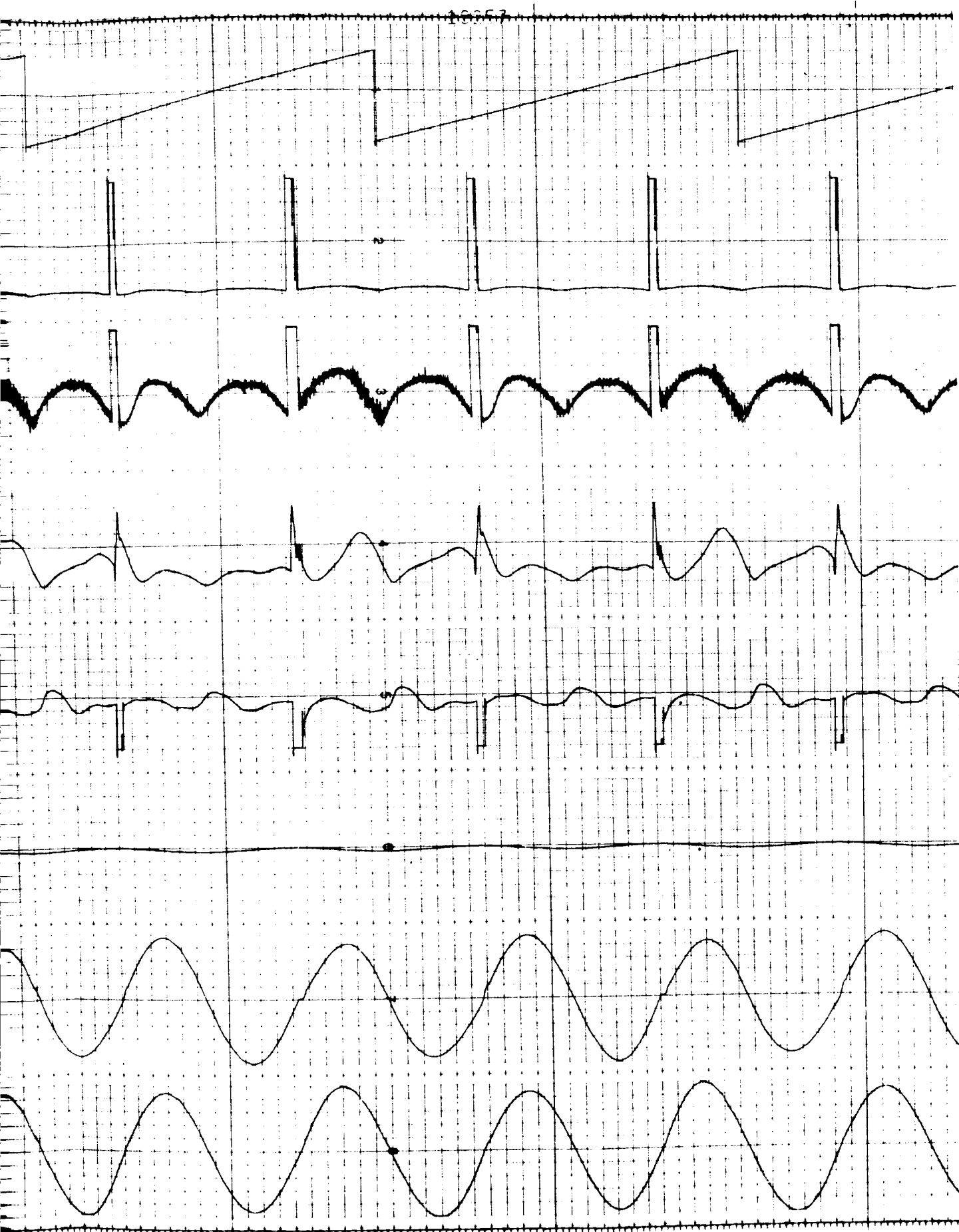


Figure 12.6. Inertial Orbital Run with

FOUR DOUT FRAME



100 SECOND TIME MARKS

θ_{oc}
 (DEG)

$||\dot{\delta}_D||$
 (RAD/SEC)

f

$||\dot{\epsilon}||$
 (DEG)

$||\dot{H}_{CMG}||$
 (FT-LB-SEC)

ω_x
 (RAD/SEC)

ω_y
 (RAD/SEC)

ω_z
 (RAD/SEC)

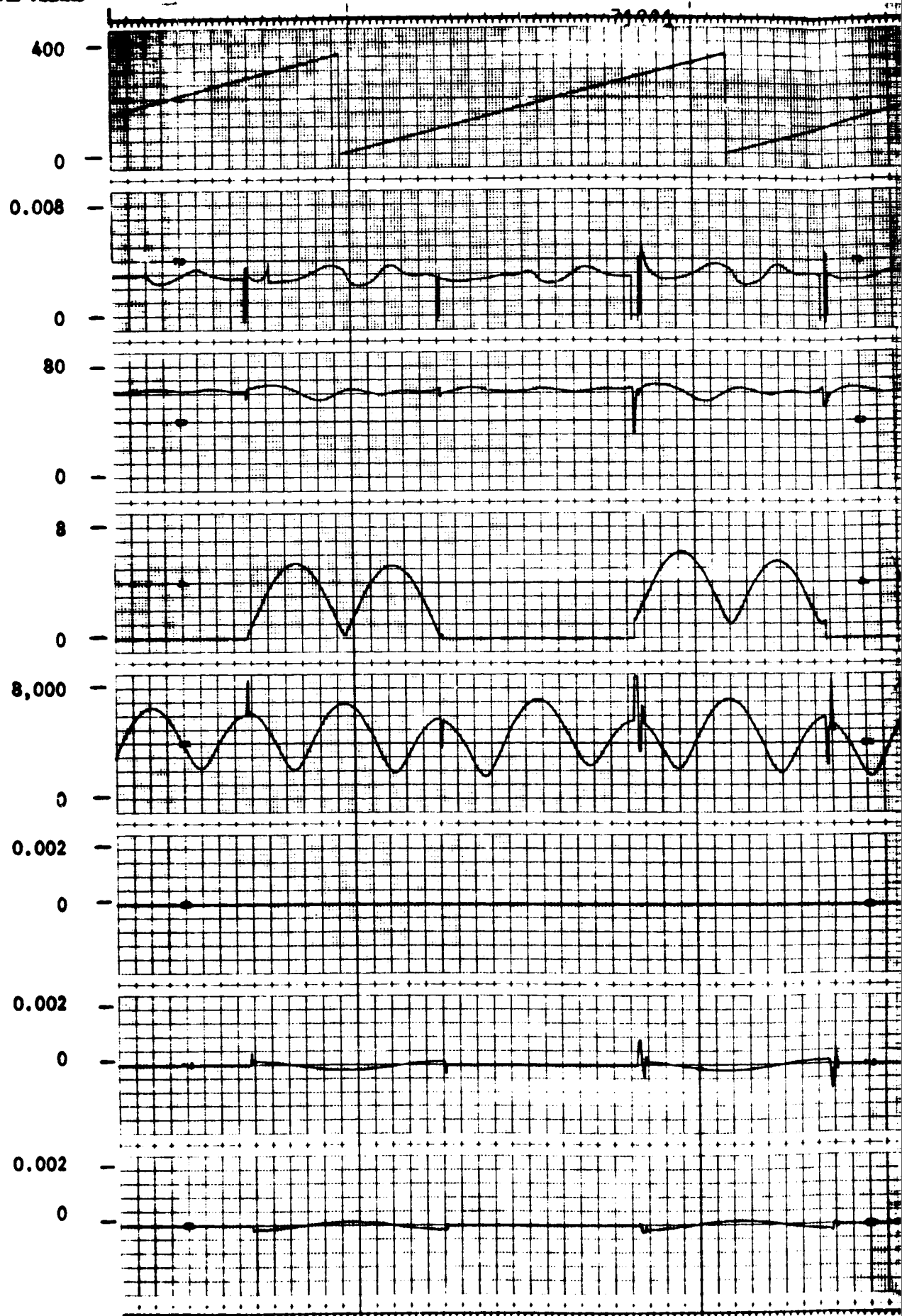
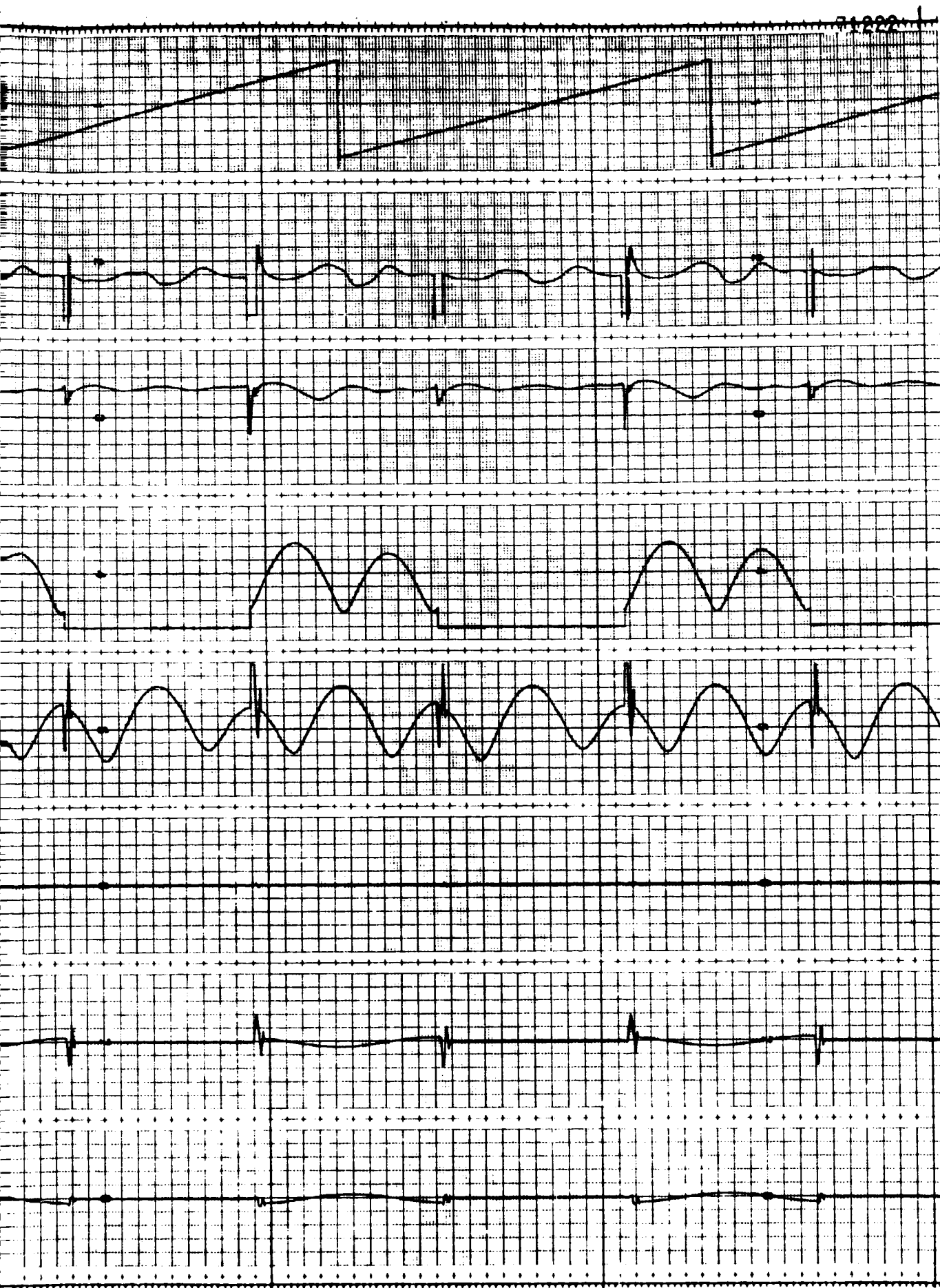


Figure 12.6. Inertial Orbital



44-38861-100

100 SECOND TIME MARKS

θ_{oc}
(DEG)

400 —

0 —

q_1

1 —

0 —

q_2

1 —

0 —

q_3

1 —

0 —

q_4

1 —

0 —

ϕ_{Ex}
(ARC-MIN)

4 —

0 —

ϕ_{Ey}
(ARC-MIN)

4 —

0 —

ϕ_{Ez}
(ARC-MIN)

4 —

0 —

FOLDOUT FRAME

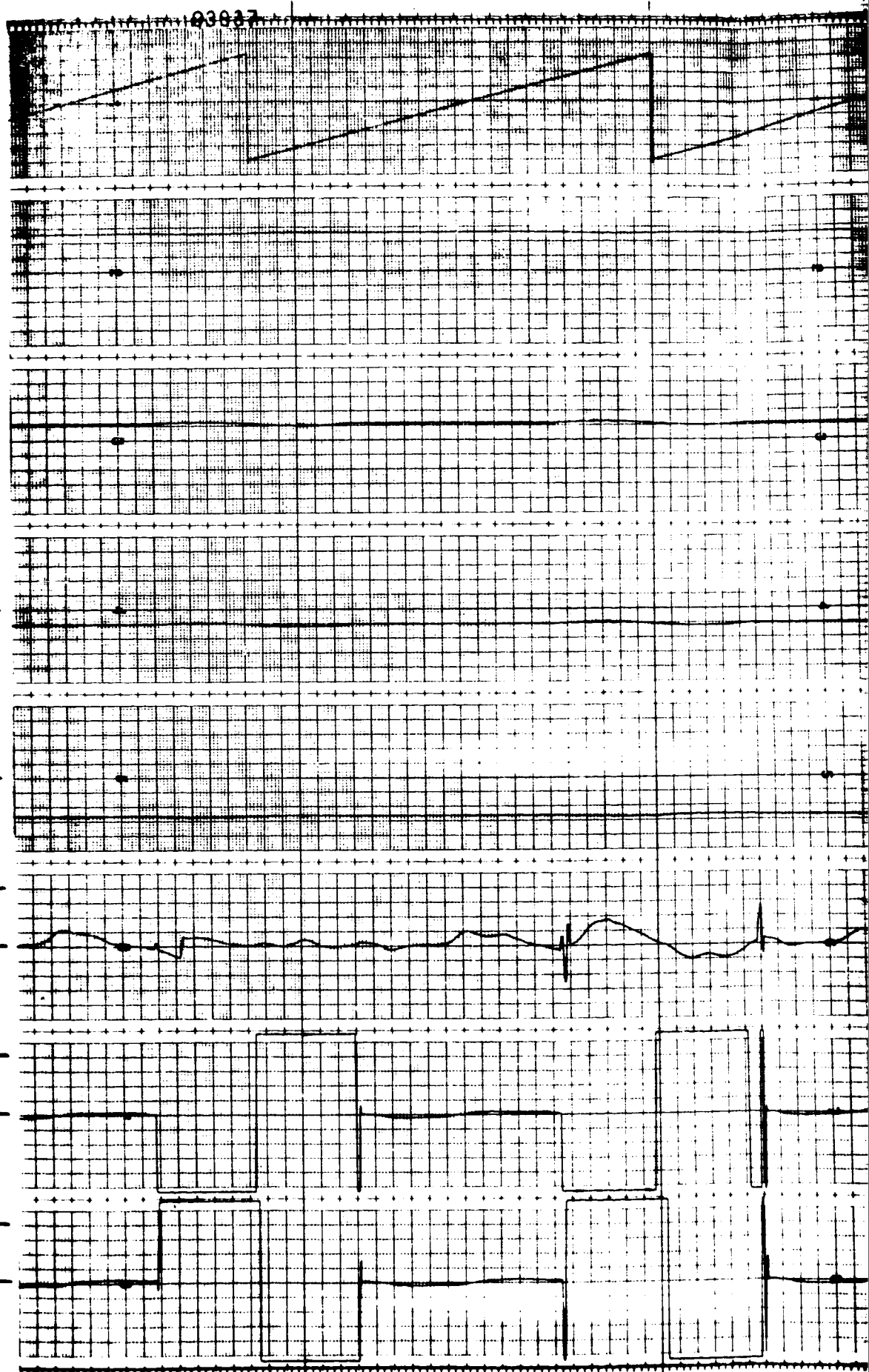


Figure 12.6. Inertial Orbital Run



100 SECOND TIME MARKS

θ_{oc}
(DEG)

400

0

$\dot{\theta}_s$
(RAD/SEC)

0.08

0

$\dot{\theta}_s$
(RAD/SEC)

0.008

0

$||\nabla f||$

40

0

$||\dot{T}_E||$
(FT-LB)

400

0

T_{gx}
(FT-LB)

8

0

T_{gy}
(FT-LB)

8

0

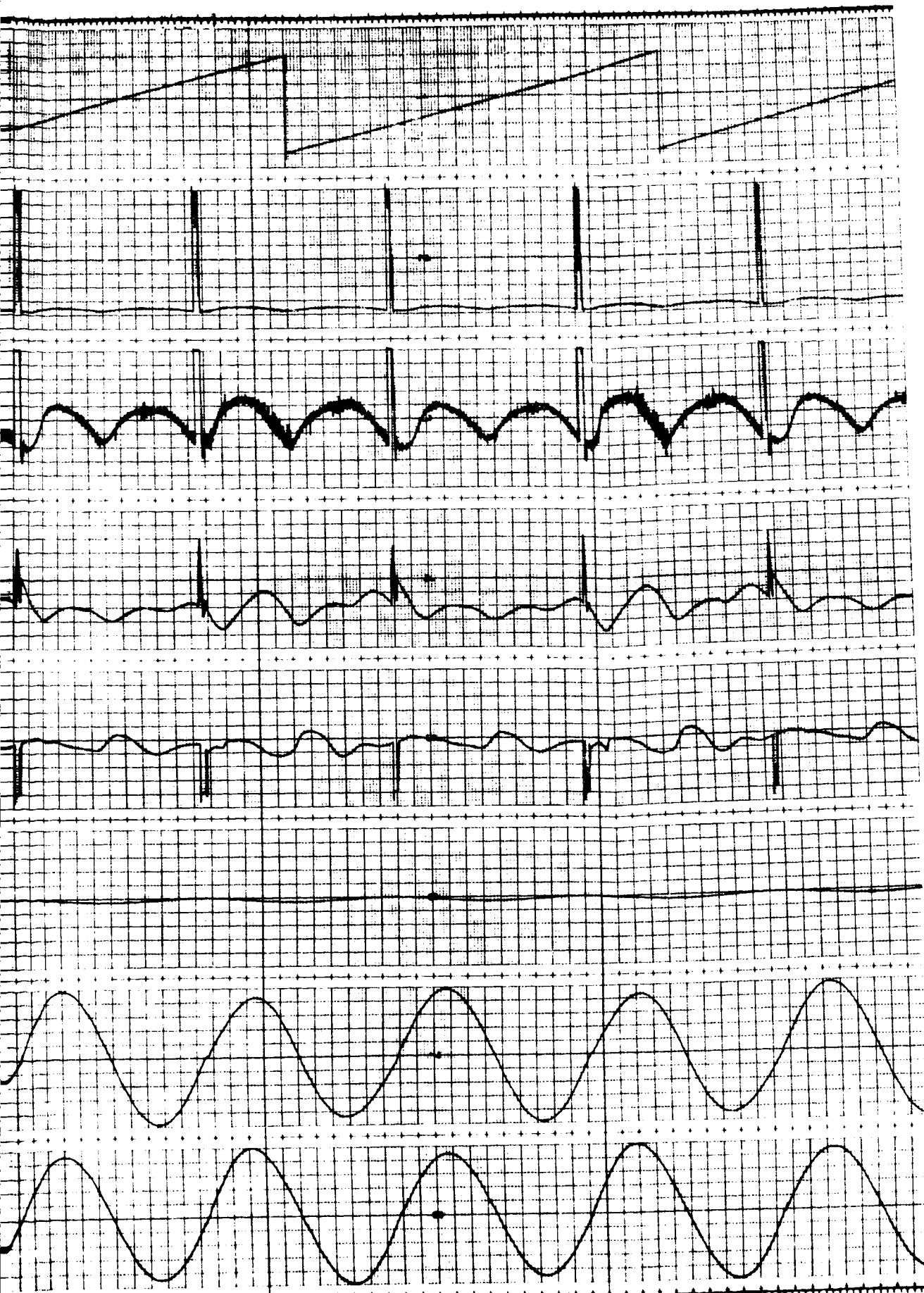
T_{gz}
(FT-LB)

8

0

FOLDOUT FRAME

Figure 12.7. Inertial Orbital Run with X-1
and 1/2 Degree Vehicle Offset



al Run with X-IOP and Z-TT (Nominally)
Vehicle Offset on Each Axis (Sheet 1 of 3)

FOLDOUT PAGE

100 SECOND TIME MARKS

θ_{oc}
 (DEG)

$\dot{\phi}_D$
 (RAD/SEC)

ϵ

ϵ
 (DEG)

\dot{H}_{CMG}
 (FT-LB-SEC)

ω_x
 (RAD/SEC)

ω_y
 (RAD/SEC)

ω_z
 (RAD/SEC)

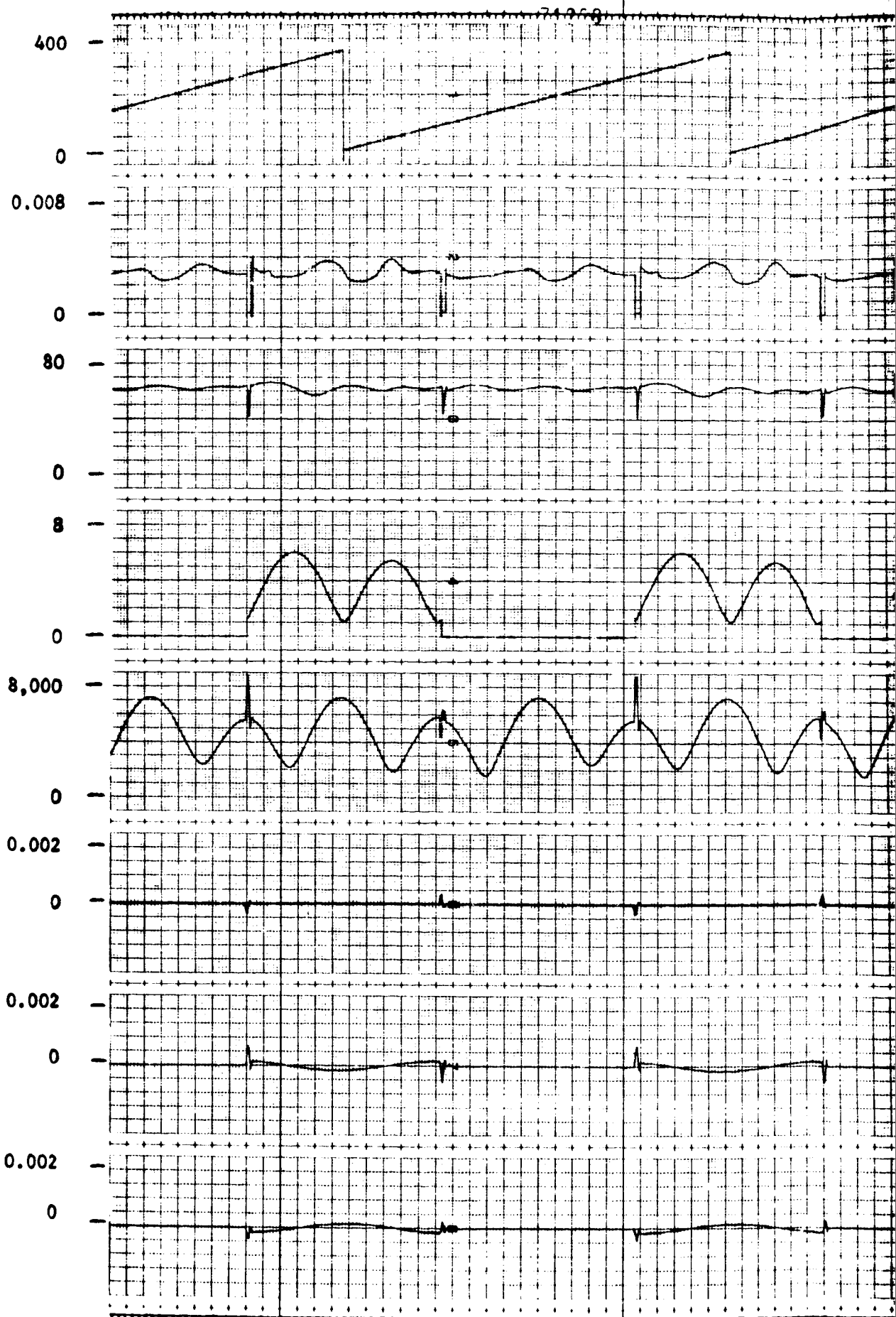
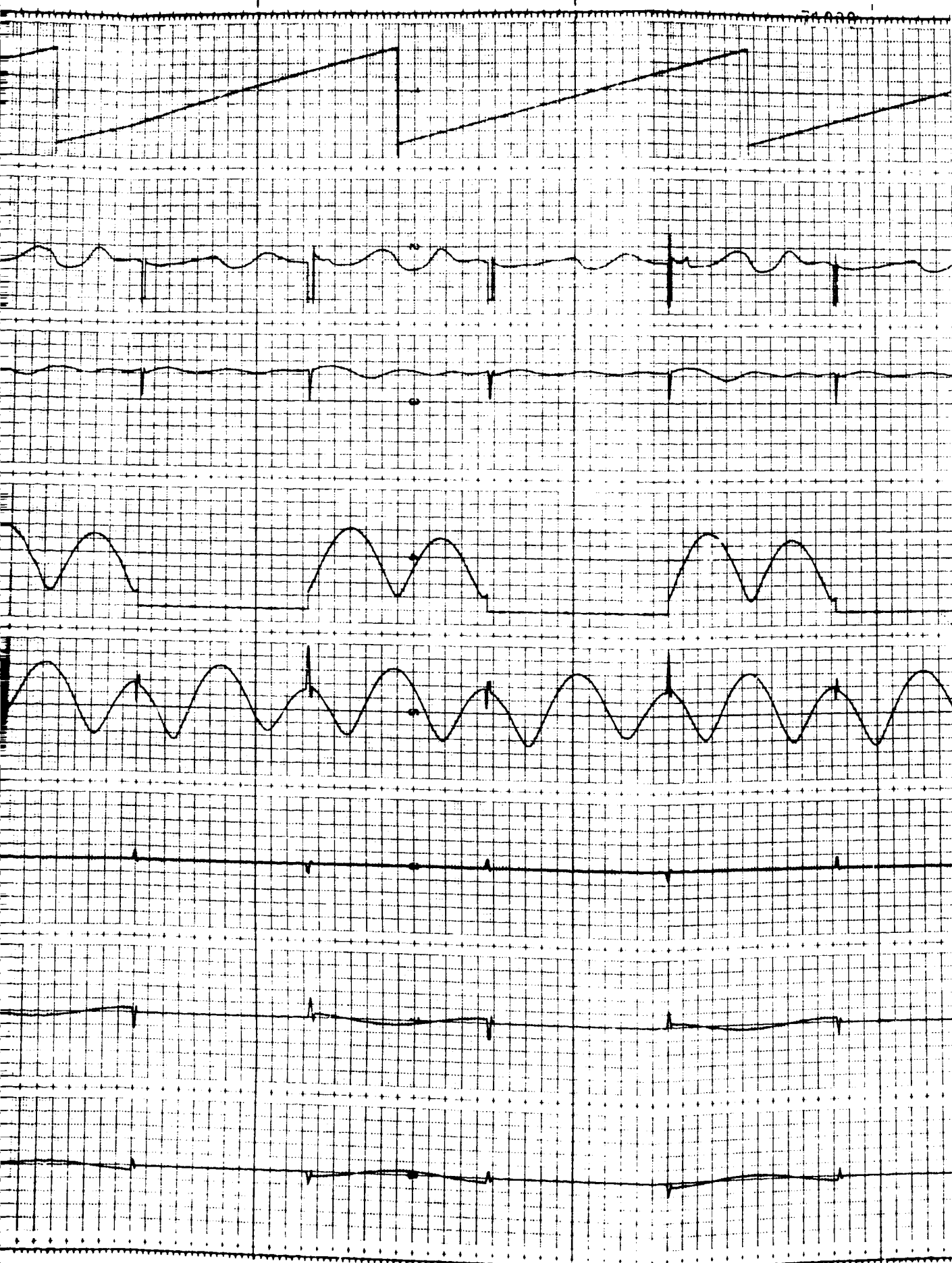


Figure 12.7. Inertial Orbital Run with 1/2 Degree Vehicle Orientation



1 Orbital Run with X-IOP and Z-TT (Nominally)
2 Degree Vehicle Offset on Each Axis (Sheet 2 of 3)

100 SECOND TIME MARKS

θ_{oc}
(DEG)

q_1

q_2

q_3

q_4

ϕ_{Ex}
(ARC-MIN)

ϕ_{Ey}
(ARC-MIN)

ϕ_{Ez}
(ARC-MIN)

FOLDOUT FRAME

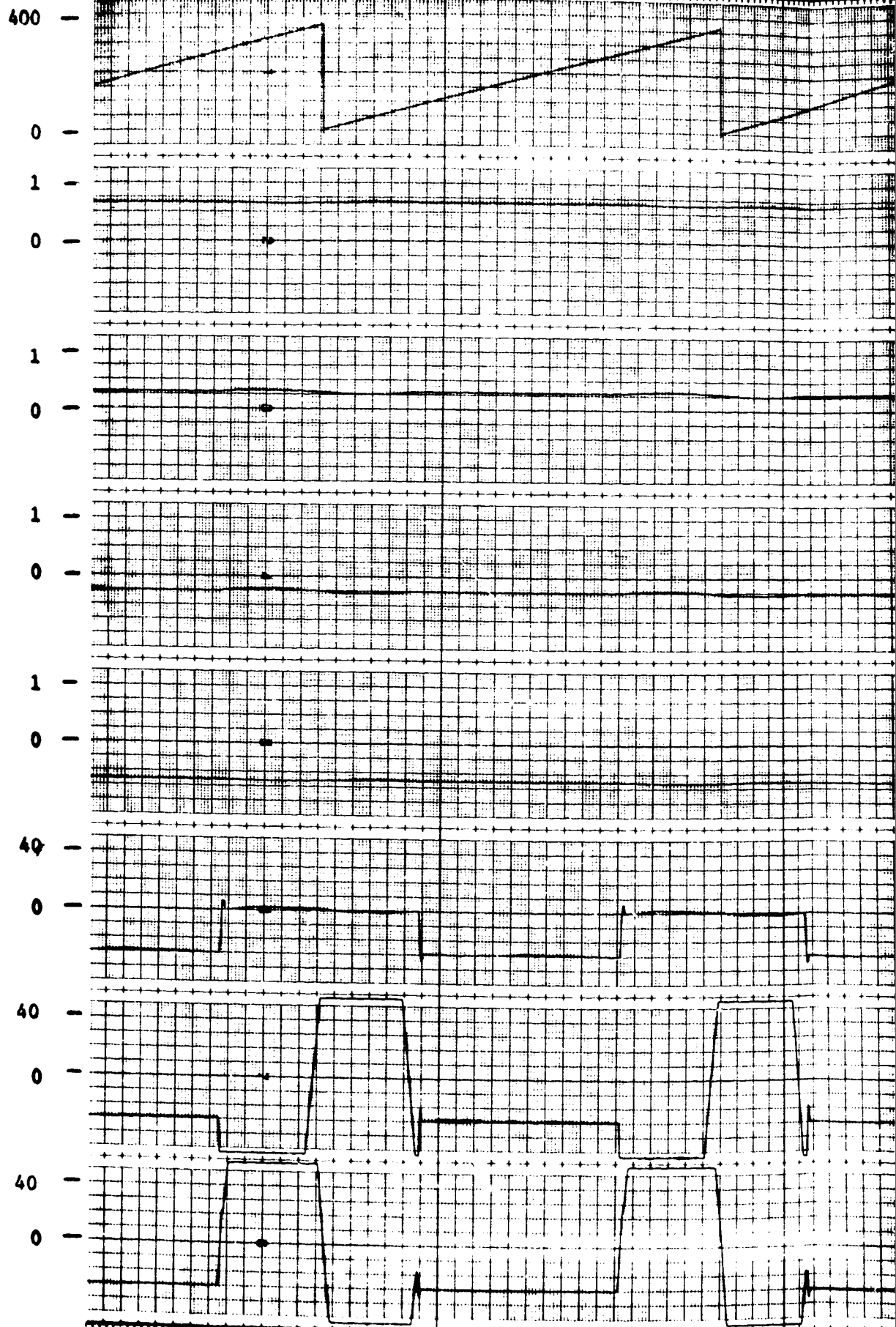


Figure 12.7 Inertial Orbital and 1/2 Degree Ve



Inertial Orbital Run with X-IOP and Z-TT (Nominally)
and 1/2 Degree Vehicle Offset on Each Axis (Sheet 3 of 3)

FOLDOUT FRAME

100 SECOND TIME MARKS

θ_{oc}
(DEG)

$\dot{\theta}_o$
(RAD/SEC)

$\dot{\theta}_s$
(RAD/SEC)

$\|\nabla f\|$

\dot{T}_E
(FT-LB)

T_{gx}
(FT-LB)

T_{gy}
(FT-LB)

T_{gz}
(FT-LB)

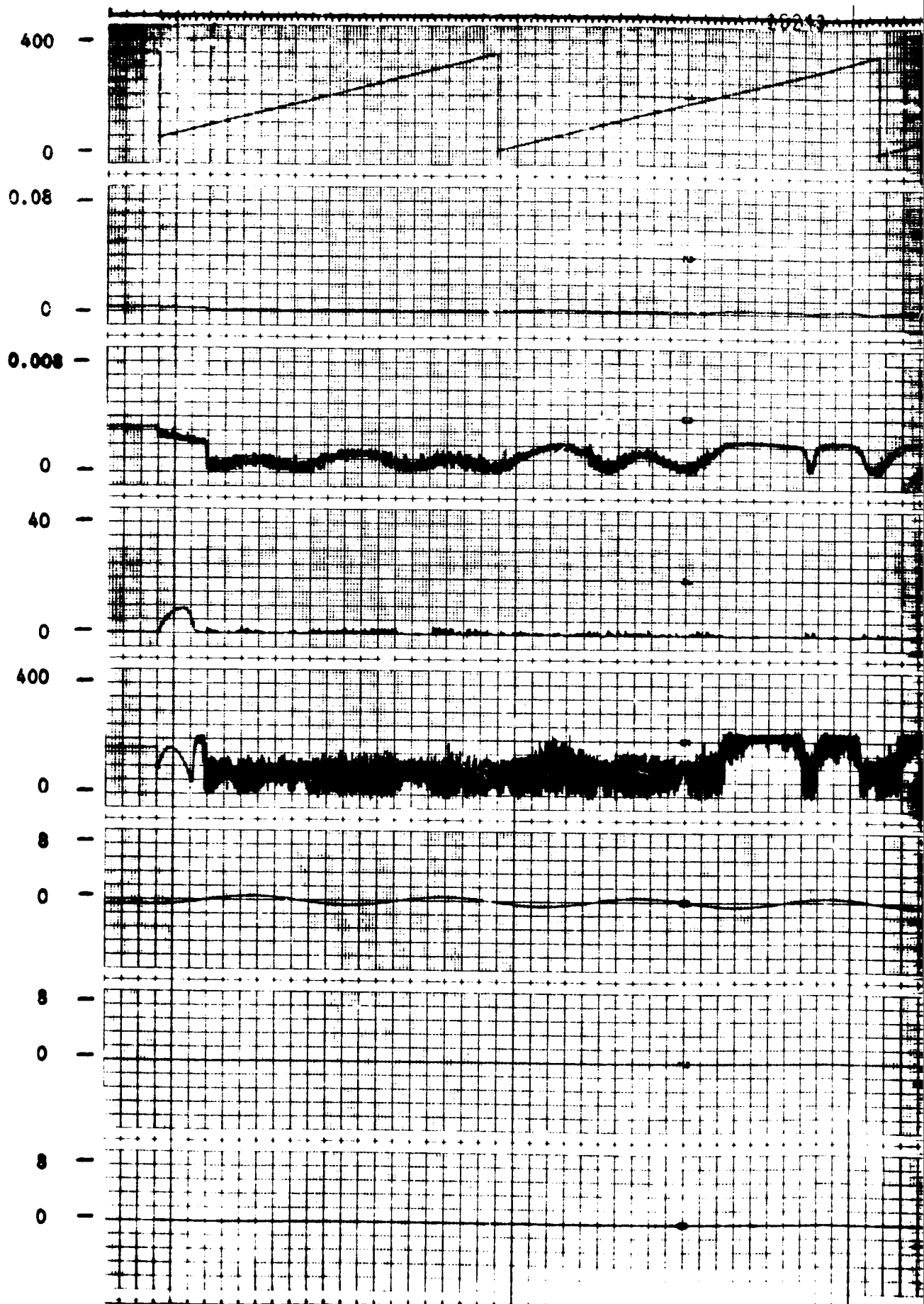
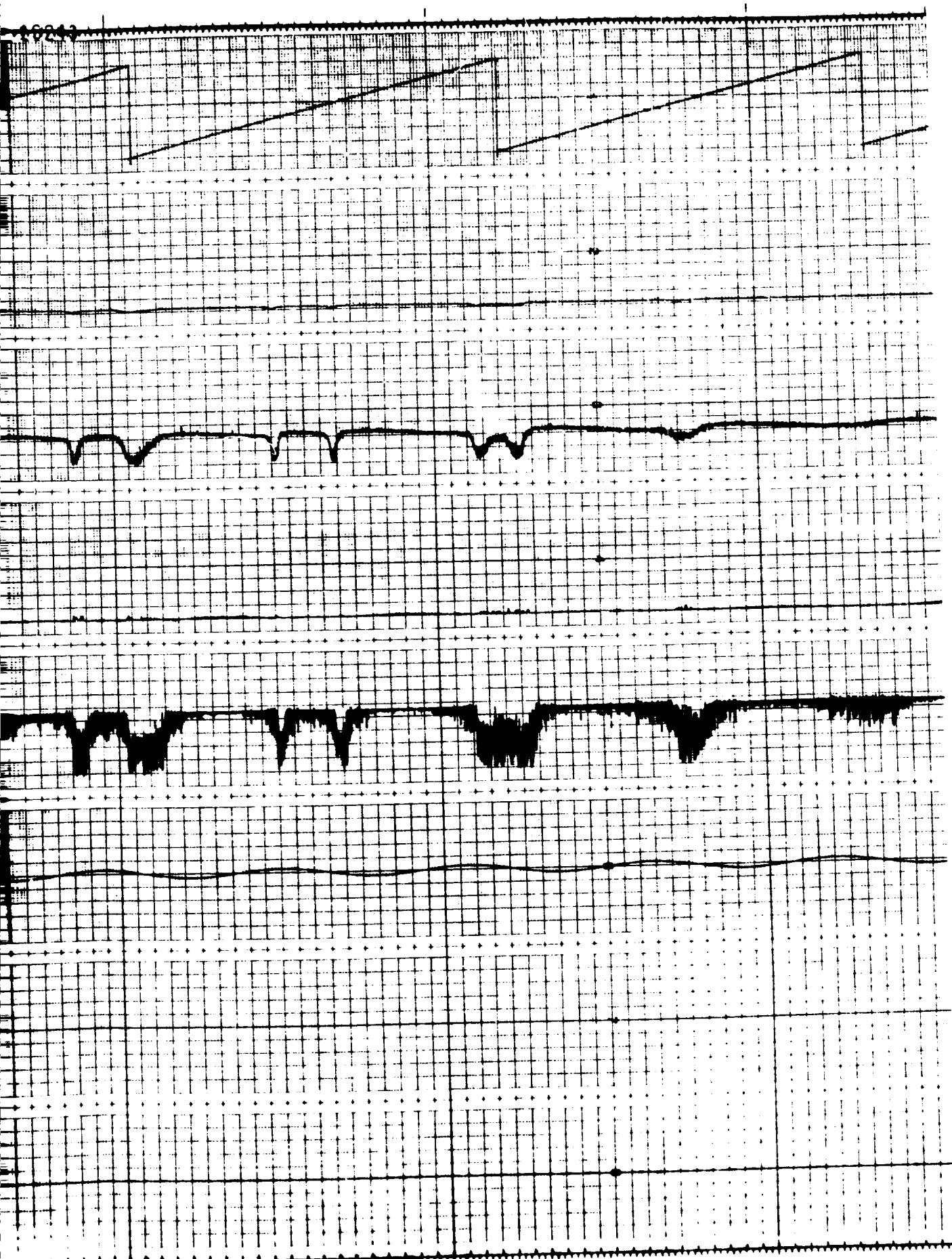


Figure 12.8 Inertial Orbital Run with X-POP and T

FOLDSIDE 11-1-66



100 SECOND TIME MARKS

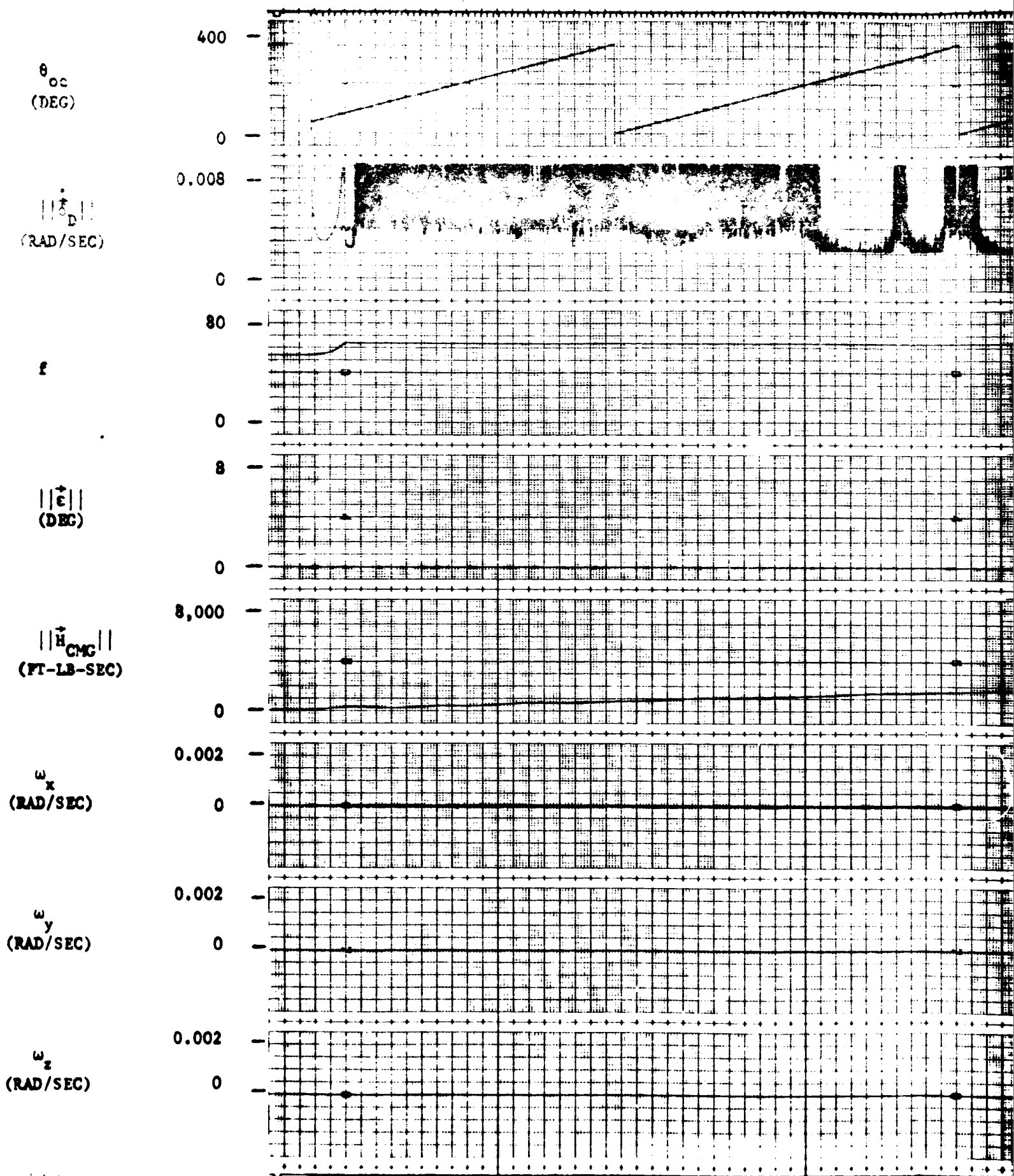
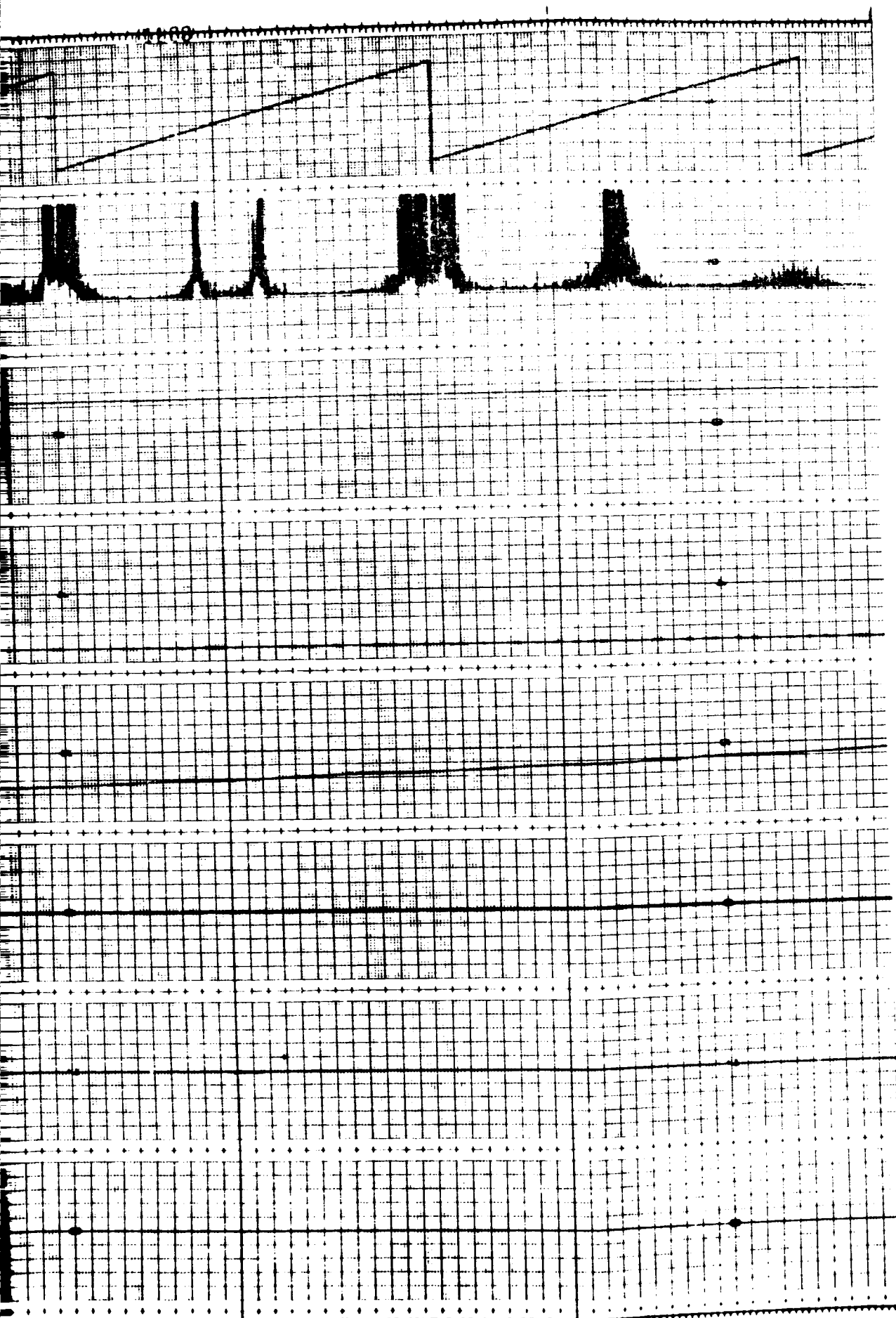


Figure 12.8. Inertial Orbital Run with X-POP and



100 SECOND TIME MARKS

θ_{oc}
(DEG)

400 —

0 —

q_1

1 —

0 —

q_2

1 —

0 —

q_3

1 —

0 —

q_4

1 —

0 —

ϕ_{Ex}
(ARC-MIN)

4 —

0 —

ϕ_{Ey}
(ARC-MIN)

4 —

0 —

ϕ_{Ez}
(ARC-MIN)

4 —

0 —

FOLDOUT FRAME

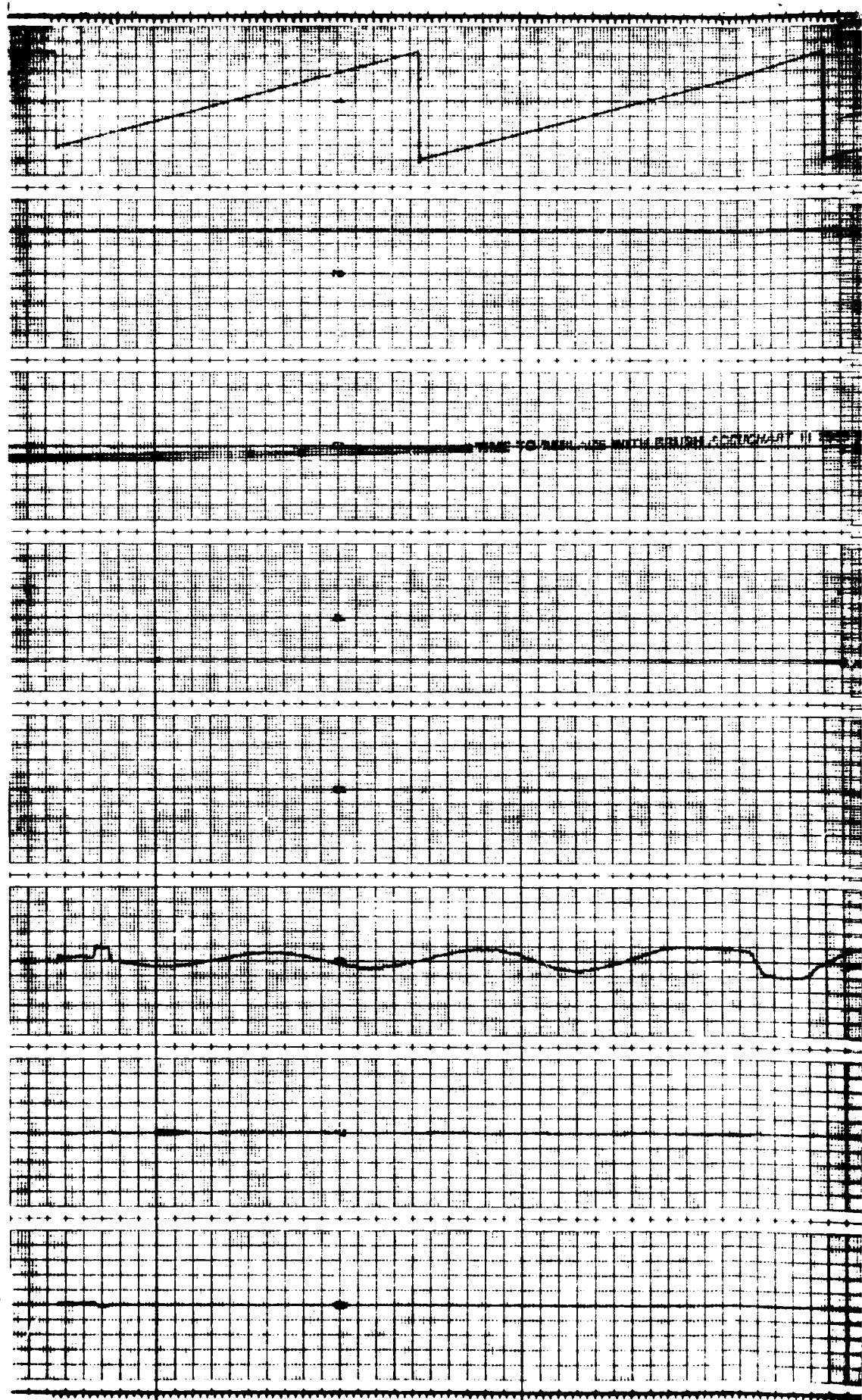
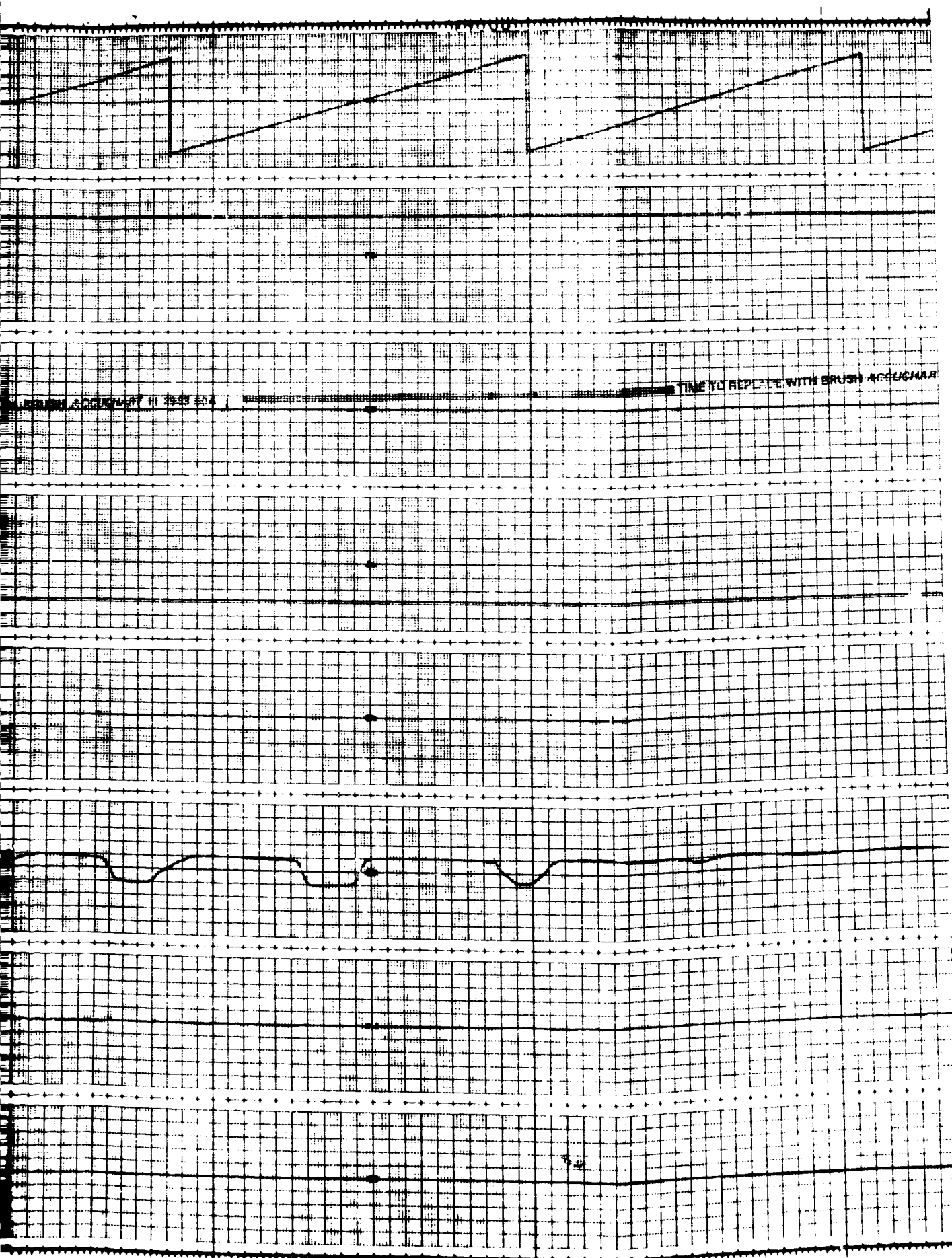


Figure 12.8. Inertial Orbital Run with R



100 SECOND TIME MARKS

θ_{oc}
(DEG)

$\dot{\theta}_s$
(RAD/SEC)

$\dot{\theta}_s$
(RAD/SEC)

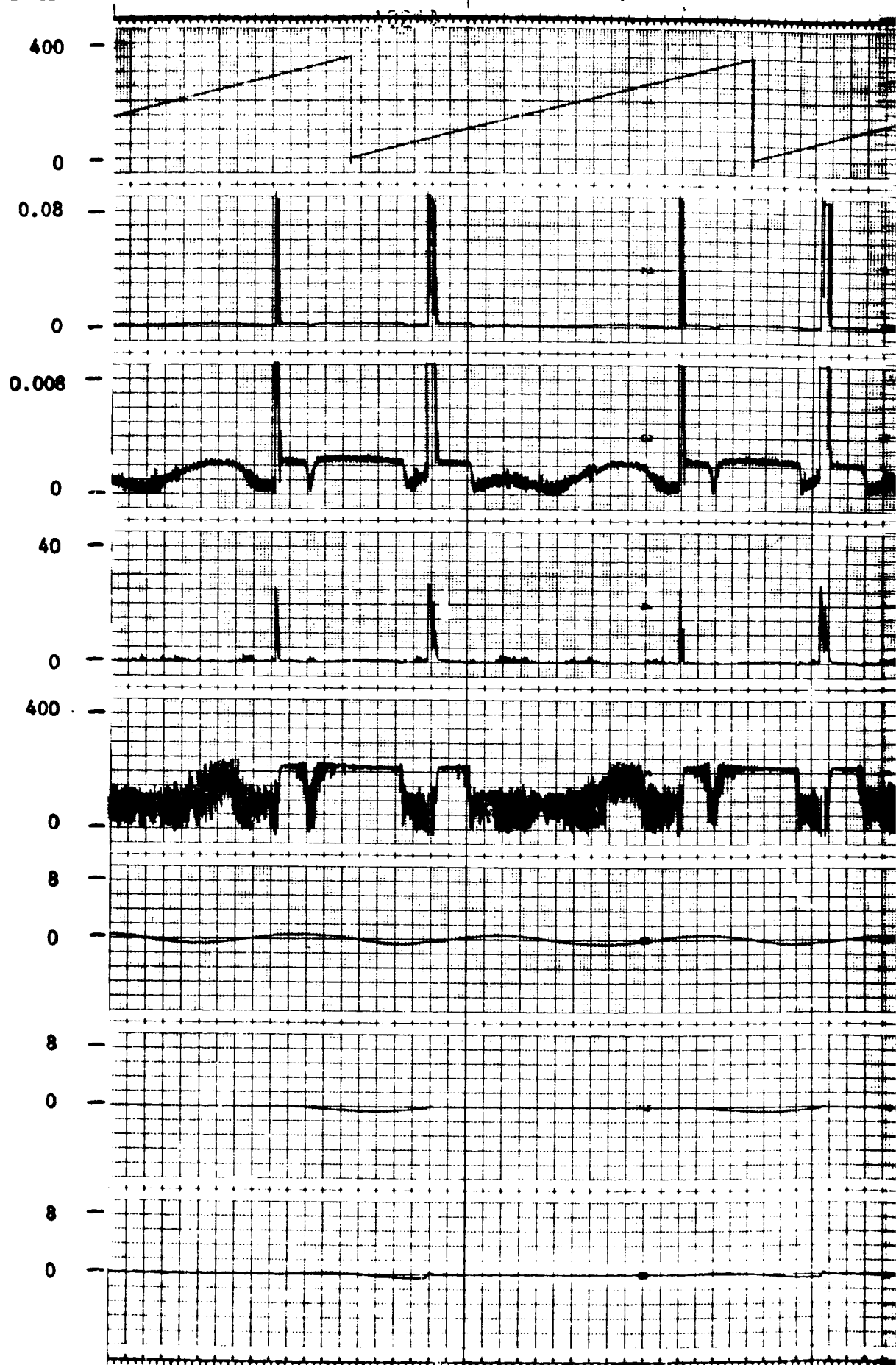
$|\nabla f|$

\dot{T}_E
(FT-LB)

T_{gx}
(FT-LB)

T_{sy}
(FT-LB)

T_{gz}
(FT-LB)



FOLDOUT FRAME

Figure 12.9. Inertial Orbit



100 SECOND TIME MARKS

θ_{oc}
(DEG)

$\|\vec{\omega}_y\|$
(RAD/SEC)

f

$\|\vec{e}\|$
(DEG)

$\|\vec{H}_{CMG}\|$
(FT-LB-SEC)

ω_x
(RAD/SEC)

ω_y
(RAD/SEC)

ω_z
(RAD/SEC)

FOLDOUT FRAME

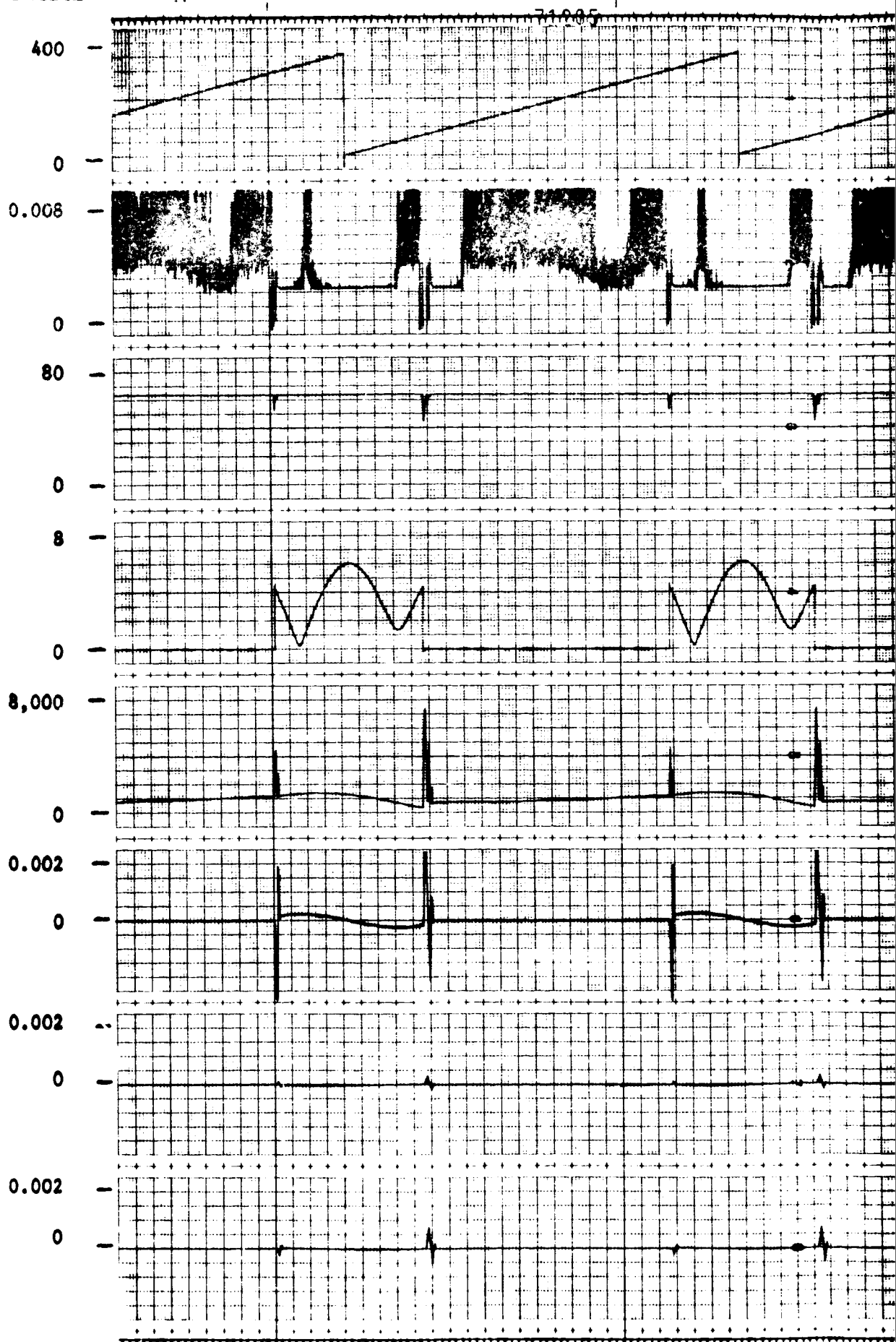
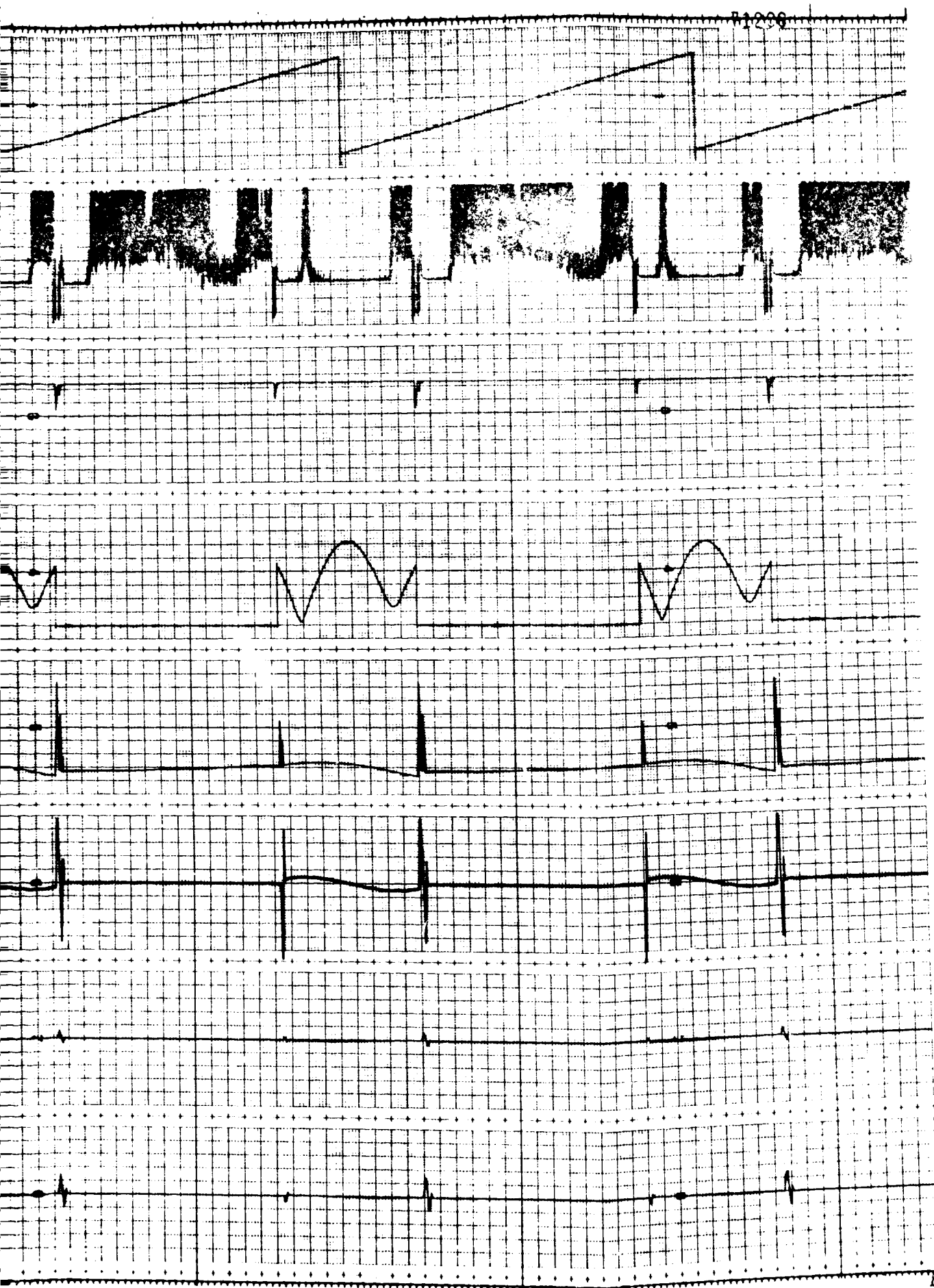


Figure 12.9. Inertial Orbital Run with



FOLDOUT FRAME

100 SECOND TIME MARKS

θ_{oc}
(DEG)

400

q_1

1

0

q_2

1

0

q_3

1

0

q_4

1

0

ϕ_{Ex}
(ARC-MIN)

4

0

ϕ_{Ey}
(ARC-MIN)

4

0

ϕ_{Ez}
(ARC-MIN)

4

0

FOLDOUT FRAME



Figure 12.9. Inertial Orbital Run wi



100 SECOND TIME MARKS

θ_{oc}
(DEG)

$\dot{\theta}_s$
(RAD/SEC)

$\dot{\theta}_s$
(RAD/SEC)

$||\nabla f||$

$||\ddot{\theta}_E||$
(FT-LB)

T_{gx}
(FT-LB)

T_{gy}
(FT-LB)

T_{gz}
(FT-LB)

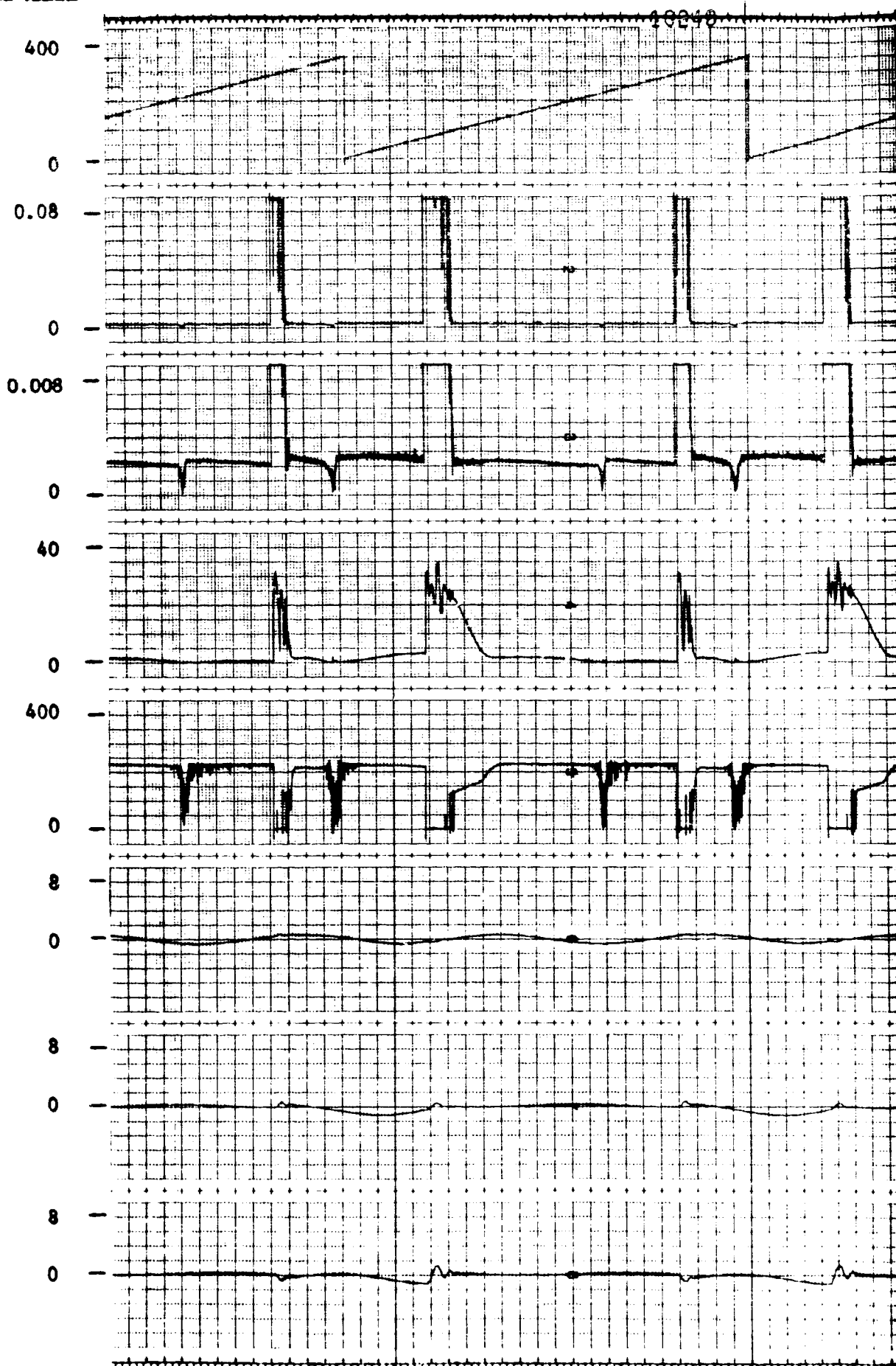
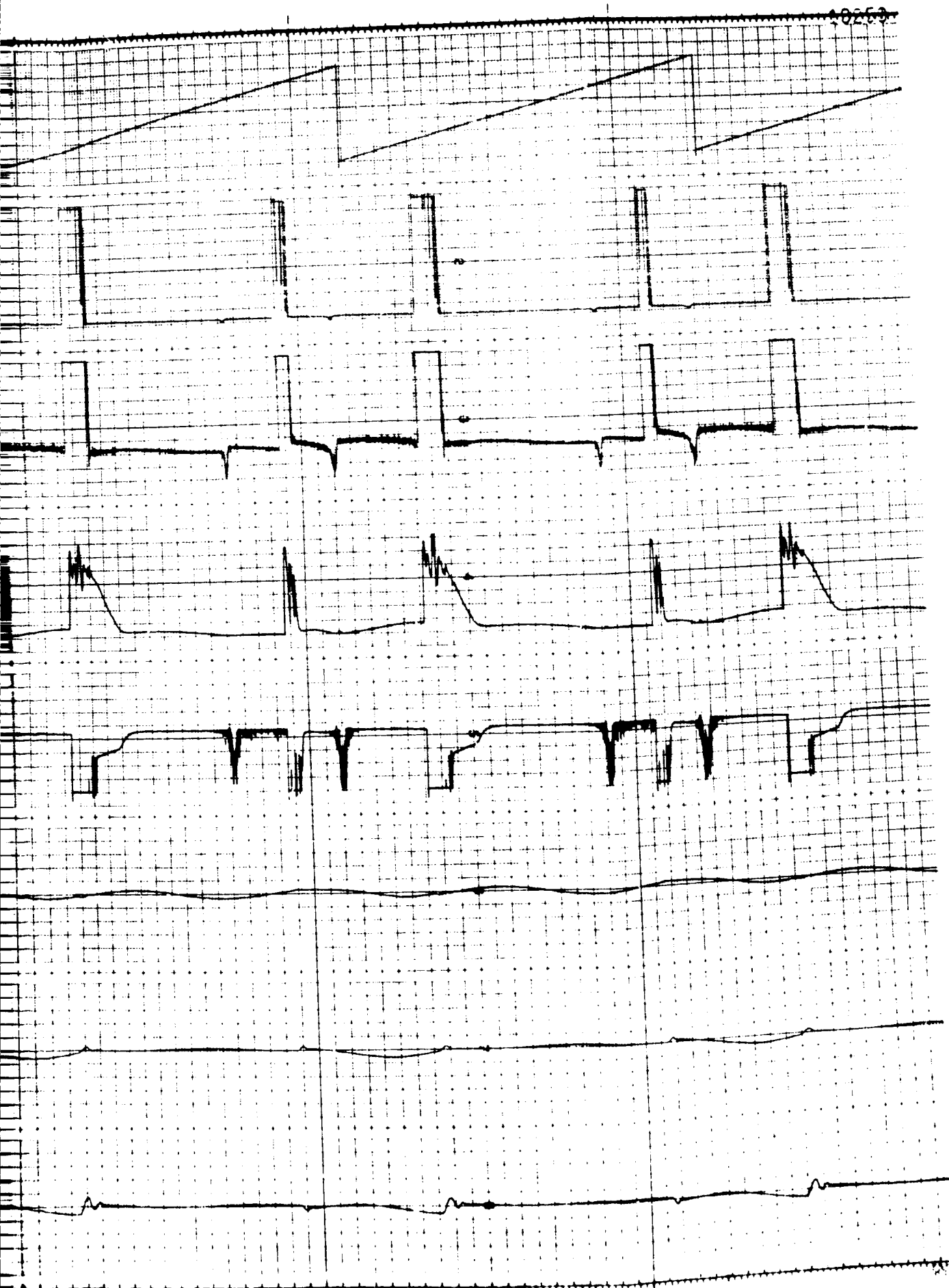
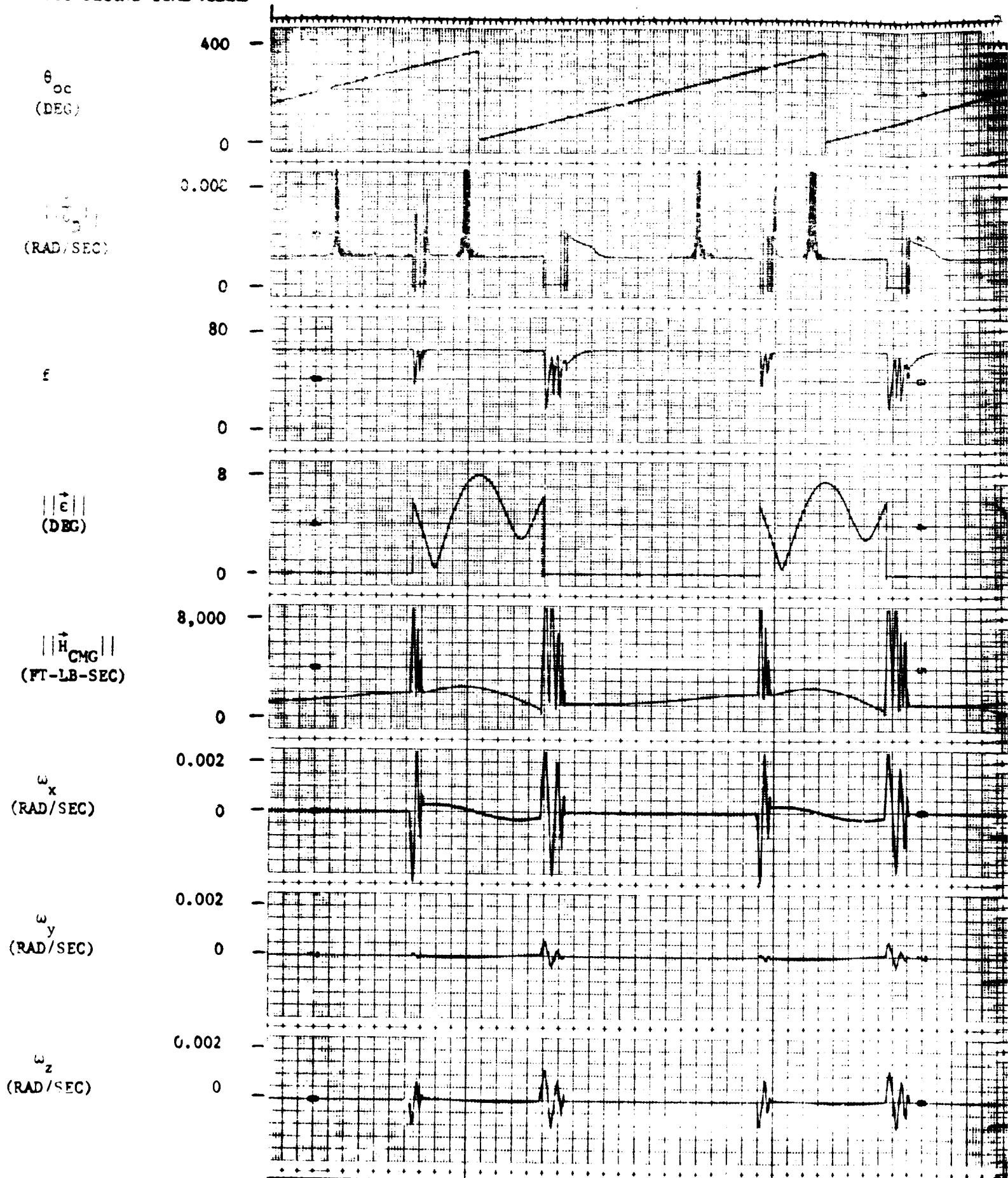


Figure 12.10. Inertial Orbital Run
1/2 Degree Vehicle



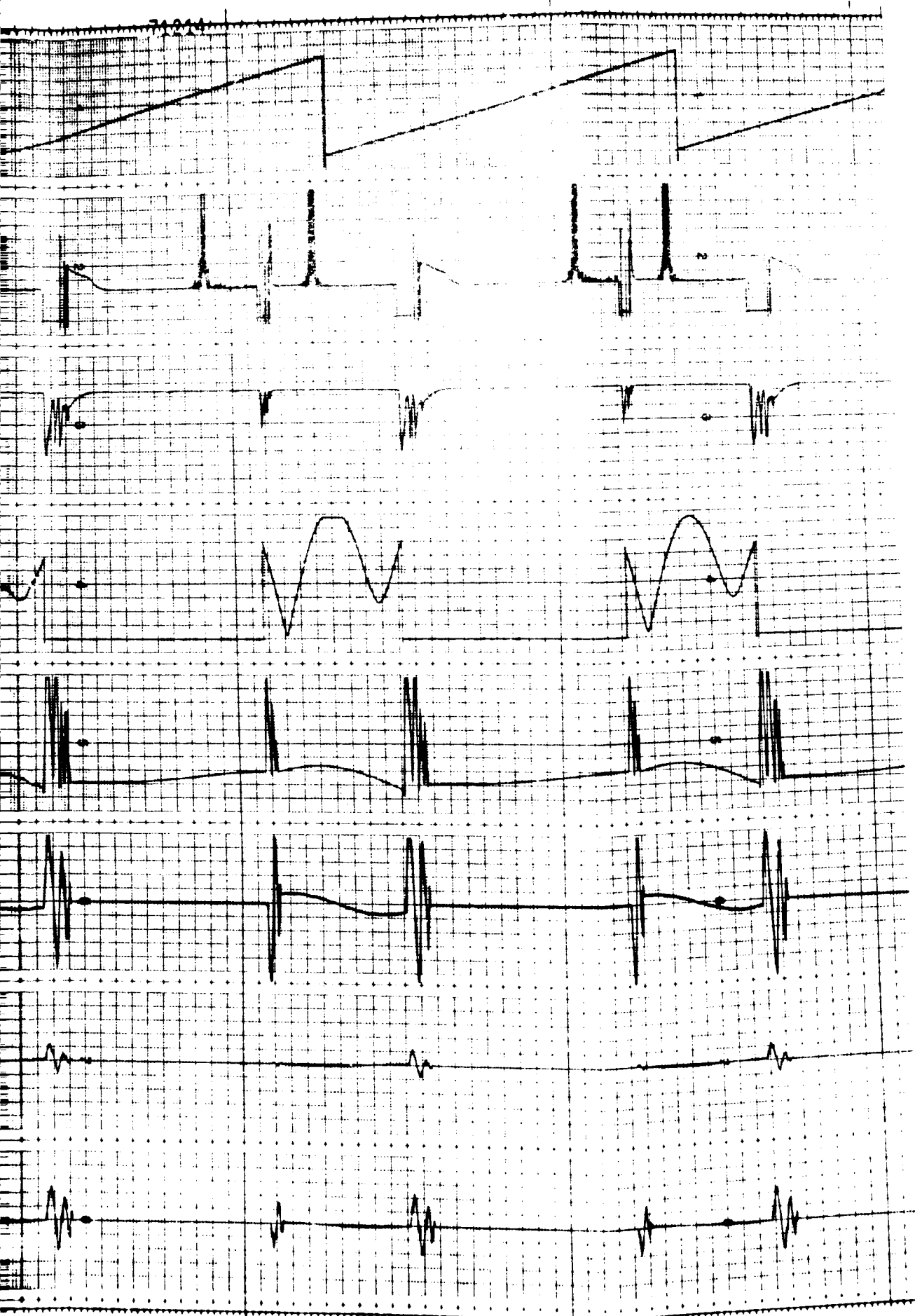
1 Orbital Run with X-POP and Z-TT (Nominally) and
Free Vehicle Offset on Each Axis (Sheet 1 of 3)

100 SECOND TIME MARKS



FOLDOUT FRAME

Figure 12.10. Inertial Orbital
1/2 Degree Vehicle



Inertial Orbital Run with X-POP and Z-TT (Nominally) and
1/2 Degree Vehicle Offset on Each Axis (Sheet 2 of 3)

FOLDOUT FRAME:

100 SECOND TIME MARKS

ϕ_{SC}
(DEG)

q_3

q_4

ϕ_{Ex}
(ARC-MIN)

ϕ_{Ey}
(ARC-MIN)

ϕ_{Ez}
(ARC-MIN)

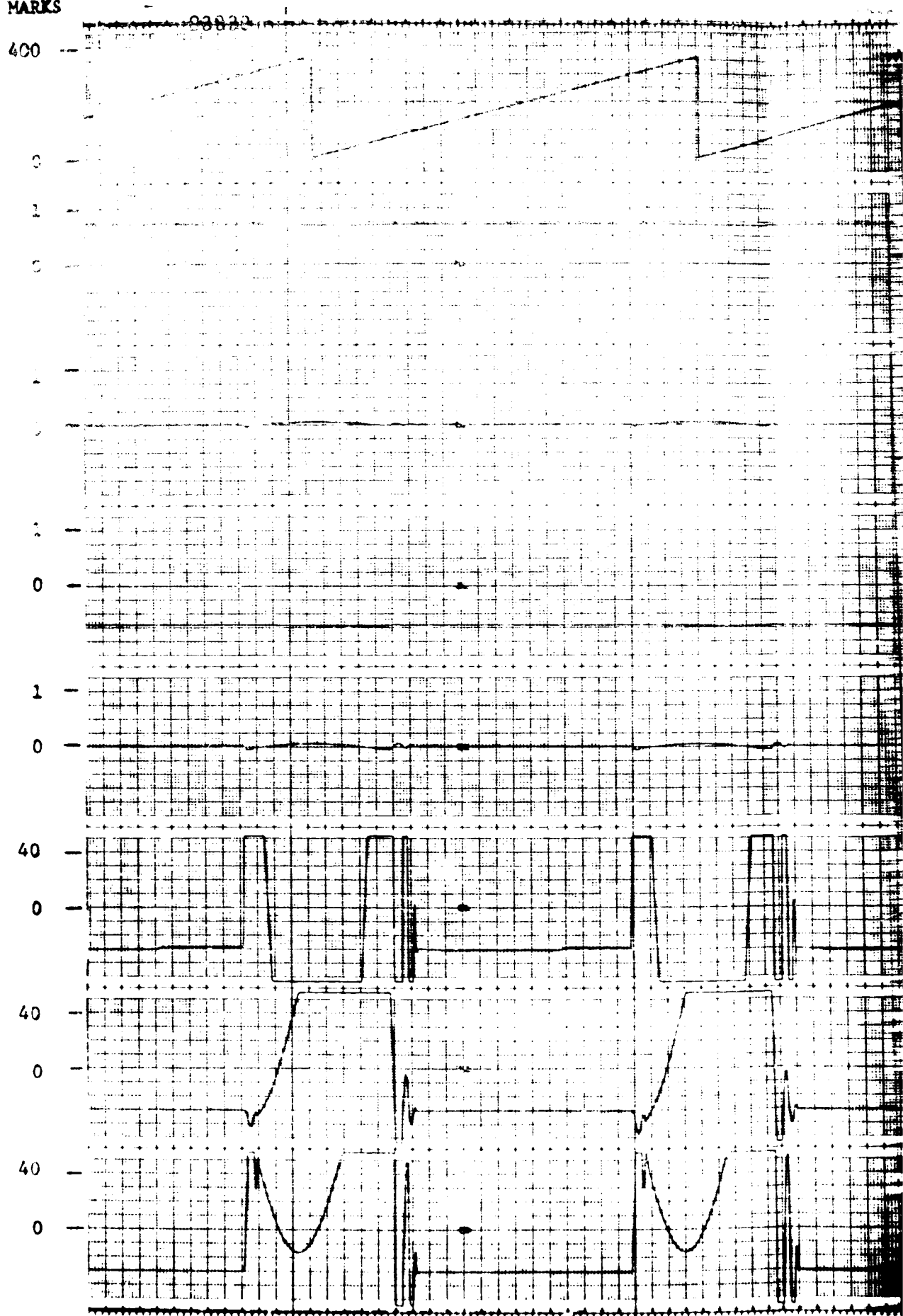


Figure 12.10. Inertial Orbital Run with
1/2 Degree Vehicle Offset

FOLDOUT FRAME



Inertial Orbital Run with X-POP and Z-TT (Nominally and
1/2 Degree Vehicle Offset on Each Axis (Sheet 3 of 3)

100 SECOND TIME MARKS

θ_{cc}
(DEG)

$\dot{\theta}_s$
(RAD/SEC)

$\dot{\delta}_s$
(RAD/SEC)

$||\dot{\gamma}_f||$

$||\dot{\gamma}_E||$
(FT-LB)

T_{gx}
(FT-LB)

T_{sy}
(FT-LB)

T_{gz}
(FT-LB)

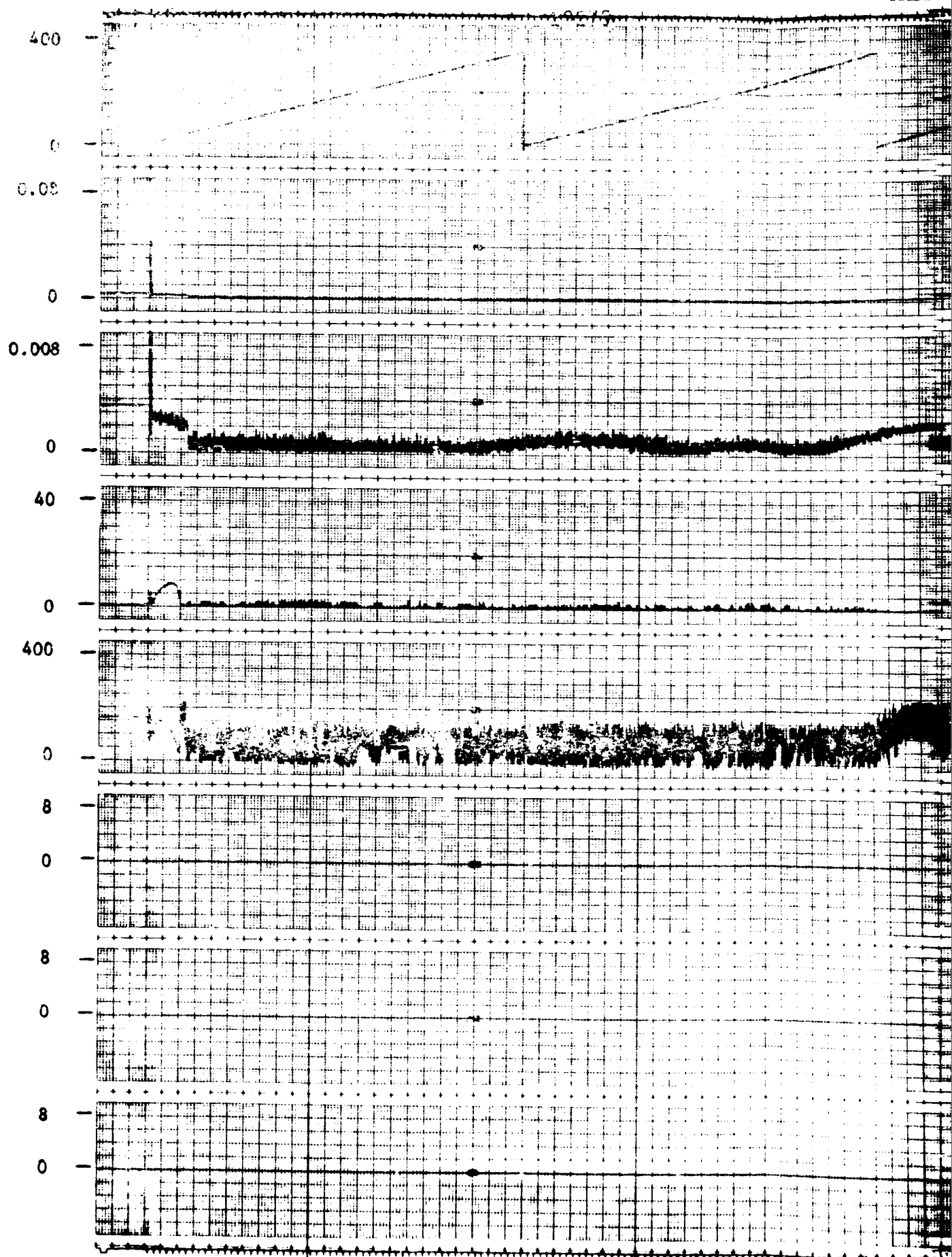
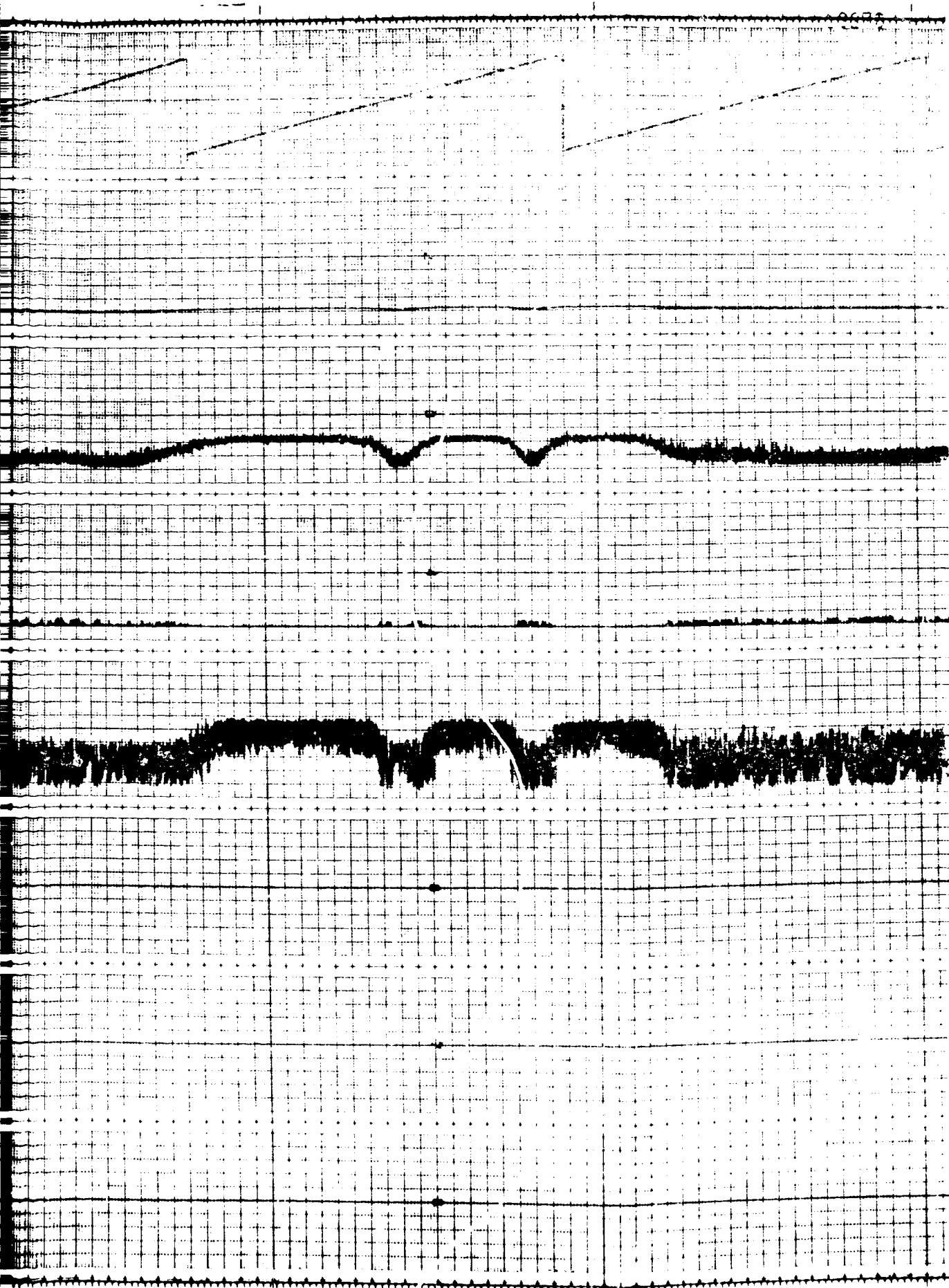
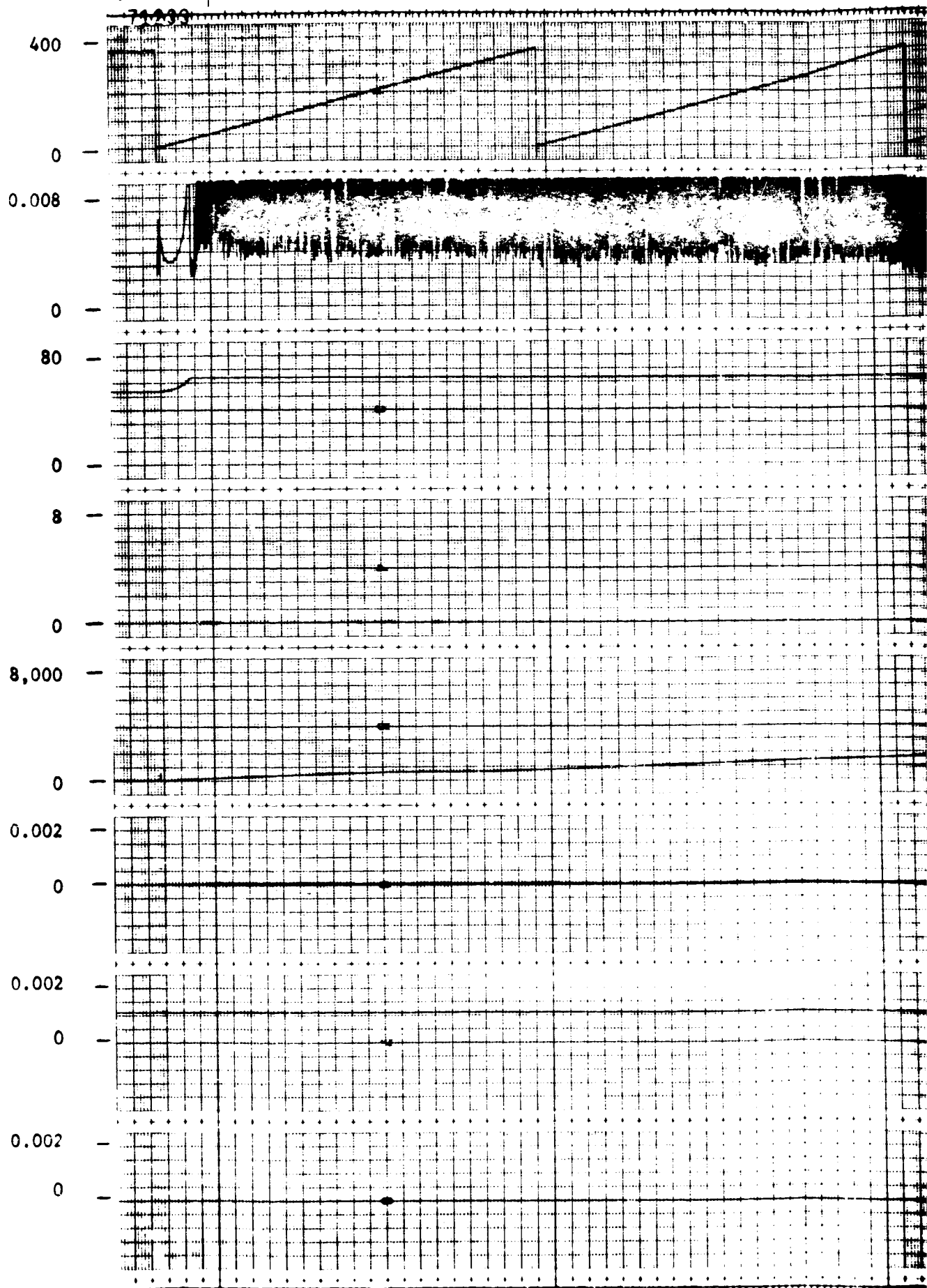


Figure 12.11. Z-LV Orbital Run with X-10P



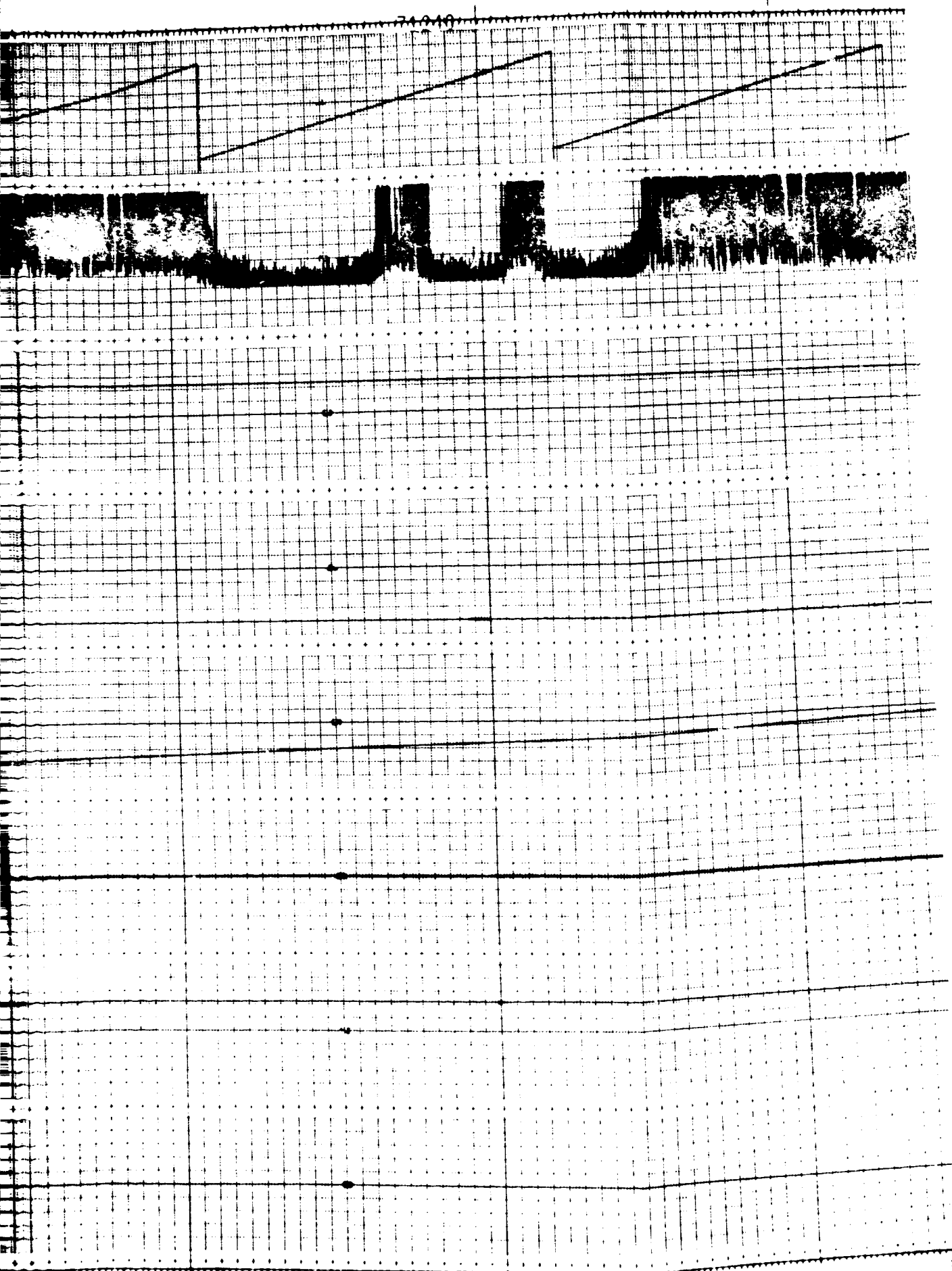
100 SECOND TIME MARKS

θ_{oc}
 (DEG)
 $\dot{\delta}_D$
 (RAD/SEC)
 f
 \vec{E}
 (DEG)
 \vec{H}_{CMG}
 (FT-LB-SEC)
 \dot{x}
 (RAD/SEC)
 \dot{y}
 (RAD/SEC)
 \dot{z}
 (RAD/SEC)



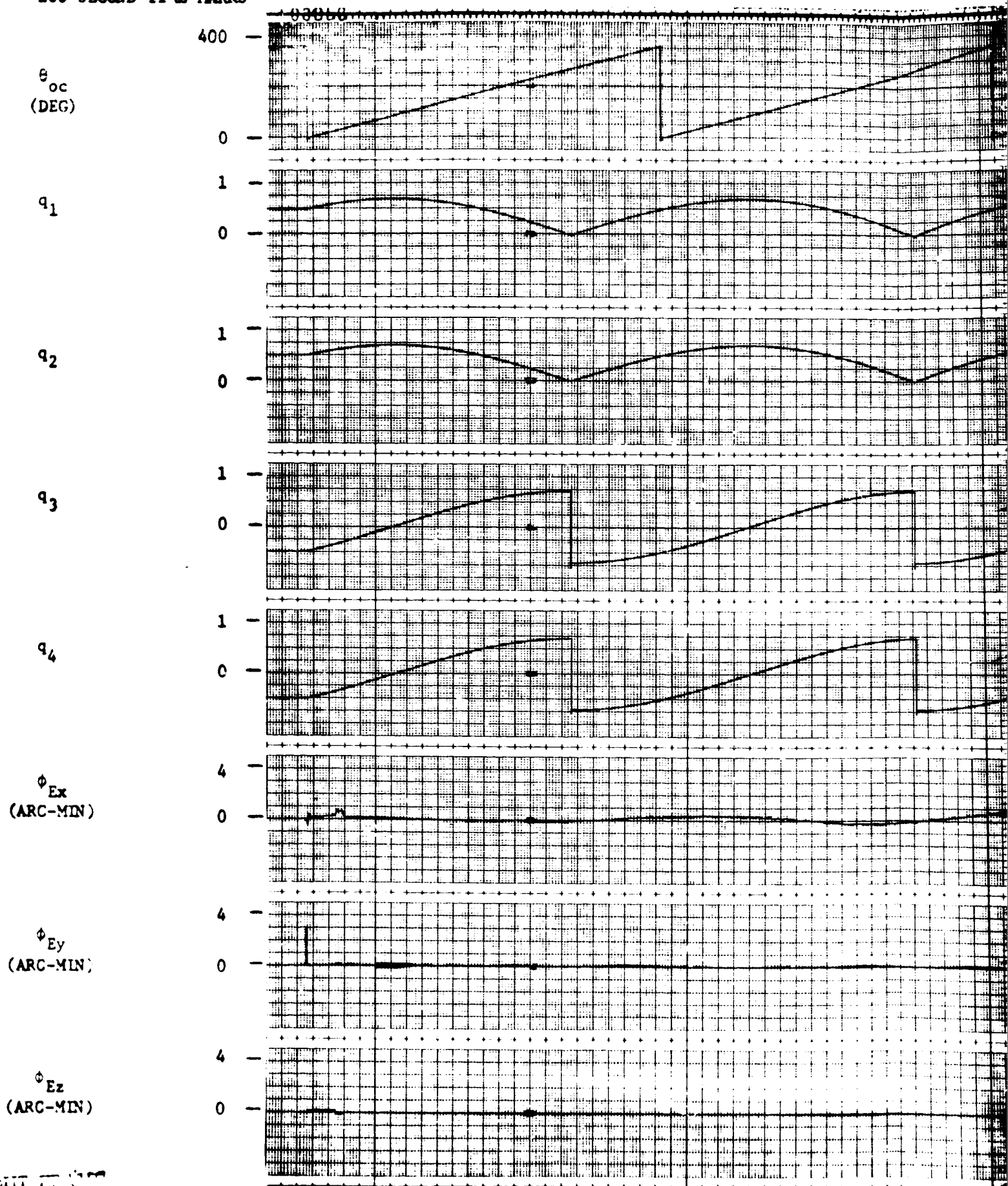
FOLDOUT FRAME

Figure 12.11. E-LV Orbital Run with X-IOP.



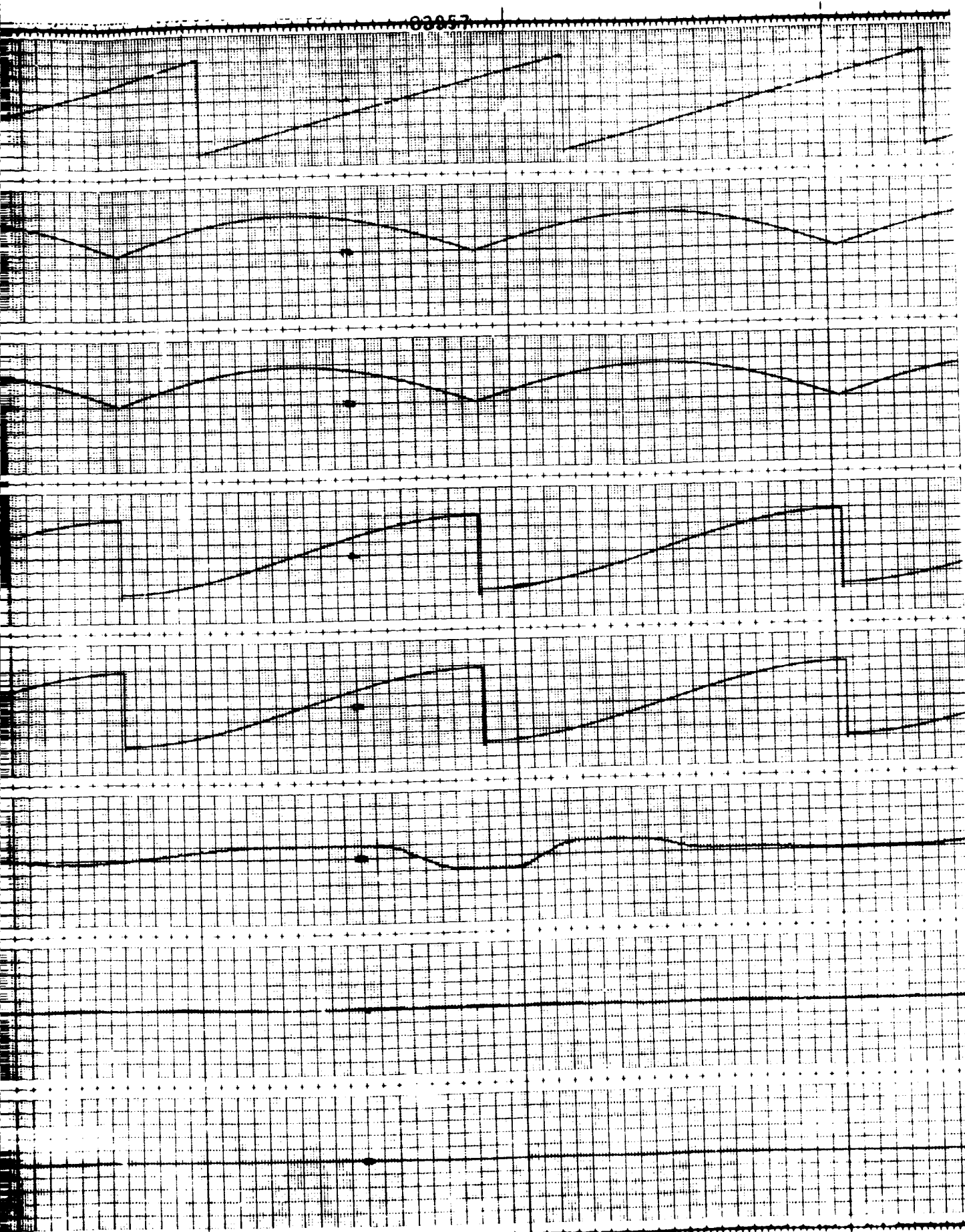
FOLDOUT TABLE

100 SECOND TIME MARKS



FOLDOUT 4-117

Figure 12.11. Z-LV Orbital Run with



OUT FRAME

100 SECOND TIME MARKS

$\dot{\phi}_{oc}$
(DEG)

400

0

$\dot{\phi}_s$
(RAD/SEC)

0.08

0

$\dot{\phi}_s$
(RAD/SEC)

0.008

0

$||\nabla f||$

40

0

$||\vec{T}_E||$
(FT-LB)

400

0

T_{gx}
(FT-LB)

8

0

T_{gy}
(FT-LB)

8

0

T_{gz}
(FT-LB)

8

0

WALDOUT FRAME

Figure 12.12. Z-LV Orbital Run with



100 SECOND TIME MARKS

θ_{oc}
 (DEG)

$\dot{\theta}_D$
 (RAD/SEC)

ϵ

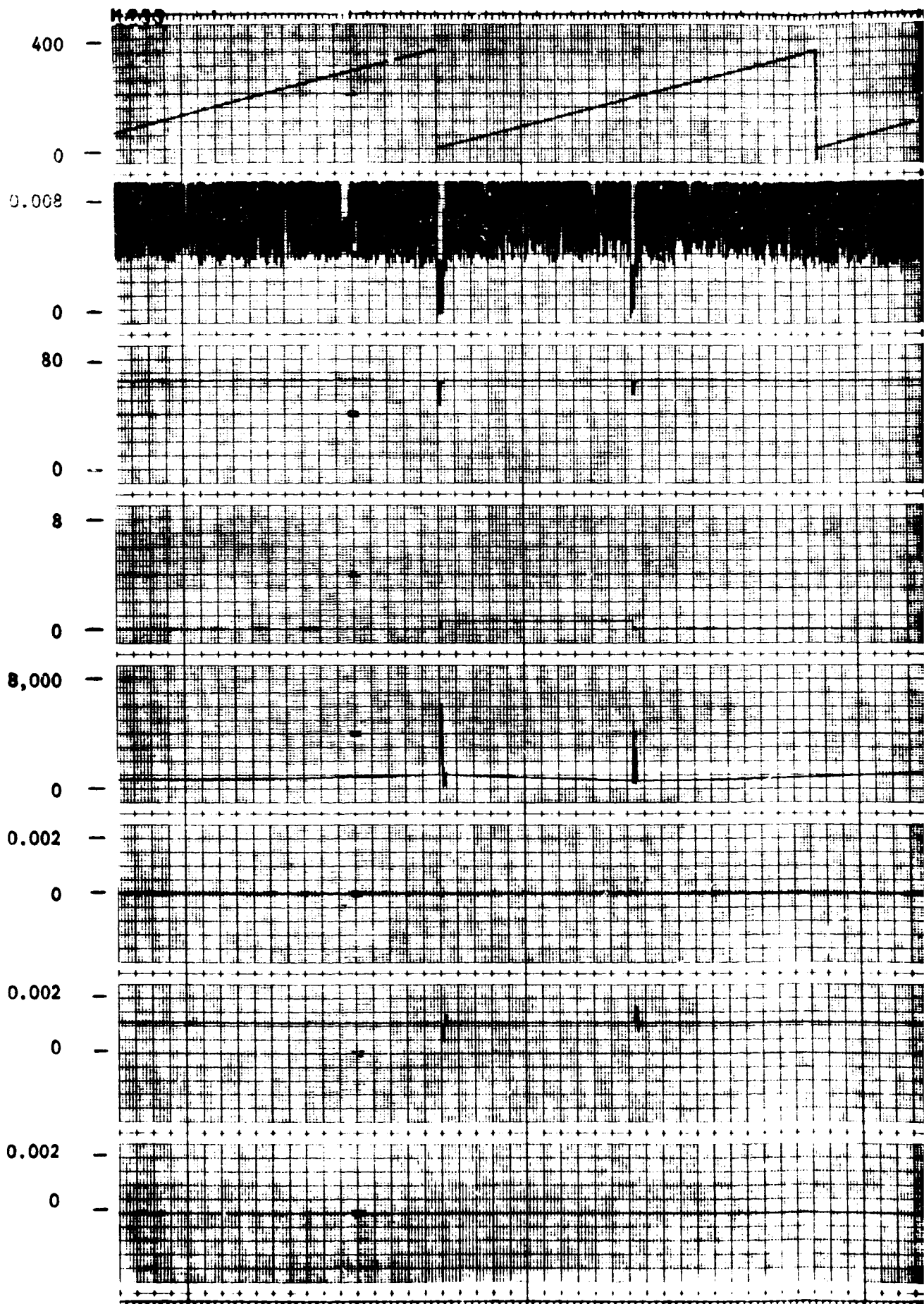
$||\vec{\epsilon}||$
 (DEG)

$||\vec{H}_{CMG}||$
 (FT-LB-SEC)

ω_x
 (RAD/SEC)

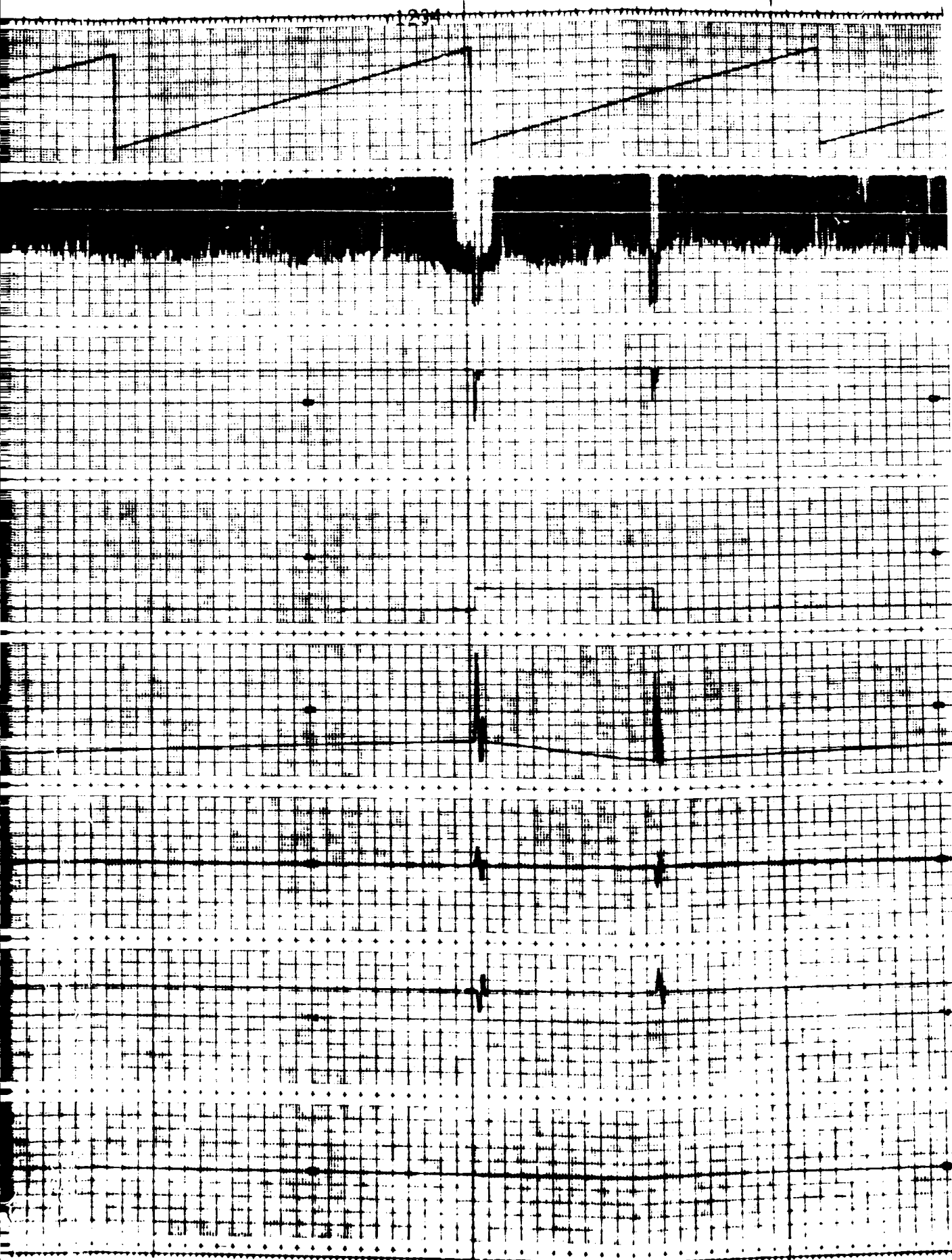
ω_y
 (RAD/SEC)

ω_z
 (RAD/SEC)



WALDOUT PL-100

Figure 12.12. E-LV Orbital Run



100 SECOND TIME MARKS

θ_{oc}
(DEG)

q_1

q_2

q_3

q_4

ϕ_{Ex}
(ARC-MIN)

ϕ_{Ey}
(ARC-MIN)

ϕ_{Ez}
(ARC-MIN)

FOLDOUT FRAME

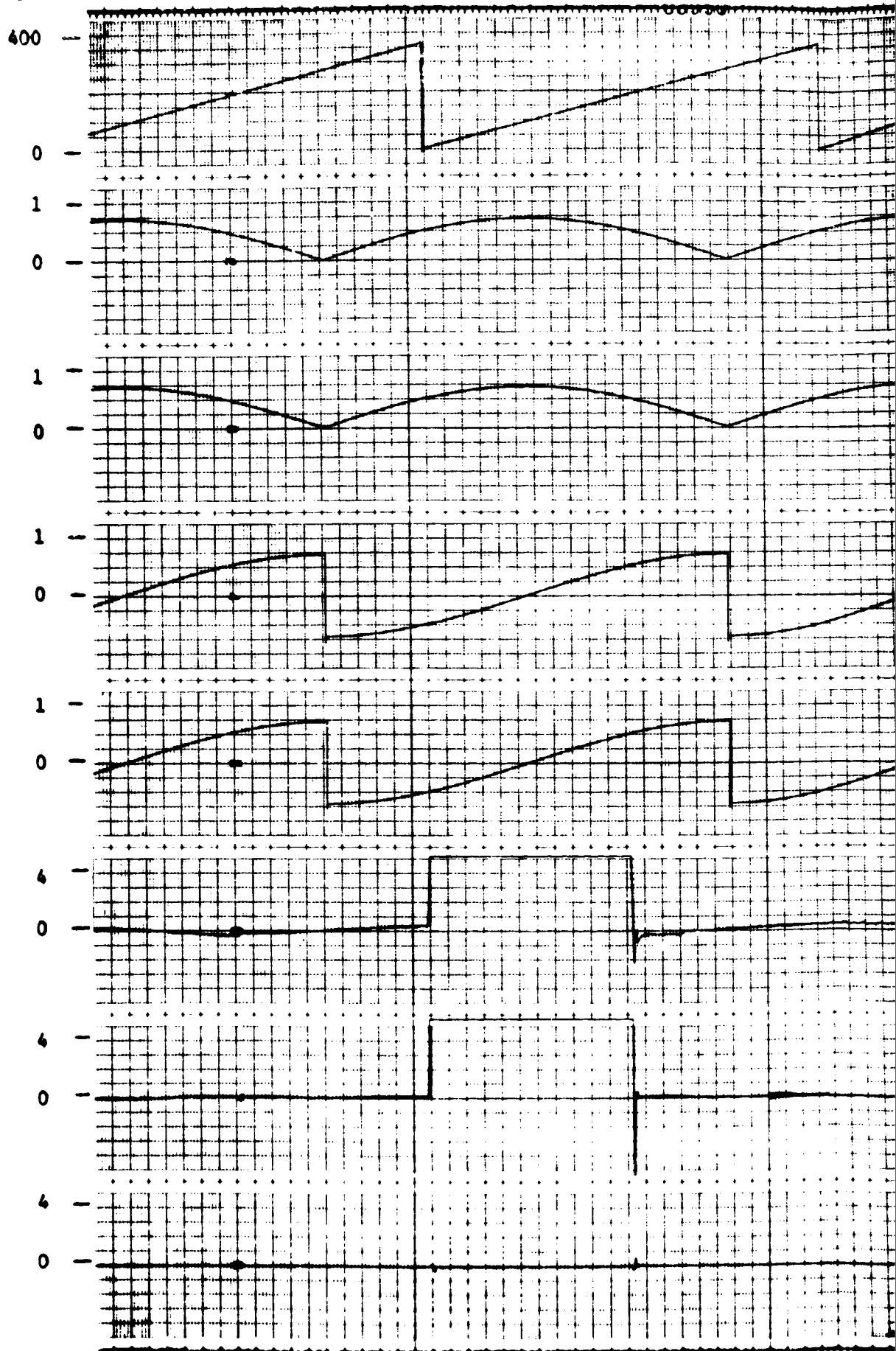
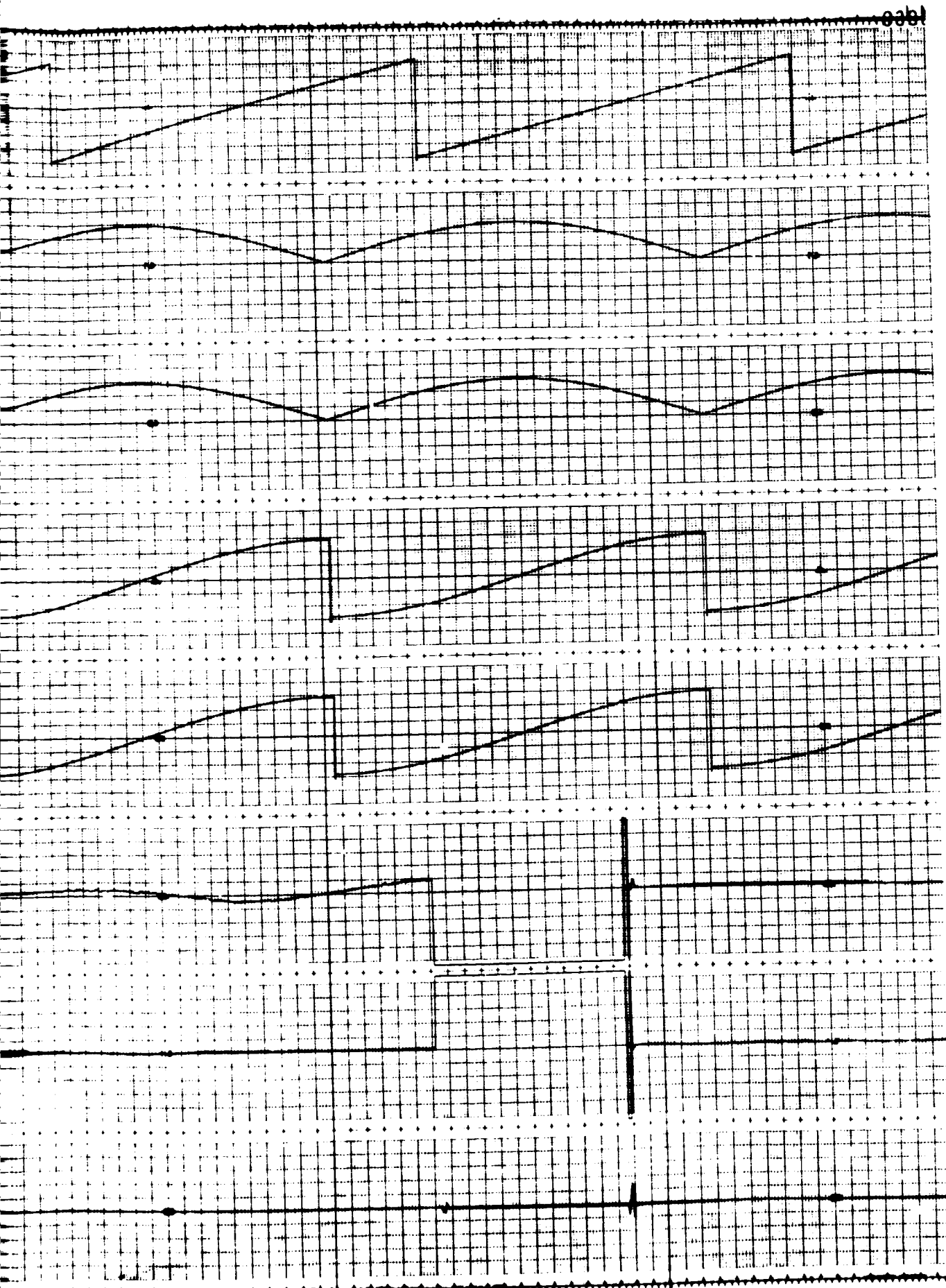


Figure 12.12. Z-LV Orbit



FOLDOUT FROM...

100 SECOND TIME MARKS

θ_{oc}
(DEG)

$\dot{\theta}_s$
(RAD/SEC)

$\dot{\theta}_s$
(RAD/SEC)

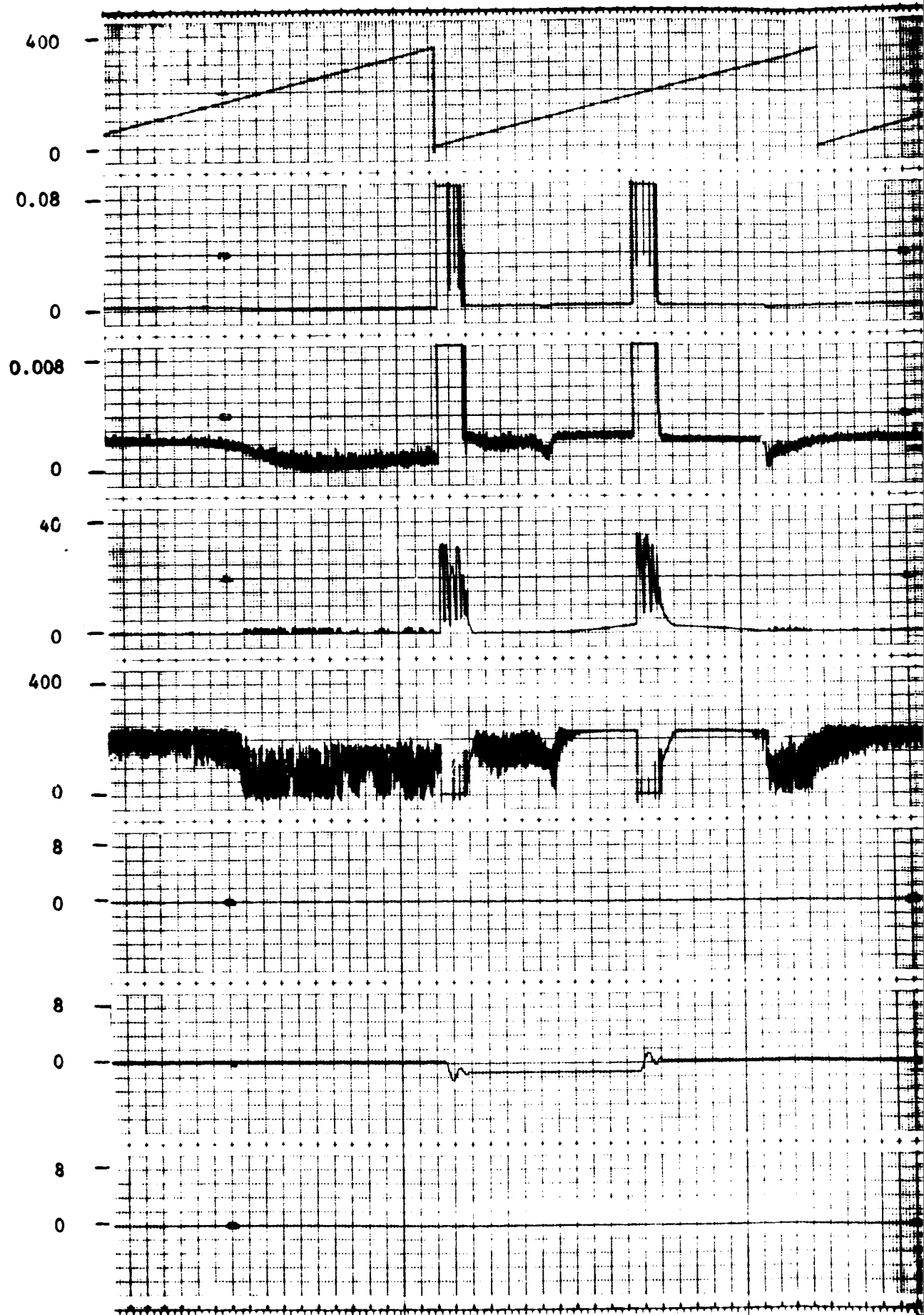
$|\dot{\theta}_f|$

$|\dot{\theta}_E|$
(FT-LB)

T_{gx}
(FT-LB)

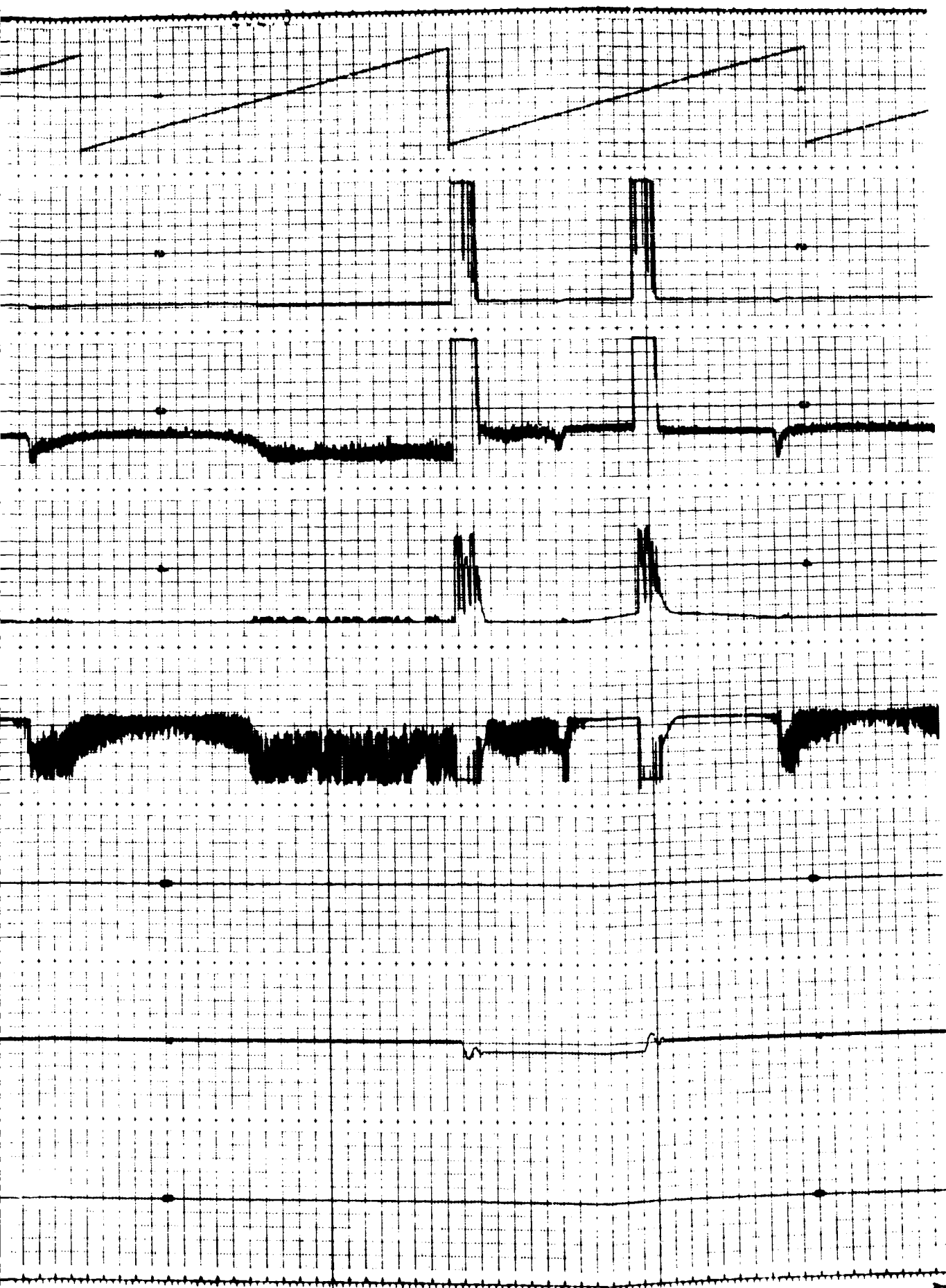
T_{gy}
(FT-LB)

T_{gz}
(FT-LB)



FOLDOUT FRAME

Figure 12.13. Z-IV Orbital Run,
1/2 Degree Vehicle



—LV Orbital Run with X-10P (Nominally) and
/2 Degree Vehicle Offset on Each Axis (Sheet 1 of 3)

FOLDOUT

100 SECOND TIME MARKS

θ_{oc}
(DEG)

$\dot{\theta}_D$
(RAD/SEC)

ϵ

$\dot{\epsilon}$
(DEG)

\dot{h}_{CMG}
(FT-LB-SEC)

ω_x
(RAD/SEC)

ω_y
(RAD/SEC)

ω_z
(RAD/SEC)

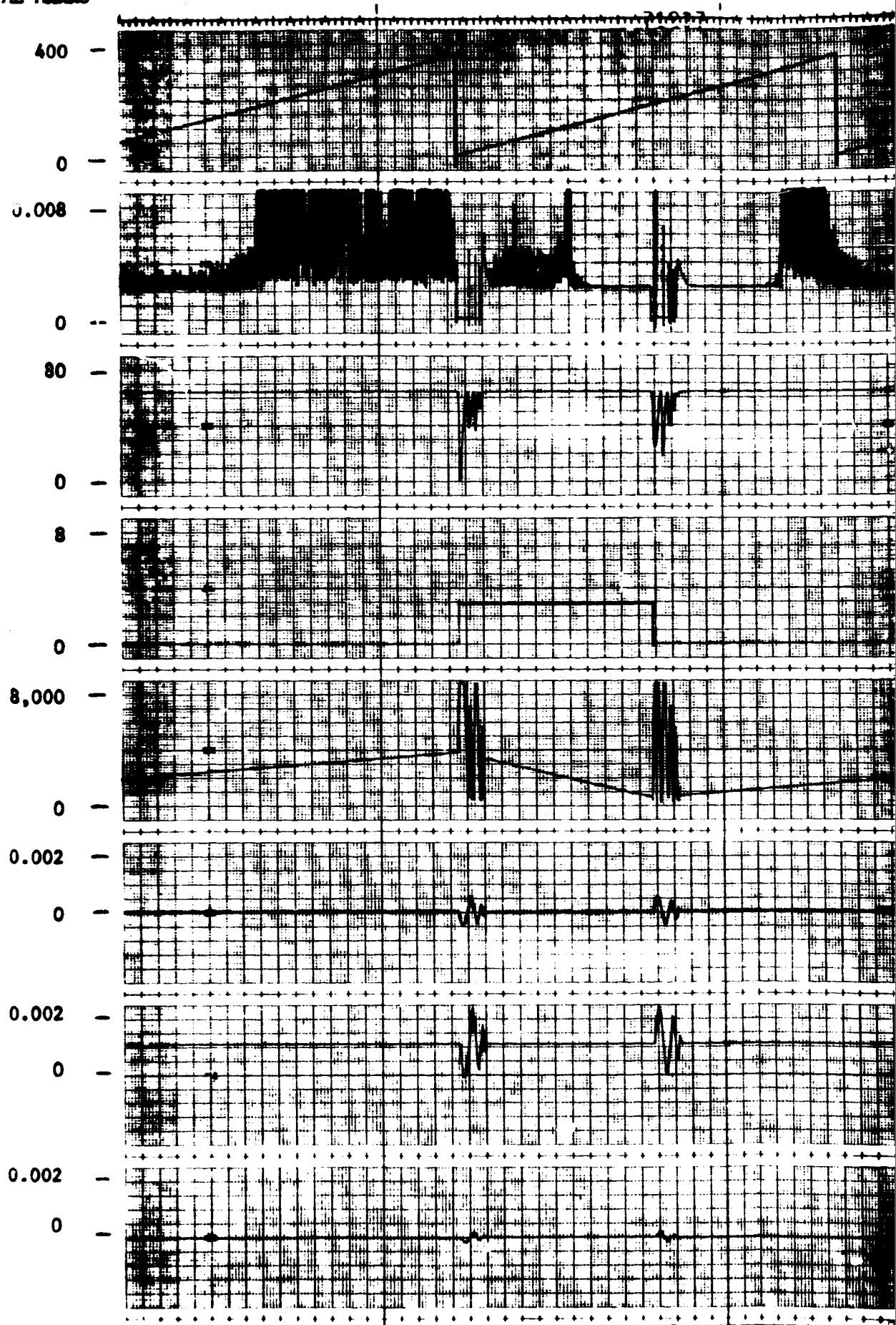


Figure 12.13. Z-LV Orbital
1/2 Degree

re 12.13. Z-LV Orbital Run with X-IOP (Nominally) and
1/2 Degree Vehicle Offset on Each Axis (Sheet 2 of 3)

100 SECOND TIME MARKS

θ_{oc}
(DEG)

q_1

q_2

q_3

q_4

ϕ_{Ex}
(ARC-MIN)

ϕ_{Ey}
(ARC-MIN)

ϕ_{Ez}
(ARC-MIN)

FOLDOUT FRAME

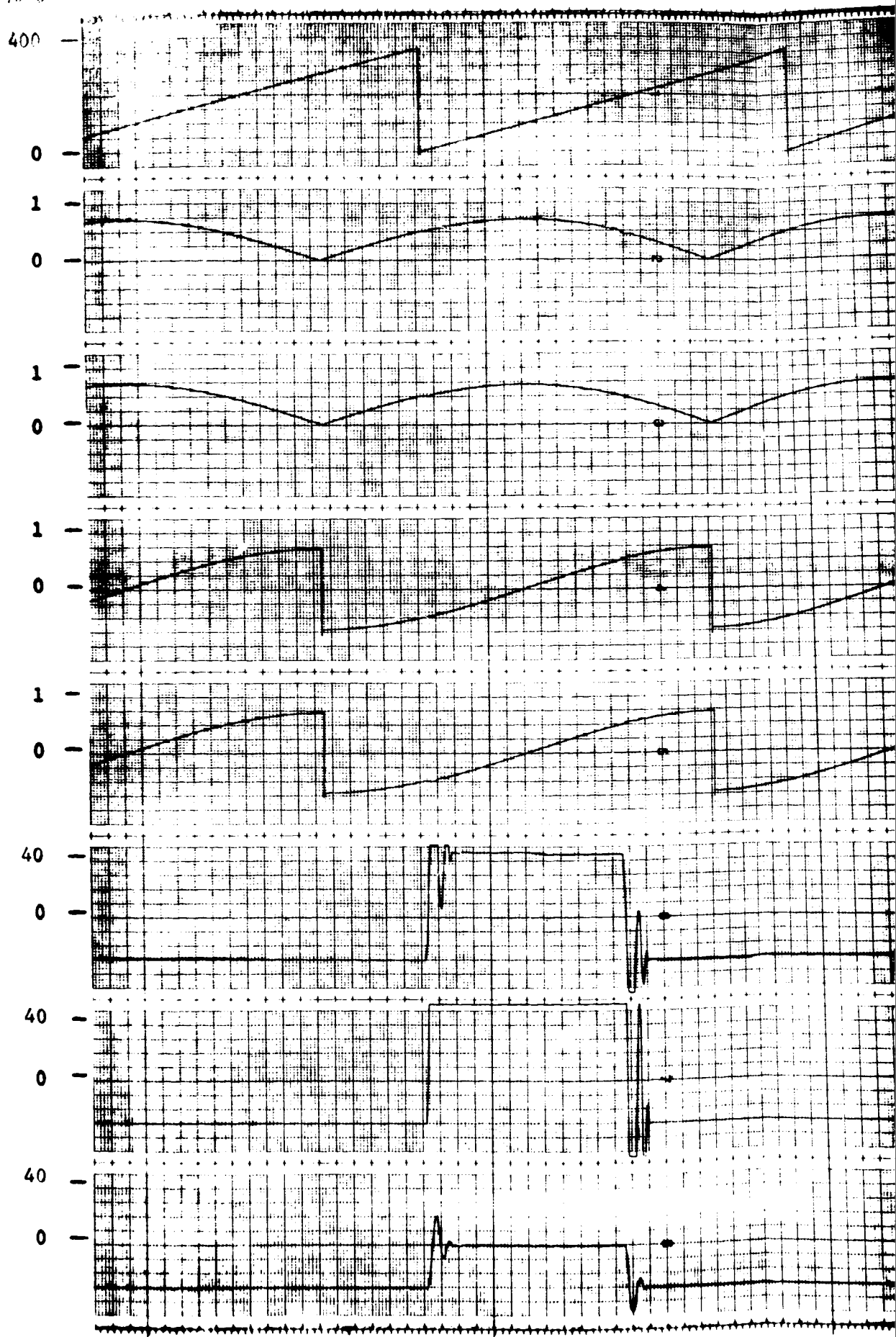
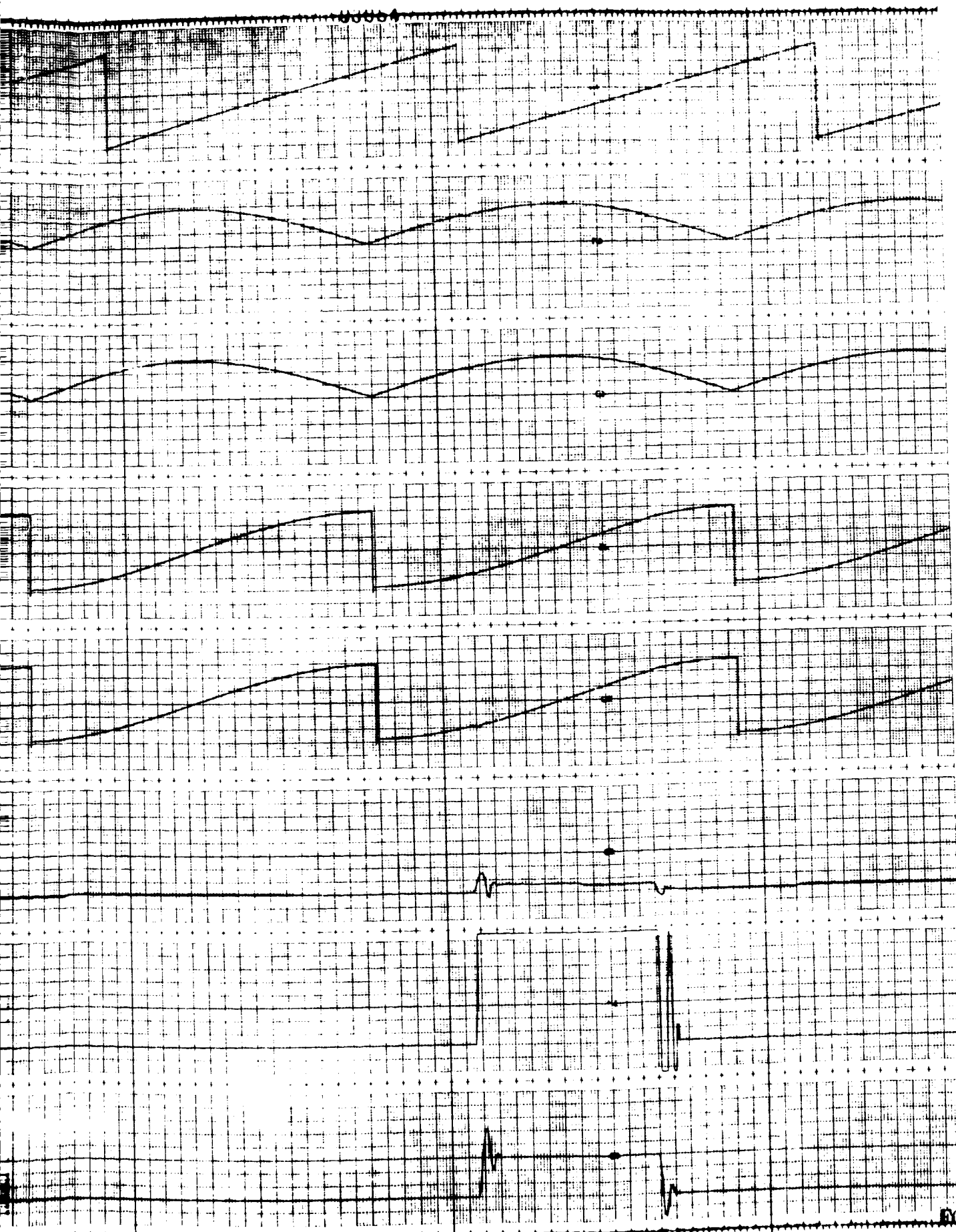


Figure 12.13. Z-LV Orbital Run
1/2 Degree Vehicle



Z-LV Orbital Run with X-IOP (Nominally) and
1/2 Degree Vehicle Offset on Each Axis (Sheet 3 of 3)

FOLDOUT

100 SECOND TIME MARKS

θ_{oc}
(DEG)

$\dot{\theta}_s$
(RAD/SEC)

$\dot{\theta}_s$
(RAD/SEC)

$\|\nabla f\|$

$\|\vec{T}_E\|$
(FT-LB)

T_{gx}
(FT-LB)

T_{gy}
(FT-LB)

T_{gz}
(FT-LB)

WINDOUT FRAME

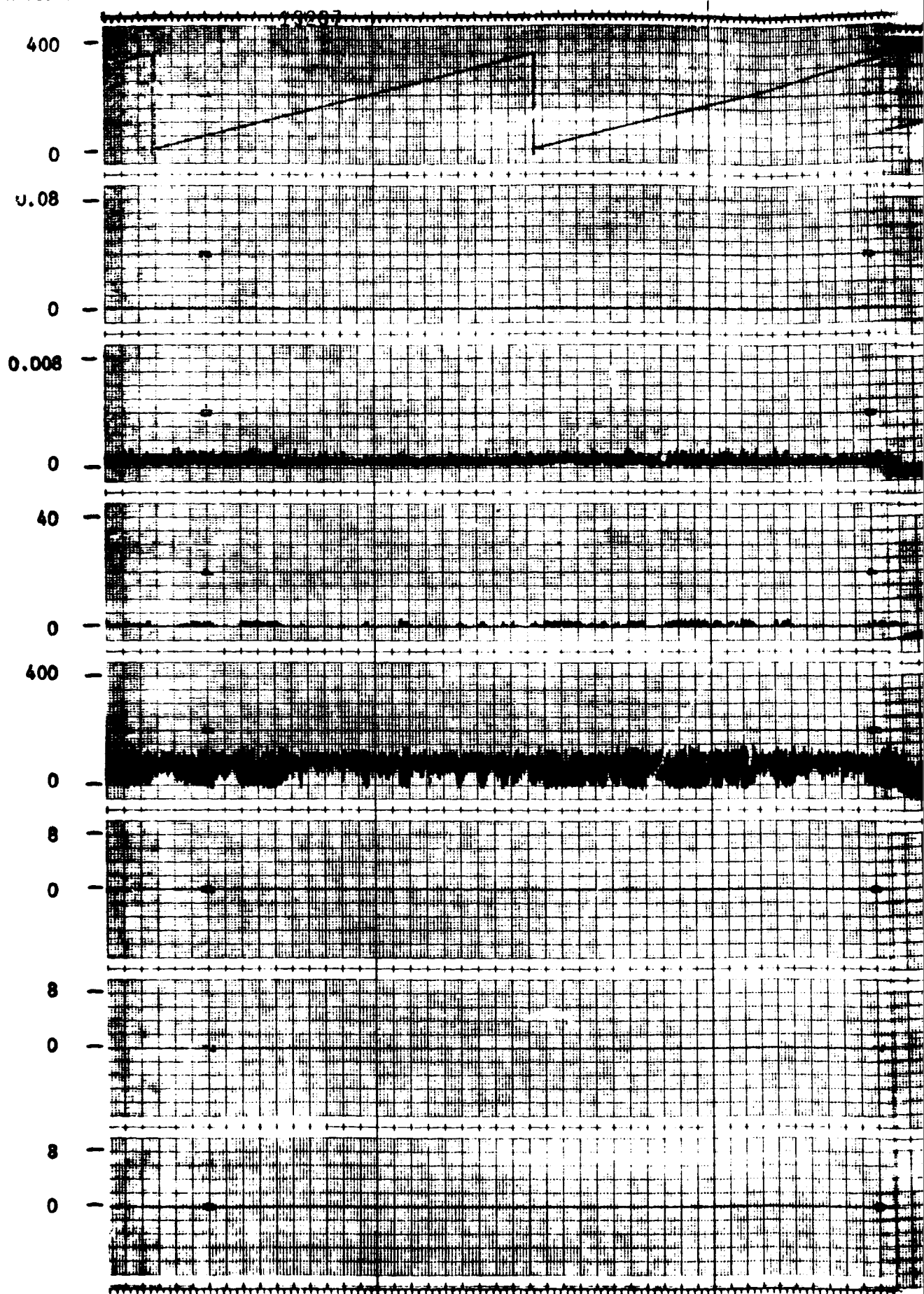
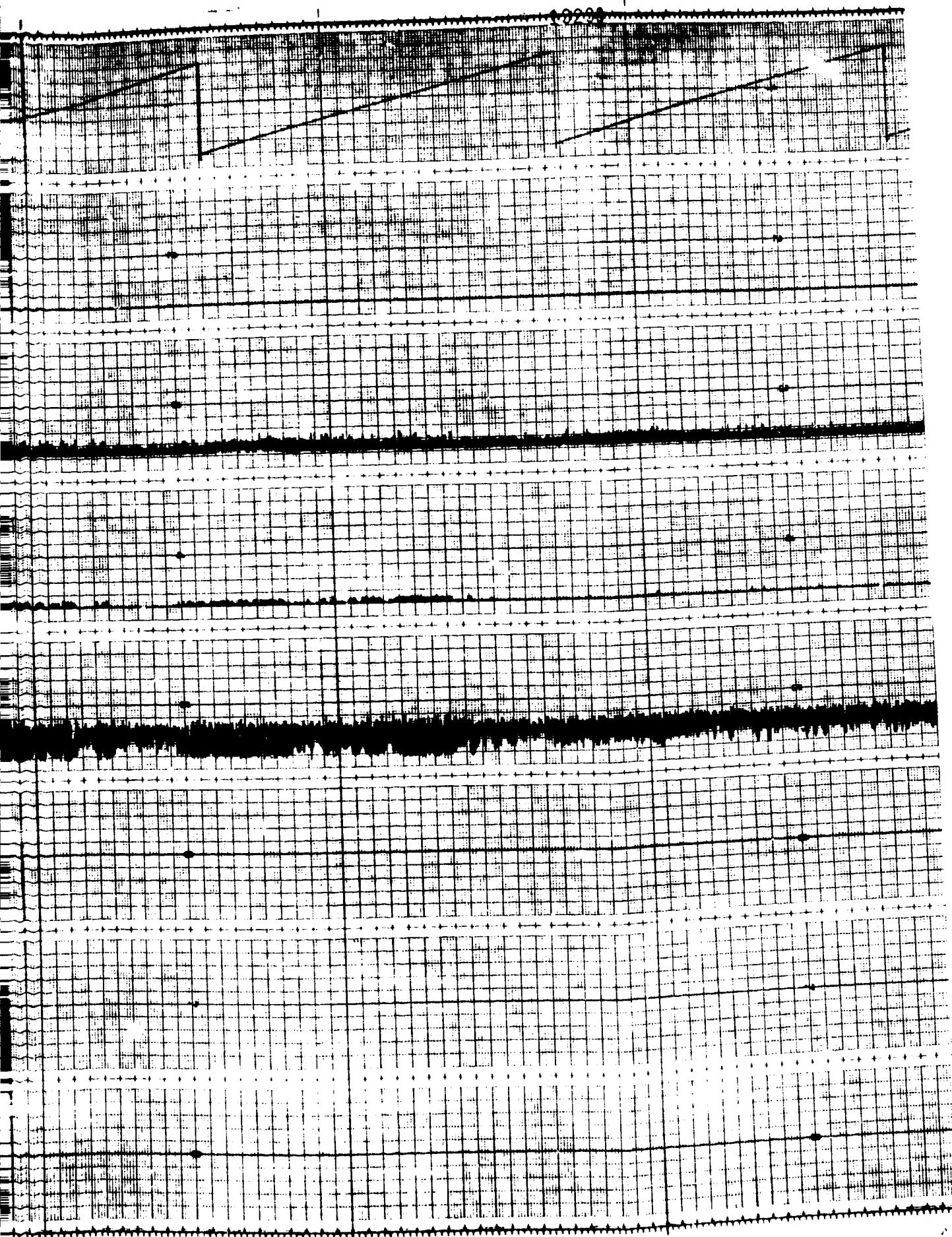


Figure 12.14. Z-LV Orbit



100 SECOND TIME MARKS

θ_{oc}
(DEG)

$\dot{\delta}_D$
(RAD/SEC)

\ddot{f}

$\dot{\epsilon}$
(DEG)

\dot{H}_{CMG}
(FT-LB-SEC)

ω_x
(RAD/SEC)

ω_y
(RAD/SEC)

ω_z
(RAD/SEC)

FOLDOUT FRAME

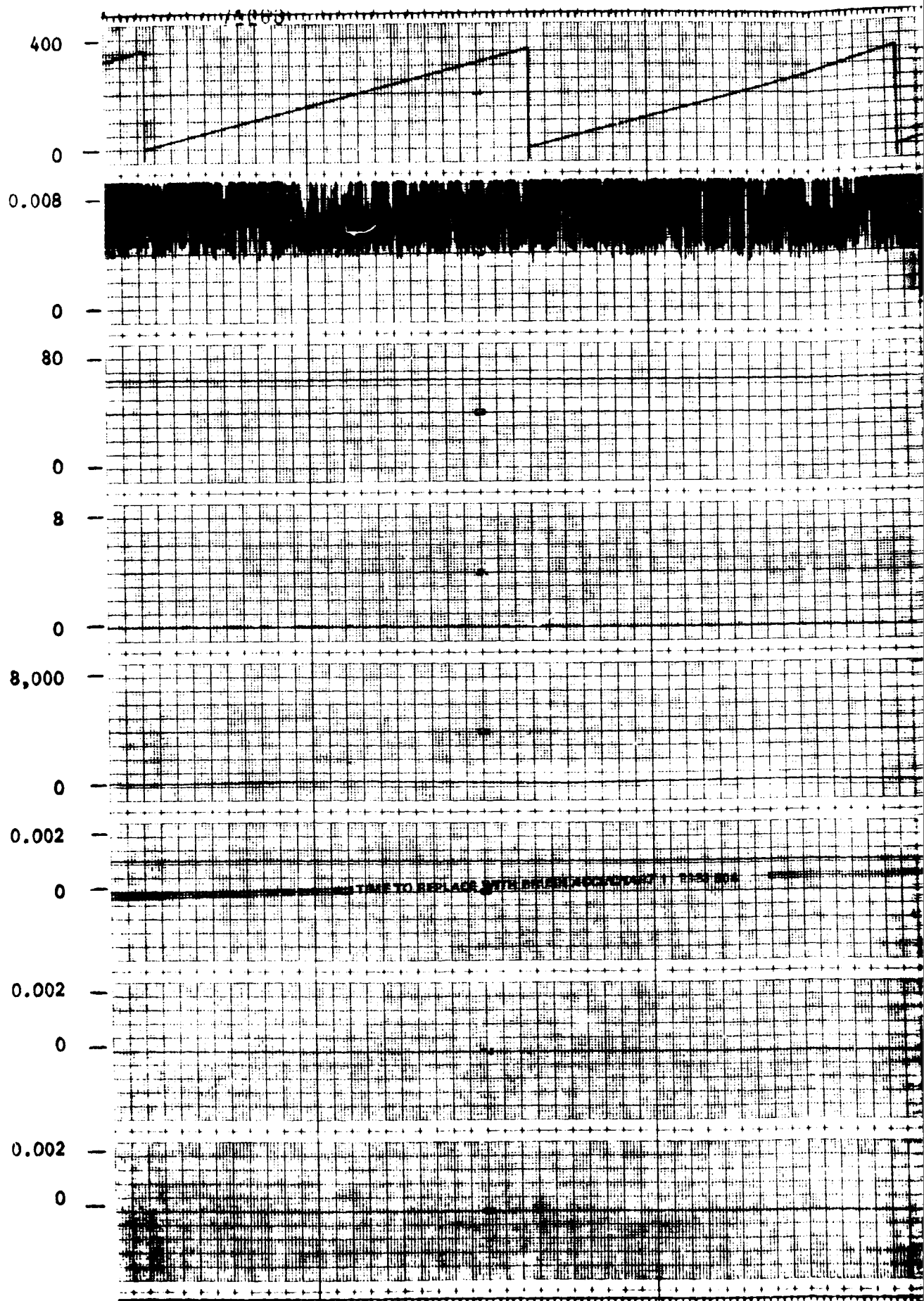
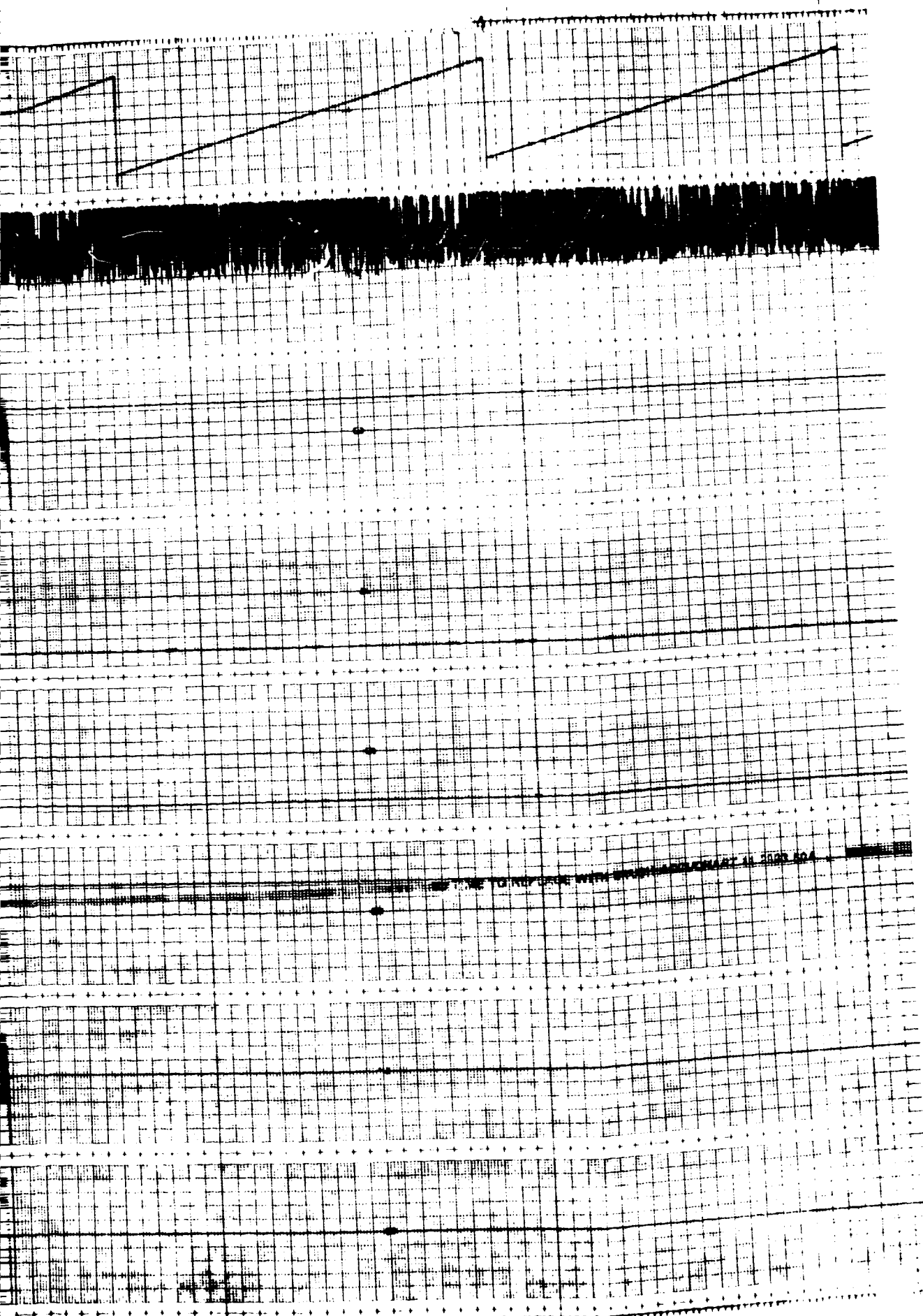


Figure 12.14. Z-LV Orbital Run

12-46



100 SECOND TIME MARKS

θ_{oc}
(DEG)

q_1

q_2

q_3

q_4

ϕ_{Ex}
(ARC-MIN)

ϕ_{Ey}
(ARC-MIN)

ϕ_{Ez}
(ARC-MIN)

FOLDOUT FRAME

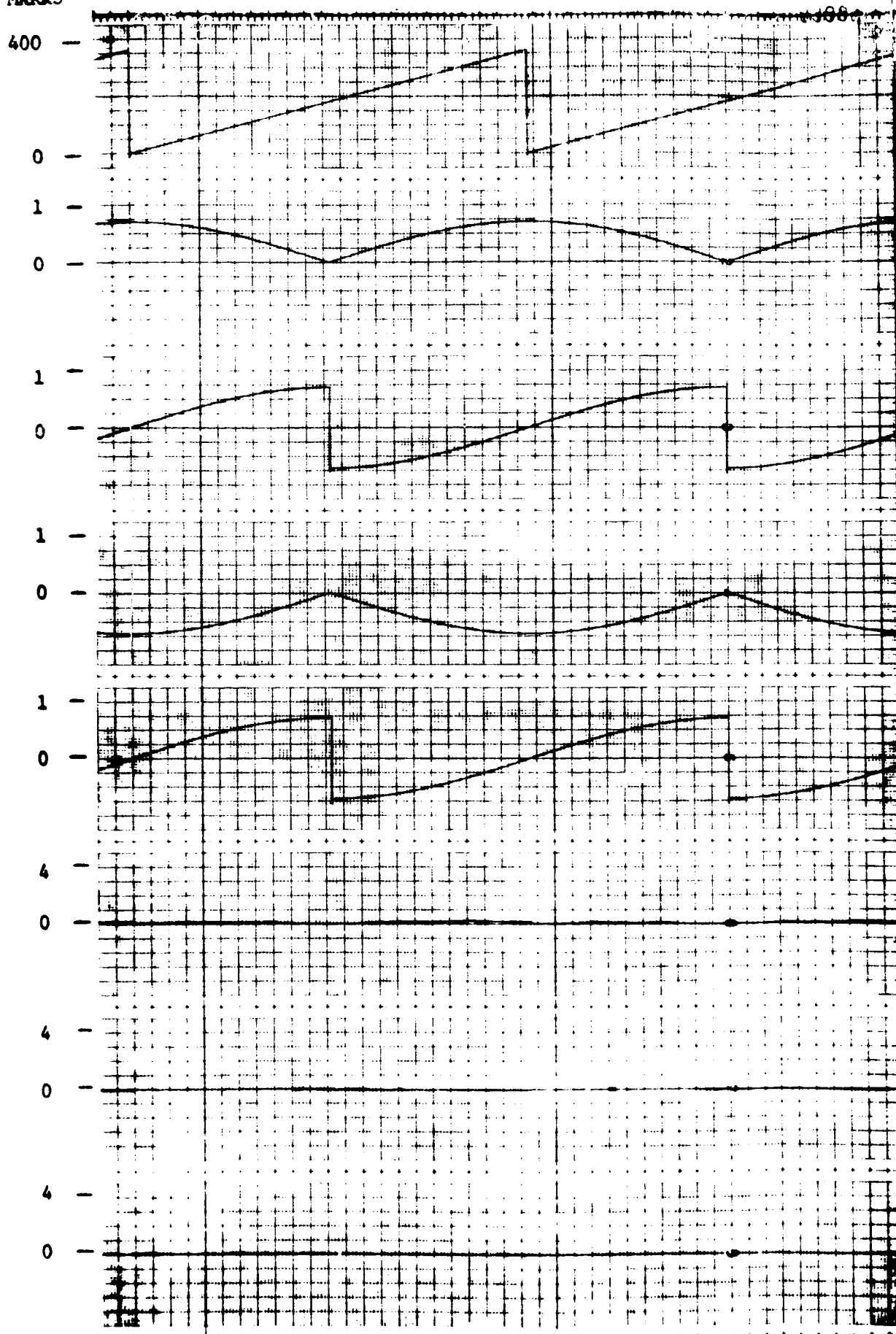
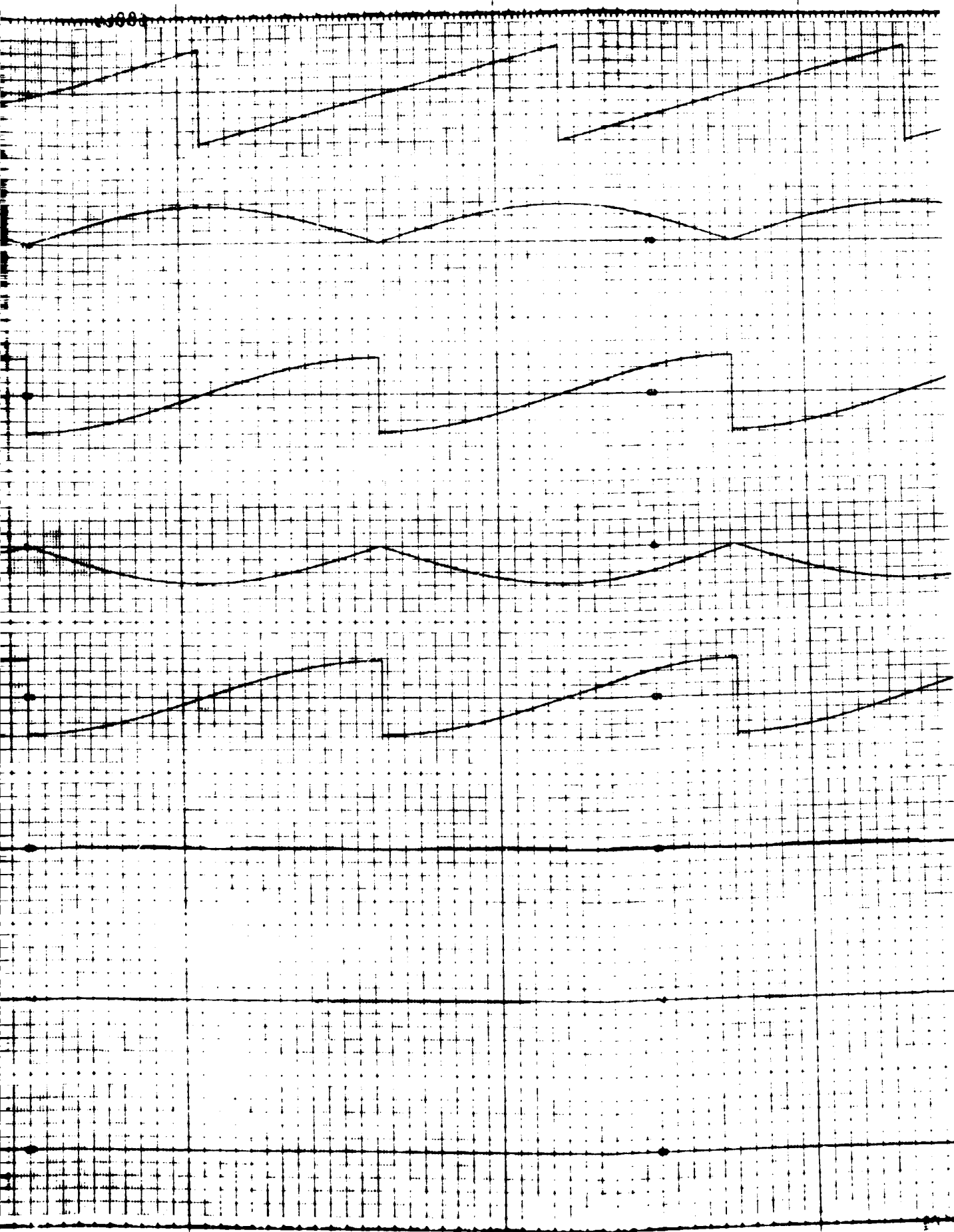


Figure 12.14. Z-LV Orb



100 SECOND TIME MARKS

θ_{oc}
(DEG)

$\dot{\delta}_s$
(RAD/SEC)

$\dot{\delta}_s$
(RAD/SEC)

$||\nabla f||$

$||\ddot{f}_E||$
(FT-LB)

T_{gx}
(FT-LB)

T_{gy}
(FT-LB)

T_{gz}
(FT-LB)

MOLDOUT FRAME

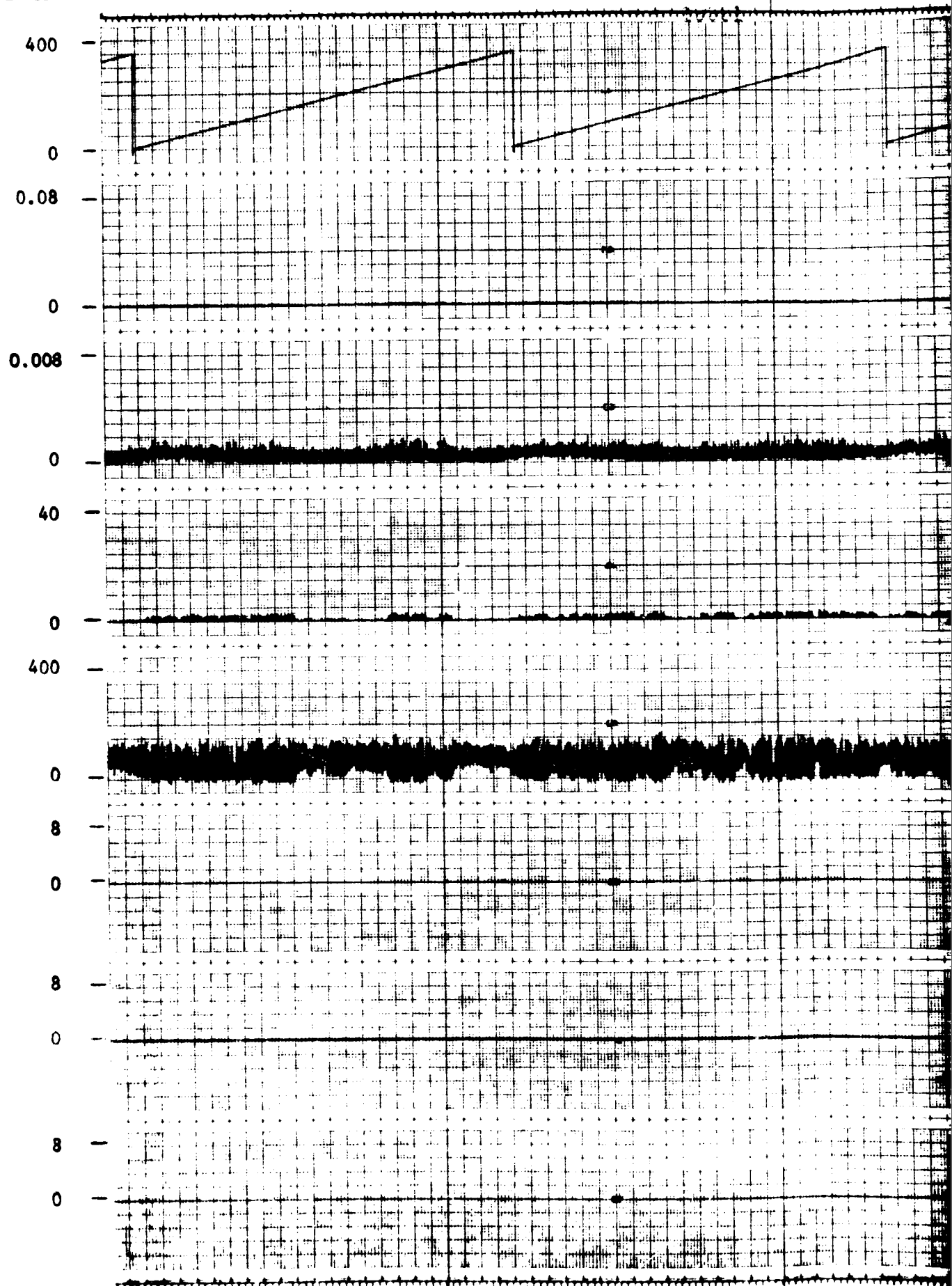
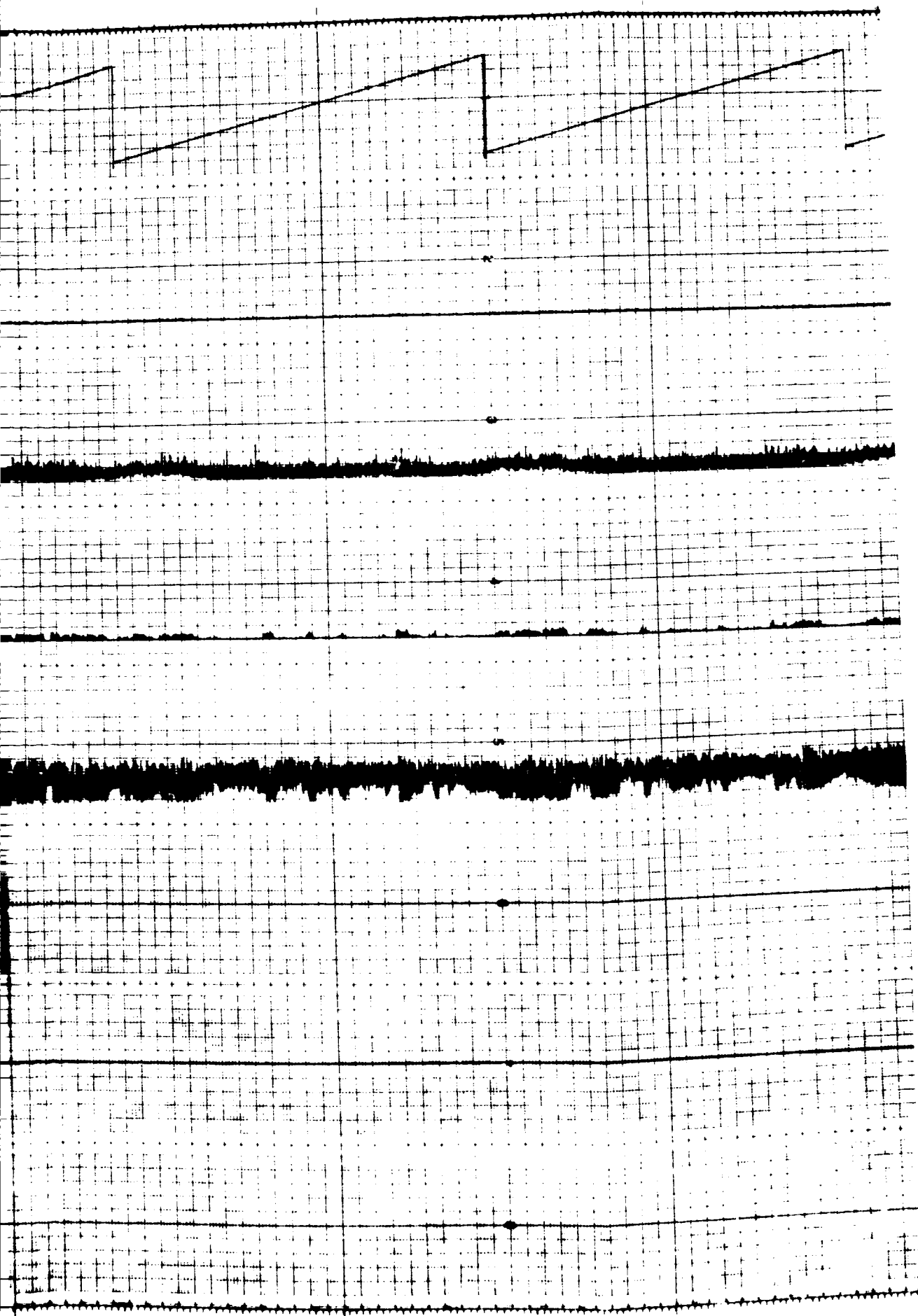


Figure 12.15. Z-LV Orbital Run w/
1/2 Degree Vehicle



100 SECOND TIME MARKS

θ_{oc}
(DEG)

400

0

$\dot{\theta}_D$
(RAD/SEC)

0.008

0

80

ϵ

0

8

$\dot{\epsilon}$
(DEG)

0

\dot{H}_{CMG}
(FT-LB-SEC)

8,000

0

0.002

ω_x
(RAD/SEC)

0

ω_y
(RAD/SEC)

0.002

0

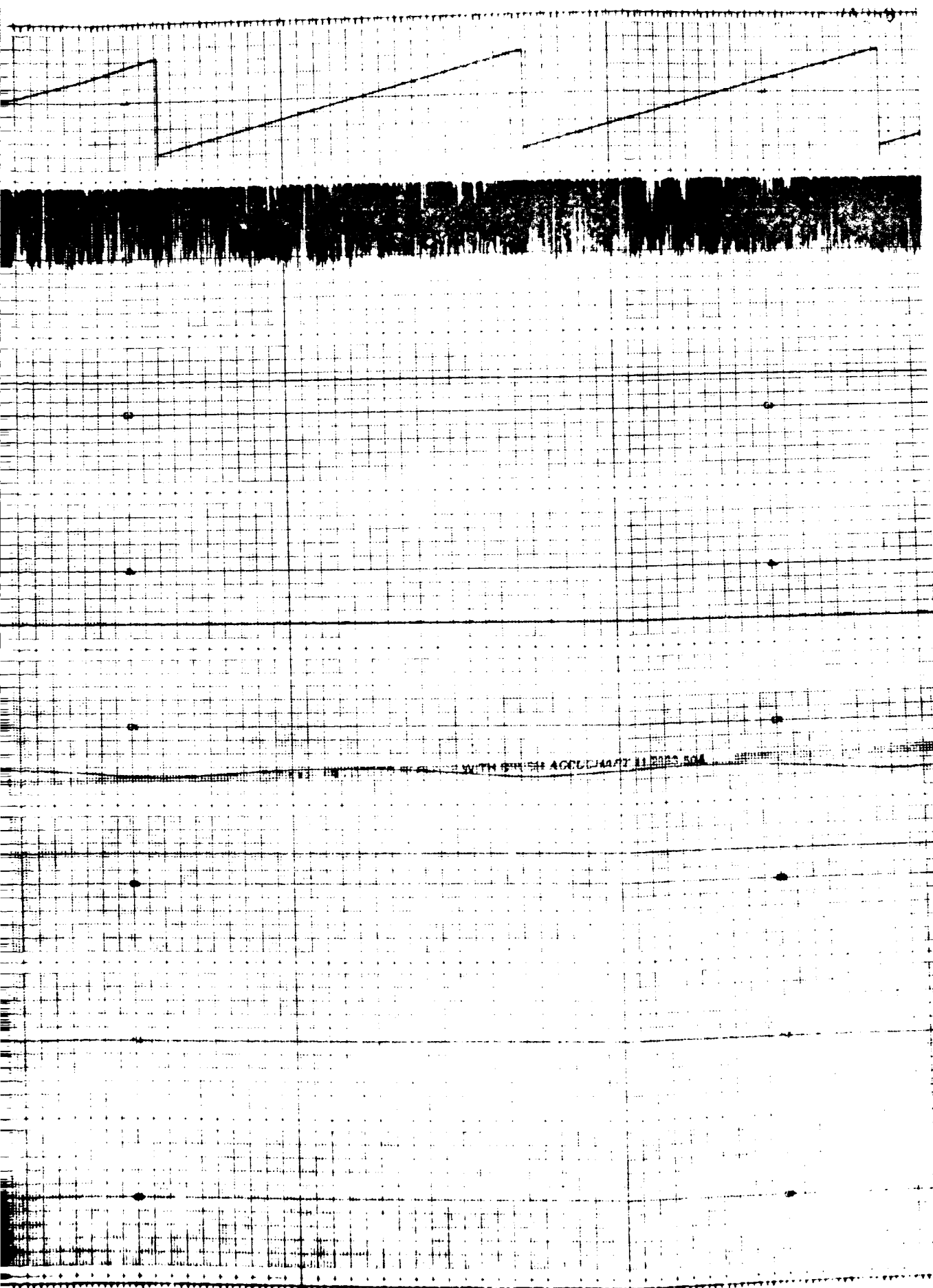
ω_z
(RAD/SEC)

0.002

0

FOLDOUT FRAME

Figure 12.15. Z-LV Orbital Run with
1/2 Degree Vehicle



FOLDOUT FRAME

100 SECOND TIME MARKS

θ_{oc}
(DEG)

q_1

q_2

q_3

q_4

ϕ_{Ex}
(ARC-MIN)

ϕ_{Ey}
(ARC-MIN)

ϕ_{Ez}
(ARC-MIN)

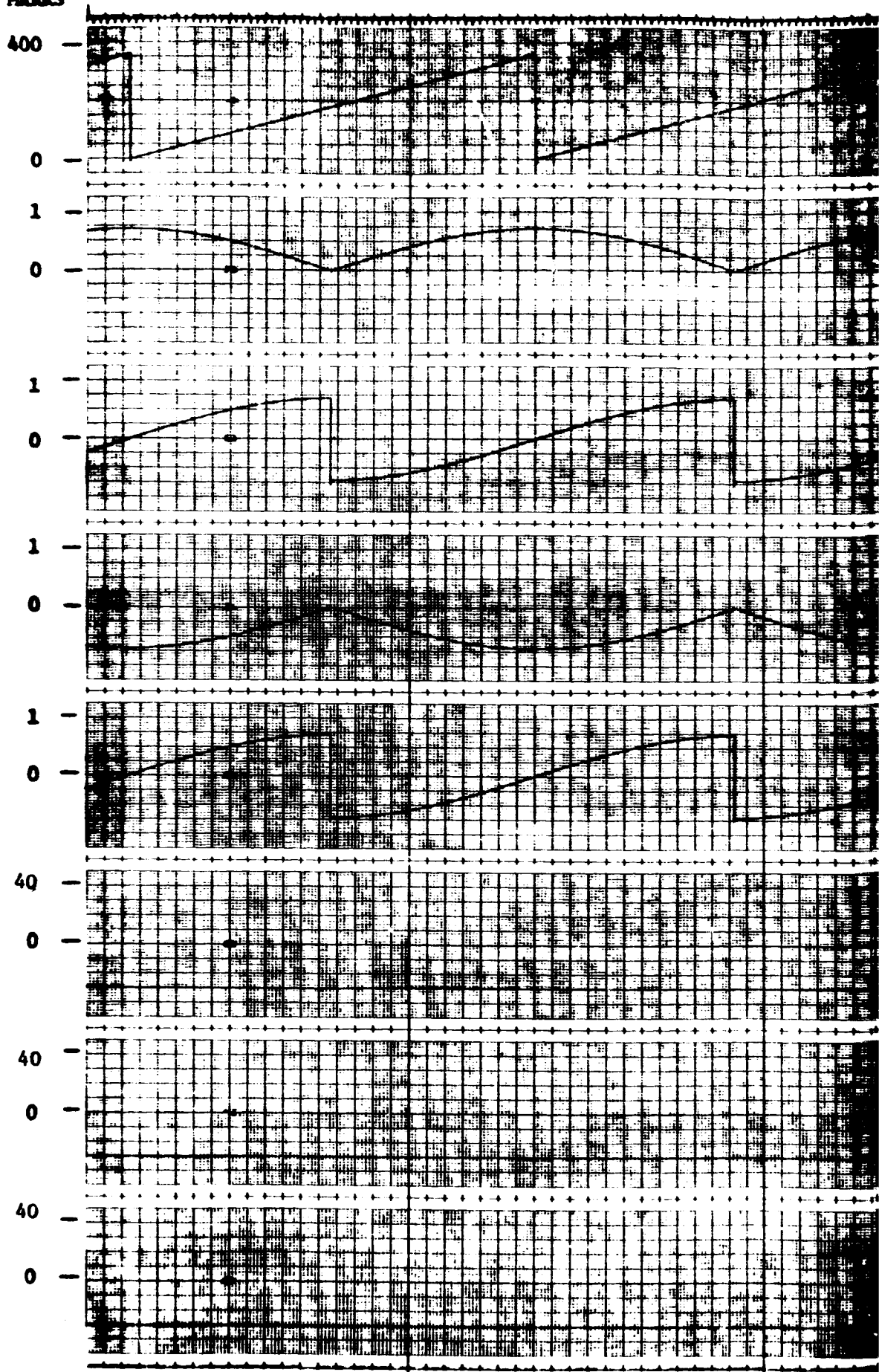
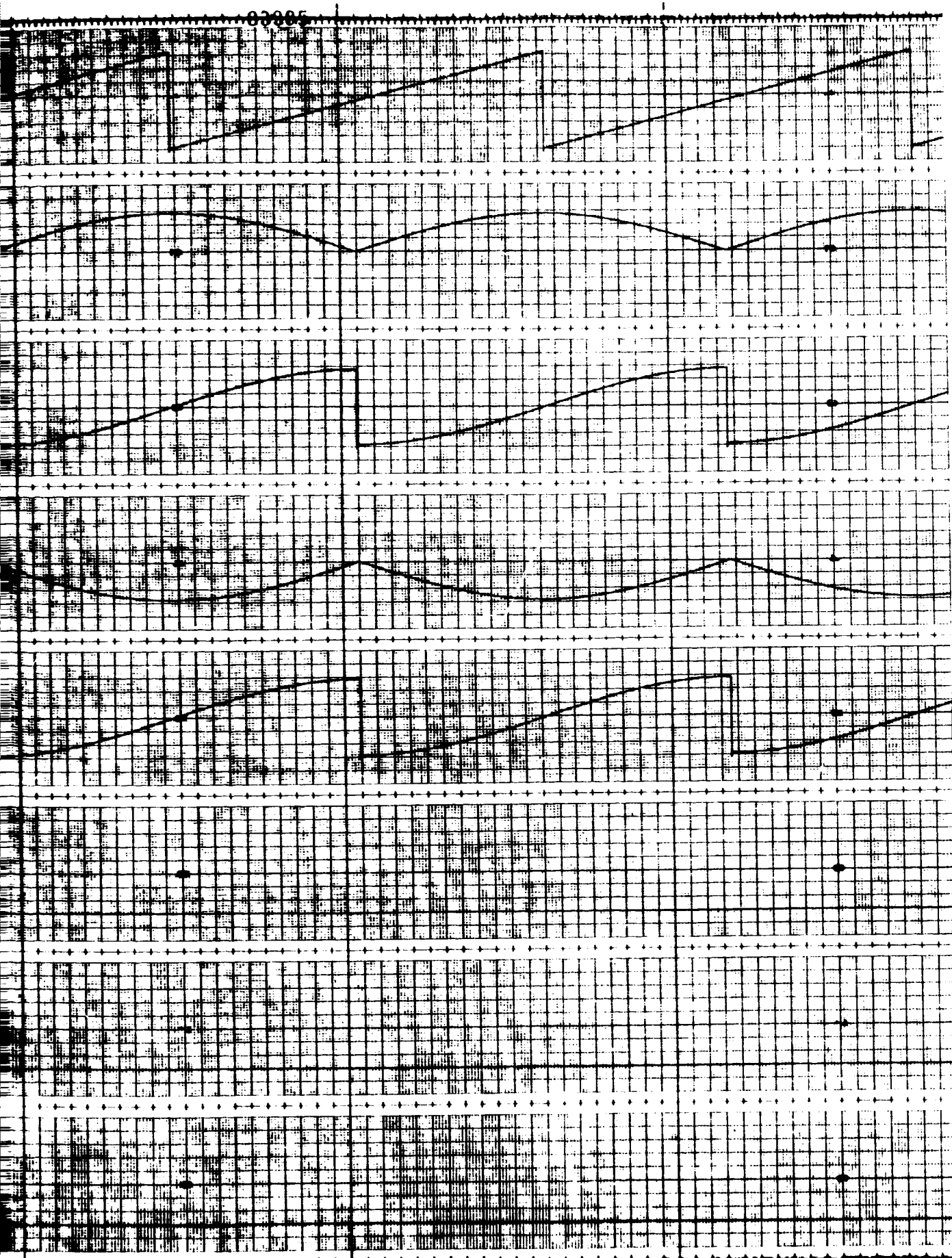


Figure 12.15. Z-LV Orbital Run with 1/2 Degree Vehicle



13. CONCLUSIONS

In this report, a control moment gyro (CMG) attitude control system is designed for a large orbiting spacecraft. The purposes of this study are: (1) to demonstrate the basic procedures that should be followed in designing a CMG control system, (2) to define the various software control options available, and (3) to verify the proper operation of the selected control logic utilizing a hybrid computer simulation of the CMG control system.

For this study, the vehicle used was the Space Shuttle. Using the Shuttle sortie missions defined in the General Dynamics/Convair Phase B Research and Application Module (RAM) program, an analysis was performed to define the vehicle mission requirements. These mission requirements are listed in table 13.1. From table 13.1, two distinct advantages of adding a CMG attitude control system to the Shuttle become apparent. The first one is that the baseline Shuttle reaction control subsystem (RCS) is too large to meet the vehicle pointing and stabilization requirements list but, that these requirements are within the projected capabilities of a CMG control system. The second and the most important advantage of a CMG system deals with the contamination control requirements listed in table 13.1. A RCS system controls the attitude of a spacecraft by expelling matter which is a potential source of experiment contamination whereas a CMG control system is a contamination free system. The contamination requirements listed in table 13.1 are fairly stringent and in all likelihood could not be met if the baseline Shuttle RCS was used for attitude control.

The next step in designing a CMG control system is to translate the mission requirements into appropriate CMG system requirements. The resulting CMG system requirements derived using the mission requirements listed in table 13.1 are:

CMG system momentum: 13,000 ft-lb-sec (spherical)

CMG system torque: 200 ft-lb about each axis

CMG redundancy: "fail operational, fail safe"

The above CMG system torque and momentum requirements were sized based on projected disturbance torques acting on the vehicle and the momentum that the CMG system must store in order for the vehicle to maintain the required vehicle attitudes for one orbit. The CMG torque and momentum requirements associated with the vehicle maneuver rate requirements listed in table 13.1 are excessive and are not reflected in the above CMG torque and

Table 13.1. Mission Requirements

Absolute Shuttle Pointing Requirement: $\widehat{3 \text{ min}}$
Shuttle Stabilization Requirement: $\widehat{3 \text{ min/observation}}$

Shuttle Attitude Requirements:

X-POP Inertial (X axis perpendicular to the orbital plane)
X-IOP Inertial (X axis in the orbital plane)
Z-LV (Z axis aligned with the local vertical)

CMG System Momentum Desaturation: once an orbit capability
Vehicle Maneuver Rate Requirement: $\widehat{0.1 \text{ degree/second}}$ about
each vehicle control axis (rate must be attainable in
15 seconds)

Contamination Control:

Particles: 10,000 class
Gas: 10^{-6} to 10^{-7} torrs

momentum requirements. A decision was made to perform all large angle Shuttle maneuvers (i.e., from a X-POP inertial attitude to a X-IOP inertial attitude) by using the baseline RCS. The CMG system is used to provide fine maneuver control by reducing system overshoots and settling times.

Using these CMG system requirements, various CMG configurations were devised to meet these requirements. Both double gimbal and single gimbal CMG systems were considered. Each configuration was evaluated on the basis of the number of CMGs needed, size, weight, power, and the impact on the system of a single CMG failure. The selected CMG system consists of six double gimbal CMGs with each CMG having a wheel momentum of 2,300 ft-lb-sec and no gimbal stops. The mounting configuration used in this study has two CMGs identically mounted along each vehicle axis. Because of the absence of gimbal stops, the mounting configuration is not critical. Logically, the CMGs should be mounted based on vehicle space and structural considerations.

Next, a vehicle control loop is designed that will result in a stable system and one that can meet the vehicle pointing and stabilization requirements listed in table 13.1. The vehicle control law used in this study is a standard rate plus position control law. The function of the vehicle control law is to generate an appropriate CMG torque command based on the sensed vehicle motion. The vehicle control law rate and position gain matrices are selected to meet the vehicle pointing and stabilization requirements.

The vehicle control system has been designed. The only remaining task is to select the CMG control logic needed to implement the CMG control system. The required CMG control logic consists of three components; they are: (1) a CMG maneuver control law, (2) a CMG gimbal rate command control law, and (3) a CMG system momentum management scheme. In each of the above categories, there are a number of possible candidates. In order to select the "most" appropriate control logic mix, a trade study is performed. From each set of candidates, a law is selected based primarily on its computational complexity and performance.

In section 8 of this report, three candidate CMG maneuver control laws are derived; they are based on (1) quaternion, (2) direction cosine, and (3) Euler angle strapdown implementations for describing the attitude of a spacecraft. The functions of these three maneuver control laws are to generate the appropriate error signals that will enable the vehicle to maintain or track specific attitudes and to perform particular maneuvers from one attitude to another. The resultant attitude error and/or rate

maneuver commands are implemented by inputting these signals into the vehicle control law. The quaternion maneuver control law was selected because (1) the vehicle maneuver produced is optimal and (2) the associated strapdown and maneuver equations can be simply and readily computed. The resultant vehicle maneuver is optimal because the vehicle is rotated about a single axis through the smallest angle required to produce the desired attitude change.

The CMG gimbal rate command law consists of two parts: (1) a CMG control law or steering law that generates a set of gimbal rate commands that will result in the desired CMG torque as computed by the vehicle control law and (2) a singularity avoidance scheme that generates another set of CMG gimbal rate commands that drives the CMG system away from singularity without producing any additional CMG torque. For a double gimbal CMG system, the singularity condition that this singularity avoidance scheme must avoid is the "anti-parallel" condition where the individual CMG wheel momentum vectors are aligned, but with some of them pointed in opposite directions. In this condition, the CMG system is physically unable to generate the desired CMG torque. The CMG control law and singularity avoidance gimbal rate commands are summed and sent to the appropriate CMG actuators as a single gimbal rate command. In section 9, four candidate CMG control laws are derived; they are: (1) the Cross Product CMG Control Law, (2) the H-Vector CMG Control Law, (3) the Scissored Pair CMG Control Law, and (4) the Pseudo-Inverse CMG Control Law. From these four candidates, the Pseudo-Inverse CMG Control Law was selected because (1) it is a decoupled control law meaning that the resultant CMG control torque generated identically equals the CMG torque command and (2) this law minimizes the CMG gimbal rate commands therefore minimizing the energy required to generate the desired CMG torque. Also in section 9, three singularity avoidance schemes are derived; they are: (1) Arbitrary Torquing of CMGs Away From Singularity, (2) Isogonal CMG Distribution Law, and (3) Optimal CMG Distribution Law. The Optimal CMG Distribution Law was selected because (1) it maximizes a singularity function that is a measure of the "distance" the CMG system is away from an "anti-parallel" condition and (2) it is very compatible with the selected Pseudo-Inverse CMG Control Law. An attempt was made to combine the Pseudo-Inverse CMG Control Law and the Optimal CMG Distribution Law into a single CMG gimbal rate command law. The obvious advantage of combining these two laws is that only a single expression is needed to generate the total CMG gimbal rate command. The resultant expression for this combined gimbal rate command is so complex that there is no computational savings or improved performance capability resulting from combining these two laws. Therefore, the recommended mode of operation is to use the individual gimbal rate command laws and then to add their corresponding gimbal rate commands to form the total command.

The function of the CMG system momentum management scheme is to insure that the CMG momentum scheme does not become saturated from a momentum storage standpoint. The primary mechanism for accomplishing this objective is a CMG momentum desaturation system. This mechanism desaturates the CMG system by applying a properly directed torque to the vehicle which reduces the momentum stored in the CMG system. In section 10, two general types of CMG desaturation systems are described; they are: (1) a reaction jet desaturation system utilizing the baseline Shuttle RCS and (2) a gravity gradient desaturation system which uses the natural gravity gradient torques acting on the vehicle. A RCS desaturation system desaturates the CMG system by sending appropriate jet firing commands to the baseline RCS. For a gravity gradient desaturation system, CMG desaturation is accomplished by sending vehicle maneuver commands and rate commands to the vehicle control law where these commands are implemented. A RCS desaturation system is more versatile than a corresponding gravity gradient system in that it can develop large desaturation torques in any direction thus desaturating the CMG system in a very short time. Its major drawback is that it expells mass during desaturation that can be a severe source of experiment contamination. For this reason the two RCS desaturation systems devised in section 10 were eliminated from consideration as the prime CMG desaturation system. Four gravity gradient desaturation laws were derived in section 10; they are: (1) a small angle multiaxis maneuver law, (2) a large single axis maneuver law, (3) a reflexive law requiring large multiaxis maneuvers, and (4) a gravity tracking law also requiring large multiaxis maneuvers. All of these laws involve maneuvering the vehicle at the start of the desaturation period to a favorable orientation where the gravity gradient torque acting on the vehicle will cause the magnitude of the CMG momentum to decrease. Of the four gravity gradient desaturation laws, the small angle multiaxis CMG desaturation law, law 1, was selected because of the following reasons: (1) the computational requirements associated with this law are fewer than those associated with the other laws and (2) the resultant small angle maneuvers can be performed by the CMG control system. This latter reason is important because the other candidate desaturation laws require at least a single large angle maneuver. To perform these large maneuvers, the baseline RCS would probably have to be used in order to generate the large torque and momentum required to perform these maneuvers in a reasonable period of time. Firing the baseline RCS to perform these maneuvers tends to defeat the principal reason for adding a CMG control system to a vehicle like the Shuttle that of reducing RCS contamination. It is recommended that a RCS desaturation system be retained as a back-up CMG desaturation system in order to give the system an emergency CMG desaturation capability.